



**FUNDAÇÃO OSWALDO CRUZ
INSTITUTO GONÇALO MONIZ**

**Curso de Pós-Graduação em Biotecnologia em Saúde e Medicina
Investigativa**

TESE DE DOUTORADO

**FÁRMACOS COM AÇÃO DUAL ANTI-*Trypanosoma cruzi* E
IMUNOMODULADORA: UMA NOVA ABORDAGEM PARA O
TRATAMENTO DA MIOCARDIOPATIA CHAGÁSICA CRÔNICA**

CÁSSIO SANTANA MEIRA

Salvador-Bahia

2018

**FUNDAÇÃO OSWALDO CRUZ
INSTITUTO GONÇALO MONIZ**

**Curso de Pós-Graduação em Biotecnologia em Saúde e Medicina
Investigativa**

**FÁRMACOS COM AÇÃO DUAL ANTI-*Trypanosoma cruzi* E
IMUNOMODULADORA: UMA NOVA ABORDAGEM PARA O
TRATAMENTO DA MIOCARDIOPATIA CHAGÁSICA CRÔNICA**

CÁSSIO SANTANA MEIRA

Tese apresentada ao Curso de Pós-Graduação em Biotecnologia em Saúde e Medicina Investigativa para a obtenção do grau de Doutor.

Orientadora: Dr^a Milena Botelho Pereira Soares

Co-orientador: Dr. Diogo Rodrigo Magalhães Moreira

Salvador-Bahia

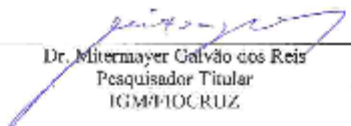
2018

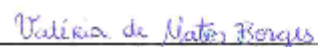
"FÁRMACOS COM AÇÃO DUAL ANTI-*TRYPANOSOMA CRUZI* E IMUNOMODULADORA: UMA NOVA ABORDAGEM PARA O TRATAMENTO DA MIOCARDIOPATIA CHAGÁSICA CRÔNICA."

CÁSSIO SANTANA MEIRA

FÓLHA DE APROVAÇÃO

COMISSÃO EXAMINADORA


Dr. Mitermayer Galvão dos Reis
Pesquisador Titular
IGM/FIOCRUZ


Dra. Valéria de Matos Borges
Pesquisadora
IGM/FIOCRUZ


Dra. Marcia Cristina Aquino Teixeira
Professora Associada II
UFBA

FONTES DE FINANCIAMENTO

Conselho Nacional de Desenvolvimento Científico e Tecnológico - CNPq

Fundação de Amparo à Pesquisa do Estado da Bahia - FAPESB

AGRADECIMENTOS

Gostaria de agradecer, inicialmente, à minha família e amigos, pelo apoio, incentivo para superar os obstáculos e amor que sempre me foram dado, em especial a minha mãe **Waldimara Silva Santana** e minha namorada **Geisa Silva Novais**, que está sempre vibrando a cada conquista minha e, acima de tudo, estendendo a mão em cada momento difícil.

À minha orientadora, **Dra. Milena Botelho Pereira Soares**, por acreditar no meu potencial, pelos ensinamentos, confiança, apoio, orientação e amizade ao longo de todos esses anos. Toda a minha admiração e respeito.

Ao **Dr. Diogo Rodrigo Magalhães Moreira** e à **Dra. Elisalva Teixeira Guimarães** por estarem sempre à disposição para ajudar em todos os momentos e por terem contribuído para a minha formação científica durante meu doutorado.

Às **Dras. Adriana Lanfredi Rangel, Juliana Vasconcelos e Simone Garcia Macambira**, pelo incentivo dado ao longo do tempo e por estarem sempre dispostas a ajudar e ensinar.

A todos os meus amigos do LETI e CBTC, em especial algumas pessoas que os laços de amizade foram mais fortes: **Emanuelle Santos, Iasmim Orge, Renan Fernandes, Tanira Matutino e Vinicius Rocha** por estarem sempre à disposição para ajudar em todos os momentos, principalmente nos experimentos; **Anna Karoline Ritt, Afrânio Evangelista, Breno Cardim, Camila Couto, Dahara Keyse, Luciano Santos, Mariana Borges, Nanashara Carvalho, Paula Ladeia, Rosane Dias, Taís Macedo, Tatiana Barbosa e Valdenizia Silva** pela amizade e pelos momentos de conversas nada científicas.

À **Rafaela Alves** e **Liliane Cunha** pela ajuda indispensável nos experimentos de citometria.

À **Edileuza Soares, Marlene Cerqueira, Lucyvera Imbroinise e Rute Vivas** pela amizade e disposição para sempre ajudar.

A **todos os professores do Programa de Pós-graduação em Biotecnologia e Medicina Investigativa**, por terem me proporcionado um ensino de excelência.

Ao **IGM** e ao **CBTC/Hospital São Rafael**, pelas estruturas que proporcionaram a minha participação em diversos projetos de pesquisa.

A **todos os membros da biblioteca do IGM** pelo apoio e suporte na revisão da presente tese.

À **CAPES** pela concessão da bolsa, imprescindível para a realização deste trabalho.

A todos que, direta ou indiretamente, contribuíram para a realização deste trabalho.

“Você nasceu para vencer, mas para ser um vencedor você precisa planejar para vencer, se preparar para vencer, e esperar vencer.”

Zig Zglar

MEIRA, Cássio Santana. **Fármacos com ação dual anti-*Trypanosoma cruzi* e imunomoduladora: Uma nova abordagem para o tratamento da miocardiopatia chagásica crônica.** 236 f. il. Tese (Doutorado em Biotecnologia em Saúde e Medicina Investigativa) – Fundação Oswaldo Cruz, Instituto Gonçalo Moniz, Salvador, 2018.

RESUMO

INTRODUÇÃO: A doença de Chagas é uma zoonose causada pelo protozoário hemoflagelado *Trypanosoma cruzi*, que afeta milhões de pessoas na América Latina. No Brasil e em muitos países, o tratamento dessa enfermidade se baseia na utilização de benzonidazol. Este fármaco tem o seu uso associado a uma série de efeitos colaterais no paciente ao longo do tratamento e uma baixa taxa de cura nos indivíduos com doença crônica. Nesse contexto, é necessário o desenvolvimento de novos medicamentos para uma quimioterapia adequada da doença de Chagas crônica, sobretudo na forma cardíaca da doença. **OBJETIVO:** Este estudo teve como objetivo testar o derivado semissintético do ácido betulínico (BA5) e o esfingolípido N,N-dimetil esfingosina (DMS), moléculas com propriedades antiparasitária e imunomoduladora, para o tratamento da cardiomiopatia chagásica crônica. **MATERIAIS E MÉTODOS:** O efeito tripanocida foi avaliado *in vitro* em tripomastigotas do *T. cruzi* e também na proliferação de formas amastigotas intracelulares em culturas de macrófagos peritoneais infectados com *T. cruzi*, com determinação de valores de concentração inibitória (CI)₅₀. A atividade imunomoduladora *in vitro* foi avaliada em cultura de macrófagos estimulados com LPS + IFN γ e em esplenócitos estimulados com concanavalina A através da quantificação de mediadores inflamatórios por ELISA e em ensaios de linfoproliferação pela incorporação de ³H-timidina. A ação imunomoduladora do BA5 foi validada *in vivo* em modelo de endotoxemia e de reação de hipersensibilidade tardia (DTH). Por último, camundongos C57BL/6 cronicamente infectados com *T. cruzi* foram tratados com BA5 ou DMS, e submetidos a avaliações de função cardíaca, quantificação de inflamação e fibrose no coração, de citocinas no soro por ELISA, e análises de PCR para avaliar a modulação da expressão gênica no coração e a carga parasitária no baço. **RESULTADOS:** Assim como o BA5 (já previamente estudado), o DMS apresentou um efeito anti-*T. cruzi* direto, porém também age através da ativação da via do inflamassoma gerando a produção de óxido nítrico e espécies reativas de oxigênio. Quando testados em culturas de macrófagos e linfócitos ativados, os compostos mostraram uma potente atividade imunomoduladora, reduzindo a produção de mediadores inflamatórios e inibindo a proliferação de linfócitos. *In vivo*, o BA5 demonstrou potente atividade imunomoduladora, conferindo proteção contra dose letal de LPS e reduzindo edema em modelo de DTH. Observamos uma redução significativa da inflamação e fibrose nos corações dos animais chagásicos crônicos tratados com BA5 ou DMS, achados estes que foram acompanhados por uma redução dos níveis séricos de TNF α e IFN γ , assim como a redução da expressão gênica de mediadores inflamatórios no coração. Nos animais tratados com BA5 observamos também um aumento significativo na produção de IL-10 e na expressão gênica de *arginase* e *CHI3*, reconhecidos marcadores de macrófagos M2. A redução de mediadores inflamatórios poderia ocasionar um aumento na carga parasitária na CCC experimental. Entretanto, através da quantificação do DNA de *T. cruzi* no baço, demonstramos que o tratamento com o BA5 não alterou a carga parasitária, enquanto o tratamento com o DMS causou a redução da carga parasitária de forma substancial, evidenciado o efeito antiparasitário desta molécula. **CONCLUSÃO:** Nossos resultados demonstram que o BA5 e o DMS,

através de ação antiparasitária e imunomoduladora, são candidatos em potencial para o desenvolvimento de novos fármacos para o tratamento da cardiomiopatia chagásica.

Palavras-chave: Doença de Chagas, *T. cruzi*, N,N-dimetil esfingosina, Ácido betulínico, cardiomiopatia chagásica.

MEIRA, Cássio Santana. **Drugs with dual anti-*Trypanosoma cruzi* and immunomodulatory actions: A new approach for the treatment of chronic chagasic myocardiopathy.** 236 f. il. Tese (Doutorado em Biotecnologia em Saúde e Medicina Investigativa) – Fundação Oswaldo Cruz, Instituto Gonçalo Moniz, Salvador, 2018.

ABSTRACT

INTRODUCTION: Chagas disease is a zoonosis caused by the protozoan hemoflagellate *Trypanosoma cruzi*, which affects millions of people in Latin America. In Brazil and in many countries, the treatment of this disease is based on the use of benznidazole. Its use is associated with a number of side effects throughout the treatment and has a low cure rate in individuals with chronic disease. In this context, the development of new drugs for a proper chemotherapy of chronic Chagas' disease is necessary, especially in the cardiac form of the disease. **OBJECTIVE:** This study aimed to test the semisynthetic derivative of betulinic acid (BA5) and sphingolipid N,N-dimethyl sphingosine (DMS), two molecules with antiparasitic and immunomodulatory properties, for the treatment of Chagas' heart disease. **MATERIALS AND METHODS:** The trypanocidal effect was evaluated *in vitro* in *T. cruzi* trypomastigotes and also in the proliferation of intracellular amastigote forms in cultures of peritoneal macrophages infected with *T. cruzi*, with determination of inhibitory concentration (IC)₅₀ values. Immunomodulatory activity *in vitro* was evaluated in culture of macrophages stimulated with LPS + IFN γ and in splenocytes stimulated with concanavalin A by the quantification of inflammatory mediators by ELISA and in lymphoproliferation assays by the incorporation of ³H-thymidine. The immunomodulatory action of BA5 was validated *in vivo* in a model of endotoxemia and delayed hypersensitivity (DTH). Finally, C57BL/6 mice chronically infected with *T. cruzi* were treated with BA5 or DMS and subjected to evaluations of cardiac function, quantification of inflammation and fibrosis in the heart, serum cytokines by ELISA, and PCR analyzes to evaluate the modulation of gene expression in the heart and the parasite load on the spleen. **RESULTS:** Similar to BA5 (already previously studied), DMS presented a direct anti-*T. cruzi* effect, but also presented a potential to activate inflammasome pathway generating the production of nitric oxide and reactive oxygen species. When tested in macrophages and lymphocyte activated cultures, both compounds showed potent immunomodulatory activity, reducing the production of inflammatory mediators and inhibiting lymphocyte proliferation. *In vivo*, BA5 demonstrated potent immunomodulatory activity, conferring protection against lethal dose of LPS and reducing edema in the DTH model. We observed a significant reduction of inflammation and fibrosis in the hearts of chronic chagasic animals treated with BA5 or DMS, which were accompanied by a reduction in serum levels of TNF α and IFN γ , as well as the reduction of the gene expression of inflammatory mediators in the heart. In BA5-treated animals we also observed a significant increase in IL-10 production and in the gene expression of *arginase* and *CHI3*, recognized markers of M2 macrophages. The reduction of inflammatory mediators could cause an increase in the parasitic load in the experimental CCC. However, through the quantification of *T. cruzi* DNA in the spleen, we demonstrated that the treatment with BA5 did not alter the parasitic load, whereas the treatment with DMS caused the reduction of the parasite load substantially, evidencing the antiparasitic effect of this molecule. **CONCLUSION:** Our results demonstrate that BA5 and DMS, through antiparasitic and immunomodulatory action, are potential candidates for the development of new drugs for the treatment of chagasic cardiomyopathy.

Keywords: Chagas disease, *T. cruzi*, N,N-dimethylsphingosine, Betulinic acid, Chagasic cardiomyopathy.

LISTA DE ILUSTRAÇÕES

Figura 1. Ciclo biológico do <i>Trypanosoma cruzi</i>	20
Figura 2. A resposta imune nas formas cardíaca e indeterminada da doença de Chagas.....	25
Figura 3. Mecanismos pelo qual o <i>T. cruzi</i> pode levar à miocardite.....	26
Figura 4. Esquema comparando a citotoxicidade e atividade anti- <i>T. cruzi</i> do ácido betulínico e seu derivado BA5.....	30
Figura 5. Esquema mostrando o mecanismo de ação do N,N-dimetil esfingosina (DMS).....	32
Figura 6. Representação esquemática da ação do BA5 no modelo de CCC experimental.....	96
Figura 7. Representação esquemática da ação do DMS no modelo de CCC experimental.....	100

LISTA DE ABREVIATURAS E SIGLAS

Arg1	Arginase-1
APC	Célula apresentadora de antígeno
BA	Ácido betulínico
BA5	Derivado semissintético do ácido betulínico
BENEFIT	Avaliação do benzonidazol para interrupção da tripanossomíase
C-3	Carbono de posição 3
C-20	Carbono de posição 20
C-28	Carbono de posição 28
CASP1	Caspase 1
CC ₅₀	Concentração citotóxica de 50%
CCC	Cardiomiopatia chagásica crônica
CCR5	Receptor da quimiocina C-C tipo 5
CD4	Grupamento de diferenciação 4
CD8	Grupamento de diferenciação 8
CD28	Grupamento de diferenciação 28
CD45	Grupamento de diferenciação 45
CHI3	do inglês <i>chitinase 3</i>
CI ₅₀	Concentração inibitória de 50%
CXCR4	Receptor de quimiocina C-X-C tipo 4
DAMPs	Padrões moleculares associados a danos
DMS	N,N-dimetil-esfingosina
DNA	Ácido desoxirribonucleico
EROs	Espécies reativas de oxigênio
FTY720	Fingolimod
Gal-3	Galectina-3
G-CSF	Fator estimulador de colônias de granulócitos
HIV	Vírus da imunodeficiência humana
ICAM-1	Molécula de adesão intracelular 1
IFN- γ	Interferon gama
IL-2	Interleucina 2

IL-4	Interleucina 4
IL-6	Interleucina 6
IL-8	Interleucina 8
IL-10	Interleucina 10
IL-12	Interleucina 12
IL-17	Interleucina 17
IL-23	Interleucina 23
IL-1 β	Interleucina 1 β
LPS	Lipopolissacarídeo
M1	Macrófago tipo I ou classicamente ativado
M2	Macrófago tipo I ou alternativamente ativado
NFAT	Fator nuclear de células T ativadas
NF- κ B	Fator de transcrição nuclear kappa B
<i>Nlrc5</i>	do inglês <i>NLR family CARD domain containing 5</i>
<i>Nlr1</i>	do inglês <i>NLR family member X1</i>
NK	do inglês <i>Natural Killer</i>
NO	Óxido nítrico
NOS2	Óxido nítrico sintase 2
PAMPs	Padrões moleculares associados a patógenos
PCR	Reação em cadeia da polimerase
SIP	Esfingosina-1-fosfato
S1P ₁	Receptor 1 da esfingosina-1-fosfato
S1P ₂	Receptor 2 da esfingosina-1-fosfato
Tbet	Fator de transcrição t-box
TGF β	Fator de crescimento de transformação β
Th1	Linfócito T auxiliar tipo 1
Th2	Linfócito T auxiliar tipo 2
Th17	Linfócito T auxiliar tipo 17
TLR	do inglês <i>Toll like receptor</i>
TNF α	Fator de necrose tumoral α
Treg	Linfócitos T regulatórios
WHO	World Health Organization

SUMÁRIO

1	INTRODUÇÃO	16
2	REVISÃO DE LITERATURA	18
2.1	A DOENÇA DE CHAGAS.....	18
2.2	CICLO DE VIDA DO <i>Trypanosoma cruzi</i>	19
2.3	EPIDEMIOLOGIA E DISTRIBUIÇÃO GEOGRÁFICA DA DOENÇA DE CHAGAS.....	21
2.4	MANIFESTAÇÕES CLÍNICAS DA DOENÇA DE CHAGAS.....	22
2.5	IMUNOPATOGÊNESE DA DOENÇA DE CHAGAS.....	24
2.6	INTERVENÇÕES TERAPÊUTICAS NA DOENÇA DE CHAGAS.....	27
2.7	ÁCIDO BETULÍNICO E O SEU DERIVADO SINTÉTICO BA5.....	29
2.8	ESFINGOLIPÍDIOS E A N,N-DIMETIL-ESFINGOSINA.....	31
3	OBJETIVOS	34
3.1	GERAL.....	34
3.2	ESPECÍFICOS.....	34
4	RESULTADOS	35
	CAPÍTULO I.....	35
	CAPÍTULO II.....	46
	CAPÍTULO III.....	77
5	DISCUSSÃO GERAL	92
6	CONCLUSÕES	101
	REFERENCIAS	102
	ANEXOS	117

1 INTRODUÇÃO

As doenças negligenciadas afetam milhões de pessoas nas diferentes regiões do planeta e são responsáveis por incapacitar uma fração significativa da população mundial, principalmente em países em desenvolvimento (WORLD HEALTH ORGANIZATION, 2017a). Dentre estas doenças se destaca a doença de Chagas, descrita no início do século XX pelo pesquisador Carlos Chagas (CHAGAS, 1909). A doença consiste em uma zoonose causada pelo protozoário hemoflagelado *Trypanosoma cruzi*, que afeta entre 6 e 7 milhões de pessoas, principalmente na Americana Latina, onde é considerada endêmica (WORLD HEALTH ORGANIZATION, 2017b).

Apesar dos avanços significativos na profilaxia da doença de Chagas gerados pelo controle da transmissão natural, pelo aumento do controle na triagem em bancos de sangue e de casos de transmissão congênita, a doença de Chagas ainda representa um problema de saúde pública grave, principalmente na América Latina (MATSUO, 2010; WHO, 2017a; PÉREZ-MOLINA; MOLINA, 2018). A intervenção terapêutica com fármacos antiparasitários é limitada a duas drogas: o benzonidazol e o nifurtimox. Estes medicamentos possuem eficácia em curar a fase aguda da doença, porém possuem baixa eficácia na fase crônica, apresentam diversos efeitos colaterais e ainda com indução de cepas resistentes a esses medicamentos (JUNIOR, 2017). Devido a essas limitações, o desenvolvimento de novas estratégias é necessário, em especial para a forma cardíaca crônica, que é responsável por uma taxa de mortalidade alta por doenças cardíacas na América Latina (BENZIGER, 2017).

Devidos aos danos teciduais causados pela resposta inflamatória na cardiomiopatia chagásica crônica (CCC), a intervenção terapêutica não deveria compreender apenas fármacos capazes de eliminar o parasito, mas também de reduzir a inflamação. Nesse contexto, o desenvolvimento de novas moléculas com propriedades farmacológicas duais, atuando como antiparasitárias e imunomoduladoras na cardiomiopatia chagásica crônica é de extrema importância.

Recentemente, nosso grupo de pesquisas demonstrou o efeito benéfico do fator estimulador de colônias de granulócitos (G-CSF) em um modelo de cardiomiopatia chagásica crônica. Através de uma ação dual, atuando como agente tripanocida e imunomodulador, o G-CSF reduziu a inflamação, a fibrose e o parasitismo no coração de animais chagásicos e contribuiu para uma melhorar funcional cardíaca dos animais

(VASCONCELOS, 2013). Estes achados reforçam a utilização de agentes imunomoduladores como uma estratégia eficaz para o tratamento da CCC.

Nesse contexto, no presente trabalho investigamos os efeitos do derivado semissintético do ácido betulínico (BA5) e do esfingolípido N,N-dimetil esfingosina (DMS) em um modelo de cardiopatia chagásica crônica. O DMS é um inibidor pantrópico de esfingosinas cinases, moléculas importantes na patogênese de inúmeras desordens de origem inflamatória e no remodelamento cardíaco (TAKUWA, 2010; MACEYKA; SPIEGEL, 2014; YANAGIDA; HLA, 2017). Já o BA5 é um derivado semissintético do ácido betulínico, um triterpenóide conhecido por sua abundância na natureza e por ter diversas atividades biológicas já reportadas, incluindo atividade antiparasitária e imunomoduladora (YOGEE SWARI; SRIRAM, 2005; Anexo I). Recentemente, o nosso grupo demonstrou que a incorporação de um grupamento amida no carbono de posição C28 resultou em uma nova série de compostos, sendo o derivado BA5 o composto com o melhor perfil antiparasitário (Anexo II).

2 REVISÃO DE LITERATURA

2.1 A DOENÇA DE CHAGAS

As doenças negligenciadas afetam milhões de pessoas nas diferentes regiões do planeta e são responsáveis por incapacitar uma fração significativa da população mundial, principalmente em países em desenvolvimento. Estimativas indicam que mais de um bilhão de pessoas são pelo menos portadoras de uma doença negligenciada, o que representa aproximadamente um sexto da população mundial e gera um grande impacto social e econômico no mundo (WORLD HEALTH ORGANIZATION, 2017a). Dentre estas, destaca-se a doença de Chagas, uma zoonose causada pelo protozoário hemoflagelado *Trypanosoma cruzi*, descrita pela primeira vez no início do século XX pelo pesquisador brasileiro Carlos Chagas (CHAGAS, 1909).

O *T. cruzi* é um protozoário pertencente à ordem Kinetoplastida e família Trypanosomatidae, cuja principal característica é a presença de flagelo e cinetoplasto, região da mitocôndria onde se concentra uma grande quantidade de DNA extranuclear (DE SOUZA, 2002). A doença é transmitida por insetos triatomíneos pertencentes à família *Reduviidae*, mais especificamente à subfamília *Triatominae*, popularmente conhecidos no Brasil como barbeiros (COURA, 2015). Existem aproximadamente 150 espécies capazes de transmitir o parasito, sendo as espécies de maior contribuição na transmissão vetorial o *Triatoma infestans*, *T. dimidiata*, *T. sordida*, *Rhodnius prolixus* e *Panstrongylus megistus* (GARCIA; AZAMBUJA, 1991).

A infecção pelo *T. cruzi* inicialmente era restrita a pequenos mamíferos de regiões de matas e campos da América, desde a Patagônia até o sul dos Estados Unidos. Esses animais (tatus, gambás, roedores) convivem com triatomíneos silvestres e, entre eles, ainda hoje circula o *T. cruzi* (TARLETON, 2007). Com a chegada do homem na América e os processos de colonização, ocorreram desequilíbrios ecológicos (desmatamentos, queimadas) e os barbeiros invadiram as habitações próximas a ambientes naturais, na procura por novas fontes de alimento. Como resultado, a infecção chegou ao homem (doença de Chagas) e aos mamíferos domésticos, sendo então classificada como uma zoonose (COURA; DIAS, 2009). A presença de exemplares de *T. infestans* em habitações humanas da era pré-colombiana e a detecção de DNA de *T. cruzi* em múmias encontradas na América do Sul datadas de 7050 anos a.C. evidenciam o estabelecimento gradual do ciclo domiciliar (AUFDERHEIDE, 2004).

2.2 CICLO DE VIDA DO *Trypanosoma cruzi*

O *T. cruzi* possui um ciclo de vida complexo que compreende diferentes formas morfológicas em hospedeiros vertebrados e invertebrados (COURA, 2015). O parasito apresenta-se sob três formas: uma forma replicante encontrada no citoplasma das células do hospedeiro vertebrado, conhecida como forma amastigota; uma forma flagelada, fusiforme, infectiva para vertebrados, incapaz de se dividir e presente nos hospedeiros vertebrados (tripomastigotas sanguíneos) e nos invertebrados (tripomastigotas metacíclicos); e uma terceira forma flagelada, que não é infectiva para vertebrados e se replica por fissão binária, presente no intestino médio do hospedeiro invertebrado, conhecida como forma epimastigota (DE SOUZA, 2002).

O ciclo de vida do *T. cruzi* se inicia quando um triatomíneo infectado, após a realização do repasto sanguíneo, elimina fezes e urina contendo formas tripomastigotas metacíclicas do parasito, que são capazes de infectar o hospedeiro vertebrado quando entram em contato com mucosas do olho, boca, ferimentos ou quando são ingeridas (BRENER; ANDRADE; BARRAL-NETO, 2000). Uma vez dentro do hospedeiro, a interação parasito-hospedeiro ocorre de forma dinâmica, resultante de múltiplos fatores ligados ao *T. cruzi* (cepa, virulência, tamanho do inóculo), ao homem (sexo, idade, raça) e ao ambiente (ANDRADE, 1985; DUTRA, 2014). Dentro do hospedeiro vertebrado, as formas tripomastigotas podem invadir macrófagos e uma variedade de outras células, permanecendo por algum tempo dentro de fagolisossomos. Quando escapam para o citoplasma, estas se diferenciam para as formas amastigotas e proliferam por divisão binária. Após sucessivas divisões, as formas amastigotas iniciam a sua diferenciação em formas tripomastigotas sanguíneas. O rompimento da célula hospedeira pode ocorrer antes da total diferenciação de formas amastigotas em formas tripomastigotas, o que gera o aparecimento de diferentes formas no meio externo. No meio extracelular, os tripomastigotas e as amastigotas podem alcançar outras regiões e infectar novas células (GARCIA; AZAMBUJA, 1991; DE SOUZA, 2002).

O ciclo de vida se completa quando o sangue contendo formas tripomastigotas sanguíneas de um hospedeiro vertebrado infectado é sugado por um triatomíneo, durante o seu repasto sanguíneo. As formas tripomastigotas sanguíneas se diferenciam em formas epimastigotas, na porção média do trato gastrointestinal do inseto e se multiplicam por fissão binária. Essa forma está adaptada para sobreviver à ação de enzimas presentes no trato gastrointestinal do inseto, através de uma cobertura resistente

a ação de proteases e glicosidades, presente na sua superfície (DE SOUZA, 2002). No intestino posterior, os parasitos sofrem uma diferenciação celular denominada metaciclogênese. Esta envolve mudanças morfológicas e metabólicas que dão origem a formas tripomastigotas metacíclicas, que são as formas liberadas nas excretas dos insetos e capazes de infectar vertebrados (**Figura 1**).

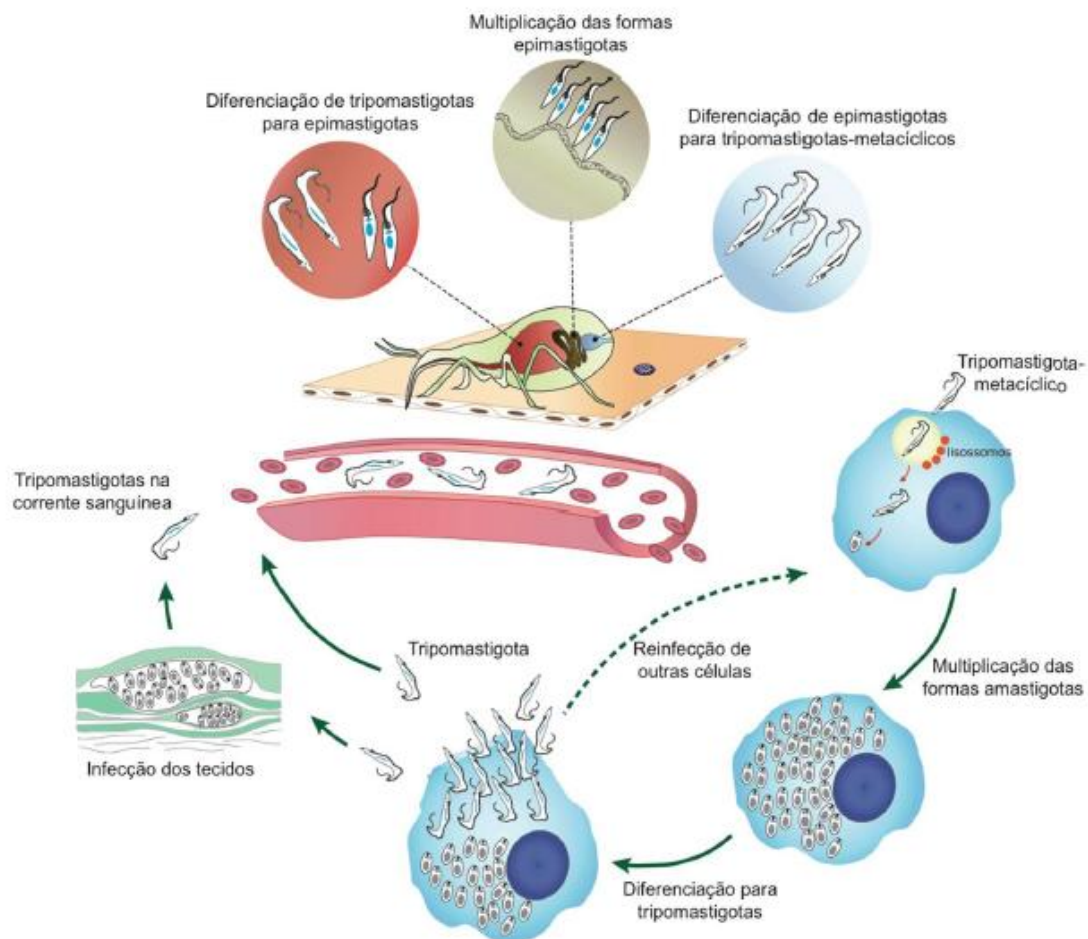


Figura 1. Ciclo biológico do *Trypanosoma cruzi*. Fonte: Elaborado pelo Dr. Nilmar Silvio Moretti.

O parasito pode ainda penetrar no hospedeiro vertebrado por outras vias, tais como: transfusão sanguínea, transplante de órgãos, acidentes em laboratório, transmissão congênita ou ingestão acidental de insetos triturados junto a alimentos (contaminação por via oral), tais como o caldo de cana de açúcar, açaí e goiaba (YOSHIDA, 2008).

Casos agudos resultantes da ingestão acidental do parasito têm sido registrados por surtos em diferentes localidades, com maior incidência na região amazônica, onde o consumo de açaí é uma frequente causa de contaminação (MONCAYO; SILVEIRA, 2009). Em 2007, em uma escola de Caracas, Venezuela, 103 crianças foram infectadas com o consumo de suco de goiaba contaminado. Destas, 75 apresentaram sintomatologia para doença de Chagas aguda e uma criança veio a óbito (ALARCÓN DE NOYA, 2010). No Brasil, em 2005, 24 casos agudos da doença foram registrados em Santa Catarina, e todos eles foram relacionados com a ingestão de caldo de cana-de-açúcar contaminado com o parasito (STEINDEL, 2008). Em 2006, outro surto de casos agudos da doença no Brasil foi registrado em duas cidades vizinhas, Macaúbas e Ibipitanga, do estado da Bahia. O surto envolveu 13 casos confirmados da doença e a contaminação ocorreu possivelmente pela ingestão de caldo de cana-de-açúcar ou água contaminada com fezes de *T. sordida* infectados (BASTOS, 2010).

2.3 EPIDEMIOLOGIA E DISTRIBUIÇÃO GEOGRÁFICA DA DOENÇA DE CHAGAS

A doença de Chagas é considerada uma condição infecciosa classificada como negligenciada pela OMS e inicialmente restrita ao continente americano em virtude da distribuição das aproximadamente 150 espécies do inseto vetor (*Triatominae*, *Hemiptera*, *Reduviidae*), e por isso é também conhecida como "tripanossomíase americana" (COURA; DIAS, 2009). A OMS estima aproximadamente 6 a 7 milhões de pessoas infectadas com o *T. cruzi* em todo o mundo, a maioria residente na América Latina, onde a doença esta presente em 21 países e é considerada endêmica (WORLD HEALTH ORGANIZATION, 2017b).

Com base em características epidemiológicas, tais como formas de transmissão, tipos de ciclos, vetores e programas de controle vetorial e transfusional, a doença de Chagas pode ser dividida em cinco grupos de países (COURA; BORGES-PEREIRA, 2010). O grupo I é formado por Argentina, Bolívia, Brasil, Chile, Equador, Honduras, Paraguai, Peru, Uruguai e Venezuela. A doença de Chagas nesses países se caracteriza por ser transmitida principalmente pelos ciclos domésticos e peridomésticos, com zonas de alta prevalência de indivíduos portadores da forma cardíaca da doença e programas de controle de vetores e transfusão na maioria dos países. No Brasil, estima-se cerca de

1,9 milhões a 4,6 milhões de pessoas infectadas, o que corresponde á variação de 1,0 a 2,4% da população (MARTINS, 2014; HOTEZ; FUJIWARA, 2014).

O grupo II é formado por Colômbia, Costa Rica e México. Nesses países, a doença é caracterizada por ciclos domésticos e peridomésticos, presença de cardiopatia chagásica crônica, ocorrências de doadores infectados e com a falta ou apenas programas de controle incipientes. O Grupo III inclui El Salvador, Guatemala, Nicarágua e Panamá. Nesses países, a doença pode ser transmitida por ciclos domésticos, peridomésticos e selvagens, existe pouca informação clínica sobre casos humanos e programas de controle são escassos, sendo encontrados apenas na Guatemala e Nicarágua. O Grupo IV, que inclui as Antilhas, Bahamas, Belize, Cuba, Estados Unidos, Guiana, Guiana Francesa, Haiti, Jamaica e Suriname, apresenta ciclos selvagens, pouca informação clínica, numerosos casos de imigrantes infectados nos Estados Unidos e uma ausência de programas de controle, com exceção dos Estados Unidos, onde existe controle transfusional (COURA; BORGES PEREIRA, 2010).

Devido ao intenso processo de globalização e fluxo migratório, é possível observar também um aumento do número de casos em países não endêmicos da América do Norte, Europa, Ásia e Oceania, em particular os Estados Unidos, Canadá, Espanha, França, Suíça, Japão, países asiáticos emergentes e Austrália (SCHMUNIS, 2007). Estima-se a presença de mais de 300.000 portadores da doença de Chagas nos Estados Unidos, 5.500 no Canadá, mais de 80.000 na Europa e região do Pacífico ocidental e mais de 1.500 na Austrália (RIBEIRO, 2012). Estes países formam o Grupo V, na classificação acima. Um agravante é o fato de que 94-96% dos imigrantes portadores da doença Chagas não têm conhecimento de que estão infectados, o que dificulta o controle da transmissão e colabora para que a doença de Chagas se torne um problema de saúde pública em países não endêmicos (BASILE, 2011).

2.4 MANIFESTAÇÕES CLÍNICAS DA DOENÇA DE CHAGAS

A infecção chagásica apresenta duas fases bem distintas: uma fase aguda, correspondente à infecção e disseminação do *T. cruzi* no organismo, e uma fase crônica, caracterizada por duas formas distintas: indeterminada e crônica sintomática. Na maioria dos casos, independente da via de transmissão, a fase aguda da doença é assintomática, provavelmente devido a uma baixa carga parasitária (RASSI; RASSI; MARIN-NETO, 2010; KIRCHHOFF, 2011). Contudo, quando a doença se manifesta, o

portador apresenta um quadro febril ou outras manifestações clínicas, tais como hipertermia ou pirexia, hepatoesplenomegalia, náuseas, vômitos, diarreia e anorexia. A fase aguda sintomática ocorre principalmente em crianças na primeira década de vida, podendo levar à morte devido a complicações decorrentes de insuficiência cardíaca e processos inflamatórios que envolvem o cérebro (BOAINAIN e RASSI, 1979; RASSI; RASSI; MARIN-NETO, 2010).

Na grande maioria das vezes, após a fase aguda, a doença de Chagas evolui para fase crônica (RASSI; RASSI; MARIN-NETO, 2010). A maioria dos indivíduos infectados (cerca de 70 %) desenvolve a forma crônica indeterminada da doença, que não apresenta sintomas clínicos. Contudo, cerca de 30% dos indivíduos infectados, após meses ou décadas da infecção evoluem para a fase crônica sintomática; cardíaca, digestiva ou mista. Essa forma da doença é caracterizada pela baixa parasitemia, porém com lesão tecidual e altos índices de anticorpos IgG (ANDRADE, 2000).

A forma cardíaca é conhecida por ser a mais séria e frequente manifestação da fase crônica da doença de Chagas. Ela se desenvolve em 20 a 30 % dos indivíduos crônicos e é caracterizada por miocardite crônica, insuficiência cardíaca e eventualmente morte súbita, por arritmia cardíaca (RASSI; RASSI; LITTLE, 2000; MARIN-NETO, 1999; MARIN-NETO, 2010).

Já a forma digestiva, que se desenvolve em 10 a 15 % dos indivíduos crônicos, ocorre quase que exclusivamente no sul da bacia amazônica (principalmente na Argentina, Brasil, Chile e Bolívia) e é rara no norte da América do Sul, América Central e México (RASSI; RASSI; MARIN-NETO, 2010). Essa distribuição geográfica bem definida é provavelmente explicada pelas diferenças existentes entre as cepas do parasito que circulam em cada uma dessas regiões (MILES, 2003; CAMPBELL; WESTENBERGER; STURM, 2004). Esta forma é caracterizada pelo desenvolvimento de disfunções gastrointestinais (principalmente megaesôfago, megacólon ou ambos). Além das duas formas descritas anteriormente, há relatos da existência de uma forma mista, que corresponde à associação entre as formas cardíaca e a digestiva. Em muitos países, o desenvolvimento de megaesôfago geralmente precede o aparecimento de megacólon e/ou da forma cardíaca. Contudo, a prevalência da forma mista é desconhecida, devido à escassez de estudos apropriados (RASSI; RASSI; MARIN-NETO, 2010).

2.5 IMUNOPATOGÊNESE DA DOENÇA DE CHAGAS

O sistema imune consiste em uma rede complexa, formada por diferentes tipos celulares e seus mediadores que atuam em conjunto no sentido de manter o equilíbrio homeostático. Durante uma infecção parasitária, o sistema imune é essencial para o controle do parasito e, algumas vezes, para conferir resistência à reinfeção. Entretanto, a resposta imune não controlada pode contribuir para a patogênese da doença (CUNHA-NETO, 2011; BONNEY; ENGMAN, 2015).

No caso da doença de Chagas, durante a fase aguda da doença, a primeira linha de defesa contra a invasão parasitária é o sistema imune inato. Componentes clássicos da imunidade inata, tais como células dendríticas e macrófagos, possuem um papel central na ativação da resposta imune anti-*T. cruzi* (TARLETON, 2007; MAYA, 2010). Essas células possuem, em sua superfície, receptores *Toll-like* (TLR), que são capazes de reconhecer padrões moleculares associados a patógenos (PAMPs), induzindo direta ou indiretamente uma resposta imune. Após a ativação via TLR, os macrófagos e células dendríticas irão produzir moléculas pró-inflamatórias envolvidas na resposta local e sistêmica contra o parasito como as citocinas IL1 β , IL-6, IL-8, IL-12 e fator de necrose tumoral alfa (TNF α), quimiocinas e a produção de substâncias microbicidas como o óxido nítrico (RODRIGUES; OLIVEIRA; BELLIO, 2012).

No controle da infecção aguda, as células *natural killer* (NK) também desempenham um importante papel ao promoverem uma conexão entre os eventos da resposta inata e adaptativa (SATHLER-AVELAR, 2009). Este tipo celular é a fonte primária de interferon- γ (IFN- γ), que aumenta a síntese de IL-12 por macrófagos (CARMAGO, 1997). A IL-12 estimula a produção de IFN γ e induz a diferenciação de linfócitos T helper (Th) 0 em Th1, promovendo uma resposta adaptativa robusta contra o parasita, porém na maioria dos casos não consegue eliminar por completo o parasita (REED, 1994).

A fase crônica sintomática é caracterizada pela presença de um intenso infiltrado inflamatório, sendo a cardiomiopatia chagásica crônica a forma de maior prevalência (BERN, 2015). A cardiomiopatia crônica é caracterizada por uma miocardite multifocal, fibrose e danos nas fibras musculares cardíacas, fruto da persistência do agente nocivo, das células inflamatórias, ou de ambos (HIGUCHI, 1987; CUNHA-NETO; CHEVILLARD, 2014). Diversos estudos observam a persistência de níveis elevados de

citocinas pró-inflamatórias, tais como $\text{IFN}\gamma$ e $\text{TNF}\alpha$ e o aumento de linfócitos T CD4 e CD8 produtores de $\text{IFN}\gamma$ no sangue periférico, além da redução de células T reguladoras, o que contribui para o desencadeamento de lesão tecidual (NOGUEIRA, 2014). Já na forma indeterminada, existe a predominância de um ambiente regulatório, uma vez que além das células ativadas produzindo citocinas inflamatórias, há também um aumento no número de células regulatórias e uma alta produção de IL-10, uma citocina anti-inflamatória responsável por desativar os macrófagos e consequentemente inibir os efeitos das células T e células NK, contribuindo para a restrição da lesão tecidual (GOMES, 2003; CUNHA-NETO, 2009). Dessa forma, fica evidente a contribuição de uma resposta Th1 exacerbada para o acometimento cardíaco. Contudo, ainda não são completamente elucidados os mecanismos que desencadeiam essa resposta em somente 30% dos indivíduos portadores da doença de Chagas.

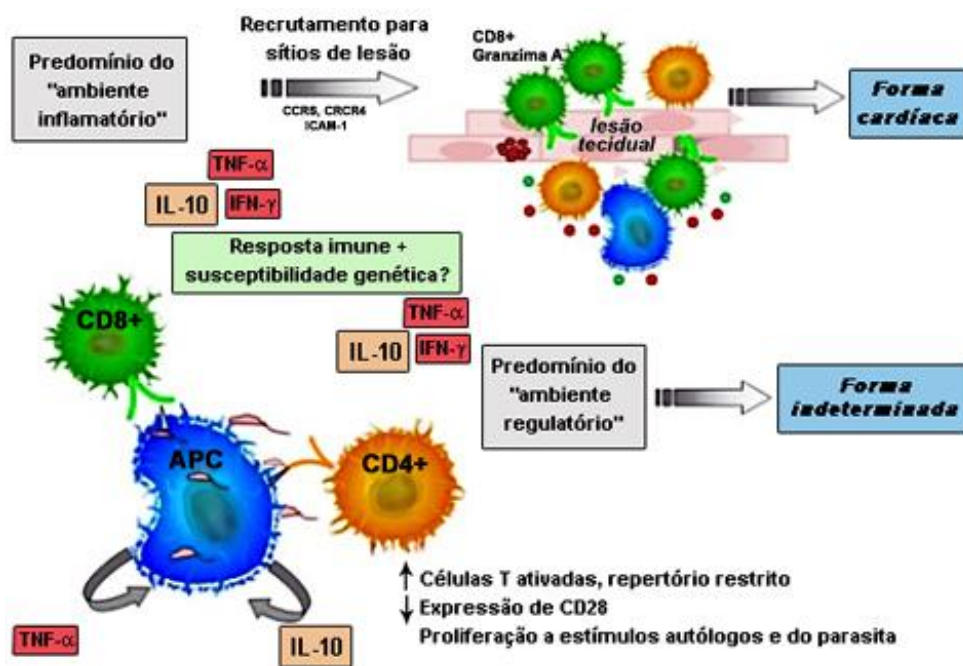


Figura 2 A resposta imune nas formas cardíaca e indeterminada da doença de Chagas.

Fonte: <http://chagas.fiocruz.br/resposta-imune>.

Diversos mecanismos têm sido propostos para explicar a cardiomiopatia crônica nos indivíduos infectados pelo *T. cruzi*. Um deles é o dano nos cardiomiócitos causado diretamente pelos parasitos (**Figura 3A**). No entanto, não foi demonstrada ainda uma correlação entre o grau de parasitismo e a gravidade da cardiomiopatia chagásica (TODOROV, 2003; BONNEY; ENGMAN, 2015).

Além da hipótese da persistência do parasito, existem hipóteses baseadas na participação da resposta imune específica contra o *T. cruzi* e de não específica. A imunidade específica contra o parasito pode contribuir para a patologia cardíaca através da destruição de miócitos, seguida por infiltração de células mononucleares e fibrose. Já a imunidade não específica é causada por resposta imune inata, ativação de granulócitos e citotoxicidade mediada por anticorpos, o que pode gerar um dano colateral nos cardiomiócitos (BONNEY; ENGMAN, 2015). A participação da microvasculopatia, conduzindo à isquemia e inflamação, também já foi previamente relatada (ROSSI, 1990). Por último, há a hipótese da autoimunidade, que sugere uma perda de tolerância a antígenos próprios. A autoimunidade pode ter origem em danos causados nos cardiomiocitos pelo parasito ou por mimetismo molecular entre proteínas cardíacas, tais como os receptores β 1 adrenérgico e M2 muscarínico por homologia a antígenos do *T. cruzi*, (SOARES; LAIN-PONTES; RIBEIRO-DOS-SANTOS, 2001; MACIEL, 2012; BONNEY; ENGMAN, 2015) (**Figura 3**). Contudo, não se pode descartar a ocorrência dos outros mecanismos, ou até mesmo uma associação entre dois ou mais mecanismos, para o estabelecimento da miocardite crônica chagásica.

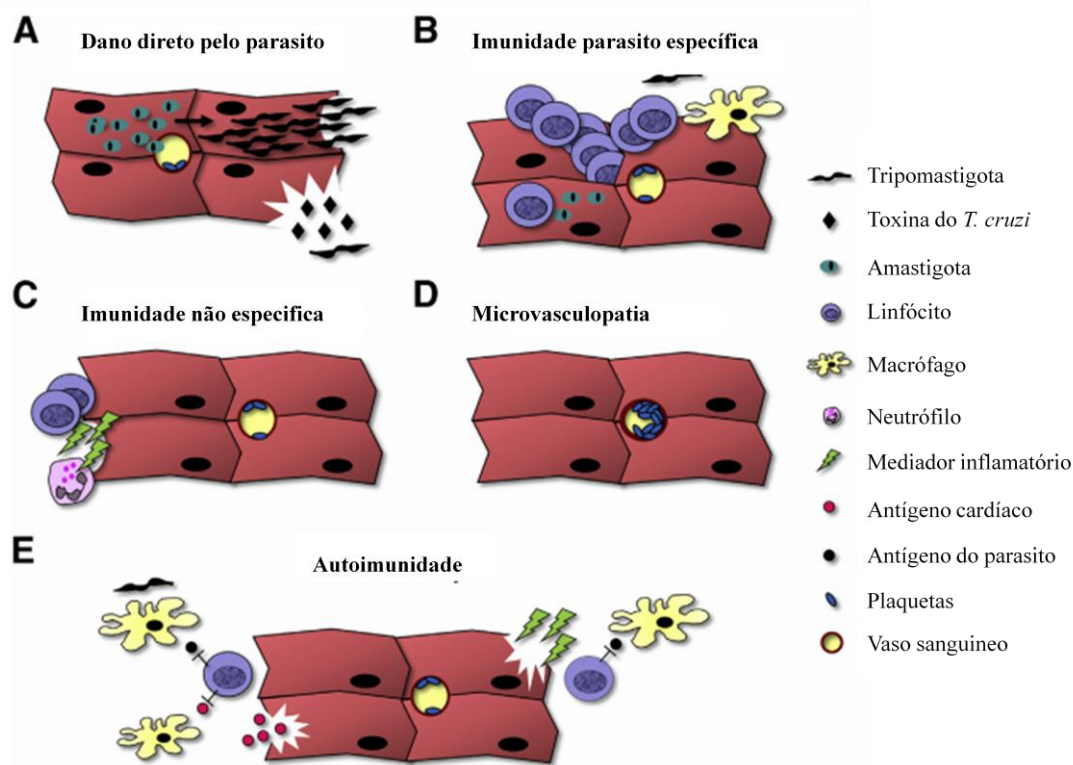


Figura 3. Mecanismos pelo qual o *T. cruzi* pode levar à miocardite. (A) Dano direto causado por parasitos que realizam o ciclo intracelular e destroem as células hospedeiras. (B) Imunidade parasito-específica pode contribuir para a patologia cardíaca através da destruição de

miócitos, seguida por infiltração de células mononucleares e fibrose. (C) Imunidade não específica causada por resposta imune inata, ativação de granulócitos e citotoxicidade mediada por anticorpos pode gerar um dano colateral nos cardiomiócitos. (D) Microvasculopatia, incluindo agregação plaquetária oclusiva, causando isquemia. (E) Autoimunidade induzida pelo parasito gerada pelo mimetismo molecular entre antígenos do *T. cruzi* e antígenos cardíacos ou ativação de células T autorreativas após a lise celular pelo *T. cruzi*. Fonte: Adaptado de BONNEY; ENGMAN, 2015.

2.6 INTERVENÇÕES TERAPÊUTICAS NA DOENÇA DE CHAGAS

Atualmente, apenas duas drogas estão disponíveis para o tratamento da doença de Chagas, o nitroimidazol benzonidazol e o nitrofurano nifurtimox, que foram introduzidos na clínica na década de 70 (JUNIOR, 2017). Ambos os medicamentos são pró-fármacos e precisam ser ativados por uma enzima conhecida como nitroreductase I de tripanosoma (HALL; WILKINSON, 2012). Estes fármacos atuam através da formação de radicais livres e/ou metabólitos eletrofílicos, que geram danos a proteínas, lipídios e ao DNA do *T. cruzi* (GARAVAGLIA, 2016). O benzonidazol, por apresentar um melhor perfil de eficácia e segurança quando comparado com o nifurtimox, é utilizado para o tratamento de primeira linha (VIOTTI, 2006). Em indivíduos adultos, a dose recomendada de benzonidazol é de 5 mg/Kg por dia, durante um período de 60 dias, enquanto que a dose recomenda de nifurtimox é de 8-10 mg/Kg por dia, durante um período de 60-90 dias (BRASIL, 2005). A intervenção com estes compostos é recomendada em pacientes com a infecção aguda, em crianças, em pessoas recém-infectadas, naqueles com a forma congênita da doença de Chagas e em casos de reagudização após a imunossupressão (ANDRADE, 2011).

Ambos os quimioterápicos apresentam elevadas taxas de cura na fase aguda da doença, sendo capazes de alcançar taxas de cura de aproximadamente 80 a 90% em casos agudos (BERN, 2015). Contudo, estes fármacos causam uma série de efeitos colaterais quando administrados por um período prolongado (CASTRO, 2006). Este fato é particularmente problemático, visto que um grande número de doses deve ser administrado por um período longo para que o tratamento obtenha sucesso. Os principais efeitos colaterais causados pela utilização destes medicamentos incluem erupções cutâneas, náuseas, insuficiência renal e hepática e neuropatia periférica (CLAYTON, 2010; URBINA, 2010).

Além da toxicidade, existe uma variação significativa na susceptibilidade de isolados do parasito à ação dessas drogas, e algumas cepas naturalmente susceptíveis e resistentes a estes compostos já foram relatadas (FILARDY; BRENER, 1987; NEAL;

VAN BUEREN, 1988; MURTA, 1998; TOLEDO, 2004). Outra limitação é a baixa eficácia destes compostos na fase crônica da infecção, na qual encontra-se a maioria dos indivíduos infectados. Apesar da limitada capacidade de erradicação do parasita na fase crônica, há evidências de um efeito benéfico do tratamento com benzonidazol nesta fase da doença de Chagas. GARCIA e colaboradores (2005) demonstraram uma relação direta entre a diminuição do parasitismo tecidual, redução do infiltrado inflamatório e da fibrose cardíaca em animais crônicos tratados com benzonidazol, que resultaram em uma melhor função cardíaca.

Recentemente foi finalizado um estudo clínico multicêntrico e duplo cego (BENEFIT – Benzinidazole Evaluation for Interrupting Trypanosomiasis) que visou avaliar o efeito do benzonidazol em 3.000 pacientes (18-75 anos) portadores da cardiomiopatia chagásica crônica (MORILLO, 2015). O estudo demonstrou benefícios do tratamento com benzonidazol com relação à carga parasitária, tendo em vista que houve uma negatização de 66% da PCR para *T. cruzi* nos indivíduos tratados com benzonidazol e apenas 33% nos indivíduos tratados com placebo. Contudo, não houve melhora do quadro clínico dentro de um período de cinco anos de seguimento (MORILLO, 2015).

Visando ao desenvolvimento de alternativas para o benzonidazol e o nifurtimox, foram investigados inibidores da cruzipafina (ou cruzafina), a principal cisteíno-protease do parasito, e da biossíntese de ergosterol. Entre os inibidores de cruzafina, o peptídeo K11777 se destaca pela potente atividade *in vitro* e pelo efeito benéfico sobre camundongos infectados em modelos de infecção aguda e crônica da doença de Chagas. Infelizmente, o avanço desse composto nos ensaios pré-clínicos foi interrompido devido à baixa tolerabilidade do mesmo em cães e primatas (DRUGS FOR NEGLECTED DISEASES, 2014). Já em relação aos compostos capazes de inibir a síntese de ergosterol, um exemplo promissor é o posaconazol, que atua sobre a enzima C14 α -esterol desmetilase do parasito. Este antifúngico apresentou uma atividade promissora em estudos pré-clínicos, porém, quando testado em um ensaio clínico de fase II, apresentou uma baixa taxa de cura (20%) em indivíduos chagásicos crônicos (BUCKNER; URBINA, 2012; MOLINA, 2014).

Considerando-se que o uso terapêutico dos compostos atualmente disponíveis é limitado, é necessário o desenvolvimento de novas estratégias para o tratamento dos pacientes chagásicos (MOREIRA, 2009). Tendo com base a importância dos mecanismos imunológicos na patogênese da doença de Chagas, nosso grupo de

pesquisa vem buscando alternativas terapêuticas para a cardiomiopatia chagásica crônica, visando à modulação da inflamação e fibrose no coração. Esta linha de pesquisa tem contemplado diferentes estratégias, tais como medicamentos, fatores de crescimento e terapia celular (VASCONCELOS, 2013; SILVA, 2014; Anexo III).

Recentemente, nosso grupo de pesquisas demonstrou o efeito imunomodulador do fator estimulador de colônias de granulócitos (G-CSF) em um modelo de cardiomiopatia chagásica crônica. Os animais tratados com G-CSF tiveram uma redução significativa do infiltrado inflamatório e da fibrose no coração quando comparados com animais tratados com solução salina (VASCONCELOS, 2013). A reversão da inflamação foi acompanhada de um aumento da migração de células Treg da medula óssea para o coração e aumento da produção de IL-10 no coração e no baço dos animais tratados, o que parece contribuir para a modulação da resposta inflamatória. Observamos também a redução da carga parasitária no coração dos animais tratados com G-CSF em comparação com o grupo controle (VASCONCELOS, 2013). Estes achados reforçam a utilização de agentes imunomoduladores como uma estratégia eficaz para o tratamento de pacientes com CCC.

2.7 ÁCIDO BETULÍNICO E O SEU DERIVADO SINTÉTICO BA5

O ácido betulínico (BA; **Figura 4**) é um triterpeno pentacíclico do tipo lupano amplamente distribuído no reino vegetal. Suas fontes tradicionais são espécies europeias do gênero *Betula*, que produzem seu álcool precursor, a betulina (KIM, 1997; FRIGHETTO, 2005) e a casca de inúmeras espécies que ocorrem em regiões tropicais e subtropicais, especialmente as pertencentes ao gênero *Clusia* (MAURYA, 1989).

Este triterpeno apresenta uma variedade de atividades farmacológicas descritas na literatura. As atividades antitumoral, antimalárica, anti-HIV, analgésica, antiinflamatória e bactericida já estão descritas (YOGESHWARI; SRIRAM, 2005; FUJIOKA, 1994; CHANDRAMU, 2003; KROGH, 1999). Dentre essas atividades, destaca-se o efeito antitumoral, visto que o ácido betulínico apresenta uma potente atividade frente a diversas linhagens neoplásicas, em especial melanomas, o que não é evidenciado quando testado em linhagens de células normais, comprovando um caráter seletivo dessa molécula (ZUCO, 2002).

O BA é considerado um protótipo promissor para a geração de moléculas mais potentes para diferentes alvos farmacológicos (YOGESHWARI; SRIRAM, 2005).

Diversos trabalhos relatam modificações estruturais nos substituintes do C-3, C-20 e C-28 do ácido betulínico (KIM, 1998). As modificações no C-20 mostraram pouca contribuição, em estudos com linhagens de células tumorais (KIM, 2001). Entretanto, as modificações no C-3 ou C-28 parecem promissoras (MULLAUER, 2010). Modificações realizadas no C-28 já contribuíram para a otimização da atividade anti-HIV, antitumoral, anti-influenza A e anti-herpes (SUN, 1998; JEONG, 1999; BALTINA, 2003; PAVLOVA, 2003).

Recentemente, o nosso grupo demonstrou a contribuição da inserção de aminas no C-28 para um aumento da atividade anti-*T. cruzi* (MEIRA, 2014; Anexo II). A inserção de um grupamento amina potencializou o efeito de uma série de derivados sobre a viabilidade de formas tripomastigotas e sobre a proliferação de formas amastigotas intracelulares. Em especial, o derivado de código BA5 que se mostrou menos citotóxico em culturas de macrófagos e mais efetivo em lisar formas tripomastigotas de *T. cruzi* do que o ácido betulínico (**Figura 4**). O tratamento de formas tripomastigotas com o derivado BA5 induziu uma série de alterações na ultraestrutura do parasito, tais como perda da integridade da membrana plasmática, deformação corporal, retração flagelar, aparecimento de vacúolos atípicos, dilatação do complexo de Golgi e a formação de autofagossomos, culminando com a morte parasitária por necrose (Anexo II). Além disso, o derivado BA5 apresentou uma potência superior à droga de referência, o benzonidazol, nos ensaios realizados com formas tripomastigotas e uma potência equipotente ao benzonidazol nos ensaios realizados com macrófagos infectados com *T. cruzi* (Anexo II).

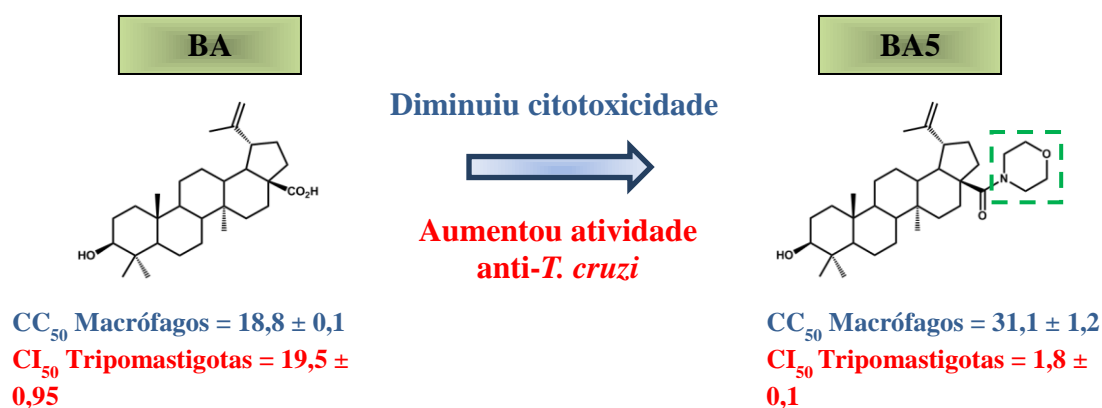


Figura 4. Esquema comparando a citotoxicidade e atividade anti-*T. cruzi* do ácido betulínico e seu derivado BA5.

2.8 ESFINGOLIPÍDIOS E A N,N-DIMETIL-ESFINGOSINA

Esfingolipídios constituem uma classe de lipídios que possuem esfingosina, um amino álcool orgânico alifático. Eles possuem uma grande diversidade estrutural para diferentes espécies, com mais de 300 tipos já identificados e com milhares de possíveis estruturas, estando presente em todos os organismos eucariontes e alguns procariontes (PATA; HANNUN, NG; 2010). Podem ser encontrados na membrana celular, onde participam de diversos processos celulares, tais como crescimento, proliferação e diferenciação (HANNUN; OBEID, 2008).

O envolvimento dessas moléculas em diversos processos celulares torna os esfingolipídios potenciais alvos terapêuticos para diversas doenças (MACEYKA; SPIEGEL, 2014). Sob esta perspectiva, já foram desenvolvidos compostos análogos às bases esfingoides para atuarem como fármacos ou como ferramentas para o estudo das funções dos esfingolipídios, modulando suas vias metabólicas. Um exemplo promissor é o FTY720, que é utilizado no tratamento de esclerose múltipla e já foi testada com sucesso na prevenção de rejeição em casos de transplante. Essa molécula atua em quatro dos cinco receptores de esfingosina-1-fosfato (GLAROS, 2008; BRINKMANN, 2010).

A esfingosina-1-fosfato (S1P) é produzida principalmente por mastócitos e fagócitos primários. Essa molécula tem um importante papel em alterações na migração de células do timo, na diferenciação de subpopulações de células T, no tráfico de linfócitos em órgãos linfoides e outros tecidos, nas interações entre células T e células dendríticas e na produção de citocinas (LEE, 1998; HLA, 2012; MACEYKA; SPIEGEL, 2014). Um inibidor potente desse mediador é o N,N-dimetil-esfingosina (DMS; **Figura 5**), que bloqueia a conversão de esfingosina em esfingosina-1-fosfato por inibir as enzimas esfingosinas cinases 1 e 2 (ARISH, 2016; YANAGIDA; HLA, 2017).

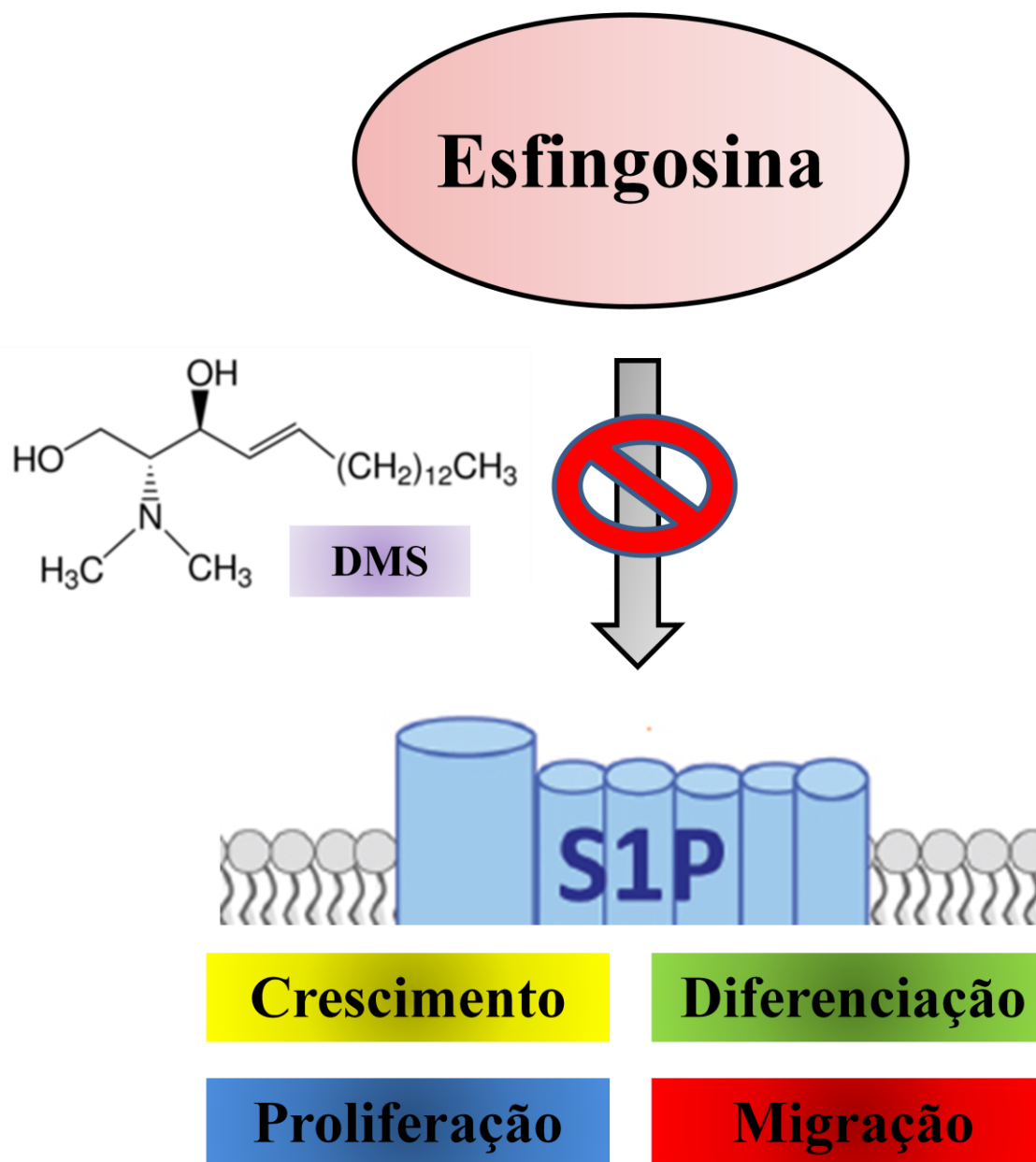


Figura 5. Esquema mostrando o mecanismo de ação N,N-dimetil-esfingosina (DMS). A molécula atua nas enzimas esfingosinas cinases 1 e 2 impedindo a conversão da esfingosina em esfingosina-1-fosfato (S1P), que é essencial em diversos processos celulares como: crescimento, diferenciação, proliferação e migração de células.

Dentre as atividades do DMS já descritas, destaca-se a ação antitumoral em células leucêmicas monoblásticas U937 e o bloqueio da ativação plaquetária (YATOMI, 1996; EDSALL, 1998). Nessas linhagens celulares, o DMS diminuiu os níveis basais de esfingosina-1-fosfato e impediu o aumento da mesma em resposta a estímulos fisiológicos conhecidos por ativar esfingosinas cinases (EDSALL, 1998). Além disso, o DMS demonstrou um efeito protetor em um modelo de lesão renal aguda isquêmica através do recrutamento de células T regulatórias ($CD4^{+}FoxP3^{+}$) (LAI; YONG; LIEN,

2012). Estas características farmacológicas do DMS demonstram o seu potencial no tratamento de doenças inflamatórias.

Tendo em vista as atividades descritas acima, no presente trabalho propomos investigar o potencial terapêutico do DMS e do BA5 em um modelo de cardiomiopatia chagásica crônica experimental.

3 OBJETIVOS

3.1 GERAL

Investigar o potencial do BA5 e do DMS em um modelo experimental de cardiomiopatia chagásica crônica.

3.2 ESPECÍFICOS

- Avaliar os efeitos imunomoduladores *in vitro* do BA5 e do DMS sobre macrófagos e linfócitos ativados
- Avaliar o potencial imunomodulador do BA5 *in vivo* em modelos de endotoxemia e de reação de hipersensibilidade tardia.
- Avaliar os efeitos do BA5 e do DMS na resposta inflamatória no coração de camundongos chagásicos crônicos;
- Avaliar os efeitos BA5 e do DMS na fibrose no coração de camundongos chagásicos crônicos;
- Avaliar os efeitos BA5 e do DMS no parasitismo na fase crônica da infecção por *T. cruzi*;
- Analisar a função cardíaca dos animais chagásicos crônicos tratados ou não com BA5 ou DMS;
- Avaliar o perfil de citocinas e expressão gênica entre os camundongos na fase crônica da infecção;
- Elucidar o mecanismo de ação do BA5 e do DMS na cardiomiopatia chagásica crônica.

4 RESULTADOS

CAPÍTULO I

Neste capítulo descrevemos a atividade imunomoduladora do derivado semissintético BA5 sobre macrófagos e linfócitos e seu efeito imunossupressor em modelo murino de endotoxemia e de hipersensibilidade do tipo tardia.

Artigo publicado na revista *European Journal of Pharmacology*, v. 815, p.156-165, 2017. Doi: 10.1016/j.ejphar.2017.09.008.

Betulinic acid derivative BA5, a dual NF- κ B/calcineurin inhibitor, alleviates experimental shock and delayed hypersensitivity

Cássio Santana Meira¹, Renan Fernandes do Espírito Santo^{1,2}, Tatiana Barbosa dos Santos^{1,3}, Iasmim Diniz Orge^{1,4}, Dahara Keyse Carvalho Silva^{1,3}, Elisalva Teixeira Guimarães^{1,3}, Luciana Souza de Aragão França⁴, José Maria Barbosa-Filho⁵, Diogo Rodrigo Magalhães Moreira¹, Milena Botelho Pereira Soares^{1,4}



Full length article

Betulinic acid derivative BA5, a dual NF- κ B/calcineurin inhibitor, alleviates experimental shock and delayed hypersensitivity

Cássio Santana Meira^a, Renan Fernandes do Espírito Santo^{a,b}, Tatiana Barbosa dos Santos^{a,c}, Iasmim Diniz Orge^{a,d}, Dahara Keyse Carvalho Silva^{a,c}, Elisalva Teixeira Guimarães^{a,c}, Luciana Souza de Aragão França^d, José Maria Barbosa-Filho^e, Diogo Rodrigo Magalhães Moreira^a, Milena Botelho Pereira Soares^{a,d,*}

^a Instituto Gonçalo Moniz, Fundação Oswaldo Cruz (FIOCRUZ), Salvador, BA, Brazil

^b Faculdade de Farmácia, Universidade Federal da Bahia, Salvador, BA, Brazil

^c Departamento de Ciências da Vida, Universidade do Estado da Bahia, Salvador, BA, Brazil

^d Centro de Biotecnologia e Terapia Celular, Hospital São Rafael, Salvador, BA, Brazil

^e Laboratório de Tecnologia Farmacêutica, Universidade Federal da Paraíba, João Pessoa, PB, Brazil

ARTICLE INFO

Keywords:

Betulinic acid derivative

T lymphocyte activation

Delayed type hypersensitivity, LPS-induced endotoxin shock

ABSTRACT

Betulinic acid (BA) is a naturally occurring triterpenoid with several biological properties already described, including immunomodulatory activity. Here we investigated the immunomodulatory activity of eight semi-synthetic amide derivatives of betulinic acid. Screening of derivatives BA1-BA8 led to the identification of compounds with superior immunomodulatory activity than BA on activated macrophages and lymphocytes. BA5, the most potent derivative, inhibited nitric oxide and TNF α production in a concentration-dependent manner, and decreased NF- κ B activation in Raw 264.7 cells. Additionally, BA5 inhibited the proliferation of activated lymphocytes and the secretion of IL-2, IL-4, IL-6, IL-10, IL-17A and IFN γ , in a concentration-dependent manner. Flow cytometry analysis in lymphocyte cultures showed that treatment with BA5 induces cell cycle arrest in pre-G1 phase followed by cell death by apoptosis. Moreover, BA5 also inhibited the activity of calcineurin, an enzyme that plays a critical role in the progression of cell cycle and T lymphocyte activation. BA5 has a synergistic inhibitory effect with dexamethasone on lymphoproliferation, showing a promising profile for drug combination. Finally, we observed immunosuppressive effects of BA5 *in vivo* in mouse models of lethal endotoxemia and delayed type hypersensitivity. Our results reinforce the potential use of betulinic acid and its derivatives in the search for potent immunomodulatory drugs.

1. Introduction

Betulinic acid (BA) is a naturally occurring pentacyclic triterpenoid found in several plant species, which can be alternatively prepared from its metabolic precursor, betulin (Yogeeswari and Sriram, 2005). This natural product holds several biological activities, including anti-cancer, anti-HIV, antiparasitic and anti-angiogenic activities (Takada and Aggarwal, 2003; Dehelean et al., 2011; Ali-Seyed et al., 2016; Li et al., 2016; Meira et al., 2016). In particular, BA has been reported to possess cytotoxic effects on several tumor cell lines of different origins, as well as in animal models of cancer (Gheorgeheosu et al., 2016).

BA has also been investigated as an immunomodulatory agent (Sultana and Saify, 2012). More specifically, BA inhibits the production of several inflammatory mediators, including nitric oxide (NO),

prostaglandin E₂ (PGE₂), tumor necrosis factor alpha (TNF α), interleukin (IL)-6 and IL-1 β (Jingbo et al., 2015; Kim et al., 2016). Most of these effects are related to the inhibition of nuclear factor- κ B (NF- κ B), a transcription factor involved in the regulation of several pro-inflammatory genes, in particular TNF α (Viji et al., 2010; Kim et al., 2016). BA is also known to suppress STAT3 signaling, which is essential transcription factor for differentiation of the CD4⁺ Th17 cells in a variety of autoimmune diseases (Blaževski et al., 2013).

In addition, in a cecal ligation and puncture mouse model, it has been demonstrated that BA treatment reduces mortality and ameliorates lung and kidney function by down-regulating NF- κ B (Lingaraju et al., 2015a, b). Furthermore, in lipopolysaccharide (LPS)-induced endotoxin shock, pre-treatment with BA significantly improves mice survival by modulating TNF α production by macrophages *in vivo*

* Correspondence to: Instituto Gonçalo Moniz, Fundação Oswaldo Cruz, Rua Waldemar Falcão, 121, Candeal, Salvador, Bahia 40296-710, Brazil.
E-mail address: milena@bahia.fiocruz.br (M.B.P. Soares).

through a mechanism dependent on IL-10 (Viji et al., 2010; Costa et al., 2014). However, in a number of *in vitro* and *in vivo* models of inflammation, the anti-inflammatory activity of BA has been considered to be moderate (Cichewicz and Kouzi, 2004; Li et al., 2017).

In view of these findings, BA has been used as a prototype for the design and synthesis of more potent immunomodulatory agents. Chemical modifications of the carboxyl group have suggested that this part of BA molecule has potential for the production of derivatives with enhanced biological activity, including immunomodulatory agents (Sultana and Saify, 2012; Chen et al., 2017). Based on these facts, the purpose of our work was to evaluate the immunomodulatory potential of new semi-synthetic amide derivatives of betulinic acid *in vitro* and *in vivo*, as well as their mechanisms of action.

2. Materials and methods

2.1. Drugs

Betulinic acid (BA) was extracted from the bark of *Ziziphus joazeiro* Mart. (Rhamnaceae) by using a previously described method (Barbosa-Filho et al., 1985). Semi-synthetic compounds (BA1 to BA8; 94–98% purity by high performance liquid chromatography) were prepared from betulinic acid, as previously described (Meira et al., 2016). Gentian violet (Synth, São Paulo, SP, Brazil) was used as positive control in the cytotoxicity assays. Dexamethasone (Sigma-Aldrich, St. Louis, MO), a synthetic glucocorticoid, was used as positive control in immunomodulatory assays. Cyclosporin A (Sigma-Aldrich) was used as positive control in calcineurin activity assay and in DTH assay. Mifepristone (RU 486; Sigma-Aldrich), an antagonist of glucocorticoid receptor, was used in mechanism assays. All compounds were dissolved in Dimethyl sulfoxide (DMSO; PanReac, Barcelona, Spain) and diluted in cell culture medium for use in the assays. The final concentration of DMSO was less than 0.1% in all *in vitro* experiments and less than 5% in all *in vivo* experiments.

2.2. Animals

BALB/c and C57BL/6 mice 4–12 weeks old) were bred and maintained at the Gonçalo Moniz Institute (Oswaldo Cruz Foundation, Bahia, Brazil) in sterilized cages, under a controlled environment and receiving a balanced rodent diet and water *ad libitum*. All animal experiments and procedures were approved by the institution's committee on the ethical handling of laboratory animals (Approved number: L-IGM-018/15).

2.3. Cytotoxicity to mammalian cells

Cytotoxicity of the compounds was determined using the rat cardiomyoblast H9c2 and the monkey kidney LCC-MK2 cell lines. Cells were seeded into 96-well plates at a cell density of 1×10^4 cells/well in Dulbecco's modified Eagle medium (DMEM; Life Technologies, GIBCO-BRL, Gaithersburg, MD) supplemented with 10% fetal bovine serum (FBS; GIBCO) and 50 µg/ml of gentamicin (Life, Carlsbad, CA) and incubated for 24 h at 37 °C and 5% CO₂. The compounds tested were then added (10 - 0.04 µM), in quadruplicate, and incubated for 72 h. One µCi of ³H-thymidine (Perkin Elmer, Waltham, MA) was added to each well, incubated for 18 h, frozen at -20 °C and subsequently thawed and the contents transferred to UniFilter-96 GF/B PEI coated plates (PerkinElmer) using a cell harvester. After drying, 50 µl of scintillation cocktail (MaxiLight, Hidex, Turku, Finland) was added in each well, sealed and plate read in a liquid scintillation microplate counter (Chameleon, Turku, Finland). Cell viability was measured as the percent of ³H-thymidine incorporation for treated-cells in comparison to untreated cells. Gentian violet was used as positive control, at concentrations ranging from 0.04 to 10 µM. Cytotoxicity concentration at 50% (CC₅₀) values were calculated using data from three independent

experiments.

In addition, the cytotoxicity of compounds was also determined in peritoneal macrophages. Cells were obtained by washing, with cold phosphate buffered saline (PBS), the peritoneal cavity of BALB/c mice 4–5 days after injection of 3% thioglycolate (Sigma-Aldrich) in saline (1.5 ml per mice). Then, cells were seeded into 96-well plates at a cell density of 2×10^5 cells/well in DMEM supplemented with 10% FBS and 50 µg/ml of gentamicin and incubated for 24 h at 37 °C and 5% CO₂. After that time each test inhibitors were added at least in six concentrations (20 - 0,15 µM) in triplicate and incubated for 24 h. 20 µl/well of AlamarBlue (Invitrogen, Carlsbad, CA) was added to the plates during 10 h. Colorimetric readings were performed at 570 and 600 nm. CC₅₀ values were calculated using data-points gathered from three independent experiments.

2.4. Macrophage cultures

Peritoneal exudate macrophages were seeded in 96-well plates at 2×10^5 cells/well in DMEM medium supplemented with 10% of FBS and 50 µg/ml of gentamicin for 2 h at 37 °C and 5% CO₂. Plates were washed to remove non-adherent cells, and the remaining cells were then stimulated with LPS (500 ng/ml, Sigma-Aldrich) and interferon gamma (IFN γ ; 5 ng/ml, Sigma-Aldrich) in the absence or presence of compounds at different concentrations, and incubated at 37 °C. Cell-free supernatants were collected 4 h (for TNF α measurement) and 24 h (for IL-1 β , IL-10 and nitrite quantifications), and kept at -80 °C until use.

2.5. NF- κ B luciferase assay

The murine mouse leukemic monocyte macrophage cell line Raw 264.7 Luc cells bearing the pBIX-luciferase (pBIX-luc) targeting vector containing the firefly luciferase gene (luc) driven by two NF- κ B binding sites from the kappa light chain enhancer in front of a minimal fos promoter (Zhong et al., 1997) were kindly provided by Maria Célia Jamur (University of São Paulo, Ribeirão Preto, Brazil). The cells were cultured in RPMI medium (Sigma) supplemented with 20% FBS and 50 µg/ml gentamicin in 24-well plates at 37 °C in a humidified environment containing 5% CO₂. For luciferase reporter assays, 5×10^5 cells/ml were pretreated with different concentrations of BA5 (20, 10 or 5 µM), BA (20 µM) or dexamethasone (20 µM) for 1 h prior to stimulation with LPS (500 ng/ml) and IFN γ (5 ng/ml) for 3 h. After washing with cold PBS, cells were lysed by adding TNT lysis buffer (200 mM Tris, pH 8.0, 200 mM NaCl, 1% Triton X-100) for 20 min at 4 °C. The determination of the luciferase activity was performed using the Promega luciferase assay system (Promega, Madison, CA), according to the manufacturer's instructions. The samples were analyzed in a Globomax 20/20 Luminometer (Promega). Data are expressed as relative light units.

2.6. Splenocyte cultures

For lymphoproliferation assays, BALB/c splenocyte suspensions were prepared in DMEM medium supplemented with 10% of FBS and 50 µg/ml of gentamicin. Splenocytes (1×10^6 cells/well) were plated in 96-well plates, in quadruplicate, and stimulated or not with concanavalin A (Con A; 2 µg/ml, Sigma-Aldrich) or Dynabeads® mouse T-activator CD3/CD28 (bead to cell ratio = 1:1; ThermoFisher Scientific, Waltham, MA). In some experiments, RU486, a glucocorticoid receptor antagonist (Sigma-Aldrich), was added to the cultures to investigate the mechanism of action of the most potent derivative. To evaluate the lymphoproliferation, splenocytes were activated in the absence or presence of various concentrations of derivatives (500–0.0005 nM). After 48 h of incubation, 1 µCi of ³H-thymidine was added to each well, incubated for 18 h and read, as described above. Cell proliferation was measured as the percent of ³H-thymidine incorporation for treated-cells in comparison to untreated cells. Dexamethasone was used as positive

control. Inhibitory concentration at 50% (IC₅₀) values were calculated using data from three independent experiments.

Splenocytes from BALB/c mice were also plated into 24-well plates at a cell density of 5×10^6 cells/ in DMEM medium supplemented with FBS containing or not 5 µg/ml of Con A in the absence or presence of different concentrations of BA5 (500, 50 and 5 nM), BA (500 nM) and dexamethasone (500 nM). After 48 h, cell-free supernatants were collected and kept at -80°C until use for cytokine quantification.

2.7. Mixed lymphocyte reaction (MLR)

BALB/c mice were weekly immunized with intraperitoneal injections of 10^7 splenocytes obtained from C57BL/6, as previously described (Soares et al., 2006). After 3 weeks of immunization, mice were euthanized for spleen cell preparation in DMEM medium supplemented with 10% of FBS and 50 µg/ml of gentamicin. Spleen cells were plated in 96 well plates at a cell density of 1×10^6 cells/well in the absence or in the presence of irradiated C57BL/6 splenocytes at 10^6 cells/well (dose of 3 Gy in a ¹³⁷Cs source irradiator purchased from CisBio International, Cordolet, France) and different concentrations of drugs in testing, in quadruplicates. After 72 h of incubation, ³H-thymidine was added to each well, and the plates were incubated for additional 18 h. The incorporation of ³H-thymidine was determined as described above.

2.8. Assessment of cytokine and nitric oxide production

Cytokine concentrations in supernatants from peritoneal macrophages cultures collected at 4 h (for TNFα) and 24 h (for IL-1β and IL-10) and from splenocyte cultures (IL-2, IL-4, IL-6, IL-10, IL-17A and IFNγ) were determined by enzyme-linked immunosorbent assay (ELISA), using DuoSet kits from R & D Systems (Minneapolis, MN), according to the manufacturer's instructions. Nitric oxide production was estimated in macrophage culture supernatants harvested at 24 h using the Griess method for nitrite quantification (Green et al., 1982).

2.9. Flow cytometry analyses

Splenocytes from BALB/c mice were plated into 24-well plates at a cell density of 5×10^6 cells/ in DMEM medium supplemented with 10% FBS containing 5 µg/ml of Con A in the absence or presence of different concentrations of BA5 (500, 50 and 5 nM) for 24 and 48 h for cell death determination and cell cycle analysis respectively. For cell death determination, cells were centrifuged and then pellet washed twice with cold PBS and initially labeled with APC anti-mouse CD3 (Biolegend, San Diego, CA) diluted 1:100 for 15 min followed by stained with propidium iodide (PI) and annexin V using the annexin V-FITC apoptosis detection kit (Sigma-Aldrich), according to the manufacturer's instructions. For cell cycle analysis, cells were labeled with APC anti-mouse CD3 followed by a second stained with a solution of PBS with propidium iodide (2 µg/ml), RNAase (100 µg/ml) and 0.1% of Triton X-100 in the dark at 37 °C for 30 min. The cell preparations were analyzed using a FACS Calibur flow cytometer (Becton Dickinson, San Diego, CA). A total of 10,000 events positive for APC anti-mouse CD3 staining was acquired and data were analyzed using FlowJo software (Tree Star, Ashland, OR).

2.10. Calcineurin activity

The calcineurin phosphatase activity was measured in cell extracts using a Calcineurin Cellular Activity assay kit (Enzo Life Sciences, Farmingdale, NY). In brief, splenocytes from BALB/c mice were plated into 24-well plates at a cell density of 5×10^6 cells/ in DMEM medium supplemented with 10% FBS containing 5 µg/ml of Con A in the absence or presence of BA5 (500, 50 and 5 nM), or cyclosporin A (500 nM) for 48 h. Then, cells were lysed in a buffer containing protease inhibitors, centrifuged and the supernatant was used for analysis.

The same amount of protein (5 µg) per sample was used in the calcineurin activity assays. Colorimetric measurements were performed at 620 nm. The amount of phosphate released by calcineurin was calculated using a standard curve.

2.11. Drug combination assay

For *in vitro* drug combinations, doubling dilutions of each drug (BA5 and dexamethasone), used alone or in fixed combinations were incubated with splenocytes followed the protocol described above. The analysis of the combined effects was performed by determining the combination index (CI), used as cutoff to determine synergism, by using Chou-Talalay CI method (Chou and Talalay, 2005) and through the construction of isobologram using the fixed ratio method, as described previously (Fivelman et al., 2004).

2.12. LPS-induced endotoxic shock

Groups of six male BALB/c mice (4 weeks of age) were used for the LPS lethality assays. Mice were treated with BA5 (50 or 25 mg/kg), dexamethasone (25 mg/kg) or vehicle (5% of DMSO in saline), by intraperitoneal (i.p.) route. Ninety min later, animals were challenged with 600 µg of LPS (from serotype O111:B4 *Escherichia coli*, Sigma-Aldrich) in saline, by i.p. route. Survival was then monitored daily, during 4 days.

2.13. Delayed type hypersensitivity (DTH) assay

BALB/c mice (8–12 weeks of age) were sensitized by injecting 50 µg of crystallized bovine serum albumin (BSA; Sigma-Aldrich) emulsified in 20 µl of complete Freund's adjuvant (CFA; Sigma-Aldrich) subcutaneously into each side of the base of tail. Seven days later, animals were randomized into five groups and mice were treated with BA5 (50 or 25 mg/kg), cyclosporin A (25 mg/kg), dexamethasone (25 mg/kg) or vehicle (5% of DMSO in saline), by the intraperitoneal route 24 and 3 h before challenge. DTH was elicited by injection of 30 µl of a 2% suspension of heat-aggregated BSA in saline subcutaneously into the footpad, according to a previously reported method (Titus and Chiller, 1981). Before and 3 h post-challenge, footpad thickness was measured with calipers and swelling was calculated by subtracting the thickness of the footpad after challenge from that before challenge.

2.14. Statistical analyses

One-way analysis of variance and Newman-Keuls multiple comparison tests were employed by using Graph Pad Prism version 5.01 (Graph Pad Software, San Diego, CA). Differences were considered significant when the values of *P* were < 0.05.

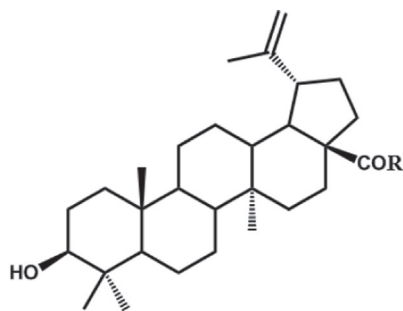
3. Results

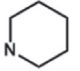
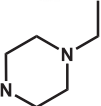
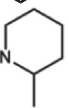
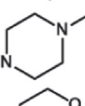
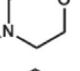
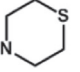
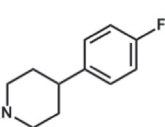
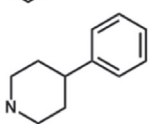
3.1. Cytotoxicity and modulation of macrophage function *in vitro* by BA derivatives

In order to test the effects of the compounds *in vitro*, first we evaluated the cytotoxicity of compounds on peritoneal macrophages, LCC-MK2 and H9c2 cells. As shown in Table 1, all compounds had no cytotoxic effect in the concentrations tested, which were used in the following *in vitro* assays.

All the compounds were initially evaluated in cultures of macrophages activated with LPS and IFNγ. Dexamethasone, a standard glucocorticoid, was used as positive control. As shown in Table 1, betulinic acid inhibited NO production in 45.1% at 10 µM. In contrast, most of derivatives showed a weak inhibitory activity of nitric oxide production, with the exception of BA5. This derivative inhibited in 53.0% the production of NO, more potently than the prototype molecule (BA) and

Table 1
Screening of cytotoxicity and immunomodulatory activity of semi-synthetic derivatives of betulinic acid.



Compounds	R	CC ₅₀ (μM) MØ ^a	CC ₅₀ (μM) MK2 cells ^b	CC ₅₀ (μM) H9c2 cells ^b	Inhibition of NO (%) production at 10 μM ^c	IC ₅₀ (nM) Mitogen Induced ^d
BA	OH	>20	> 10	> 10	45.1±1.9	284.5±32.8
BA1		>20	> 10	> 10	11.1±0.1	> 500
BA2		>20	> 10	> 10	7.2±0.9	> 500
BA3		>20	> 10	> 10	15.9±0.7	> 500
BA4		>20	> 10	> 10	7.7±0.1	> 500
BA5		>20	> 10	> 10	53.0±2.2	14.3±0.91
BA6		>20	> 10	> 10	25.9±2.7	27.6±2.1
BA7		>20	> 10	> 10	0±0.00	> 500
BA8		>20	> 10	> 10	16.7±1.4	58.7±4.9
Dexa	-	>20	> 10	> 10	57.6±3.2	6.9±0.4
GV	-	-	1.1±0.01	1.5±0.32	-	-

^a Determined 24 h after incubation with compounds. ^b Determined 72 h after incubation with compounds. ^c Percent inhibition determined 24 h after incubation with compounds and LPS plus IFN-γ. ^d Determined 48 h after incubation with compounds and Con A. Values represents the mean ± S.E.M. and were calculated from three independent experiments performed. IC₅₀ = inhibitory concentration at 50%. CC₅₀ = cytotoxic concentration at 50%. MØ = peritoneal macrophages Dexa = Dexamethasone. GV = gentian violet. S.E.M. = standard error of mean.

close to that found for dexamethasone (57.6% of inhibition at 10 μM). BA5 caused a concentration-dependent inhibition of NO and TNFα production (Figs. 1A and B). Additionally, the production of IL-10 was significantly reduced by BA5 and dexamethasone, while it was increased by BA (Fig. 1C).

LPS-induced Toll-like receptor-4 (TLR4) activation leads to

triggering of intracellular signaling pathways, including NF-κB activation, consequently causing the transcriptional regulation of several inflammatory genes, including *Tnf* and *Nos2* (Bartuzi et al., 2013). To investigate whether BA5 modulates NF-κB activation in macrophages, we performed an assay using RAW cells transduced with a reporter gene under the control of a promoter regulated by NF-κB. Addition of BA5

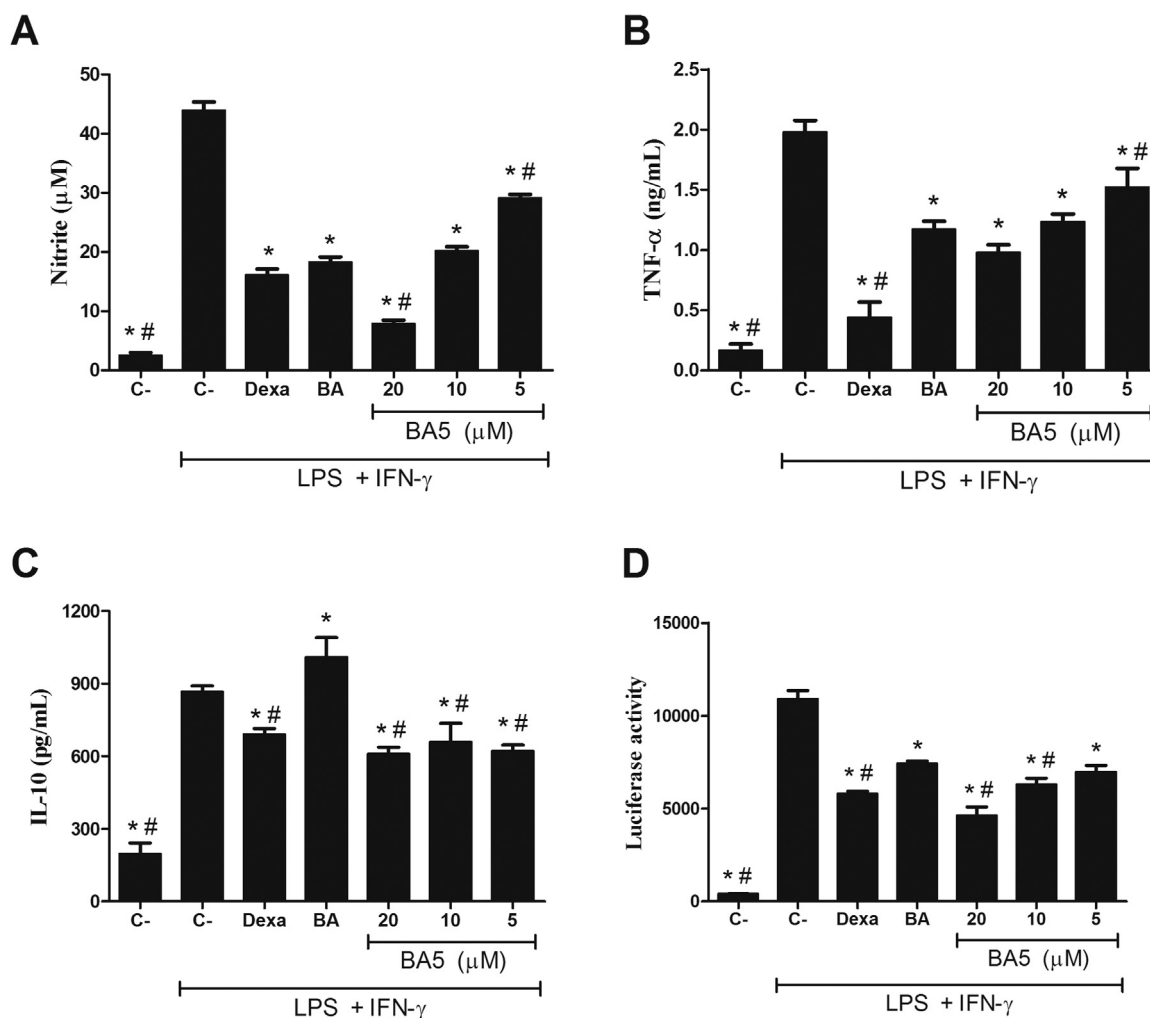


Fig. 1. Modulation of nitric oxide, cytokines and NF- κ B activity in BA5-treated macrophages. Effect of BA5 (20, 10 or 5 μ M), BA (20 μ M) or dexamethasone (20 μ M) on nitrite (A), TNF α (B), IL-10 (C) production and NF- κ B activity (D). C- is untreated cells. Values represent the means \pm S.E.M. of four determinations obtained in one of two experiments performed. * $P < 0.05$ compared to stimulated and untreated cells; # $P < 0.05$ compared to BA-treated cells.

caused the reduction of NF- κ B activation, in a concentration-dependent manner, in RAW cells stimulated with LPS and IFN γ . BA and dexamethasone also caused a significant reduction of luciferase activity (Fig. 1D).

3.2. BA derivatives inhibit T cell proliferation

To evaluate the immunosuppressive effects of BA derivatives on lymphocytes, we first performed a Con A-induced lymphoproliferation assay. Screening of BA derivatives led to the identification of three compounds more active than BA (Table 1). The most active derivatives were BA5, BA6 and BA8, which present a morpholyl, thiomorpholyl and 4-methylphenylpiperidine groups, presented increased potency, especially the BA5 derivative, which had an IC₅₀ value of 14.3 nM, close to that of dexamethasone (IC₅₀ = 6.9 nM). Dexamethasone has a potent T cell proliferation inhibition activity (Table 1).

We further evaluated in splenocyte cultures activated with anti-CD3/anti-CD28 coated-beads to evaluate the effect of BA5 on the proliferation of CD4⁺ T lymphocytes. As shown in Fig. 2A, BA5 caused a concentration-dependent inhibition of lymphoproliferation, with higher potency ($P < 0.05$) than the prototype BA and similar to the activity observed for dexamethasone. Additionally, BA5 treatment inhibits *in vitro* alloreactive T cell response as demonstrated by a concentration-dependent reduction of proliferation in a mixed lymphocyte reaction (Fig. 2B).

3.3. BA5 modulates cytokine production and induces cell cycle arrest in activated T cells

As a potential immunotherapeutic agent, it was also important to determine the effect of BA5 on cytokine secretion. To this end, cytokine production by splenocytes stimulated with Con A and treated with BA5 was investigated (Fig. 3). Compared to untreated and stimulated cultures, treatment with BA5 decreased the secretion of IL-2, IL-4, IL-6, IL-10, IL-17A and IFN- γ in a concentration dependent manner. Under the same conditions, dexamethasone also promoted a significant decrease in cytokine production. BA also decreased the production of most cytokines but less efficient when compared with BA5. Once again, BA treatment increased IL-10 production (Fig. 3D).

Flow cytometry analysis was carried out in splenocyte cultures in order to determine the effect of BA5 on cell cycle progression and cell death. Treatment with BA5 induced, in a concentration-dependent manner, cell cycle arrest on G0/G1 phase, accompanied by an increase in PreG1 phase (Figs. 4A and B). Moreover, the cell cycle arrest was accompanied by a significant and concentration-dependent increase in annexin V positive cells, which is a hallmark of apoptosis (Fig. 4C).

3.4. BA5 effects on lymphocytes is independent of glucocorticoid receptor, but affects calcineurin activity

To understand the mechanisms by which BA5 inhibits lymphocyte

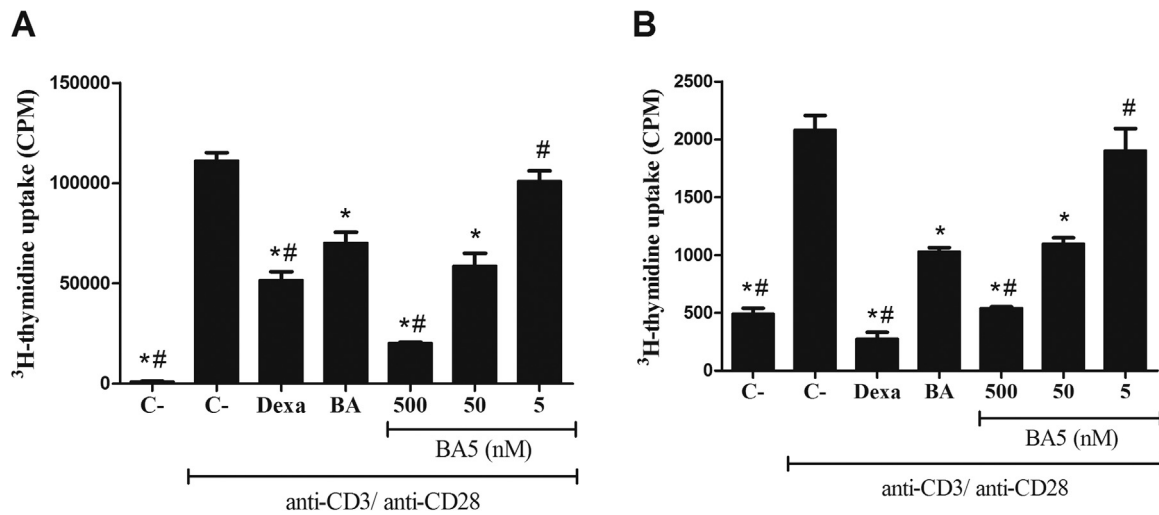


Fig. 2. Inhibition of lymphocyte proliferation by BA5. (A) Effect of BA5 (500, 50 and 5 nM), BA (500 nM) or dexamethasone (500 nM) on lymphoproliferation induced by anti-CD3 + anti-CD28 for 48 h. (B) Splenocytes from BALB/c mice sensitized with C57BL/6 cells were cultured in the absence (unstimulated) or presence (stimulated) of irradiated C57BL/6 spleen cells, with or without BA5 (500, 50 and 5 nM), BA (500 nM) or dexamethasone (500 nM) for 72 h. C- is untreated cells. Proliferation rates were assessed through ³H-thymidine incorporation. Values represent means ± S.E.M. of four determinations. Results shown were obtained in one representative of three experiments performed. **P* < 0.05 compared to cells stimulated anti-CD3/anti-CD28 (A) or irradiated C57BL/6 spleen cells (B); #*P* < 0.05 compared to BA-treated cultures.

activation, we tested the ability of RU486, a glucocorticoid receptor antagonist, to reverse the effect of BA5 in Con A-stimulated splenocyte cultures. As shown in Fig. 5, addition of RU486 inhibited spleen cell proliferation. This is a glucocorticoid receptor (GR) antagonist which can block the effect of GR agonists, such as dexamethasone. However, it presents off-targets effects, which lead to an attenuation of T cell proliferation (Chien et al., 2009). When co-treated with dexamethasone,

addition of RU486 promoted a partial block of dexamethasone activity. In contrast, the inhibition of spleen cell proliferation upon Con A activation by BA5 was not reversed under RU486 co-treatment.

We also investigated the effect of BA5 on calcineurin activity, which leads to the activation of Nuclear factor of activated T-cells (NFAT), a transcription factor involved in T cell activation (Macian, 2005). As shown in Fig. 6, treatment with BA5 decreased the activity of this

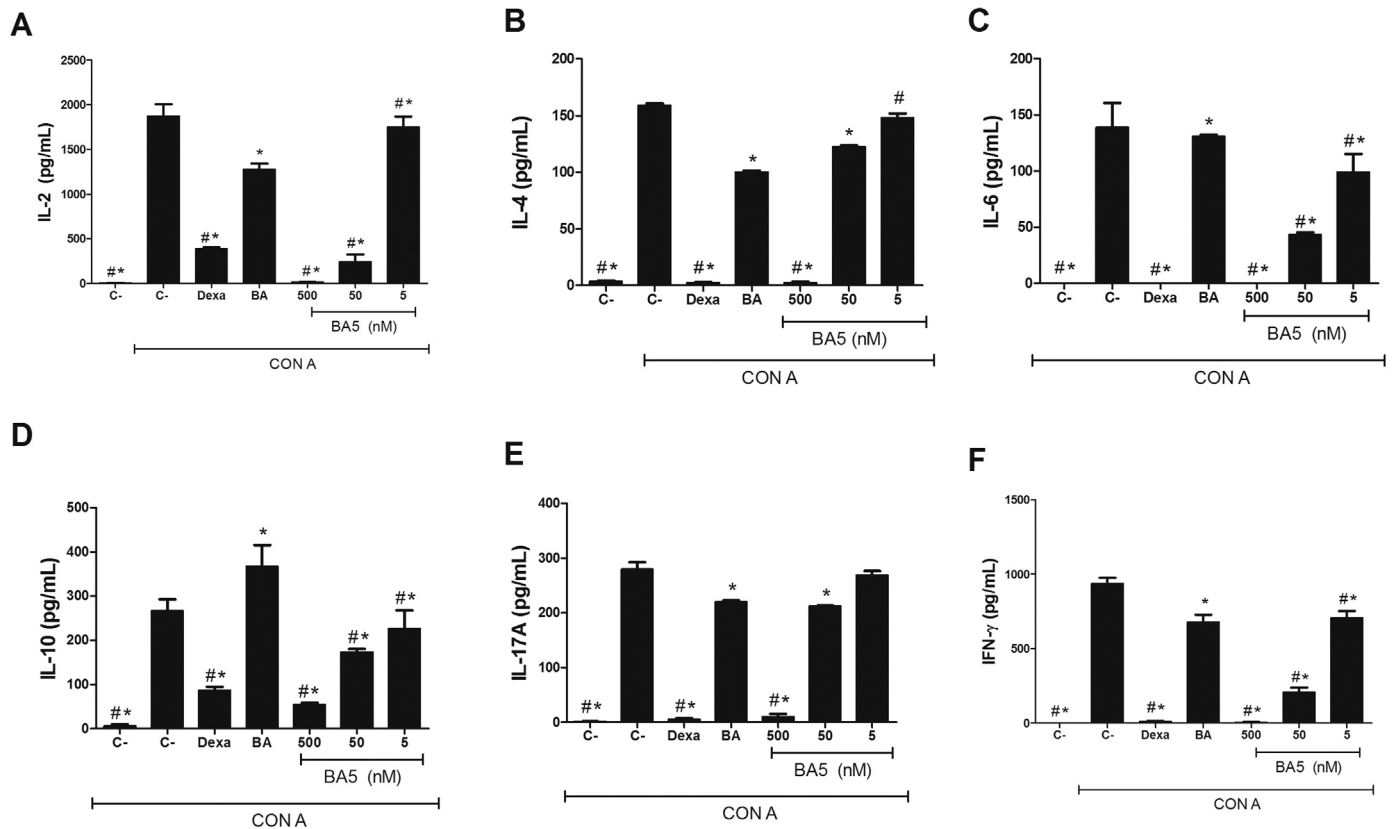


Fig. 3. Assessment of cytokine production by splenocytes treated with BA5. Concentrations of IL-2 (A), IL-4 (B), IL-6 (C), IL-10 (D), IL-17A (E) and IFN- γ (F) were determined in splenocytes treated or not with BA (500 nM), dexamethasone (500 nM) or BA5 (500, 50 and 5 nM) in the presence of concanavalin A (Con A; 5 μ g/ml) for 48 h. C- is untreated cells. Cell-free supernatants were then collected for cytokine measurement by ELISA. Values represent the means ± S.E.M. of four determinations obtained in one of three experiments performed. **P* < 0.05 compared to stimulated and untreated cells; #*P* < 0.05 compared to BA-treated cells.

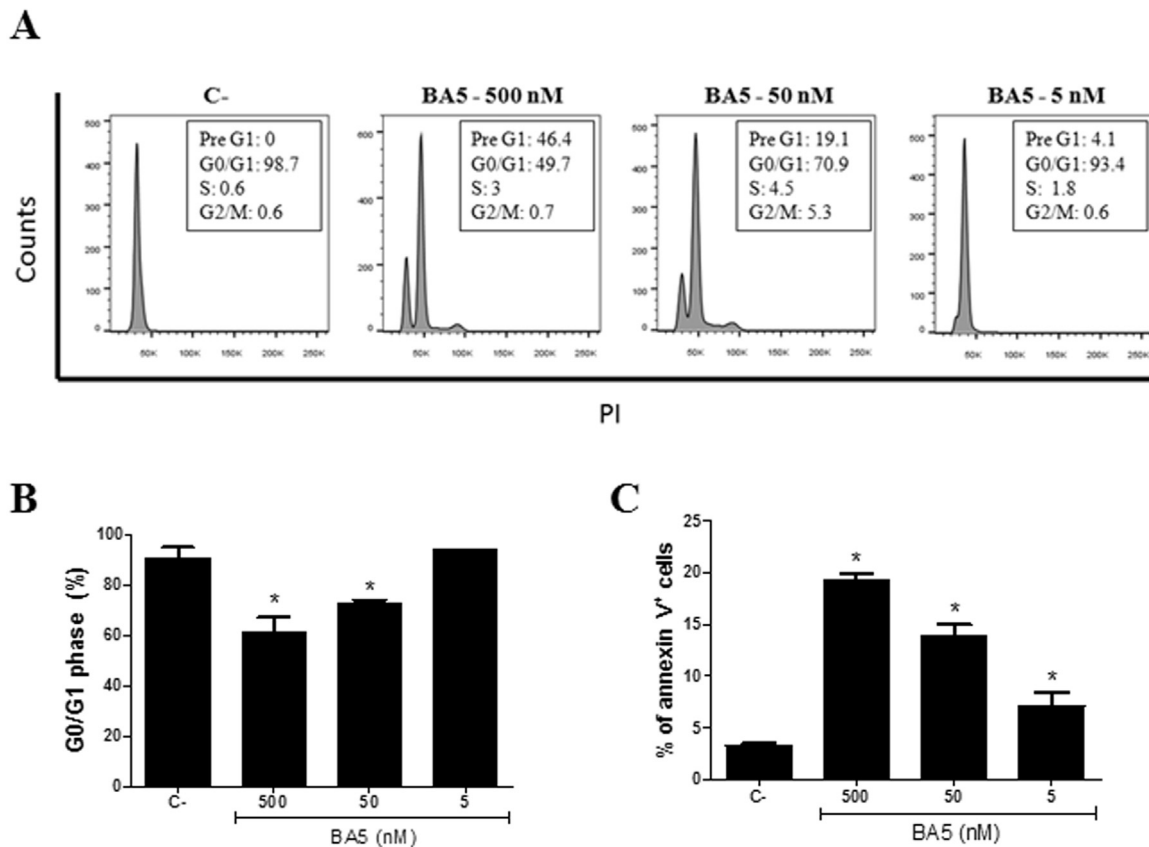


Fig. 4. Analysis of cell cycle progression and cell death after treatment with BA5. (A and B) Splenocytes were treated or not with BA5 (500, 50 or 5 nM) for 24 and 48 h for cell death determination and cell cycle analysis respectively. After staining with propidium iodide (2 µg/ml), DNA content was analyzed by flow cytometry. The distribution and percentage of cells in pre-phase, G0/G1, S and G2/M phase of the cell cycle are indicated. (C) Percentage of stained cells for annexin V after 24 h of treatment with BA5. Values represent the means ± S.E.M. of four determinations obtained in one of two experiments performed. *P < 0.05 compared to stimulated and untreated cells.

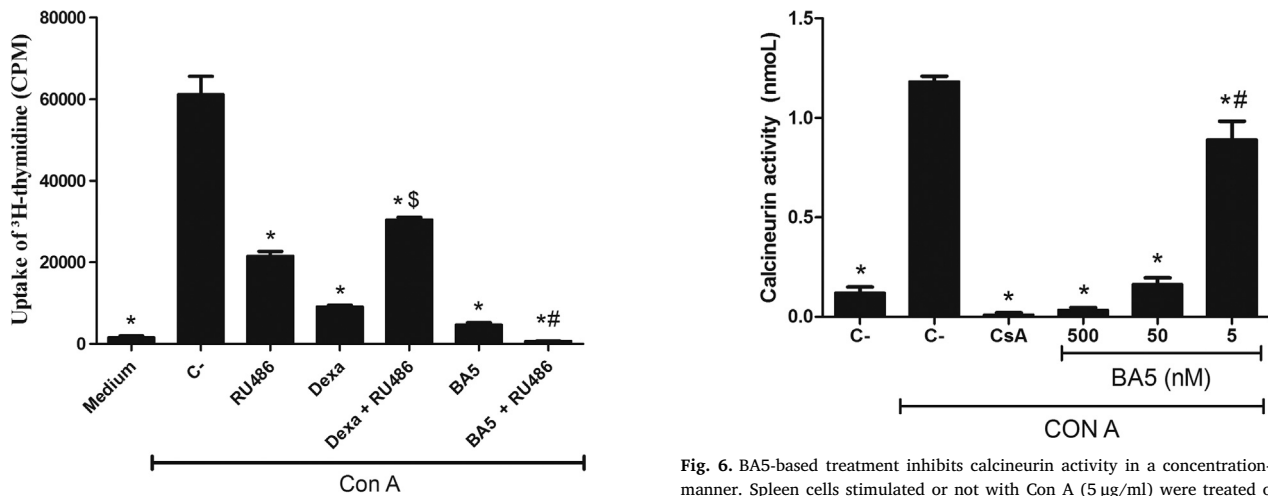


Fig. 5. Effects of RU486 on BA5 activity on Con A-induced lymphoproliferation. BALB/c splenocytes were stimulated with Con A alone or in the presence of dexamethasone (Dexa; 50 nM), BA5 (50 nM) and RU486 (10 µM). C- is untreated cells Proliferation was assessed 48 h later by ³H-thymidine incorporation. Values represent the means ± S.E.M. of 4 determinations. *P < 0.05 compared to Con A; #P < 0.05 compared to BA5 + Con A; §P < 0.05 compared to Dexa + Con A.

enzyme in a concentration-dependent manner, when compared to control untreated cultures. At 500 nM, BA5 caused the inhibition of calcineurin activity comparable to that of cyclosporin A, a reference inhibitor of calcineurin (Fig. 6).

Fig. 6. BA5-based treatment inhibits calcineurin activity in a concentration-dependent manner. Splen cells stimulated or not with Con A (5 µg/ml) were treated or not with different concentrations of BA5 (500, 50 and 5 nM) or cyclosporin A (Csa; 500 nM) for 48 h. C- is untreated cells Then, cells were lysed and cellular calcineurin phosphatase activity was measured in cell extracts, as described in the methods Values represent the means ± S.E.M. of four determinations obtained in one of two experiments performed. *P < 0.05 compared to stimulated and untreated cells; #P < 0.05 compared to cyclosporin A-treated cells.

3.5. Synergistic effects of BA5 and dexamethasone

Drug combinations are often employed in the clinical setting for treatment of immune-mediated diseases. Thus, we investigated the immunosuppressive effects of BA5 and dexamethasone in combination on lymphocyte proliferation induced by Con A. Compared to each drug

Table 2
Concentration reductions and combination indexes for immunosuppression by BA5 and dexamethasone.

Compounds	IC ₅₀ ± S.E.M. (nM) ^a		IC ₉₀ ± S.E.M. (nM) ^a		CI ^b	
	Drug alone	Combination	Drug alone	Combination	IC ₅₀	IC ₉₀
BA5	13.7 ± 0.9	0.4 ± 0.05	205 ± 7.7	10 ± 2.5	0.13 ± 0.01	0.14 ± 0.03
Dexa	4.2 ± 0.1	0.5 ± 0.06	76 ± 8.7	8.1 ± 2.8		

^a IC₅₀ and IC₉₀ values were calculated using concentrations in quadruplicates and two independent experiments were performed.

^b Combination index (CI). Cutoff: CI value of 0.1–0.7, synergism; 0.7–0.85, moderate synergism; 0.85–0.9, slight synergism; 0.9–1.1, additivity; > 1.1, antagonism. S.E.M. = standard error of the mean.

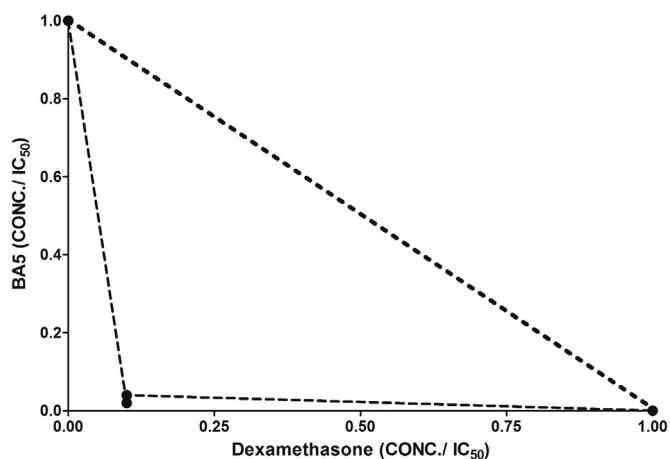


Fig. 7. Isobologram describing the synergistic effects of BA5 and dexamethasone on lymphocyte proliferation induced by Con A. Broken lines correspond to the predicted positions of the experimental points for additive effects.

alone, the combination of BA5 and dexamethasone reduced both IC₅₀ and IC₉₀ values. In fact, the IC₅₀ and IC₉₀ of both drugs decreased at least eight times (Table 2). The combination index values associated with a concave isobologram revealed that BA5 and dexamethasone have synergistic effects (Table 2; Fig. 7).

3.6. BA5 protects mice against a lethal LPS challenge and reduces edema in delayed-type hypersensitivity reaction

To investigate the effects of BA5 in a model of endotoxic shock, groups of BALB/c mice were treated with BA5 or vehicle (5% of DMSO in saline) and challenged with a lethal dose of LPS. Treatment with 50 mg/kg BA5 induced protection to 83% of the animals (Fig. 8). Mice treated with BA5 at a lower dose (25 mg/kg) had, at the end of the observed period (four days), a survival rate of 33%, similar to the vehicle-treated group. Administration of dexamethasone protected 100%

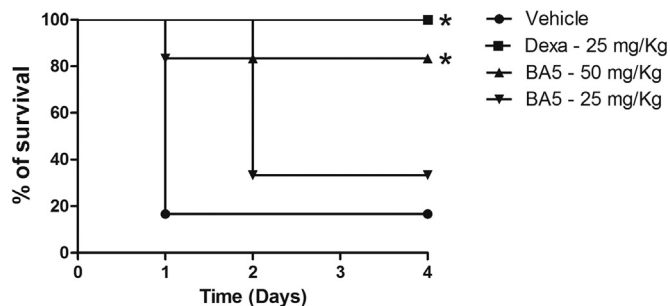


Fig. 8. Survival curve of mice treated with BA5 and submitted to endotoxic shock. Male BALB/c mice (n = 6) were treated with BA5 (25 and 50 mg/Kg) or dexamethasone (25 mg/Kg) or vehicle (5% DMSO in saline) and challenged with LPS 90 min later, intraperitoneally administered. Survival was monitored during 4 days after LPS challenge. Results are from one experiment of two experiments performed. *P < 0.05 compared to vehicle group. Statistical analysis was carried out using Logrank (Mantel Cox).

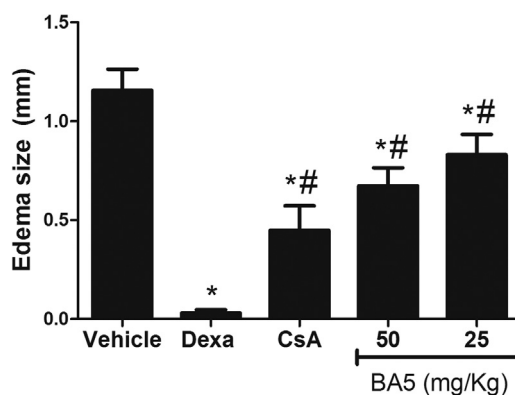


Fig. 9. BA5 reduces BSA-induced DTH in mice. Male BALB/c mice (n = 6) were treated with BA5 (25 and 50 mg/Kg) or dexamethasone (Dexa; 25 mg/Kg) or cyclosporin A (CsA; 25 mg/Kg) or vehicle (5% DMSO in saline) and challenged with 30 µl of a 2% suspension of heat-aggregated BSA in saline administered in the footpad. At 3 h post-challenge, footpad thickness was measured with calipers and the extent of swelling was calculated by subtracting the thickness of the footpad after challenge from that before challenge. Values represent the means ± S.E.M. of six determinations obtained in one of two experiments performed. *P < 0.05 compared to vehicle group; #P < 0.05 compared to dexamethasone group.

of animals at 25 mg/kg. Animals from all groups displayed signs of shock, such as piloerection, shivering, and lethargy.

Finally, we investigated the effect of BA5 on BSA-induced DTH reaction in BALB/c mice. Following sensitization, groups of mice were treated with different doses of BA5 and thicknesses of paw measured before and after challenge were used as clinical signs of hypersensitivity. As shown in Fig. 9, treatment with BA5 at 50 and 25 mg/kg caused a reduction of paw edema of 41.7% and 27.8% respectively. Treatment with dexamethasone or cyclosporin A (25 mg/kg) caused a reduction of 97.4% and 61.7%, respectively.

4. Discussion

Natural products are still a promising source for drug discovery through the continuous process of prospection of new compounds or synthesis of derivatives based on natural products (Newman and Cragg, 2016). This is exemplified by betulinic acid, a natural product with pleiotropic biologic effects and used successfully to generate more active compounds, such as antitumor and anti-HIV agents (Smith et al., 2007; Willmann et al., 2009; Ali-Seyed et al., 2016). In the present study, we investigated the immunomodulatory activity of amide semi-synthetic betulinic acid derivatives containing substituents attached in the lupane backbone. We showed that the incorporation of an amide on C-28 enhanced the immunomodulatory effects on macrophage activation and lymphocyte function. The investigation led to the identification of a potent immunomodulatory agent, the semi-synthetic derivative BA5.

It is well-known that TNFα and NO play critical roles in inflammatory conditions. TNFα recruits and activates macrophages and T cells and modulates the secretion of other pro-inflammatory cytokines

(Elenkov et al., 2005). Nitric oxide, due to its over production on inflammatory conditions, causes vasodilation (Xu et al., 2013). Here, we demonstrated a potent inhibitory activity of BA5 on TNF α and NO production in a concentration-dependent manner without affect cell viability in the tested concentrations. Consistent with these findings, BA5 also suppressed NF- κ B activity, an important transcription factor that regulates several pro-inflammatory genes, such as TNF α (Lawrence et al., 2002). Moreover, the anti-inflammatory mechanism of BA5 differs from that of BA, the prototype molecule, which is IL-10 dependent (Fiorentino et al., 1991; Costa et al., 2014).

Although there are several reports about the anti-inflammatory activity of betulinic acid and its derivatives, little is known about the effects of these molecules on lymphocyte function. In the present work, we showed that betulinic acid is a potent inhibitor of lymphocyte proliferation and production of key cytokines in the proliferation and activation of lymphocytes, such as IL-2 and IFN γ (Kohno et al., 1997; Boyman and Sprent, 2012). In addition, we showed that these properties are enhanced in BA5 derivative. In fact, the antiproliferative effect of BA and other terpenoids is well recognized in different tumor cell lines, especially in leukemia lineages, such as Jurkat cells, in which BA treatment induced cell cycle arrest in pre-G1 phase followed by cell death by apoptosis (Chen et al., 2008). Interestingly, a similar pathway of cell death was observed in lymphocytes treated with BA5. In addition, BA5 also potently inhibited calcineurin activity, an enzyme that plays a critical role in the progression of cell cycle and T lymphocyte activation through activation of NFAT (Rusnak and Mertz, 2000; Lipskaia and Lompré, 2004; Cen et al., 2013).

Despite the large number of immunosuppressive drugs available, most have side effects associated to a prolonged use and are not efficient in certain conditions (Garcia et al., 2004; Malvezzi et al., 2015). Combined drug therapy may be a valuable tool to improve treatment efficacy and reduce dose levels and toxicity immune disorders, as well as to prevent the potential development of resistance (Vedtofte et al., 2017; Kavishe et al., 2017). In our study, BA5 had synergistic effects with dexamethasone on the inhibition of lymphocyte proliferation, showing a promising profile for drug combination.

Previous studies detected the potential of betulinic acid and others triterpenoids in inflammatory mouse models (Costa et al., 2014; Niu et al., 2014; Lingaraju et al., 2015b). In the present work, we observed the effects of BA5 in a mouse model of endotoxemia induced through intraperitoneally LPS administration. In this model of lethal shock, LPS binds to CD14 receptors of macrophages and triggers the release of proinflammatory cytokines, including IL-1 and TNF- α that can in turn induce lethal shock (Blank et al., 1997). Despite having protective effects in T-cell mediated shock models, classic calcineurin inhibitors such as cyclosporin A didn't have protective effects in LPS mediated shock models (Gonzalo et al., 1993). In contrast, BA5 proven to be a potent inhibitor of calcineurin and also able to protect animals from a lethal dose of LPS, showing a advantage when compared to others calcineurin inhibitors. We also observed a reduction of paw edema in a mouse model of BSA-induced DTH, a expected feature for a calcineurin inhibitor. Our results reinforce the potential use of betulinic acid and its derivatives in the searching for more potent and selective immunomodulatory drugs

In conclusion, betulinic acid can be successfully used for the generation of more active compounds, such as the derivative BA5, identified herein with a potent immunomodulatory *in vitro* and *in vivo*. BA5 also proved to be a suitable partner for drug combination, evidencing its potential use for the treatment of immune-mediated disorders.

Conflict of interest

All authors have no conflict of interest to disclose.

Acknowledgements

This work was supported by grants from CNPq (# 400910/2013-6), PRONEX (# PN0002/2014) and FAPESB (# PET0042/2013).

References

- Ali-Seyed, M., Jantan, I., Vijayaraghavan, K., Bukhari, S.N., 2016. Betulinic acid: recent advances in chemical modifications, effective delivery, and molecular mechanisms of a promising anticancer therapy. *Chem. Biol. Drug Des.* 87 (4), 517–536.
- Barbosa-Filho, J.M., Trigueiro, J.A., Cheriyan, U.O., Bhattacharyya, J., 1985. Constituents of the stem-bark of *Ziziphus joazeiro*. *Nat. Prod. Res.* 48, 152–153.
- Bartuzi, P., Hofker, M.H., Sluis, B.V., 2013. Turning NF- κ B activity: a touch of COMMD proteins. *Biochim. Biophys. Acta* 1832 (12), 215–2321.
- Blank, C., Luz, A., Bendigs, S., Endmann, A., Wagner, H., Heeg, K., 1997. Superantigen and endotoxin synergize in the induction of lethal shock. *Eur. J. Immunol.* 27, 825–833.
- Blaževski, J., Petković, F., Momčilović, M., Paschke, R., Kaluderović, G.N., Mostarica Stojković, M., Miljković, D., 2013. Betulinic acid regulates generation of neuroinflammatory mediators responsible for tissue destruction in multiple sclerosis *in vitro*. *Acta Pharm. Sin.* 34 (3), 424–431.
- Boyman, O., Sprent, J., 2012. The role of interleukin-2 during homeostasis and activation of the immune system. *Nat. Rev. Immunol.* 12, 180–190.
- Cen, J., Shi, M., Yang, Y., Fu, Y., Zhou, H., et al., 2013. Isogarcinol is a new immunosuppressant. *PLoS One* 8 (6), e66503.
- Chen, S., Bai, Y., Li, Z., Jia, K., Jin, Y., et al., 2017. A betulinic acid derivative SH479 inhibits collagen-induced arthritis by modulating T cell differentiation and cytokine balance. *Biochem. Pharmacol.* S0006-2952 (16), 30368–30473.
- Chen, Z., Wu, Q.L., Chen, Y., He, J., 2008. Effect of betulinic acid on proliferation and apoptosis in Jurkat cells and its mechanism. *Zhonghua Zhong Liu Za Zhi* 30 (8), 588–592.
- Chien, C.H., Lai, J.N., Liao, C.F., Wang, O.Y., LM, L.U., Huang, M.I., Lee, W.F., Shie, M.C., Chien, E.J., 2009. Mifepristone acts as progesterone antagonist of non-genomic responses but inhibits phytohemagglutinin-induced proliferation in human T cells. *Hum. Reprod.* 24 (8), 1968–1975.
- Chou, T.C., Talalay, P., 2005. Quantitative analysis of dose-effect relationships: the combined effects of multiple drugs or enzyme inhibitors. *Adv. Enzym. Regul.* 22, 27–55.
- Cichewicz, R.H., Kouzi, S.A., 2004. Chemistry, biological activity and chemotherapeutic potential of betulinic acid for the prevention and treatment of cancer and HIV infection. *Med. Res. Rev.* 24, 90–114.
- Costa, J.F.O., Barbosa-Filho, J.M., Maia, G.L.A., Guimarães, E.T., Meira, C.S., Ribeiro-dos-Santos, R., Carvalho, L.P., Soares, M.B.P., 2014. Potent anti-inflammatory activity of betulinic acid treatment in a model of lethal endotoxemia. *Int. Immunopharmacol.* 23, 469–474.
- Dehelean, C.A., Feflea, S., Ganta, S., Amiji, M., 2011. Anti-angiogenic effects of betulinic acid administered in nanoemulsion formulation using chorioallantoic membrane assay. *J. Biomed. Nanotechnol.* 7 (2), 317–324.
- Elenkov, I.J., Iezzoni, D.G., Daly, A., Harris, A.G., Chrousos, G.P., 2005. Cytokine dysregulation, inflammation and well-being. *Neuroimmunomodulation* 12, 255–269.
- Fiorentino, D.F., Zlotnik, A., Mosmann, T.R., Howard, M., O'Garra, A., 1991. IL-10 inhibits cytokine production by activated macrophages. *J. Immunol.* 147, 3815–3822.
- Fivelman, Q.L., Adagu, I.S., Warhurst, D.C., 2004. Modified fixed-ratio isobologram method for studying *in vitro* interactions between atovaquone and proguanil or dihydroartemisinin against drug-resistant strains of *Plasmodium falciparum*. *Antimicrob. Agents Chemother.* 48, 4097–4102.
- Garcia, S.C., Lopes, L.S., Schott, K.L., Beck, S.T., Pombum, V.J., 2004. Cyclosporine A and tacrolimus: a review. *J. Bras. Patol. Med. Lab.* 40 (6), 393–401.
- Gheorgheso, D., Duicu, O., Dehelean, C., Soica, C., Muntean, D., 2016. Betulinic acid as a potent and complex antitumor phytochemical: a minireview. *Anticancer Agents Med. Chem.* 14 (7), 936–945.
- Gonzalo, J.A., González-García, A., Kalland, T., Hedlund, G., Martínez-A, C., Linomide, Kroemer G., 1993. a novel immunomodulator that prevents death in four model of septic shock. *Eur. J. Immunol.* 23, 2372–2374.
- Green, L.C., Wagne, D.A., Glogowski, J., Skipper, P.L., Wishnok, J.S., Tannenbaum, S.R., 1982. Analysis of nitrate, nitrite, and [15N] nitrate in biological fluids. *Anal. Biochem.* 126, 131–138.
- Jingbo, W., Aimin, C., Qi, W., Xin, L., Huaining, L., 2015. Betulinic acid inhibits IL-1 β -induced inflammation by activating PPAR- γ in human osteoarthritis chondrocytes. *Int. Immunopharmacol.* 29 (2), 687–692.
- Kavishe, R.A., Koenderink, J.B., Alifrangis, M., 2017. Oxidative stress in malaria and artemisinin combination therapy: pros and cons. *FEBS J.* <http://dx.doi.org/10.1111/febs.14097>.
- Kim, K.S., Lee, D.S., Kim, D.C., Yoon, C.S., Ko, W., Oh, W., Oh, H., Kim, Y.C., 2016. Anti-inflammatory effects and mechanisms of action of coussaric and betulinic acids isolated from *Diospyros kaki* in lipopolysaccharide-stimulated RAW 264.7 macrophages. *Molecules* 21 (9), E1206.
- Kohno, K., Kataoka, J., Ohtsuki, T., Suemoto, T., Okamoto, I., Usui, M., Ikeda, M., Kurimoto, M., 1997. IFN-gamma-inducing factor (IGIF) is a costimulatory factor on the activation of Th1 but not Th2 cells and exerts its effect independently of IL-12. *J. Immunol.* 158 (4), 1541–1550.
- Lawrence, T., Willoughby, D.A., Gilroy, D.W., 2002. Anti-inflammatory lipid mediators and insights into the resolution of inflammation. *Nat. Rev. Immunol.* 123, 97–105.
- Li, J., Goto, M., Yang, X., Morris-Natschke, S.L., Huang, L., Chen, C.H., Lee, K.H., 2016.

- Fluorinated betulinic acid derivatives and evaluation of their anti-HIV activity. *Bioorg. Med. Chem. Lett.* 26 (1), 68–71.
- Li, J., Jing, J., Bai, Y., Li, Z., Xing, R., Tan, B., Ma, X., Qiu, W.W., Du, C., Du, B., Yang, F., Tang, J., Siwko, S., Li, M., Chen, H., Luo, J., 2017. SH479, a betulinic acid derivative, ameliorates experimental autoimmune encephalomyelitis by regulating the T helper 17/Regulatory T cell balance. *Mol. Pharmacol.* 91 (5), 464–474.
- Lingaraju, M.C., Pathak, N.N., Begum, J., Balaganur, V., Bhat, R.A., Ramachandra, H.D., Ayanur, A., Ram, M., Singh, V., Kumar, D., Kumar, D., Tandan, S.K., 2015a. Betulinic acid attenuates lung injury by modulation of inflammatory cytokine response in experimentally-induced polymicrobial sepsis in mice. *Cytokine* 71 (1), 101–108.
- Lingaraju, M.C., Pathak, N.N., Begum, J., Balaganur, V., Bhat, R.A., Ram, M., Singh, V., Kandasamy, K., Kumar, D., Kumar, D., Tandan, S.K., 2015b. Betulinic acid attenuates renal oxidative stress and inflammation in experimental model of murine polymicrobial sepsis. *Eur. J. Pharm. Sci.* 70, 12–21.
- Lipskaia, L., Lompré, A.M., 2004. Alteration in temporal kinetics of Ca²⁺ signaling and control of growth and proliferation. *Biol. Cell* 96 (1), 55–64.
- Macian, F., 2005. NFAT proteins: key regulators of T-cell development and function. *Nat. Rev. Immunol.* 5 (6), 472–484.
- Malvezzi, P., Rostaing, L., 2015. The safety of calcineurin inhibitors for kidney-transplant patients. *Expert Opin. Drug Saf.* 14 (10), 1531–1546.
- Meira, C.S., Barbosa-Filho, J.M., Lanfredi-Rangel, A., Guimarães, E.T., Moreira, D.R.M., Soares, M.B.P., 2016. Antiparasitic evaluation of betulinic acid derivatives reveals effective and selective anti-*Trypanosoma cruzi* inhibitors. *Exp. Parasitol.* 166, 108–115.
- Newman, D.J., Cragg, G.M., 2016. Natural products as sources of new drugs from 1981 to 2014. *J. Nat. Prod.* 79 (3), 629–661.
- Niu, X., Mu, Q., Li, W., Yao, H., Li, H., Huang, H., 2014. Esculentin acid, a novel and selective COX-2 inhibitor with anti-inflammatory effect *in vivo* and *in vitro*. *Eur. J. Pharm.* 740, 532–538.
- Rusnak, F., Mertz, P., 2000. Calcineurin: form and function. *Physiol. Rev.* 80, 1483–1521.
- Smith, P.F., Ogundele, A., Forrest, A., Wilton, J., Salzwedel, K., Doto, J., Allaway, G.P., Martin, D.E., 2007. Phase I and phase II study of the safety, virologic effect, and pharmacokinetics/pharmacodynamics of single-dose 3-*o*-(3',3'-dimethylsuccinyl)betulinic acid (bevirimat) against human immunodeficiency virus infection. *Antimicrob. Agents Chemother.* 51 (10), 3574–3581.
- Soares, M.B.P., Brustolim, D., Santos, L.A., Bellintani, M.C., Paiva, F.P., et al., 2006. Physalins B, F and G, *seco-steroids* purified from *Physalis angulata* L., inhibit lymphocyte function and allogeneic transplant rejection. *Int. Immunopharmacol.* 6, 408–414.
- Sultana, N., Saify, Z.F., 2012. Naturally occurring and synthetic agents as potential anti-inflammatory and immunomodulators. *Antiinflamm. Antiallergy Agents Med. Chem.* 11 (1), 3–19.
- Takada, Y., Aggarwal, B.B., 2003. Betulinic acid suppresses carcinogen-induced NF-kappa B activation through inhibition of I Kappa B alpha kinase and p65 phosphorylation: abrogation of cyclooxygenase-2 and matrix metalloproteinase-9. *J. Immunol.* 17 (6), 3278–3286.
- Titus, R.G., Chiller, J.M., 1981. A simple and effective method to assess murine delayed type hypersensitivity to proteins. *J. Immunol. Methods* 45, 65–78.
- Vedtofte, L., Knop, F.K., Vilsboll, T., 2017. Efficacy and safety of fixed-ratio combination of insulin degludec and liraglutide (IDegLira) for the treatment of type 2 diabetes. *Expert Opin. Drug Saf.* 16 (3), 387–396.
- Viji, V., Shobha, B., Kavitha, S.K., Ratheesh, M., Kripa, K., Helen, A., 2010. Betulinic acid isolated from *Bacopa monniera* (L.) Wettst suppresses lipopolysaccharide stimulated interleukin-6 production through modulation of nuclear factor-kappaB in peripheral blood mononuclear cells. *Int. Immunopharmacol.* 10 (8), 843–849.
- Willmann, M., Wacheck, V., Buckley, J., Nagy, K., Thalhammer, J., Paschke, R., Triche, T., Jansen, B., Selzer, E., 2009. Characterization of NVX-207, a novel betulinic acid-derived anti-cancer compound. *Eur. J. Clin. Invest.* 39 (5), 384–394.
- Xu, J., Jia, Y.Y., Chen, S.R., Ye, J.T., Bu, X.Z., Hu, Y., Ma, Y.Z., Guo, J.L., Liu, P.Q., 2013. (E)-1-(4-ethoxyphenyl)-3-(4-nitrophenyl)-prop-2-en-1-one suppresses LPS-induced inflammatory response through inhibition of NF-κB signaling pathway. *Int. Immunopharmacol.* 15, 743–751.
- Yogeewari, P., Sriram, D., 2005. Betulinic acid and its derivatives: a review on their biological properties. *Curr. Med. Chem.* 12, 657–666.
- Zhong, H., SuYang, H., Erdjument-Bromage, H., Tempst, P., Ghosh, S., 1997. The transcriptional activity of NF-kappaB is regulated by the IkappaB-associated PKAc subunit through a cyclic amp-independent mechanism. *Cell* 89 (3), 413–424.

CAPÍTULO II

Neste capítulo demonstramos que o composto BA5, através de uma ação dual anti-*T. cruzi* e imunomoduladora, é benéfico no modelo experimental de cardiomiopatia chagásica crônica.

Artigo a ser submetido para publicação.

Betulinic acid derivative BA5, attenuates inflammation and fibrosis in experimental chronic Chagas disease cardiomyopathy by inducing IL-10 and M2 polarization

Cássio Santana Meira¹, Emanuelle De Souza Santos¹, Renan Fernandes do Espírito Santo^{1,2}, Juliana Fraga Vasconcelos^{1,3}, Iasmim Diniz Orge^{1,3}, Carolina Kymie Vasques Nonaka^{1,3}, Breno Cardim Barreto³, Alex Cleber Improta Caria³, Daniela Nascimento Silva^{1,3}, José Maria Barbosa-Filho⁴, Simone Garcia Macambira^{3,5}, Diogo Rodrigo Magalhães Moreira¹, Milena Botelho Pereira Soares^{1,3}

Betulinic acid derivative BA5, attenuates inflammation and fibrosis in experimental chronic Chagas disease cardiomyopathy by inducing IL-10 and M2 polarization

Cássio Santana Meira¹, Emanuelle De Souza Santos¹, Renan Fernandes do Espírito Santo^{1,2}, Juliana Fraga Vasconcelos^{1,3}, Iasmim Diniz Orge^{1,3}, Carolina Kymie Vasques Nonaka^{1,3}, Breno Cardim Barreto³, Alex Cleber Improta Caria³, Daniela Nascimento Silva^{1,3}, José Maria Barbosa-Filho⁴, Simone Garcia Macambira^{3,5}, Diogo Rodrigo Magalhães Moreira¹, Milena Botelho Pereira Soares^{1,3}

¹ Instituto Gonçalo Moniz, Fundação Oswaldo Cruz (FIOCRUZ), Salvador, BA, Brazil;

² Faculdade de Farmácia, Universidade Federal da Bahia, Salvador, BA, Brazil;

³ Centro de Biotecnologia e Terapia Celular, Hospital São Rafael, Salvador, BA, Brazil;

⁴ Laboratório de Tecnologia Farmacêutica, Universidade Federal da Paraíba, João Pessoa, PB, Brazil;

⁵ Departamento de Bioquímica e Biofísica, Instituto de Ciências da Saúde, Universidade Federal da Bahia, Salvador, BA, 40110-100, Brazil.

*Corresponding author: Milena Botelho Pereira Soares. Instituto Gonçalo Moniz, Fundação Oswaldo Cruz. Rua Waldemar Falcão, 121, Candeal, Salvador, Bahia, Brazil. Zip code: 40296-710. Phone: (+55) 71 31762260; fax: (+55) 71 31762272. Email address: milena@bahia.fiocruz.br

Abstract

Chronic Chagas disease cardiomyopathy (CCC) is a major cause of heart disease in Latin America and treatment for this condition is unsatisfactory. Here we investigated the effects of BA5, an amide semi-synthetic derivative betulinic acid, in a model of CCC. Mice chronically infected with *T. cruzi* were treated orally with BA5 (10 or 1 mg/Kg), three times per week, for two months. BA5 treatment decreased inflammation and fibrosis in heart sections but did not improve exercise capacity or ameliorate cardiac electric disturbances in infected mice. Serum concentrations of TNF- α , IFN- γ and IL-1 β , as well as cardiac gene expression of pro-inflammatory mediators, were reduced after BA5 treatment. In contrast, a significant increase in the anti-inflammatory cytokine IL-10 concentration was observed in BA5-treated mice in both tested doses compared to vehicle-treated mice. Moreover, polarization to anti-inflammatory/M2 macrophage phenotype was evidenced by a decrease in the expression of NOS2 and proinflammatory cytokines and the increase in M2 markers, such as Arg1 and CHI3 in mice treated with BA5. In conclusion, BA5 had a potent anti-inflammatory activity on a model of parasite-driven heart disease related to IL-10 production and a switch from M1 to M2 subset of macrophages.

KeyWords: *Trypanosoma cruzi*, Betulinic acid derivative, Chagas disease cardiomyopathy.

Introduction

Chagas disease, caused by the flagellate protozoan *Trypanosoma cruzi*, affects 7 million people worldwide (WHO, 2017). Endemic in Latin American countries, it is increasingly found in non-endemic countries due to intense flow of migration, representing a major public health problem (Connors *et al.*, 2016). The acute phase of Chagas disease is characterized by the presence of *T. cruzi* parasites in the bloodstream, which trigger an intense inflammatory response in several tissues, especially in the cardiac tissue (Boscardin *et al.*, 2010). The majority of *T. cruzi*-infected patients survive in the acute phase and develop a chronic asymptomatic infection (Lewis & Kelly, 2016). Nonetheless, after a variable period of time (10-30 years after the onset infection), about 30% of chronically-infected patients become symptomatic (Marin-Neto *et al.*, 2010).

Chronic Chagasic cardiomyopathy (CCC) is the most common symptomatic form of Chagas disease and may evolve with several manifestations, including heart failure, arrhythmias and thromboembolism (Benziger *et al.*, 2017). CCC is a major cause of heart disease and a cardiovascular-related death in Latin America, and causes a significant economic and social burden in affected countries (Cunha-Neto & Chevillard, 2014).

Antiparasitic treatment is based on the use of two drugs, benznidazole and nifurtimox. Although benznidazole has good cure rates when administered during the acute phase, its prolonged use is related to severe side effects, and has limited efficacy during the chronic phase (Rassi *et al.*, 2000; Morillo *et al.*, 2015). New candidate drugs are being tested, including the inhibitor of ergosterol posaconazole, which failed to promote cure in patients in the chronic stage of disease (Molina *et al.*, 2014). This

scenario makes the search for new drugs with a better profile of safety and efficiency an important issue for Chagas disease.

In addition to eliminating the parasites, an ideal treatment for chronic stage must be able to modulate the inflammatory process responsible for the establishment of myocarditis, causing loss of cardiomyocytes and fibrosis deposition, ultimately leading to heart failure, arrhythmias and death of Chagasic patients (González-Herrera *et al.*, 2017). In this context, the compound BA5, an amide semi-synthetic betulinic acid derivative, is an attractive option. Recently, our group reported the antiparasitic activity against *T. cruzi* trypomastigotes and intracellular amastigotes, with potency similar to benznidazole (Meira *et al.*, 2016). We also found a potent immunomodulatory activity of BA5 *in vitro*, decreasing the production of crucial inflammatory mediators, including nitric oxide (NO), tumor necrosis factor alpha (TNF- α) and inhibiting the activation of nuclear factor- κ B (NF- κ B), a transcription factor that regulates the expression of several pro-inflammatory genes (Meira *et al.*, 2017). Moreover, BA5 conferred protection against a lethal dose of LPS and decreased edema in a delayed type hypersensitivity model (Meira *et al.*, 2017).

In the present study we tested the therapeutic effects of BA5, a compound with combined antiparasitic and immunomodulatory activities, in a mouse model of chronic *T. cruzi* infection, which reproduces key features of CCC.

Materials and methods

Drugs

Semi-synthetic compound BA5 (95% purity by HPLC) was prepared from betulinic acid, as previously described (Meira *et al.*, 2016). Benznidazole (LAFEPE, Recife, Brazil) was used as a positive control.

Animals

C57BL/6 mice (4 weeks old) were bred and maintained in the animal facility of the Center for Biotechnology and Cell Therapy, Hospital São Rafael (Salvador, Bahia, Brazil), and provided with rodent diet and water *ad libitum*. All experiments were carried out in accordance with the recommendations of Ethical Issues Guidelines, and were approved by the local ethics committee for animal use under number 001/15 (FIOCRUZ, Bahia, Brazil).

***Trypanosoma cruzi* infection and BA5 treatment**

Trypomastigotes of the myotropic Colombian *T. cruzi* strain were obtained from culture supernatants of infected LLC-MK2 cells. Infection was performed by intraperitoneal inoculation of 10^3 parasites in 100 μ L of saline solution and parasitemia was monitored during infection, using standard protocols (Brenner, 1962). After six months of infection, mice were divided into groups of 10 and received treatments, as follows: 10 or 1 mg/kg of BA5, 100 mg/Kg benznidazole or vehicle (10% DMSO in saline), given orally three times per week for two months (Figure 1). A naive group (n=5) was also included as a control. Mice were euthanized one week after therapy, under anesthesia with 5% ketamine and 2% xylazine (Vetanarcol® and Sedomin®, respectively; Konig, Avellaneda, Argentina).

Exercise capacity analysis and electrocardiography

A motor-driven treadmill chamber for one animal (LE 8700; Panlab, Barcelona, Spain) was used to exercise the animals. The speed of the treadmill and the intensity of the shock (mA) were controlled by a potentiometer (LE 8700 treadmill control; Panlab). Total running distance and time of exercise were recorded. Electrocardiography was performed using the Bio Amp PowerLab System (PowerLab 2/20; ADInstruments, Castle Hill, NSW, Australia), recording the bipolar lead I. All data were acquired for computer analysis using Chart 5 for Windows (PowerLab). The EKG analysis included heart rate, PR interval, P wave duration, QT interval, QTc, and arrhythmias. The QTc was calculated as the ratio of QT interval by square roots of RR interval (Bazett's formula) (Berul *et al.*, 1996).

Morphometric analysis

The hearts of all mice were removed and half of each heart was fixed in 10% buffered formalin. Sections of paraffin-embedded tissue were stained by the standard hematoxylin-eosin and Sirius red staining methods for evaluation of inflammation and fibrosis, respectively, by optical microscopy. Images were digitized using a color digital video camera (CoolSnap, Montreal, Canada) adapted to a BX41 microscope (Olympus, Tokyo, Japan). Morphometric analyses were performed using the software Image Pro Plus v.7.0 (Media Cybernetics, San Diego, CA). The inflammatory cells were counted in 10 fields (400x magnification) per heart. The percentage of fibrosis was determined using Sirius red-stained heart sections and the Image Pro Plus v.7.0 Software to integrate the areas, 10 random fields per animal were captured using a 200x magnification.

Real time reverse transcription polymerase chain reaction (qRT-PCR)

RNA was extracted of the heart samples using TRIzol (Invitrogen, Molecular Probes, Eugene, OR). cDNA was synthesized using High Capacity cDNA Reverse Transcription Kit (Applied Biosystems). The qPCR was prepared with TaqMan® Universal PCR Master Mix (Applied Biosystems). qRT-PCR assays were performed to detect the expression levels of, *Lgals3* (Mm_00802901_m1), *Tnf* (Mm_00443258_m1), *IFN- γ* (Mm_00801778_m1), *Il10* (Mm_00439616_m1), *Tbet* (Mm_00450960_m1), *Foxp3* (Mm_00475162_m1), *Gata-3* (Mm_00484683_m1), *TGF- β* (Mm_00441724_m1), *Nos2* (Mm_01309898_m1), *Chi3l3* (Mm_00657889_m1), *Il1 β* (Mm_0044228_m1) and *Arg1* (Mm_00475988_m1). All reactions were run in triplicate on an ABI 7500 Real Time PCR System (Applied Biosystems) under standard thermal cycling conditions. A non-template control (NTC) and non-reverse transcription controls (No-RT) were also included. The samples were normalized with *Gpdh* (mm99999915_g1). The threshold cycle ($2^{-\Delta\Delta Ct}$) method of comparative PCR was used to analyse the results (Schmittgen & Livak, 2008).

Parasitemia and quantification of parasite load

Blood parasitemia of infected mice was monitored weekly in the period of treatment by counting the number of motile parasites in 5 μ L of fresh blood sample drawn from the lateral tail veins, as recommended by standard protocol (Brener, 1962).

To evaluate the tissue parasitism, *T. cruzi* DNA was quantified in spleen samples by qPCR analysis. For DNA extraction, spleen pieces were submitted to DNA extraction using the Mini Spin plus Kit (Biopur, Cambridge, USA), as recommended by the manufacturer. Spleen samples was submitted to DNA extraction, and the DNA amount and purity (260/280 nm) were analyzed by Nanodrop 2000 spectrophotometry

(Thermo Fisher Scientific, Waltham, MA, USA). Primers were designed based on the literature (Schijman *et al*, 2011) and the quantification of parasite load was performed as described previously (Vasconcelos *et al*, 2013). To calculate the number of parasites per milligram of tissue, each plate contained a 7-log standard curve of DNA extracted from trypomastigotes of the Colombian *T. cruzi* strain (ranging from 10^{-1} to 10^6) in triplicate. Data were analyzed using 7500 software 2.0.1 (Applied Biosystems).

Assessment of cytokine production

Blood samples was collected via the brachial plexus, centrifuged (1200 g, 10 min, 4 °C) and the serum supernatant transferred to microcentrifuge tube and stored at -80 °C until subsequent analysis. Serum samples from the *in vivo* study were used for TNF- α , IFN- γ , IL-1 β and IL-10 determination. Quantification of cytokines was performed by ELISA, using specific antibody kits (R&D Systems, Minneapolis, MN), according to manufacturer's instructions.

Statistical analyses

All continuous variables are presented as means \pm SEM. Data were analyzed using one-way ANOVA, followed by Newman-Keuls multiple-comparison test with Prism 5.01 (GraphPad Software, San Diego, CA). Differences were considered significant when the values of *P* were < 0.05 .

Results

BA5 decreases cardiac inflammation and fibrosis in *T. cruzi*-infected mice

To investigate the effects of BA5 in chronic Chagas disease, we treated *T. cruzi*-infected mice with BA5 (1 or 10 mg/Kg) benznidazole (100 mg/Kg) or vehicle (Figure 1A). First, we performed functional evaluation by ergometry and ECG before and after treatment. The exercise capacity of mice from both BA5-treated groups showed no improvements compared to saline treated chagasic controls (Figures 1B and C). Treatment with benznidazole caused only a small improvement in time run (Figure 1B). The evaluation of conduction disturbances did not show significant differences between the groups infected with *T. cruzi* before and after treatment, which presented alterations such as atrioventricular block, atrioventricular dissociation and tachycardia (Table 1).

We next evaluated the effects of BA5 administration in the cardiac tissue, by analyzing heart sections stained with hematoxylin and eosin and Sirius red for quantification of inflammation and fibrosis, respectively. A multifocal inflammatory response, mainly composed of mononuclear cells, was found in vehicle-treated infected mice (Figure 2B and 2I). BA5 administration at the highest dose (10 mg/Kg), but not at 1 mg/Kg, decreased the number of inflammatory cells (Figure 2D and 2I). Treatment with the standard drug, benznidazole, promoted a more pronounced reduction in inflammation (Figure 2C and 2I). In addition, the gene expression of CD45, a pan leukocyte marker, was increased in *T. cruzi* infected mice treated with vehicle, but not in BA5 (10 mg/Kg) and benznidazole-treated mice (Figure 2J).

Similarly, fibrosis deposition was increased in chronic chagasic hearts compared to naïve controls (Figure 2F and 2K). A significant reduction of fibrosis was found in mice treated with BA5 at 10 and 1 mg/Kg, although the highest dose promoted a more pronounced effect (Figure 2H and 2K). Benznidazole also reduced cardiac fibrosis compared to vehicle-treated mice, as revealed by Sirius red staining (Figure 2G and 2K).

BA5 modulates the production of inflammatory mediators in chagasic mice

The inflammatory response in CCC has been associated with an elevated production of proinflammatory cytokines, such as TNF- α and IFN- γ (Abel *et al.*, 2001). Thus, we evaluated the effects of BA5 in cytokine production in the sera and in the hearts of chagasic mice. *T. cruzi* chronic infection caused a significant increase in serum concentrations of proinflammatory cytokines TNF- α , IFN- γ and IL-1 β (Figure 4A-C). BA5 promoted a marked reduction in the production of TNF- α in both doses tested (10 and 1 mg/Kg), and a significant decrease in the production of IFN- γ and IL-1 β in the highest dose (Figures 4A-C). Benznidazole administration significantly inhibited serum TNF- α and IFN- γ , but not IL-1 β . In contrast, a significant increase in the concentration of IL-10, an antiinflammatory cytokine, was observed in BA5-treated mice in both doses tested, compared to vehicle-treated mice. Benznidazole treatment did not induce an increase in IL-10 production (Figure 4D).

To evaluate the effects of BA5 treatment in the heart, we performed RT-qPCR analysis in samples from the different experimental groups. As expected, infection upregulated the expression of several inflammation-related genes, including TNF- α , IFN- γ , IL-1 β , galectin-3, TGF β and IL-10, compared to naïve controls (Figures 5A-F). Treatment with BA5 (10 mg/Kg) or benznidazole promoted a significant reduction in the gene expression of IFN- γ , TGF β and Gal-3, but not in gene expression of TNF- α , and IL- β and (Figure 5). In contrast, IL-10 was significantly increased by BA5, while treatment with benznidazole reduced IL-10 transcripts (Figure 5E). Moreover, the gene expression levels of T-bet, GATA-3, and FoxP3, transcription factors associated with T-cell subtypes T helper 1, T helper 2 and Treg cells, respectively, was investigated. These transcription factors were significantly increased in vehicle-treated mice compared to naïve controls. BA5 promoted a significant reduction in Tbet and FoxP3 gene

expression, but not on GATA-3 gene expression, while benznidazole reduced the transcription of all three factors (Figures 5G-I).

Based on the critical role of macrophages in the heart inflammatory infiltrate in Chagas disease, we evaluated the gene expression of markers for M1 and M2 macrophages. Treatment with BA5, but not with benznidazole, promoted a significant reduction in the M1 marker iNOS (Figure 5J). Conversely, a marked increase in the M2 markers Arg1 and CHI3 was seen after BA5 treatment, while this marker was reduced in benznidazole group (Figure 5K and 5L).

Assessment of parasite load in mice treated with BA5

The use of immunosuppressive drugs during chronic Chagas disease has been associated with parasitemia resurgence (Bocchi, 1995). Thus, we evaluated blood samples during the course of the treatment with BA5. All samples evaluated at different time points were negative for *T. cruzi* trypomastigotes (data not shown). In order to determine if BA5 treatment affected the residual parasite load, we performed RT-qPCR in spleen samples from infected mice submitted to the different treatments. As shown in Figure 6, treatment with BA5 at 10 mg/Kg did not influence the parasite load. In contrast, treatment with benznidazole caused a significant reduction in the parasite load when compared to vehicle-treated mice.

Discussion

Current treatment for Chagas disease is based on trypanocidal drugs in the intention of eliminate parasitic load (Sales-Junior *et al.*, 2017). This approach has proven to be useful in the management of acute Chagas disease, but inefficient in the majority of patients, which are in the chronic stage of the disease (Rassi *et al.*, 2000;

Morillo *et al.*, 2015). Regarding chronic Chagas disease cardiomyopathy, the main problem is the persistence of an intense inflammatory response, which leads to a permanent structural damage in myocardium and culminates with heart dysfunctions (Bern, 2015; Bonney & Engman, 2015). Therefore, the development of strategies to attenuate inflammatory response without affecting parasite control can be of great value for CCC patients. In the present study, we investigated the effects of BA5, an amide semi-synthetic derivative betulinic acid, in a mouse model of chronic Chagas cardiomyopathy which reproduces the pathological findings observed in human hearts (Vasconcelos *et al.*, 2013). We found here a potent immunomodulatory potential of BA5, reducing inflammation and fibrosis in the hearts, as well as the expression of important inflammatory mediators which participate in the regulation of pathogenesis of CCC. Importantly, this immunomodulatory action was not accompanied by an increase in parasite load.

In a previous study we have shown that BA5 modulates the *in vitro* activation of T lymphocytes through a mechanism related to the inhibition of calcineurin (Meira *et al.*, 2017), an enzyme that regulates the activation of the nuclear factor of activated T cells, NFAT which is involved in T cell activation (Rusnak & Mertz, 2000). *In vivo*, BA5 was shown to inhibit edema formation in a delayed type hypersensitivity model (Meira *et al.*, 2017), which is a T cell dependent reaction. The finding that BA5 inhibits chagasic myocarditis, which is an inflammatory reaction similar to DTH response, composed mainly by macrophages and lymphocytes, reinforces its modulatory role upon T cell-mediated immune responses.

Inflammation and disease severity in CCC has been associated with high levels of IFN- γ . We found here a marked reduction in IFN- γ after BA5, both in the serum as well as in the heart tissue, having thus systemic and local modulatory effects. The

modulation of Th1-type responses was reinforced by the reduction of gene expression of Tbet, a Th1 associated transcription factor, in the hearts of infected mice after BA5 treatment. Similar results were found in mice treated with benznidazole.

A marked increase in IL-10 production was seen after BA5 treatment, both in the sera and hearts of chronic chagasic mice, a feature which was not achieved with benznidazole treatment. IL-10 is a crucial regulatory cytokine, and its production is associated with a better outcome of chronic Chagas disease, since asymptomatic individuals were found to produce higher IL-10 levels than patients with cardiomyopathy (Mendes-da-Silva *et al.*, 2017). IL-10 negatively correlated with IFN- γ levels in chronic chagasic individuals, suggesting a protective effect against the type 1 inflammatory response (Gomes *et al.*, 2003).

Macrophage activation and production of pro-inflammatory mediators, such as TNF- α , have been well demonstrated to play a critical role for parasite control during the acute phase of infection. During the chronic phase, however, these cytokines are well associated with chronic inflammation and cardiac dysfunction in Chagas disease. BA5 and its prototype betulinic acid down regulate key inflammatory mediators such as TNF- α *in vitro* and *in vivo*, regulating the activation of the transcription factor NF- κ B in activated macrophages (Costa *et al.*, 2014; Meira *et al.*, 2017). In the present study we confirmed the anti-TNF- α action of BA5 in chronic *T. cruzi* infection.

An interesting observation in our study was a switching in macrophage polarization from M1 to M2, evidenced by a decrease in the expression of NOS2 and proinflammatory cytokines and the increase in the M2 markers, Arg1 and CHI3, in the hearts of mice treated with BA5. This effect was not achieved by treatment with benznidazole. M2 macrophages play a protective role in several disease settings, including cardiovascular diseases, due to their anti-inflammatory properties (Bolego *et*

al., 2013). IL-10 production is elevated in M2 macrophages, and greatly contributes to their anti-inflammatory action. Thus, it is likely that the increase in IL-10 production seen after BA5 treatment is in part due to the M2 polarization.

The balance between the parasite-mediated immune response and the inflammation detrimental to host tissues probably determines the course of CCC (Rassi *et al.*, 2010). We have previously shown that BA5 presents anti-*T. cruzi* activity (Meira *et al.*, 2016). In the present study, however, by quantifying the *T. cruzi* DNA in the spleen we found that treatment with BA5 did not affect parasite load. The lack of parasite reduction by BA5 may be explained by a low efficacy of parasite clearance during the chronic phase, or alternatively, the antiparasitic effects of BA5 may be surpassed by its immunosuppressive effects. Moreover, our data reinforce the hypothesis that heart inflammation does not correlate directly with parasite load (Soares *et al.*, 2001).

In agreement with a previous study (Vilar-Pereira *et al.*, 2016), we observed a reduction in parasite load in benznidazole-treated chronic chagasic mice, accompanied by a reduction of cardiac inflammation, fibrosis and crucial inflammatory mediators such as TNF- α and IFN- γ . Several studies have shown immunomodulatory effects of benznidazole. More specifically, benznidazole inhibits the production of inflammatory mediators, including IL-6, NO and TNF- α (Pascutti *et al.*, 2004; Manarin *et al.*, 2008; Ronco *et al.*, 2011). In addition, in a cecal ligation and puncture mouse model, it has been demonstrated that benznidazole treatment reduces mortality by down-regulating NF- κ B and mitogen-activated protein kinase (MAPK) (p38 and extracellular signal-regulated kinase - ERK) (Ronco *et al.*, 2011). In fact, benznidazole acts as an immunomodulator agent, suggesting that the beneficial properties of benznidazole are

related on both trypanocidal action and immunomodulatory effects (Cutrullis *et al.*, 2011; Piaggio *et al.*, 2001).

Despite the reduction of inflammation and fibrosis, we did not observe any significant gains in cardiac function by EKG and ergometry analyses, both in BA5 or benznidazole treated mice. Since *in vitro* drug combination showed a synergistic effect (Meira *et al.*, 2016), it is possible that a combined therapy may result in a better recovery, especially if given earlier.

Finally, we conclude that the betulinic acid derivative BA5 had a potent anti-inflammatory activity on a model of parasite-driven heart disease, being related to elevated IL-10 production and a switch from M1 to M2 macrophage subset. More importantly, decrease in inflammation and fibrosis was achieved without affect parasite control, making BA5 an interesting molecule for development of alternative treatments for patients with CCC.

Conflict of interest

Authors have no conflict of interest to disclose.

Acknowledgements

This work was supported by grants from CNPq (grant number 562655/2010-7), PRONEX (grant number 0002/2014), CAPES and FAPESB (grant number 0042/2013).

References

1. Abel, L. C., Rizzo, L. V., Ianni, B., Albuquerque, F., Bacal, F., Carrada, D., Bocchi, E. A., Teixeira, H. C., Mady, C., Kalil, J., Cunha-Neto, E., 2001.

- Chronic Chagas' disease cardiomyopathy patients display an increased IFN-gamma response to *Trypanosoma cruzi* infection. *J Autoimmun.* 17, 99-107.
2. Araújo-Jorge, T. C., Waghbi, M. C., Bailly, S., Feige, J. J., 2012. The TGF- β pathway as an emerging target for Chagas disease therapy. *Clin Pharmacol Ther.* 92, 613-621.
 3. Bartuzi, P., Hofker, M. H., Sluis, B. V., 2013. Turning NF- κ B activity: A touch of COMMD proteins. *Biochim Biophys Acta.* 1832, 215-2321.
 4. Bern, C., 2015. Chagas' Disease. *N Engl J Med.* 373, 456-466.
 5. Benziger, C. P., Do Carmo, G. A. L., Ribeiro, A. L. P., 2017. Chagas cardiomyopathy: Clinical presentation and management in the Americas. *Cardiol. Clin.* 35, 31-47.
 6. Berul, C. I., Aronovitz, M. J., Wang, P. J., Mendelsohn, M. E., 1996. *In vivo* cardiac electrophysiology studies in the mouse. *Circulation.* 94, 2641-2648.
 7. Bocchi, E. A., 1995. Heart transplants for patients with Chagas' heart disease. *São Paulo Med J.* 113, 873-879.
 8. Bolego, C., Cignarella, A., Staels, B., Chinetti-Gbaguidi, G., 2013. Macrophage function and polarization in cardiovascular disease: a role of estrogen signaling? *Arterioscler Thromb Vasc Biol.* 33, 1127-1134.

9. Bonney K. M., Engman, D. M., 2015. Autoimmune pathogenesis of Chagas heart disease. *Am J Pathol.* 185, 1537-1547.
10. Boscardin, S. B., Torrecilhas, A. C., Manarin, R., Revelli, S., Rey, E. G., Tonelli, R. R., Silber, A. M., 2010. Chagas´disease: an update on immune mechanisms and therapeutic strategies. *J Cell Mol Med.* 14, 1373-1384.
11. Brener, Z., 1962. Therapeutic activity and criterion of cure in mice experimentally infected with *Trypanosoma cruzi*. *Rev. Inst. Med. Trop. São Paulo.* 4, 386-396.
12. Chistiakov, D. A., Myasoedova, V. A., Revin, V. V., Orekhov, A. N., Bobryshev Y. V., 2018. The impact of interferon-regulatory factors to macrophage differentiation and polarization into M1 and M2. *Immunobiology.* 1, 101-111.
13. Connors, E. E., Vinetz, J. M., Weeks, J. R., Brouwer, K. C., 2016. A global systematic review of Chagas disease prevalence among migrants. *Acta Trop.* 156, 68-79.
14. Costa, J. F. O., Barbosa-Filho, J. M., Maia, G. L. A., Guimarães, E. T., Meira, C. S., Ribeiro-dos-Santos, R., Carvalho, L. P., Soares, M. B. P., 2014. Potent anti-inflammatory activity of betulinic acid treatment in a model of lethal endotoxemia. *Int Immunopharmacol.* 23, 469-474.

15. Cunha-Neto, E., Chevillard, C., 2014. Chagas disease cardiomyopathy: immunopathology and genetics. *Mediators Inflamm.* v. 2014:683230.
16. Cutrullis, R. A., Moscatelli, G. F., Moroni, S., Volta, B. J., Cardoni, R. L., Altcheh, J. M., Corral, R. S., Freilij, H. L., Petray, P. B., 2011. Benznidazole therapy modulates interferon- γ and M2 muscarinic receptor autoantibody responses in *Trypanosoma cruzi*-infected children. *Plos one.* 6, e27133.
17. Gomes, J. A. S., Bahia-Oliveira, L. M. G., Rocha, M. O. C., Martins-Filho, O. A., Gazzinelli, G., Correa-Oliveira, R., 2003. Evidence that development of severe cardiomyopathy in human Chagas' disease is due to a Th1-specific response. *Infect Immun.* 71, 1185-1193.
18. González-Herrera, F., Cramer, A., Pimentel, P., Castillo, C., Liempi, A., Kemmerling, U., Machado, F. S., Maya, J. D., 2017. Simvastatin attenuates endothelial activation through 15-Epi-Lipoxin A4 production in murine chronic Chagas cardiomyopathy. *Antimicrob. Agents Chemother.* 61, e02137-16.
19. Lewis, M. D., Kelly, J. M., 2016. Putting infection dynamics at the heart of Chagas disease. *Trends Parasitol.* 32, 899-911.
20. Manarin, R., Pascutti, M. F., Ruffino, J. P., De Las, H. B., Bosca, L., Bottasso, O., Revelli, S., Serra, E., 2010. Benznidazole blocks NF-kappaB activation but not AP-1 through inhibition of IKK. *Mol. Immunol.* 47, 2485–2491.

21. Meira, C. S., Barbosa-Filho, J. M., Lanfredi-Rangel, A., Guimarães, E.T., Moreira, D. R. M., Soares, M. B. P., 2016. Antiparasitic evaluation of betulinic acid derivatives reveals effective and selective anti-*Trypanosoma cruzi* inhibitors. *Exp Parasitol.* 166, 2016.
22. Meira, C. S., Santo, R. F. E., Santos, T. B.; Orge, I. D., Silva, D. K. C., Guimarães, E. T., França, L. S. A., Barbosa-Filho, J. M., Moreira, D. R. M., Soares, M. B. P., 2017. Betulinic acid derivative BA5, a dual NF- κ B/calcineurin inhibitor, alleviates experimental shock and delayed hypersensitivity. *Eur J Pharmacol.* 815, 156-165.
23. Marin-Neto, J. A. *et al.*, 2010. Chagas heart disease. In: Yusuf S, Cairns JA, Camm AJ, Fallen EL, Gersh BJ, eds. Evidence-based cardiology, 3rd edn. London: BMJ Books, p. 823-841.
24. Mendes da Silva, L. D., Gatto, M., Teodoro, M. A. M., 2017. Participation of TLR2 and TLR4 in cytokines production by patients with symptomatic and asymptomatic chronic Chagas disease. *Scand J Immunol.* 85, 58-65.
25. Molina, I., Gómez I Pra, J., Salvador, F. *et al.*, 2014. Randomized trial of posaconazole and benznidazole for chronic Chagas' disease. *N Engl J of Med.* 370, 1889-1908.

26. Morillo, C. A., Marin-Neto, J. A., Avezum, A. *et al.*, 2015. Randomized trial of benznidazole for chronic Chagas' cardiomyopathy. *N Engl J of Med.* 373, 1295-1306.
27. Rassi, A. Jr., Rassi, A., Little, W. C., 2000. Chagas heart disease. *Clin Cardiol.* 23, 883-889.
28. Rassi, A, Jr., Rassi, A., Marin-Neto, J. A., 2010. Chagas disease. *Lancet.* 375, 1388-1402.
29. Ronco, M. T., Manarin, R., Francés, D., Serra, E., Revelli, S., Carnovale, C., 2016. Benznidazole treatment attenuates liver NF- κ B activity and MAPK in a cecal ligation and puncture model of sepsis. *Molecular Immunol.* 48, 867-873.
30. Rusnak, F., Mertz, P., 2000. Calcineurin: form and function. *Physiol Rev.* 80, 1483-1521.
31. Sales-Junior, P. A., Molina, I., Murta, S. M. F., Sánchez-Montalvá, A. S., Salvador, R, F., Corrêa-Oliveira, R., Carneiro, C. M., 2017. Experimental and Clinical treatment of Chagas disease: A review. *Am. J. Trop. Med. Hyg.* 97, 1289-1303.
32. Schijman, A. G., Bisio, M., Orellana, L. *et al.*, 2011. International study to evaluate PCR methods for detection of *Trypanosoma cruzi* DNA in blood samples from Chagas disease patients. *Plos Negl. Trop. Dis.* 5, e931.

33. Schmittgen, T. D., Livak, K. J., 2008. Analyzing real-time PCR data by the comparative C (T) method. *Nat. Protoc.* 3, 1101-1108.
34. Soares, M. B. P., Pontes-Carvalho, L. C., Ribeiro-dos-Santos, R., 2001. The pathogenesis of Chagas' disease: when autoimmune and parasitic-specific immune responses meet. *An Acad Bras Cienc.* 73, 547-559.
35. Piaggio, E., Roggero, E., Pitashny, M., Wietzerbin, J., Bottasso, O. A., Revelli, S. S., 2001. Treatment with benznidazole and its immunomodulating effects on *Trypanosoma cruzi*-infected rats. *Parasitol Res.* 87, 538-547.
36. Pascutti, M. F., Pitashny, M., Nocito, A. L., Guermonprez, P., Amigorena, S., Wietzerbin, J., Serra, E., Bottasso, O., Revelli, S., 2004. Benznidazole, a drug use for Chagas' disease, ameliorates LPS-induced inflammatory response in mice. *Life Sci.* 76, 685-597.
37. Tanowitz, H. B., Machado, F. S., Spray, D.C. *et al.*, 2015. Developments in the management of Chagas cardiomyopathy. *Expert Rev Cardiovasc Ther.* 13, 1393-1409.
38. Vasconcelos, J. F., Souza, B. F., Lins, T. F., Garcia, L. M., Kaneto, C. M., Sampaio, G. P., DE Alcântara, A. C., Meira, C. S., Macambira, S. G., Ribeiro-dos-Santos, R., Soares, M. B. P., 2013. Administration of granulocyte colony-stimulating factor induces immunomodulation, recruitment of T regulatory cells,

reduction of myocarditis and decrease of parasite load in a mouse model of chronic Chagas disease cardiomyopathy. *FASEB J.* 27, 4691-4702.

39. Vilar-Pereira, G., Pereira, I. R., Ruivo, L. A. S., Moreira, O. C., Silva, A. A., Britto, C., Lannes-Viera, J., 2016. Combination chemotherapy with suboptimal doses of benznidazole and pentoxifylline sustains partial reversion of experimental Chagas' heart disease. *Antimicrob Agents Chemother.* 60, 4297-4309.

40. WORLD HEALTH ORGANIZATION. Chagas disease (American trypanosomiasis). <http://www.who.int/mediacentre/factsheets/fs340/en>. Accessed 2 December 2017.

Table 1. ECG analysis in naive and *T. cruzi*-infected mice.

ECG findings	Naïve (n = 5)	Vehicle (n = 10)	Bdz 100 mg/Kg (n = 8)	BA5 10 mg/Kg (n = 10)	BA5 1 mg/Kg (n = 10)
No alterations	5/5	0/10	0/8	0/10	0/10
AVB	0/5	2/10	0/8	6/10	3/10
AVD	0/5	4/10	6/8	10/10	10/10
EXTS	0/5	0/10	1/8	0/10	0/10
IVCD	0/5	2/10	1/8	0/10	0/10
JR	0/5	0/10	1/8	0/10	0/10
PVT	0/5	2/10	0/8	0/10	1/10
SVT	0/5	2/10	0/8	0/10	0/10

AVB, atrioventricular block; AVD, atrioventricular dissociation; Bdz, benznidazole; ECG, electrocardiography; EXTS, extrastystole; IVCD, intraventricular conduction delay; JR, junctional rhythm; PVT, polymorphic ventricular tachycardia; SVT, supraventricular tachycardia.

Figure legends

Figure 1. Experimental design and exercise capacity of mice from the different experimental groups. (A) C57BL/6 mice were infected with 10^3 Colombian strain *T. cruzi* trypomastigotes and treated during the chronic phase (6 months after infection) with 10 or 1 mg/kg of BA5 or benznidazole (100 mg/Kg), as indicated. (B and C) Distance run and time of exercise on a motorized treadmill. Values represent the means \pm S.E.M. of 5-10 mice per group. * $P < 0.05$ compared to vehicle-treated mice; # $P < 0.05$ compared to naive group. \$ $P < 0.05$ compared to benznidazole-treated group.

Figure 2. Reduction of inflammation and fibrosis by BA5 in cardiac tissue of chagasic mice. (A and E) heart sections of naive group. (B and F) heart sections of mice infected with *T. cruzi* and treated with vehicle. (C and G) heart sections of infected mice treated with 10 mg/Kg of BA5. (D and H) heart sections of mice infected and treated with 100 mg/Kg of benznidazole. (A-D) staining with hematoxylin & eosin. (E-H) staining with picosirius red. (I) Inflammatory cells were quantified in heart sections of naive mice, vehicle-treated mice, BA5-treated mice or benznidazole-treated mice and integrated by area. (J) The expression of CD45 was evaluated by real-time qRT-PCR using cDNA samples prepared from mRNA extracted from hearts of experimental groups. (K) Fibrotic area is represented by percentage of collagen deposition in heart sections. Values represent the means \pm S.E.M. of ten determinations. * $P < 0.05$ compared to vehicle-treated mice; # $P < 0.05$ compared to naive group. \$ $P < 0.05$ compared to benznidazole-treated group.

Figure 3. BA5 promoted a significant reduction of fibrosis in the hearts of chagasic mice. Heart sections of mice from naive (A), vehicle (B), 100 mg/Kg benznidazole (C)

and heart sections of infected mice treated with 10 mg/Kg of BA5 (D), stained with Sirius red. (E) Fibrosis area was quantified in heart sections by morphometric analysis and integrated by area. Values represent the means \pm S.E.M. of 5-10 mice per group. * $P < 0.05$ compared to vehicle-treated mice; # $P < 0.05$ compared to naive group. \$ $P < 0.05$ compared to benznidazole-treated group. & $P < 0.05$ compared to group treated with 10 mg/Kg of BA5.

Figure 4. Modulation of systemic cytokine production in chronic chagasic mice treated with BA5 or benznidazole. Effects of BA5 (10 or 1 mg/Kg) or benznidazole (Bdz; 100 mg/Kg) in serum concentrations of TNF- α (A), IFN- γ (B), IL-1 β (C) and IL-10 (D). Values represent the means \pm S.E.M. of 5-10 mice per group. * $P < 0.05$ compared to vehicle-treated mice; # $P < 0.05$ compared to naive group. \$ $P < 0.05$ compared to benznidazole-treated group.

Figure 5. Gene expression in the hearts of infected mice after BA5 or benznidazole treatment. Analysis of gene expression was performed by real-time qRT-PCR using cDNA samples prepared from mRNA extracted from hearts of naive and chronic Chagasic mice treated with vehicle (Saline), BA5 (10 mg/Kg) or Benznidazole (Bdz; 100 mg/Kg). (A) *Tnfa*, (B) *Ifng*, (C) *IL1b*, (D) *Tgfb*, (E) *Il10*, (F) *Lgals3*, (G) *FoxP3*, (H) *Tbet* (I) *Gata3* (J) *Nos2*, (K) *Arg1* and (L) *Chi3* gene expression. Values represent the means \pm S.E.M. of 5-10 mice per group. * $P < 0.05$ compared to vehicle-treated mice; # $P < 0.05$ compared to naive group. \$ $P < 0.05$ compared to benznidazole-treated group.

Figure 6. Effects of BA5 treatment in the residual parasite load. Spleen fragments obtained from uninfected and *T. cruzi*-infected mice treated with vehicle, Bdz or BA5

were used for DNA extraction and RT-qPCR analysis for quantification of parasite load, as described in the Materials and Methods section. Values represent the means \pm S.E.M. of 5-10 mice per group. * $P < 0.05$ compared to vehicle-treated mice; # $P < 0.05$ compared to naive group. \$ $P < 0.05$ compared to benznidazole-treated group.

Figure 1

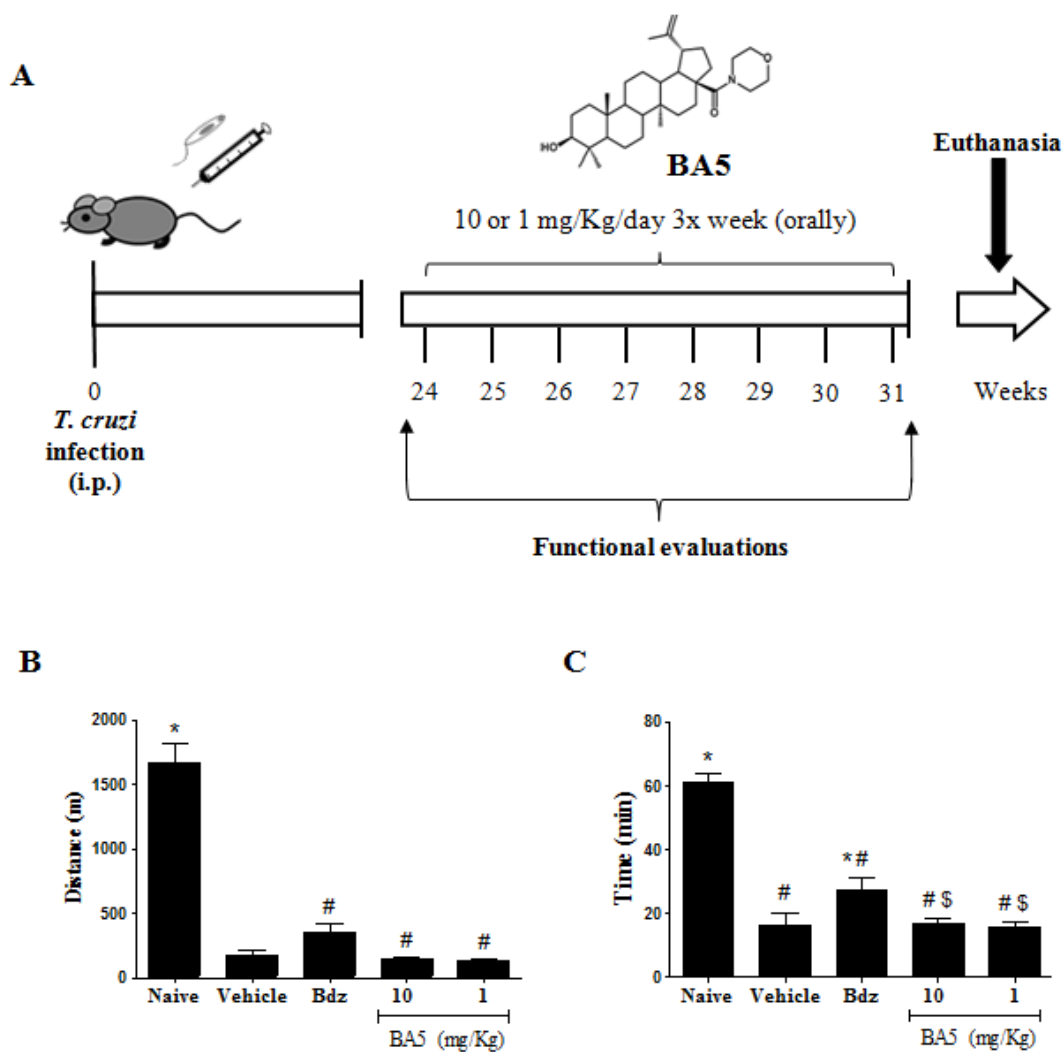


Figure 2

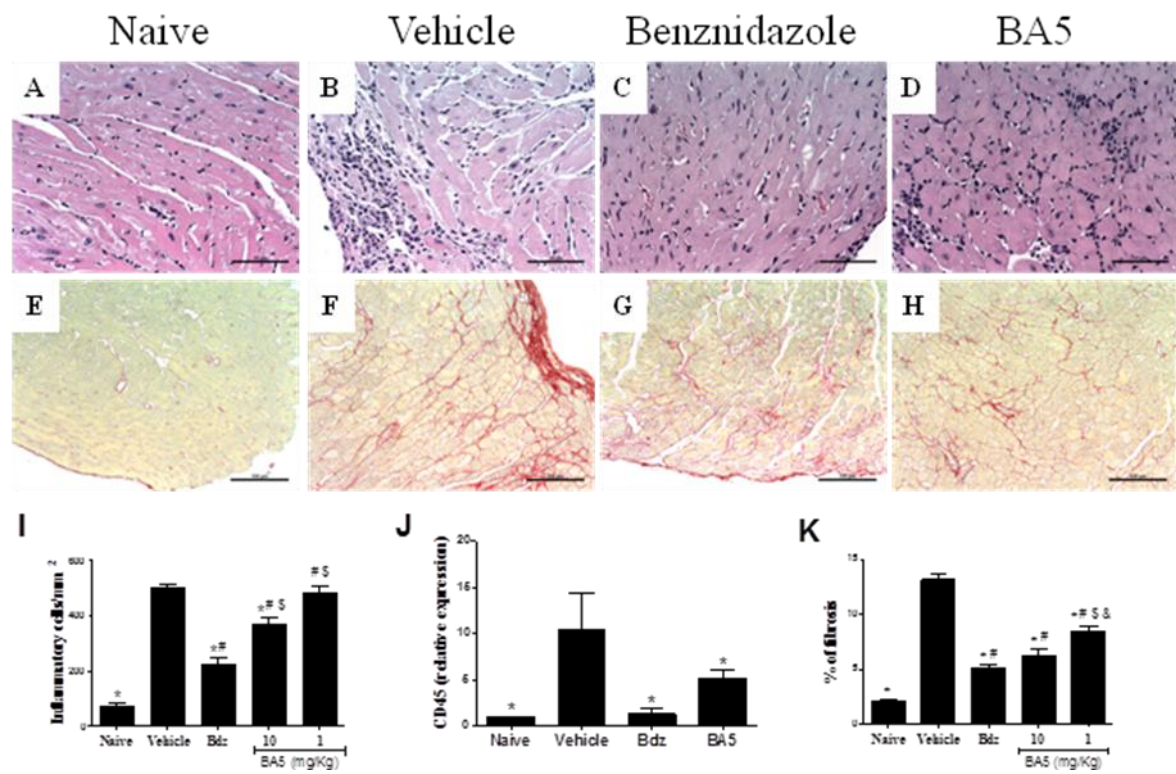


Figure 3

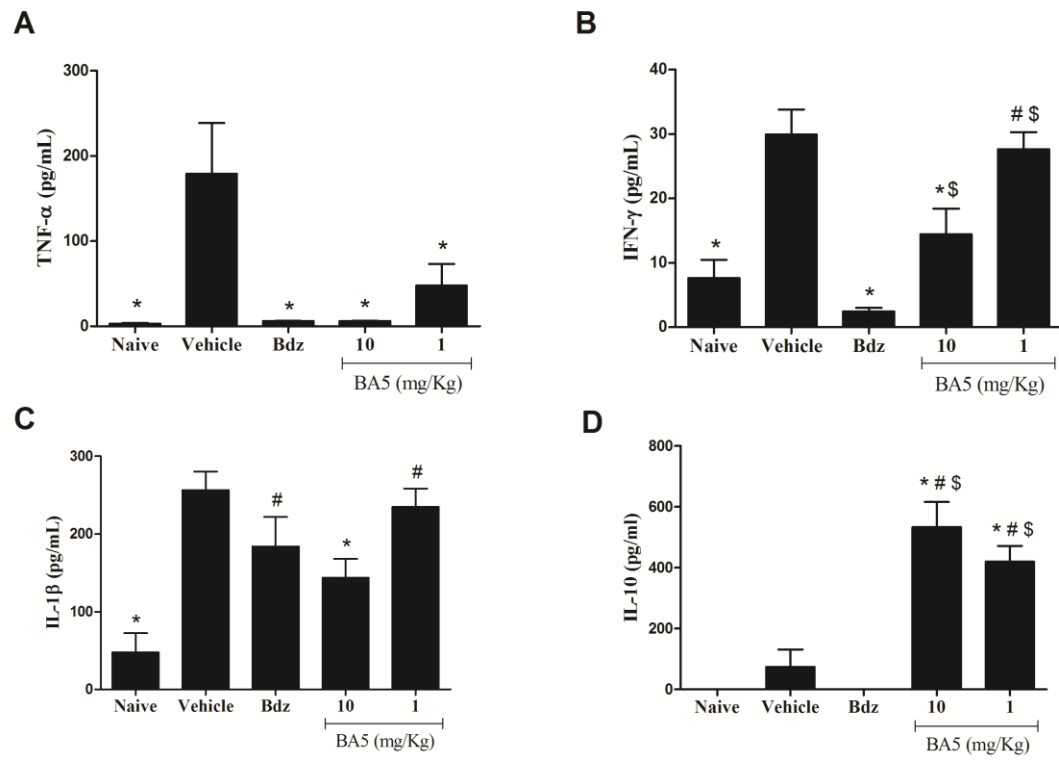


Figure 4

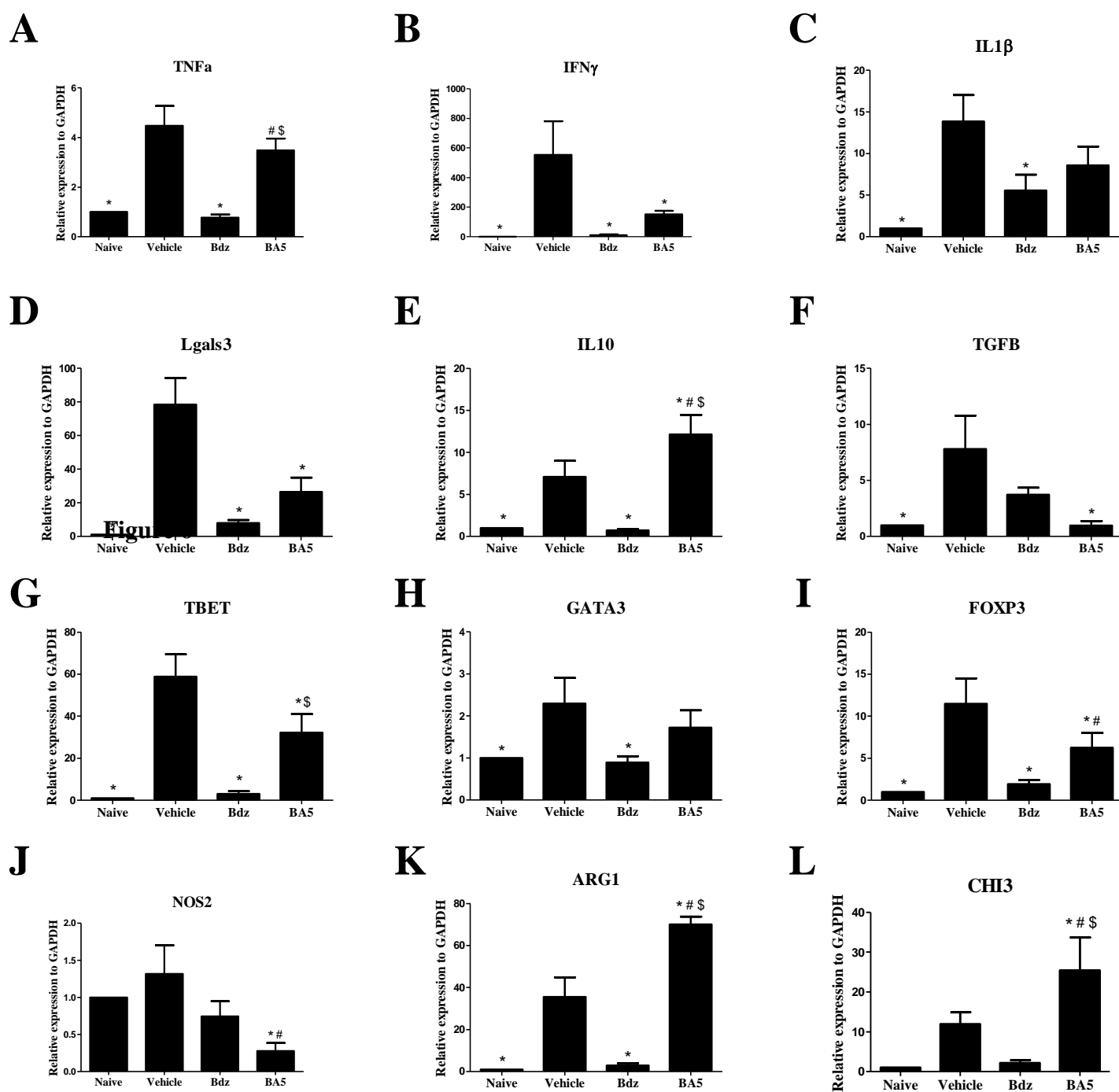
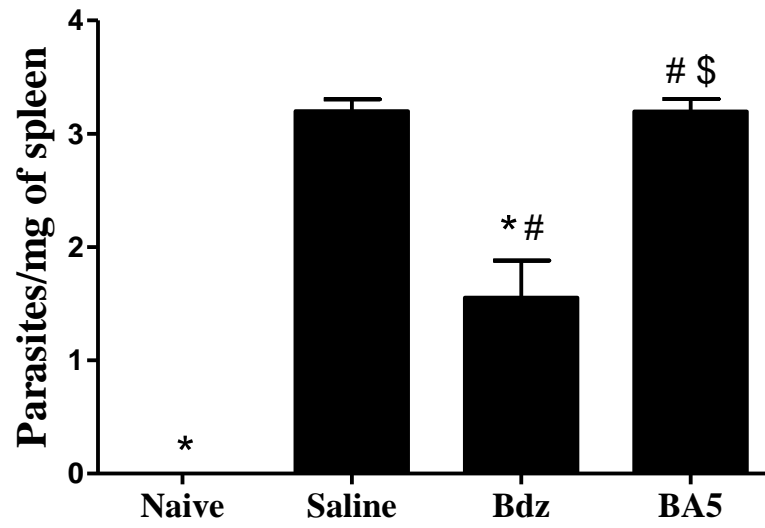


Figure 5



CAPÍTULO III


Neste capítulo demonstramos que o N,N dimetil esfingosina (DMS), através de uma ação anti-*T. cruzi* e imunomoduladora, é benéfico no modelo experimental de cardiomiopatia chagásica crônica.

Artigo publicado na revista *Scientific Reports*, v. 7, p. 1-14, 2017. Doi:10.1038/s41598-017-06275-z.

Therapeutic effects of sphingosine kinase inhibitor N,N-dimethylsphingosine (DMS) in experimental chronic Chagas disease cardiomyopathy

Juliana Fraga Vasconcelos^{1,2,3}, Cássio Santana Meira^{1,2}, Daniela Nascimento Silva², Carolina Kymie Vasques Nonaka², Pâmela Santana Daltro², Simone Garcia Macambira^{2,4}, Pablo Daniel Domizi⁵, Valéria Matos Borges¹, Ricardo Ribeiro-dos-Santos², Bruno Solano de Freitas Souza^{1,2} & Milena Botelho Pereira Soares^{1,2}

SCIENTIFIC REPORTS



OPEN

Therapeutic effects of sphingosine kinase inhibitor N,N-dimethylsphingosine (DMS) in experimental chronic Chagas disease cardiomyopathy

Juliana Fraga Vasconcelos^{1,2,3}, Cássio Santana Meira^{1,2}, Daniela Nascimento Silva², Carolina Kymie Vasques Nonaka², Pâmela Santana Daltró², Simone Garcia Macambira^{2,4}, Pablo Daniel Domizi⁵, Valéria Matos Borges¹, Ricardo Ribeiro-dos-Santos², Bruno Solano de Freitas Souza^{1,2} & Milena Botelho Pereira Soares^{1,2}

Chagas disease cardiomyopathy is a parasite-driven inflammatory disease to which there are no effective treatments. Here we evaluated the therapeutic potential of N,N-dimethylsphingosine(DMS), which blocks the production of sphingosine-1-phosphate(S1P), a mediator of cellular events during inflammatory responses, in a model of chronic Chagas disease cardiomyopathy. DMS-treated, *Trypanosoma cruzi*-infected mice had a marked reduction of cardiac inflammation, fibrosis and galectin-3 expression when compared to controls. Serum concentrations of galectin-3, IFN γ and TNF α , as well as cardiac gene expression of inflammatory mediators were reduced after DMS treatment. The gene expression of M1 marker, iNOS, was decreased, while the M2 marker, arginase1, was increased. DMS-treated mice showed an improvement in exercise capacity. Moreover, DMS caused a reduction in parasite load *in vivo*. DMS inhibited the activation of lymphocytes, and reduced cytokines and NO production in activated macrophage cultures *in vitro*, while increasing IL-1 β production. Analysis by qRT-PCR array showed that DMS treatment modulated inflammasome activation induced by *T. cruzi* on macrophages. Altogether, our results demonstrate that DMS, through anti-parasitic and immunomodulatory actions, can be beneficial in the treatment of chronic phase of *T. cruzi* infection and suggest that S1P-activated processes as possible therapeutic targets for the treatment of Chagas disease cardiomyopathy.

The pathological manifestations of chronic Chagas disease, caused by *Trypanosoma cruzi* infection, both in the cardiac and in the digestive form, are associated with the occurrence of an inflammatory reaction¹. Chronic Chagas disease cardiomyopathy (CCC) involves cardiac myocytes undergoing necrosis and cytolysis via various mechanisms, and areas of myocellular hypertrophy and mononuclear cell infiltration occur²⁻⁴. In response to the myocardial damage, fibrotic areas occur and may contribute to the disruption of the cardiac conduction system and appearance of dysrhythmias, as well as to myocardial thinning and cardiac hypertrophy⁵. Given the lack of an effective specific therapy, CCC is treated similarly to all other heart failure syndromes using therapies to mitigate symptoms⁶. Therefore, the development of new alternative treatments for CCC is needed.

¹Instituto Gonçalo Moniz, Fundação Oswaldo Cruz, FIOCRUZ, Salvador, BA, 40296-710, Brazil. ²Centro de Biotecnologia e Terapia Celular, Hospital São Rafael, Salvador, BA, 41253-190, Brazil. ³Escola de Ciências da saúde, Universidade Salvador, Salvador, BA, 41720-200, Brazil. ⁴Departamento de Bioquímica e Biofísica, Instituto de Ciências da Saúde, Universidade Federal da Bahia, Salvador, BA, 40110-100, Brazil. ⁵Centro de Ciências da Saúde, Instituto de Biofísica Carlos Chagas Filho, Universidade Federal do Rio de Janeiro, Rio de Janeiro, RJ, 21944-970, Brazil. Juliana Fraga Vasconcelos and Cássio Santana Meira contributed equally to this work. Correspondence and requests for materials should be addressed to M.B.P.S. (email: milena@bahia.fiocruz.br)

Sphingolipid metabolites are emerging as important lipid signaling molecules in both health and disease⁷. Among them, sphingosine-1-phosphate (S1P), produced by phosphorylation of sphingosine (Sph) by sphingosine kinases (SphK1 and SphK2) in response to various stimuli, plays important roles in several cellular processes, including cell growth and cell trafficking^{8,9}. The balance of Sph and S1P determines the progress of many diseases and there is evidence that sphingolipid metabolism and the expression of S1P receptors (S1PR1-5) are altered in inflammatory processes¹⁰. S1P drives the differentiation of different immune cell types, inducing changes in their functional phenotypes and regulating production of pro-inflammatory cytokines and eicosanoids. In particular, S1P has emerged as a central regulator of lymphocyte egress^{11,12}.

Due to the persistent inflammation found in CCC, which is a hallmark of the disease, and the critical role of S1P-activated pathways on the regulation of inflammation, we hypothesized that N,N-dimethylsphingosine (DMS), a pan SphK inhibitor, has a beneficial effect in chronic Chagas disease. Thus, in the present study we investigated the effects of DMS in a murine model of chronic Chagas disease cardiomyopathy, as well as its mechanisms of action on *in vitro* assays.

Results

Treatment with DMS reduces heart inflammation and fibrosis in *T. cruzi*-infected mice. Groups of mice chronically infected with *T. cruzi* were treated with DMS or vehicle (saline) (Fig. 1A). Inflammation and fibrosis were evaluated in heart sections two months after the first dose. A diffuse inflammatory response, mainly composed of mononuclear cells, was found in saline-treated infected controls (Fig. 1B). Administration of DMS caused a marked reduction in the number of inflammatory cells, which was statistically significant when compared to vehicle-treated mice (Fig. 1B,C). Gene expression of CD45, a pan-leukocyte marker, which was increased in *T. cruzi* infected mice treated with saline, was also significantly reduced after DMS treatment (Fig. 1D). Similarly, heart sections from DMS-treated mice had a reduced percentage of fibrosis when compared with vehicle-treated mice (Fig. 1B,E).

Galectin-3 reduction in the heart and sera of chagasic mice after DMS treatment. We have previously shown the overexpression of galectin-3 in the hearts of chronic chagasic mice¹³. To evaluate the effects of DMS on the expression of this important mediator of inflammation and fibrosis, we performed confocal microscopy analysis in the heart tissue. Vehicle-treated, *T. cruzi*-infected mice had a high expression of galectin-3, while a reduction of galectin-3 expression was seen after DMS treatment (Fig. 1B). Morphometrical analyses revealed a statistically significant difference between the groups (Fig. 1F). Moreover, DMS treatment also caused a significant reduction in the concentration of galectin-3 in the serum of *T. cruzi*-infected mice (Fig. 2C), as well as in the expression of galectin-3 gene in the hearts (Fig. 3A).

DMS administration modulates the production of inflammatory mediators in *T. cruzi*-infected mice. CCC has been associated with an increase of IFN γ and TNF α production in mice, as well as in humans^{14,15}. We observed, both in the sera as well as in the heart, an up regulation in the expression of these two proinflammatory cytokines in the saline-treated chagasic mice, compared to uninfected mice (Figs 2 and 3). The administration of DMS promoted a significant reduction in the concentrations of both cytokines in the sera (Fig. 2A,B), as well as in the expression of their genes in the heart tissue (Fig. 3B,C). We also investigated the production of regulatory cytokines IL-10 and TGF β , which are increased in *T. cruzi*-infected mice. TGF β concentrations in the sera were similar in both vehicle and DMS-treated infected groups, and increased compared to naive mice (Fig. 2D). The expression of IL-10 gene in the hearts, also increased by *T. cruzi* infection, was reduced after DMS treatment compared to saline group (Fig. 3D). Since macrophages are one of the main cell populations composing the heart inflammatory infiltrate in Chagas disease¹⁵, we investigated the expression of genes associated with macrophage activation. IL-1 β expression in the heart was found to be increased by *T. cruzi* infection and significantly reduced by DMS treatment (Fig. 3F). The expression of iNOS, a marker of M1 activation increased in the hearts of *T. cruzi*-infected mice, was reduced after DMS treatment (Fig. 3G). When M2 activation markers were analyzed, we observed an up regulation of Arg1 gene expression after DMS, while CHI3 was down-regulated in the hearts of DMS-treated mice, when compared to saline-treated controls (Fig. 3H,I).

DMS improves exercise capacity, reduces parasitism but does not ameliorate cardiac electric disturbances. The exercise capacity of the experimental groups was evaluated before and after treatment. *T. cruzi*-infected mice ran less time and smaller distance when compared to naive controls (Fig. 4A,B). DMS-treated mice, however, showed a better performance in the treadmill test when compared to saline-treated controls. The majority of *T. cruzi*-infected mice presented severe cardiac conduction disturbances in the EKG records, such as AV blockage, intraventricular conduction disturbances and abnormal cardiac rhythm, six months after infection. At the end of treatment, no improvements were observed in DMS-treated mice, and all *T. cruzi*-infected mice aggravated the conduction disturbances during the observed time (Table 1). To investigate whether the anti-inflammatory response induced by DMS treatment affected the immune response against the parasite, we analyzed the residual *T. cruzi* infection by qRT-PCR in the spleens of infected mice. As shown in Fig. 4C, a significant reduction of parasite load was observed in DMS-treated mice compared to saline-treated controls.

Modulation of lymphocyte and macrophage functions *in vitro* by DMS. The inflammatory infiltrate in the hearts of *T. cruzi*-infected mice is mainly composed by T lymphocytes and macrophages¹⁵. Thus, we tested the effects of DMS *in vitro* in these two cell populations. To investigate whether DMS can directly modulate the activation of lymphocytes, we assessed the proliferation of splenocytes stimulated by concanavalin A (Con A) or anti-CD3 plus anti-CD28. A concentration-dependent inhibition of lymphoproliferation was seen when DMS was added to the cultures (See Supplementary Fig. S1A and B). Additionally, the production of IL-2 and IFN γ upon Con A stimulation was significantly reduced by DMS (See Supplementary Fig. S1C and D). Dexamethasone,

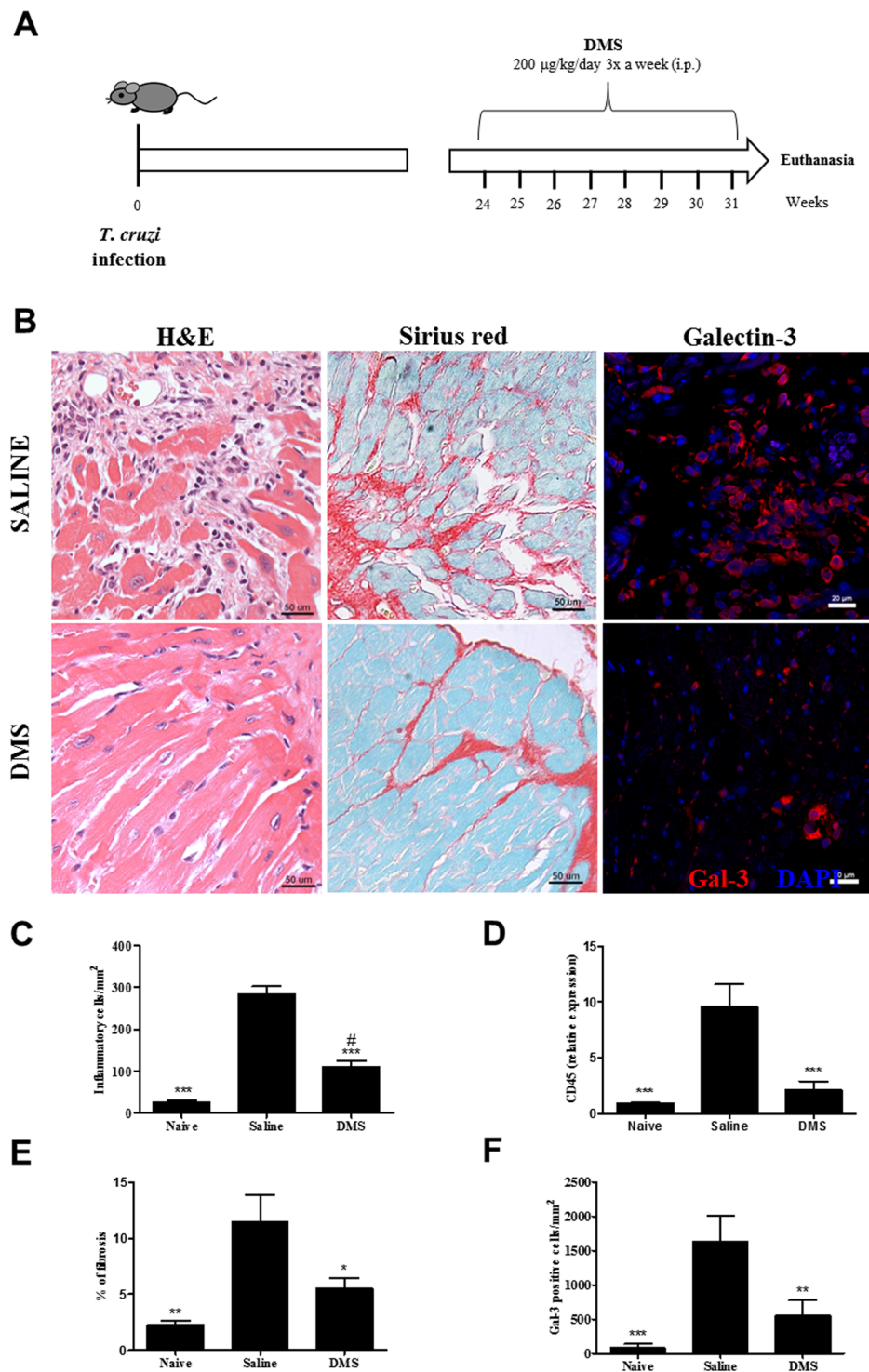


Figure 1. Reduction of inflammation, fibrosis and galectin-3 was found in the hearts of DMS-treated mice. (A) Experimental design of *in vivo* treatment. C57BL/6 mice infected with trypomastigotes (Colombian strain) were treated during the chronic phase of infection (6 months post-infection) with DMS (200 µg/Kg/day; 3x week; i.p.). (B) Microphotographs of heart sections stained with hematoxylin and eosin or sirius red or anti-galectin-3 (1:50; red) and DAPI (blue). (C) Inflammatory cells were quantified in heart sections of naive mice, saline-treated chagasic mice, or DMS-treated chagasic mice and integrated by area. (D) The expression of CD45 was evaluated by real-time qRT-PCR using cDNA samples prepared from mRNA extracted from hearts of experimental groups. (E) Fibrotic area is represented by percentage of collagen deposition in heart sections. (F) Quantifications of galectin-3⁺ cells in heart sections were performed in ten random fields captured under 400x magnification, using the Image Pro Plus v.7.0 software. Bars represent means ± SEM of 10 mice/group. ****P* < 0.001; ***P* < 0.01; **P* < 0.05 compared to saline group; #*P* < 0.05 compared to naive group.

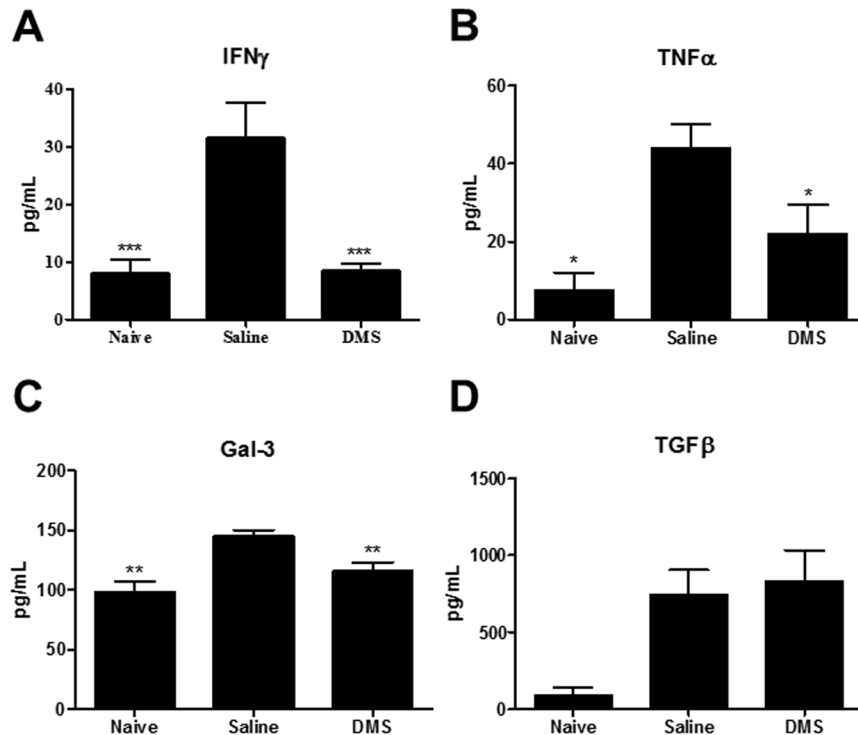


Figure 2. Modulation of systemic cytokine production in chronic chagasic mice treated with DMS. Concentrations of IFN γ (A), TNF α (B), Gal-3 (C) and TGF β (D) in the sera from naive and chagasic mice treated with saline or DMS. Values represent means \pm SEM of 10 mice/group. *** $P < 0.001$; ** $P < 0.01$; * $P < 0.05$ compared to saline group.

a known immunosuppressive agent, reduced proliferation and cytokine production (See Supplementary Fig. S1). Moreover, the addition of DMS to macrophage cultures activated by LPS plus IFN γ caused an increase in IL-1 β production (See Supplementary Fig. S2A). In contrast, the production of other inflammatory mediators, such as TNF α , IL-6, IL-10 and nitric oxide was reduced in a concentration-dependent manner (See Supplementary Fig. S2B–E). NF- κ B activation participates in the regulation of several pro-inflammatory genes, including TNF α . To investigate whether DMS acted through the modulation of NF- κ B activation, we performed an assay using RAW cells transduced with a reporter gene under the control of a promoter regulated by NF- κ B. As shown in Supplementary Fig. S2F, DMS at 10 and 5 μ M caused about 20% reduction of luciferase activity induced by activation with LPS and IFN γ . To understand if DMS effects in macrophages has off-targets effects by the inhibition of PKC and MAPK, we tested the action of DMS in the presence of specific inhibitors of ERK-1/2 (PD98059) and MAPK (BIS). The inhibition of IL-6 and iNOS production by DMS was not affected by the inhibitors (See Supplementary Fig. S2G and H).

Antiparasitic effects of DMS *in vitro*. To investigate the mechanisms by which DMS caused the reduction on parasite load *in vivo*, we evaluated the antiparasitic activity of DMS *in vitro*. To determine whether DMS acts directly on the parasite, we analyzed the effects of DMS on *T. cruzi* trypomastigote cultures (Table 2). Addition of DMS at various concentrations in axenic cultures of *T. cruzi* trypomastigotes allowed the determination of the EC₅₀ value at 1.98 μ M, while benznidazole presented an EC₅₀ of 12.53. Regarding the cytotoxicity of DMS, we determined the CC₅₀ in mouse macrophage cultures at 9.02 μ M. Next, we investigated the mechanisms of cell death in trypomastigotes forms of *T. cruzi* induced by DMS, by flow cytometry analysis. Incubation with DMS induced apoptosis of trypomastigotes in a concentration-dependent manner, as shown by the increase in annexin positive cells (see Supplementary Fig. S3). Furthermore, we evaluated the morphology and ultrastructure of trypomastigotes incubated with DMS. Compared with untreated trypomastigotes, parasites exposed to DMS for 24 h exhibited the formation of numerous and atypical vacuoles within the cytoplasm, a large loss of density degeneration of mitochondria and intense vacuolization (Fig. 5A–E). Interestingly, we also observed the presence of myelin-like figures within the cytoplasm (Fig. 5F), which is suggestive of parasite starvation or autophagy induced by DMS. The antiparasitic effects of DMS on the intracellular form of the parasite were also investigated. Macrophages infected *in vitro* by *T. cruzi* had a concentration-dependent reduction in the number of amastigotes and in percentage of infection (Fig. 6A,B). DMS at 5 μ M presented a similar effect when compared to benznidazole, a standard anti-*T. cruzi* chemotherapy agent (Fig. 6A,B). *T. cruzi*-infected macrophage cultures had an increased production of nitric oxide (Fig. 6C). Addition of DMS caused a concentration-dependent increase of nitric oxide by infected macrophages (Fig. 6C). The transcription of inducible nitric oxide synthase (iNOS) gene, however, was not altered by DMS treatment (Fig. 6D). We also evaluated the production of reactive oxygen species (ROS) in *T. cruzi*-infected macrophage cultures. DMS induced a concentration-dependent increase of ROS

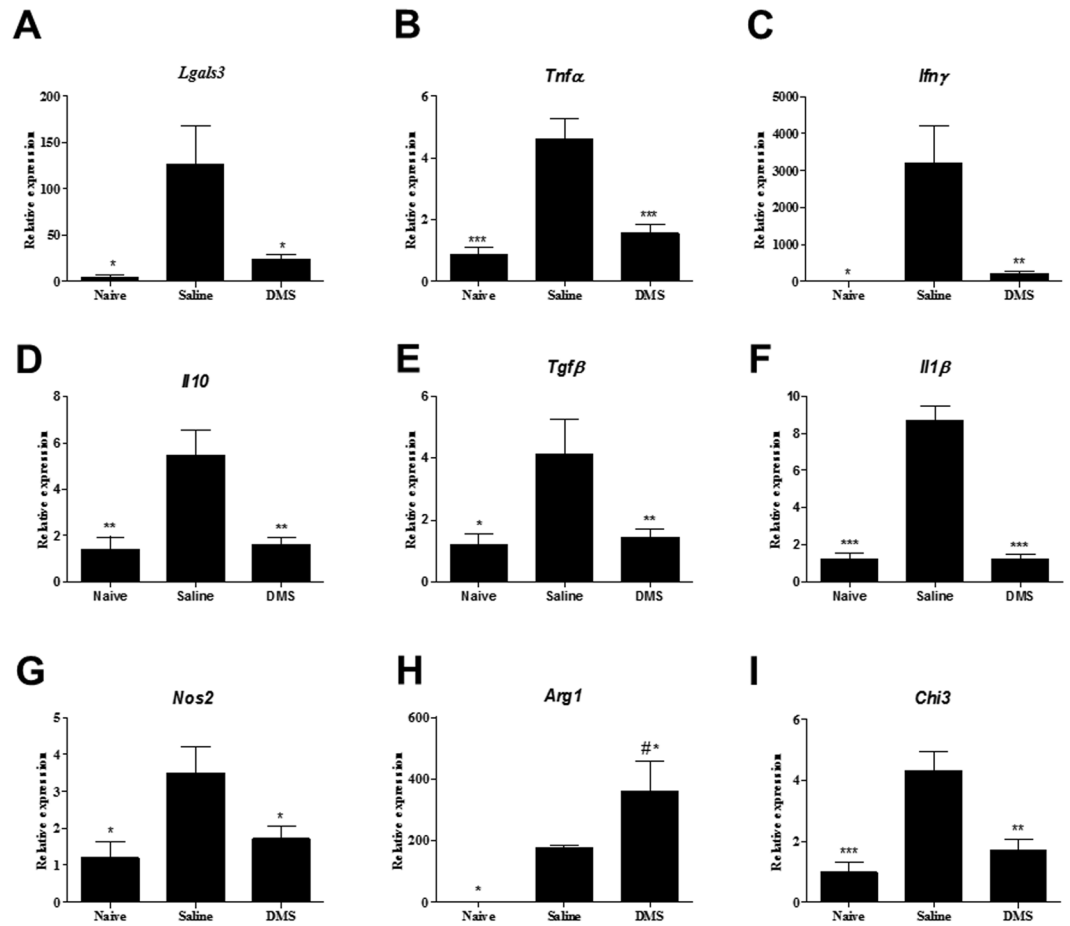


Figure 3. Gene expression in the hearts of infected mice after DMS treatment. Analysis of gene expression was performed by real-time qRT-PCR using cDNA samples prepared from mRNA extracted from hearts of naive and chronic Chagasic mice treated with saline or DMS. (A) Gal-3, (B) TNF α , (C) IFN γ , (D) IL-10, (E) TGF β , (F) IL-1 β , (G) NOS2, (H) ARG1 and (I) CHI3 gene expression. Bars represent means \pm SEM of 10 mice/group. *** $P < 0.001$; ** $P < 0.01$; * $P < 0.05$ compared to saline group; # $P < 0.05$ compared to naive group.

(Fig. 6E), as well as the transcription factor NFE2L2, which regulates the expression of key protective enzymes against ROS (Fig. 6F). Additionally, the gene expression of catalase and superoxide dismutase 1, two enzymes involved in ROS degradation, was increased by DMS treatment (Fig. 6G,H).

Activation of inflammasome pathways in *T. cruzi*-infected macrophages. *T. cruzi*-infected macrophages incubated with DMS increased IL-1 β production, in a concentration-dependent manner (Fig. 6I), suggesting involvement of an inflammasome pathway activation. To confirm that DMS induced inflammasome activation in *T. cruzi*-infected macrophages, we performed a caspase 1 activity assay. Addition of DMS (5 μ M) to *T. cruzi*-infected macrophages significantly increased the activation of caspase 1, whereas infection by *T. cruzi* alone induced a slight increase of caspase 1 activity (Fig. 6J). The effects of DMS on caspase 1 activation were abrogated by the addition of the caspase 1 inhibitor YVAD (Fig. 6J). To evaluate the regulation of inflammasome pathways by DMS, we performed a qRT-PCR array for inflammasome, including genes involved in innate immunity and NOD-like receptor (NLR) signaling. Macrophages infected with *T. cruzi* for 24 h were incubated with DMS (5 μ M) during 1 and 24 h and total RNA was extracted for gene expression analysis, compared to uninfected macrophage cultures (see Supplementary Tables 1–7). *T. cruzi* infection alone activated the transcription of genes related to inflammasome pathways, including *Nlrp3*, as well as several genes coding for chemokines and cytokines. Additionally, several genes related to signaling transduction pathways, including Mapk and NF- κ B pathway were upregulated (Fig. 7A). Analysis using the reactome pathway database highlighted the main pathways activated by *T. cruzi* infection, which include immune system related genes, NF- κ B and TLR pathways (Fig. 8A). The transcription of 17 genes were regulated by *T. cruzi* infection at the two time points evaluated. When changes in *T. cruzi*-infected macrophages at the two time points were compared, we found the expression of 15 genes altered only at 1 h time point (25 h of infection), whereas 2 genes were found altered only at 24 h time point (48 h of infection) (Fig. 7A). DMS treatment alone (24 h) did not induce any gene transcription change (see Supplementary Table S1). When *T. cruzi*-infected macrophages treated or not with DMS were compared, however, we found that DMS treatment suppressed the *T. cruzi* upregulated expression of *Mapk13* (Fig. 7C), *Il6*, *Il33*, *Nfkbib* and *Nlrp1a* (Fig. 7D). Additionally, DMS treatment increased the activation of *Nlr5* and *Nlr1* genes,

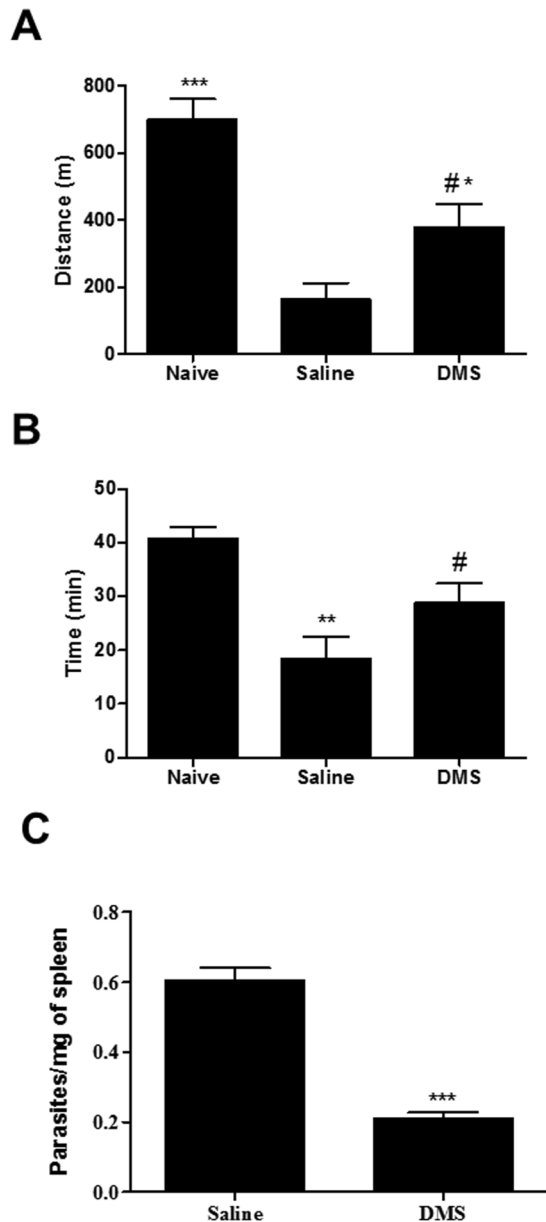


Figure 4. Effects of DMS treatment in cardiac function and parasite load. After an adaptation period in the treadmill chamber, naive and saline-treated or DMS-treated chronic Chagasic mice exercised at 5 different velocities (7.2, 14.4, 21.6, 28.8 and 36.0 m/min), with increasing velocity after 5 min of exercise at a given speed. (A) Distance run and (B) Time of exercise on a motorized treadmill. (C) Spleen fragments obtained from normal and *T. cruzi*-infected mice treated with saline or DMS were used for DNA extraction and qRT-PCR analysis for quantification of parasite load (primer 1 5'-GTTTCACACACTGGACACCAA-3' and primer 2 5'-TCGAAAACGATCAGCCGAST-3'). The standard curve of DNA ranged from 4.7×10^{-1} to 4.7×10^6). Bars represent means \pm SEM of 8–10 mice/group. *** $P < 0.001$; ** $P < 0.01$; * $P < 0.05$ compared to saline group; # $P < 0.05$ compared to naive group.

and had an increasing trend of expression of *Nlrp4*, *Nlrp5*, *Nlrp6*, *Nlrp9* genes when compared to *T. cruzi*-infected cells (Fig. 7B). Analysis using the reactome pathway database showed that, in addition to the pathways induced by *T. cruzi* infection, DMS treatment favoured the activation of RIG and NOD signaling pathways (Fig. 8B).

Discussion

Persistent inflammation is one of the hallmarks of chronic Chagas disease cardiomyopathy, and leads to a progressive destruction of the myocardium and heart dysfunction^{5,6}. Therefore, the development of therapeutic strategies aiming at modulation of inflammation without affecting parasite control is of great interest. Here we show, using a mouse model of chronic Chagas cardiomyopathy which reproduces the pathological findings observed in human hearts, a potent effect of DMS, causing reduction of heart inflammation and fibrosis, modulation of

	NSR		1 st AVB		IACD		JR		IVCD		VB		TAVB	
	Pre	Post	Pre	Post	Pre	Post	Pre	Post	Pre	Post	Pre	Post	Pre	Post
CTRL (n = 05)	05	05	—	—	—	—	—	—	—	—	—	—	—	—
INF + Saline (n = 11)	—	—	07	02	—	01	01	—	03	—	01	—	03	06
INF + DMS (n = 11)	03	—	02	01	—	01	02	02	03	—	03	02	02	04

Table 1. Number of animals per arrhythmias before treatment (Pre) and at the end of treatment (Post) in naive (CTRL), chronic infected and vehicle-treated (INF + Saline) and chronic infected, DMS-treated (INF + DMS) groups. In infected groups, some animals developed more than one type of arrhythmias. NSR = Normal sinus rhythm, 1st AVB = 1st degree atrio-ventricular block, IACD = Intra-atrial conduction disturbance, JR = Junctional rhythm, IVCD = Intra-ventricular conduction disturbance, VB = Ventricular bigeminism, TAVB = Total atrio-ventricular dissociation.

Compound	CC ₅₀ MO (μM) ^a	EC ₅₀ Try. (μM) ^b	SI
DMS	9.02 (±0.12)	1.98 (±0.47)	4.5
BDZ	>50	12.53 (±0.55)	>4
GV	0.48 (±0.05)	—	—

Table 2. Host cell cytotoxicity and trypanocidal activity of DMS on trypomastigotes forms of *T. cruzi* (Colombian strain). ^aCell viability of mouse macrophages determined 72 h after treatment. ^bTrypanocidal activity determined 24 h after incubation with compounds. ^bValues represent the mean ± SEM of triplicate. Three independent experiments were performed. EC₅₀ = effective concentration at 50%. CC₅₀ = cytotoxic concentration at 50%. BDZ = benznidazole. GV = Gentian violet.

pro-inflammatory mediators and improvement of exercise capacity. Importantly, the residual parasite load found in mice chronically infected with *T. cruzi* was reduced by DMS treatment.

In our study, a marked reduction of inflammation was seen after DMS treatment, as shown by two different analyses, morphometry and qRT-PCR for quantification of CD45 expression. Moreover, the production of IFN γ and TNF α , two cytokines known to promote the chronic Chagas myocarditis, were significantly reduced in the heart, as well as in the serum, showing a local and a systemic effect of DMS. The fact that DMS modulates the activation of lymphocytes and macrophages *in vitro* reinforces that, in addition to a reduction of cell migration, a direct effect of the drug on immune cells may cause the potent immunomodulatory effect of DMS observed *in vivo* in our model. In line with this idea, it was recently shown that FTY720, a recently approved drug that inhibits the S1P pathway, also modulates the activation of human T lymphocytes and leads to a reduction of IFN γ production¹⁶.

All of the three major S1P receptor (1–3) subtypes are also expressed in cardiac fibroblasts and participate in cardiac remodeling by the activation of signaling pathways through S1P. Moreover, both FTY720 and DMS have been shown to reduce fibrosis^{17–19}. The expression of SphK1 is an important factor regulating the proliferation of cardiac fibroblasts²⁰. SphK1-transgenic mice which overproduces endogenous S1P showed 100% occurrence of cardiac fibrosis, involved with activation of the S1P3-Rho family small G protein signaling pathway and increased ROS production²¹. Additionally, DMS-treated mice had a reduced expression of TGF β and galectin-3, two pro-fibrogenic factors that stimulate the proliferation and production of extracellular matrix proteins by cardiac fibroblasts^{22,23}. Here we observed a reduction on fibrotic area in the heart of DMS-treated mice, corroborating the importance of S1P signaling for heart fibrosis.

An important finding was the antiparasitic effect of DMS, leading to a reduction of parasite load *in vivo*, despite causing a reduction on the production of pro-inflammatory factors, such as IFN γ and TNF α , known to play important roles in resistance to *T. cruzi* infection^{24,25}. We showed here that DMS has not only a direct effect on the parasite, causing several cellular alterations and death of trypomastigote forms, but also an indirect effect, by inducing the increase of NO and ROS production in infected macrophages *in vitro*. These results are in accordance with a previous report showing S1P down regulating iNOS expression in macrophages through the inhibition of NF- κ B, AP-1 and/or STAT-1 activation²⁶. This suggests that the inhibition of S1P production by DMS treatment may lead to an increased NO production, also contributing to the *in vivo* antiparasitic mechanisms of DMS.

Chagas disease cardiomyopathy may result from multiple pathological mechanisms, including immune responses against the parasite, as well as self-reactive responses against cardiac antigens²⁷. The reduction of parasitism by benznidazole, a drug used to treat Chagas disease, reduces cardiac alterations during the chronic phase of infection²⁸. Additionally, the reinforcement of immunological tolerance to myocardial antigens also caused reduction of inflammation in a mouse model of *T. cruzi* infection²⁹. Thus, the fact that DMS affects both inflammatory cells as well as the parasite suggests that these effects may contribute to the modulation of inflammation seen after DMS treatment.

SphK is a highly conserved enzyme in eukaryotes, and while there are two isoforms in mammals, only one is found in trypanosomatids. Depletion of *Trypanosoma brucei* SphK causes attenuation of cell division, microtubule elongation at the posterior tip, and altered organelle positioning. SphK inhibitors, such as DMS and safingol,

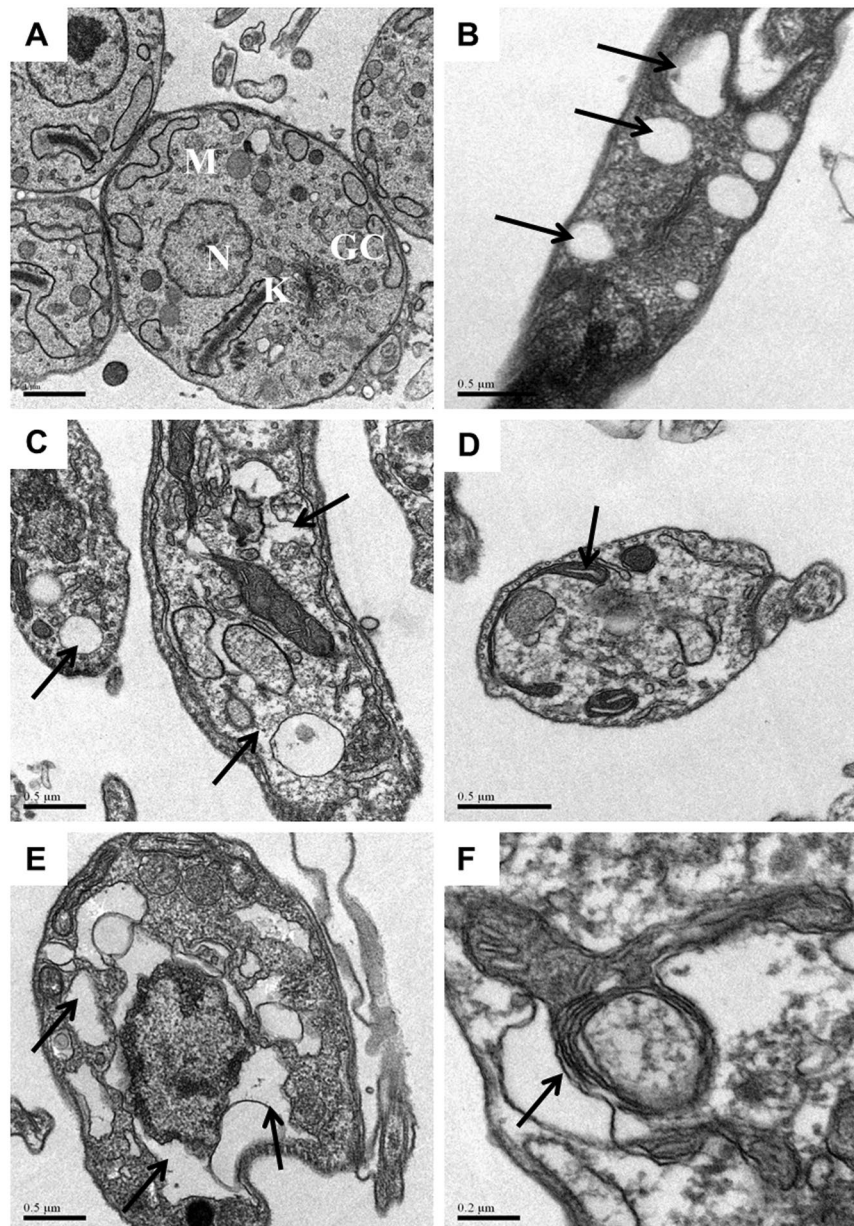


Figure 5. Transmission electron micrographs of trypomastigotes treated or not with DMS for 24 h. (A) Untreated trypomastigotes presenting a typical morphology of the nucleus (N), kinetoplast (K), mitochondria (M) and Golgi complex (GC). (B,C) Trypomastigotes treated with DMS (1 μ M) causes the formation of numerous and atypical vacuoles within the cytoplasm accompanied by a large loss of density. (D,E) Trypomastigotes treated with DMS (2 μ M) shows degeneration of mitochondria and intense vacuolization. (F) Trypomastigotes treated with DMS (4 μ M) shows myelin-figures. Black arrows indicate alterations cited. Scale bars: A = 1 μ m; B–E = 0.5 μ m; F = 0.2 μ m.

are toxic to *T. brucei*, both of them having a 10-fold therapeutic index versus human cells, suggesting their potential use against *T. brucei* infection³⁰. Here we demonstrated that DMS also induces morphological alterations and death in *T. cruzi*, suggesting that TcSphK may be a candidate target for drug development against *T. cruzi*. The reduced parasite load on infected macrophages may be also an important mechanism to reduce the dissemination of parasites, since it is likely that *T. cruzi*-infected macrophages circulate *in vivo*³¹.

A previous study has shown that Sph and its analogues DMS and FTY720 act as a danger-associated molecular patterns (DAMPs), inducing mature IL-1 β secretion and promoting inflammasome activation³². Both Sph analogues are capable of inducing IL-1 β production, and our data reinforces the ability of DMS to activate the inflammasome pathway. *T. cruzi* infection has also been shown to induce inflammasome activation in mice, being a resistance factor to infection by regulating the production of nitric oxide and ROS^{33–35}. Here we found that DMS induced inflammasome activation in *T. cruzi*-infected macrophages, as shown by increased caspase-1 activation and IL-1 β production. Moreover, DMS increased the production of ROS and NO, which may be

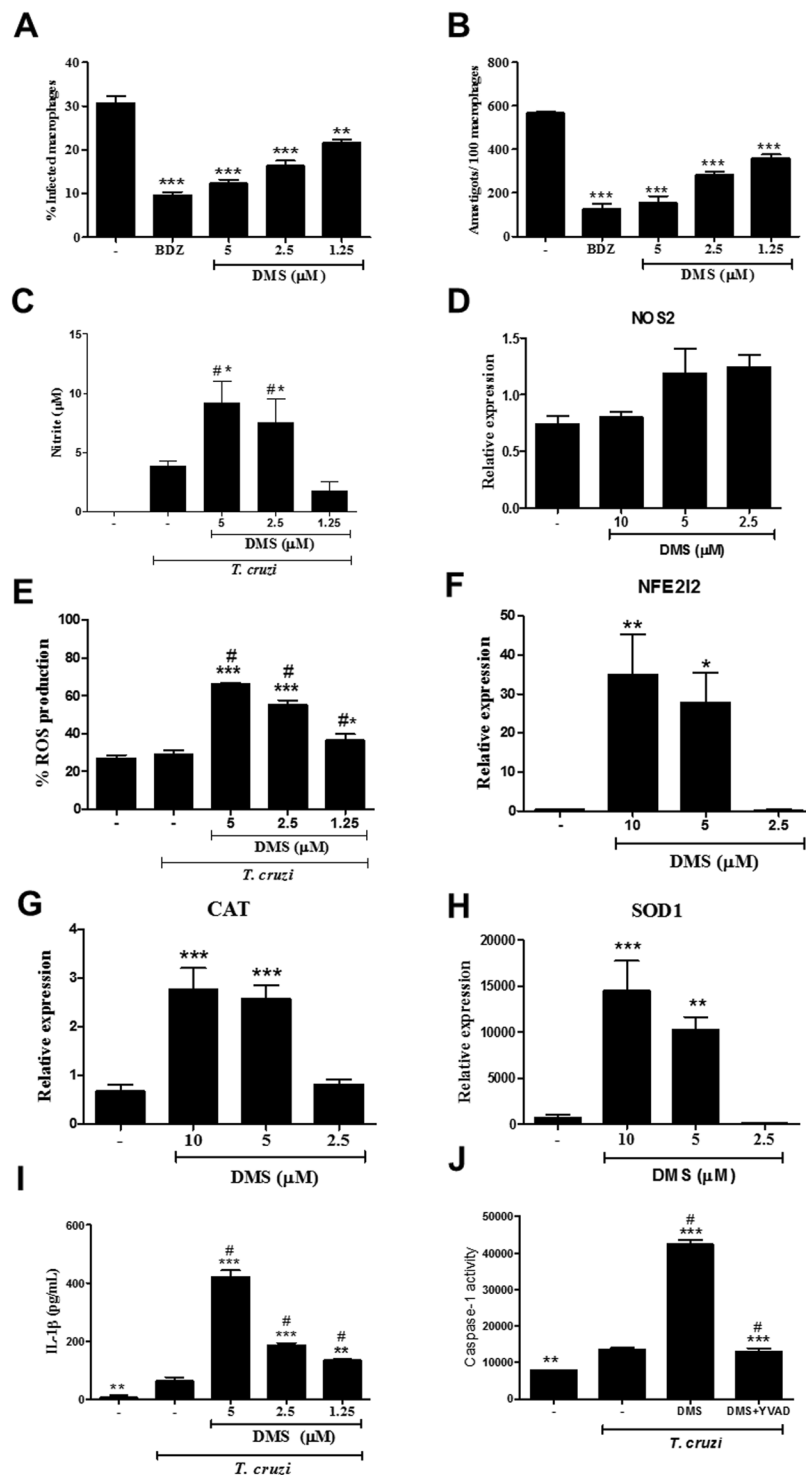


Figure 6. DMS inhibits amastigote proliferation in *T. cruzi*-infected macrophages, increases NO and ROS and activates caspase 1. The percentage of infected macrophages (A) and the relative number of amastigotes per 100 macrophages (B) were determined by counting hematoxylin and eosin-stained cultures after 72 hours of treatment. (C) Nitric oxide was determined by Griess method after 72 hours of treatment. (D) Relative expression of NOS2 gene in infected macrophages treated or not with DMS. (E) Reactive oxygen species was quantified by stained with 2',7'-dichlorofluorescein diacetate after 30 minutes of treatment. (F–H) Relative expression of NFE2I2, CAT and SOD1 genes in infected macrophages treated or not with DMS. (I) IL-1 β production quantified by ELISA. (J) Caspase-1 activity measured using caspase-Glo 1 inflammasome assay in cultures incubated with complete medium alone, with DMS (5 μ M) or with DMS and YVAD (a caspase-1 inhibitor) in triplicate for 2 h. Values represent means \pm SEM of 4 determinations. *** P < 0.001; ** P < 0.01; * P < 0.05 compared to infected and untreated group; # P < 0.05 compared to uninfected and untreated group.

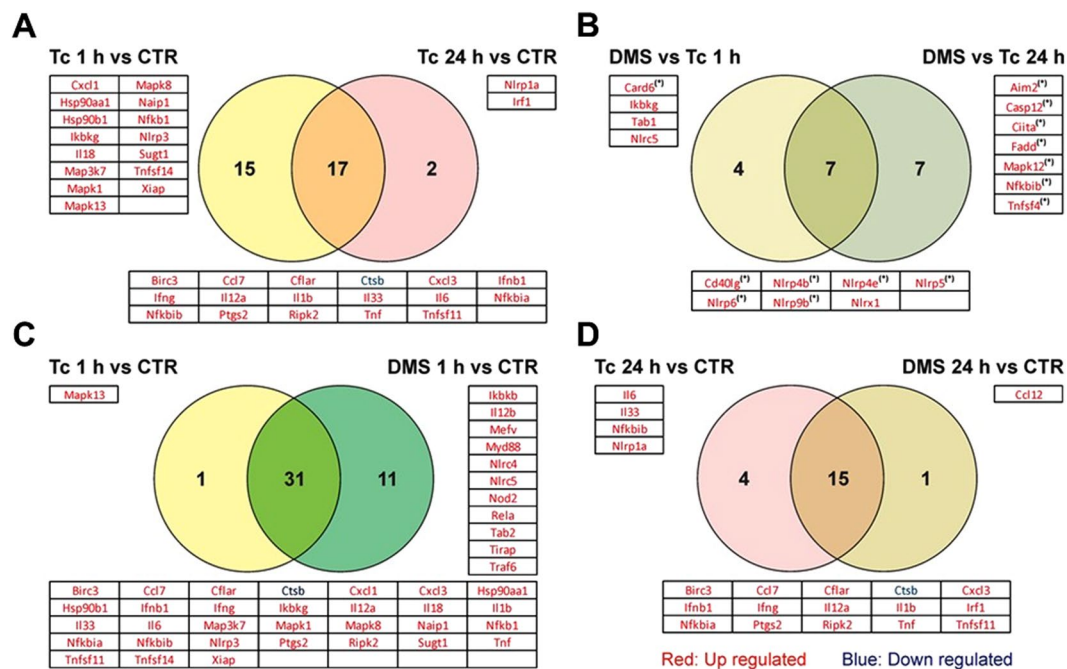


Figure 7. Venn diagrams representing differentially expressed genes (DEG) through *T. cruzi* infection with or without DMS treatment. (A) Comparison between DEG after 25 h (Tc 1 h condition) or 48 h (Tc 24 h condition) after *T. cruzi* infection with respect to uninfected macrophages (CTR condition). (B) Analysis of common DEG by DMS treatment for 1 h (DMS 1 h) and 24 h (DMS 24 h) when compared to infected macrophages. (C) Comparison between DEG by *T. cruzi* infection with or without 1 h DMS treatment with respect to uninfected macrophages. (D) Comparison between DEG during 48 h infection with or without 24 h DMS treatment with respect to uninfected macrophages. (*) indicates genes with $|FC| \geq 2$ but p-values > 0.05 .

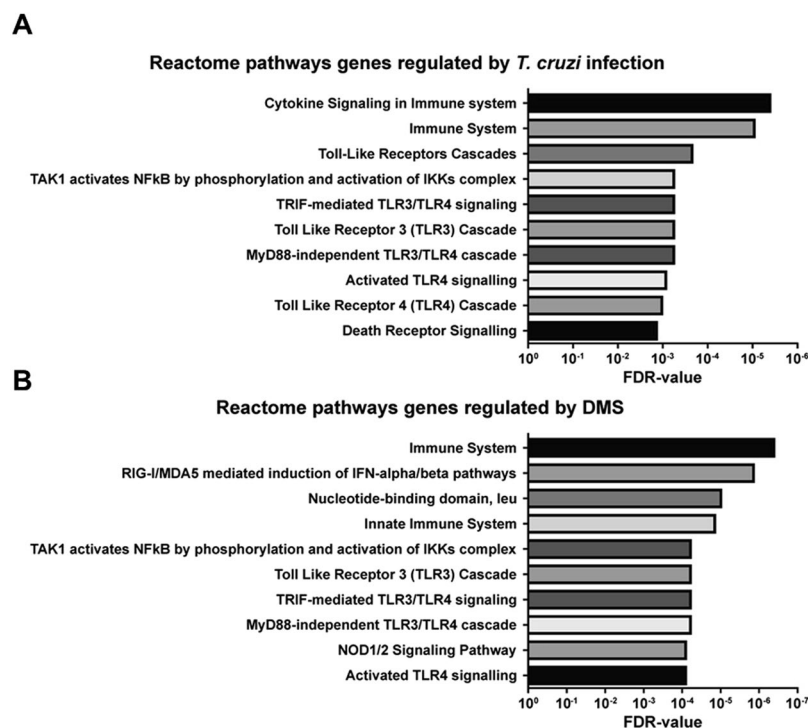


Figure 8. Reactome pathway analysis of DEG by *T. cruzi* infection or DMS treatment. (A) Graph representing the 10 most significant pathways in which common DEG by *T. cruzi* at 25 h (Tc 1 h condition) and 48 h (Tc 24 h condition) after infection are involved. (B) Graph representing the 10 most significant pathways in which genes induced by DMS treatment are involved.

contributing to parasite clearance by infected macrophages. Interestingly, the increase on production of nitric oxide was not accompanied by an upregulation of iNOS gene transcription, suggesting that post-transcriptional and post-translational mechanisms are responsible for DMS-induced NO production³⁶. The transcription of genes activated in response to ROS production, however, were increased in DMS-treated macrophages, such as NFE2L1, SOD-1 and catalase 1.

In addition to its effects on Sphk, DMS was shown to inhibit the activity of protein kinase C and mitogen-activated protein kinase (MAPK)^{37,38}. Although we did not see interference of PKC and MAPK inhibitors on the effects of DMS in macrophage cultures, further studies are required to demonstrate whether the beneficial effects of DMS *in vivo* are solely dependent on Sphk inhibition. The fact that DMS may have off-target effects, however, may not be detrimental, since FTY720 and other approved drugs are known to have off-target effects³⁹.

Despite the increased production of IL-1 β by DMS-treated macrophages, a reduction of TNF α and IL-6, two proinflammatory cytokines, was found. This may be due to a modulation of NF- κ B activation by DMS, as observed in our study and in previous reports^{40,41}. The analysis by PCR array performed in our study indicates that DMS induces the expression of inflammasome genes known to repress NF- κ B activation, such as *Nlr5* and *Nlr1*^{42,43}, which suggests that inhibition of *T. cruzi*-induced NF- κ B may be linked to the activation of these inflammasome mediators. Both Sph and its analogue FTY720 have already been described as regulators of the NLRP3-inflammasome and IL-1 β release from macrophages³². Although NLRP3-inflammasome activation plays a significant role in the activation of IL-1 β /ROS and NF- κ B signaling of cytokine gene expression for *T. cruzi* control in human and mouse macrophages, it was observed that NLRP3-mediated IL-1 β /NF- κ B activation is dispensable since it is compensated by ROS-mediated control of *T. cruzi* replication and survival in macrophages³⁵. Therefore, our results suggest that, in addition to the NLRP3 inflammasome previously described³², DMS activates other inflammasome pathways.

In conclusion, our results demonstrate a potent effect of DMS *in vitro* and *in vivo* by its antiparasitic and immunomodulatory effects and suggest that inflammasome activation is a promising strategy for the development of anti-Chagas disease treatment. Further studies are required to demonstrate the usefulness of inhibitors of S1P pathway, which are being already used in the clinical setting, as potential candidates for the treatment of Chagas disease cardiomyopathy.

Methods

Animals. Four weeks-old male C57BL/6 mice were used in all experiments. They were raised, maintained in the animal facility of the Center for Biotechnology and Cell Therapy, Hospital São Rafael (Salvador, Bahia, Brazil), and provided with rodent diet and water *ad libitum*. All experiments were carried out in accordance with the recommendations of Ethical Issues Guidelines, and were approved by the local ethics committee for animal use under number 001/15 (FIOCRUZ, Bahia, Brazil).

Trypanosoma cruzi infection and DMS treatment. Trypomastigotes of the myotropic Colombian *T. cruzi* strain were obtained from culture supernatants of infected LLC-MK2 cells. Infection was performed by intraperitoneal (i.p.) injection of 1000 *T. cruzi* trypomastigotes in saline and parasitemia was monitored during infection. Groups of chronically infected mice were treated i.p. with N,N-dimethylsphingosine (DMS; 200 μ g/kg; Cayman Chemical, Ann Arbor, MI) based on a previous report by Lai and col. (2008)⁴⁴, 3 \times /week during two months (Fig. 1A). Control infected mice received vehicle (saline solution) in the same regimen. Groups of mice were euthanized one week after therapy, under anesthesia with 5% ketamine (Vetanarcol[®]; Konig, Avellaneda, Argentina) and 2% xylazine (Sedomin[®]; Konig).

Exercise capacity and electrocardiography analysis. A motor-driven treadmill chamber for one animal (LE 8700; Panlab, Barcelona, Spain) was used to exercise the animals. The speed of the treadmill and the intensity of the shock (mA) were controlled by a potentiometer (LE 8700 treadmill control; Panlab). Total running distance and time of exercise were recorded.

Electrocardiography was performed using the Bio Amp PowerLab System (PowerLab 2/20; ADInstruments, Castle Hill, NSW, Australia), recording the bipolar lead I. All data were acquired for computer analysis using Chart 5 for Windows (PowerLab). The EKG analysis included heart rate, PR interval, P wave duration, QT interval, QTc, and arrhythmias. The QTc was calculated as the ratio of QT interval by square roots of RR interval (Bazett's formula)⁴⁵.

Morphometric analysis. The hearts of all mice were removed and half of each heart was fixed in buffered 10% formalin. Sections of paraffin-embedded tissue were stained by the standard hematoxylin-eosin and Sirius red staining methods for evaluation of inflammation and fibrosis, respectively, by optical microscopy. Images were digitized using a color digital video camera (CoolSnap, Montreal, Canada) adapted to a BX41 microscope (Olympus, Tokyo, Japan). Morphometric analyses were performed using the software Image Pro Plus v.7.0 (Media Cybernetics, San Diego, CA), as described before⁴⁶.

Confocal immunofluorescence analyses. Sections of formalin-fixed paraffin embedded hearts were used for detection of galectin-3 expression by immunofluorescence as described before⁴⁶. Sections were incubated overnight with anti-galectin-3, diluted 1:50 (Santa Cruz Biotechnology, Santa Cruz, CA) followed by incubation, for 1 h, with Alexa fluor 633 (1:200) (Molecular Probes, Carlsbad, CA) Nuclei were stained with 4,6-diamidino-2-phenylindole (Vector Laboratories, Burlingame, CA). The presence of fluorescent cells was determined by observation on a FluoView 1000 confocal microscope (Olympus).

Quantification of parasite load. For DNA extraction, spleen fragments were submitted to DNA extraction using the NucleoSpin Tissue Kit (Macherey-Nagel, Düren, Germany), as recommended by the manufacturer. Primers were designed based on the literature⁴⁷, and the quantification of parasite load was performed as described previously⁴⁶. To calculate the number of parasites per milligram of tissue, each plate contained an 8-log standard curve of DNA extracted from trypomastigotes of the Colombian *T. cruzi* strain in duplicate. Data were analyzed using 7500 software 2.0.1 (Applied Biosystems).

Macrophage infection *in vitro*. Peritoneal exudate macrophages obtained from C57BL/6 mice, four days after thioglycollate injection, were seeded at a cell density of 2×10^5 cells/mL in a 24 well-plate with rounded coverslips on the bottom in RPMI-1640 medium (Sigma-Aldrich, St. Louis, MD) supplemented with 10% fetal bovine serum (FBS; Gibco Laboratories, Gaithersburg, MD) and 50 $\mu\text{g}/\text{mL}$ of gentamycin (Novafarma, Anápolis, GO, Brazil) and incubated for 24 h. Cells were then infected with trypomastigotes (1:10) for 2 h. Free trypomastigotes were removed by successive washes using saline solution. Cultures were incubated for 24 h to allow full internalization and differentiation of trypomastigotes into amastigotes. Cultures were then incubated in complete medium alone or with test inhibitors for 72 h. Cells were fixed, then stained with hematoxylin and eosin, and submitted to manual counting using an optical microscope (Olympus).

Real time reverse transcription polymerase chain reaction (qRT-PCR). RNA was extracted of the heart samples and macrophage cultures using TRIzol (Invitrogen, Molecular Probes, Eugene, OR). cDNA was synthesized using High Capacity cDNA Reverse Transcription Kit (Applied Biosystems). The qPCR was prepared with TaqMan[®] Universal PCR Master Mix (Applied Biosystems). qRT-PCR assays were performed to detect the expression levels of *Ptprc*, *Lgals3*, *Tnf*, *Ifn γ* , *Il10*, *Tgf β* , *Nos2*, *Chi3l3*, *Il1 β* , *Arg1*, *Nfe2l2*, *Cat* and *Sod1*. All reactions were run in triplicate on an ABI 7500 Real Time PCR System (Applied Biosystems) under standard thermal cycling conditions. A non-template control (NTC) and non-reverse transcription controls (No-RT) were also included. The samples were normalized with 18S and *Hprt*. The threshold cycle ($2^{-\Delta\Delta\text{Ct}}$) method of comparative PCR was used to analyse the results⁴⁸.

PCR array. Peritoneal exudate macrophages (2×10^6 cells/mL) were incubated in 24 well-plates with supplemented RPMI for 24 h. After washing with saline solution to discard non-adherent cells, infection was performed with trypomastigotes (1:10), for 24 h. Free trypomastigotes were removed by successive washes. Cultures were then incubated with complete medium alone or with DMS (5 μM) in triplicate for 24 h. RNA was extracted using the Rneasy Plus Mini Kit (Qiagen, Valencia, CA). Quantification of RNA and degree of purity were performed in a spectrophotometer (NanoDrop[™] 1000, Thermo Fisher Scientific, Wilmington, DE). Sample integrity was observed using a 1% agarose gel. cDNA synthesis was performed using the RT2 First Strand kit (Qiagen). For target gene expression analysis, we used RT2 Profiler PCR Arrays Mouse Inflammasome (Qiagen), the SYBR[®]Green system and 96-well plates. The 7500 Real Time PCR was used (Applied Biosystems). All experiments were performed in DNase/RNase free conditions. The analysis was performed by Threshold Cycle Method⁴⁸, obtained by calculating $2^{-\Delta\Delta\text{Ct}}$. The QIAGEN's qPCR analysis web portal date, available on <http://pcrdataanalysis.sabiosciences.com/pcr/arrayanalysis.php> was used to assist in the analysis, and analysis of differentially expressed genes and pathways prediction were done through free online bioinformatic sites BioVenn (www.cmbi.ru.nl/cdd/bioenn) and Enrichr (amp.pharm.mssm.edu/Enrichr).

Lymphoproliferation assay. Spleen cell suspensions from naive C57BL/6 mice were prepared in DMEM medium (Life Technologies, GIBCO-BRL, Gaithersburg, MD) supplemented with 10% FBS and 50 $\mu\text{g}/\text{mL}$ of gentamycin. Splenocytes were cultured in 96-well plates at 1×10^6 cells per well, in a final volume of 200 μL , in triplicate, in the presence of 2 $\mu\text{g}/\text{mL}$ concanavalin A (Con A; Sigma-Aldrich) only or with anti-CD3 and anti-CD28 (Thermo Fisher Scientific), in the absence or presence of DMS at different concentrations (2.5, 1.25 or 0.62 μM). After 48 h, plates were pulsed with 1 μCi of methyl-³H-thymidine (Perkin Elmer, Waltham, MA) for 18 h. The plates were harvested and the ³H-thymidine uptake was determined using a β -plate counter (Multilabel Reader, Finland). Dexamethasone (Sigma-Aldrich) was used as positive control.

ELISA assays and determination of nitric oxide production. Serum samples from the *in vivo* study were used for galectin-3, TNF α and IFN γ and TGF β determination. Quantification of cytokines was performed by ELISA, using specific antibody kits (R&D Systems, Minneapolis, MN), according to manufacturer's instructions. To estimate the amount of nitric oxide (NO) produced, macrophage culture supernatants were used for nitrite determination by the Griess reaction, as previously described⁴⁹.

Reactive oxygen species (ROS) production assay. Thioglycollate-elicited peritoneal exudate macrophages (1×10^6) were obtained and infected with *T. cruzi*. Cultures were then incubated with complete medium alone or with DMS for 30 min. After incubation, macrophages were removed from each well using 0.01% trypsin and labeled with 10 μM of 2',7'-dichlorofluorescein diacetate (Sigma-Aldrich) for 30 minutes at 37 °C. Cells were then washed and analyzed using a cell analyzer (LSRFortessa; BD Biosciences, San Jose, CA) with FlowJo software (Tree Star, Ashland, OR).

Caspase 1 activity assay. Thioglycollate-elicited peritoneal exudate macrophages (1×10^6) were obtained and infected with *T. cruzi* as described above. Cultures were then incubated with reagents for 2 h and after that, caspase-1 activity was measured using caspase-Glo[®] 1 inflammasome assay (Promega, Madison, WI), according to the manufacturer's instructions. The luminescence of each sample was measured in a Glomax 20/20 luminometer (Promega).

Transmission electron microscopy analysis. *T. cruzi* trypomastigotes (5×10^7) were treated with DMS (1, 2 or 4 μM) and incubated for 24 h at 37°C. After incubation, parasites were fixed for 1 h at room temperature with 2% formaldehyde and 2.5% glutaraldehyde (Electron Microscopy Sciences, Hatfield, PA) in sodium cacodylate buffer (0.1 M, pH 7.2) for 1 h at room temperature. After fixation, parasites were processed for transmission electron microscopy as previously described⁵⁰. Images were obtained in a JEOL TEM-1230 transmission electron microscope.

Statistical analyses. All continuous variables are presented as means \pm SEM. Data were analyzed using 1-way ANOVA, followed by Newman-Keuls multiple-comparison test with Prism 5.0 (GraphPad Software, San Diego, CA). All differences were considered significant at values of $P < 0.05$.

References

1. Dutra, W. O. *et al.* Cellular and genetic mechanisms involved in the generation of protective and pathogenic immune responses in human Chagas disease. *Mem. Inst. Oswaldo Cruz* **104**(Suppl. 1), 208–218 (2009).
2. Andrade, Z. A. Immunopathology of Chagas disease. *Mem Inst Oswaldo Cruz* **94**(Suppl 1), 71e80 (1999).
3. Fuenmayor, C. *et al.* Acute Chagas' disease: immunohistochemical characteristics of T cell infiltrate and its relationship with *T. cruzi* parasitic antigens. *Acta Cardiol* **60**(1), 33–37 (2005).
4. Bonney, K. M. & Engman, D. M. Autoimmune pathogenesis of Chagas heart disease: looking back, looking ahead. *Am J Pathol* **185**(6), 1537–1547 (2015).
5. Tanowitz, H. B. *et al.* Chagas' disease. *Clin Microbiol Rev* **5**(4), 400–419 (1992).
6. Rassi, A. Jr., Rassi, A. & Marin-Neto, J. A. Chagas disease. *Lancet* **375**(9723), 1388–1402 (2010).
7. Arana, L., Gangoiti, P., Ouro, A., Trueba, M. & Gómez-Muñoz, A. Ceramide and ceramide 1-phosphate in health and disease. *Lipids Health Dis* **9**, 15 (2010).
8. Yanagida, K. & Hla, T. Vascular and immunobiology of the circulatory sphingosine 1-phosphate gradient. *Annu Rev Physiol* **79**, 67–91 (2017).
9. Arish, M. *et al.* sphingosine-1-phosphate signaling: unraveling its role as a drug target against infectious diseases. *Drug Discov Today* **21**(1), 133–142 (2016).
10. Maceyka, M. & Spiegel, S. Sphingolipid metabolites in inflammatory disease. *Nature* **510**(7503), 58–67 (2014).
11. Rivera, J., Proia, R. L. & Olivera, A. The alliance of sphingosine-1-phosphate and its receptors in immunity. *Nat Rev Immunol* **8**(10), 753–763 (2008).
12. Cyster, J. G. & Schwab, S. R. Sphingosine-1-phosphate and lymphocyte egress from lymphoid organs. *Annu Rev Immunol* **30**, 69–94 (2012).
13. Soares, M. B. *et al.* Reversion of gene expression alterations in hearts of mice with chronic chagasic cardiomyopathy after transplantation of bone marrow cells. *Cell Cycle* **10**(9), 1448–1455 (2011).
14. Gomes, J. A. *et al.* Evidence that development of severe cardiomyopathy in human Chagas' disease is due to a Th1-specific immune response. *Infect Immun* **71**(3), 1185–1193 (2003).
15. Soares, M. B. *et al.* Gene expression changes associated with myocarditis and fibrosis in hearts of mice with chronic chagasic cardiomyopathy. *J Infect Dis* **202**(3), 416–426 (2010).
16. Mazzola, M. A. *et al.* Identification of a novel mechanism of action of fingolimod (FTY720) on human effector T cell function through TCF-1 upregulation. *J Neuroinflammation* **12**, 245 (2015).
17. Takuwa, Y., Ikeda, H., Okamoto, Y., Takuwa, N. & Yoshioka, K. Sphingosine-1-phosphate as a mediator involved in development of fibrotic diseases. *Biochim Biophys Acta* **1831**(1), 185–192 (2013).
18. Shiohira, S. *et al.* Sphingosine-1-phosphate acts as a key molecule in the direct mediation of renal fibrosis. *Physiol Rep* **1**(7), e00172 (2013).
19. Landeen, L. K., Aroonsakool, N., Haga, J. H., Hu, B. S. & Giles, W. R. Sphingosine-1-phosphate receptor expression in cardiac fibroblasts is modulated by *in vitro* culture conditions. *Am J Physiol Heart Circ Physiol* **292**(6), H2698–2711 (2007).
20. Kacimi, R., Vessey, D. A., Honbo, N. & Karliner, J. S. Adult cardiac fibroblasts null for sphingosine kinase-1 exhibit growth dysregulation and an enhanced proinflammatory response. *J Mol Cell Cardiol* **43**(1), 85–91 (2007).
21. Takuwa, N. *et al.* S1P3-mediated cardiac fibrosis in sphingosine kinase 1 transgenic mice involves reactive oxygen species. *Cardiovasc Res* **85**(3), 484–493 (2010).
22. Araújo-Jorge, T. C. *et al.* Pivotal role for TGF- β in infectious heart disease: the case of *Trypanosoma cruzi* infection and its consequent chagasic cardiomyopathy. *Cytok Growth Factors Rev* **19**(5–6), 405–413 (2008).
23. Azibani, F., Fazal, L., Chatziantoniou, C., Samuel, J. L. & Delcayre, C. Hypertension-induced fibrosis: a balance story. *Ann Cardiol Angeiol* **61**(3), 150–155 (2012).
24. Machado, F. S. *et al.* *Trypanosoma cruzi*-infected cardiomyocytes produce chemokines and cytokines that trigger potent nitric oxide-dependent trypanocidal activity. *Circulation* **102**(24), 3003–3008 (2000).
25. Boscardin, S. B. *et al.* Chagas' disease: an update on immune mechanisms and therapeutic strategies. *J Cell Mol Med* **14**(6B), 1373–1384 (2010).
26. Hughes, J. E. *et al.* Sphingosine-1-phosphate induces an antiinflammatory phenotype in macrophages. *Circ Res* **102**(8), 950–958 (2008).
27. Soares, M. B., Pontes-De-Carvalho, L. & Ribeiro-Dos-Santos, R. The pathogenesis of Chagas' disease: when autoimmune and parasite-specific immune responses meet. *An Acad Bras Cienc* **73**(4), 547–559 (2001).
28. Garcia, S. *et al.* Treatment with benznidazole during the chronic phase of experimental Chagas' disease decreases cardiac alterations. *Antimicrob Agents Chemother* **49**(4), 1521–1528 (2005).
29. Pontes-de-Carvalho, L. *et al.* Experimental chronic Chagas' disease myocarditis is an autoimmune disease preventable by induction of immunological tolerance to myocardial antigens. *J Autoimmun* **18**(2), 131–138 (2002).
30. Pasternack, D. A., Sharma, A. I., Olson, C. L., Epting, C. L. & Engman, D. M. Sphingosine kinase regulates microtubule dynamics and organelle positioning necessary for proper G1/S cell cycle transition in *Trypanosoma brucei*. *MBio* **6**(5), e01291–1315 (2015).
31. Lewis, M. D., Francisco, A. F., Taylor, M. C. & Kelly, J. M. A new experimental model for assessing drug efficacy against *Trypanosoma cruzi* infection based on highly sensitive *in vivo* imaging. *J Biomol Screen* **20**(1), 36–43 (2015).
32. Luheshi, N. M., Giles, J. A., Lopez-Castejon, G. & Brough, D. Sphingosine regulates the NLRP3-inflammasome and IL-1 β release from macrophages. *Eur J Immunol* **42**(3), 716–725 (2012).
33. Silva, G. K. *et al.* Apoptosis-associated speck-like protein containing a caspase recruitment domain inflammasomes mediate IL-1 β response and host resistance to *Trypanosoma cruzi* infection. *J Immunol* **191**(6), 3373–3383 (2013).
34. Gonçalves, V. M. *et al.* NLRP3 controls *Trypanosoma cruzi* infection through a caspase-1-dependent IL-1R-independent NO production. *PLoS Negl Trop Dis* **7**(10), e2469 (2013).
35. Dey, N. *et al.* Caspase-1/ASC inflammasome-mediated activation of IL-1 β -ROS-NF κ B pathway for control of *Trypanosoma cruzi* replication and survival is dispensable in NLRP3-/- macrophages. *Plos One* **9**(11), e111539 (2014).
36. Pautz, A. *et al.* Regulation of the expression of inducible nitric oxide synthase. *Nitric Oxide* **23**(2), 75–93 (2010).

37. Sakakura, C. *et al.* Selectivity of sphingosine-induced apoptosis. Lack of activity of DL-erythro-dihydrosphingosine. *Biochem Biophys Res Commun* **246**(3), 827–830 (1998).
38. Kim, J. W. *et al.* Synthesis and evaluation of sphingoid analogs as inhibitors of sphingosine kinases. *Bioorg Med Chem* **13**(10), 3475–3485 (2005).
39. Patmanathan, S. N., Yap, L. F., Murray, P. G. & Paterson, I. C. The antineoplastic properties of FTY720: evidence for the repurposing of fingolimod. *J Cell Mol Med* **19**(10), 2329–2340 (2015).
40. Billich, A. *et al.* Basal and induced sphingosine kinase 1 activity in A549 carcinoma cells: function in cell survival and IL-1beta and TNF-alpha induced production of inflammatory mediators. *Cell Signal* **17**(10), 1203–1217 (2005).
41. Zhang, Z. *et al.* SPHK1 inhibitor suppresses cell proliferation and invasion associated with the inhibition of NF- κ B pathway in hepatocellular carcinoma. *Tumour Biol* **36**(3), 1503–1509 (2015).
42. Cui, J. *et al.* NLRX5 negatively regulates the NF-kappaB and type I interferon signaling pathways. *Cell* **141**(3), 483–496 (2010).
43. Xia, X. *et al.* NLRX1 negatively regulates TLR-induced NF- κ B signaling by targeting TRAF6 and IKK. *Immunity* **34**(6), 843–853 (2011).
44. Lai, W. Q. *et al.* The role of sphingosine kinase in a murine model of allergic asthma. *J Immunol* **15** **180**(6), 4323–4329 (2008).
45. Berul, C. I., Aronovitz, M. J., Wang, P. J. & Mendelsohn, M. E. *In vivo* cardiac electrophysiology studies in the mouse. *Circulation* **94**(10), 2641–2648 (1996).
46. Vasconcelos, J. F. *et al.* Administration of granulocyte colony-stimulating factor induces immunomodulation, recruitment of T regulatory cells, reduction of myocarditis and decrease of parasite load in a mouse model of chronic Chagas disease cardiomyopathy. *FASEB J* **27**(12), 4691–4702 (2013).
47. Schijman, A. G. *et al.* International study to evaluate PCR methods for detection of *Trypanosoma cruzi* DNA in blood samples from Chagas disease patients. *Plos Negl Trop Dis* **5**(1), e931 (2011).
48. Schmittgen, T. D. & Livak, K. J. Analyzing real-time PCR data by the comparative C(T) method. *Nat Protoc* **3**(6), 1101–1108 (2008).
49. Green, L. C., Wagner, D. A., Glogowski, K., Skipper, P. L. & Wishnok, J. S. Analysis of nitrate, nitrite and [15N] nitrate in biological fluids. *Anal Biochem* **126**(1), 131–138 (1982).
50. Meira, C. S. *et al.* Physalins B and F, seco-steroids isolated from *Physalis angulata* L., strongly inhibit proliferation, ultrastructure and infectivity of *Trypanosoma cruzi*. *Parasitology* **140**(14), 1811–1821 (2013).

Acknowledgements

This study was supported by funds from the National Council for Scientific and Technological Development (CNPq) and Bahia Research Foundation (FAPESB). The authors thank Adriano Costa de Alcântara for technical assistance in qPCR analysis for parasite load quantification.

Author Contributions

J.F.V. and C.S.M. performed *in vivo* and *in vitro* experiments, P.S.D. and S.G.M. performed functional analysis, J.F.V. and B.S.F.S. performed morphometric analysis, C.K.V.N., V.M.B. and P.D.D. performed inflammasome analysis, D.N.S. performed genic expression analysis, C.S.M. performed transmission electron microscopy analysis and flow cytometry analysis. M.B.P.S. and J.F.V. wrote the manuscript, and designed figures. All authors contributed to experimental design and conceived experiments. R.R.S. and M.B.P.S. provided overall guidance, funding and assisted in manuscript completion.

Additional Information

Supplementary information accompanies this paper at doi:[10.1038/s41598-017-06275-z](https://doi.org/10.1038/s41598-017-06275-z)

Competing Interests: The authors declare that they have no competing interests.

Publisher's note: Springer Nature remains neutral with regard to jurisdictional claims in published maps and institutional affiliations.



Open Access This article is licensed under a Creative Commons Attribution 4.0 International License, which permits use, sharing, adaptation, distribution and reproduction in any medium or format, as long as you give appropriate credit to the original author(s) and the source, provide a link to the Creative Commons license, and indicate if changes were made. The images or other third party material in this article are included in the article's Creative Commons license, unless indicated otherwise in a credit line to the material. If material is not included in the article's Creative Commons license and your intended use is not permitted by statutory regulation or exceeds the permitted use, you will need to obtain permission directly from the copyright holder. To view a copy of this license, visit <http://creativecommons.org/licenses/by/4.0/>.

© The Author(s) 2017

5. DISCUSSÃO

Uma questão central relacionada à CCC é a persistência de uma resposta inflamatória característica, que é responsável pelas lesões no miocárdio. Este dano é, em última instância, responsável pelo desenvolvimento da insuficiência cardíaca e eventualmente morte súbita, por arritmia cardíaca (MARIN-NETO *et al.*, 2010). A terapia convencional é baseada no uso de antiparasitários, eficientes em reduzir a carga parasitária, contudo não conseguem parar ou reverter o dano ao miocárdio (JÚNIOR *et al.*, 2017). Assim, é necessário desenvolver novas estratégias terapêuticas que permitam modificar os mecanismos imunológicos do hospedeiro e reverter o curso da doença. Nesse contexto, o nosso grupo de pesquisa vem buscando identificar compostos com atividade imunomoduladora e anti-*T. cruzi*, visando encontrar alternativas terapêuticas capazes de controlar a inflamação e a carga parasitária na CCC (Anexo IV-X). O presente estudo reforça os efeitos benéficos de duas moléculas com efeito dual antiparasitário e imunomodulador sobre a modulação da fibrose e inflamação no coração em modelo de cardiomiopatia chagásica crônica, já descrito anteriormente para o G-CSF (VASCONCELOS *et al.*, 2013).

Inicialmente investigamos os efeitos imunomoduladores do BA5 e identificamos um efeito potente sobre a ativação de macrófagos e linfócitos. O BA5, em uma potência superior ao BA, diminuiu a produção de mediadores inflamatórios, tais como NO e TNF α , em cultura de macrófagos. Consistente com estes dados, o BA5 também suprimiu a ativação do NF- κ B, um fator de transcrição essencial na regulação gênica de inúmeros mediadores inflamatórios, como o TNF α (LAWRENCE; WILLOUGHBY; GILROY, 2002). Além disso, em um modelo experimental de ligação e perfuração cecal, demonstrou-se que o tratamento com BA reduz a taxa de mortalidade e melhora a função pulmonar e renal através da regulação negativa de NF κ B (LINGARAU, 2015a, b). Em concordância com esses dados, observamos um efeito protetor do BA5 em um modelo de choque endotóxico induzido por LPS.

Embora existam vários relatos sobre a atividade antiinflamatória do ácido betulínico e seus derivados, pouco se sabe sobre os efeitos dessas moléculas na função dos linfócitos. Nós demonstramos que o BA5 possui uma atividade antiproliferativa em culturas de linfócitos e sobre citocinas chaves, tais como IL-2 e IFN γ , para a ativação e proliferação de linfócitos (BOYMAN; SPRENT, 2012; SILVA *et al.*, 2015), sendo este

efeito aproximadamente 20 vezes maior do que o ácido betulínico e relacionado ao direcionamento do linfócito para uma morte celular por apoptose.

O efeito antiproliferativo desta molécula está relacionado à inibição da atividade da calcineurina, uma enzima que desempenha um papel crítico na ativação de linfócitos T por meio da ativação do fator nuclear das células T ativadas, o NFAT (RUSNAK; MERTZ, 2000). Com base nos resultados *in vitro*, avaliamos o efeito do BA5 em um modelo de hipersensibilidade do tipo tardia induzida por albumina, que é mediado por linfócitos T. Animais pré-tratados com o BA5 tiveram uma inibição do edema quando comparados aos animais tratados com a solução veículo.

Considerando a semelhança na resposta inflamatória entre a hipersensibilidade do tipo tardia e a CCC, o efeito anti-inflamatório do BA5 observado no modelo de hipersensibilidade do tipo tardia subsidiou a avaliação da resposta farmacológica do BA5 em nosso modelo de CCC (SOARES; PONTES-DE-CARVALHO; RIBEIRO-DOS-SANTOS, 2001).

Um quadro característico da CCC reproduzido no modelo de infecção crônica pela cepa Colombiana de *T. cruzi* é a inflamação e a fibrose no coração (SOARES *et al.*, 2004; ROCHA *et al.*, 2006). Em nosso estudo, um exame de seções cardíacas de camundongos tratados com BA5 mostrou uma redução na inflamação multifocal. Associado à redução de células inflamatórias, o tratamento com o BA5 reduziu a expressão de CD45, um importante marcador pantrópico de leucócitos. De fato, os linfócitos e macrófagos possuem um papel central na CCC, tanto experimental como humana, participando da agressão que leva à destruição e à hipertrofia dos cardiomiócitos, o que desencadeia o remodelamento cardíaco através de um reparo tecidual com fibrogênese (ANDRADE, 1983. HIGUCHI *et al.*, 2003).

Concomitantemente com a redução da inflamação, observamos um decréscimo nos níveis sistêmicos e cardíacos de TNF α e IFN γ , citocinas relacionados ao desenvolvimento da miocardite na doença de Chagas (GOMES *et al.*, 2003). Este decréscimo está associado ao efeito imunomodulador do BA5 no infiltrado celular, pois observamos que *in vitro* o BA5 regula mediadores inflamatórios, tais como o TNF α , NO e NF- κ B em culturas de macrófagos. Além disso, o BA5 possui um efeito antiproliferativo em cultura de linfócitos, que é acompanhado da redução da produção de IL-2 e IFN γ , moléculas chaves na proliferação e ativação de linfócitos (BOYMAN; SPRENT, 2012; SILVA *et al.*, 2015).

O tratamento com o BA5 também resultou em uma redução da fibrose cardíaca, achado este corroborado com a redução da expressão gênica de TGF β e galectina-3, dois fatores pró-fibrogênicos que aumentam a produção e deposição de proteínas da matriz extracelular por meio de fibroblastos (ARÁUJO-JORGE *et al.*, 2012; Anexo III).

Tendo em vista que mediadores inflamatórios como o TNF α e o IFN γ desempenham papéis importantes no controle da infecção por *T. cruzi* (MACHADO *et al.*, 2000; BOSCARDIN *et al.*, 2010), um agente imunomodulador poderia aumentar a carga parasitária na CCC experimental. Entretanto, através da quantificação do DNA de *T. cruzi* no coração, demonstramos que o tratamento com o BA5 não induziu um descontrole da infecção.

Em contrapartida à redução de mediadores pró-inflamatórios, o tratamento com BA5 aumentou a concentração de IL-10 no soro e no coração dos animais chagásicos. Este efeito não foi observado nos animais chagásicos tratados com o DMS ou benzonidazol. De fato, a IL-10 é reconhecida como uma citocina central na regulação da resposta imune em indivíduos assintomáticos com infecção por *T. cruzi* (MENDES-DASILVA *et al.*, 2017). Devido ao papel da IL-10 como imunossupressor, um aumento na produção de IL-10 induzida pelo tratamento com BA5 durante a fase crônica está possivelmente associado a um efeito protetor do hospedeiro contra a resposta inflamatória do tipo 1 (GOMES *et al.*, 2003). Em concordância com os nossos resultados, estudos anteriores demonstraram um aumento da produção de IL-10 induzida pelo tratamento com o ácido betulínico em modelos de sepse induzida por LPS e artrite reumatoide induzida por colágeno do tipo II (Anexo I; MATHEW; RAJAGOPAL, 2017). É possível, que no modelo de CCC, a IL-10 esteja sendo produzida por células T regulatórias, como já observado pelo tratamento com o derivado do ácido betulínico SH479 em um modelo de artrite reumatoide (CHEN *et al.*, 2017).

Tendo em vista o papel dos macrófagos no desenvolvimento da miocardite característica da doença de Chagas, aliado aos níveis elevados de IL-10 induzido pelo tratamento com BA5, uma hipótese é que o tratamento com BA5 altera as subpopulações de macrófagos. Macrófagos com fenótipo M1 são importantes no controle de infecções e são caracterizados pela produção de citocinas pró-inflamatórias, tais como IL-1 β , IL-6, IL-12, IL-23 e TNF α (MOGHADDAM *et al.*, 2018). Contudo, a ativação excessiva ou não resolvida de macrófagos M1 pode causar inflamação crônica e danos teciduais (VALLEDOR *et al.*, 2010). Uma mudança do perfil de macrófagos

M1 para M2 ocorre naturalmente durante a resolução da inflamação e estes são caracterizados por terem um perfil anti-inflamatório ou reparador e pela produção de IL-10 e TGF β (JABLONSKI *et al.*, 2015; MOGHADDAM *et al.*, 2018). Em nosso trabalho, a polarização ao fenótipo anti-inflamatório/macrófago M2 foi evidenciada por uma diminuição na expressão da *NOS2* e demais citocinas pró-inflamatórias e o aumento da expressão de marcadores M2 como *Arg1* e *CHI3* em camundongos tratados com BA5.

Embora o tratamento com BA5 tenha promovido uma diminuição na inflamação e na fibrose, o ganho funcional não foi observado nas doses testadas. No entanto, é possível que um tratamento mais precoce ou uma terapia combinada com benzonidazol, previamente consolidado como sinérgica, traga ganhos adicionais (Anexo III).

Dessa forma, apresentamos mecanismos múltiplos de ação do BA5, sumarizados na **figura 6**, que promovem a redução da inflamação e fibrose no nosso modelo de cardiomiopatia chagásica crônica. Os dados apresentados demonstram um potente efeito anti-inflamatório do BA5 relacionado à produção de IL-10 e uma transição de uma subpopulação de macrófagos M1 com perfil inflamatório, para uma subpopulação M2 com um perfil anti-inflamatório.

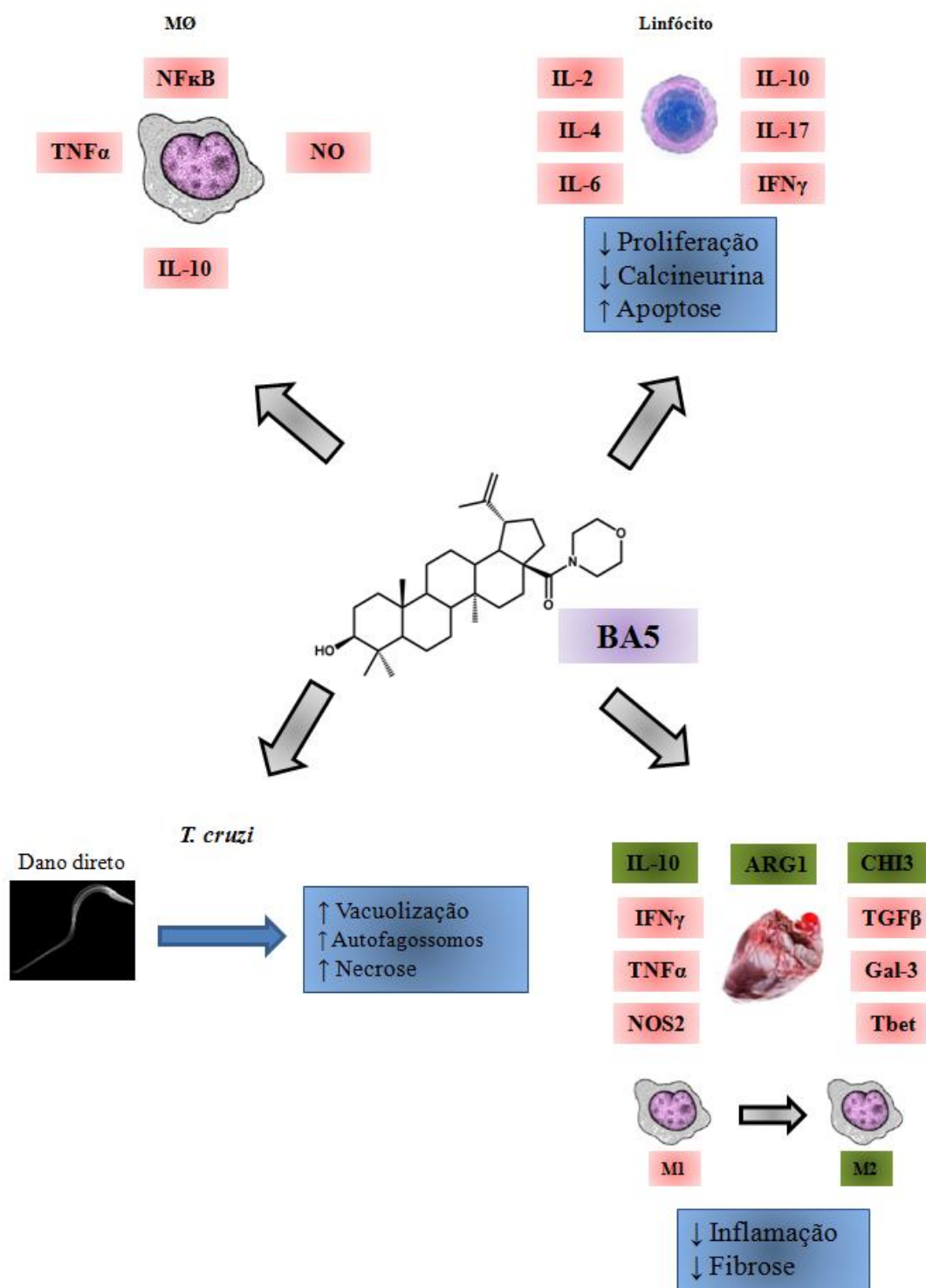


Figura 6. Representação esquemática da ação do BA5 no modelo de CCC experimental. Os mediadores em verde foram modulados positivamente pelo BA5, enquanto os mediadores em vermelho apresentaram uma modulação negativa pelo BA5.

Testamos, a seguir, o DMS, uma molécula com propriedades farmacológicas duais, atuando como antiparasitário e imunomodulador, no modelo de cardiomiopatia chagásica crônica. De modo semelhante ao observado com o BA5, o DMS reduziu a fibrose e o infiltrado inflamatório no coração dos animais chagásicos crônicos. Esses efeitos foram correlacionados à redução na produção de mediadores inflamatórios, tais como $IFN\gamma$ e $TNF\alpha$, importantes para o desenvolvimento da miocardite chagásica (GOMES *et al.*, 2003). Em consonância com este achado, foi recentemente demonstrado que o FTY720, uma droga que também inibe a via S1P, modula a ativação de linfócitos T humanos e reduz os níveis de $IFN\gamma$ (MAZZOLA *et al.*, 2015).

A expressão gênica de $TGF\beta$ e galectina-3, dois fatores pró-fibrogênicos (ARÁUJO-JORGE *et al.*, 2012), também foi modulada pelo DMS. Sabe-se que, no miocárdio, a S1P induz o remodelamento cardíaco através da ativação de proteínas da família GTPase Rho, que por meio dos receptores $S1P_2$ e/ou $S1P_3$, levam à transativação da via do $TGF\beta$. Esta citocina desencadeia a sinalização da esfingosina cinase 1 com consequente aumento na expressão do receptor S1P, o que agrava ainda mais os danos cardíacos (TAKUWA *et al.*, 2010). Camundongos transgênicos superexpressando a esfingosina cinase 1 apresentam fibrose no coração (TAKUWA *et al.*, 2010). Em concordância com os nossos dados obtidos na CCC, a atenuação da fibrose pelo DMS e FTY720 já foi descrita em um modelo de obstrução uretral unilateral, o que sugere uma correlação entre os níveis de S1P e de fibrose (SHUNJI *et al.*, 2013).

A redução dos mediadores inflamatórios $TNF\alpha$ e o $IFN\gamma$ poderia aumentar a carga parasitária na CCC experimental (MACHADO *et al.*, 2000; BOSCARDIN *et al.*, 2010). Entretanto, através da quantificação do DNA de *T. cruzi* no coração, demonstramos que o tratamento com o DMS causou a redução da carga parasitária de forma substancial, sugerindo uma atividade antiparasitária dessa molécula. Utilizando formas tripomastigotas, observamos que o DMS induz a morte celular do parasita por apoptose. Foi possível identificar também diversas alterações na ultraestrutura induzidas pelo tratamento com o DMS, em especial alterações na mitocôndria, uma intensa vacuolização e o aparecimento de figuras mielínicas, estruturas sugestivas de morte celular por autofagia (VANNIER-SANTOS; DE CASTRO, 2009). Em comparação com o benzonidazol, o DMS é cerca de cinco vezes mais potente, confirmando que este composto é não apenas um modulador de inflamação, mas também um agente antiparasitário eficaz. Trabalhos anteriores demonstram que a depleção de esfingosinas

cinases, induzida pelo DMS, reduziu seletivamente a viabilidade celular das formas infectantes do *T. brucei* (PASTERNAK *et al.*, 2015).

Embora ainda não esteja completamente elucidado o mecanismo de ação antiparasitária, uma possibilidade é que o bloqueio de esfingosina cinases do parasita com o DMS altere a composição de fosfolípidios na membrana plasmática. Estudos anteriores demonstram a atividade antiparasitária de outros inibidores de esfingosina cinases. O CAY10621, o PF543 e o SKI 2 são inibidores seletivos da esfingosina cinase 1 e possuem atividade tripanocida *in vitro* contra o *T. brucei*, com valores de CI_{50} variando de 0,002 a 0,5 μ M. Contudo, não existe uma correlação entre o papel das esfingosina cinases e a atividade tripanocida (JONES; KAISES; AVERY, 2015). O esfingolípido FTY720, um reconhecido inibidor da SIP, também possui uma atividade tripanocida potente frente a diferentes cepas do *T. brucei*, com valores de CI_{50} variando entre 0,072 a 1,98 μ M. Entretanto, quando testado em um modelo murino de infecção aguda por *T. brucei rhodesiense*, a depleção da SIP induzida por este fármaco não foi suficiente para reduzir os parasitos circulantes (JONES; KAISES; AVERY, 2015).

Além de um efeito direto em células parasitárias, o DMS também demonstrou um efeito antiparasitário indireto, através da indução da produção de NO e espécies reativas de oxigênio (EROs) em macrófagos infectados *in vitro*. De fato, sabe-se que a esfingosina e seus análogos DMS e FTY720 atuam como padrões moleculares associados ao dano (DAMPs), induzindo secreção de IL-1 β e promovendo a ativação de inflamassoma (LUHESHI *et al.*, 2013). Tanto o DMS quanto o FTY720 são capazes de induzir a produção de IL-1 β , e nossos dados reforçam a capacidade do DMS para ativar a via do inflamassoma (GONÇALVES *et al.*, 2013; DEY *et al.*, 2014). A infecção por *T. cruzi* também induziu a ativação do inflamassoma em camundongos, sendo um fator importante de controle da infecção pela regulação da produção de óxido nítrico e EROs (SILVA *et al.*, 2013).

No presente estudo demonstramos que o DMS induz a ativação da via do inflamassoma em macrófagos infectados, fato evidenciado pelo aumento da ativação de caspase 1 e produção de IL-1 β . A ativação do inflamassoma tem se mostrando essencial para a defesa do hospedeiro contra uma grande gama de agentes infecciosos, dentre eles: *Staphylococcus aureus*, *Legionella pneumophila*, *Bacillus anthrax*, *Salmonella entérica* e *Candida albicans* (FRANCHI; MUNOZ-PLANILLO; NUNEZ, 2012). Recentemente, o inflamassoma Nlrp3 dependente de IL-1 β mostrou promover resistência a *L. amazonensis* em camundongos B/6 induzindo a produção de NO mediada por NOS2

(LIMA-JUNIOR *et al.*, 2013). Estes estudos também descobriram que o inflamassoma foi importante para o controle da infecção *in vivo* por *L. braziliensis* e *L. infantum*. No presente trabalho, observamos que a ativação do inflamassoma induzida pelo DMS contribui para o controle da infecção pelo *T. cruzi* através da indução da produção de NO e ROS em macrófagos infectados.

Em contrapartida ao aumento da citocina pro-inflamatória IL-1 β , o tratamento de macrófagos com o DMS reduziu a produção de TNF α e a IL-6, moléculas pro-inflamatórias *in vitro* e *in vivo*. Isto pode estar relacionado a modulação do NF- κ B observada em nosso estudo e em trabalhos anteriores CUI *et al.*, 2010; ZHANG *et al.*, 2015). A análise por microarranjo de PCR indicou que o DMS induz a expressão de genes do inflamassoma conhecidos por suprimirem a ativação do NF- κ B, tais como Nlrc5 e Nlr1, evidenciando a correlação da ativação do inflamassoma com o efeito anti-inflamatório do DMS (CUI *et al.*, 2010; ZHANG *et al.*, 2015).

Dessa forma, apresentamos mecanismos múltiplos de ação do DMS, sumarizados na **figura 7**, que promovem a redução da inflamação, fibrose e parasitismo no modelo de cardiomiopatia chagásica crônica. Os dados apresentados demonstram um potente efeito do DMS sobre diferentes formas do *T. cruzi* e sobre a ativação de linfócitos e macrófagos, células com um papel central no estabelecimento da cardiomiopatia chagásica. As propriedades antiparasitárias e imunomoduladoras do DMS refletiram em um potente efeito na modulação da fibrose, inflamação e parasitismo em um modelo de cardiomiopatia chagásica crônica.

Diversos estudos vêm demonstrando os efeitos benéficos do uso de imunomoduladores, visando ao reposicionamento da resposta inflamatória na CCC (BRAZÃO *et al.*, 2015; VILAR-PEREIRA *et al.*, 2016; GONZÁLEZ-HERRERA *et al.*, 2017). A combinação de benzonidazol com pentoxifilina, uma metilxantina inibidora de fosfodiesterase, reduz os níveis de NO e TNF α no coração. Este efeito, atrelado à atividade antiparasitária do benzonidazol, diminui a inflamação, a fibrose e a carga parasitária no coração, o que resulta em uma melhora funcional da atividade elétrica do coração (VILAR-PEREIRA *et al.*, 2016). O uso associado do benzonidazol com sinvastatina, estatina utilizado no tratamento de dislipidemias, também induz a redução de inflamação e fibrose no coração de animais chagásicos crônicos (GONZÁLEZ-HERRERA *et al.*, 2017). Estes achados, juntamente com os dados apresentados no presente trabalho, reforçam a ideia de que esquemas terapêuticos visando à diminuição

da carga parasitária e a modulação da inflamação consiste em uma estratégia promissora para o tratamento da CCC.

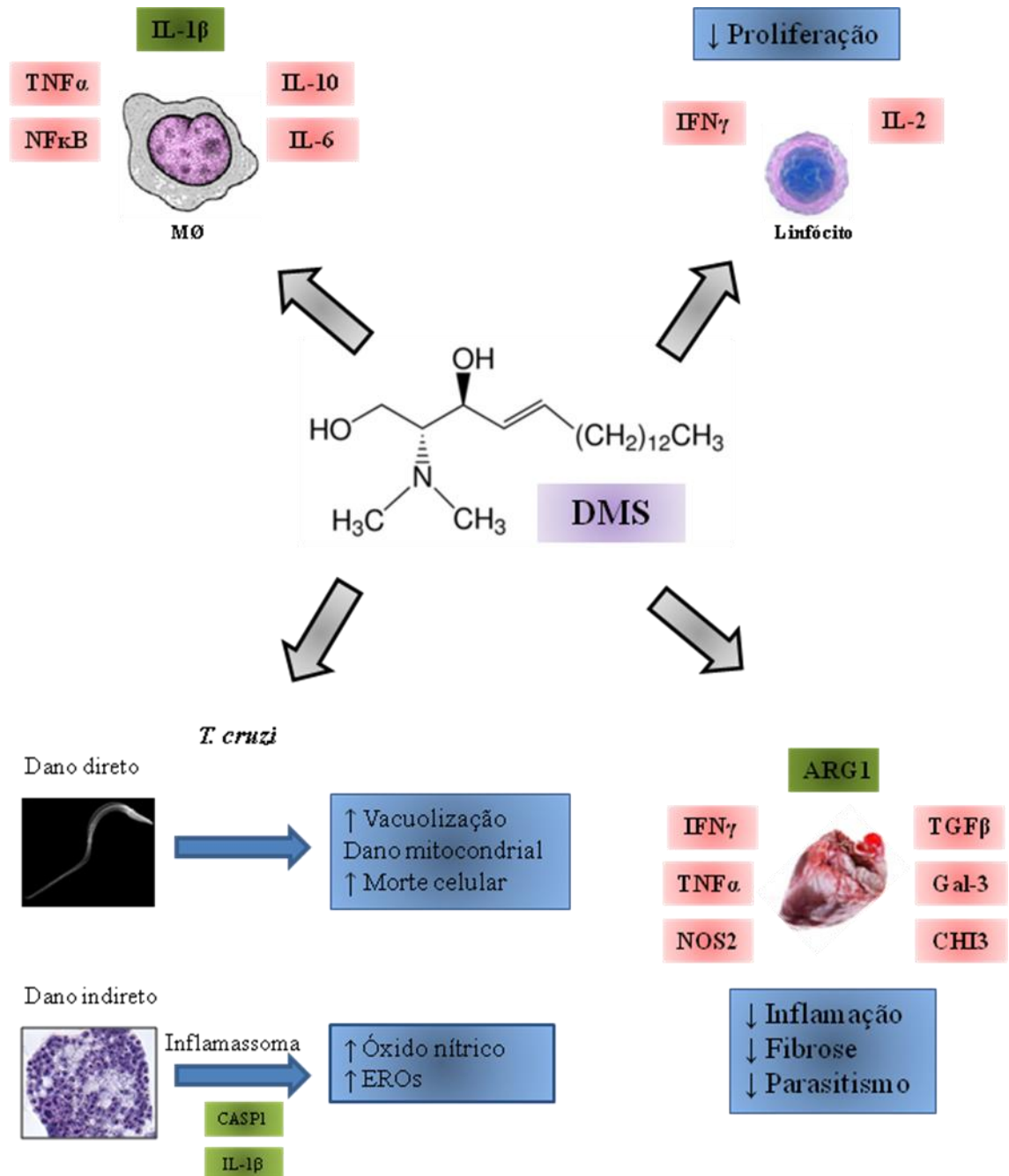


Figura 7. Representação esquemática da ação do DMS no modelo de CCC experimental.

Os mediadores em verde foram modulados positivamente pelo DMS, enquanto os mediadores em vermelho apresentaram uma modulação negativa pelo DMS.

6. CONCLUSÃO

O presente estudo reforça a ideia de que moléculas com propriedades farmacológicas duais, antiparasitárias e imunomoduladoras, podem ser benéficas no tratamento da cardiomiopatia chagásica crônica. A utilização do BA5 e do DMS reduziu a inflamação e fibrose no coração de animais chagásicos. A modulação da resposta imune patogênica foi alcançada sem afetar o controle da infecção, característica altamente desejada no cenário da clínica. Sendo assim, o nosso estudo valida a utilização de moléculas com mecanismos múltiplos de ação para o tratamento da CCC.

REFERÊNCIAS

ALARCÓN DE NOYA, B. et al. Large urban outbreak of orally acquired acute Chagas disease at a school in Caracas, Venezuela. **Journal of Infectious Disease**, v. 201, n. 9, p. 1308-1315, 2010.

ANDRADE, S. G. Morphological and behavioral characterization of *Trypanosoma cruzi* strains. **Revista da Sociedade Brasileira de Medicina Tropical**, v. 18, p. 29-46, 1985.

ANDRADE, Z. Mechanisms of myocardial damage in *Trypanosoma cruzi* infection. **Ciba Foundation Symposium**, v. 99, p. 214-233, 1983.

ANDRADE, Z. **Patologia da doença de Chagas**. In: BRENER, Z.; ANDRADE, Z.; BARRAL- NETO, M. (Eds.), *Trypanosoma cruzi* e Doença de Chagas, 2 ed. Rio de Janeiro: Guanabara Koogan, 2000, p. 201–230.

ANDRADE, J. P. et al. Latin American Guidelines for the diagnosis and treatment of Chagas heart disease: executive summary. **Arquivos Brasileiros de Cardiologia**, v. 96, p. 434-442, 2011.

ARAÚJO-JORGE, T. C. et al. Pivotal role for TGF- β in infectious disease: the case of *Trypanosoma cruzi* infection and its consequent chagasic cardiomyopathy. **Cytokines Growth Factors Review**, v. 19, n. 5-6, p. 405-413, 2012.

ARISH, M. et al. Sphingosine-1-phosphate signaling: unraveling its role as a drug target against infectious disease. **Drug Discovery Today**, v. 21, n. 1, p. 133-142, 2016.

AUFDERHEIDE, A. C. et al. A 9,000-year record of Chagas' disease. **Proceedings of the National Academy of Sciences of the United States of America**, v. 101, n. 7, p. 2034-2039, 2004.

BALTINA, L. A. *et al.* Lupane triterpenes and derivatives with antiviral activity. **Bioorganic & Medicinal Chemistry Letters**, v. 13, n. 20, p. 3549-3552, 2003.

BASILE, L. et al. The current screening programme for congenital transmission of Chagas disease in Catalonia, Spain. **Europe's Journal on Infectious Disease Surveillance, Epidemiology, Prevention and Control**, v. 16, n. 38, p. 19972, 2011.

BASTOS, C. J. C. et al. Clinical outcomes of thirteen patients with acute Chagas disease acquired through oral transmission from two urban outbreaks in northeastern Brazil. **PLOS Neglected Diseases**, v. 4, n. 6, p. e711, 2010.

BENVENUTI, L. A. et al. Chronic American trypanosomiasis: parasite persistence in endomyocardial biopsies is associated with high-grade myocarditis. **Annals Tropical Medicine and Parasitology**, v. 102, n. 6, p. 481-7, 2008.

BENZIGER, C. P.; DO CARMO, G. A. L.; RIBEIRO, A. L. P. Chagas cardiomyopathy: Clinical presentation and management in the Americas. **Cardiology Clinics**, v. 35, n. 1, p. 31-47, 2017.

BERN, C. Chagas' disease. **New England Journal of Medicine**, v. 373, n. 5, p. 456-466, 2015.

BONNEY, K. M.; ENGMAN, D. M. Autoimmune pathogenesis of Chagas heart disease. **The American Journal of Pathology**, v. 185, n. 6, p. 1537, 1547, 2015.

BOSCARDIN, S. B. et al. Chagas' disease: an update on immune mechanisms and therapeutic strategies. **Journal of Cellular and Molecular Medicine**, v. 14, n. 6B, p. 1373–1384, 2010.

BOYMAN, O.; SPRENT J. The role of interleukin-2 during homeostasis and activation of the immune system. **Nature Reviews Immunology**, v. 12, n. 3, p. 180-190, 2012.

BRAZÃO, V. et al. Immunomodulatory properties and anti-apoptotic effects of zinc and melatonin in an experimental model of chronic Chagas disease. **Immunobiology**, v. 220, n. 5, p. 626-633, 2015.

BRENER, Z.; ANDRADE, Z. A.; BARRAL-NETO, M. *Trypanosoma cruzi e a doença de Chagas*. 2 ed. Rio de Janeiro: Guanabara Koogan, 2000, p. 152-174.

BRINKMANN, V. et al. Fingolimod (FTY720): discovery and development of an oral drug to treat multiple sclerosis. **Nature Review Drug Discovery**, v. 9, n. 11, p. 883-897, 2010.

BUCKNER, F. S.; URBINA, J. A. Recent developments in sterol 14-demethylase inhibitors for Chagas disease. **International Journal of Parasitology: Drugs and Drug Resistance**, v. 2, p. 236-242, 2012.

CAMARGO, M. M. et al. Glycoconjugates isolated from *Trypanosoma cruzi* but not from *Leishmania* species membranes trigger nitric oxide synthesis as well as microbicidal activity in IFN-gamma-primed macrophages. **Journal of Immunology**, v. 159, p. 6131- 6139, 1997.

CAMPBELL, D. A.; WESTENBERGER, S. J.; STURM, N. R. The determinants of Chagas disease: connecting parasite and host genetics. **Current Molecular Medicine**, v. 4, n. 6, p. 549-562, 2004.

CASTRO, J. A.; DE MECCA, M. M.; BATERL, L. C. Toxic side effects of drugs used to treat Chagas' disease (American trypanosomiasis). **Human Experimental Toxicology**, v. 25, n. 8, p. 471-479, 2006.

CHAGAS, C. Nova tripanozomiaze humana: estudos sobre a morfologia e o ciclo evolutive do *Schizotrypanum cruzi* n. gen. n. sp., agente etiológico de nova entidade mórbida do homem. **Memórias do Instituto Oswaldo Cruz**, v. 1, n. 2, p. 159-218, 1909.

CHANDRAMU, C. et al. Isolation, characterization and biological activity of betulinic acid and ursolic acid from *Vitex negundo* L. **Phytotherapy Research**, v. 17, p. 127-134, 2003.

CHEN, S. et al. A betulinic acid derivative SH479 inhibits collagen-induced arthritis by modulating T cell differentiation and cytokine balance. **Biochemical Pharmacology**, v. S0006-2952, n. 16, p. 30368-30473, 2017.

CLAYTON, J. Chagas disease: pushing through the pipeline. **Nature**. v. 465, suppl. S12-S15, 2010.

COURA, J. R. The main sceneries of Chagas disease transmission. The vectors, blood and oral transmissions - A comprehensive review. **Memórias do Instituto Oswaldo Cruz**, v. 110, n. 3, p. 277-282, 2015.

COURA, J. R.; Borges-Pereira, J. Chagas disease: 100 years after its discovery. A systematic review. **Acta Tropica**, v. 115, p. 5-13, 2010.

COURA, J. R.; DIAS, J. C. P. Epidemiology, control and surveillance of Chagas disease: 100 years after its discovery. **Memórias do Instituto Oswaldo Cruz**, v. 104, n. i, p. 31, p. 227-282, 2009.

CUI, J. et al. NLRC5 negatively regulates the NF-kappBA and type I interferon signaling pathways. **Cell**, v. 141, n. 3, p. 483–496, 2010.

CUNHA-NETO, E. et al. Immunological and non-immunological effects of cytokines and chemokines in the pathogenesis of chronic Chagas disease cardiomyopathy. **Memórias do Instituto Oswaldo Cruz**, v. 104, p. 252–258, 2009.

CUNHA-NETO, E. et al. Autoimmunity. **Advances in Parasitology**, v. 76, p. 129-152, 2011.

CUNHA-NETO, E.; CHEVILLARD C. Chagas disease cardiomyopathy: immunopathology and genetics. **Mediators Inflammation**, v. 2014, ID 683230, 2014.

DE SOUZA, W. Basic cell biology of *Trypanosoma cruzi*. **Current Pharmaceutical Design**, v. 8, n. 4, p. 269-85, 2002.

DEY, N. et al. Caspase-1/ASC inflammasome-mediated activation of IL-1 β -ROS-NF κ B pathway for control of *Trypanosoma cruzi* replication and survival is dispensable in NLRP3-/- macrophages. **PLOS One**, v. 9, n. 11, p. e111539, 2014.

DRUGS FOR NEGLECTED DISEASES, INICIATIVE. **Drug trial for leading parasitic killer of the Americas shows mixed results but provides new evidence for improved therapy.** Disponível em: <http://www.dndi.org/media-centre/press-releases/1700-e1224.html?highlight=WyJIMTyNCJd>. Acesso em: 20 dez. 2017.

DUTRA, W. O.; MENEZES, C. A. S.; MAGALHÃES, L. M. D.; GOLLOB, K. J. Immunoregulatory networks in human Chagas disease. **Parasite immunology**, v. 36, n. 8, p. 377-387, 2014.

EDSALL, L. C. et al. N-N-dimethylsphingosine is a potent competitive inhibitor of sphingosine kinase but not of protein kinase C: modulation cellular levels of sphingosine-1-phosphate ceramide. **Biochemistry**, v. 37, p. 12892-12898, 1998.

FILARDY, L. S.; BRENER, Z. Susceptibility and natural resistance of *Trypanosoma cruzi* strains to drugs used clinically in Chagas disease. **Transactions of the Royal Society of Tropical Medicine Hygiene**, v. 81, n. 5, p. 755-759, 1987.

FRANCHI, L.; MUNOZ-PLANILLO, R.; NUNEZ, G. Sensing and reacting to microbes through the inflammasomes. **Nature Immunology**, v. 13, p. 325-332, 2012.

FRIGHETTO, N. et al. Purification of betulinic acid from *Eugenia florida* (Myrtaceae) by high-speed counter-current chromatography. **Phytochemical Analysis**, v. 16, p. 411-414, 2005.

FUJIOKA, T. et al. Anti-AIDS agents, 11. Betulinic acid and platanic acid as anti-HIV principles from *Syzygium claviflorum*, and the anti-HIV activity of structurally related triterpenoids. **Journal of Natural Products**, v. 57, p. 243-247, 1994.

GARAVAGLIA, P. A. et al. Putative role of the aldo-keto reductase from *Trypanosoma cruzi* in benznidazole metabolism. **Antimicrobial Agents and Chemotherapy**, v, 60, n. 5, p. 2664-2670, 2016.

GARCIA, E. S.; AZAMBUJA, P. Development and interactions of *Trypanosoma cruzi* within the insect vector. **Parasitology Today (Personal ed.)**, v. 7, n. 9, p. 240-244, 1991.

GARCIA, S. et al. Treatment with benznidazole during the chronic phase of experimental Chagas' disease decreases cardiac alterations. **Antimicrobial Agents and Chemotherapy**, v. 49, p. 1-7, 2005.

GLAROS, E. N. et al. Myriocin slows the progression of established atherosclerotic lesions in apolipoprotein E gene knockout mice. **Journal of Lipid Research**, v. 49, n. 2, p. 324-331, 2007.

GOMES, J. A. et al. Evidence that development of severe cardiomyopathy in human Chagas' disease is due to a Th1-specific immune response. **Infection and Immunity**, v. 71, n. 3, p. 1185-1193, 2003.

GONÇALVES, V. M. et al. NLRP3 controls *Trypanosoma cruzi* infection through a caspase-1-dependent IL-1R-independent NO production. **PLOS Neglected Tropical Disease**, v. 7, n. 10, p. e2469, 2013.

GONZÁLEZ-HERRERA, F. et al. Simvastatin attenuates endothelial activation through 15-Epi-Lipoxin A4 production in murine chronic Chagas cardiomyopathy. **Antimicrobial Agents and Chemotherapy**, v. 61, n. 3, p. e02137-16.

HALL, B. S.; WILKINSON, S. R. Activation of benznidazole by trypanosomal type I nitroreductases results in glyoxal formation. **Antimicrobial Agents and Chemotherapy**, v.56, n. 1, p. 115-123, 2012.

HIGUCHI, M. L. et al. The role of active myocarditis in the development of heart failure in chronic Chagas' disease: a study based on endomyocardial biopsies. **Clinical Cardiology**, v. 10, n. 11, p. 665-70, 1987.

HIGUCHI, M. L. et al. Pathophysiology of the heart in Chagas' disease: current status and new development. **Cardiovascular Research**, v. 60, p. 96-107, 2003.

HLA, T.; DANNENBERG, A. J. Sphingolipid signaling in metabolic disorders. **Cell Metabolism**, v. 16, n. 4, p. 420-434, 2012.

HOTEZ, P. J.; Fujiwara, R. T. Brazil's neglected tropical diseases: an overview and a report card. **Microbes and Infection**, v. 16, n. 8, p. 601-606, 2014.

JABLONSKI, K. A. et al. Novel markers to delineate murine M1 and M2 macrophages. **PLOS One**, v. 10, n. 12, p. e0145342, 2015.

JEONG, H. J. et al. Preparation of amino acid conjugates of betulinic acid with activity against human melanoma. **Bioorganic & Medicinal Chemistry Letters**, v. 9, 1201-1204, 1999.

JONES A. J.; KAISER, M.; AVERY, V. M. Identification and characterization of FTY720 for the treatment of human African trypanosomiasis. **Antimicrobial Agents and Chemotherapy**, v. 60, n. 03, p. 1859-1861, 2015.

JUNIOR, P. A. S. et al. Experimental and clinical treatment of Chagas disease: A review. **American Journal of Tropical Medicine Hygiene**, v. 97, n. 5, p. 1289-1303, 2017.

KIM, D. S. H. L. et al. A concise semi-synthetic approach to betulinic acid from betulin. **Synthetic Communications**, v. 27, p. 1607-1612, 1997.

KIM, D. S. et al. Synthesis of betulinic acid derivatives with activity against human melanoma. **Bioorganic & Medicinal Chemistry Letters**, v. 8, p. 1707-1712, 1998.

KIM, J. Y. et al. Development of C-20 modified betulinic acid derivatives as antitumor agents. **Bioorganic & Medicinal Chemistry Letters**, v. 11, p. 2405-2408, 2001.

KIRCHHOFF, L. V. Epidemiology of American trypanosomiasis (Chagas disease). **Advances in Parasitology**, v. 75, p. 1-18, 2011.

KROGH, R. et al. Isolation and identification of compounds with antinociceptive action from *Ipomea pes-caprae* (L.) R. Br. **Pharmazie**, v. 54, p. 464-466, 1999.

LAWRENCE, T.; WILLOUGHBY, D.A.; GILROY, D. W. Anti-inflammatory lipid mediators and insights into the resolution of inflammation. **Nature Reviews Immunology**, v. 2, n. 10, p. 787-795, 2002.

LEE, M. J. et al. Sphingosine-1-phosphate as a ligand for the G protein-coupled receptor EDG-1. **Science**, v. 6, p. 1552-1555, 1998.

LIMA-JUNIOR, D. S. et al. Inflammasome-derived IL-1 β production induces nitric oxide-mediated resistance to *Leishmania*. **Nature Medicine**, v. 19, n. 7, p. 909-915, 2013.

LINGARAJU, M. C. et al. Betulinic acid attenuates lung injury by modulation of inflammatory cytokine response in experimentally-induced polymicrobial sepsis in mice. **Cytokine**, v. 71, n. 1, p. 101-108, 2015a.

LINGARAJU, M. C. et al. Betulinic acid attenuates renal oxidative stress and inflammation in experimental model of murine polymicrobial sepsis. **European Journal of Pharmaceutical Sciences**, v. 70, p. 12-21, 2015b.

LUSHESHI, N. M. et al. Sphingosine regulates the NLRP3-inflammasome and IL-1 β release from macrophages. **European Journal of Immunology**, v. 42, n. 3, p. 716-725, 2012.

MACEYKA, M.; SPIEGEL, S. Sphingolipid metabolites in inflammatory diseases. **Nature**, v. 510, p. 58-67, 2014.

MACHADO, F. S. et al. *Trypanosoma cruzi*-infected cardiomyocytes produce chemokines and cytokines that trigger potent nitric oxide dependent trypanocidal activity. **Circulation**, v. 102, n. 24, p. 3003–3008, 2000.

MACIEL, L. et al. Ventricular arrhythmias are related to the presence of autoantibodies with adrenergic activity in chronic chagasic patients with preserved left ventricular function. **Journal of Cardiac Failure**, v. 18, n. 5, p. 423-31, 2012.

MARIN-NETO, J. A.; SIMÕES, M. V.; SARABANDA, A. V. Chagas heart disease. **Arquivos Brasileiros de Cardiologia**, v. 72, p. 247-80, 1999.

MARIN-NETO, J. A. et al. Chagas heart disease. In: Yusuf S, Cairns JA, Camm AJ, Fallen EL, Gersh BJ, eds. Evidence-based cardiology, 3rd edn. London: BMJ Books, p. 823-841, 2010.

MARTINS-MELO, F. R. et al. Prevalence of Chagas disease in Brazil: a systematic review and meta-analysis. **Acta Tropica**, v. 130, p. 167-174, 2014.

MATHEW, L. E.; RAJAGOPAL, V.; A, H. Betulinic acid and fluvastatin exhibits synergistic effect on toll-like receptor-4 mediated anti-atherogenic mechanism in type II collagen induced arthritis. **Biomedicine & Pharmacotherapy**, v. 93, p. 681-694, 2017.

MATSUO, A. L. et al. *In vitro* and *in vivo* trypanocidal effects of the cyclopalladated compound 7a, a drug candidate for treatment of Chagas disease. **Antimicrobial Agents and Chemotherapy**, v. 54, n. 8, p. 3318-3325, 2010.

MAURYA, S. K. et al. Content of betulin and betulinic acid, antitumor agents of *Zizyphus* species. **Fitoterapia**, v. 60, p. 468-469, 1989.

MAYA, J. D. et al. Chagas disease: Present status of pathogenic mechanisms and chemotherapy. **Biologia Research**, v. 43, p. 323-31, 2010.

MAZZOLA, M. A. et al. Identification of a novel mechanism of action of fingolimod (FTY720) on human effector T cell function through TCF-1 upregulation. **Journal of Neuroinflammation**, v. 12, p. 245, 2015.

MEIRA, C. S. **Investigação da atividade anti-*Trypanosoma cruzi* de esteroides isolados de plantas e derivados sintéticos**. Dissertação (Mestrado em Biotecnologia em Saúde e Medicina Investigativa) – Fundação Oswaldo Cruz, Instituto Gonçalo Moniz, Salvador, 2014.

MENDES-DA-SILVA, L. D. et al. Participation of TLR2 and TLR4 in cytokines production by patients with symptomatic and asymptomatic chronic Chagas disease. **Scandinavian Journal of Immunology**, v. 85, n. 1, p. 58-65, 2017.

MILES, M. A. et al. American trypanosomiasis (Chagas's disease) and the role of molecular epidemiology in guiding control strategies. **British Medicine Journal**, v. 326, p. 1444-1448, 2003.

MINISTÉRIO DA SAÚDE DA BRASIL. Brazilian Consensus on Chagas disease. **Revista da Sociedade Brasileira de Medicina Tropical**, v. 38, p. 7-29, 2005.

MOGHADDAM, A. S. et al. Macrophage plasticity, polarization and function in health and disease. **Journal of Cell Physiology**, in press, 2018, doi: 10.1002/jcp.26429.

MOLINA, I. et al. Randomized trial of posaconazole and benznidazole for chronic Chagas disease. **New England Journal of Medicine**, v. 370, p. 1889-1908, 2014.

MONCAYO, À.; SILVEIRA, A. C. Current epidemiological trends for Chagas disease in Latin America and future challenges in epidemiology, surveillance and health policy. **Memórias do Instituto Oswaldo Cruz**, v. 104, n. Suppl. 1, p. 17-30, 2009.

MOREIRA, D. R. M. et al. Approaches for the development of new anti-*Trypanosoma cruzi* agents. **Current Drug Targets**, v. 10, n. 3, p. 212-231, 2009.

MORILLO, C. A. et al. Randomized trial of benznidazole for chronic Chagas' cardiomyopathy. **New England Journal of Medicine**, v. 373, p. 1295-1306, 2015.

MULLAUER, F. B. et al. Betulinic acid, a natural compound with potent anticancer effects. **Anti-Cancer Drug**, v. 21, p. 215-227, 2010.

MURTA, S. M. et al. Molecular characterization of susceptible and naturally resistant strains of *Trypanosoma cruzi* to benznidazole and nifurtimox. **Molecular and Biochemical Parasitology**, v. 93, n. 2, p. 203-214, 1998.

NEAL, R. A.; VAN BUEREN, J. Comparative studies of drug susceptibility of five strains of *Trypanosoma cruzi* *in vivo* and *in vitro*. **Transactions of the Royal Society of Tropical Medicine Hygiene**, v. 82, n. p. 709-714, 1988.

NOGUEIRA, L. G. et al. Myocardial gene expression of T-bet, GATA-3, Ror- γ t, FoxP3, and hallmark cytokines in chronic Chagas disease cardiomyopathy: an essentially unopposed THI-type response. **Mediators Inflammation**, v. 2014, ID 914326, 2014.

PASTERNAK, D. A. et al. Sphingosine kinase regulates microtubule dynamics and organelle positioning necessary for proper G1/S cell cycle transition in *Trypanosoma brucei*. **mBio**, v. 6, n. 6, p. 1291-1295, 2015.

PATA, M.; HANNUN, Y.; NG, C. K. Y. Plant sphingolipids: decoding the enigma of the Sphinx. **New Phytologist**, v. 185, n. 3, p. 611-630, 2010.

PAVLOVA, N. I. et al. Antiviral activity of betulin, betulinic and betulonic acids against some enveloped and non-enveloped viruses. **Fitoterapia**, v. 74, p. 489-492, 2003.

PÉREZ-MOLINA, J. A.; MOLINA, I. Chagas disease. **Lancet**, v. 391, n. 10115, p. 82-94, 2018.

RASSI, A. Jr.; RASSI, A.; LITTLE, W. C. Chagas heart disease. **Clinical Cardiology**, v. 23, n. 12, p. 883-889, 2000.

RASSI, A. Jr.; RASSI, A.; MARIN-NETO, J. A. Chagas disease. **Lancet**. v. 375, p. 1388-1402, 2010.

REED, S. IL-10 mediates susceptibility to *Trypanosoma cruzi* infection. **Journal of Immunology**, v. 153, n. 7, p. 3135-3140, 1994.

RIBEIRO, A. L. et al. Diagnosis and management of Chagas disease and cardiomyopathy. **Nature Reviews Cardiology**, v. 9, n. 10, p. 576-589, 2012.

ROCHA, N. et al. Characterization of cardiomyopathy function and cardiac muscarinic and adrenergic receptor density adaptation in C57BL/6 mice with chronic *Trypanosoma cruzi* infection. **Parasitology**, v. 133, n. 6, p. 729-737, 2006.

RODRIGUES, M. M.; OLIVEIRA, A. C.; BELLIO, M. The immune response to *Trypanosoma cruzi*: Role of toll-like receptors and perspectives for vaccine development. **Journal of Parasitology Research**, v. 2012, ID 507874, 2012.

ROSSI, M. A. Microvascular changes as a cause of chronic cardiomyopathy in Chagas' disease. **American Heart Journal**, v. 120, n. 1, p. 233-236, 1990.

SATHLER-AVELAR, R. et al. Innate immunity and regulatory T-cells in human Chagas disease: what must be understood? **Memórias do Instituto Oswaldo Cruz**, v. 104, n. SUPPL I, p. 246-51, 2009.

SCHMUNIS, JR. et al. Epidemiology of Chagas disease in non-endemic countries: the role of international migration. **Memórias do Instituto Oswaldo Cruz**, v. 102, n. SUPPL. 1, p. 31-40, 2009.

SCHUNJI, S. et al. Sphingosine-1-phosphate acts as a key molecule in the direct mediation of renal fibrosis. **Physiological Reports**, v. 1, n. 7, p. e00172, 2013.

SILVA, G. K. et al. Apoptosis-associated speck-like protein containing a caspase recruitment domain inflammasomes mediate IL-1 β response and host resistance to *Trypanosoma cruzi* infection. **Journal of Immunology**, v. 191, n. 6, p. 3373–3383, 2013.

SILVA, D. N. et al. Intramyocardial transplantation of cardiac mesenchymal stem cells reduces myocarditis in a model of chronic Chagas disease cardiomyopathy. **Stem Cells Research & Therapy**, v. 5, n. 4, p. 81, 2014.

SILVA, H. B. et al. IFN γ priming effects on the maintenance of effector memory CD4+ T cells and on phagocyte function: evidences from infectious diseases. **Journal of Immunology Research**, v. 2015, p. 202816, 2015.

SOARES, M. B. P.; PONTES-DE-CARVALHO, L.; RIBEIRO-DOS-SANTOS, R. The pathogenesis of Chagas' disease: when autoimmune and parasitic-specific immune responses meet. **Anais da Academia Brasileira de Ciências**, v. 73, n. 4, p. 547-59, 2001.

SOARES, M. B. P. et al. Transplanted bone marrow cells repair heart tissue and reduce myocarditis in chronic chagasic mice. **American Journal of Pathology**, v. 164, n. 2, p. 441-447, 2004.

STEINDEL, M. et al. Characterization of *Trypanosoma cruzi* isolated from humans, vectors, and animal reservoirs following an outbreak of acute human Chagas disease in Santa Catarina State, Brazil. **Diagnostic Microbiology and Infectious Disease**, v. 60, n. 1, p. 25-32, 2008.

SUN, I. C. et al. Anti-AIDS agents. 34. Synthesis and structure-activity relationships of betulin derivatives as anti-HIV agents. **Journal of Medicine Chemistry**, v. 41, p. 4648-4657, 1998.

SUTARIYA, B.; TANEJA, N.; SARAF, M. Betulinic acid, isolated from the leaves of *Syzygium cumuni* (L.) Skeels, ameliorates the proteinuria in experimental membranous

nephropathy through regulating Nrf2/NF- κ B pathways. **Chemical-Biological Interactions**, v. 274, p. 124-137, 2017.

TARLETON, R. L. Immune system recognition of *Trypanosoma cruzi*. **Current Opinion in Immunology**, v. 19, n. 4, p. 430-4, 2007.

TARLETON, R. L. et al. The challenges of Chagas disease-grim outlook or glimmer of hope. **PLOS Medicine**, v. 12, p. e332, 2007.

TEIXEIRA, A. R.; NASCIMENTO, R. J. STURM, N. R. Evolution and pathology in Chagas disease: a review. **Memórias do Instituto Oswaldo Cruz**, v. 101, n. 5, p. 463-491, 2006.

TODOROV, A. G. et al. *Trypanosoma cruzi* induces edematogenic responses in mice and invades cardiomyocytes and endothelial cells *in vitro* by activating distinct kinin receptor (B1/B2) subtypes. **FAPESB Journal**, v. 17, n. 1, p. 73-75, 2003.

TOLEDO, M. J. et al. Effects of specific treatment on parasitological and histopathological parameters in mice infected with different *Trypanosoma cruzi* clonal genotypes. **Journal of Antimicrobial Chemotherapy**, 53, p. 1045-1053, 2004.

URBINA, J. A. Specific chemotherapy of Chagas disease: relevance, current limitations and new approaches. **Acta Tropica**, v. 115, n. 1-2, p. 55-68, 2010.

VALLEDOR, A. F. et al. Macrophages proinflammatory activation deactivation: a question of balance. **Advances in Immunology**, v. 108, n., p. 108-120, 2010.

VANNIER-SANTOS, M. A.; DE CASTRO, S. L. Electron microscopy in antiparasitic chemotherapy: A (close) view to a kill. **Current Drug Targets**, v. 10, n. 3, p. 246-260, 2009.

VILAR-PEREIRA, G. et al. Combination chemotherapy with suboptimal doses of benznidazole and pentoxifylline sustains partial reversion of experimental Chagas' heart disease. **Antimicrobial Agents and Chemotherapy**, v. 60, n. 7, p. 4297-4309, 2016.

VIOTTI, R. et al. Long-term cardiac outcomes of treating chronic Chagas disease with benznidazole versus no treatment: a nonrandomized trial. **Annals of Internal Medicine**, v. 144, n. 10, p.724-734, 2006.

XIE, R. et al. The protective effect of betulinic acid (BA) diabetic nephropathy on streptozotocin (STZ)-induced diabetic rats. **Food & Function**, v. 8, n. 1, p. 299-306, 2017.

WORLD HEALTH ORGANIZATION. **Neglected tropical diseases**. Disponível em: [HTTP://www.who.int/neglected_diseases/diseases/en/](http://www.who.int/neglected_diseases/diseases/en/). Acesso em: 21 dez. 2017a.

WORLD HEALTH ORGANIZATION. **Chagas disease (American trypanosomiasis)**. Disponível em: <http://www.who.int/mediacentre/factsheets/fs340/en>>. Acesso em: 2 dez. 2017b.

YATOMI, Y. et al. N,N-dimethylsphingosine inhibition of sphingosine kinase and sphingosine-1-phosphate activity in human platelets. **Biochemistry**, v. 35, n. 2, p. 626-633, 1996.

YOGEE SWARI, P.; SRIRAM, D. Betulinic acid and its derivatives: A review on their biological properties. **Current Medicinal Chemistry**, v. 12, n. 6, p. 657-666, 2005.

YOSHIDA, N. *Trypanosoma cruzi* infection by oral route: how the interplay between parasite and host components modulates infectivity. **Parasitology International**, v. 57, n. 02, p. 105-109, 2008.

ZHANG, Z. et al. SPHK1 inhibitor suppresses cell proliferation and invasion associated with the inhibition of NF- κ B pathway in hepatocellular carcinoma. **Tumour Biology**, v. 36, n. 3, p. 1503–1509, 2015.

ZUCO, V. Selective cytotoxicity of betulinic acid on tumor cell lines, but not on normal cells. **Cancer Letters**. v. 175, p. 17-25, 2002.

ANEXOS

ANEXO 1

COSTA, J. F. O.; BARBOSA-FILHO, J. M.; MAIA, G. L. A.; GUIMARÃES, E. T.; MEIRA, C. S.; RIBEIRO-DOS-SANTOS, R.; SOARES, M. B. P. Potent anti-inflammatory activity of betulinic acid treatment in a model of lethal endotoxemia. **International Immunopharmacology**, v. 23, p. 469-474, 2014.



Potent anti-inflammatory activity of betulinic acid treatment in a model of lethal endotoxemia



José Fernando Oliveira Costa^a, José Maria Barbosa-Filho^b, Gabriela Lemos de Azevedo Maia^b,
Elisalva Teixeira Guimarães^{a,c}, Cássio Santana Meira^a, Ricardo Ribeiro-dos-Santos^{a,d},
Lain Carlos Pontes de Carvalho^a, Milena Botelho Pereira Soares^{a,d,*}

^a Laboratory of Tissue Engineering and Immunopharmacology Gonçalo Moniz Research Center, Oswaldo Cruz Foundation, Rua Waldemar Falcão, 121, 40296–750, Salvador, Bahia, Brazil

^b Laboratory of Pharmaceutical Technology, Federal University of Paraíba, João Pessoa, Cidade Universitária, s/n, 58051–900, João Pessoa, PB, Brazil

^c Department of Life Sciences, State University of Bahia, Rua Silveira Martins, 2555, 41150–000, Salvador, BA, Brazil

^d Center of Biotechnology and Cell Therapy, São Rafael Hospital, Av. São Rafael, 2152, São Marcos 41253–190, Salvador, BA, Brazil

ARTICLE INFO

Article history:

Received 24 February 2014

Received in revised form 4 September 2014

Accepted 17 September 2014

Available online 1 October 2014

Keywords:

Betulinic acid

Endotoxemia

Anti-inflammatory activity

Macrophages

Cytokines

ABSTRACT

Betulinic acid (BA) is a lupane-type triterpene with a number of biological activities already reported. While potent anti-HIV and antitumoral activities were attributed to BA, it is considered to have a moderate anti-inflammatory activity. Here we evaluated the effects of BA in a mouse model of endotoxic shock. Endotoxemia was induced through intraperitoneally LPS administration, nitric oxide (NO) and cytokines were assessed by Griess method and ELISA, respectively. Treatment of BALB/c mice with BA at 67 mg/kg caused a 100% survival against a lethal dose of lipopolysaccharide (LPS). BA treatment caused a reduction in TNF- α production induced by LPS but did not alter IL-6 production. Moreover, BA treatment increased significantly the serum levels of IL-10 compared to vehicle-treated, LPS-challenged mice. To investigate the role of IL-10 in BA-induced protection, wild-type and IL-10^{-/-} mice were studied. In contrast to the observations in IL-10^{+/+} mice, BA did not protect IL-10^{-/-} mice against a lethal LPS challenge. Addition of BA inhibited the production of pro-inflammatory mediators by macrophages stimulated with LPS, while promoting a significant increase in IL-10 production. BA-treated peritoneal exudate macrophages produced lower concentrations of TNF- α and NO and higher concentrations of IL-10 upon LPS stimulation. Similarly, macrophages obtained from BA-treated mice produced less pro-inflammatory mediators and increased IL-10 when compared to non-stimulated macrophages obtained from vehicle-treated mice. In conclusion, we have shown that BA has a potent anti-inflammatory activity *in vivo*, protecting mice against LPS by modulating TNF- α production by macrophages *in vivo* through a mechanism dependent on IL-10.

© 2014 Elsevier B.V. All rights reserved.

1. Introduction

Betulinic acid (3 β -hydroxy-lup-20(29)-en-28-oic acid; BA), a C-30 carboxylic acid derivative of the ubiquitous triterpene betulin, is a member of the class of lupane-type triterpenes. The molecule is abundant in the plant kingdom and has been isolated from several plant species, including *Zizyphus joazeiro* [1], *Syzigium clariflorum* [2], and *Dolioscarpus schottianus* [3]. A number of reports have shown diverse biological activities of BA, such as anticancer [4], anti-HIV, anti-HSV-1 [5], anti-HBV [6], antihelmintic [6], antinociceptive [7], and antiplasmodial [1,8]. Of particular interest, in view of the large prevalence of chronic inflammatory-degenerative diseases, is the BA anti-inflammatory

activity [9,10]. However, in a number of *in vitro* and *in vivo* models of inflammation, the intensity of the BA anti-inflammatory activity has been considered only moderate (reviewed by [5]).

Sepsis is one of the most frequent complications in surgical patients and one of the leading causes of mortality in intensive care units. Severe sepsis is an important cause of mortality worldwide, and is estimated as directly responsible for 9% of all deaths in the United States [11]. It is defined as an infection-induced syndrome characterized by a generalized inflammatory state and can be caused by infection with Gram-negative or Gram-positive bacteria, fungi, or viruses. Sepsis can also occur in the absence of detectable bacterial invasion and, in these cases, microbial toxins (lipopolysaccharide; LPS) and endogenous cytokines have been implicated as initiators and mediators of the condition [12].

Macrophage activation by LPS results in the release of several inflammatory mediators, including proinflammatory cytokines such as tumor necrosis factor (TNF)- α , interleukin (IL)-1, IL-6, IL-8, and IL-12,

* Corresponding author at: Centro de Pesquisas Gonçalo Moniz, Fundação Oswaldo Cruz, Rua Waldemar Falcão, 121 – Candeal, Salvador, BA, 40296–710. Tel.: +55 71 3176 2260; fax: +55 71 3176 2272.

E-mail address: milena@bahia.fiocruz.br (M.B.P. Soares).

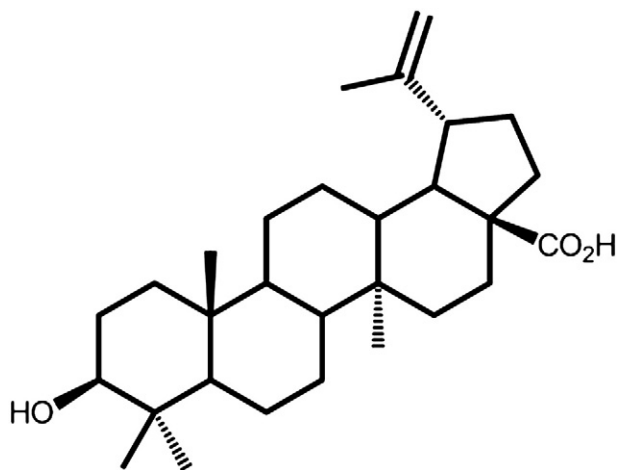


Fig. 1. Molecular structure of betulinic acid.

as well as nitric oxide. The exacerbated production of these mediators by activated macrophages are the main cause of the deleterious consequences of septicemia or endotoxemia, and may lead to hypotension, disseminated intravascular coagulation, neutrophil extravasation to tissues, tissue hypoxia, and death. Conversely, IL-4, IL-10 and IL-13 may function as anti-inflammatory cytokines, modulating macrophage and monocyte responses and inhibiting the production of TNF- α , IL-1, and IL-8 [11–13]. The discovery of new agents capable of down-modulating the production of the inflammatory mediators that play key roles in the installation of sepsis is therefore of great interest for the development of effective treatments. Since BA has been shown to inhibit the TNF- α -induced activation of NF- κ B [14], in this work we investigated the effects of BA in a mouse model of endotoxic shock and on the production of cytokines by activated macrophages.

2. Materials and methods

2.1. General experimental procedures

Melting points were determined using a Geahaka model PF1500 version 1.0 apparatus and were not corrected. The NMR spectra were acquired on a Varian System 500 spectrometer, equipped with a XW4100 HP workstation. High-resolution mass spectra were recorded on a microTOF spectrometer (LC-ITTOF model 225–07 100–34, Bruker) with positive ionization modes of the ESI source. Silica gel 60 (Merck) was used for column chromatography, and Si gel 60 PF254 (Merck)

was used for purification of compounds by preparative TLC. All solvents used were analytical grade (Merck).

2.2. Plant material

Tabebuia aurea (Manso) S. Moore was collected in March 2002 in the surroundings of São João do Cariri, State of Paraíba, Brazil, and identified by botanist Dr. Maria de Fátima Agra of the Universidade Federal da Paraíba. A Voucher specimen (Agra 2337) is deposited at the Herbarium Prof. Lauro Pires Xavier (JPB), Universidade Federal da Paraíba.

2.3. Extraction and isolation of betulinic acid

Five kg of air-dried ground bark of *Tabebuia aurea* (Manso) S. Moore were exhaustively extracted with 95% ethanol. The solvent was evaporated to yield a dark syrup residue (167 g, 3.3%), which was partitioned with water and successively treated with hexane, chloroform, ethyl acetate and n-butanol, yielding 8.5 g (0.2%), 4.1 g (0.08%), 6.2 g (0.13%) and 74 g (1.5%), respectively. The chloroform residue was also subjected to column chromatography over silica gel, and eluted with a chloroform-hexane gradient. Seventy five 100-mL fractions were collected, after analysis by TLC silica gel-60 F254 developed with either I₂ reagent. Combined fractions 41–50 were rechromatographed on CC column silica gel (with a chloroform-methanol gradient) to afford pure betulinic acid (BA) (0.015 g, 0.0003%; Fig. 1). Identification of the betulinic acid was performed by analyzing 1H e 13C NMR spectral data and high-resolution mass spectra compared with those published in the literature [1,15].

2.4. Animals

Male 4- to 6-week old BALB/c, wild-type C57BL/6, and IL-10^{-/-} C57BL/6 mice were used. All mice were raised and maintained at the animal facilities of the Gonçalo Moniz Research Center, Fundação Oswaldo Cruz, Salvador, Brazil, in rooms with controlled temperature (22 ± 2 °C) and humidity (55 ± 10%) and continuous air renovation. Animals were housed in a 12 h light/12 h dark cycle (6 am–6 pm) and provided with rodent diet and water *ad libitum*. All mice, when necessary, were subjected to euthanasia and treated according to the Oswaldo Cruz Foundation guidelines for laboratory animals. The work had prior approval by the institutional Ethics Committee in Laboratory Animal Use.

2.5. Endotoxic shock model

Groups of 11 BALB/c or C57BL/6 mice were used for the lethality assays and groups of 6 BALB/c mice were used for *in vivo* cytokine studies.

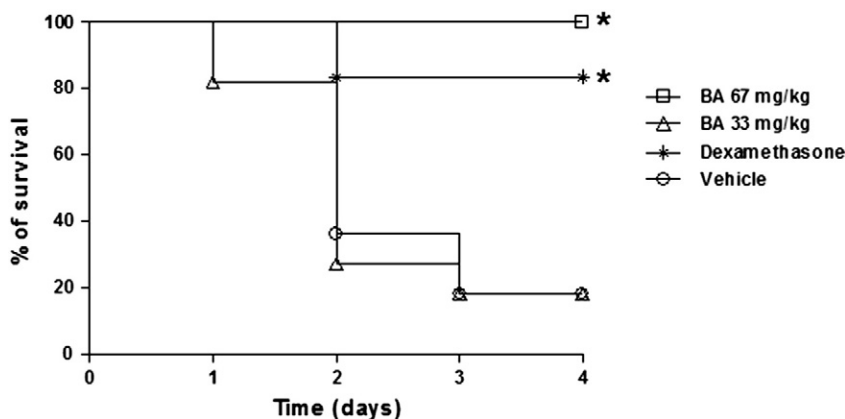


Fig. 2. Survival curve of mice treated with betulinic acid and submitted to endotoxic shock. Male BALB/c mice (n = 11) were treated with betulinic acid (33 and 67 mg/kg) or vehicle (5% DMSO in saline) and challenged with LPS 90 min later, intraperitoneally administered. Survival was monitored during 96 hours after LPS challenge. Results are from one experiment of two replicates performed. *P < 0.05 compared to vehicle group. Statistical analysis was carried out using Logrank (Mantel Cox).

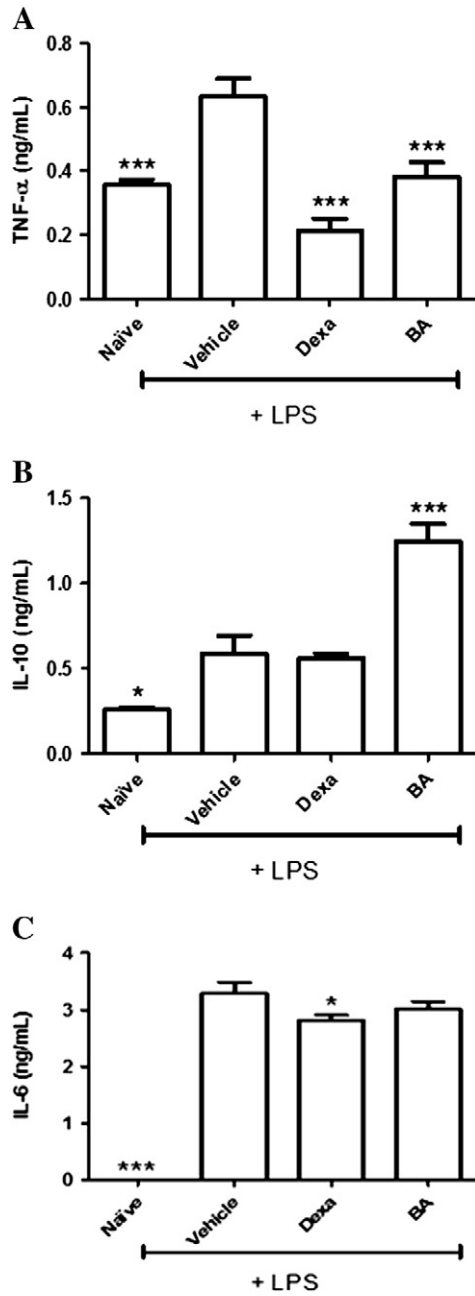


Fig. 3. Assessment of cytokine production after bacterial lipopolysaccharide (LPS) challenge. BALB/c mice (6 animals per group) were injected intraperitoneally with betulinic acid (BA, 67 mg/kg), dexamethasone (Dexa, 0.5 mg/kg) or vehicle (5% DMSO in saline), 90 min prior to intraperitoneal LPS administration. The mice were sacrificed 90 min later, to collect sera for assessment of TNF- α (A), IL-10 (B), and IL-6 (C), by ELISA. Values represent the means \pm SEM of six determinations obtained in one of two experiments performed. * $P < 0.05$, *** $P < 0.001$ compared to untreated group stimulated with LPS. ANOVA followed by Newman-Keuls multiple comparison test.

Mice were treated with BA at different doses (see figure legends), dexamethasone (0.5 mg/kg, Sigma-Aldrich, St. Louis, MO) or vehicle (5% of DMSO in saline), by the intraperitoneal (i.p.) route. Ninety minutes later, animals were challenged with 600 μ g of LPS (LPS from serotype 0111:B4 *Escherichia coli*, Sigma-Aldrich; previously determined LD_{90–100} = 42.8 mg/kg) in saline by the i.p. route. Mice were monitored daily for 4 days. To evaluate the serum cytokine levels, mice were anesthetized with a combination of ketamine (100 mg/kg) and xilazine (10 mg/kg), 60 min after injection of 600 μ g of LPS, for blood collection via the brachial plexus. Serum samples were immediately used or stored at -80°C until use.

2.6. Macrophage cell cultures

Peritoneal exudate cells were obtained by washing, with cold Dulbecco's modified Eagle's medium (DMEM; Life Technologies, GIBCO-BRL, Gaithersburg, MD), the peritoneal cavity of mice 4–5 days after injection of 3% thioglycolate in saline (1.5 mL per mouse). Cells were washed twice with DMEM, resuspended in DMEM supplemented with 10% fetal bovine serum (Cultilab, Campinas, Brazil) and 50 μ g/mL of gentamycin (Novafarma, Anápolis, Brazil), and plated in 96-well tissue culture plates at 2×10^5 cells per 0.2 mL per well. After 2 hours of incubation at 37°C , non-adherent cells were removed by two washes with DMEM. Macrophages were then treated with LPS (500 ng/mL) in the absence or presence of BA (10 or 20 μ M) or dexamethasone (20 μ M), and incubated at 37°C . Cell-free supernatants were collected 4 or 24 h after incubation and kept at -80°C for cytokine and nitric oxide determinations.

To assess cytokine production by resident macrophages, groups of male BALB/c mice were injected with BA (67 mg/kg), dexamethasone (0.5 mg/kg) or 5% of DMSO in saline, by the i.p. route. After 90 min, the mice were subjected to euthanasia for macrophage collection by means of peritoneal wash using cold DMEM. Cells were washed twice with DMEM, resuspended in DMEM supplemented with 10% fetal bovine serum and 50 μ g/ml of gentamycin, and plated in 96-well tissue culture plates at 2×10^5 cells per 0.2 mL per well. After 2-hour incubation at 37°C , non-adherent cells were removed by two medium changes. Macrophages were then stimulated or not with LPS (500 ng/mL), as indicated in the text and figure legends and further incubated at 37°C and 5% CO₂. Cell-free supernatants were collected 4 and 24 h after incubation for cytokines and nitric oxide measurement.

2.7. Measurement of cytokines and nitric oxide concentrations

TNF- α , IL-6, and IL-10 concentrations in serum samples or in supernatants from macrophage cultures, were determined by enzyme-linked immunosorbent assay (ELISA), using the DuoSet kit from R&D Systems (Minneapolis, MN), according to the manufacturer's instructions. After incubation with a streptoavidin-peroxidase conjugate (Sigma-Aldrich), the reaction was developed using H₂O₂ and 3,3',5,5'-tetramethylbenzidine (Sigma-Aldrich) and the absorbance to 450 nm-wave length light read in a spectrophotometer. Quantification of nitric oxide was done indirectly through determination of nitrite concentrations 24 h after incubation, using the Griess method [16].

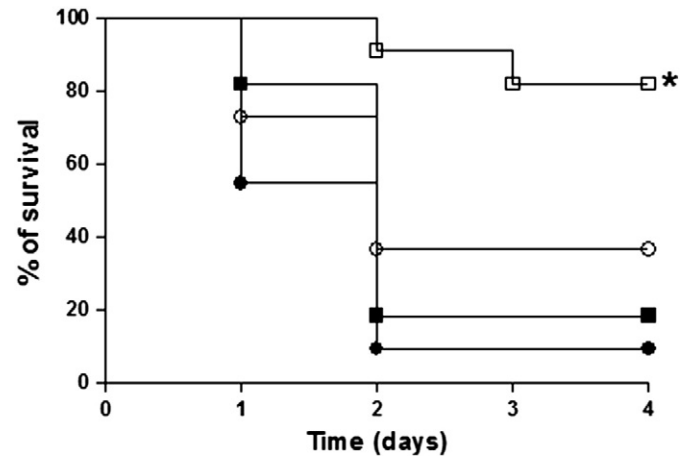


Fig. 4. Survival curve of IL-10^{+/+} and IL-10^{-/-} mice treated with betulinic acid and submitted to endotoxic shock. Groups of male IL-10^{+/+} and IL-10^{-/-} C57BL/6 mice (n = 11) were treated with betulinic acid (67 mg/kg) or vehicle (5% DMSO in saline) and challenged with intraperitoneal LPS administration 90 min later. Survival was monitored during 96 hours after LPS challenge. Results are from one of two experiments performed. * $P < 0.05$ compared to IL-10^{+/+} vehicle group. Statistical analysis was carried out using Logrank (Mantel Cox).

2.8. Statistical analyses

The statistical analysis of the differences in survival curves was made using the Logrank test. Comparisons among the experimental groups were performed by one-way analysis of variance and Newman-Keuls multiple comparison tests using Graph Pad Prism version 5.01 (Graph Pad Software, San Diego, CA). Differences were considered significant when the values of *P* were < 0.05.

3. Results

To investigate the effects of BA on endotoxic shock, groups of BALB/c mice were treated with the compound or vehicle (5% of DMSO in saline) and challenged with a lethal dose of LPS. Treatment with 67 mg of BA per kg induced protection to 100% of the animals (Fig. 2). BA at a lower dose (33 mg/kg) did not protect mice against the lethal LPS challenge and at the end of the observed period (four days), only 18% of animals were alive, similar to the vehicle-treated group. Dexamethasone, a control antiinflammatory drug, protected 83% at 0.5 mg/kg. Animals from all groups displayed signs of shock, such as piloerection, shivering, and lethargy.

To further investigate the effects of BA administration on endotoxemia, we measured the serum levels of cytokines in BA-treated animals after LPS challenge. Treatment with 67 mg of BA per kg decreased the TNF- α concentration significantly, when compared to treatment with vehicle, in LPS challenged mice, although less than dexamethasone, the reference drug (Fig. 3A). In contrast, the IL-10 concentration was significantly higher in animals treated with BA and challenged with LPS (Fig. 3B) than in vehicle-treated, LPS-challenged mice. The dexamethasone

treatment did not increase the production of IL-10 when compared to vehicle-treated mice (Fig. 3B). The concentration of IL-6 following LPS challenge was significantly reduced only by treatment with dexamethasone (Fig. 3C).

To evaluate the role of IL-10 in the BA-induced protection against LPS challenge, we carried out a lethality experiment using IL-10-deficient and wild-type C57BL/6 mice. IL-10^{-/-} mice treated with BA had an elevated mortality rate after LPS challenge, similar to vehicle-treated IL-10^{-/-} mice. In contrast, the IL-10^{+/+} control mice were significantly protected against the LPS challenge by the BA treatment (Fig. 4).

To assess the effects of BA on macrophages, we first measured nitric oxide levels in cultures of peritoneal exudate macrophages. Incubation of macrophages with BA (10 or 20 μ M), or with dexamethasone (20 μ M), significantly inhibited nitric oxide production induced by LPS stimulation, compared to LPS-stimulated untreated cultures (Fig. 5A). We next evaluated the effects of BA on TNF- α , IL-6 and IL-10 production. BA significantly decreased the production of TNF- α and modestly of IL-6, whereas dexamethasone significantly inhibited both cytokines (Fig. 5B and C). In contrast, a significant increase in IL-10 concentration was observed in BA-treated cultures (20 μ M) compared to LPS-stimulated untreated cultures (Fig. 5D) which was not observed in macrophage cultures treated with dexamethasone.

Finally, the effects of *in vivo* treatment with BA on macrophages were evaluated. For this purpose, nitric oxide and TNF- α , IL-6 and IL-10 were measured on resident macrophages from animals previously treated with BA. As revealed in Fig. 6, treatment with 67 mg/Kg of BA significantly reduced nitric oxide (Fig. 6A) and TNF- α (Fig. 6B) relative to the LPS-stimulated vehicle-treated cultures. A reduction of IL-6 levels

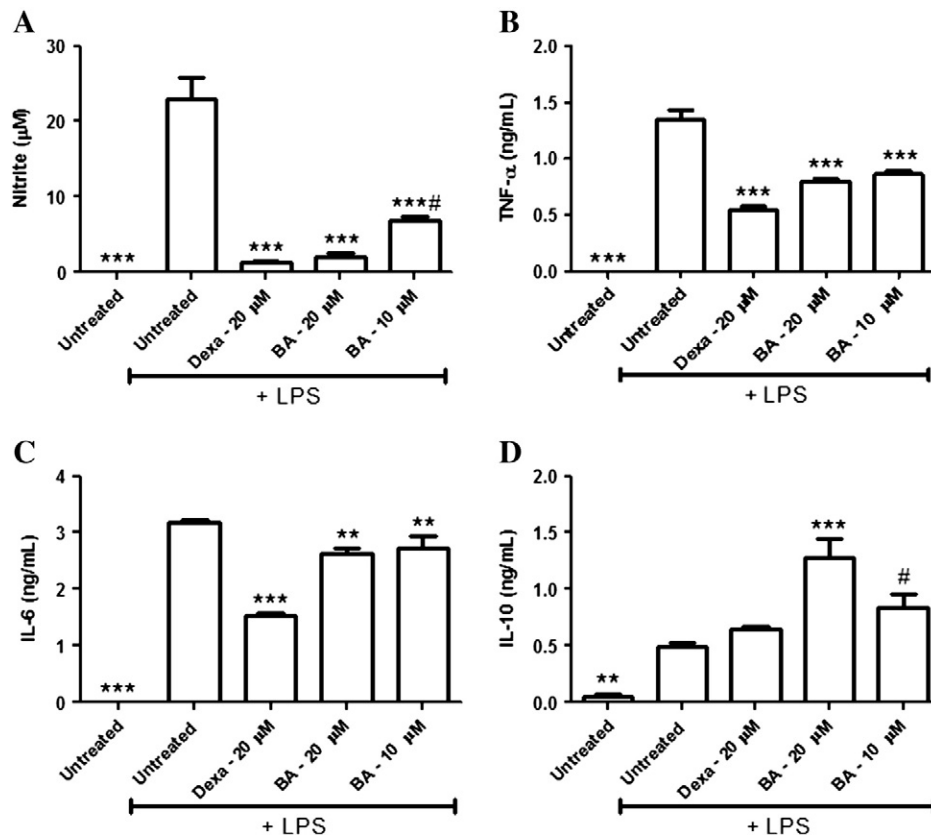


Fig. 5. Assessment of nitric oxide and cytokine production by peritoneal macrophages treated *in vitro* with betulinic acid. Concentrations of nitrite (A), TNF- α (B), IL-6 (C) and IL-10 (D) were determined in peritoneal macrophages treated or not with BA (10 or 20 μ M) or dexamethasone (20 μ M) in the presence of LPS (500 ng/mL) during 4 or 24 h. Cell-free supernatants were then collected for nitrite quantification by the Griess method and cytokine measurement by ELISA. Values represent the means \pm SEM of four determinations obtained in one of two experiments performed. ***P* < 0.01, ****P* < 0.001 compared to untreated cultures stimulated with LPS. # *P* < 0.01 compared to BA 20 μ M; ANOVA followed by Newman-Keuls multiple comparison test.

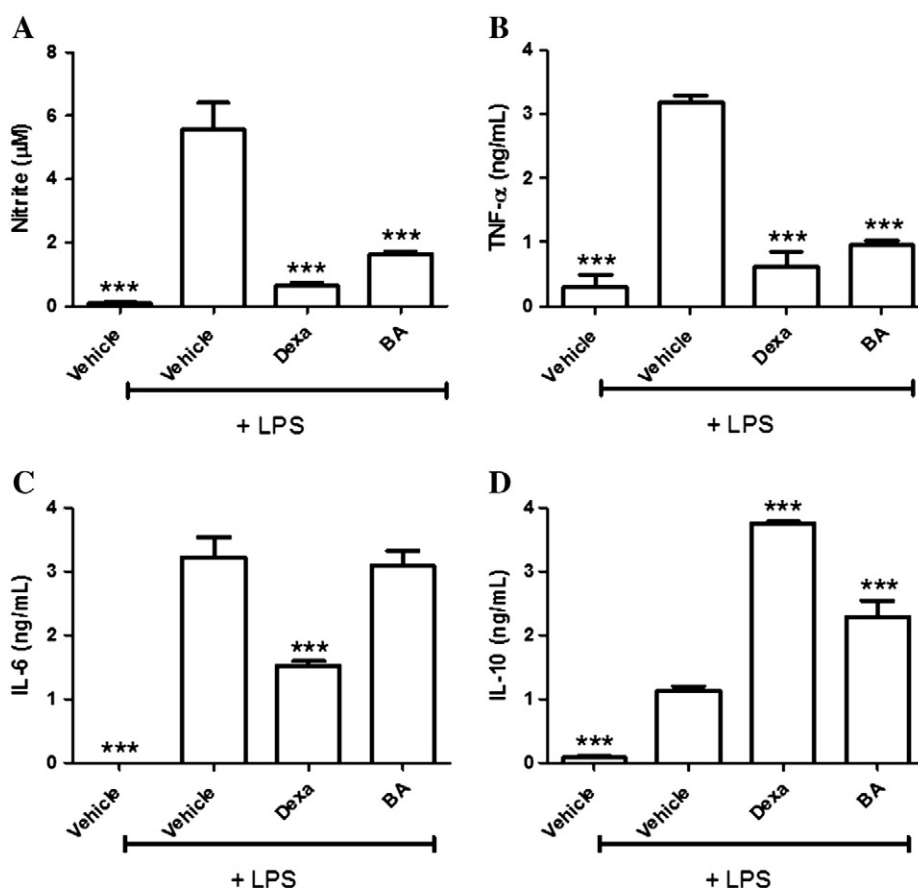


Fig. 6. In vivo treatment with betulinic acid (BA) decreases nitric oxide and TNF- α production and increases IL-10 production by LPS-stimulated macrophages. BALB/c mice (6 animals per group) were treated with BA (67 mg/kg), dexamethasone (Dexa; 0.5 mg/kg) or vehicle (5% DMSO in saline) and, after 90 min, were euthanized to harvest resident peritoneal macrophages. Cells were cultured in 96-well plates in the presence or absence of LPS (500 ng/mL) and, after 4 or 24 h, cell-free supernatants were collected. Concentrations of nitrite (A), TNF- α (B), IL-6 (C) and IL-10 (D) were obtained through Griess method and cytokines measurement by ELISA respectively. Values represent the means \pm SEM of six determinations obtained in 1 of 2 experiments performed. *** $P < 0.001$ compared to macrophages stimulated with LPS from vehicle-treated group; ANOVA followed by Newman-Keuls multiple comparison test.

was observed in macrophages derived from dexamethasone-treated, but not from BA-treated mice (Fig. 6C). In contrast, IL-10 production was significantly increased in macrophages obtained from mice treated with BA or dexamethasone.

4. Discussion

Sepsis, a life-threatening clinical condition, is associated with an overproduction of cytokines, including tumor necrosis factor and interleukins, as well as increased expression of adhesion molecules, as a result of stimulation by pathogenic agents or endotoxins [17]. Interaction between these various cytokines results in the activation of a cascade reaction that triggers an excessive inflammation, being a major cause of organ failure [18]. Recent studies have made considerable progress on antibiotic therapies and critical care techniques for sepsis treatment [19]. However, little progress was done about the anti-inflammatory treatment of sepsis.

Here we demonstrated the protective effects of BA, a triterpenoid found in many plant species, in a mouse model of endotoxemia. Administration of BA (67 mg/kg) prevented the mortality against a lethal dose of LPS. This protection followed the suppression of TNF- α production, one of the main soluble mediators involved in several aspects of the pathophysiology of endotoxemia. Altogether, our data demonstrate a potent *in vivo* anti-inflammatory activity of BA.

IL-10, a cytokine with potent anti-inflammatory properties, inhibits LPS-induced TNF- α release *in vitro* [20] and *in vivo*, and protects mice against lethal endotoxemia [21]. An increase in the levels of serum IL-10 was observed in mice treated with BA, suggesting an important role of

this cytokine in BA-induced protection. To confirm this hypothesis, we carried out an experiment using wild-type and IL-10^{-/-} C57BL/6 subjected to LPS-induced endotoxemia. Differing from wild-type mice, IL-10^{-/-} mice treated with BA had an elevated mortality rate after LPS challenge, suggesting a role for IL-10 in the protection against lethal endotoxemia conferred by BA. However, the fact that BA modulates I κ B α phosphorylation [22] suggests that its action on TNF- α inhibition may also be related to alterations in signaling pathways, such as NF- κ B activation.

A previous report has shown that BA inhibits the expression of cyclooxygenase 2 (COX-2) expression in cultures of human peripheral blood mononuclear cells, leading to a decrease in PGE₂ production [22]. The increase in IL-10 induced by BA described in our study may be related to the inhibition of PGE₂ production, another inflammatory mediator in LPS-challenged mice, since IL-10 is known to inhibit COX2 expression by LPS-stimulated monocytes [23]. Thus, we are establishing the role of another molecule involved in the anti-inflammatory activity produced by BA.

Since lethal endotoxemia results from an undesirable overproduction of cytokines by activated mononuclear phagocytes, we carried out *in vitro* experiments aiming to observe the effects of BA treatment in LPS-activated macrophages. Thus, addition of BA to macrophage cultures inhibited the production of inflammatory mediators, such as NO and TNF- α , and increased IL-10 production, in agreement with our *in vivo* findings. These data were also confirmed using macrophages harvested from mice previously treated with BA. Altogether, our data indicate that BA-induced IL-10 production by macrophages suggests a role of this anti-inflammatory cytokine in the protection against lethal

LPS challenge. The mechanisms leading to the increase in IL-10 production induced by BA remain still to be determined.

In contrast to the inhibition of TNF- α , BA did not significantly affect IL-6 production induced by LPS. IL-6 is a pleiotropic cytokine with both pro and anti-inflammatory actions. Although a number of agents, including dexamethasone, cause the down-modulation of both TNF- α and IL-6, selective inhibition of TNF- α may occur. In fact, a previous report has shown that a vasoactive sand fly peptide (maxadilan) exerts its anti-inflammatory action by a mechanism dependent on IL-6 [24].

A number of natural compounds have immunomodulatory activity in experimental models of LPS-induced endotoxemia, where TNF- α plays an important effector role [25,26]. Plant-derived polyphenols, alkaloids, terpenes, sterols, and fatty acids are reported in literature as inhibitors of TNF- α signaling [26], and may exert protective effects in endotoxemia. Physalins B, F and G, which are seco-steroids isolated from *Physalis angulata*, are examples of natural compounds with TNF- α suppressing activity which are able to prevent LPS-induced lethality [13]. BA, however, is a well-studied molecule that has originated a new class of antiretroviral drugs, named inhibitors of maturation and which has been evaluated in phase II clinical studies [27]. In addition, BA is a very well tolerated drug and its use is safe in doses higher than 500 mg/kg, according to studies on antineoplastic activity [5,28,29]. Indeed, the anti-inflammatory activity of BA should be taken into consideration in the context of the antineoplastic therapy.

4.1. Conclusion

The present findings reinforce the potential of BA, a natural compound as an anti-inflammatory drug candidate consider the role of IL-10 as another important mediator involved in the immune regulation produced by the drug and indicate the carrying out of future clinical evaluations involving BA effect on severe sepsis.

Acknowledgements

The authors would like to thank Tatiana Barbosa dos Santos for experimental support in ELISA assays. This work was supported by CNPq, PRONEX, FAPESB, FINEP and RENORBIO.

References

- [1] Sá MS, Costa JFO, Krettli AU, Zalis MG, Maia GLA, Sette IMF, et al. Antimalarial activity of betulinic acid and derivatives *in vitro* against *Plasmodium falciparum* and *in vivo* in *P. berghei*-infected mice. *Parasitol Res* 2009;105:275–9.
- [2] Yun Y, Han S, Park E, Yim D, Lee S, Lee CK, et al. Immunomodulatory activity of betulinic acid by producing pro-inflammatory cytokines and activation of macrophages. *Arch Pharm Res* 2003;26:1087–95.
- [3] Oliveira BH, Santos CA, Espíndola AP. Determination of the triterpenoid, betulinic acid, in *Doliocarpus schottianus* by HPLC. *Phytochem Anal* 2002;13:95–8.
- [4] Fulda S, Kroemer G. Targeting mitochondrial apoptosis by betulinic acid in human cancers. *Drug Discov Today* 2009;14:885–90.
- [5] Cichewicz RH, Kouzi SA. Chemistry, biological activity and chemotherapeutic potential of betulinic acid for the prevention and treatment of cancer and HIV infection. *Med Res Rev* 2004;24:90–114.
- [6] Yao D, Li H, Gou Y, Zhang H, Vlessidis AG, Zhou H, et al. Betulinic acid-mediated inhibitory effect on hepatitis B virus by suppression of manganese superoxide dismutase expression. *FEBS J* 2009;276:2599–614.
- [7] Krogh R, Berti C, Madeira AO, Souza MM, Cechinel-Filho V, Delle-Monache F, et al. Isolation and identification of compounds with antinociceptive action from *Ipomoea pes-caprae* (L.) R. Br. *Pharmazie* 1999;54:464–6.
- [8] Steele JCP, Warhurst DC, Kirby GC, Simmonds MSJ. *In vitro* and *in vivo* evaluation of betulinic acid as an antimalarial. *Phytother Res* 1999;13:115–9.
- [9] Mukherjee PK, Saha K, Das J, Pal M, Saha BP. Studies on the anti-inflammatory activity of rhizomes of *Nelumbo nucifera*. *Planta Med* 1997;63:367–9.
- [10] Recio MC, Giner RM, Mániz S, Gueho J, Julien HR, Hostettmann K, et al. Investigations on the steroidal anti-inflammatory activity of triterpenoids from *Diospyros leucomelas*. *Planta Med* 1995;61:9–12.
- [11] Lamontagne F, Meade M, Ondiveeran HK, Lesur O, Robichaud AR. Nitric oxide donors in sepsis: a systematic review of clinical and *in vivo* preclinical data. *Shock* 2008;30:653–9.
- [12] Tsiotou AG, Sakorafas GH, Anagnostopoulos G, Bramis J. Septic shock; current pathogenic concepts from a clinical perspective. *Med Sci Monit* 2005;11:RA76–85.
- [13] Soares MBP, Bellintani MC, Ribeiro IM, Tomassini TCB, Santos RR. Inhibition of macrophage activation and lipopolysaccharide-induced death by seco-steroids purified from *Physalis angulata* L. *Eur J Pharmacol* 2003;459:107–12.
- [14] Takada Y, Aggarwal BB. Betulinic acid suppresses carcinogen-induced NF- κ B activation through inhibition of I κ B kinase and p65 phosphorylation: abrogation of cyclooxygenase-2 and Matrix Metalloproteinase-9. *J Immunol* 2003;171:3278–86.
- [15] Barbosa-Filho JM, Lima CSA, Amorim ELC, Sena KXF, Almeida JRGS, Cunha EVL, et al. Botanical study, phytochemistry and antimicrobial activity of *Tabebuia aurea*. *Phyton* 2004;53:221–8.
- [16] Green LC, Wagne DA, Glogowski J, Skipper PL, Wishnok JS, Tannenbaum SR. Analysis of nitrate, nitrite, and [15 N] nitrate in biological fluids. *Anal Biochem* 1982;126:131–8.
- [17] Van der Poll T. Immunotherapy of sepsis. *Lancet Infect Dis* 2001;3:165–74.
- [18] Payen D, Monneret G, Hotchkiss R. Immunotherapy—a potential new way forward in the treatment of sepsis. *Crit Care* 2013;17:118.
- [19] Levy MM, Dellinger RP, Townsend SR, Linde-Zwirble WT, Marshall JC, Brion J, et al. The Surviving Sepsis Campaign: results of an international guideline-based performance improvement program targeting severe sepsis. *Intensive Care Med* 2010;36:222–31.
- [20] Fiorentino DF, Zlotnik A, Mosmann TR, Howard M, O'Garra A. IL-10 inhibits cytokine production by activated macrophages. *J Immunol* 1991;147:3815–22.
- [21] Howard M, Muchamuel T, Andrade SS. Interleukin 10 protects mice from lethal endotoxemia. *J Exp Med* 1993;177:1205–8.
- [22] Viji V, Helen A, Luxmi VR. Betulinic acid inhibits endotoxin-stimulated phosphorylation cascade and pro-inflammatory prostaglandin E2 production in human peripheral blood mononuclear cells. *Br J Pharmacol* 2011;162:1291–303.
- [23] Niiru H, Otsuka T, Tanabe T, Hara S, Kuga S, Nemoto Y, et al. Inhibition by interleukin-10 of inducible cyclooxygenase expression in lipopolysaccharide-stimulated monocytes: its underlying mechanism in comparison with interleukin-4. *Blood* 1995;85:3736–45.
- [24] Soares MB, Titus RG, Shoemaker CB, David JR, Bozza M. The vasoactive peptide maxadilan from sand fly saliva inhibits TNF-alpha and induces IL-6 by mouse macrophages through interaction with the pituitary adenylate cyclase-activating polypeptide (PACAP) receptor. *J Immunol* 1998;160:1811–6.
- [25] Son HJ, Lee HJ, Yun-Choi HS, Ryu JH. Inhibitors of nitric oxide synthesis and TNF- α expression from *Magnolia obovata* in activated macrophages. *Planta Med* 2000;66:469–71.
- [26] Atish TP, Vikrantsinh MG, Kamlesh KB. Modulating TNF- α signaling with natural products. *Drug Discov Today* 2006;11:725–32.
- [27] Adamson CS, Sakali M, Salzwedel K, Freed EO. Polymorphisms in Gag spacer peptide 1 confer varying levels of resistance to the HIV-1 maturation inhibitor bevirimat. *Retrovirology* 2010;7:36.
- [28] Nakagawa-Goto K, Yamada K, Taniguchi M, Tokuda H, Lee KH. Cancer preventive agents. Betulinic acid derivatives as potent cancer chemopreventive agents. *Bioorg Med Chem Lett* 2009;19:3378–81.
- [29] Yogeewari P, Siram D. Betulinic acid and its derivatives: a review on their biological properties. *Curr Med Chem* 2005;12:657–66.

ANEXO 2

MEIRA, C. S.; BARBOSA-FILHO, J. M.; LANFREDI-RANGEL, A.; TEIXEIRA, E. T.; MOREIRA, D. R. M.; SOARES, M. B. P. Antiparasitic evaluation of betulinic acid derivatives reveals effective and selective anti-*Trypanosoma cruzi* inhibitors. **Experimental Parasitology**, v. 166, p. 108-115, 2016.



Full length article

Antiparasitic evaluation of betulinic acid derivatives reveals effective and selective anti-*Trypanosoma cruzi* inhibitors

Cássio Santana Meira ^a, José Maria Barbosa-Filho ^b, Adriana Lanfredi-Rangel ^a,
Elisalva Teixeira Guimarães ^{a, c}, Diogo Rodrigo Magalhães Moreira ^a,
Milena Botelho Pereira Soares ^{a, d, *}

^a Centro de Pesquisas Gonçalo Moniz, Fundação Oswaldo Cruz (FIOCRUZ), Salvador, BA, Brazil

^b Laboratório de Tecnologia Farmacêutica, Universidade Federal da Paraíba, João Pessoa, PB, Brazil

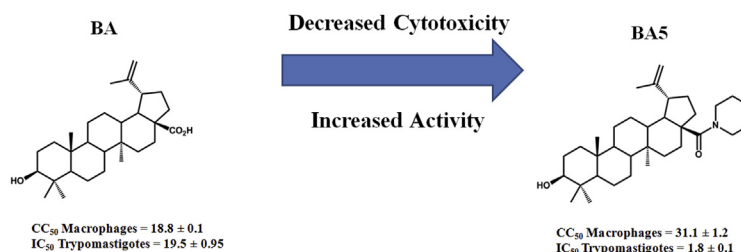
^c Universidade do Estado da Bahia, Departamento de Ciências da Vida, Salvador, BA, Brazil

^d Hospital São Rafael, Centro de Biotecnologia e Terapia Celular, Salvador, BA, Brazil

HIGHLIGHTS

- Terpenoids are potent and selective trypanocidal agents.
- BA5 destroys parasite cells by necrotic death.
- Betulinic acid derivatives inhibit the growth of intracellular amastigotes of *T. cruzi*.
- Combination of BA5 and benznidazole showed synergistic effects.

GRAPHICAL ABSTRACT



ARTICLE INFO

Article history:

Received 26 November 2015

Received in revised form

6 April 2016

Accepted 10 April 2016

Available online 11 April 2016

Keywords:

Chagas disease

Trypanosoma cruzi

Natural compounds

Semi-synthetic

Triterpenoids

Betulinic acid

ABSTRACT

Betulinic acid is a pentacyclic triterpenoid with several biological properties already described, including antiparasitic activity. Here, the anti-*Trypanosoma cruzi* activity of betulinic acid and its semi-synthetic amide derivatives (BA1–BA8) was investigated. The anti-*Trypanosoma cruzi* activity and selectivity were enhanced in semi-synthetic derivatives, specially on derivatives BA5, BA6 and BA8. To understand the mechanism of action underlying betulinic acid anti-*T. cruzi* activity, we investigated ultrastructural changes by electron microscopy. Ultrastructural studies showed that trypomastigotes incubated with BA5 had membrane blebbing, flagella retraction, atypical cytoplasmic vacuoles and Golgi cisternae dilatation. Flow cytometry analysis showed that parasite death is mainly caused by necrosis. Treatment with derivatives BA5, BA6 or BA8 reduced the invasion process, as well as intracellular parasite development in host cells, with a potency and selectivity similar to that observed in benznidazole-treated cells. More importantly, the combination of BA5 and benznidazole revealed synergistic effects on trypomastigote and amastigote forms of *T. cruzi*. In conclusion, we demonstrated that BA5 compound is an effective and selective anti-*T. cruzi* agent.

© 2016 Elsevier Inc. All rights reserved.

* Corresponding author. Centro de Pesquisas Gonçalo Moniz, Fundação Oswaldo Cruz, Rua Waldemar Falcão, 121, Candeal, Salvador 40296-710, BA, Brazil.

E-mail address: milena@bahia.fiocruz.br (M.B.P. Soares).

1. Introduction

Chagas disease is a neglected disease caused by the protozoan parasite *Trypanosoma cruzi* and constitutes a serious public health problem worldwide (Pinto-Dias, 2006). It affects about 8–10

million people, mainly in Latin American countries, where this disease is endemic (Rassi et al., 2010). Pharmacotherapy is based on nifurtimox and benznidazole, which are recommended to treat all infected people (Urbina and Docampo, 2003). Treatment with benznidazole is associated with side effects, prolonged treatment time and low and variable efficacy in chronic phase of infection, which is the most prevalent form of the disease (Urbina and Docampo, 2003; Viotti et al., 2009; Morillo et al., 2015). This scenario emphasizes a need to develop safer and more effective drugs.

Natural products play an important role in drug discovery and development (Newman and Cragg, 2012). Naturally occurring terpenoids represent an important class of bioactive compounds that exhibit several medicinal properties (Yin, 2015). This is exemplified by betulinic acid, a lupane-type pentacyclic triterpenoid abundant in the plant kingdom, which can be isolated from several plant species or obtained from its metabolic precursor, betulin (Yogeeswari and Sriram, 2005). Betulinic acid and its derivatives possess anti-HIV activity, anti-bacterial, antihelminthic, anti-inflammatory and a potent cytotoxic activity against a large panel of tumor cell lines (Baglin et al., 2003; Chandramu et al., 2003; Yogeeswari and Sriram, 2005; Drag et al., 2009; Costa et al., 2014; Chakraborty et al., 2015).

Betulinic acid and other triterpenoids, both naturally-occurring and semi-synthetic, have also been investigated as antiparasitic agents (Hoet et al., 2007; Innocente et al., 2012). More specifically, the activity of betulinic acid and its derivatives against the erythrocytic stage of a chloroquine-resistant *Plasmodium falciparum* strain, as well as antileishmanial activity on different *Leishmania* species, were reported (Alakurtti et al., 2010; Chen et al., 2010; Innocente et al., 2012; Sousa et al., 2014). Regarding the anti-*Trypanosoma cruzi* activity, it was previously shown that betulinic acid and ester derivatives inhibit epimastigote proliferation (Domínguez-Carmona et al., 2010). In view of these findings, betulinic acid is considered to be a prototype for the design and synthesis of antiprotozoal agents. Chemical modifications of the carboxyl group have suggested that this part of the molecule can produce derivatives with enhanced antiprotozoal activity when compared to betulinic acid (Gros et al., 2006; Domínguez-Carmona et al., 2010; Da Silva et al., 2011; Sousa et al., 2014; Spivak et al., 2014). Based on these facts, the purpose of our work was to evaluate the trypanocidal potential of new semi-synthetic amide derivatives of betulinic acid.

2. Material and methods

2.1. Chemistry

Betulinic acid (BA) was extracted from the bark of *Ziziphus joazeiro* Mart. (Rhamnaceae) by using a previously described method (Barbosa-Filho et al., 1985). Semi-synthetic compounds (BA1 to BA8) were prepared from betulinic acid (Fig. 1). Betulinic acid was initially converted to mixed anhydride by using isobutyl chloroformate (Sigma-Aldrich), followed by addition of the respective secondary amines. This methodology allowed the synthesis of compounds BA1 to BA8 (Fig. 1), with yields varying from 30 to 41% after HPLC purification.

2.2. General procedure for the synthesis

Two mmol (0.1 g) of betulinic acid were added to a 100 mL round bottom flask under magnetic stirring and dissolved in dichloromethane (10 mL). The mixture was cooled to -10°C and then 4-dimethylaminopyridine isobutyl chloroformate (3.0 mmol, 0.4 g) in dichloromethane (1 mL) was slowly added during 30 min. The mixture was maintained under stirring for 3 h. The reaction

was transferred to a separating funnel, to which 50 mL of ethyl ether were added and the organic phase was quickly washed with a saturated solution of sodium bisulfite (1×50 mL), washed with water and with saturated NaCl solution (2×50 mL). The organic phase was separated, dried over MgSO_4 , and evaporated under reduced pressure to give a white thick oily residue, which was crystallized in cyclohexane. Purity was analyzed by HPLC and structures examined by HRESIMS. Mass spectrometry was performed in a Q-TOF spectrometer (nanoUPLC-Xevo G2 Tof, Waters). ESI was carried out in the positive ion mode. HPLC analysis was carried out in Beckmann Coulter using UV detector in a C_{18} column (100 \AA , 2.14×25 cm) with a linear gradient of 5–95% MeCN/ H_2O in 0.1% TFA. Compound **BA1**, 95% (HPLC). HRESIMS Anal. Calc. (Found)/Error for $\text{C}_{34}\text{H}_{55}\text{NO}_2$: 509.4232 (510.4713, $[\text{M}+\text{H}^+]$)/6.5 ppm. Compound **BA2**, 94% (HPLC). HRESIMS Anal. Calc. (Found)/Error for $\text{C}_{35}\text{H}_{58}\text{N}_2\text{O}_2$: 538.4498 (539.4491, $[\text{M}+\text{H}^+]$)/5.7 ppm. Compound **BA3**, 98% (HPLC). HRESIMS Anal. Calc. (Found)/Error for $\text{C}_{35}\text{H}_{57}\text{NO}_2$: 523.4389 (524.5031, $[\text{M}+\text{H}^+]$)/5.0 ppm. Compound **BA4**, 98% (HPLC). HRESIMS Anal. Calc. (Found)/Error for $\text{C}_{34}\text{H}_{56}\text{N}_2\text{O}_2$: 524.4341 (524.4249, $[\text{M}+\text{H}^+]$)/4.0 ppm. Compound **BA5**, 95% (HPLC). HRESIMS Anal. Calc. (Found)/Error for $\text{C}_{33}\text{H}_{53}\text{NO}_3$: 511.4025 (512.3177, $[\text{M}+\text{H}^+]$)/10 ppm. Compound **BA6**, 94% (HPLC). HRESIMS Anal. Calc. (Found)/Error for $\text{C}_{33}\text{H}_{53}\text{NSO}_2$: 527.3797 (529.1641, $[\text{M}+\text{H}^+]$)/20 ppm. Compound **BA7**, 95% (HPLC). HRESIMS Anal. Calc. (Found)/Error for $\text{C}_{40}\text{H}_{58}\text{NFO}_2$: 603.4451 (604.4085, $[\text{M}+\text{H}^+]$)/4.0 ppm. Compound **BA8**, 98% (HPLC). HRESIMS Anal. Calc. (Found)/Error for $\text{C}_{40}\text{H}_{59}\text{NO}_2$: 585.4545 (589.7109, $[\text{M}+\text{H}^+]$)/10 ppm.

2.3. Cytotoxicity to mammalian cells

Peritoneal exudate macrophages were obtained by washing, with cold RPMI medium, the peritoneal cavity of BALB/c mice 4–5 days after injection of 3% thioglycolate in saline (1.5 mL per mice). Then, cells were placed into 96-well plates at a density 1×10^5 cells/well in RPMI-1640 medium without phenol red (Sigma-Aldrich, St. Louis, MO) supplemented with 10% of fetal bovine serum (FBS; Cultilab, Campinas, Brazil), and 50 $\mu\text{g}/\text{mL}$ of gentamycin (Novafarma, Anápolis, Brazil) and incubated for 24 h at 37°C and 5% CO_2 . After that time, each compound was added in triplicate at eight concentrations ranging from 0.04 to 100 μM and incubated for 6 or 72 h. Twenty $\mu\text{L}/\text{well}$ of AlamarBlue (Invitrogen, Carlsbad, CA) was added to the plates during 10 h. Colorimetric readings were performed at 570 and 600 nm. CC_{50} values were calculated using data-points gathered from three independent experiments. Gentian violet (Synth, São Paulo, Brazil) was used as a cytotoxicity control, at concentrations ranging from 0.04 to 10 μM .

2.4. Cytotoxicity for trypomastigotes

Bloodstream trypomastigotes forms of *T. cruzi* (Y strain) were obtained from supernatants of LLC-MK2 cells previously infected and maintained in RPMI-1640 medium supplemented with 10% FBS, and 50 $\mu\text{g}/\text{mL}$ gentamycin at 37°C and 5% CO_2 . Parasites (4×10^5 cells/well) were dispensed into 96-well plates and the test inhibitors were added at eight concentrations ranging from 0.04 to 100 μM in triplicate, and the plate was incubated for 24 h at 37°C and 5% of CO_2 . Aliquots of each well were collected and the number of viable parasites was assessed in a Neubauer chamber and compared to untreated cultures. Benznidazole (LAFEPE, Recife, Brazil) was used as positive control in the anti-*Trypanosoma cruzi* studies. Three independent experiments were performed.

2.5. In vitro T. cruzi infection assay

Peritoneal exudate macrophages were plated at a cell density of

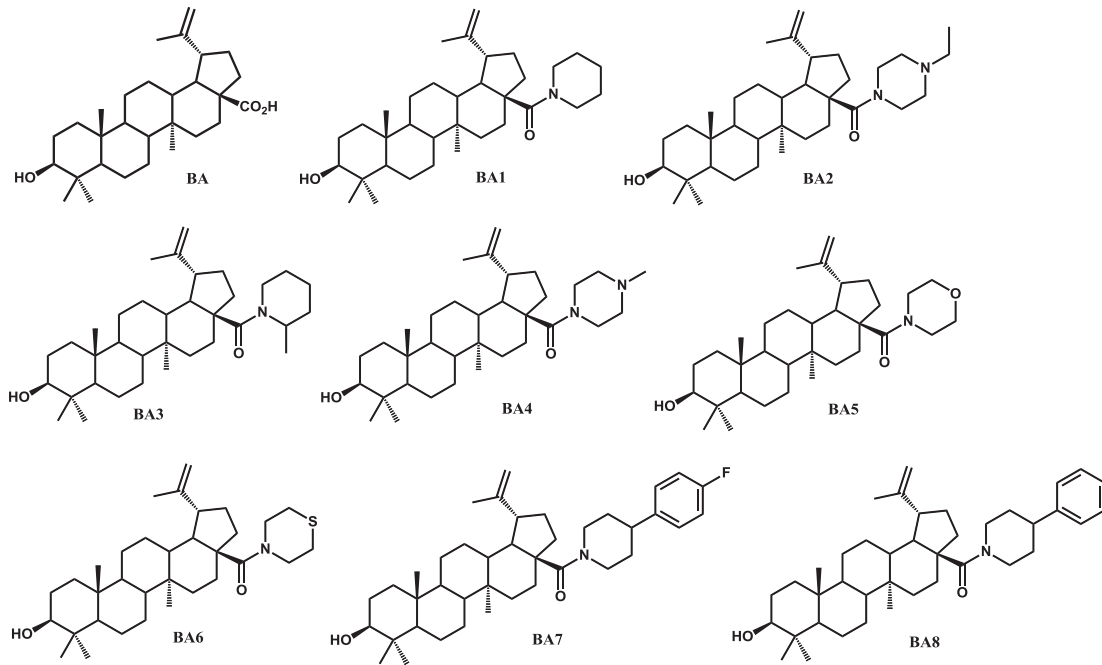


Fig. 1. Structure of betulinic acid and its derivatives.

2×10^5 cells/well in 24-well plates with sterile coverslips on the bottom in RPMI supplemented with 10% FBS and incubated for 24 h at 37 °C and 5% CO₂. Cells were then infected with trypomastigotes at a ratio of 10 parasites per macrophage for 2 h. Free trypomastigotes were removed by successive washes using saline solution. Cultures were incubated in complete medium alone or with the compounds under investigation in different concentrations for 6 h. The medium was replaced with fresh medium and the plate was incubated for 3 days (Soares et al., 2012). Cells were fixed in absolute alcohol and the percentage of infected macrophages and the mean number of amastigotes/100 macrophages was determined by manual counting after hematoxylin and eosin staining in an optical microscope (Olympus, Tokyo, Japan). The percentage of infected macrophages and the relative number of amastigotes per macrophage was determined by counting 100 cells per slide. Experiments were performed three times.

2.6. *Trypanosoma cruzi* invasion assay

Peritoneal exudate macrophages (10^5 cells) were plated onto sterile coverslips in 24-well plates and kept for 24 h. Plates were washed with saline solution and trypomastigotes were then added at a cell density of 1×10^7 parasites/well along with the addition of BA5, or BA6 or BA8 (50 μM). The plate was incubated for 2 h at 37 °C and 5% CO₂, followed by successive washes with saline solution to remove extracellular trypomastigotes. Plates were maintained in RPMI medium supplemented with 10% FBS at 37 °C for 2 h. Infected macrophages were examined for the presence of amastigotes by optical microscopy using a standard hematoxylin and eosin staining. Amphotericin B (Gibco Laboratories, Gaithersburg, MD) was used as a positive control in this assay. Three independent experiments were performed.

2.7. Ultrastructural studies

Trypomastigotes at a cell density of 1×10^7 cells/mL in 24 well-plates were treated with test inhibitor BA5 (2 or 4 μM) or not for

24 h. Parasites were then fixed with 2% formaldehyde and 2.5% glutaraldehyde (Electron Microscopy Sciences, Hatfield, PA) in sodium cacodylate buffer (0.1 M, pH 7.2) for 1 h at room temperature. After fixation, parasites were washed 3 times with sodium cacodylate buffer (0.1 M, pH 7.2), and post-fixed with a 1.0% solution of osmium tetroxide containing 0.8% potassium ferrocyanide (Sigma) for 1 h. Cells were subsequently dehydrated in increasing concentrations of acetone (30, 50, 70, 90 and 100%) for 10 min at each step and embedded in polybed resin (PolyScience family, Warrington, PA). Ultrathin sections on copper grids were contrasted with uranyl acetate and lead citrate and observed under a ZEISS 109 transmission electron microscope. For scanning electron microscopy, trypomastigotes treated with or without BA 505 (2 or 4 μM) and fixed in the same conditions were washed in 0.1 M cacodylate buffer, and allowed to adhere in coverslips pre-coated with poly-L-lysine (Sigma). Cells were then post-fixed with a solution of osmium tetroxide containing 0.8% of potassium ferrocyanide for 30 min and dehydrated in crescent concentrations of ethanol (30, 50, 70, 90 and 100%). The samples were dried until the critical point, metallized with gold and analyzed in a JEOL JSM-6390LV scanning electron microscope. Two independent experiments were performed.

2.8. Propidium iodide and annexin V staining

Trypomastigotes 1×10^7 /mL in 24 well-plates were treated with 5 or 10 μM of BA5 in RPMI supplemented with FBS at 37 °C for 24 or 72 h and labeled for propidium iodide (PI) and annexin V using the annexin V-FITC apoptosis detection kit (Sigma), according to the manufacturer's instructions. Acquisition and analyses was performed using a FACS Calibur flow cytometer (Becton Dickinson, San Diego, CA), with FlowJo software (Tree Star, Ashland, OR). A total of 10,000 events were acquired in the region previously established as that corresponding to trypomastigotes forms of *T. cruzi*. Two independent experiments were performed.

Table 1
Cytotoxicity against macrophages and anti-*Trypanosoma cruzi* activity against trypomastigotes forms of betulinic acid and its derivatives.

Compound	CC ₅₀ (μM) ^a	IC ₅₀ Try. (μM)	SI
BA	18.8 (±0.1)	19.5 (±0.9)	0
BA1	>100	>100	–
BA2	>100	>100	–
BA3	>100	13.7 (±2.3)	7.3
BA4	39.7 (±0.5)	10.2 (±1.0)	3.9
BA5	31.1 (±1.2)	1.8 (±0.1)	17.3
BA6	28.7 (±1.1)	5.4 (±1.3)	5.3
BA7	>100	55 (±0.6)	1.8
BA8	53.5 (±0.4)	5 (±0.5)	10.7
Gentian violet	0.5 (±0.1)	–	–
Benznidazole	>100	11.4 (±1.4)	8.8

CC₅₀ = cytotoxicity concentration 50%. IC₅₀ = inhibitory concentration. SI = Selective index. 50%. Values are means ± SD of three independent experiments performed in triplicate.

^a Cell viability of BALB/c mouse macrophages determined 72 h after treatment.

2.9. Drug combination

For *in vitro* drug combinations, doubling dilutions of each drug (BA5 and benznidazole), used alone or in fixed combinations were incubated with trypomastigotes or intracellular parasites followed the protocols described above. The analysis of the combined effects was performed by determining the combination index (CI), used as

cutoff to determine synergism, by using Chou-Talalay CI method (Chou and Talalay, 2005) and through the construction of isobologram using the fixed ratio method, as described previously (Fivelman et al., 2004).

2.10. Statistical analyses

To determine the cytotoxicity concentration 50% of BALB/c mice macrophages (CC₅₀) and the inhibitory concentration 50% (IC₅₀) of the trypomastigotes and amastigotes forms of *T. cruzi*, we used nonlinear regression. The selectivity index (SI) was defined as the ratio of CC₅₀ by IC₅₀ (trypomastigotes or amastigotes). The one-way ANOVA followed by Bonferroni's multiple comparison test was used to determine the statistical significance of the group comparisons in the *in vitro* infection studies and cell invasion study. Results were considered statistically significant when $P < 0.05$. All analyses were performed using Graph Pad Prism version 5.01 (Graph Pad Software, San Diego, CA).

3. Results

3.1. Trypanocidal and cytotoxicity activity

First the compounds had their anti-*T. cruzi* activity determined against trypomastigote forms (Table 1). The structural design of the

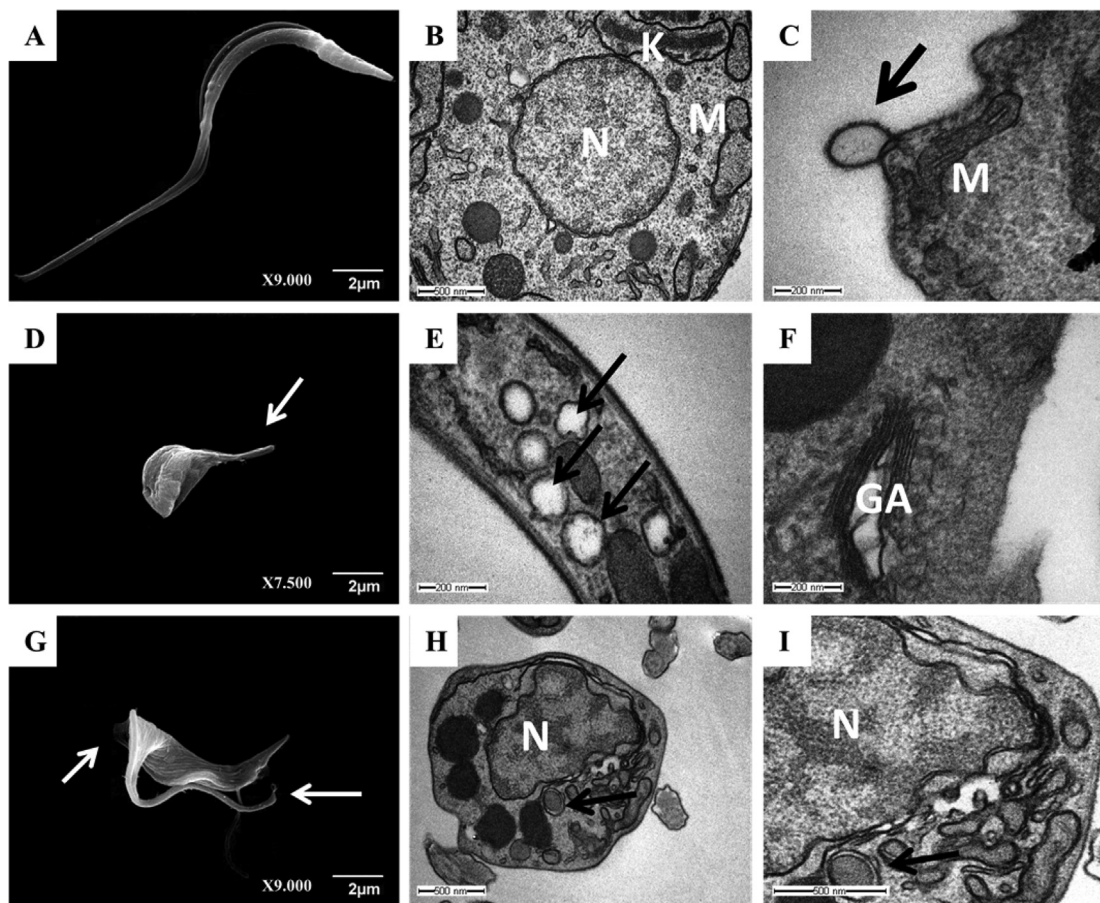


Fig. 2. Electron microscopy of trypomastigotes of *T. cruzi* treated with BA5 for 24 h. Using SEM, we observed alterations in cell shape and flagella retraction (2 μM; D) and loss of plasma membrane integrity and body deformation (4 μM; G), untreated cells (A). White arrows indicate the alterations reported. Scale bars = 2 μm. Using TEM, we observed appearance of membrane blebbing (2 μM; C), the formation of numerous and atypical vacuoles within the cytoplasm (2 μM; E), dilatation of some Golgi cisternae (2 μM; F) and (4 μM; H and I) appearance of profiles of endoplasmic reticulum involving organelles accompanied by the formation of autophagosomes, (B) untreated cells. Black arrows indicate changes in the organelles.

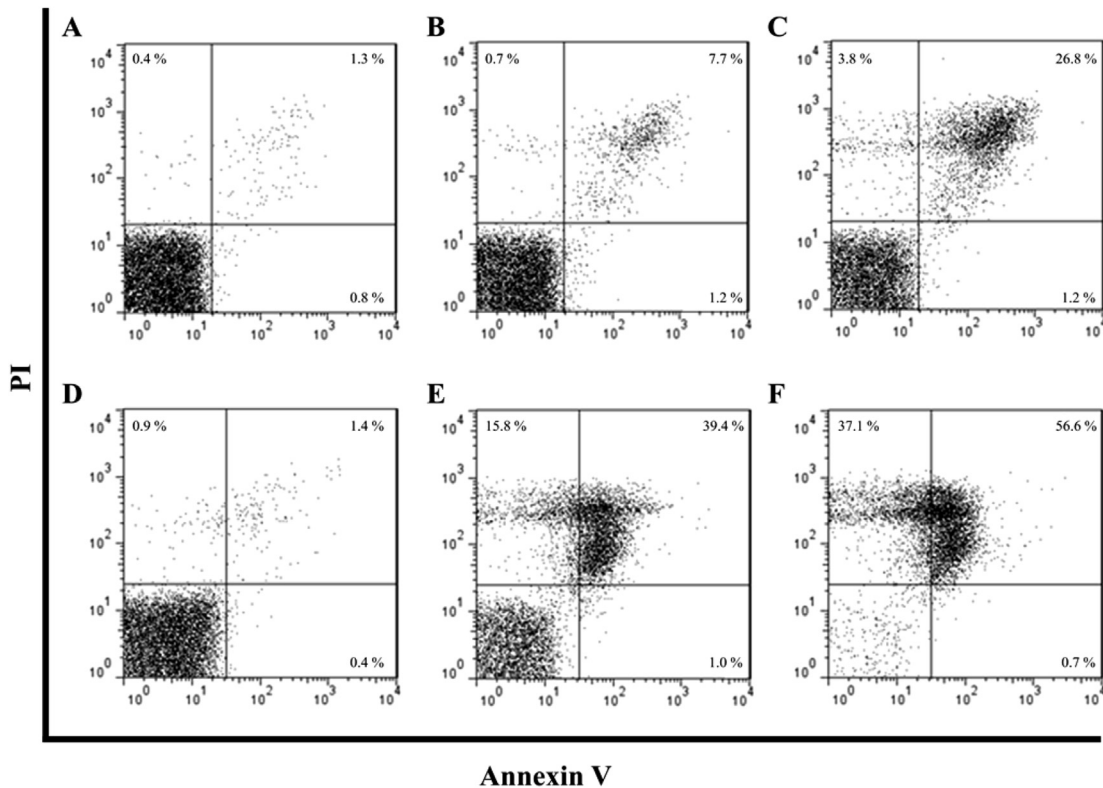


Fig. 3. Flow cytometry analysis of trypomastigotes treated with BA5 and incubated with propidium iodide (PI) and annexin V. (A) Untreated trypomastigotes after 24 h of incubation; (B and C) trypomastigotes treated with 5 and 10 μM of BA5, respectively by 24 h. (D) Untreated trypomastigotes after 72 h of incubation. (E and F) Trypomastigotes treated with 5 or 10 μM of BA5, respectively, for 72 h.

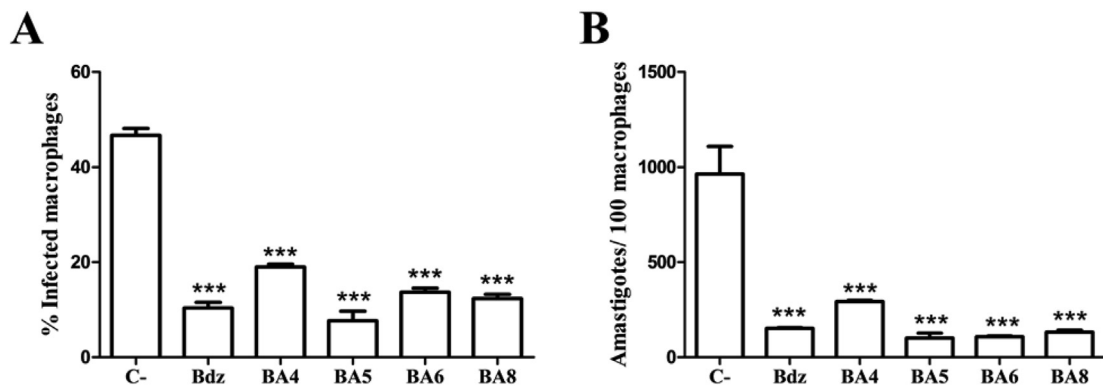


Fig. 4. The betulinic acid derivatives inhibit the growth of intracellular amastigotes of *T. cruzi*. Mouse peritoneal macrophages were infected with Y strain trypomastigotes for 2 h and treated with betulinic acid derivatives (50 μM) or benznidazole (50 μM) for 6 h. Infected cells were stained with hematoxylin and eosin and analyzed by optical microscopy. Bdz = benznidazole. Values represent the mean \pm SEM of triplicate. ***, $P < 0.001$ compared with untreated cultures.

Table 2
Antiparasitic activity in intracellular parasite, host cells cytotoxicity and selectivity index of derivatives.

Comp.	Amastigotes $\text{IC}_{50} \pm \text{S.D.}(\mu\text{M})^a$	Macrophages $\text{CC}_{50} \pm \text{S.D.}(\mu\text{M})^b$	Selectivity index ^c
BA4	18.9 (± 1.2)	>100	>5.3
BA5	10.6 (± 0.8)	>100	>9.4
BA6	12.4 (± 1.7)	>100	>8
BA8	13.2 (± 1.6)	>100	>7.6
Bdz	13.5 (± 1.3)	>100	>7.4

IC_{50} and CC_{50} values were calculated using concentrations in triplicate, in three independent experiments. IC_{50} = inhibitory concentration at 50%. CC_{50} = cytotoxic concentration at 50%. S.D. = standard deviation. Bdz = benznidazole.

^a Cells were exposed to derivatives for 6 h and activity was determined 3 days after incubation with derivatives.

^b Cell viability of BALB/c mouse macrophages determined 6 h after treatment.

^c SI is selectivity index, calculated by the ratio of CC_{50} (macrophages) and IC_{50} (amastigotes).

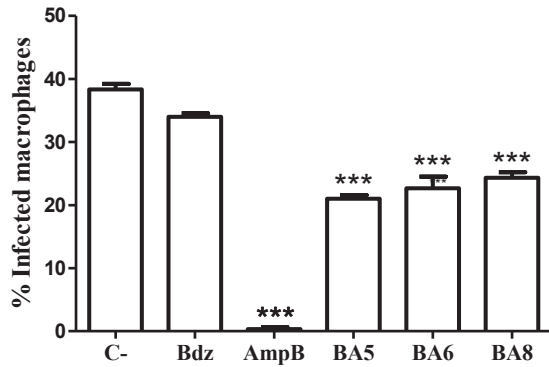


Fig. 5. The betulinic acid derivatives impair *T. cruzi* trypomastigote invasion in macrophages. Mouse macrophages were simultaneously infected with 10^7 Y strain trypomastigotes and treated with betulinic acid derivatives ($50 \mu\text{M}$) or benznidazole ($50 \mu\text{M}$) for 2 h. Bdz = benznidazole; AmpB = amphotericin B. ***, $P < 0.001$ compared with untreated cultures.

betulinic acid derivatives was performed to investigate the piperidinyl moiety attached to the C28 position of carboxylic acid function, varying thus the hydrogen-bond sites. In fact, most of semi-synthetic derivatives had IC_{50} values lower than betulinic acid and, in some cases (BA4, BA5, BA6 and BA8), the values of IC_{50} was also lower than benznidazole, the reference drug. More specifically, the attachment of morpholyl, thiomorpholyl or a 4-methylphenylpiperidine group produced the most potent compounds.

Next, the cytotoxicity of the compounds to mouse macrophages was analyzed. As shown in Table 1, all semi-synthetic derivatives presented values of CC_{50} higher than betulinic acid. The derivatives BA5 and BA8 showed the best profiles of selectivity with values of SI of 17.3 and 8.8 respectively.

3.2. Investigating the mechanism of action

We used scanning electron microscopy (SEM) to study the morphology of trypomastigotes treated or not with the most potent derivative (BA5). Untreated trypomastigotes had the typical elongated shape of the parasite without visible alterations in the plasma membrane or in cell volume (Fig. 2A). On the other hand, trypomastigotes treated for 24 h with BA5 (2 or $4 \mu\text{M}$) had flagella retraction (Fig. 2D), loss of plasma membrane integrity and body deformation (Fig. 2G).

Transmission electron microscopy (TEM) was also used to examine ultrastructural alterations. Thin sections of untreated trypomastigotes observed by TEM revealed normal appearance of organelles, intact plasma membrane and cytoplasm without alterations (Fig. 2B). However, treatment with BA5 (2 or $4 \mu\text{M}$) caused plasma membrane alterations (Fig. 2C), the formation of numerous atypical vacuoles within the cytoplasm (Fig. 2E), dilatation of Golgi cisternae (Fig. 2F) and profiles of endoplasmic reticulum involving organelles as nucleus accompanied by the formation of autophagosomes (Fig. 2H and I).

To understand the mechanism by which compound BA5 causes parasite death, a double staining with annexin V and propidium iodide (PI) was performed for flow cytometry analysis. In untreated cultures, most cells were negative for annexin V and PI staining, demonstrating cell viability. In contrast, a significant increase in the number of PI-positive parasites was observed in cultures treated with BA5 at 5 and $10 \mu\text{M}$. Treatment with $5 \mu\text{M}$ of BA5 for 72 h resulted in 15.8% and 39.4% of cells positively stained for PI and PI^+ annexin V^+ , respectively (Fig. 3). These results suggest that the BA5 derivative induces a necrotic process in *Trypanosoma cruzi* trypomastigotes.

3.3. In vitro infection studies

We next investigated the ability of BA4, BA5, BA6 and BA8

Table 3

Concentration reductions and combination indexes for anti-*T. cruzi* activity by BA5 and benznidazole on trypomastigotes and amastigotes forms of *T. cruzi*.

Compounds	$\text{IC}_{50} \pm \text{S.D.} (\mu\text{M})^a$ Trypomastigotes		$\text{IC}_{50} \pm \text{S.D.} (\mu\text{M})^a$ Amastigotes		CI^b	
	Drug alone	Combination	Drug alone	Combination	Trypo	Ama.
BA5	2.6 ± 0.2	0.9 ± 0.1	11.2 ± 0.9	3.7 ± 0.8	0.45 ± 0.1	0.84 ± 0.1
Bdz	10.6 ± 0.9	1.3 ± 0.4	13.6 ± 0.1	5.8 ± 0.6		

^a IC_{50} values were calculated using concentrations in triplicates and two independent experiments were performed.

^b Combination index (CI). Cutoff: CI value of 0.3–0.7, synergism; 0.7–0.85, moderate synergism; 0.85–0.9, slight synergism; 0.9–1.1, additively; > 1.1, antagonism. S.D = standard deviation.

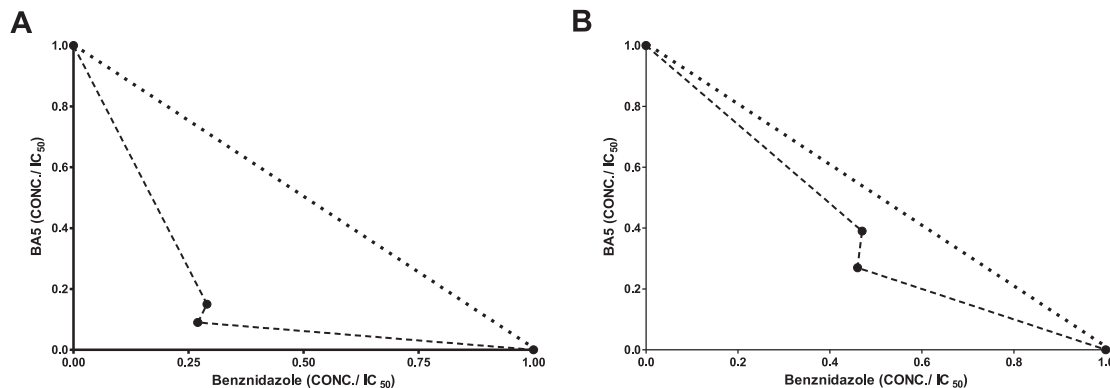


Fig. 6. Isobologram describing the synergistic effects of BA5 and benznidazole on *T. cruzi* trypomastigotes (A) and amastigotes (B). Dotted lines correspond to the predicted positions of the experimental points for additive effects.

derivatives to inhibit the development of parasites in host cells. Macrophages infected with *Trypanosoma cruzi* trypomastigotes treated with 50 μM of the compounds were stained with hematoxylin and eosin for analysis by optical microscopy. As shown in Fig. 4, treatment with the semi-synthetic compounds significantly decreased the percentage of infected macrophages ($P < 0.001$) and the relative number of amastigotes per 100 macrophages ($P < 0.001$) when compared with untreated cultures. When tested at different concentrations, it was possible to calculate the IC_{50} value of the derivatives against intracellular parasites. As shown in Table 2, the derivatives had an equipotent activity when compared to benznidazole. Cytotoxicity measured at 6 h of drug exposure demonstrated that benznidazole, as well as all derivatives tested are not cytotoxic at the tested concentrations ($\text{CC}_{50} > 100 \mu\text{M}$). These data demonstrate that the derivatives are selective compounds.

We also evaluated the effect of the most potent derivatives on the invasion process. In this assay, peritoneal macrophages were exposed to trypomastigotes and at the same time treated with the semi-synthetic BA5, BA6 and BA8 derivatives (50 μM) for 2 h. After this time, the cells were washed with saline solution to remove extracellular parasites and incubated for 2 additional hours. Cells were stained with hematoxylin and eosin and analyzed by optical microscopy. Amphotericin B was used as a positive control for this experiment. As shown in Fig. 5, the derivatives significantly inhibited the parasite invasion in comparison to untreated cells ($P < 0.001$), but not as efficiently as the positive control amphotericin B, although they were more effective than benznidazole, that show no significant activity on this assay.

Finally, the antiparasitic effect of BA5 and benznidazole in combination was investigated against trypomastigote and amastigote forms of *Trypanosoma cruzi*. In comparison to the drugs alone, the combination of BA5 and benznidazole reduced IC_{50} values in both forms of the parasite. In fact, the IC_{50} of benznidazole decreased in average by 88% and 43% when combined with EEPA BA5 against trypomastigotes and amastigotes forms of *T. cruzi* respectively (Table 3).

An isobologram analysis and CI calculation, which can distinguish between the synergistic, additive and antagonistic effects of two compounds, confirmed that the combination of BA5 and benznidazole resulted in a remarkable synergistic effect on trypomastigotes and a moderate synergistic effect on amastigotes (Table 3; Fig. 6).

4. Discussion

Terpenoids, such as betulinic acid, are some of the most investigated source of antiparasitic compounds in terms of potency and selectivity (Newman and Cragg, 2012). In the present study, we investigated the anti-*Trypanosoma cruzi* activity of amide semi-synthetic betulinic acid derivatives containing substituents attached in the lupane backbone. We observed that an incorporation of an amide on C-28 enhanced the anti-*T. cruzi* activity. This led to the identification of compound BA5, which exhibited a potency superior to benznidazole, the current standard drug. Several reports describe the chemical modifications of betulinic acid at C-28 position to produce semi-synthetic derivatives with enhanced antimalarial, anti-tumor and anti-viral activities (Jeong et al., 1999; Baltina et al., 2003; Domínguez-Carmona et al., 2010). This is the first report, however, regarding the contribution of the incorporation of amides on C-28 as drug design strategy to enhance the anti-*T. cruzi* activity.

An examination of parasite morphology revealed that compound BA5 is parasitocidal, by altering parasite ultrastructure. It induced flagella retraction, loss of plasma membrane integrity and notable cell body deformation. Interestingly, the treatment with

BA5 also led to the formation of numerous and atypical vacuoles within the cytoplasm, as well as the dilatation of Golgi cisternae. Lack of membrane integrity and cytoplasmic vacuolization are often associated to necrotic parasitic death (Rodríguez et al., 2006; Zong and Thompson, 2006). Through flow cytometry assays, we confirmed the parasitic death by necrosis. In addition, we observed that the treatment produced endoplasmatic reticulum profiles involving organelles as nucleus accompanied by the formation of autophagosomes, typical features of autophagy (Tsujimoto and Shimizu, 2005; Fernandes et al., 2012).

Most importantly, the semi-synthetic derivatives were able to prevent the parasite development and invasion into host cells, crucial events for *T. cruzi* infection establishment, with potency similar to benznidazole. As a limitation, these compounds didn't eliminate intracellular amastigotes even in the highest concentration tested. However, the derivative BA5 exhibited synergistic activity when used in combination to benznidazole. These results encourage further investigations, since the combination of drugs is becoming increasingly attractive to combat parasitic diseases (Alirol et al., 2013; Diniz et al., 2013; Sousa et al., 2014).

Altogether, these findings reinforce that terpenoids are potent and selective trypanocidal agents. Therefore, the screening for structurally-related BA5 derivative for Chagas disease treatment is an attractive line of drug development.

5. Conclusion

Here, we have reported the synthesis and anti-*T. cruzi* evaluation of betulinic acid and its new amide semi-synthetic derivatives. By varying substituents attached to the amide group, we could find substituents that retain, enhance or greatly increase the trypanocidal activity, in comparison to betulinic acid. Specifically, we identified the betulinic acid derivative BA5 as a selective anti-*T. cruzi* agent, which destroys parasite cells by necrotic death and acts synergistically in combination to benznidazole.

Acknowledgements

This work was supported by grants from CNPq (grant number 562655/2010-7), PRONEX (grant number 0002/2014), FAPESP (grant number 0042/2013) and FINEP (grant number 01.04.0320-00).

References

- Alakurtti, S., Heiska, T., Kiriaziz, A., Sacerdoti-Sierra, N., Jaffe, C.L., Yli-Kauhaluoma, J., 2010. Synthesis and anti-leishmanial activity of heterocyclic betulin derivatives. *Bioorg. Med. Chem.* 18, 1573–1582.
- Alirol, E., Schrupf, D., Amici-Heradi, J., Riedel, A., de Patoul, C., Quere, M., Chappuis, F., 2013. Nifurtimox-eflornithine combination therapy for second-stage gambiense human African trypanosomiasis: Médecins Sans Frontières experience in the Democratic Republic of the Congo. *Clin. Infect. Dis.* 56, 195–203.
- Baglin, I., Mitaine-Offer, A.C., Nour, M., Tan, K., Cave, C., Lacaile-Dubois, M.A., 2003. A review of natural and modified betulinic, ursolic and echinocystic acid derivatives as potential antitumor and anti-HIV agents. *Mini Rev. Med. Chem.* 3, 525–539.
- Baltina, L.A., Flekhter, O.B., Nigmatullina, L.R., Boreko, E.I., Pavlova, N.I., Nikolaeva, S.N., Savinova, O.V., Tolstikov, G.A., 2003. Lupane triterpenes and derivatives with antiviral activity. *Bioorg. Med. Chem. Lett.* 13, 3549–3552.
- Barbosa-Filho, J.M., Trigueiro, J.A., Cheryan, U.O., Bhattacharyya, J., 1985. Constituents of the stem-bark of *Ziziphus joazeiro*. *J. Nat. Prod.* 48, 152–152.
- Chen, Y., Li, S., Sun, F., Han, H., Zhang, X., Fan, Y., Tai, G., Zhou, Y., 2010. In vivo antimalarial activities of glycoalkaloids isolated from Solanaceae plants. *Pharm. Biol.* 48, 1018–1024.
- Chakraborty, B., Dutta, D., Mukherjee, S., Das, S., Maiti, C., Das, P., Chowdhury, C., 2015. Synthesis and biological evaluation of a novel betulinic acid derivative as an inducer of apoptosis in human colon carcinoma cells (HT-29). *Eur. J. Med. Chem.* 102, 93–105.

- Chandramu, C., Monohar, R.D., Krupadanam, D.G., Dashavantha, R.V., 2003. Isolation, characterization and biological activity of betulinic acid and ursolic acid from *Vitex negundo* L. *Phytother. Res.* 27, 129–134.
- Chou, T.C., Talalay, P., 2005. Quantitative analysis of dose-effect relationships: the combined effects of multiple drugs or enzyme inhibitors. *Adv. Enzyme Regul.* 22, 27–55.
- Costa, J.F.O., Barbosa-Filho, J.M., Maia, G.L.A., Guimarães, E.T., Meira, C.S., Ribeiros-Santos, R., Carvalho, L.C.P., Soares, M.B.P., 2014. Potent anti-inflammatory activity of betulinic acid treatment in a model of lethal endotoxemia. *Int. Immunopharmacol.* 23, 469–474.
- Da Silva, C.F., Junqueira, A., Lima, M.M., Romanha, A.J., Junior, P.A.S., Stephens, C.E., Som, P., Boykin, D.W., Soeiro, M.N.C., 2011. *In vitro* trypanocidal activity of DB745B and other novel arylimidamides against *Trypanosoma cruzi*. *J. Antimicrobiol. Chemother.* 66, 1295–1297.
- Drag, M., Surowiak, P., Drag-Zelesinska, M., Diétel, M., Lage, H., Oleksyzyn, L., 2009. Comparison of the cytotoxicity effects of birch bark extract, betulin and betulinic acid towards human gastric carcinoma and pancreatic carcinoma drug-sensitive and drug resistant cell lines. *Molecules* 14, 1639–1651.
- Diniz, L.F., Urbina, J.A., De Andrade, I.M., Mazzeti, A.L., Martins, T.A., Caldas, I.S., Talvani, A., Ribeiro, I., Bahia, M.T., 2013. Benznidazole and posaconazole in experimental Chagas disease: positive interaction in concomitant and sequential treatments. *PLoS Negl. Trop. Dis.* 7, e2367.
- Domínguez-Carmona, D.B., Escalante-Erosa, F., García-Sosa, K., Ruiz-Pinell, G., Gutierrez-Yapu, D., Chan-Bacab, M.J., Giménez-Turba, A., Peña-Rodríguez, L.M., 2010. Antiprotozoal activity of betulinic acid derivatives. *Phytomedicine* 17, 379–382.
- Fernandes, M.C., Da Silva, E.N., Pinto, A.V., De Castro, S.L., Menna-Barreto, R.F., 2012. A novel triazolic naphthofuranquinone induces autophagy in reservosomes and impairment of mitosis in *Trypanosoma cruzi*. *Parasitology* 139, 26–36.
- Fivelman, Q.L., Adagu, I.S., Warhurst, D.G., 2004. Modified fixed-ratio isobologram method for studying in vitro interactions between atovaquone and proguanil or dihydroartemisinin against drug-resistant strain of *Plasmodium falciparum*. *Antimicrob. Agents Chemother.* 48, 4097–4102.
- Gros, L., Lorente, S.O., Jimenez, C.J., Yardley, V., Rattray, L., Wharton, H., Little, S., Croft, S.L., Ruiz-Perez, L.M., Gonzalez-Pacanowska, D., Gilbert, I.H., 2006. Evaluation of azasterols as anti-parasitics. *J. Med. Chem.* 49, 6094–6103.
- Hoet, S., Pieters, L., Muccioli, G.G., Habib-Jiwan, J.L., Opperdoes, F.R., Quetin-Leclercq, J., 2007. Antitrypanosomal activity of triterpenoids and sterols from the leaves of *Strychnos spinosa* and related compounds. *J. Nat. Prod.* 70, 1360–1363.
- Innocente, A.M., Silva, G.N., Cruz, L.N., Moraes, M.S., Nakabashi, M., Sonnet, P., Gosmann, G., Garcia, C.R., Gnoatto, S.C., 2012. Synthesis and antiplasmodial activity of betulinic acid and ursolic acid analogues. *Molecules* 17, 12003–12014.
- Jeong, H.J., Chai, H.B., Park, S.Y., Kim, D.S., 1999. Preparation of amino acid conjugates of betulinic acid with activity against human melanoma. *Bioorg. Med. Chem. Lett.* 9 (8), 1201–1204.
- Morillo, C.A., Marin-Neto, J.A., Avezum, A., et al., 2015. Randomized trial of benznidazole for chronic chagas'cardiomyopathy. *N. Engl. J. Med.* 373, 1295–1306.
- Newman, D.J., Cragg, G.M., 2012. Natural products as sources of new drugs over the 30 years from 1981 to 2010. *J. Nat. Prod.* 75, 311–335.
- Pinto-Dias, J.C., 2006. The treatment of Chagas disease (South American trypanosomiasis). *Ann. Intern. Med.* 144, 722–774.
- Rassi Jr, A., Rassi, A., Marin-Neto, J.A., 2010. Chagas disease. *Lancet* 375, 1388–1402.
- Rodrigues, J.C., Seabra, S.H., De Souza, W., 2006. Apoptosis-like death in parasitic protozoa. *Braz. J. Morphol. Sci.* 23, 87–98.
- Soares, M.B.P., Silva, C.V., Bastos, T.M., Guimarães, E.T., Figueira, C.P., Smirlis, D., Azevedo Jr, W.F., 2012. Anti-*Trypanosoma cruzi* activity of nicotinamide. *Acta Trop.* 122, 224–229.
- Sousa, M.C., Varandas, R., Santos, R.C., Santos-Rosa, M., Alvez, V., 2014. Anti-leishmanial activity of semisynthetic lupane triterpenoids betulin and betulinic acid derivatives: synergic effects with miltefosine. *PLoS One* 9, e89939.
- Spivak, A.Y., Keiser, J., Vargas, M., Gubaidullin, R.R., Nedopekina, D.A., Shakurova, E.R., Khalitova, R.R., Odinkov, V.N., 2014. Synthesis and activity of new triphenylphosphonium derivatives of betulin and betulinic acid against *Schistosoma mansoni* in vitro and in vivo. *Bioorg. Med. Chem.* 22, 6297–5304.
- Tsujimoto, Y., Shimizu, S., 2005. Another way to die: autophagic programmed cell death. *Cell Death Differ.* 12, 1528–1534.
- Urbina, J.A., Docampo, R., 2003. Specific chemotherapy of Chagas disease: controversies and advances. *Trends Parasitol.* 19, 495–501.
- Viotti, R., Vigliano, C., Lococo, B., Alvarez, M.G., Petti, M., Bertocchi, G., Armenti, A., 2009. Side effects of benznidazole as treatment in chronic Chagas disease: fears and realities. *Expert Rev. Anti Infect. Ther.* 7, 157–163.
- Yin, M.C., 2015. Inhibitory effects and actions of pentacyclic triterpenes upon glycation. *Biomed. (Taipei)* 5, 13.
- Yogeeswari, P., Sriram, D., 2005. Betulinic acid and its derivatives: a review on their biological properties. *Curr. Med. Chem.* 12, 657–666.
- Zong, W.X., Thompson, C.B., 2006. Necrotic death as a cell fate. *Genes Dev.* 20, 1–15.

ANEXO 3

SOUZA, B. S. F.; SILVA, D. N.; CARVALHO, R. H.; SAMPAIO, G. L. A.; PAREDES, B. D.; FRANÇA, L. A.; AZEVEDO, C. M.; VASCONCELOS, J. F.; **MEIRA, C. S.**; NETO, P. C.; MACAMBIRA, S. G.; SILVA, K. N.; ALLABHDADI, K. J.; TAVORA, F.; NETO, J. D. S.; RIBEIRO-DOS-SANTOS, R.; SOARES, M. B. P. Association of cardiac galectin-3 expression, myocarditis, and fibrosis in chronic Chagas disease cardiomyopathy. **The American Journal of Pathology**, v. 187, p. 1134-1146, 2017.



IMMUNOPATHOLOGY AND INFECTIOUS DISEASES

Association of Cardiac Galectin-3 Expression, Myocarditis, and Fibrosis in Chronic Chagas Disease Cardiomyopathy



Bruno Solano de Freitas Souza,^{*†} Daniela Nascimento Silva,[†] Rejane Hughes Carvalho,[†] Gabriela Louise de Almeida Sampaio,[†] Bruno Diaz Paredes,[†] Luciana Aragão França,[†] Carine Machado Azevedo,^{*†} Juliana Fraga Vasconcelos,^{*†} Cassio Santana Meira,^{*†} Paulo Chenaud Neto,[†] Simone Garcia Macambira,^{*†‡} Kátia Nunes da Silva,[†] Kyan James Allahdadi,[†] Fabio Tavora,[§] João David de Souza Neto,[§] Ricardo Ribeiro dos Santos,[†] and Milena Botelho Pereira Soares^{*†}

From the Gonçalo Moniz Research Center, * Oswaldo Cruz Foundation (FIOCRUZ), Salvador; the Center for Biotechnology and Cell Therapy,[†] São Rafael Hospital, Salvador; the Health Sciences Institute,[‡] Federal University of Bahia, Salvador; and Messejana Heart and Lung Hospital,[§] Fortaleza, Brazil

Accepted for publication
January 19, 2017.

Address correspondence to
Milena Botelho Pereira Soares,
Ph.D., Centro de Pesquisas
Gonçalo Moniz, Fundação
Oswaldo Cruz, Rua Waldemar
Falcão, 121, Candeal, Salvador,
Bahia, Brazil CEP: 40296-
710. E-mail: [milena@bahia.
fiocruz.br](mailto:milena@bahia.fiocruz.br).

Chronic Chagas disease cardiomyopathy, caused by *Trypanosoma cruzi* infection, is a major cause of heart failure in Latin America. Galectin-3 (Gal-3) has been linked to cardiac remodeling and poor prognosis in heart failure of different etiologies. Herein, we investigated the involvement of Gal-3 in the disease pathogenesis and its role as a target for disease intervention. Gal-3 expression in mouse hearts was evaluated during *T. cruzi* infection by confocal microscopy and flow cytometry analysis, showing a high expression in macrophages, T cells, and fibroblasts. *In vitro* studies using Gal-3 knockdown in cardiac fibroblasts demonstrated that Gal-3 regulates cell survival, proliferation, and type I collagen synthesis. *In vivo* blockade of Gal-3 with N-acetyl-D-lactosamine in *T. cruzi*-infected mice led to a significant reduction of cardiac fibrosis and inflammation in the heart. Moreover, a modulation in the expression of proinflammatory genes in the heart was observed. Finally, histological analysis in human heart samples obtained from subjects with Chagas disease who underwent heart transplantation showed the expression of Gal-3 in areas of inflammation, similar to the mouse model. Our results indicate that Gal-3 plays a role in the pathogenesis of experimental chronic Chagas disease, favoring inflammation and fibrogenesis. Moreover, by demonstrating Gal-3 expression in human hearts, our finding reinforces that this protein could be a novel target for drug development for Chagas cardiomyopathy. (*Am J Pathol* 2017, 187: 1134–1146; <http://dx.doi.org/10.1016/j.ajpath.2017.01.016>)

Chronic Chagas disease cardiomyopathy (CCC), caused by *Trypanosoma cruzi* infection, is an important cause of morbidity and mortality in endemic countries. It is estimated that approximately 7 million people are infected worldwide, with high prevalence in Latin America and growing incidence in developed countries because of globalization.^{1,2} It is estimated that the cardiac form of the disease occurs in approximately 20% to 30% of infected subjects.² Antiparasitic drugs are effective during acute infection, but fail to improve established CCC.^{3,4} Besides standard heart failure treatment, patients with advanced CCC rely on heart transplantation, which is limited because of organ availability and complications relative to parasite reactivation after immunosuppression therapy.⁵

During CCC, cardiomyocytes are lost as a result of damage caused by immune responses directed to the parasites that persist in the heart, as well as to autoreactive cells directed to heart antigens.^{6,7} Although the mechanisms of pathogenesis are not completely understood, several studies indicate the involvement of type 1 helper T-cell lymphocytes associated with high production of interferon- γ (IFN- γ), resembling a delayed hypersensitivity reaction.⁶ An association between progression to severe chronic forms and a high production of IFN- γ was observed in

Supported by National Council for Scientific and Technological Development and Bahia Research Foundation.

Disclosures: None declared.

patients with Chagas disease.⁸ Macrophages, a major cell population found in the inflammatory sites, can be activated by IFN- γ and tumor necrosis factor- α , two inflammatory cytokines overexpressed in the hearts of mice chronically infected with *T. cruzi*. Furthermore, several genes related to the inflammatory response are up-regulated in heart tissue during the chronic phase of *T. cruzi* infection.⁹

Previous studies suggested that activated macrophages secrete galectin-3 (Gal-3), a molecule involved in the pathogenesis of cardiac dysfunction.¹⁰ Gal-3 is a soluble β -galactoside binding lectin involved in a variety of cellular processes, including proliferation, migration, and apoptosis.¹¹ The importance of this protein in the regulation of cardiac fibrosis and remodeling has been highlighted by the demonstration of its contribution to the development and progression of heart failure in different experimental settings.^{12–14} Serum Gal-3 concentrations are also increased in patients with acute decompensated heart failure. On the basis of these findings, the value of Gal-3 as a prognostic biomarker in patients with chronic heart failure has been investigated.¹⁵

Previously, we performed transcriptomic analysis in the cardiac tissue of mice chronically infected with *T. cruzi*, and found that *Lgals3*, the gene encoding for Gal-3, is among the most overexpressed genes.¹⁶ By immunofluorescence analysis, we showed that Gal-3 is mainly expressed in inflammatory cells in the hearts of *T. cruzi*-infected mice. We hypothesized that Gal-3 plays a role in the pathogenesis of CCC, contributing to the progression of inflammation and fibrosis. In the present study, we evaluated the expression of Gal-3 during *T. cruzi* infection in mice. Gal-3 expression was also investigated in human heart samples, to validate the expression of this protein in the human disease setting. Finally, we conducted *in vitro* and *in vivo* studies involving genetic and pharmacological blockades of Gal-3 to investigate its potential role in disease pathogenesis and its usefulness as a target for therapeutic development.

Materials and Methods

Animal Procedures

Six- to eight-week-old female C57BL/6 mice were used for *T. cruzi* infection and as normal controls. Galectin-3 C57BL/6 mice were used in cell adhesion experiments. All animals were raised and maintained at the animal facility of the Center for Biotechnology and Cell Therapy, Hospital São Rafael, in rooms with controlled temperature (22°C \pm 2°C) and humidity (55% \pm 10%), and continuous air flow. Animals were housed in a 12-hour light/12-hour dark cycle (6AM to 6PM) and provided with standard rodent diet and water ad libitum. Animals were handled according to the NIH guidelines for animal experimentation.¹⁷ All procedures described had prior approval from the local institutional animal ethics committee at Hospital São Rafael (01/13).

Trypanosoma cruzi Infection

Trypomastigotes of the myotropic Colombian *T. cruzi* strain were obtained from culture supernatants of infected LLC-MK2 cells, as previously described.⁹ Infection of C57BL/6 mice was performed by i.p. injection of 1000 *T. cruzi* trypomastigotes in saline, and was confirmed through evaluation of parasitemia at different time points after infection.

Pharmacological Blockade of Gal-3 with N-Lac

C57BL/6 female mice ($n = 11$) chronically infected with *T. cruzi* [6 months postinfection (m.p.i.)] were treated with N-acetyl-D-lactosamine (N-Lac) (Sigma-Aldrich, St. Louis, MO), 5 mg/kg per day, i.p. injections 3 \times per week, for 60 days. Chronically infected mice injected with saline ($n = 10$) and same age naïve mice ($n = 8$) served as controls. Functional analyses were performed, as described below. Mice were euthanized, by cervical dislocation under anesthesia with 5% ketamine (König, São Paulo, Brazil) and 2% xylazine (König Lab), the week after the final N-Lac injection. Heart samples were collected for real-time quantitative PCR and histological analysis. In another experiment, sucrose (Sigma-Aldrich) was administered in the same regimen as N-Lac to C57BL/6 mice, after 6 months of infection with *T. cruzi*. Heart samples were collected for histological analysis.

Functional Analysis

Electrocardiography was performed using the Bio Amp PowerLab System (PowerLab 2/20; ADInstruments, Sydney, Australia), recording the bipolar lead I. All animals were anesthetized by i.p. injection of 10 mg/kg xylazine and 100 mg/kg ketamine to obtain the records. All data were acquired for computer analysis using Chart 5 for Windows (ADInstruments). The electrocardiographic analysis included heart rate, PR interval, P wave duration, QT interval, QTc, and arrhythmias. The QTc was calculated as the ratio of QT interval by square roots of RR interval.

A motor-driven treadmill chamber for one animal (LE 8700; Panlab, Barcelona, Spain) was used to exercise the animals. The speed of the treadmill and the intensity of the shock (mA) were controlled by a potentiometer (LE 8700 treadmill control; Panlab). After an adaptation period in the treadmill chamber, the mice exercised at five different velocities (7.2, 14.4, 21.6, 28.8, and 36.0 m/minute), with increasing velocity after 5 minutes of exercise at a given speed. Velocity was increased until the animal could no longer sustain a given speed and remained >5 seconds on an electrified stainless-steel grid. Total running distance was recorded.

Morphometric Analysis

Two months after the therapy, mice were euthanized as mentioned before and hearts were collected and fixed in 10% buffered formalin. Heart sections were analyzed by

light microscopy after paraffin embedding, followed by standard hematoxylin and eosin staining. Inflammatory cells infiltrating heart tissue were counted using a digital morphometric evaluation system. Images were digitized using the slide scanner ScanScope (Leica, Wetzlar, Germany). Morphometric analyses were performed using Image Pro Plus software version 7.0 (Media Cybernetics, Rockville, MD). The inflammatory cells were counted in 10 fields ($\times 400$ magnification) per heart sample. The percentage of fibrosis was determined using Sirius red–stained heart sections and the Image Pro Plus version 7.0. Two blinded investigators performed the analyses (J.F.V. and C.M.A.).

Immunofluorescence Analysis

Frozen (10 μm thick) or formalin-fixed, paraffin-embedded (3 μm thick) heart sections were obtained. Paraffin-embedded tissues were deparaffinized and submitted to a heat-induced antigen retrieval step by incubation in citrate buffer (pH = 6.0). Then, sections were incubated overnight at 4°C with the following primary antibodies: anti-Gal-3, diluted 1:400 (Santa Cruz Biotechnology, Dallas, TX) and anti-CD11b, diluted 1:400 (BD Biosciences, San Jose, CA). Next, the sections were incubated for 1 hour with secondary antibodies anti-goat IgG Alexa Fluor 488-conjugated and anti-rat IgG Alexa Fluor 594-conjugated (1:400; ThermoFisher Scientific, Waltham, MA). Immunostaining for *in vitro* experiments was performed in cardiac fibroblasts or bone marrow–derived macrophages plated on coverslips. The cells were fixed with paraformaldehyde 4% and incubated with the primary antibodies: goat anti-Gal-3, diluted 1:400 (Santa Cruz Biotechnology), or rabbit anti-collagen type I, diluted 1:50 (Novotec, Lyon, France). On the following day, sections were incubated for 1 hour with phalloidin conjugated with Alexa Fluor 633 or 488 conjugated, diluted 1:50, mixed with the secondary antibodies anti-goat IgG Alexa Fluor 488-conjugated (1:400) or anti-rabbit IgG Alexa Fluor 568-conjugated (1:200; all from ThermoFisher Scientific), respectively. Nuclei were stained with DAPI (VectaShield mounting medium with DAPI H-1200; Vector Laboratories, Burlingame, CA). The presence of fluorescent cells was determined by observation on a FluoView 1000 confocal microscope (Olympus, Tokyo, Japan) and A1+ confocal microscope (Nikon, Tokyo, Japan). Quantifications of Gal-3⁺ cells were performed in 10 random fields captured under $\times 400$ magnification, using the Image Pro Plus software version 7.0.

Flow Cytometry Analysis

Control and *T. cruzi*–infected mice were euthanized, hearts were collected, perfused with phosphate-buffered saline (PBS) to remove blood cells, and processed by enzymatic digestion using 0.1% collagenase IV (Sigma-Aldrich) and 10 $\mu\text{g}/\text{mL}$ DNase (Roche, Basel, Switzerland), for 40 minutes, at 37°C. To evaluate the subpopulations of digested cardiac tissue

samples, cell suspensions were allowed to pass through a 70- μm cell strainer (BD Biosciences) and counted. Aliquots of 10^6 cells were used for each test tube and 1 μL of Fc blocking reagent (BD Biosciences) was added. The fluorochrome-conjugated antibody panels used for each subpopulation were: i) T lymphocytes: CD45-APC-Cy7, CD3-APC, CD4-PE-Cy5, CD8-PE (BD Biosciences); ii) macrophages: CD45-APC-Cy7, CD11b-APC (eBiosciences, San Diego, CA); iii) fibroblast/fibrocyte: CD45-APC-Cy7, vimentin-APC (Cell Signaling, Danvers, MA). Each antibody was diluted as suggested on the product data sheet. Samples were incubated for 20 minutes at room temperature in the dark. For intracellular staining of Gal-3, samples were washed once in PBS and CytoFix/CytoPerm kit (BD Biosciences) were used as directed on data sheet protocol. Anti-Gal-3-PE (R&D Systems, Minneapolis, MN) antibody was added to macrophages and fibroblast/fibrocyte sample tubes, whereas nonconjugated anti-Gal-3 (Santa Cruz Biotechnology) was added on T lymphocyte sample tube and its detection was performed by addition of anti-mouse IgG-Alexa Fluor 488 (ThermoFisher Scientific). Each incubation step was performed during 30 minutes at room temperature in the dark. Samples were washed twice and resuspended in PBS and added with Hoechst 33258 to exclude cell debris from analysis. Apoptosis was evaluated by annexin V-PI assay. Cells were harvested from culture flasks by adding TrypLE solution (ThermoFisher Scientific) and incubating for 5 minutes at 37°C. Cell suspensions were collected and washed with PBS by centrifugation at $300 \times g$. After discarding supernatant, pellets were resuspended in binding buffer (ThermoFisher Scientific) and cells were counted. Apoptosis assays were performed using annexin-V-APC and PI (BD Biosciences) according to the manufacturer's recommendations. Sample acquisition was performed using a BD LSRFortessa SORP cytometer (BD Biosciences) using BD FACS Diva software version 6.2 (BD Biosciences). Ten thousand events were acquired per sample, and the data were analyzed using FlowJo software version 7.5 (FlowJo Enterprise, Ashland, OR).

Real-Time RT-PCR

Total RNA was isolated from heart samples with TRIzol reagent (ThermoFisher Scientific) and the concentration was determined by spectrophotometry. High Capacity cDNA Reverse Transcription Kit (ThermoFisher Scientific) was used to synthesize cDNA of 1 μg RNA following manufacturer's recommendations. Real-time RT-PCR assays were performed to detect the expression levels of *Tbet* (Mm_00450960_m1), *Gata3* (Mm_00484683_m1), *Tnf* (Mm_00443258_m1), *Ifng* (Mm_00801778_m1), *Il10* (Mm_00439616_m1), *Foxp3* (Mm_00475162_m1), *Lgals3* (Mm_00802901_m1), and *MMP9* (Mm_00444299_m1). Other primer sequences used in real-time PCR analyses: *Coll1*: 5'-GTCCCTCGACTCCTACATCTTCTGA-3' (forward) and 5'-AAACCCGAGGTATGCTTGATCTGTA' (reverse); *Ccnd1*: 5'-TCCGCAAGCATGCACAGA-3'

(forward) and 5'-GGTGGGTTGGAAATGAACTTCA-3' (reverse); *Cav1*: 5'-GGCACTCATCTGGGGCATTTA-3' (forward) and 5'-CTCTTGATGCACGGTACAACC-3' (reverse). The real-time RT-PCR amplification mixtures contained a 20 ng template cDNA, TaqMan Master Mix (10 μ L) and probes, constituting a final volume of 20 μ L (all from ThermoFisher Scientific). All reactions were run in duplicate on an ABI7500 Sequence Detection System (ThermoFisher Scientific) under standard thermal cycling conditions. The mean Ct values from duplicate measurements were used to calculate expression of the target gene, while normalized to an internal control (*Gapdh*) using the 2⁻DCt formula. Experiments with CVs >5% were excluded. A nontemplate control and nonreverse transcription controls were also included.

Design of shRNAs and Production of Lentiviral Vectors

To stably knock down *Lgals3* expression, we designed shRNA against different regions of the *Lgals3* coding sequence, and a scramble shRNA as control. Target sequences were designed using the online tool siRNA Wizard software version 3.1 (Invivogen, San Diego, CA). All suggested sequences were blasted against the mouse RNA reference sequence database, and the three with the lowest degree of homology to other sequences were selected: *Lgals3*_shRNA1 5'-GATTTTCAGGAGAGGGAATGAT-3'; *Lgals3*_shRNA2 5'-GGTCAACGATGCTCACCTACT-3'; *Lgals3*_shRNA3 5'-CATGCTGATCACAATCATGG-3'; and one *Lgals3*_scrbl_shRNA 5'-AGGTATGAGTCGA-GATTGAGA-3'. Sense and antisense single strands, containing the target sequence, a loop sequence (TCAAGAG), and restriction enzyme sites for MluI at the sense sequence and ClaI at the antisense sequence, were synthesized separately. The annealing of both strands to form double-stranded shRNAs was performed by incubating 2.5 μ mol/L from the sense and antisense strand of each shRNA in 10 mmol/L Tris-HCl (pH 7.5), 0.1 mol/L NaCl, and 1 mmol/L EDTA at 95°C for 5 minutes and then allowing the reaction to cool down to room temperature for at least 2 hours. The double-stranded shRNAs were then phosphorylated using T4 PNK (New England Biolabs, Ipswich, MA) following manufacturer protocol. The shRNAs were cloned into the pLVTHM lentiviral vector (Addgene plasmid 12247), specifically designed for gene knockdown with shRNAs,¹⁸ after the vector was linearized by digestion with MluI and ClaI (New England Biolabs) according to the manufacturer instructions. Each of the produced shRNA constructs were confirmed by sequencing using ABI 3500 platform (ThermoFisher Scientific).

For lentiviral vector production, HEK293 FT cells were cotransfected with each of the shRNA constructs, plus psPAX2 (Addgene plasmid 12260) and pMD2.G (Addgene plasmid 12247) for production of the lentivirus particles, in a proportion of 3:2:1. Viral supernatants were harvested 48 and 72 hours later, pooled, centrifuged to remove cell debris, filtered through 0.45- μ m filters (Millipore, Billerica, MA), and concentrated by ultracentrifugation. Cardiac

fibroblasts were transduced with the lentivirus by overnight incubation in medium containing lentiviral particles and 6 μ g/mL polybrene. Knockdown efficiency for each shRNA was evaluated by real-time quantitative PCR using TaqMan probes for *Lgals3* (mm00802901_m1), *Gapdh* (mm99999915_g1), *Actb* (mm00607939_s1), and *Hprt* (mm00496968_m1) and TaqMan Universal PCR master mix (ThermoFisher Scientific), according to the manufacturer's instructions. Assay was performed in triplicate, and the empty vector was used as control. Ct for *Lgals3* was normalized taking into account the geometric mean of the Ct for *Gapdh*, *Actb*, and *Hprt* (Δ Ct). The relative expression was then calculated by the normalized Ct between each *Lgals3* shRNA construct and the empty vector ($\Delta\Delta$ Ct).

In Vitro Studies with Cardiac Fibroblasts and Bone Marrow-Derived Macrophages

Cardiac fibroblasts were isolated from hearts of adult C57BL/6 mice, euthanized as described above. Hearts were minced into pieces of 1 mm and incubated with 0.1% collagenase type A (Sigma-Aldrich) at 37°C for 30 minutes, under constant stirring. The cell suspension was passed through a 70- μ m cell strainer (BD Biosciences), and plastic-adherent cells were selected by 1 hour incubation in gelatin-coated flasks (Sigma-Aldrich). Nonadherent cells from supernatant were removed and adherent cells were cultured with Dulbecco's modified Eagle's medium supplemented with 10% fetal bovine serum and 1% penicillin and streptomycin (all from ThermoFisher Scientific), in a humidified incubator at 37°C with 5% CO₂. Culture medium was changed every 3 days, and cells were trypsinized (trypsin-EDTA 0.05%; ThermoFisher Scientific) when 80% confluence was reached. Cell cycle studies were performed with CFSE Cell Proliferation Kit (ThermoFisher Scientific), according to the manufacturer's instructions. Proliferation of cardiac fibroblasts was assessed by the measurement of ³H-thymidine uptake. Cells were plated in 96-well plates, at a density of 10⁴ cells/well, in a final volume of 200 μ L, in triplicate, and cultured in the absence or presence of 30 μ g/mL rmGal-3 (R&D Systems), with or without 1% modified citrus pectin (ecoNugenics, Santa Rosa, CA). After 24 hours, plates were pulsed with 1 μ Ci of methyl-³H thymidine (PerkinElmer, Waltham, MA) for 18 hours, and proliferation was assessed by measurement of ³H-thymidine uptake by using a Chameleon β -plate counter (Hydrex, Turku, Finland). Proliferation capacity of Gal-3 knockdown and control cell lines was compared by ³H-thymidine incorporation, using the same procedures.

To obtain macrophages, bone marrow cells were harvested from femurs of C57BL/6 mice by flushing with cold RPMI 1640 medium. Bone marrow cells were induced to differentiate into macrophages by culture in RPMI 1640 supplemented with 10% fetal bovine serum (ThermoFisher Scientific), 50 U/mL of penicillin, 50 μ g/mL of streptomycin, 2.0 g/L of sodium bicarbonate, 25 mmol/L HEPES, 2 mmol/L

glutamine, and 30% supernatant obtained from X63-GM-CSF¹⁹ cell line culture, at 37°C and 5% CO₂. Cells were cultured for 7 days, with half medium changes every 3 days. Differentiated macrophages were plated onto 24-well plates and incubated in medium alone or with 1 µg/mL lipopolysaccharide (Sigma-Aldrich) with or without 50 ng/mL IFN-γ (R&D Systems). After 24 hours, macrophages were detached using a cell scraper and analyzed for Gal-3 expression by flow cytometry, as described above.

Human Samples

The procedures involving human samples received prior approval by the local Ethics committee at Hospital São Rafael (approval number 51025115.3.0000.0048). Samples were obtained at Messejana Hospital in Fortaleza, Ceará, a medical center specialized for heart transplantation in Brazil. Fragments of explanted hearts from three patients with Chagas disease, confirmed by serological assay, were obtained from left ventricle and septum. Samples were processed in paraffin and stained with hematoxylin and eosin and Sirius Red, or used for immunostaining for detection of Gal-3, as described above.

Lymphoproliferation Assay

Splenocyte suspensions, obtained from C57Bl/6 mice, were prepared in Dulbecco's modified Eagle's medium supplemented with 10% fetal bovine serum and 50 µg/mL of

gentamicin. Splenocytes were cultured in 96-well plates at 1 × 10⁶ cells/well, in triplicate, and lymphocyte proliferation was stimulated or not with concanavalin A (2 µg/mL; Sigma-Aldrich) or Dynabeads mouse T-activator CD3/CD28 (ThermoFisher Scientific), according to the manufacturer's instructions. Cell proliferation was induced in the absence or presence of various concentrations of N-Lac (10, 1, and 0.1 µmol/L). After 48 hours of incubation, 1 µCi of ³H-thymidine was added to each well, and the plate was incubated for 18 hours. Plates were frozen at -70°C, then thawed and transferred to UniFilter-96 GF/B PEI coated plates (PerkinElmer) with the assistance of a cell harvester. After drying, 50 mL of scintillation cocktail was added in each well, sealed and plate read at liquid scintillation microplate counter. Dexamethasone (Sigma-Aldrich; 10 µmol/L) was used as positive control. Three independent experiments were performed.

En Face Leukocyte Adhesion Assay

The aorta from the thoracic region and spleens were removed from wild-type and galectin-3 knockout C57Bl/6 mice. Fragments of approximately 1 mm² were placed with the intimal side up in 96-well plates previously coated with Matrigel (Corning Inc., Corning, NY) for 30 minutes at 37°C. Endothelium was activated by incubation with 500 ng/mL lipopolysaccharide (Sigma), whereas the splenocyte suspension with 2 µg/mL concanavalin A (Sigma)

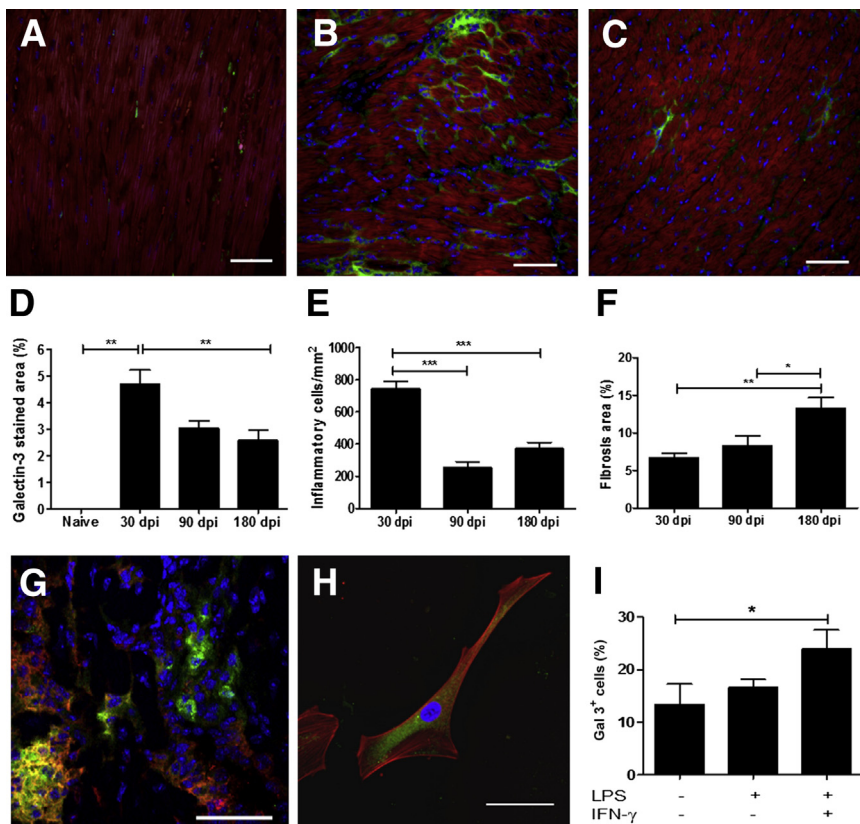


Figure 1 Gal-3 is overexpressed in mouse hearts after *Trypanosoma cruzi* infection. Confocal microscopy analysis demonstrated the presence of Gal-3⁺ cells (green), mainly in areas of inflammatory infiltrates, in naïve (A), at 1 (B) and 6 (C) months postinfection (m.p.i.). Cardiac muscle was stained for actin-F (red), and nuclei were stained with DAPI (blue). D: The cardiac expression of Gal-3 peaked at 1 m.p.i., but remained elevated during the chronic phase of infection, when compared to naïve mice. E: A similar pattern is observed for the number of inflammatory cells infiltrating the heart. F: However, the percentage of fibrosis increased with time. G: Most cells expressing Gal-3 (green) coexpressed the monocyte/macrophage marker CD11b (red). H: Cardiac fibroblasts isolated by enzymatic digestion of heart tissue also express Gal-3 (green). Actin-F is seen in red, and nucleus in blue. I: Bone marrow-derived macrophages stimulated *in vitro* with proinflammatory (M1) inducers interferon-γ (IFN-γ) and lipopolysaccharide (LPS) increase the expression of Gal-3. Data are expressed as means ± SEM. *P < 0.05, **P < 0.01, and ***P < 0.001. Scale bars = 50 µm. dpi, days postinfection.

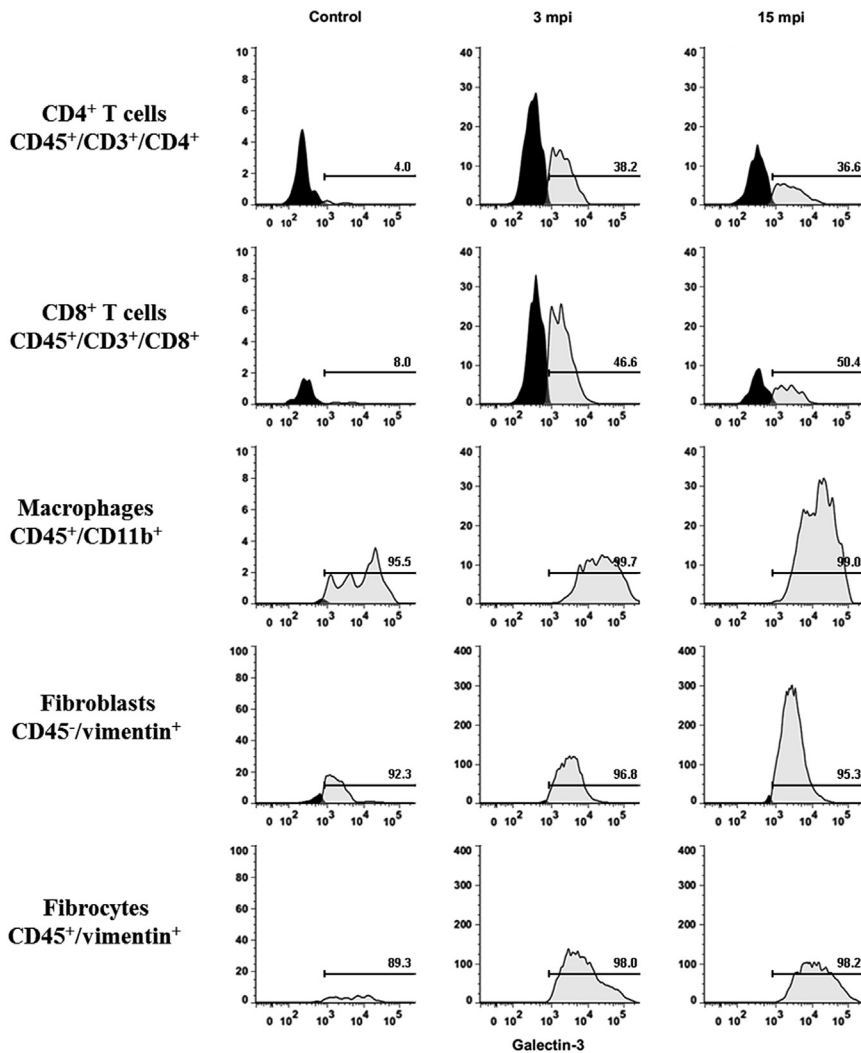


Figure 2 Gal-3 is increased in different cell types involved in inflammation and tissue repair. Histograms showing flow cytometry analysis from digested heart tissue, obtained from naïve and infected mice, at 3 and 15 months postinfection (m.p.i.). Gal-3⁺ T CD4⁺ and CD8⁺ lymphocytes expressing Gal-3 are increased at 3 and 15 m.p.i. when compared to naïve controls. Most macrophages (CD45⁺/CD11b⁺), fibroblasts (CD45⁻/vimentin⁺), and bone marrow-derived fibrocytes (CD45⁺/vimentin⁺) express Gal-3 (>90%) in all groups, but the mean fluorescence intensity increases with time of infection.

and 500 ng/mL lipopolysaccharide, during a period of 6 hours.

Activated splenocytes were incubated with 1 $\mu\text{mol/L}$ Celltracker Fluorescent Probes (Life Technologies) in serum-free RPMI 1640 medium (Gibco) for 30 minutes and washed three times, before adhesion to the endothelium. Splenocytes (5×10^5 /well) were plated and incubated with the aortic endothelium fragments for 30 minutes at 37°C in the presence or absence of 10 $\mu\text{mol/L}$ N-Lac (Sigma-Aldrich). Plates were then carefully washed three times with warm Hanks' balanced salt solution to remove the nonadherent cells. Three replicates were used for each treatment. Different random areas per well were acquired using a digital camera from an inverted fluorescence microscope. Fluorescent cells were quantified using ImagePro.

Inhibition of Cell Migration Assay

C57BL/6 mice, 8 to 12 weeks old, were submitted to euthanasia by cervical dislocation under anesthesia. Spleens

were collected, minced, cells were resuspended in PBS and passed through a 70- μm cell strainer. The cells were resuspended and maintained in RPMI 1640 medium (ThermoFisher Scientific), without serum, supplemented with 2 mmol/L L-glutamine (ThermoFisher Scientific), 0.1% RPMI 1640 vitamin solution (Sigma Aldrich), 1 mmol/L sodium pyruvate, 10 mmol/L HEPES, 50 $\mu\text{mol/L}$ 2-mercaptoethanol, and penicillin/streptomycin solution (all from ThermoFisher Scientific). Splenocytes were incubated in starvation during 24 hours at 37°C and 5% CO₂, in the presence or absence of 10 $\mu\text{mol/L}$ N-Lac. Migration assay was performed using the QCM Chemotaxis Cell Migration Assay, 24-well 3- μm pore (Millipore), according to the manufacturer's instructions. Briefly, splenocytes were counted and 10^7 cells in 250 μL were placed in the upper chamber, in serum-free medium, in the presence or absence of N-Lac. RPMI 1640 medium supplemented with 10% fetal bovine serum (ThermoFisher Scientific) with or without 10 $\mu\text{mol/L}$ N-Lac was placed in the bottom chamber. Cells present in the bottom chamber were counted after overnight incubation.

Statistical Analysis

All continuous variables are presented as means \pm SEM. Continuous variables were tested for normal distribution using Kolmogorov-Smirnov test. Parametric data were analyzed using unpaired *t* tests, for comparisons between two groups, and one-way analysis of variance, followed by Bonferroni post hoc test for multiple-comparison test, using Prism 6.0 (GraphPad, La Jolla, CA). $P < 0.05$ was considered statistically significant.

Results

Gal-3 Expression Is Increased during Experimental *T. cruzi* Infection

We first analyzed the expression of Gal-3 in mouse heart sections obtained at different time points of infection. *Trypanosoma cruzi* infection led to increased expression of Gal-3⁺ cells in the myocardium compared to naïve controls, as shown by confocal microscopy (Figure 1, A–C). Quantification of Gal-3 expression showed a significant increase in all time points analyzed, in comparison with uninfected controls (Figure 1D). The number of Gal-3⁺ cells was higher at the peak of parasitemia (1 m.p.i.), when an intense acute inflammatory response is found in the heart (Figure 1E). The numbers of Gal-3⁺ cells during the chronic phase were sustained, whereas the percentage of fibrosis increased with time (Figure 1F). The population of Gal-3⁺ cells in the heart included macrophages (CD11b⁺ cells) (Figure 1G) and cardiac fibroblasts (Figure 1H). To investigate the role of proinflammatory signals in the expression of Gal-3 by macrophages, we performed *in vitro* studies to analyze the expression of Gal-3 in activated macrophages. Bone marrow–derived macrophages activated with IFN- γ and Toll-like receptor 4 ligand lipopolysaccharide had an increased expression of Gal-3, as demonstrated by flow cytometry analysis (Figure 1I).

To better characterize the cell populations expressing Gal-3, we performed flow cytometry analysis of cells isolated from hearts of *T. cruzi*–infected mice (Figure 2). Both CD4⁺ and CD8⁺ T cells had increased Gal-3 expression at 3 and 15 m.p.i. when compared to uninfected controls. In addition, macrophages, characterized as CD45⁺/CD11b⁺, composed the cell populations expressing the higher mean fluorescence intensity of Gal-3 (Figure 2). Gal-3 was expressed at low levels in fibroblasts (vimentin⁺/CD45[−]) in control hearts, and was increased by 52.5% at 3 m.p.i. Gal-3 expression intensity in fibroblasts at 15 m.p.i. returned to levels similar to those found in controls. However, a significant increase in Gal-3 expression was detected in a population of vimentin⁺/CD45⁺ cells, characterized as bone marrow–derived fibrocytes, at 3 and 15 m.p.i., when compared to controls (Figure 2).

Expression of Gal-3 in the Hearts of Subjects with CCC

To evaluate if the presence of Gal-3⁺ cells in the myocardium of infected mice could be translatable to the human

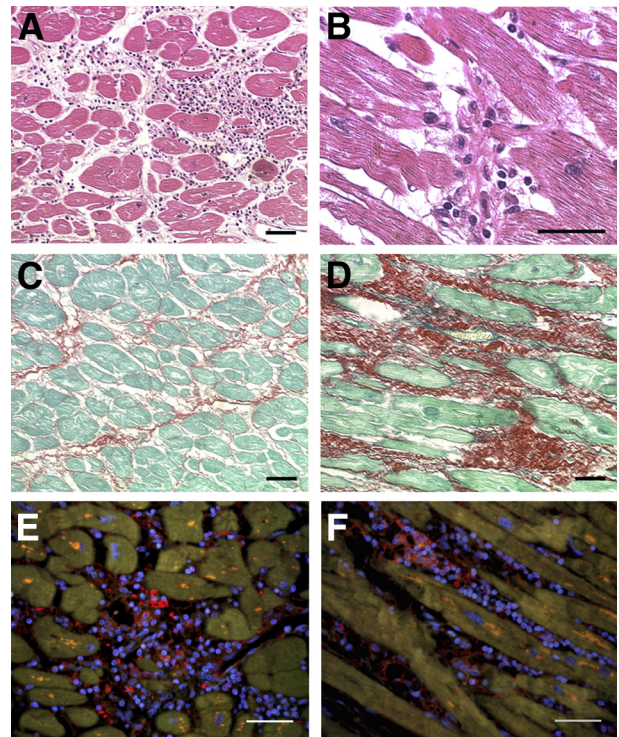


Figure 3 Gal-3 expression in heart samples from subjects with end-stage Chagas cardiomyopathy. Representative images obtained from explanted heart sections of two subjects with end-stage Chagas cardiomyopathy who underwent heart transplantation. Heart sections were stained with hematoxylin and eosin, showing inflammatory infiltrates composed of mononuclear cells surrounding myofibers (A) and in areas of myocytolysis (B). Heart sections stained with Sirius red showing areas of mild (C) and extensive (D) cardiac fibrosis. E and F: Confocal microscopy analysis from two different subjects, showing Gal-3⁺ cells (red) in areas of inflammatory infiltrates. Nuclei are stained with DAPI (blue). Scale bars = 50 μ m (A–C, E, and F); 25 μ m (D).

disease, we performed analysis in human heart samples obtained from explants of subjects with chronic Chagas disease cardiomyopathy who underwent heart transplantation. Heart sections were prepared and stained with hematoxylin and eosin for histological analysis, demonstrating the presence of foci of myocarditis, with an inflammatory infiltrate composed mainly of mononuclear cells, leading to the destruction of myofibers (Figure 3, A and B). In addition, an extensive area of diffuse fibrotic scar was found in Sirius red–stained sections (Figure 3, C and D). The expression of Gal-3 in human heart samples was evaluated by analysis using confocal microscopy. We observed the presence of cells, within the inflammatory foci and surrounding the myofibers, expressing variable levels of Gal-3 (Figure 3, E and F).

Gal-3 Is a Major Regulator of Fibroblast Function

On the basis of the findings of increased Gal-3 expression in fibroblasts during the development of CCC, we performed *in vitro* studies aiming at investigating the role of Gal-3 on different aspects of the biology of these cells. Cardiac

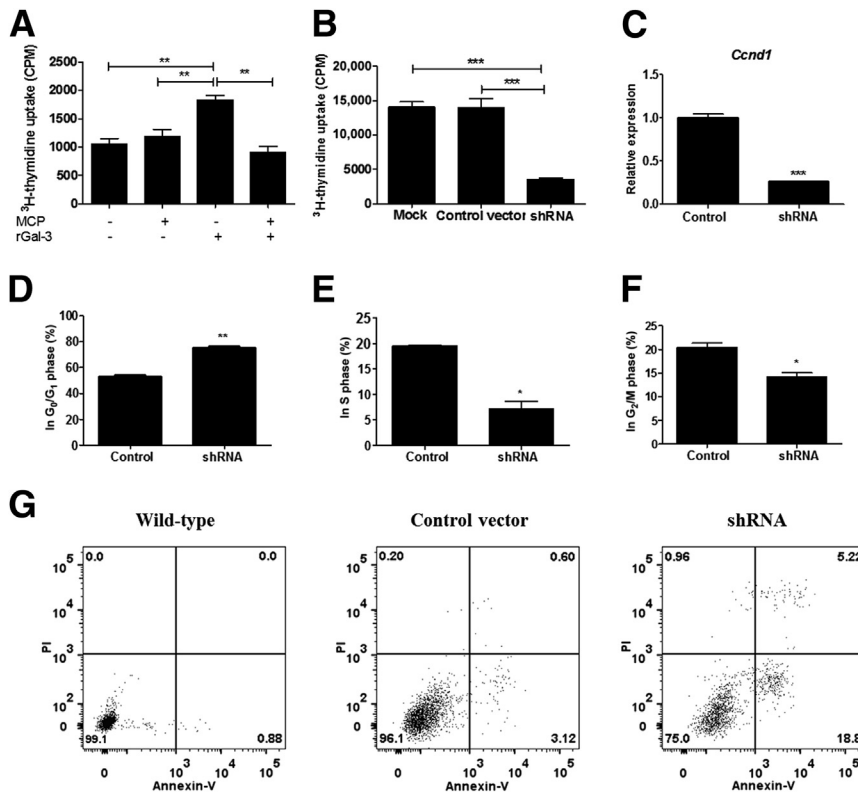


Figure 4 Gal-3 is crucial for cardiac fibroblast proliferation and survival. Recombinant Gal-3 was added to the cardiac fibroblast culture medium and cell proliferation was measured by ^3H -thymidine incorporation assay. **A:** Extracellular Gal-3 induced cardiac fibroblast proliferation, which is abolished by addition of modified citrus pectin, a Gal-3 binding partner. **B:** Gal-3 knockdown in cardiac fibroblasts markedly reduces cell proliferation, as evaluated by ^3H -thymidine incorporation assay. **C:** A reduction in gene expression of cyclin D1 is found by real-time quantitative PCR analysis. Cell cycle analysis was performed by flow cytometry with carboxyfluorescein succinimidyl ester assay, demonstrating that Gal-3 knockdown in cardiac fibroblasts is associated with cell cycle arrest in G_0/G_1 phases (**D**) and reduced number of cells in the S (**E**) and G_2/M (**F**) phases. **G:** Gal-3 knockdown is associated with increased frequency of apoptosis, as evaluated by annexin V assay. Data are expressed as means \pm SEM. * $P < 0.05$, ** $P < 0.01$, and *** $P < 0.001$. CPM, counts per minute; PI, propidium iodide.

fibroblasts isolated from mouse hearts were incubated with mouse recombinant Gal-3 to evaluate their proliferative rate. We found that exogenous recombinant Gal-3, at a micromolar concentration, increased the proliferation of cardiac fibroblasts, whereas addition of modified citrus pectin, a binding partner of Gal-3, blocked the effect of Gal-3 (Figure 4A).

Considering that this effect was observed at high concentrations of exogenous Gal-3, and given the high expression of intracellular Gal-3 in cardiac fibroblasts in experimental CCC, we evaluated the role of endogenous Gal-3 in cardiac fibroblasts. We generated lentiviral vectors encoding shRNA targeting the *Lgals3*, together with green fluorescence protein expression as a reporter gene. Then, cardiac fibroblasts were transduced by lentiviral infection, resulting in the knockdown of Gal-3. The efficiencies of lentiviral infection and knockdown were confirmed by green fluorescence protein reporter gene expression and by quantification of Gal-3 gene and protein expressions by real-time quantitative PCR and immunofluorescence analysis, respectively (>90%) (Supplemental Figure S1, A–E). More important, Gal-3 knockdown in cardiac fibroblasts led to a down-regulation of type I collagen expression (Supplemental Figure S1, F–H).

Gal-3 knockdown was associated with a significant reduction in the proliferative rate of cardiac fibroblasts (Figure 4B). This finding was accompanied by a reduction of cyclin D1 gene expression (Figure 4C). Analysis of caveolin-1 gene expression did not show alterations when

control or Gal-3 knockdown cells were compared (data not shown). Flow cytometry analysis showed cell cycle arrest in Gal-3 knockdown when compared to control cells (increased percentage of G_0/G_1 and decreased S and G_2/M phases) (Figure 4, D–F).

To determine whether Gal-3 knockdown also affects cell survival, we evaluated the frequency of apoptosis in the culture of cardiac fibroblasts, by annexin V/PI staining and flow cytometry analysis. A higher percentage of apoptotic cells was detected in cultures of cardiac fibroblasts with Gal-3 knockdown when compared to controls (Figure 4G).

Treatment with the Gal-3 Blocking Agent N-Lac Reduces Inflammation and Fibrosis in Experimental CCC

To study the role of Gal-3 on the pathogenesis of CCC, we performed a pharmacological blockade of Gal-3 using N-Lac (Figure 5A), during the chronic phase of the infection, when cardiac fibrosis is significantly increased (6 and 8 m.p.i.). We performed functional evaluations (electrocardiographic analysis and treadmill test) before treatment (6 m.p.i.) and after the treatment with N-Lac (8 m.p.i.). *Trypanosoma cruzi* infection caused the development of arrhythmias and cardiac conduction disturbances, such as atrioventricular block, ventricular tachycardia, and ventricular bigeminy. Treatment with N-Lac did not alter the frequencies or the severity of arrhythmias when compared to those found in saline-treated controls (Table 1). Regarding

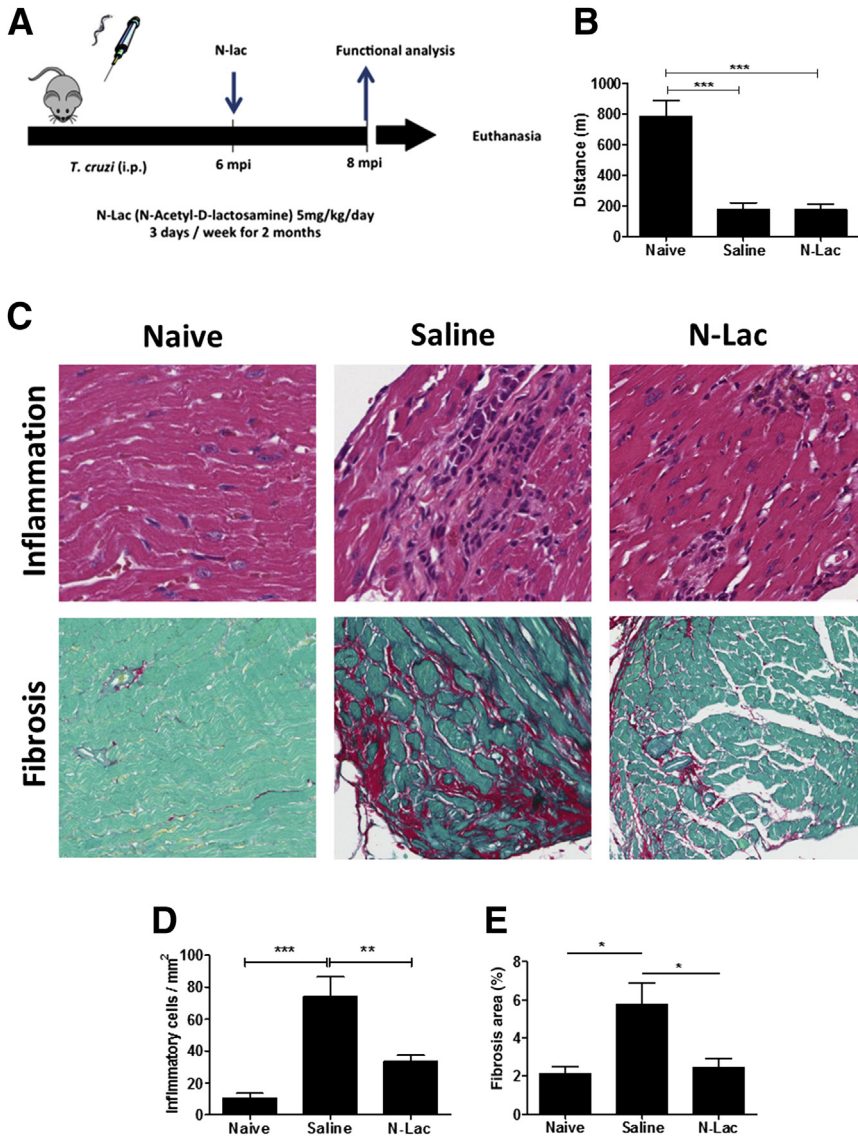


Figure 5 *In vivo* pharmacological blockade of Gal-3 during the chronic phase of experimental *Trypanosoma cruzi* infection reduces inflammation and fibrosis. **A:** Experimental design. **B:** A lack of functional recovery was observed by analysis of performance in treadmill test 2 months after the beginning of treatment with N-Lac. **C:** A significant reduction in the intensity of cardiac inflammation and fibrosis is observed in heart sections of mice treated with N-Lac stained with hematoxylin and eosin (**top row**) and Sirius red (**bottom row**). Quantifications of the number of inflammatory cells infiltrating the heart (**D**), cardiac fibrosis area (**E**), showing histological improvement in N-Lac treated mice. Data are expressed as means \pm SEM. * $P < 0.05$, ** $P < 0.01$, and *** $P < 0.001$. Original magnification, $\times 200$ (**C**). m.p.i., months postinfection.

the exercise capacity, *T. cruzi*-infected mice had an impaired performance when compared to uninfected controls 6 months after infection (data not shown). N-Lac treatment did not cause any improvement in exercise capacity, because mice treated with this Gal-3 blocker had similar performance in treadmill test to saline-treated mice and a reduced capacity when compared to uninfected controls (**Figure 5B**).

Histological analysis demonstrated the presence of inflammatory infiltrate in the hearts of mice infected with *T. cruzi*, mainly composed of mononuclear cells. The number of inflammatory cells infiltrating the heart, however, was significantly reduced in N-Lac-treated mice, compared to saline-treated controls (**Figure 5, C and D**). In addition, the percentage of heart fibrosis was significantly reduced after N-Lac treatment when compared to saline-treated mice (**Figure 5, C and E**). In addition, a control experiment was performed in which *T. cruzi*-infected mice were treated in

the same regimen with sucrose. Morphometric analysis in the hearts of sucrose-treated mice did not show reduction of inflammatory cells and the fibrotic area in sucrose-treated mice when compared to those treated with saline (**Supplemental Figure S2**).

To investigate whether N-Lac caused modulation of inflammatory mediators, we performed gene expression analysis in the heart tissue (**Figure 6**). N-Lac-treated mice had reduced gene expression of the inflammatory cytokines tumor necrosis factor- α and IFN- γ when compared to saline-treated mice. The regulatory cytokine IL-10 was increased in *T. cruzi*-infected mice when compared to uninfected controls, both in saline as well as in N-Lac-treated mice. Moreover, the gene expression of transcription factors T-bet, GATA-3, and FoxP3, associated with T-cell subtypes type 1 helper T cell, type 2 helper T cell, and T regulatory cell, respectively, was increased by *T. cruzi* infection and reduced in mice treated with N-Lac. The gene

Table 1 ECG Analysis in Uninfected and *Trypanosoma cruzi*-Infected Mice

ECG findings	Uninfected (n = 7)	Pretreatment (n = 19)	Saline (n = 9)	N-Lac (n = 10)
No alterations	7/7	1/19		
Atrial overload		1/19	1/9	
IACD			2/9	
JR		1/19	1/9	
AVB first degree		6/19	3/9	2/10
AVB third degree		5/19	2/9	3/10
SVT		2/19	1/9	1/10
Ventricular bigeminy				3/10
Isorhythmic AVD		2/19	1/9	1/10
AVD			1/9	
IVCD		1/19	1/9	

AVB, atrioventricular block; AVD, atrioventricular dissociation; ECG, electrocardiography; IACD, intra-atrial conduction delay; IVCD, intraventricular conduction delay; JR, junctional rhythm; N-Lac, N-acetyl-D-lactosamine; SVT, supraventricular tachycardia.

expression of chemokine ligand 8 (modified citrus pectin 2) and the chemokine receptor CCR5, which are increased by *T. cruzi* infection, was also reduced after N-Lac treatment. More important, treatment with N-Lac reduced the gene expression of Gal-3 in the hearts of *T. cruzi*-infected mice (Figure 6).

To better investigate the mechanisms by which N-Lac caused reduction of inflammation, we performed lymphoproliferation and migration assays. Mouse splenocytes were stimulated *in vitro* with concanavalin A or anti-CD3/CD28.

Addition of N-Lac at the highest concentration tested (10 $\mu\text{mol/L}$) caused a small reduction of lymphoproliferation stimulated by both polyclonal activators (Figure 7, A and B). In contrast, the positive control dexamethasone inhibited the proliferation induced by both stimuli. Last, we tested the effects of N-Lac in adhesion of leukocytes to the endothelium and in cell migration. The adhesion of leukocytes to aorta endothelium in an *en face* assay was significantly blocked by N-Lac using cells and endothelium from wild-type mice, but not from galectin-3 knockout mice (Figure 7C). In fact, cell adhesion of galectin-3 knockout mice was similar to that of pharmacological blockade with N-Lac in wild-type cells (Figure 7C). In addition, the presence of N-Lac significantly inhibited leukocyte migration in a transwell system (Figure 7D).

Discussion

Gal-3 is a multifunctional lectin that can be found in various cells and tissues, and is detected in the nucleus, cytoplasm, as well as in the extracellular compartment.¹¹ Notably, Gal-3 may have different, concordant, or opposite actions depending on the cell type and whether it is present in the extracellular or intracellular compartments.¹¹ Previous studies from our group and others have shown a correlation between inflammation and fibrosis in the heart and Gal-3 expression.^{16,32,34} Moreover, host expression of Gal-3 is required for *T. cruzi* adhesion and invasion in human cells.²⁰ In the present study, we demonstrated the expression of Gal-3 in different cell populations and its role in the promotion

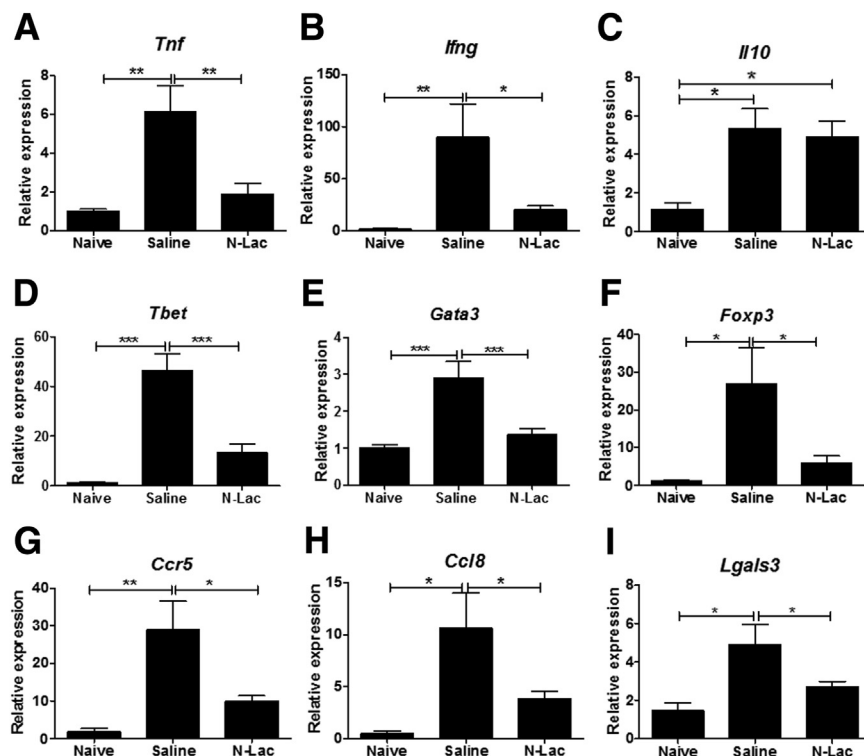


Figure 6 Modulation of gene expression in chagasic heart after N-Lac treatment. real-time RT-PCR analysis of gene expression in the heart tissue demonstrates that N-Lac treatment is associated with a reduction of inflammatory cytokines tumor necrosis factor (TNF)- α (A) and interferon (IFN)- γ (B), and does not alter the expression of IL-10 (C), when compared to saline-treated mice. T-lymphocyte subtype-specific transcription factors associated with type 1 helper T cell (T-bet; D), type 2 helper T cell (GATA-3; E), and T regulatory cell (FOXP3; F) are reduced in N-Lac-treated mice. The expression of genes associated with leukocyte migration and chemotaxis CCR5 (G), chemokine ligand 8 (H), and Gal-3 (I) is also reduced after N-Lac treatment. Data are expressed as means \pm SEM. * $P < 0.05$, ** $P < 0.01$, and *** $P < 0.001$.

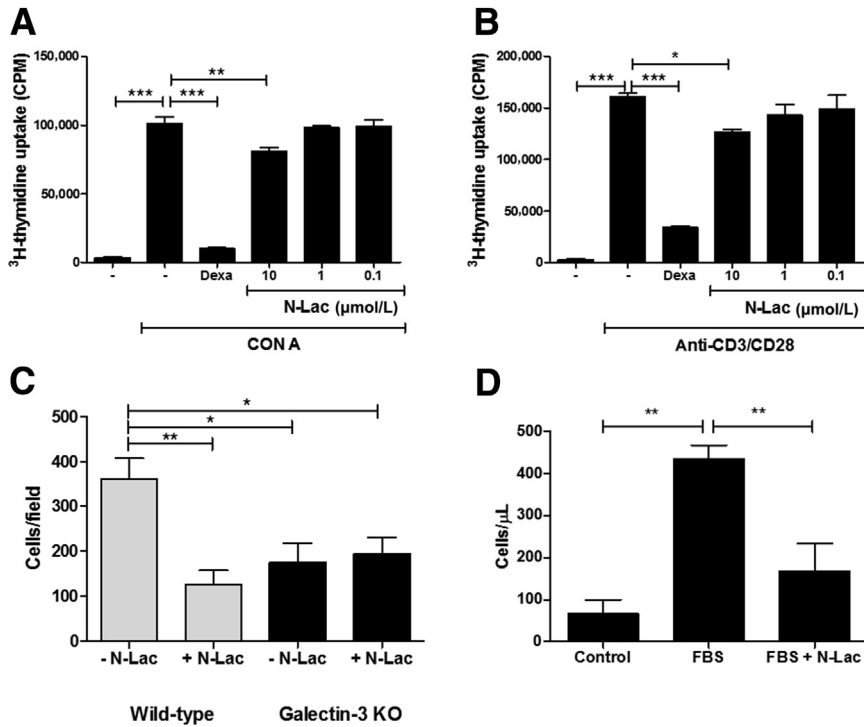


Figure 7 Effects of N-Lac on splenocyte proliferation and migration *in vitro*. Mouse splenocytes obtained from naïve C57Bl/6 mice were stimulated with concanavalin A (Con A; **A**) or anti-CD3/CD28 (**B**) in the absence or presence of N-Lac or dexamethasone (Dexa; 10 μmol/L). Lymphoproliferation was assessed by ³H-thymidine uptake. **C:** *En face* adhesion assay was performed using aorta fragments and splenocytes from wild-type or Gal-3 knockout mice, in the absence or presence of N-Lac. Data show the frequency of adherent cells 30 minutes after incubation. **D:** Mouse splenocytes were submitted to starvation and placed in the upper compartment of a transwell system in the presence or absence of 10 μmol/L N-Lac. Medium with or without fetal bovine serum (FBS) was placed in the lower chamber as a chemoattractant. Cell concentration in the lower chamber after overnight incubation. Data are expressed as means ± SEM (**A–D**). **P* < 0.05, ***P* < 0.01, and ****P* < 0.001. CPM, counts per minute.

of heart inflammation and fibrosis in *T. cruzi*-infected mice. This was achieved by the following: i) immunostaining in chronic Chagas disease human and mouse heart samples showing the presence of Gal-3⁺ cells, including macrophages, T cells, fibroblasts, and fibrocytes; ii) blockade of Gal-3 expression in cardiac fibroblasts, showing its role on proliferation and collagen production; and iii) pharmacological blockade *in vivo* in the experimental model, showing significant reduction of inflammation, fibrosis, and production of key inflammatory mediators in the heart.

Previous studies have highlighted a role for Gal-3 in the cardiac remodeling process in different experimental settings, including experimental models of hypertrophic cardiomyopathy and myocardial infarction.^{12–14} These reports have focused on Gal-3 effects in cardiac fibroblasts, contributing to cell survival, proliferation, and extracellular matrix synthesis. In CCC, however, a massive infiltration of immune cells is observed in the heart, which leads to persistent immune-mediated myocyte damage, ultimately triggering a progressive fibrogenic response.^{6–9}

In the present study, we demonstrated the dynamic expression of Gal-3 in different periods during *T. cruzi* experimental infection and correlated with the findings of human heart analysis, in sections obtained from hearts of subjects with end-stage heart failure due to CCC. Gal-3 expression was observed in a similar pattern in human and mouse heart samples, mainly in areas of inflammatory infiltrates. Gal-3 has been previously described in immune cells and to participate in different aspects of innate and adaptive immune responses.^{21–26} In the experimental model, we showed expression of Gal-3 in macrophages and

T cells, two main cell types present in the inflammatory foci in Chagas disease hearts. Moreover, we demonstrated that inflammatory stimuli increase the expression of Gal-3 in macrophages *in vitro*. Because IFN-γ and tumor necrosis factor-α are produced in mouse hearts chronically infected with *T. cruzi*, their action may account for the increased Gal-3 expression in macrophages. The described roles for Gal-3 in T-cell biology include the promotion of cell survival, proliferation, T-cell receptor signaling, and migration.²⁷ In our study, we observed reduction of cell adhesion to endothelium and migration, but not of lymphocyte proliferation, by the Gal-3 inhibitor N-Lac, suggesting that the reduction of inflammation in the hearts of infected mice after N-Lac treatment is mainly because of reduction of cell migration.

In our study, we found that *T. cruzi* infection also increased the expression of Gal-3 in cardiac fibroblasts and, even more intensely, in a population of bone marrow-derived fibrocytes. Although cardiac fibroblasts have been classically described as the most important cell type involved in cardiac fibrosis, different studies have shown that bone marrow-derived fibrocytes play relevant roles in fibrogenesis and remodeling.^{28–30} Our data provided from *in vitro* assays in cardiac fibroblasts demonstrated the role of exogenous and endogenous Gal-3 in cell survival, proliferation, and type I collagen synthesis, which is supported by the current literature.^{12–14} The fact that extracellular Gal-3 increased cell proliferation only in high concentration and the marked reduction of proliferation in Gal-3 knockdown cells indicate that intracellular Gal-3 has a critical role in cell proliferation regulation. Interestingly, Gal-3 has been

previously shown to enhance cyclin D1 promoter activity,³¹ correlating with the cell cycle arrest and decreased expression of cyclin D1 gene in Gal-3 knockdown fibroblasts found in our study. The fact that caveolin-1 gene expression was not increased in Gal-3 knockdown cells reinforces a direct action of Gal-3 in the regulation of cyclin D1 gene transcription.

We have previously shown that *Lgals3* gene expression is up-regulated in the hearts of mice during chronic *T. cruzi* infection.^{9,16} The correlation between intensity of myocarditis and presence of collagen type I, Gal-3, and α -smooth muscle actin—positive cells was also seen in a mouse model of *T. cruzi* infection.³² Gal-3 was implicated in the process of *T. cruzi* invasion.³³ Altogether, these data suggest that Gal-3 is involved in different aspects of the pathogenesis of CCC, from *T. cruzi* infection to immune response, inflammation, and tissue repair. Interestingly, a reduction of Gal-3 expression in the heart was observed accompanying decreased fibrosis and myocarditis after granulocyte colony-stimulating factor treatment or cell therapy in chronically infected mice.^{16,34} In the present study, we showed that the Gal-3 pharmacological blockade with N-Lac significantly modulated the immune response in the hearts from CCC mice, reducing migration of immune cells to the myocardium and decreasing the expression of inflammatory type 1 helper T-cell cytokines and markers of type 2 helper T-cell and T regulatory cell lymphocyte subtypes, to the level of naïve control mice. Notably, the anti-inflammatory cytokine IL-10 was increased when compared to naïve mice. This finding, together with the observed reduced levels of *IFNG* and *TNFA* gene expression, demonstrates a potent anti-inflammatory effect of N-Lac. Moreover, N-Lac treatment was associated with a significant reduction of myocardial fibrosis, which is in accordance with a previous report in a different experimental model.¹⁴ Despite the reduction of inflammation and fibrosis, our results did not correlate with any improvement in functional parameters after N-Lac treatment. This finding does not exclude the possibility of long-term beneficial effects of Gal-3 blockade, nor that N-Lac treatment, at an earlier stage of the infection, which may prevent the deterioration of cardiac function.

The strong binding affinity between galectin-3 and N-acetyl-D-lactosamine has been previously reported.³⁵ Moreover, in previous studies, similar dose and administration regimen of N-acetyl-D-lactosamine were used to block galectin-3 in mouse models of viral myocarditis³⁶ and hypertensive cardiac remodeling.¹⁴ The reduction of inflammation and fibrosis observed after N-Lac treatment were not observed in mice treated with sucrose in the same dose and regimen. Moreover, pharmacological (by N-Lac) and genetic (gene knockout) blockade of Gal-3 had similar effects in cell adhesion to endothelium, and indicate that N-Lac does not interfere with selectin binding.

In a translational perspective, Gal-3 could be used in the clinical setting as either a novel biomarker or a therapeutic target. Although the identification of novel noninvasive

biomarkers that adequately predict cardiac fibrosis would be highly desired, in a recent report we showed that plasma Gal-3 levels do not correlate with the intensity of fibrosis, as measured by magnetic resonance imaging, in a recently published transversal study in subjects with CCC.³⁷ Nonetheless, these data do not exclude the possibility of Gal-3 being useful as a biomarker for prognosis determination, which is currently under investigation in chronic heart failure caused by other etiologies.³⁸ Thus, the conduction of a longitudinal study in Chagas disease subjects would be required to validate the use of plasma Gal-3 as prognosis biomarker.

In conclusion, herein, we demonstrated that Gal-3 plays an important role in the pathogenesis of experimental chronic Chagas disease, acting in different cell compartments and promoting cardiac inflammation and fibrosis. The finding of Gal-3 expression in human heart samples, in a similar pattern as observed in the mouse model, reinforces its potential as a novel target for drug and therapy development for CCC.

Acknowledgments

We thank Pamela Daltro for technical assistance in the cardiac functional analysis, Didier Trono for pLVTHM lentiviral vector, Dr. Luiz R. Goulart for providing galectin-3 knockout mice, and Drs. Igor Correia de Almeida and Washington Luis Conrado dos Santos for helpful discussions.

Supplemental Data

Supplemental material for this article can be found at <http://dx.doi.org/10.1016/j.ajpath.2017.01.016>.

References

- Andrade DV, Gollob KJ, Dutra WO: Acute Chagas disease: new global challenges for an old neglected disease. *PLoS Negl Trop Dis* 2014, 8:e3010
- WHO: Chagas disease in Latin America: an epidemiological update based on 2010 estimates. *Wkly Epidemiol Rec* 2015, 90:33–44
- Bern C, Montgomery SP, Herwaldt BL, Rassi A Jr, Marin-Neto JA, Dantas RO, Maguire JH, Acquatella H, Morillo C, Kirchhoff LV, Gilman RH, Reyes PA, Salvatella R, Moore AC: Evaluation and treatment of Chagas disease in the United States: a systematic review. *JAMA* 2007, 298:2171–2181
- Morillo CA, Marin-Neto JA, Avezum A; BENEFIT Investigators: Randomized trial of Benznidazole for chronic Chagas' cardiomyopathy. *N Engl J Med* 2015, 373:1295–1306
- Burgos JM, Diez M, Vigliano C, Bisio M, Risso M, Duffy T, Cura C, Bruses B, Favaloro L, Leguizamón MS, Lucero RH, Laguens R, Levin MJ, Favaloro R, Schijman AG: Molecular identification of *Trypanosoma cruzi* discrete typing units in end-stage chronic Chagas heart disease and reactivation after heart transplantation. *Clin Infect Dis* 2010, 51:485–495
- Soares MB, Pontes-De-Carvalho L, Ribeiro-Dos-Santos R: The pathogenesis of Chagas' disease: when autoimmune and parasite-specific immune responses meet. *An Acad Bras Cienc* 2001, 73:547–559

7. Bonney KM, Engman DM: Autoimmune pathogenesis of Chagas heart disease: looking back, looking ahead. *Am J Pathol* 2015, 185:1537–1547
8. Gomes JA, Bahia-Oliveira LM, Rocha MO, Martins-Filho OA, Gazzinelli G, Correa-Oliveira R: Evidence that development of severe cardiomyopathy in human Chagas' disease is due to a Th1-specific immune response. *Infect Immun* 2003, 71:1185–1193
9. Soares MB, de Lima RS, Rocha LL, Vasconcelos JF, Rogatto SR, dos Santos RR, Iacobas S, Goldenberg RC, Iacobas DA, Tanowitz HB, de Carvalho AC, Spray DC: Gene expression changes associated with myocarditis and fibrosis in hearts of mice with chronic chagasic cardiomyopathy. *J Infect Dis* 2010, 202:416–426
10. de Boer RA, Voors AA, Muntendam P, van Gilst WH, van Veldhuisen DJ: Galectin-3: a novel mediator of heart failure development and progression. *Eur J Heart Fail* 2009, 11:811–817
11. Krześlak A, Lipińska A: Galectin-3 as a multifunctional protein. *Cell Mol Biol Lett* 2004, 9:305–328
12. Sharma U, Pokharel S, van Brakel TJ, van Berlo JH, Cleutjens JP, Schroen B, André S, Crijns HJ, Gabius HJ, Maessen J, Pinto YM: Galectin-3 marks activated macrophages in failure-prone hypertrophied hearts and contributes to cardiac dysfunction. *Circulation* 2004, 110:3121–3128
13. González GE, Cassaglia P, Noli Truant S, Fernández MM, Wilensky L, Volberg V, Malchiodi EL, Morales C, Gelpi RJ: Galectin-3 is essential for early wound healing and ventricular remodeling after myocardial infarction in mice. *Int J Cardiol* 2014, 176:1423–1425
14. Yu L, Ruyfrok WP, Meissner M, Bos EM, van Goor H, Sanjabi B, van der Harst P, Pitt B, Goldstein II, Koerts JA, van Veldhuisen DJ, Bank RA, van Gilst WH, Silljé HH, de Boer RA: Genetic and pharmacological inhibition of galectin-3 prevents cardiac remodeling by interfering with myocardial fibrogenesis. *Circ Heart Fail* 2013, 6:107–117
15. Chen A, Hou W, Zhang Y, Chen Y, He B: Prognostic value of serum galectin-3 in patients with heart failure: a meta-analysis. *Int J Cardiol* 2015, 182:168–170
16. Soares MBP, Lima RS, Souza BSF, Vasconcelos JF, Rocha LL, dos Santos RR, Iacobas S, Goldenberg RC, Lisanti MP, Iacobas DA, Tanowitz HB, Spray DC, Campos-de-Carvalho AC: Reversion of gene expression alterations in hearts of mice with chronic chagasic cardiomyopathy after transplantation of bone marrow cells. *Cell Cycle* 2011, 10:1448–1455
17. Committee for the Update of the Guide for the Care and Use of Laboratory Animals; National Research Council: *Guide for the Care and Use of Laboratory Animals: Eighth Edition*. Washington, DC, National Academies Press, 2011
18. Wiznerowicz M, Trono D: Conditional suppression of cellular genes: lentivirus vector-mediated drug-inducible RNA interference. *J Virol* 2003, 77:8957–8961
19. Karasuyama H, Melchers F: Establishment of mouse cell lines which constitutively secrete large quantities of interleukins 2, 3, 4, or 5 using modified cDNA expression vectors. *Eur J Immunol* 1988, 18:97–104
20. Kleshchenko YY, Moody TN, Furtak VA, Ochieng J, Lima MF, Villalta F: Human galectin-3 promotes *Trypanosoma cruzi* adhesion to human coronary artery smooth muscle cells. *Infect Immun* 2004, 72:6717–6721
21. Henderson NC, Sethi T: The regulation of inflammation by galectin-3. *Immunol Rev* 2009, 230:160–171
22. Hsu DK, Yang RY, Pan Z, Yu L, Salomon DR, Fung-Leung WP, Liu FT: Targeted disruption of the galectin-3 gene results in attenuated peritoneal inflammatory responses. *Am J Pathol* 2000, 156:1073–1083
23. Jeon SB, Yoon HJ, Chang CY, Koh HS, Jeon SH, Park EJ: Galectin-3 exerts cytokine-like regulatory actions through the JAK-STAT pathway. *J Immunol* 2010, 185:7037–7046
24. MacKinnon AC, Farnworth SL, Hodkinson PS, Henderson NC, Atkinson KM, Leffler H, Nilsson UJ, Haslett C, Forbes SJ, Sethi T: Regulation of alternative macrophage activation by galectin-3. *J Immunol* 2008, 180:2650–2658
25. Yang RY, Hsu DK, Liu FT: Expression of galectin-3 modulates t-cell growth and apoptosis. *Proc Natl Acad Sci U S A* 1996, 93:6737–6742
26. Chen SS, Sun LW, Brickner H, Sun PQ: Downregulating galectin-3 inhibits proinflammatory cytokine production by human monocyte-derived dendritic cells via RNA interference. *Cell Immunol* 2015, 294:44–53
27. Tribulatti MV, Figini MG, Carabelli J, Cattaneo V, Campetella O: Redundant and antagonistic functions of galectin-1, -3, and -8 in the elicitation of t cell responses. *J Immunol* 2012, 188:2991–2999
28. Chu PY, Mariani J, Finch S, McMullen JR, Sadoshima J, Marshall T, Kaye DM: Bone marrow-derived cells contribute to fibrosis in the chronically failing heart. *Am J Pathol* 2010, 176:1735–1742
29. van Amerongen MJ, Bou-Gharios G, Popa E, van Ark J, Petersen AH, van Dam GM, van Luyn MJ, Harmsen MC: Bone marrow-derived myofibroblasts contribute functionally to scar formation after myocardial infarction. *J Pathol* 2008, 214:377–386
30. Haudek SB, Cheng J, Du J, Wang Y, Hermosillo-Rodriguez J, Trial J, Taffet GE, Entman ML: Monocytic fibroblast precursors mediate fibrosis in angiotensin-II-induced cardiac hypertrophy. *J Mol Cell Cardiol* 2010, 49:499–507
31. Lin HM, Pestell RG, Raz A, Kim HR: Galectin-3 enhances cyclin d(1) promoter activity through sp1 and a camp-responsive element in human breast epithelial cells. *Oncogene* 2002, 21:8001–8010
32. Ferrer MF, Pascuale CA, Gomez RM, Leguizamón MS: DTU I isolates of *Trypanosoma cruzi* induce upregulation of galectin-3 in murine myocarditis and fibrosis. *Parasitology* 2014, 141:849–858
33. Machado FC, Cruz L, da Silva AA, Cruz MC, Mortara RA, Roque-Barreira MC, da Silva CV: Recruitment of galectin-3 during cell invasion and intracellular trafficking of *Trypanosoma cruzi* extracellular amastigotes. *Glycobiology* 2014, 24:179–184
34. Vasconcelos JF, Souza BS, Lins TF, Garcia LM, Kaneto CM, Sampaio GP, de Alcântara AC, Meira CS, Macambira SG, Ribeiro-dos-Santos R, Soares MB: Administration of granulocyte colony-stimulating factor induces immunomodulation, recruitment of T regulatory cells, reduction of myocarditis and decrease of parasite load in a mouse model of chronic Chagas disease cardiomyopathy. *FASEB J* 2013, 27:4691–4702
35. von Mach T, Carlsson MC, Straube T, Nilsson U, Leffler H, Jacob R: Ligand binding and complex formation of galectin-3 is modulated by pH variations. *Biochem J* 2014, 457:107–115
36. Jaquenod De Giusti C, Ure AE, Rivadeneyra L, Schattner M, Gomez RM: Macrophages and galectin 3 play critical roles in CVB3-induced murine acute myocarditis and chronic fibrosis. *J Mol Cell Cardiol* 2015, 85:58–70
37. Noya-Rabelo MM, Larocca TF, Macêdo CT, Torreão JA, Souza BS, Vasconcelos JF, Souza LE, Silva AM, Ribeiro Dos Santos R, Correia LC, Soares MB: Evaluation of Galectin-3 as a novel biomarker for Chagas cardiomyopathy. *Cardiology* 2017, 136:33–39
38. Peacock WF: How galectin-3 changes acute heart failure decision making in the emergency department. *Clin Chem Lab Med* 2014, 52:1409–1412

ANEXO 4

BASTOS, T. M.; BARBOSA, M. I. F.; SILVA, M. M.; JÚNIOR, J. W. C.; **MEIRA, C. S.**; GUIMARÃES, E. T.; ELLENA, J.; MOREIRA, D. R. M.; BATISTA, A. A.; SOARES, M. B. P. Nitro/Nitrosyl-Ruthenium complexes are potent and selective anti-*Trypanosoma cruzi* agents causing autophagy and necrotic parasite death. **Antimicrobial Agents and Chemotherapy**, v. 58, p. 6044-6054, 2014.

Nitro/Nitrosyl-Ruthenium Complexes Are Potent and Selective Anti-*Trypanosoma cruzi* Agents Causing Autophagy and Necrotic Parasite Death

Tanira M. Bastos,^a Marília I. F. Barbosa,^b Monize M. da Silva,^b José W. da C. Júnior,^b Cássio S. Meira,^a Elisalva T. Guimaraes,^{a,c} Javier Ellena,^d Diogo R. M. Moreira,^{a,e} Alzir A. Batista,^b Milena B. P. Soares^{a,e}

FIOCRUZ, Centro de Pesquisas Gonçalo Moniz, Salvador, Bahia, Brazil^a; UFSCAR, Departamento de Química, São Carlos, São Paulo, Brazil^b; UNEB, Departamento de Ciências da Vida, Salvador, Bahia, Brazil^c; USP, Instituto de Física de São Carlos, São Carlos, São Paulo, Brazil^d; Centro de Biotecnologia e Terapia Celular, Hospital São Rafael, Salvador, Bahia, Brazil^e

cis-[RuCl(NO₂)(dppb)(5,5'-mebipy)] (complex 1), *cis*-[Ru(NO₂)₂(dppb)(5,5'-mebipy)] (complex 2), *ct*-[RuCl(NO)(dppb)(5,5'-mebipy)](PF₆)₂ (complex 3), and *cc*-[RuCl(NO)(dppb)(5,5'-mebipy)](PF₆)₂ (complex 4), where 5,5'-mebipy is 5,5'-dimethyl-2,2'-bipyridine and dppb is 1,4-bis(diphenylphosphino)butane, were synthesized and characterized. The structure of complex 2 was determined by X-ray crystallography. These complexes exhibited a higher anti-*Trypanosoma cruzi* activity than benznidazole, the current antiparasitic drug. Complex 3 was the most potent, displaying a 50% effective concentration (EC₅₀) of 2.1 ± 0.6 μM against trypomastigotes and a 50% inhibitory concentration (IC₅₀) of 1.3 ± 0.2 μM against amastigotes, while it displayed a 50% cytotoxic concentration (CC₅₀) of 51.4 ± 0.2 μM in macrophages. It was observed that the nitrosyl complex 3, but not its analog lacking the nitrosyl group, releases nitric oxide into parasite cells. This release has a diminished effect on the trypanosomal protease cruzain but induces substantial parasite autophagy, which is followed by a series of irreversible morphological impairments to the parasites and finally results in cell death by necrosis. In infected mice, orally administered complex 3 (five times at a dose of 75 μmol/kg of body weight) reduced blood parasitemia and increased the survival rate of the mice. Combination index analysis of complex 3 indicated that its *in vitro* activity against trypomastigotes is synergic with benznidazole. In addition, drug combination enhanced efficacy in infected mice, suggesting that ruthenium-nitrosyl complexes are potential constituents for drug combinations.

Chagas disease, caused by the protozoan parasite *Trypanosoma cruzi*, affects approximately 10 million people worldwide, with a high prevalence in Latin America (1). The main drugs used against this disease are benznidazole and nifurtimox (2), both of which are effective in curing the disease when administered during the acute phase but are less effective in patients that have progressed to the chronic phase (3). Furthermore, these drugs are not considered ideal, due to severe side effects, and drug resistance to *T. cruzi* strains has been reported (4). Thus, research aimed at identifying molecules with anti-*T. cruzi* activity is urgently need for the treatment of Chagas disease.

In recent years, a variety of anti-*T. cruzi* drug targets have been identified, including the enzymes lanosterol 14α-demethylase, *trans*-sialidase, trypanothione reductase, and cysteine protease (5). *T. cruzi* contains a cysteine protease homologous to cathepsin L in mammalian cells, called cruzipain or cruzain, which is responsible primarily for the proteolytic activity involved in all stages of the parasite's life cycle (6, 7). Cruzain is important for parasite survival, cell growth, and differentiation (8, 9). Furthermore, this enzyme plays an important role in the process of parasite internalization in mammalian cells and in the intracellular replication of *T. cruzi* (7, 9).

Nitric oxide (NO) is a well-known endogenous trypanocidal molecule which contributes to host control of acute infection (10, 11). NO inactivates cruzain by *S*-nitrosylation of the binding site (12), but *T. cruzi* uses trypanothione reductase to convert NO into a harmless species (13). Therefore, it has been hypothesized that NO donor drugs may be useful against *T. cruzi* infection by producing exogenous NO (14). Organic NO donor molecules have

been investigated as anti-*T. cruzi* agents, but compounds with *in vivo* efficacy have not been identified (15). In recent years, ruthenium-nitrosyl complexes have been evaluated as anti-*T. cruzi* agents, demonstrating potent and selective antiparasitic activity, including in *T. cruzi*-infected mice (16–19). In addition, this class of complexes exhibited inhibitory activity against the *T. cruzi* glyceraldehyde 3-phosphate dehydrogenase, suggesting that ruthenium-nitrosyl complexes may have pleiotropic effects (19). From the point of view of medicinal chemistry, ruthenium complexes have been explored as an alternative to platinum complexes in the context of anticancer and anti-infective chemotherapy (20–22). More specifically, ruthenium complexes are described as outstanding bioactive agents because of the phosphine ligands, which provide great stability for these compounds (23–26). Nevertheless, only a few ruthenium complexes containing these ligands have been fully examined against *T. cruzi* (19).

Therefore, in this study we evaluated the *in vitro* and *in vivo* anti-*T. cruzi* activity of four new ruthenium complexes: *cis*-[RuCl

Received 11 March 2014 Returned for modification 16 April 2014

Accepted 18 July 2014

Published ahead of print 4 August 2014

Address correspondence to Milena B. P. Soares, milenabpsoares@gmail.com.

Supplemental material for this article may be found at <http://dx.doi.org/10.1128/AAC.02765-14>.

Copyright © 2014, American Society for Microbiology. All Rights Reserved.

doi:10.1128/AAC.02765-14

(NO₂)(dppb)(5,5'-mebipy)] (complex 1), *cis*-[Ru(NO₂)₂(dppb)(5,5'-mebipy)] (complex 2), *ct*-[RuCl(NO)(dppb)(5,5'-mebipy)] (PF₆)₂ (complex 3), and *cc*-[RuCl(NO)(dppb)(5,5'-mebipy)] (PF₆)₂ (complex 4). All the synthesized compounds are mononuclear complexes and contain 5,5'-dimethyl-2,2'-bipyridine (5,5'-mebipy) and 1,4-bis(diphenylphosphino)butane (dppb) ligands. To ascertain the importance of the nitrosyl group in antiparasitic activity, the synthesized complexes contained a nitrosyl group in two different positions (*cis* and *trans*), and two complexes contained a nitro group in the place of nitrosyl. Also, a complex lacking the nitro/nitrosyl groups, *cis*-[RuCl₂(dppb)(bipy)] (complex 5), was prepared and tested. By testing complexes 1 to 5 *in vitro*, a potent anti-*T. cruzi* activity was observed in the nitro/nitrosyl complexes (1 to 4), which was higher than that observed for benznidazole. In contrast, complex 5 did not show antiparasitic activity. Complex 3, the most potent compound, exhibited strong trypanocidal activity, through the release of NO, which subsequently induced the formation of vacuoles typical of the autophagy process. Moreover, complex 3 decreased blood parasitemia in *T. cruzi*-infected mice, strengthening the hypothesis that ruthenium complexes are promising drugs for Chagas disease therapy.

MATERIALS AND METHODS

Synthesis and drug dilution. Synthesis, structural characterization, and X-ray analysis of complexes 1 to 5 are described in the supplemental material. All complexes as well as the reference drugs were dissolved in dimethyl sulfoxide (DMSO) (Sigma-Aldrich, St. Louis, MO, USA) and then diluted in cell culture medium. The final concentration of DMSO was less than 1% in all *in vitro* experiments.

Animals. Female BALB/c mice (18 to 20 g) were maintained in sterilized cages under a controlled environment, receiving a rodent balanced diet and water *ad libitum* at Centro de Pesquisas Gonçalo Moniz (Fundação Oswaldo Cruz, Bahia, Brazil). All experiments were carried out in accordance with the recommendations of Ethical Issues Guidelines and were approved by the local Animal Ethics Committee (protocol number 002/2011).

Parasites. All experiments were performed with the Y strain of *T. cruzi*. The epimastigote form was maintained in axenic medium at 28°C, with weekly transfers into liver infusion tryptose (LIT) medium supplemented with 10% fetal bovine serum (FBS; Cultilab, Campinas, Brazil), 1% hemin (Sigma-Aldrich), 1% R9 medium (Sigma-Aldrich), and 50 µg/ml of gentamicin (Novafarma, Anápolis, Brazil). For *in vitro* assays, the metacyclic trypomastigote form of *T. cruzi* was obtained from the supernatant of infected LLC-MK2 cells and maintained in RPMI 1640 medium (Sigma-Aldrich) supplemented with 10% FBS (Cultilab, Campinas, Brazil) and 50 µg/ml of gentamicin (Novafarma, Anápolis, Brazil) at 37°C with 5% CO₂. For *in vivo* assays, bloodstream trypomastigotes were obtained from infected BALB/c mice at the peak of parasitemia.

Activity against epimastigotes. The effect of the treatment on epimastigotes proliferation was observed 5 days after incubation with the complexes at six concentrations. Epimastigote forms were resuspended at 5 × 10⁶ cells/ml in supplemented LIT medium. The number of viable parasites was counted in a hemocytometer, and complex activity was expressed as 50% inhibitory concentration (IC₅₀), in comparison to untreated parasites. Each drug concentration was carried out in triplicate, and three independent experiments were performed. The reference drug, benznidazole (Lafepe, Pernambuco, Brazil), was used as the positive control.

Activity against trypomastigotes. Trypomastigotes were cultured in 96-well plates (2 × 10⁶ cells/ml) in enriched RPMI 1640 medium, in the presence or absence of the complexes at different concentrations for 24 h. Viable parasites were counted in a hemocytometer, and complex activity was expressed as 50% effective concentration (EC₅₀), in comparison to

untreated parasites. Each drug concentration was carried out in triplicate, and three independent experiments were performed. The reference drug, benznidazole, was used as the positive control. For *in vitro* drug combinations, doubling dilutions of each drug (ruthenium complex 3 and benznidazole) used alone or in fixed combinations were incubated with 2 × 10⁶ cells/ml trypomastigotes for 24 h. The analysis of the combined effects was performed by calculating the median effect principle using CompuSyn software.

Host cell toxicity. Five days after 3% sodium thioglycolate injection (Sigma-Aldrich), macrophages were obtained by washing with saline solution in the peritoneal cavity of BALB/c mice. Macrophages in RPMI 1640 medium supplemented with 10% FBS were seeded on 96-well plates at 5 × 10⁵ cells/ml and treated with the complexes for 6 h or 24 h of incubation time. Following this, cells were washed with phosphate-buffered saline (PBS) twice, and cell viability was determined by alamarBlue assay (Invitrogen, Carlsbad, CA, USA) according to the manufacturer's instructions. Colorimetric readings were performed after 10 h at 570 and 600 nm. Fifty-percent cytotoxic concentration (CC₅₀) values were calculated using data points gathered from three independent experiments.

***In vitro T. cruzi* infection assay.** Peritoneal macrophages stimulated with 3% sodium thioglycolate (Sigma-Aldrich) were transferred to 24-well plates at 2 × 10⁵ cells/well in supplemented RPMI 1640 medium and maintained overnight at 37°C with 5% CO₂. The cultures were washed with saline solution and infected with trypomastigotes (10 parasites:1 host cell). Following 2 h of incubation, the noninternalized parasites were removed by washing with saline solution, and fresh medium, with or without drugs (25, 10, 5, and 1.0 µM), was added to the cultures and incubated for 6 h. Afterward, the culture was washed with saline, and drug-free medium was added and incubated for 4 days. Cells were fixed in absolute ethanol, stained with hematoxylin and eosin, and analyzed in an optical microscope (Olympus, Tokyo, Japan). The percentage of infected macrophages and the percentage of intracellular parasites per 100 macrophages were determined and compared to the negative control. The IC₅₀ of proliferation inhibition of amastigotes was calculated using the number of parasites/100 cells. The reference drug, benznidazole, was used as the positive control. Each drug concentration was carried out in triplicate, and three independent experiments were performed.

Cruzain inhibition. Recombinant cruzain was activated in acetate buffer (0.1 M; pH 5.5) containing 5.5 mM dithiothreitol (DTT) (Invitrogen), and the protein concentration was adjusted to a final concentration of 0.1 µM. Protein was incubated in phosphate buffer containing 0.01% Triton 100 and transferred to a 96-well plate. Following complex addition, the plate was incubated for 10 min at 35°C. A solution containing the Z-FR-AMC (Sigma-Aldrich) protease substrate was then added, incubated for 10 min, and read using the EnVision multilabel reader (PerkinElmer, Connecticut, USA). The percentage of cruzain inhibition was calculated by using the following equation: 100 - (A1/A × 100), where A1 represents the cruzain relative fluorescence units (RFU) in the presence of the test inhibitor and A refers to the control RFU (cruzain and substrate only). IC₅₀s of cruzain activity inhibition were also calculated. (2S,3S)-*trans*-Epoxy succinyl-L-leucylamido-3-methylbutane (E-64c) (Sigma-Aldrich) was used as the reference cruzain inhibitor. Each drug concentration was carried out in triplicate, and two independent experiments were performed.

Nitric oxide production. Peritoneal macrophages stimulated with 3% sodium thioglycolate (10⁶ cells/well) were incubated in a 24-well plate and infected with trypomastigotes (10⁶ parasites/well) for 2 h. This experiment was also performed using J774 macrophages at 10⁶ cells/well, which were incubated in a 24-well plate and infected with trypomastigotes (2 × 10⁵ parasites/well) for 3 h. Cells were washed with saline solution and treated with complex 3 or 5 at a concentration of 10 µM for 24 h. For the positive control, cells were stimulated with 5.0 ng/ml of gamma interferon (IFN-γ; R&D Systems, Minneapolis, MN, USA) and 500 ng/ml of lipopolysaccharide (LPS; Sigma-Aldrich). Nitrite levels were determined 24 h after incubation using the Griess method (27).

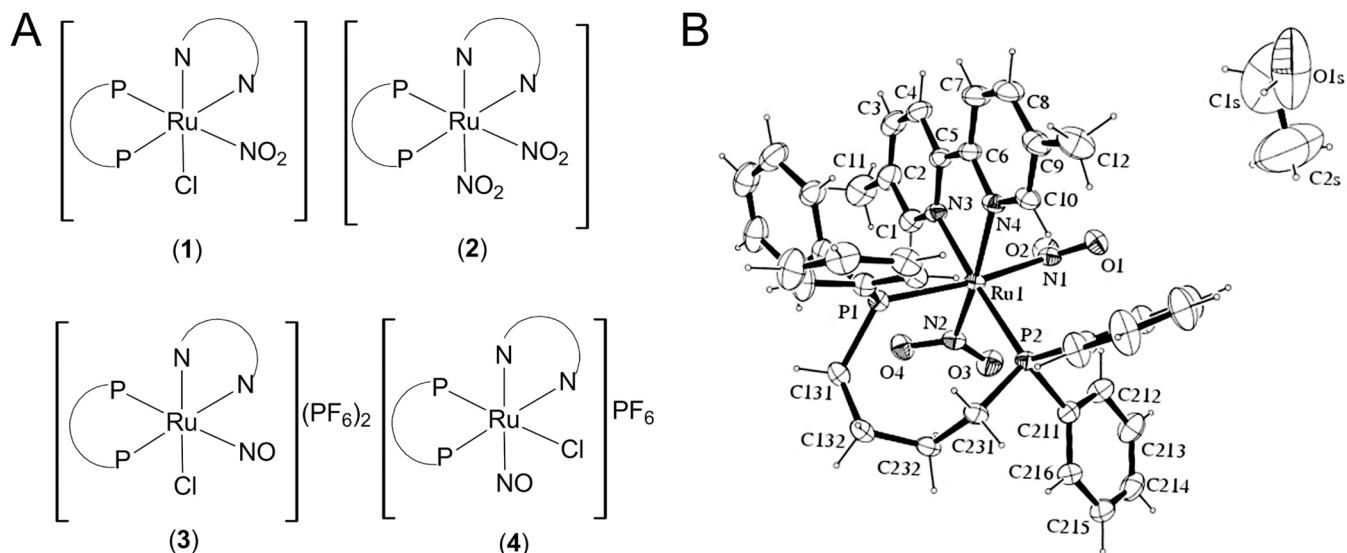


FIG 1 Ruthenium complexes 1 to 4. (A) Representation of the complexes: *cis*-[RuCl(NO₂)(dppb)(5,5-mebipy)] (1), *cis*-[Ru(NO₂)₂(dppb)(5,5-mebipy)] (2), *ct*-[RuCl(NO)(dppb)(5,5-mebipy)](PF₆)₂ (3), *cc*-[RuCl(NO)(dppb)(5,5-mebipy)](PF₆)₂ (4). N-N is 5,5'-dimethyl-2,2'-bipyridine (5,5'-mebipy), and P-P is 1,4-bis(diphenylphosphino)butane (dppb). (B) ORTEP-3 view of complex 2 and the atom numbering scheme. Ellipsoids are drawn at the 30% probability level.

Transmission and scanning electron microscopy analysis. Trypomastigotes (10⁷ cells/ml) were treated with 2.1 μM complex 3 and incubated for 24 h at 37°C with 5% CO₂. Infected macrophages were treated with 2.1 μM complex 3 and incubated for 6 h. After incubation, parasites were fixed for 1 h at room temperature with 2% formaldehyde and 2.5% glutaraldehyde (Electron Microscopy Sciences, Hatfield, PA, USA) in sodium cacodylate buffer (0.1 M, pH 7.2). Fixed parasites were then washed 4 times with sodium cacodylate buffer (0.1 M, pH 7.2) and postfixed with a 1% solution of osmium tetroxide (Sigma-Aldrich). The cells were dehydrated in an ascending acetone series (30, 50, 70, 90, and 100%) and embedded in PolyBed resin (PolyScience Family, Warrington, PA, USA). Ultrathin sections were prepared on a Leica UC7 ultramicrotome and collected on 300-mesh copper grids, contrasted with uranyl acetate and lead citrate. Images were captured in a JEOL TEM-1230 transmission electron microscope. Alternatively, trypomastigotes were dried by using the critical-point method with CO₂, mounted on aluminum stubs, coated with a 20-nm-thick gold layer, and examined under a JEOL JSM-6390LV scanning electron microscope.

Monodansylcadaverine labeling. Trypomastigotes (10⁷ cells/ml) were treated with complex 3 at a concentration of 2.1 μM. After incubation for 24 h, 0.05 mM monodansylcadaverine (MDC; Sigma-Aldrich) was added and incubated for 15 min in the absence of light. For the positive control, cells were treated with 0.1 mg/ml of rapamycin (Sigma-Aldrich). The autophagy inhibitor wortmannin (Sigma-Aldrich) was used at 0.5 μM and added simultaneously with complex 3 to the cell culture. The parasites were washed twice with PBS and analyzed in an FV1000 confocal microscope (Olympus).

LC3B immunolocalization. Infected macrophages (as described above) were treated with complex 3 at a concentration of 2.1 μM. Following 6 h of incubation, cells were washed in PBS and fixed with 4% paraformaldehyde (Electron Microscopy Sciences) for 20 min, permeabilized with 0.2% Triton X-100 (Sigma-Aldrich) in PBS for 15 min at room temperature, and blocked with background blocker (Diagnostic BioSystem, Pleasanton, CA, USA). Cells were incubated overnight with rabbit polyclonal antibody against LC3B (Invitrogen) (1/100 dilution) diluted in 1% PBS-bovine serum albumin (BSA), rinsed, and incubated for 1 h at room temperature with Alexa Fluor 568-conjugated goat anti-rabbit IgG (Molecular Probes, Carlsbad, CA, USA) diluted to 1:400. Subsequently, cells were washed in PBS and mounting medium with 4',6-diamidino-2-phenylindole (DAPI) (Vector Laboratories, Burlingame, CA, USA). Cells were analyzed by confocal microscopy (FV1000; Olympus).

Flow cytometry analysis. Trypomastigotes (10⁷ cells/ml) were resuspended in supplemented RPMI 1640 medium and treated with complex 3 (2.1 or 5 μM) for 36 h at 37°C with 5% CO₂. Parasites were labeled with propidium iodide (PI) and annexin V using the annexin V-fluorescein isothiocyanate (FITC) apoptosis detection kit (Sigma-Aldrich) according to the manufacturer's instructions. The experiment was performed using a BD FACSCalibur flow cytometer (San Jose, CA, USA) by acquiring 10,000 events, and data were analyzed by BD CellQuest software (San Jose, CA, USA).

In vivo anti-*T. cruzi* activity. Female BALB/c mice (18 to 20 g) were infected by intraperitoneal injection of 10⁴ bloodstream trypomastigotes of the *T. cruzi* Y strain in a 100-μl solution per mouse. Only mice with positive blood parasitemia were included in the experiment. Each drug was solubilized in DMSO-saline (10:90 [vol/vol]) prior to administration. Mice were randomly divided into groups (*n* = 6 mice per group). Treatment was initiated within 5 days postinfection and given once per day orally by gavage for five consecutive days. Complex 3 doses were administered at 25 (26.6 mg/kg of body weight) or 75 μmol/kg (80 mg/kg), and benznidazole was given at 384 μmol/kg (100 mg/kg). According to recommendations (28, 29), the following parameters were evaluated: (i) microscopic parasitemia analysis at 5, 8, 10, and 12 days postinfection and (ii) animal survival 30 days postinfection. The percentage of parasitemia reduction was calculated as follows: [(average vehicle group - average treated group)/average vehicle group] × 100%. Two independent experiments were carried.

In vivo drug combinations. The same *in vivo* protocol described above was performed. The four groups included were (i) vehicle DMSO-saline (10:90 [vol/vol]), (ii) complex 3 alone at 75 μmol/kg (80 mg/kg), (iii) benznidazole alone at 38 μmol/kg (10 mg/kg), and (iv) simultaneous treatment with complex 3 at 75 μmol/kg and benznidazole at 38 μmol/kg. Two independent experiments were performed.

Statistical analyses. Nonlinear regression analysis was used to calculate CC₅₀, EC₅₀, and IC₅₀ values. The selectivity index (SI) was defined as the ratio of CC₅₀ (macrophages) to IC₅₀ (amastigote form). One-way analysis of variance (ANOVA) and Bonferroni multiple comparison tests were used to determine the statistical significance of group comparisons in the *in vitro* infection assay, and two-way ANOVA with Bonferroni

multiple comparison tests was used in the *in vivo* assay (parasitemia). Results were considered statistically significant when *P* values were <0.05. Analyses were performed using GraphPad Prism version 5.01 (Graph Pad Software, San Diego, CA, USA) and OriginPro version 8.5 (OriginLab, Northampton, MA, USA) (cruzain IC₅₀s only). Animal survival rates were analyzed with GraphPad Prism 1.5 (GraphPad Software). Combined drug analysis was calculated by using CompuSyn (ComboSyn, Inc., Paramus, NJ, USA).

RESULTS

Compound characterization. Figure 1A shows the structures of ruthenium complexes investigated here. Complex 1 is the prototype compound, since it was used as the basis for synthesis of all other compounds. The differences among the complexes are based on the presence or absence of the nitro/nitrosyl group or chlorine. Complex 1 has a nitro group and a chlorine ligand; complex 2 was formed by replacing the chlorine by a nitro group. Complexes 3 and 4 are nitrosyl species. The difference between complexes 3 and 4 is the NO position; in complex 3, the NO is *cis* to chlorine and *trans* to phosphorus atoms, whereas in complex 4, NO is *cis* to chlorine and *cis* to phosphorus atoms.

All complexes were subjected to chemical and spectroscopic analysis. The elemental composition (C, H, and N) of the complexes corresponded closely to the calculated values. The ³¹P{¹H} nuclear magnetic resonance (NMR) spectra of complexes 1 to 4 exhibited a pair of doublets that indicated the magnetic inequivalence of the phosphorus atoms present in the dppb (30). The observed doublets showed chemical shifts different from those of the starting material *cis*-[RuCl₂(dppb)(5,5'-mebipy)], suggesting that the presence of the nitro or nitrosyl groups coordinated to the metal shifted the electron density of the phosphorus atoms from the dppb.

In the infrared (IR) spectrum of *cis*-[RuCl(NO₂)(dppb)(5,5'-mebipy)] (complex 1), there were strong bands at 1,349 cm⁻¹ and 1,298 cm⁻¹, which can be assigned to ν_{as}NO₂ and ν_sNO₂, respectively. For *cis*-[Ru(NO₂)₂(dppb)(5,5'-mebipy)] (complex 2), these bands were at 1,360 cm⁻¹ and 1,310 cm⁻¹ for ν_{as}NO₂ and at 1,294 cm⁻¹ and 1,269 cm⁻¹ for ν_sNO₂. The presence of four bands for this complex indicates that nitro groups are nonequivalent, one being *trans* to the nitrogen of 5,5'-mebipy, while the other is *trans* to the phosphorus of dppb. The nitrosyl complexes *ct*-[RuCl(NO)(dppb)(5,5-mebipy)](PF₆)₂ (complex 3) and *cc*-[RuCl(NO)(dppb)(5,5-mebipy)](PF₆)₂ (complex 4) exhibited strong bands at 1,891 cm⁻¹ and at 1,895 cm⁻¹, respectively, which were assigned to the NO⁺ stretching (31). Nitro group can be bound to metal through either nitrogen or oxygen, which may produce geometric isomers (32). Complex 1 exhibits its ρ_wNO₂ band at 572 cm⁻¹, while complex 2 has two bands, at 566 and 610 cm⁻¹, suggesting that in both complexes the nitro group is bound to the ruthenium through the nitrogen atom (32, 33). In addition to IR, the electronic absorption spectra for all complexes were characterized by an intense high-energy band centered at about 300 nm, which can be assigned to an intraligand π-π* transition. Also, these complexes exhibited low-energy bands in the range of 316 to 488 nm, which can be assigned to a metal-to-ligand charge transfer (MLCT) transition, Ru (dπ) to ligand (π*).

The crystal structure of complex 2 was solved by X-ray crystallography (Table 1), and its ORTEP view was prepared with ORTEP-3 for Windows (Fig. 1B). Selected bond lengths (Å) and angles (°) in the complex are listed in Table S1 in the supplemental material. Complex 2 exhibits a distorted octahedral geometry, and it crystallized in a triclinic system, space group *P*-1, with the metal

TABLE 1 Crystal data and structure refinement of complex 2

Characteristic	Value
Empirical formula	[RuC ₄₂ H ₄₆ N ₄ O ₅ P ₂]·CH ₃ CH ₂ OH
Formula wt	849.84
Temp (K)	293(2)
Wavelength (Å)	0.71073
Crystal system	Triclinic
Space group	<i>P</i> -1
Unit cell dimensions	
a (Å)	10.2261(7)
b (Å)	12.2153(5)
c (Å)	17.4217(10)
α (°)	74.904(2)
β (°)	74.660(3)
γ (°)	76.827(3)
Vol (Å ³)	1996.5(2)
Z	2
Density (calculated) (mg/m ³)	1.414
Absorption coefficient (mm ⁻¹)	0.522
F(000)	880
Crystal size (mm ³)	0.30 by 0.26 by 0.10
Theta range for data collection (°)	3.13 to 26.41
Index ranges	-11 ≤ <i>h</i> ≤ 12, -15 ≤ <i>k</i> ≤ 15, -21 ≤ <i>l</i> ≤ 21
No. of reflections collected	15,073
No. of independent reflections	8,129 [<i>R</i> (int) = 0.0217]
% completeness to theta = 25.00°	99.0
Absorption correction	Gaussian
Max and min transmission	0.950 and 0.847
Refinement method	Full-matrix least-squares on F ²
Computing	COLLECT, HKL Denzo and Scalepack, SHELXL-97, SHELXS-97 ^a
Data/restraints/parameters	8,129/2/491
Goodness of fit on F ²	1.056
Final R index [<i>I</i> > 2σ(<i>I</i>)]	R1 = 0.0378, wR2 = 0.1010
R index (all data)	R1 = 0.0442, wR2 = 0.1045
Largest diff peak and hole (e Å ⁻³)	0.611 and -0.640

^a Data collection, data processing, structure solution, and structure refinement, respectively.

center coordinated to two bidentate ligands and two NO₂ groups. The nitro groups are *cis*-positioned relative to each other and coordinated through the nitrogen atoms, as suggested by the IR data. From the data in Table S1, it can be seen that the Ru-N_(NO₂) [Ru-N_(NO₂) *trans* P] bond length is about 0.5 Å longer than the bond Rui-N(2) [Ru-N_(NO₂) *trans* N_(bipy)], which is consistent with the stronger *trans* effect of the phosphorus atoms, relative to the *trans* effect of the nitrogen atoms. Also, this difference explains the two bands for νNO₂ observed in the infrared spectrum of complex 2.

Anti-*T. cruzi* activity and host cell cytotoxicity. Anti-*T. cruzi* activity was determined in epimastigotes and trypomastigotes of the Y strain, and results were expressed as IC₅₀ and EC₅₀, respectively. Cell toxicity in BALB/c mice macrophages was performed under identical drug incubation times for antiparasitic assay in trypomastigotes (i.e., 24-h drug exposure) and expressed as CC₅₀. Benznidazole was used as the reference drug in these assays, and results are reported in Table 2. Benznidazole exhibited an IC₅₀ of 10.7 ± 1.6 μM in epimastigote proliferation. Similarly, it was observed that ruthenium complexes 2, 3, and 4 greatly inhibited

TABLE 2 Antiparasitic activity, host cell cytotoxicity, and cruzain inhibition of ruthenium complexes 1 to 5^e

Compound	<i>T. cruzi</i> Y strain			
	Epimastigote IC ₅₀ ± SEM (μM) ^a	Trypomastigote EC ₅₀ ± SEM (μM) ^b	Macrophage CC ₅₀ ± SEM (μM) ^c	Cruzain IC ₅₀ ± SD (μM) ^d
Complex 1	>100	8.4 ± 1.1	>100	30.2 ± 7.3
Complex 2	16.6 ± 0.6	2.9 ± 0.2	50.5 ± 0.1	>100
Complex 3	5.7 ± 0.6	2.1 ± 0.6	28.5 ± 2.0	14.4 ± 6.6
Complex 4	26.7 ± 2.0	5.9 ± 1.0	25.4 ± 0.1	0.4 ± 0.1
Complex 5	ND	>100	>100	59.8 ± 4.6
Bdz	10.7 ± 1.6	11.4 ± 1.0	>100	
E-64c				1.0 ± 0.8 nM

^a Determined 5 days after incubation with complexes.

^b Determined 24 h after incubation with complexes.

^c Cell viability of BALB/c mouse macrophages determined 24 h after treatment.

^d Cruzain activity was determined 10 min after incubation.

^e Values were calculated using concentrations in triplicate, and two independent experiments were performed. IC₅₀, inhibitory concentration at 50%; EC₅₀, effective concentration at 50%; CC₅₀, cytotoxic concentration at 50%; ND, not determined owing to lack of activity; Bdz, benznidazole; E-64c, standard cruzain inhibitor.

epimastigotes. In contrast, complex 1 did not inhibit epimastigote proliferation. Complexes 1 to 4 decreased trypomastigote viability, with EC₅₀s lower than that of benznidazole. Complex 5, which lacks a nitro/nitrosyl group, did not exhibit antitrypomastigote activity, while complex 3 was the most active compound among them, with an EC₅₀ of 2.1 ± 0.6 μM. Complexes 1 and 5 did not demonstrate cytotoxicity in macrophages following the drug exposure, and complex 2 displayed relatively low cytotoxicity. Complexes 3 and 4 had CC₅₀ values of 28.5 ± 2.0 and 25.4 ± 0.1 μM, respectively.

Evaluation of cruzain inhibition. Due to the previous findings that ruthenium complexes inhibit cruzain, inhibitory activity was measured here for all five complexes in an assay based on competition with Z-Phe-Arg 7-amido-4-methylcoumarin hydrochloride (Z-FR-AMC). (2*S*,3*S*)-*trans*-Epoxy succinyl-L-leucylamido-3-methylbutane (E-64c), which is a high-affinity cruzain inhibitor, was used as the reference inhibitor and displayed an IC₅₀ of 1.0 ± 0.8 nM. As demonstrated in Table 2, complex 2 did not inhibit cruzain, while complexes 1 and 5 presented weak potency, with IC₅₀s as high as 30 μM. Complexes 3 and 4 showed stronger potency against cruzain, with IC₅₀s of 14.4 ± 6.6 and 0.4 ± 0.1 μM, respectively. Although complex 4 was the most potent ruthenium complex, it had lower potency than E-64c.

In vitro infection. After observing that ruthenium complexes inhibit the extracellular parasite, we investigated their activity against the intracellular parasite. It was observed that all the nitro/nitrosyl complexes at 10 μM caused a statistically significant reduction in the percentage of *T. cruzi*-infected macrophages compared to untreated infected cells (Fig. 2A). Complex 3 was the most potent of the four compounds tested in reducing the *in vitro* infection. Additionally, all the complexes decreased the mean number of intracellular parasites (Fig. 2B) as well as the parasite burden (Fig. 2C). Amastigote IC₅₀ was calculated by analyzing the percentage of infected cells (Table 3). Ruthenium complex 3 greatly inhibited this percentage, displaying an IC₅₀ of 1.3 ± 0.2 μM, while benznidazole displayed an IC₅₀ of 14.0 ± 0.3 μM. Cytotoxicity of ruthenium complexes incubated for 6 h in macrophages demonstrated that neither benznidazole nor complex 1 are cytotoxic at the tested concentrations (CC₅₀s of >100 μM). Complex 2 exhibited a low cytotoxicity (CC₅₀ = 93.1 ± 7.7 μM), and complexes 3 and 4 were approximately 2-fold more cytotoxic than

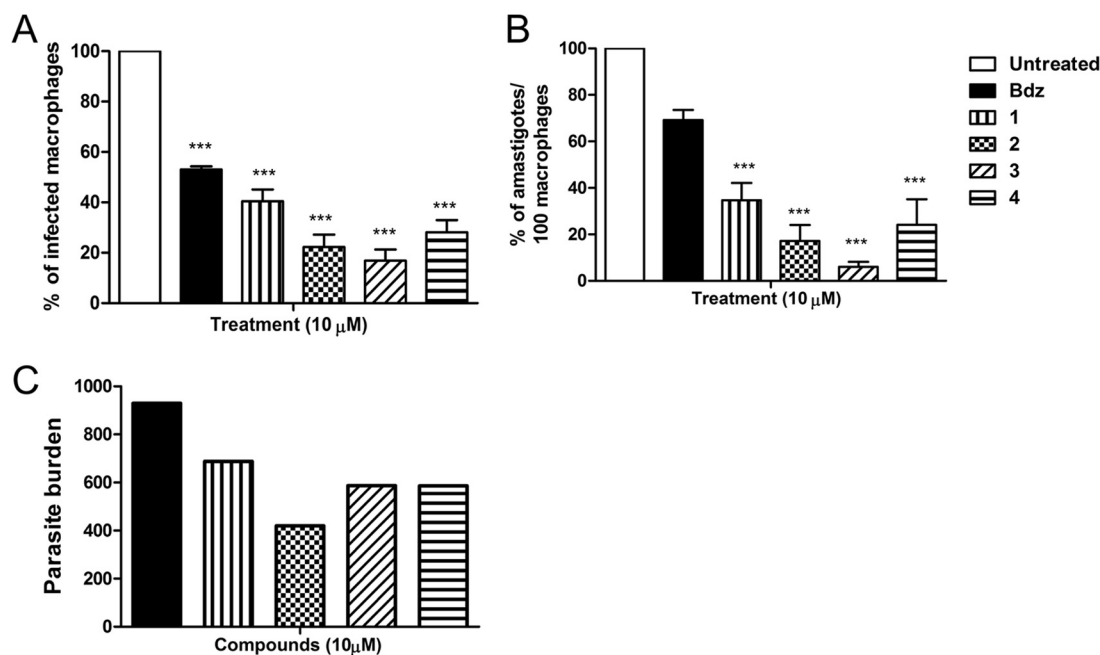


FIG 2 Ruthenium complexes reduce the *in vitro* infection. (A) Percentage of infection in comparison to untreated infected cells; (B) percentage of amastigotes/100 macrophages in comparison to untreated controls; (C) parasite burden, calculated as the percentage of infected cells × the mean number of amastigotes. Infected macrophages were treated for 6 h and then incubated for 4 days. Three independent experiments were performed. Error bars represent the standard errors of the means. ***, $P < 0.0001$ compared to untreated controls.

TABLE 3 Antiparasitic activity in intracellular parasite, host cell cytotoxicity, and selectivity index of ruthenium complexes 1 to 5^d

Compound	Amastigote IC ₅₀ ± SEM (μM) ^a	Macrophage CC ₅₀ ± SEM (μM) ^b	SI ^c
Complex 1	4.2 ± 1.6	>100	>24
Complex 2	2.6 ± 0.7	93.1 ± 7.7	36
Complex 3	1.3 ± 0.2	51.4 ± 0.2	40
Complex 4	2.7 ± 0.6	38.3 ± 2.3	14
Complex 5	ND	>100	ND
Bdz	14.0 ± 0.3	>100	>7

^a Cells were exposed to complexes for 6 h, and activity was determined 4 days after incubation with complexes.

^b Cell viability of BALB/c mouse macrophages determined 6 h after treatment.

^c SI is selectivity index, calculated by the ratio of CC₅₀ (macrophages) to IC₅₀ (amastigotes).

^d IC₅₀ and CC₅₀ values were calculated using concentrations in triplicate, and two independent experiments were performed. IC₅₀, inhibitory concentration at 50%; CC₅₀, cytotoxic concentration at 50%; ND, not determined owing to lack of activity; Bdz, benznidazole.

nitro complex 2. The selectivity index (SI) of the ruthenium complexes was calculated, and it was observed that, among the complexes tested, complex 3 showed the highest SI.

NO level in infected cells. Complex 3 was the most potent and selective antiparasitic ruthenium complex. To investigate whether complex 3 is an NO donor drug, NO levels in infected macrophages were inferred by determining nitrite content. In this assay, infected cells were incubated for 24 h with drugs, and the nitrite content was estimated by the Griess method. As shown in Fig. 3A, untreated infected BALB/c macrophages produced low levels of NO, whereas stimulus with IFN-γ and LPS induced a significant production of NO. In comparison to untreated infected cells, treatment with 10 μM complex 3 presented a significantly elevation in NO ($P < 0.001$). In contrast, treatment with complex 5 did not result in significant production of NO. No measurable NO concentration was observed in a cell-free experiment containing only complex 3 plus culture medium (data not shown). The same conditions were used in infected J774 cell lines, and similar results were observed (Fig. 3B).

Electron microscopy analysis. Trypomastigotes were treated with complex 3 and analyzed by scanning electron microscopy (SEM). In comparison with untreated parasites (Fig. 4A), treatment resulted in parasite shrinkage and caused cell membrane

discontinuity and fragmentation (Fig. 4B). Morphological changes following complex 3 treatment were observed in 76% of the parasite cells. Among these cells, 74% showed cell shrinkage, 21% displayed membrane discontinuity, and 21% had membrane fragmentation (data not shown). Next, transmission electron microscopy (TEM) experiments were performed in trypomastigotes and intracellular amastigotes. In comparison with untreated trypomastigotes (Fig. 4C), parasites in the presence of complex 3 exhibited swollen mitochondria (Fig. 4D) and loss of the nuclear membrane (Fig. 4E). In most of the treated trypomastigotes, the presence of atypical cytoplasmic vacuoles and the formation of myelin-like structures (Fig. 4F) were observed. The presence of these atypical cytoplasmic vacuoles was also observed in intracellular amastigotes following treatment with the ruthenium complex (Fig. 4H).

Autophagy markers. The observations by transmission micrographs that ruthenium complex induces the formation of atypical cytoplasmic vacuoles led us to investigate whether the mechanism of action involves autophagy. Trypomastigotes were treated with the complex 3 and then incubated with monodansylcadaverine (MDC) to label the autophagic cytosolic vacuoles. In this experiment, untreated parasites were not stained with MDC (Fig. 5A), while parasites treated with rapamycin, a standard autophagy inducer, were stained (Fig. 5B). Parasites treated with complex 3 were positively stained with MDC (Fig. 5C). In order to distinguish between autophagic and lysosomal vacuoles, an additional experiment was carried out using the autophagy inhibitor wortmannin. MDC staining during complex 3 treatment was blocked in the presence of 0.5 μM wortmannin (data not shown). The presence of microtubule-associated protein 1b light chain 3 (LC3B) was detected in untreated and treated *T. cruzi*-infected macrophages by incubating with anti-LC3B polyclonal antibody. In this controlled experiment, nuclei were stained with 4',6-diamidino-2-phenylindole (DAPI), and cells were analyzed by immunofluorescence under a confocal microscope. Untreated infected macrophages did not demonstrate LC3B labeling (Fig. 5A). In contrast, infected macrophages treated with 0.1 mg/ml rapamycin displayed intracellular parasites labeled for LC3B (Fig. 5B). Similarly, infected macrophages treated with ruthenium complex 3 at 2.1 μM displayed intracellular parasites labeled for LC3B (Fig. 5C).

Parasite cell death. After observing that ruthenium complexes induce autophagy, we wanted to know the consequence of au-

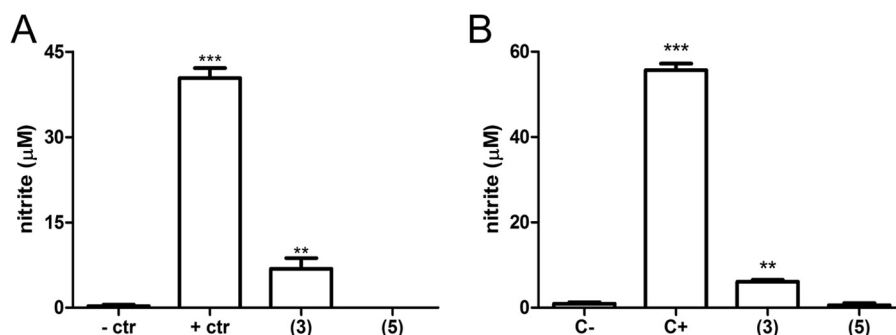


FIG 3 Ruthenium complex 3 increases NO in infected macrophages. Nitrite levels in infected macrophages determined 24 h after treatment. BALB/c peritoneal (A) and J774 (B) macrophages were infected with trypomastigotes and treated with 10 μM of complexes 3 and 5. A positive-control culture (+ ctr) was stimulated with IFN-γ and LPS. The negative-control culture (- ctr) received no treatment or stimulus. Nitrite contents in the supernatant were estimated by the Griess nitrite test 24 h later. Values represent the means ± SEM from three independent experiments. ***, $P < 0.0001$ compared to negative control; **, $P < 0.001$ compared to -ctr.

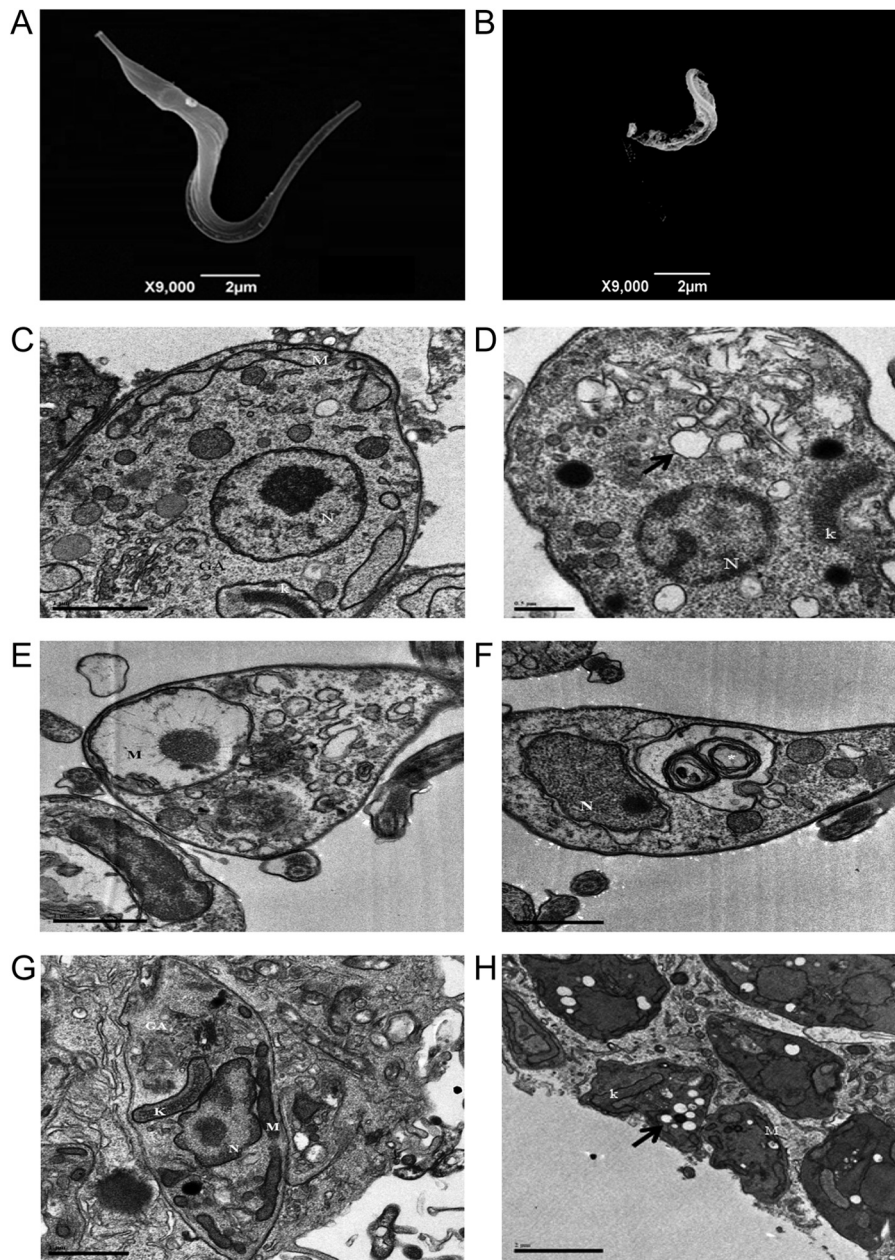


FIG 4 Ruthenium complex 3 causes irreversible morphological impairments to the parasite. Scanning electron micrograph in panel A shows untreated trypomastigote, and panel B shows treated parasite. Transmission electron micrographs in panels C to F are trypomastigotes and in panels G and H are infected macrophages. Panel C shows untreated trypomastigotes, panels D to F are treated parasites. Arrow in panel D indicates cytoplasmic vacuoles; arrow in panel E indicates mitochondrial swelling; arrow and asterisk in panel F indicate nuclear membrane disruption and myelin-like figures, respectively. Panel G shows untreated infected cells, while panel H shows treated infected cells. Arrow in panel H indicates cytoplasmic vacuoles. Complex 3 was added at 2.1 μM and incubated for 24 h in trypomastigotes and 6 h in infected macrophages. GA, Golgi apparatus; K, kinetoplast; N, nucleus; M, mitochondria.

trophagy to the parasite cells. To this end, trypomastigotes were incubated with two different concentrations (2.5 and 5.0 μM) of complex 3 for 36 h at 37°C and then double labeled with annexin V-fluorescein isothiocyanate (FITC) and propidium iodide (PI). Individual cell data were acquired and analyzed by flow cytometry. In comparison to untreated parasites (Fig. 6A), a concentration-related increase in the percentage of stained parasites was observed after complex 3 treatment (Fig. 6B and C). Parasites treated with complex 3 at 5.0 μM showed 34.6% positively stained

cells, of which 26.1% were necrotic (PI stain alone), 5.6% were late apoptotic (PI-annexin V), and 2.9% were early apoptotic (annexin staining alone). As shown in Fig. 6D, this ruthenium complex significantly increased the proportion of necrotic *T. cruzi* cells in a concentration-dependent manner.

In vivo efficacy study. Complex 3 was tested in *T. cruzi*-infected mice during the acute phase. Control groups, receiving either benznidazole or vehicle, were included in this experiment. In this assay, 10^4 Y strain trypomastigotes in a 100- μl solution were

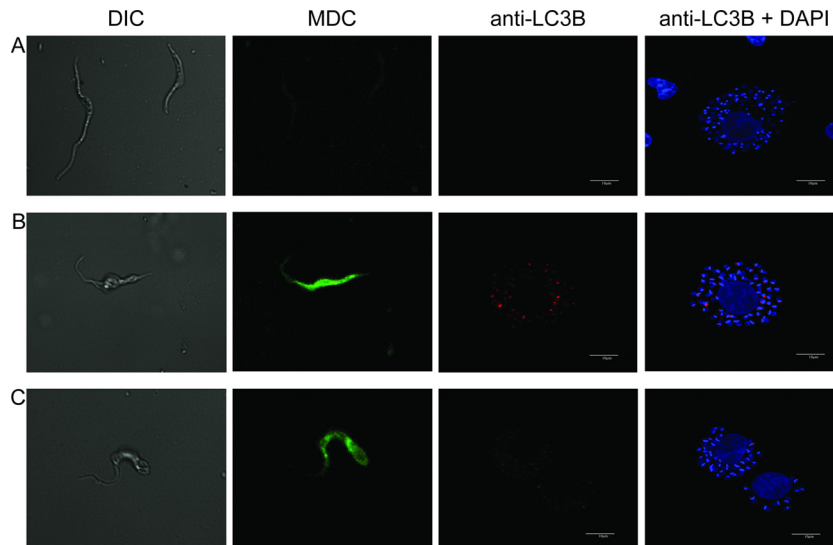


FIG 5 Ruthenium complex 3 induces parasite autophagy. Panel A shows untreated parasites, panel B shows treatment with 0.1 mg/ml rapamycin, and panel C is treatment with 2.1 μ M ruthenium complex 3. Axenic trypomastigotes were incubated for 24 h and stained with MDC, and infected macrophages were incubated for 6 h and then stained with anti-LC3B antibody and DAPI. Images were captured using a confocal microscope with a 60 \times oil-immersion objective at $\times 3$ zoom. DIC, differential interference contrast.

intraperitoneally inoculated in female BALB/c mice ($n = 6$ /group). Treatments were given orally by gavage. Blood parasitemia and survival rates were analyzed. Complex 3 at 25 and 75 μ mol/kg was able to decrease the blood parasitemia peak by 25% ($P < 0.001$) and 46% ($P < 0.001$), respectively (Fig. 7A), in comparison to the blood parasitemia in the untreated group. On day 12 postinfection, no parasites were detected by microscopic examination in benznidazole group blood samples, indicating negative parasitemia. But the same was not observed for infected mice receiving 75 μ mol/kg of complex 3. Mice mortality rates were monitored up to 30 days postinfection. Complex 3 at 75 μ mol/kg significantly decreased mortality compared to that of the untreated group (log rank, $P < 0.01$). The group treated with benznidazole had 100% survival, while the group treated with the highest dose of complex 3 showed a survival rate of 50% (Fig. 7B).

Drug combination. Considering that complex 3 and benznidazole exhibit different mechanism of antiparasitic actions, the possibility of drug combination was studied. Complex 3 and benznidazole alone or in fixed combinations were evaluated against trypomastigote cell cultures, and results were analyzed by CompuSyn software and listed in Table 4. In comparison to individual drug incubation, the combination of complex 3 and benznidazole reduced both EC_{50} and EC_{90} values. Combination index (CI) calculations were used as cutoffs and revealed that this combination has synergistic effects against trypomastigotes. It was observed that drug combinations at the EC_{50} s reduced the percentage of viable trypomastigotes (Fig. 7C) but did not reduce the percentage of viable macrophages (Fig. 7D). Of note, macrophage cytotoxicity was observed when drug combinations were evaluated in concentrations equal or higher than the EC_{90} values.

Based on the *in vitro* synergism, we evaluated the efficacy of ruthenium complex 3 in combination with a suboptimal dose of benznidazole. Complex 3 at 75 μ mol/kg (80 mg/kg) and benznidazole at 38 μ mol/kg (10 mg/kg) were administered individually or in combination using the *in vivo* protocol described above.

Benznidazole at this suboptimal dose reduced blood parasitemia compared to that of the untreated group but did not eliminate circulating parasites. The group receiving the drug combination presented lower parasitemia than the untreated group and groups receiving each individual drug (Fig. 7E). When monitored for up to 30 days postinfection, the group treated with drug combination had 100% survival, while the groups treated with each drug alone showed a survival rate of 60% (Fig. 7F).

DISCUSSION

Identification of new pharmaceuticals is vital for Chagas disease treatment. In order to reach this objective, investigations cannot be limited to small organic molecules but should also include metallic compounds. In fact, coordination complexes and organometallics are recognized as notable anti-*T. cruzi* agents. For instance, the coordination of trypanocidal molecules with metals increases anti-*T. cruzi* activity in comparison with the metal-free molecules. This enhanced activity can be explained by the gain in lipophilicity. This strategy has been performed to enhance the potency of ketoconazole, clotrimazole, benznidazole, risidronate, and quinolones (34–39). Alternatively, metal complexes which are composed of ligands with unique chemical properties (redox and electrochemical behavior based on ligand reductions) exhibit anti-*T. cruzi* properties, possibly due to parasite membrane accumulation, in addition to effects on DNA and enzymes (40–43).

Here, the *in vitro* screening of anti-*T. cruzi* activity demonstrated that both nitro and nitrosyl ruthenium complexes are toxic for trypomastigotes and inhibited epimastigote proliferation at noncytotoxic concentrations in host cells. In contrast, the ruthenium complex lacking nitro and nitrosyl groups did not display anti-*T. cruzi* activity. Regarding structure-activity relationships, the complex containing two nitro groups was more potent than the complex containing only one. However, the nitrosyl complexes showed greater activity than nitro complexes. This suggests that a nitrosyl group contributes more to antiparasitic activity

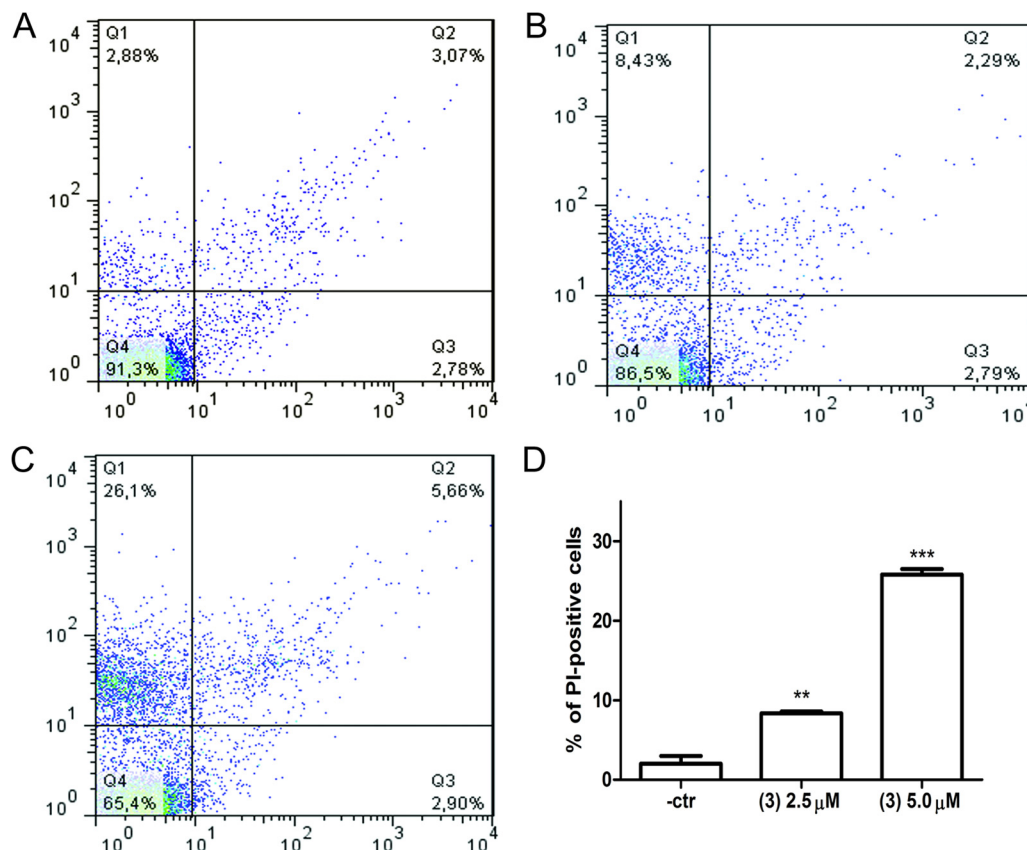


FIG 6 Ruthenium-based treatment causes parasite death by inducing necrosis. Trypomastigotes were treated with complex 3 for 36 h. Parasites were examined by flow cytometry with annexin V and PI staining. Cells plotted in each quadrant represent the following: lower left, double negative; upper left, PI single positive; lower right, annexin V single positive; upper right, PI and annexin V double positive. (A) Untreated; (B) complex 3 at 2.5 μM ; (C) complex 3 at 5.0 μM ; (D) percentage of PI-positive cells. Values are means \pm SD from triplicate tests. -ctr, negative control. **, $P < 0.05$ compared to negative control (ANOVA); ***, $P < 0.0001$ compared to negative control (ANOVA).

than a nitro group. For cruzain, nitro complexes exhibited weak or no inhibitory activity, while nitrosyl complexes exhibited greater inhibitory activity. The nitrosyl complex 4 was only twice less potent as an antiparasitic than its isomer, complex 3, but it presented much higher potency against cruzain than complex 3. These observations indicate that the environment surrounding the metal is important for biological activity.

After determining that these ruthenium complexes inhibit extracellular *T. cruzi*, we examined their activity in infected macrophages. The complexes were able to reduce the number of infected cells more efficiently than benznidazole, and they clearly arrested parasite growth and differentiation inside the host cells. Given the potency of complex 3 against amastigotes, we investigated its mechanism of action in parasites. We observed that nitrosyl complex 3 increased the NO levels in infected macrophages, while the complex lacking the nitrosyl group did not. The antiparasitic activity of ruthenium complex 3 is likely due to its NO-releasing ability or alternatively by indirectly inducing NO production. According to the literature, NO release leads to the inactivation of the protease cruzain in parasite cells. However, complex 3 did not present potency as strong as the powerful cruzain inhibitor E-64c. Therefore, we believe that while complex 3 is an NO donor drug, this property is not related to its ability to inhibit cruzain. Further evidence regarding the mechanism of action of complex 3 was

found by analyzing the parasite ultrastructure and morphology. Two main effects were observed in the treated parasites: first, cell membrane discontinuity and fragmentation and, to a lesser extent, nuclear membrane alterations; second, the appearance of atypical cytoplasmic vacuoles, as well as the formation of myelin-like figures.

Lack of cell membrane integrity is very often associated with necrotic parasite death (44). In fact, parasites treated with complex 3 exhibited a cell death pattern via necrosis rather than apoptosis. Our results are consistent with previous findings demonstrating that ruthenium bipyridyl complexes are prone to accumulate in the cell membrane (22). The presence of cytoplasmic vacuoles and myelin-like figures suggested that ruthenium complexes induce parasite autophagy. By assaying MDC staining and LC3B immunolocalization (45, 46), it was observed that trypomastigotes were stained with MDC after ruthenium complex treatment, and this process was blocked by the presence of the autophagy inhibitor wortmannin. Similar to the literature (47, 48), here, ruthenium complex treatment resulted in the accumulation of LC3B in intracellular amastigotes. The findings observed here support the overall idea that nitrosyl-ruthenium complexes release NO, which triggers cellular events, including parasite autophagy. As a result, a number of irreversible morphological im-

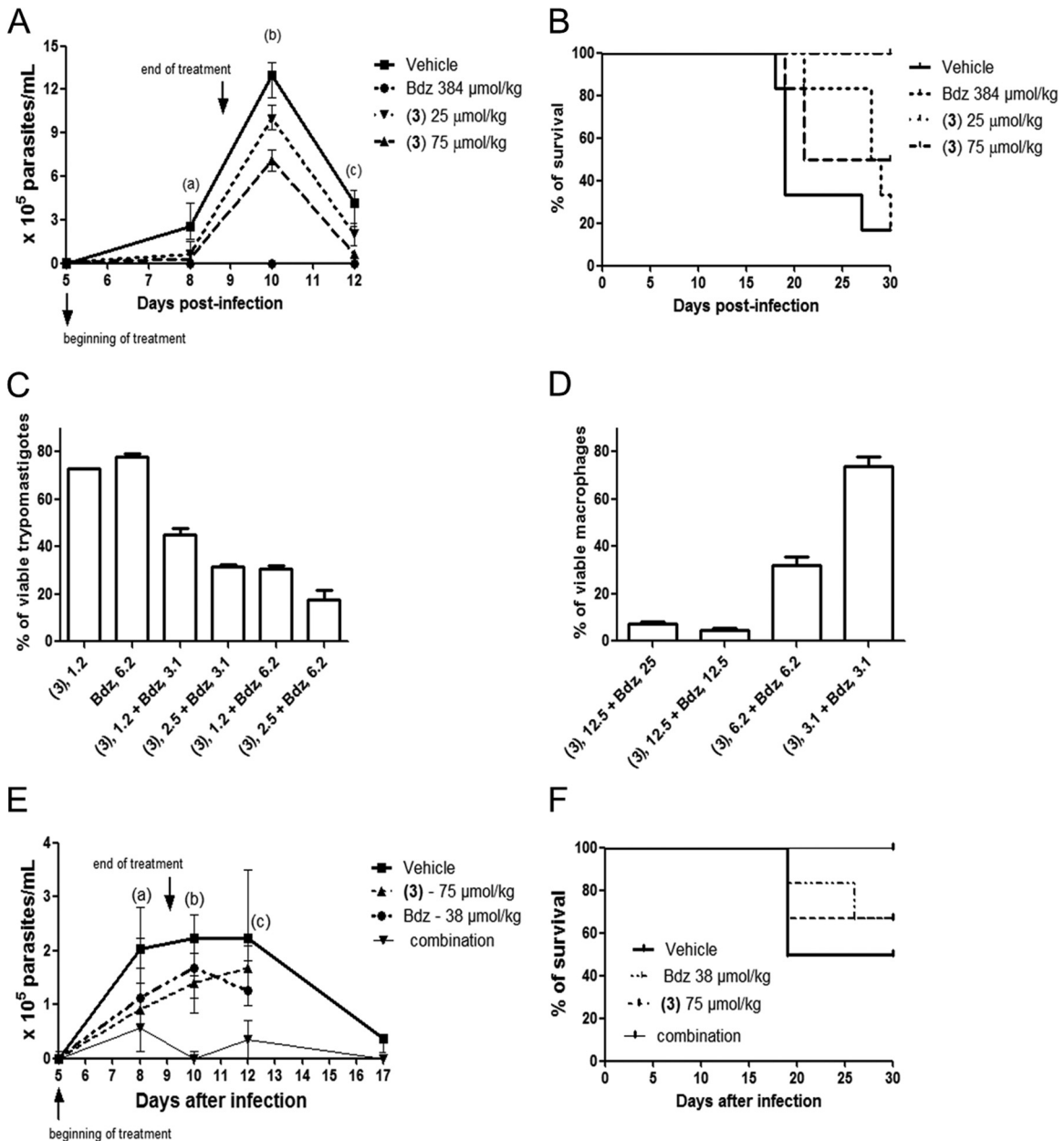


FIG 7 Ruthenium complex 3 reduces acute infection, and this is enhanced under drug combination with benznidazole. Parasitemia (A) and survival (B) of *T. cruzi*-infected mice ($n = 6$ /group) orally treated once per day for 5 consecutive days with 25 μ mol/kg (26.6 mg/kg) or 75 μ mol/kg (80 mg/kg) of complex 3. Benznidazole (Bdz) was given at 384 μ mol/kg (100 mg/kg). (A) Sets a, b, c, vehicle versus Bdz ($P < 0.001$), vehicle versus complex 3 at 25 μ mol/kg ($P < 0.001$), vehicle versus complex 3 at 75 μ mol/kg ($P < 0.001$), respectively. (B) Log rank analysis, vehicle versus complex 3 at 75 μ mol/kg ($P < 0.01$), vehicle versus Bdz ($P < 0.001$). Percentage of viable trypomastigotes (C) and macrophages (D). Drug concentration is indicated on the x axis in μ M, and cell viability was recorded 24 h after incubation. (E) Parasitemia and survival of infected mice ($n = 6$ /group) orally treated once per day with a drug combination of complex 3 and benznidazole. (a) Vehicle versus complex 3 ($P < 0.001$), vehicle versus Bdz ($P < 0.01$), vehicle versus drug combination ($P < 0.001$); (b) vehicle versus complex 3 ($P < 0.05$), vehicle versus drug combination ($P < 0.001$); (c) vehicle versus complex 3 ($P < 0.05$), vehicle versus Bdz ($P < 0.001$), vehicle versus drug combination ($P < 0.001$). (F) Log rank analyses revealed curves are not significantly different.

pairments occur to the parasite cells, finally leading to cell death by necrosis.

Due to the strong antiparasitic activity of complex 3, it was evaluated in mice during the acute phase of Chagas disease. Complex 3 had a dose-dependent effect and presented an optimal efficacy when given orally at 75 μ mol/kg. This reduced the blood parasitemia and increased mice survival; however, it did not elim-

inate parasites present in the bloodstream, while the benznidazole regime did. Given the substantial dedication to identifying optimal drug combinations for the treatment of Chagas disease (49, 50), a combination of ruthenium complex 3 and benznidazole would offer a potential therapy to reduce the benznidazole dosage required to cure infection. This is supported by the fact that combination would target *T. cruzi* at two different modes of action:

TABLE 4 Concentration reduction and combination indexes in trypomastigotes treated with ruthenium complex 3 and benznidazole^a

Compound	EC ₅₀ ± SD (μM)		CRI at EC ₅₀	EC ₉₀ ± SD (μM)		CRI at EC ₉₀	CI at:	
	Alone	Combination		Alone	Combination		EC ₅₀	EC ₉₀
Complex 3	2.1 ± 0.6	0.8 ± 0.02	2.7 ± 0.2	4.9 ± 0.1	1.7 ± 0.02	2.6 ± 0.2	0.65 ± 0.03	0.56 ± 0.09
Bdz	11.4 ± 1.0	4.1 ± 0.1	3.5 ± 0.1	25.8 ± 0.8	8.7 ± 0.1	4 ± 0.8		

^a EC₅₀ and EC₉₀ values were calculated using concentrations in duplicate, and two independent experiments were performed. Cutoff: CI value of 0.3 to 0.7, synergism; 0.7 to 0.85, moderate synergism; 0.85 to 0.9, slight synergism; 0.9 to 1.1, additivity; >1.1, antagonism. CRI, concentration reduction index; CI, combination index; Bdz, benznidazole.

NO release and autophagy induction mediated by complex 3 and nitroreductase inhibition and oxidative stress induction mediated by benznidazole (51, 52). *In vitro*, combinations of complex 3 and benznidazole were synergic in killing trypomastigotes. In infected mice, combination of ruthenium complex with a suboptimal dose of benznidazole exhibited enhanced efficacy in terms of reducing infection and increasing survival compared to each drug used alone. Overall, these findings indicate that ruthenium complexes are a class of suitable constituents for drug combination.

Conclusions. We investigated the NO donor drug strategy by synthesizing new ruthenium complexes that feature nitro or nitrosyl groups. These complexes exhibited a broad spectrum of activities (vector-borne stage, bloodstream form, intracellular stage) against *T. cruzi*. This activity is abolished once nitro and nitrosyl groups are removed from the complex, indicating these groups are structural determinants for activity. By examining the underlying mechanism of action of these complexes, it was observed that they release NO, causing autophagy, which is followed by a series of irreversible morphological impairments to the parasites, culminating in necrotic cell death. More striking, ruthenium-nitrosyl complex 3 was efficient in reducing blood parasitemia in acutely infected mice and presented synergic effects when in combination with benznidazole.

ACKNOWLEDGMENTS

This research was funded by CNPq, FAPESB, and FAPESP. A.A.B., J.E., and M.B.P.S. are recipients of a CNPq fellowship. T.M.B received a CAPES scholarship; C.S.M. and D.R.M.M. are receiving FAPESP scholarships.

We are thankful to Carine Azevedo for assistance with confocal microscopy, Adriano Alcantara for providing cruzain, and Marcos Vannier dos Santos for providing MDC and rapamycin. We are thankful to the electron microscopy unit of CPqGM.

We declare no competing financial interests.

T.M.B. designed and performed most experimental studies and analyses; M.I.F.B., J.W.D.C.J., and M.M.D.S. synthesized and validated the complexes; J.E. assisted with X-ray crystallography; C.S.M. assisted with the transmission electron microscopy analyses and cell culture; E.T.G. assisted with flow cytometry; D.R.M.M. provided guidance and assisted with experimental design and assisted with manuscript preparation; A.A.B. and M.B.P.S. initiated the project and provided guidance for experimental design, interpretation of data, and preparation of the manuscript. All authors have read and approved the final manuscript.

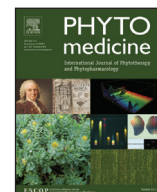
REFERENCES

- Schofield CJ, Jannin J, Salvatella R. 2006. The future of Chagas disease control. *Trends Parasitol.* 12:583–588. <http://dx.doi.org/10.1016/j.pt.2006.09.011>.
- Rodrigues Coura J. 2013. Chagas disease: control, elimination and eradication. Is it possible? *Mem. Inst. Oswaldo Cruz* 108:962–967. <http://dx.doi.org/10.1590/0074-0276130565>.
- Pinazo MJ, Muñoz J, Posada E, López-Chejade P, Gállego M, Ayala E, del Cacho E, Soy D, Gascon J. 2010. Tolerance of benznidazole in treatment of Chagas' disease in adults. *Antimicrob. Agents Chemother.* 54:4896–4899. <http://dx.doi.org/10.1128/AAC.00537-10>.
- Urbina JA. 2010. Specific chemotherapy of Chagas disease: relevance, current limitations and new approaches. *Acta Trop.* 115:55–68. <http://dx.doi.org/10.1016/j.actatropica.2009.10.023>.
- Moreira DRM, Leite ACL, dos Santos RR, Soares MBP. 2009. Approaches for the development of new anti-*Trypanosoma cruzi* agents. *Curr. Drug Targets* 10:212–231. <http://dx.doi.org/10.2174/138945009787581140>.
- Scharfstein J, Schechter M, Senna M, Peralta JM, Mendonça-Previato L, Miles MA. 1986. *Trypanosoma cruzi*: characterization and isolation of a 57/51,000 m.w. surface glycoprotein (GP57/51) expressed by epimastigotes and bloodstream trypomastigotes. *J. Immunol.* 137:1336–1341.
- Souto-Padrón T, Campetella OE, Cazzulo JJ, de Souza W. 1990. Cysteine proteinase in *Trypanosoma cruzi*: immunocytochemical localization and involvement in parasite-host cell interaction. *J. Cell Sci.* 96:485–490.
- McKerrow JH, Caffrey C, Kelly B, Loke P, Sajid M. 2006. Proteases in parasitic diseases. *Annu. Rev. Pathol.* 1:497–536. <http://dx.doi.org/10.1146/annurev.pathol.1.110304.100151>.
- Doyle PS, Zhou YM, Hsieh I, Greenbaum DC, McKerrow JH, Engel JC. 2011. The *Trypanosoma cruzi* protease cruzain mediates immune evasion. *PLoS Pathog.* 7:e1002139. <http://dx.doi.org/10.1371/journal.ppat.1002139>.
- Gazzinelli RT, Oswald IP, Hieny S, James SL, Sher A. 1992. The microbicidal activity of interferon-gamma-treated macrophages against *Trypanosoma cruzi* involves an L-arginine-dependent, nitrogen oxide-mediated mechanism inhibitable by interleukin-10 and transforming growth factor-beta. *Eur. J. Immunol.* 22:2501–2506. <http://dx.doi.org/10.1002/eji.1830221006>.
- Vespa GN, Cunha FQ, Silva JS. 1994. Nitric oxide is involved in control of *Trypanosoma cruzi*-induced parasitemia and directly kills the parasite *in vitro*. *Infect. Immun.* 62:5177–5182.
- Venturini G, Salvati L, Muolo M, Colasanti M, Gradoni L, Ascenzi P. 2000. Nitric oxide inhibits cruzipain, the major papain-like cysteine proteinase from *Trypanosoma cruzi*. *Biochem. Biophys. Res. Commun.* 270:437–441. <http://dx.doi.org/10.1006/bbrc.2000.2447>.
- Bocedi A, Dawood KF, Fabrini R, Federici G, Gradoni L, Pedersen JZ, Ricci G. 2010. Trypanothione efficiently intercepts nitric oxide as a harmless iron complex in trypanosomatid parasites. *FASEB J.* 24:1035–1042. <http://dx.doi.org/10.1096/fj.09-146407>.
- Tfouni E, Truzzi DR, Tavares A, Gomes AJ, Figueiredo LE, Franco DW. 2012. Biological activity of ruthenium nitrosyl complexes. *Nitric Oxide* 26:38–53. <http://dx.doi.org/10.1016/j.niox.2011.11.005>.
- Ascenzi P, Bocedi A, Gentile M, Visca P, Gradoni L. 2004. Inactivation of parasite cysteine proteinases by the NO-donor 4-(phenylsulfonyl)-3-((2-(dimethylamino)ethyl)thio)-furoxan oxalate. *Biochim. Biophys. Acta* 1703:69–77. <http://dx.doi.org/10.1016/j.bbapap.2004.09.027>.
- Silva JJ, Osakabe AL, Pavanelli WR, Silva JS, Franco DW. 2007. *In vitro* and *in vivo* antiproliferative and trypanocidal activities of ruthenium NO donors. *Br. J. Pharmacol.* 152:112–121. <http://dx.doi.org/10.1038/sj.bjp.0707363>.
- Silva JJ, Pavanelli WR, Pereira JC, Silva JS, Franco DW. 2009. Experimental chemotherapy against *Trypanosoma cruzi* infection using ruthenium nitric oxide donors. *Antimicrob. Agents Chemother.* 53:4414–4421. <http://dx.doi.org/10.1128/AAC.00104-09>.
- Guedes PM, Oliveira FS, Gutierrez FR, da Silva GK, Rodrigues GJ, Bendhack LM, Franco DW, Do Valle Matta MA, Zamboni DS, da Silva RS, Silva JS. 2010. Nitric oxide donor *trans*-[RuCl([15]aneN)NO] as a possible therapeutic approach for Chagas' disease. *Br. J. Pharmacol.* 160:270–282. <http://dx.doi.org/10.1111/j.1476-5381.2009.00576.x>.
- Silva JJ, Guedes PM, Zottis A, Balliano TL, Nascimento Silva FO, França Lopes LG, Ellena J, Oliva G, Andricopulo AD, Franco DW, Silva JS. 2010. Novel ruthenium complexes as potential drugs for Chagas's disease: enzyme inhibition and *in vitro/in vivo* trypanocidal activity. *Br. J. Pharmacol.* 160:260–269. <http://dx.doi.org/10.1111/j.1476-5381.2009.00524.x>.

20. Levina A, Mitra A, Lay PA. 2009. Recent developments in ruthenium anticancer drugs. *Metallomics* 1:458–470. <http://dx.doi.org/10.1039/b904071d> <http://dx.doi.org/10.1039/b904071d>.
21. Bergano A, Sava G. 2011. Ruthenium anticancer compounds: myths and realities of the emerging metal-based drugs. *Dalton Trans.* 40:7817–7823. <http://dx.doi.org/10.1039/c0dt01816c>.
22. Zava O, Zakeeruddin SM, Danelon C, Vogel H, Grätzel M, Dyson PJ. 2009. A cytotoxic ruthenium tris(bipyridyl) complex that accumulates at plasma membranes. *ChemBioChem* 10:1796–1800. <http://dx.doi.org/10.1002/cbic.200900013>.
23. Groessel M, Zava O, Dyson PJ. 2011. Cellular uptake and subcellular distribution of ruthenium-based metallodrugs under clinical investigation versus cisplatin. *Metallomics* 3:591–599. <http://dx.doi.org/10.1039/c0mt00101e>.
24. Heinrich TA, Von Poelhsitz G, Reis RI, Castellano EE, Neves A, Lanznaster M, Machado SP, Batista AA, Costa-Neto CM. 2011. A new nitrosyl ruthenium complex: synthesis, chemical characterization, *in vitro* and *in vivo* antitumor activities and probable mechanism of action. *Eur. J. Med. Chem.* 46:3616–3622. <http://dx.doi.org/10.1016/j.ejmech.2011.04.064>.
25. Pavan FR, Poelhsitz GV, Barbosa MI, Leite SR, Batista AA, Ellena J, Sato LS, Franzblau SG, Moreno V, Gambino D, Leite CQ. 2011. Ruthenium(II) phosphine/diimine/picolinate complexes: inorganic compounds as agents against tuberculosis. *Eur. J. Med. Chem.* 46:5099–5107. <http://dx.doi.org/10.1016/j.ejmech.2011.08.023>.
26. Santos ER, Mondelli MA, Pozzi LV, Corrêa RS, Salistre-de-Araújo SS, Pavan FR, Leite CQF, Ellena J, Malta VRS, Machado SP, Batista AA. 2013. New ruthenium(II)/phosphines/diimines complexes: promising antitumor (human breast cancer) and *Mycobacterium tuberculosis* fighting agents. *Polyhedron* 51:292–297. <http://dx.doi.org/10.1016/j.poly.2013.01.004>.
27. Green LC, Wagner DA, Glogowski J, Skipper PL, Wishnok JS, Tannenbaum SR. 1982. Analysis of nitrate, nitrite, and [¹⁵N]nitrate in biological fluids. *Anal. Biochem.* 126:131–138.
28. Brener Z. 1962. Therapeutic activity and criterion of cure on mice experimentally infected with *Trypanosoma cruzi*. *Rev. Inst. Med. Trop. Sao Paulo* 4:386–396.
29. Romanha AJ, Castro SL, Soeiro MN, Lannes-Vieira J, Ribeiro I, Talvani A, Bourdin B, Blum B, Olivieri B, Zani C, Spadafora C, Chiari E, Chatelain E, Chaves G, Calzada JE, Bustamante JM, Freitas-Junior LH, Romero LI, Bahia MT, Lotrowska M, Soares MBP, Andrade SG, Armstrong T, Degreve W, Andrade ZA. 2010. *In vitro* and *in vivo* experimental models for drug screening and development for Chagas disease. *Mem. Inst. Oswaldo Cruz* 105:233–238. <http://dx.doi.org/10.1590/S0074-02762010000200022>.
30. Barbosa MIF, Corrêa RS, Oliveira KM, Rodrigues C, Ellena J, Nascimento OR, Rocha VPC, Nonato FR, Macedo TS, Barbosa-Filho JM, Soares MBP, Batista AA. 2014. Antiparasitic activities of novel ruthenium/lapachol complexes. *J. Inorg. Biochem.* 136:33–39. <http://dx.doi.org/10.1016/j.jinorgbio.2014.03.009>.
31. Richter-Addo GB, Legzdins P. 1992. Metal nitrosyls, p 383. Oxford University Press, New York, NY.
32. Godwin JB, Meyer TJ. 1971. Nitrosyl-nitrite, interconversion in ruthenium complexes. *Inorg. Chem.* 10:2150–2153. <http://dx.doi.org/10.1021/ic50104a012>.
33. Nakamoto K. 1997. Infrared and Raman spectra of inorganic and coordination compounds, p 384, 5th ed, part B. Wiley-Interscience, New York, NY.
34. Navarro M, Cisneros-Fajardo EJ, Lehmann T, Sánchez-Delgado RA, Atencio R, Silva P, Lira R, Urbina JA. 2001. Toward a novel metal-based chemotherapy against tropical diseases. 6. Synthesis and characterization of new copper(II) and gold(I) clotrimazole and ketoconazole complexes and evaluation of their activity against *Trypanosoma cruzi*. *Inorg. Chem.* 40:6879–6884. <http://dx.doi.org/10.1021/ic0103087>.
35. Nogueira Silva JJ, Pavanelli WR, Gutierrez FR, Alves Lima FC, Ferreira da Silva AB, Santana Silva J, Wagner Franco D. 2007. Complexation of the anti-*Trypanosoma cruzi* drug benzimidazole improves solubility and efficacy. *J. Med. Chem.* 51:4104–4114. <http://dx.doi.org/10.1021/jm701306r>.
36. Demoro B, Caruso F, Rossi M, Benítez D, Gonzalez M, Cerecetto H, Parajón-Costa B, Castiglioni J, Galizzi M, Docampo R, Otero L, Gambino D. 2010. Risedronate metal complexes potentially active against Chagas disease. *J. Inorg. Biochem.* 104:1252–1258. <http://dx.doi.org/10.1016/j.jinorgbio.2010.08.004>.
37. Reis DC, Pinto MC, Souza-Fagundes EM, Rocha LF, Pereira VR, Melo CM, Beraldo H. 2011. Investigation on the pharmacological profile of antimony(III) complexes with hydroxyquinoline derivatives: antitrypanosomal activity and cytotoxicity against human leukemia cell lines. *Biometals* 24:595–601. <http://dx.doi.org/10.1007/s10534-011-9407-8>.
38. Martínez A, Carreon T, Iniguez E, Anzellotti A, Sánchez A, Tyan M, Sattler A, Herrera L, Maldonado RA, Sánchez-Delgado RA. 2012. Searching for new chemotherapies for tropical diseases: ruthenium-clotrimazole complexes display high *in vitro* activity against *Leishmania major* and *Trypanosoma cruzi* and low toxicity toward normal mammalian cells. *J. Med. Chem.* 55:3867–3877. <http://dx.doi.org/10.1021/jm300070h>.
39. Iniguez E, Sánchez A, Vasquez MA, Martínez A, Olivas J, Sattler A, Sánchez-Delgado RA, Maldonado RA. 2013. Metal-drug synergy: new ruthenium(II) complexes of ketoconazole are highly active against *Leishmania major* and *Trypanosoma cruzi* and nontoxic to human or murine normal cells. *J. Biol. Inorg. Chem.* 18:779–790. <http://dx.doi.org/10.1007/s00775-013-1024-2>.
40. Lowe G, Droz AS, Vilaivan T, Weaver GW, Tweedale L, Pratt JM, Rock P, Yardley V, Croft SL. 1999. Cytotoxicity of (2,2':6',2'-terpyridine)platinum(II) complexes to *Leishmania donovani*, *Trypanosoma cruzi*, and *Trypanosoma brucei*. *J. Med. Chem.* 42:999–1006. <http://dx.doi.org/10.1021/jm981074c>.
41. Vieites M, Smircich P, Parajón-Costa B, Rodríguez J, Galaz V, Oleazar C, Otero L, Aguirre G, Cerecetto H, González M, Gómez-Barrio A, Garat B, Gambino D. 2008. Potent *in vitro* anti-*Trypanosoma cruzi* activity of pyridine-2-thiol *N*-oxide metal complexes having an inhibitory effect on parasite-specific fumarate reductase. *J. Biol. Inorg. Chem.* 13:723–735. <http://dx.doi.org/10.1007/s00775-008-0358-7>.
42. Donnici CL, Araujo MH, Oliveira HS, Moreira DRM, Pereira VRA, Souza MA, De-Castro MCAB, Leite ACL. 2009. Ruthenium complexes endowed with potent anti-*Trypanosoma cruzi* activity: synthesis, biological characterization and structure-activity relationships. *Bioorg. Med. Chem.* 17:5038–5043. <http://dx.doi.org/10.1016/j.bmc.2009.05.071>.
43. Benítez J, Becco L, Correia I, Leal SM, Guiseth H, Pessoa JC, Lorenzo J, Tanco S, Escobar P, Moreno V, Garat B, Gambino D. 2011. Vanadium polypyridyl compounds as potential antiparasitic and antitumoral agents: new achievements. *J. Inorg. Biochem.* 105:303–312. <http://dx.doi.org/10.1016/j.jinorgbio.2010.11.001>.
44. Vannier-Santos MA, de Castro SL. 2009. Electron microscopy in antiparasitic chemotherapy: a (close) view to a kill. *Curr. Drug Targets* 10:246–260. <http://dx.doi.org/10.2174/138945009787581168>.
45. Jimenez V, Paredes R, Sosa MA, Galanti N. 2008. Natural programmed cell death in *T. cruzi* epimastigotes maintained in axenic cultures. *J. Cell. Biochem.* 105:688–698. <http://dx.doi.org/10.1002/jcb.21864>.
46. Veiga-Santos P, Barrias ES, Santos JF, de Barros-Moreira TL, de Carvalho TM, Urbina JA, de Souza W. 2012. Effects of amiodarone and posaconazole on the growth and ultrastructure of *Trypanosoma cruzi*. *Int. J. Antimicrob. Agents* 40:61–71. <http://dx.doi.org/10.1016/j.ijantimicag.2012.03.009>.
47. Tan C, Lai S, Wu S, Hu S, Zhou L, Chen Y, Wang M, Zhu Y, Lian W, Peng W, Ji L, Xu A. 2010. Nuclear permeable ruthenium(II) β-carboline complexes induce autophagy to antagonize mitochondrial-mediated apoptosis. *J. Med. Chem.* 53:7613–7624. <http://dx.doi.org/10.1021/jm1009296>.
48. Castonguay A, Doucet C, Juhas M, Maysinger D. 2012. New ruthenium(II)-letrozole complexes as anticancer therapeutics. *J. Med. Chem.* 55:8799–8806. <http://dx.doi.org/10.1021/jm301103y>.
49. Cencig S, Coltel N, Truyens C, Carlier Y. 2012. Evaluation of benzimidazole treatment combined with nifurtimox, posaconazole or AmBisome in mice infected with *Trypanosoma cruzi* strains. *Int. J. Antimicrob. Agents* 40:527–532. <http://dx.doi.org/10.1016/j.ijantimicag.2012.08.002>.
50. Bustamante JM, Craft JM, Crowe BD, Ketchie SA, Tarleton RL. 2014. New, combined, and reduced dosing treatment protocols cure *Trypanosoma cruzi* infection in mice. *J. Infect. Dis.* 209:150–162. <http://dx.doi.org/10.1093/infdis/jit420>.
51. Hall BS, Wilkinson SR. 2012. Activation of benzimidazole by trypanosomal type I nitroreductases results in glyoxal formation. *Antimicrob. Agents Chemother.* 56:115–123. <http://dx.doi.org/10.1128/AAC.05135-11>.
52. Rajão MA, Furtado C, Alves CL, Passos-Silva DG, de Moura MB, Schamber-Reis BL, Kunrath-Lima M, Zuma AA, Vieira-da-Rocha JP, Borio Ferreira Garcia J, Mendes IC, Junho Pena SD, Macedo AM, Franco GR, de Souza-Pinto NC, de Medeiros MH, Cruz AK, Machado Motta MC, Ribeiro Teixeira SM, Machado CR. 2014. Unveiling benzimidazole's mechanism of action through overexpression of DNA repair proteins in *Trypanosoma cruzi*. *Environ. Mol. Mutagen.* 55:309–321. <http://dx.doi.org/10.1002/em.21839>.

ANEXO 5

MEIRA, C. S.; GUIMARÃES, E. T.; SANTOS, J. A. F.; MOREIRA, D. R. M.; NOGUEIRA, R. C.; TOMASSINI, T. C. B.; RIBEIRO, I. M.; SOUZA, C. V. C.; RIBEIRO-DOS-SANTOS, R.; SOARES, M. B. P. *In vitro* and *in vivo* antiparasitic activity of *Physalis angulata* L. concentrated ethanolic extract against *Trypanosoma cruzi*. **Phytomedicine**, v. 22, p. 969-974, 2015.



In vitro and *in vivo* antiparasitic activity of *Physalis angulata* L. concentrated ethanolic extract against *Trypanosoma cruzi*



Cássio Santana Meira^a, Elisalva Teixeira Guimarães^{a,b}, Jamyle Andrade Ferreira dos Santos^{a,b}, Diogo Rodrigo Magalhães Moreira^a, Renata Campos Nogueira^a, Therezinha Coelho Barbosa Tomassini^c, Ivone Maria Ribeiro^c, Claudia Valeria Campos de Souza^c, Ricardo Ribeiro dos Santos^d, Milena Botelho Pereira Soares^{a,d,*}

^a Centro de Pesquisas Gonçalo Moniz, Fundação Oswaldo Cruz, Salvador, Bahia, Brazil

^b Universidade do Estado da Bahia, Salvador, Bahia, Brazil

^c Laboratório de Química de Produtos Naturais-PN2-Extração, Isolamento e Purificação, Farmanguinhos-Fiocruz, Rio de Janeiro, RJ, Brazil

^d Centro de Biotecnologia e Terapia Celular, Hospital São Rafael, Salvador, BA, Brazil

ARTICLE INFO

Article history:

Received 23 March 2015

Revised 3 July 2015

Accepted 6 July 2015

Keywords:

Chagas disease

Trypanosoma cruzi

Physalis angulata

Plant extract

Drug combination

ABSTRACT

Background: The current treatment of Chagas disease, endemic in Latin America and emerging in several countries, is limited by the frequent side effects and variable efficacy of benznidazole. Natural products are an important source for the search for new drugs.

Aim/hypothesis: Considering the great potential of natural products as antiparasitic agents, we investigated the anti-*Trypanosoma cruzi* activity of a concentrated ethanolic extract of *Physalis angulata* (EEPA).

Methods: Cytotoxicity to mammalian cells was determined using mouse peritoneal macrophages. The antiparasitic activity was evaluated against axenic epimastigote and bloodstream trypomastigote forms of *T. cruzi*, and against amastigote forms using *T. cruzi*-infected macrophages. Cell death mechanism was determined in trypomastigotes by flow cytometry analysis after annexin V and propidium iodide staining. The efficacy of EEPA was examined *in vivo* in an acute model of infection by monitoring blood parasitaemia and survival rate 30 days after treatment. The effect against trypomastigotes of EEPA and benznidazole acting in combination was evaluated.

Results: EEPA effectively inhibits the epimastigote growth (IC_{50} $2.9 \pm 0.1 \mu\text{M}$) and reduces bloodstream trypomastigote viability (EC_{50} $1.7 \pm 0.5 \mu\text{M}$). It causes parasite cell death by necrosis. EEPA impairs parasite infectivity as well as amastigote development in concentrations nontoxic to mammalian cells. In mice acutely-infected with *T. cruzi*, EEPA reduced the blood parasitaemia in 72.7%. When combined with benznidazole, EEPA showed a synergistic anti-*T. cruzi* activity, displaying CI values of 0.8 ± 0.07 at EC_{50} and 0.83 ± 0.1 at EC_{90} .

Conclusion: EEPA has antiparasitic activity against *T. cruzi*, causing cell death by necrosis and showing synergistic activity with benznidazole. These findings were reinforced by the observed efficacy of EEPA in reducing parasite load in *T. cruzi*-mice. Therefore, this represents an important source of antiparasitic natural products.

© 2015 Elsevier GmbH. All rights reserved.

Introduction

Chagas disease, a zoonosis caused by the hemoflagellate protozoan *Trypanosoma cruzi*, remains a serious health problem in many Latin American countries, where it is an endemic disease that affects approximately 10 million people (Rassi et al. 2010). It is estimated that over 400,000 individuals are infected in non-endemic areas, mainly in the USA and in European countries (Coura and Viñas 2010). Once the individual has been infected by *T. cruzi*, there is no effective treatment and the development of a vaccine is still in experimental stage (Gupta et al. 2013; Maya et al. 2007). The current treatment is based on the 2-nitroimidazole benznidazole (LAFEPE, Brazil), which

Abbreviations: EEPA, ethanolic extract from *P. angulata*; DMSO, dimethyl sulfoxide; DTU, discrete typing unit; LIT, liver infusion tryptose; FBS, fetal bovine serum; RPMI, Roswell park memorial institute; PI, propidium iodide; CC_{50} , cytotoxicity concentration of 50%; IC_{50} , inhibitory concentration of 50%; EC_{50} , effective concentration at 50%; ANOVA, analysis of variance; EC_{90} , effective concentration of 90%; CI, combination index; GV, gentian violet; BDZ, benznidazole; SEM, standard error of the mean; SD, standard deviation; DPI, days post-infection.

* Corresponding author at: Centro de Pesquisas Gonçalo Moniz, Fundação Oswaldo Cruz. 121, Rua Waldemar Falcão, Candeal, Salvador 40296-710, Bahia, Brazil. Tel.: +55 71 3176 2260; fax: +55 71 3176 2272.

E-mail address: milenabpsoares@gmail.com, milena@bahia.fiocruz.br (M.B.P. Soares).

<http://dx.doi.org/10.1016/j.phymed.2015.07.004>

0944-7113/© 2015 Elsevier GmbH. All rights reserved.

is recommended for all acute, early chronic and reactivated cases (Da Silva et al. 2011). Its inefficacy against the chronic phase of the disease, allied to many side effects which frequently lead to treatment interruption (Bahia et al. 2012; Urbina 2009) encourages the search for alternative compounds for a better treatment for Chagas disease.

In the continuous search for new drugs, natural products are an important source of compounds to a large number of illnesses (Newman and Cragg 2012). A considerable number of plant-derived compounds are nowadays recognized for their antiparasitic properties (Negi et al. 2014; Rocha et al. 2005; Singh et al. 2014; Wink 2012). An example of plant species with active compounds is the Solanaceae *Physalis angulata* L., an annual herb widespread in many tropical countries and widely used in folk medicine (Soares et al. 2003; Tomassini et al. 2000). Previously, our research group demonstrated the antiparasitic properties of *seco*-steroids physalins isolated from *P. angulata* against *Plasmodium falciparum* and different *Leishmania* species (Guimarães et al. 2009,2010; Sá et al. 2011). More recently, it was also reported that physalins, specifically B and F, are endowed with a strong anti-*T. cruzi* activity against different evolutive forms of *T. cruzi* (Meira et al. 2013). Isolating physalins is quite costly, time consuming and affords low yields, aspects which hamper the use of isolated physalins for a neglected disease. To overcome this, a feasible alternative is the use of a *Physalis angulata* extract. In fact, the concentrated ethanolic extract from *P. angulata* (EEPA) is nonmutagenic, presents low toxicity in mice and is effective against different *Leishmania* species (Nogueira et al. 2013). Therefore, in the present work the anti-*T. cruzi* activity *in vitro* and *in vivo* of EEPA was evaluated.

Material and methods

Plant material

P. angulata specimens were collected and identified during the drier season (from June until November) in Belém, Pará State, Brazil. A voucher specimen was deposited in the Herbarium of the Department of Physiology from the University Federal of Pará (Voucher number 15).

Extraction and phytochemical analysis of *P. angulata*

Stems of *P. angulata* (1 kg) were dried and crushed. Then, extraction was carried out with ethanol at 50–60 °C during 6 h. The extract was concentrated under reduced pressure, yielding 100 g (10%) of crude ethanolic extract. It was maintained in a desiccator under vacuum until weight stabilized. HPLC–UV analysis was determined in an Agilent HP 1100 series system consisting of an auto-sampler, high-pressure mixing pump and UV detector (Agilent Technologies, Santa Clara, CA). Samples were run in a reverse phase C-18 column 5 µm (250 mm × 4 mm, Hibar® LiChrosorb®, Merck, Germany) and UV absorbance was measured at 225 nm by injecting 10 µl of EEPA dissolved in 10 mg/ml in MeOH at flow rate 1 ml/min. Physalins in the EEPA were confirmed by comparing with standard isolated physalin previously characterized. These procedures were performed as described by Nogueira et al. (2013) and executed in accordance with European Medicines Agency guidelines for herbal products.

Drugs

Benznidazole (LAFEPE, Recife, Brazil) was used as reference drug in the anti-*T. cruzi* assays. Gentian violet (Synth, São Paulo, Brazil) was used as positive control in the cytotoxicity assays. All compounds were dissolved in DMSO (Sigma–Aldrich, St. Louis, MO) and diluted in cell culture medium for use in the assays. The final concentration of DMSO was less than 1% in all *in vitro* experiments.

Parasites

The *T. cruzi* strains Y (DTU II; Silva and Nussenzweig 1953) and Colombian (DTU I; Federici et al. 1964) were used in this study. *T. cruzi* epimastigotes were grown in liver infusion tryptose (LIT) medium supplemented with 10% fetal bovine serum (FBS; CultiLab, Campinas, Brazil), 1% hemin (Sigma–Aldrich), 1% R9 medium (Sigma–Aldrich) and 50 µg/ml of gentamycin (Novafarma, Anápolis, Brazil) at 26 °C. Tissue culture trypomastigotes were obtained from the supernatants of 5- to 6-day-old infected LLC-MK2 cells maintained in RPMI-1640 medium supplemented with 10% FBS and 50 µg/ml gentamycin at 37 °C in a 5% humidified CO₂ atmosphere.

Animals

Female BALB/c mice (18–22 g) were provided by the animal breeding facility and maintained in sterilized cages under a controlled environment, water *ad libitum* and receiving a balanced diet for rodent at Centro de Pesquisa Gonçalo Moniz (Fundação Oswaldo Cruz, Bahia, Brazil). All experiments were carried out in accordance with the recommendations of Ethical Issues Guidelines, and were approved by the local Animal Ethics Committee.

Assessment of cytotoxicity to macrophages

Peritoneal exudate macrophages were obtained by washing, with cold RPMI medium, the peritoneal cavity of BALB/c mice 4–5 days after injection of 3% thioglycolate in saline (1.5 ml per mice). Then, cells were seeded into 96-well plates at a cell number 1×10^5 cells/well in RPMI-1640 medium supplemented with 10% of FBS and 50 µg/ml of gentamycin and incubated for 24 h at 37 °C and 5% CO₂. After that time each sample was added at eight concentrations (0.02–50 µg/ml) in triplicate and incubated for 72 h. Twenty microliters/well of AlamarBlue (Invitrogen, Carlsbad, CA) were added to the plates during 10 h. Colorimetric readings were performed at 570 and 600 nm. CC₅₀ values were calculated using data-points gathered from three independent experiments. Gentian violet was used as positive control.

Antiparasitic activity

Epimastigotes (1×10^6 cells/well) were seeded in fresh medium in LIT medium in the absence or presence of the EEPA at eight concentrations (0.02–50 µg/ml) in triplicate. Cell growth was determined after culture for 5 days by counting viable forms in a Neubauer chamber. Bloodstream trypomastigotes forms of *T. cruzi* from the supernatants of previously infected LLC-MK2 cells were dispensed into 96-well plates (4×10^5 cell/well) in RPMI medium supplemented with 10% FBS and 50 µg/ml of gentamycin in the absence or presence of different concentrations (0.02–50 µg/ml) of the plant extract, in triplicate. Viable parasites were counted in a Neubauer chamber 24 h after incubation. The percentage of inhibition was calculated in relation to untreated cultures. To determine the inhibitory concentration of 50% (IC₅₀) and the effective concentration at 50% (EC₅₀) for epimastigote and trypomastigote forms of *T. cruzi*, respectively, a nonlinear regression on Prism 5.02 GraphPad software was employed. Experiments were performed in both Y and Colombian strains and benznidazole was used as anti-*T. cruzi* reference drug. For *in vitro* drug combinations, doubling dilutions of each drug (EEPA and benznidazole), used alone or in fixed combinations were incubated with 4×10^5 cells/well trypomastigotes (Y strain) for 24 h. The analysis of the combined effects was performed by determining the combination index (CI) by using Chou–Talalay CI method and the CompuSyn software version 1.0 (ComboSyn Inc., Paramus, NJ), as described previously (Chou and Talalay 2005). CI values were used as cutoff to determine synergism.

T. cruzi-infected macrophages

Peritoneal exudate macrophages (2×10^5 cells/well) obtained from BALB/c mice were seeded in a 24 well-plate with rounded coverslips on the bottom in RPMI supplemented with 10% FBS and incubated for 24 h. Cells were then infected with trypomastigotes (10:1) for 2 h. Free trypomastigotes were removed by successive washes using saline solution and the cells were incubated for 24 h to allow full internalization and differentiation of trypomastigotes to amastigotes. Next, cultures were incubated in complete medium alone or with the EEPA or benznidazole (0.1–2.5 $\mu\text{g/ml}$) for 72 h. Cells were fixed in absolute alcohol and the percentage of infected macrophages and the number of amastigotes/100 macrophages was determined by manual counting after hematoxylin and eosin staining using an optical microscope (Olympus, Tokyo, Japan). The percentage of infected macrophages and the number of amastigotes per 100 macrophages was determined by counting 100 cells per slide. The one-way ANOVA and Bonferroni for multiple comparisons were used to determine the statistical significance of the group comparisons. Experiment was done with both strains (Y and Colombian) and benznidazole was used as positive control.

Propidium iodide and annexin V staining

T. cruzi trypomastigotes from Y strain (1×10^7) were incubated for 24 and 72 h at 37 °C in the absence or presence of EEPA (1.7, 3.4 or 5 $\mu\text{g/ml}$). After incubation, the parasites were labeled for propidium iodide (PI) and annexin V using the annexin V-FITC apoptosis detection kit (Sigma–Aldrich), according to the manufacturer's instructions. Acquisition and analyses was performed using a FACS Calibur flow cytometer (Becton Dickinson, San Diego, CA), with FlowJo software (Tree Star, Ashland, OR). A total of 30,000 events were acquired in the region previously established as that corresponding to trypomastigotes forms of *T. cruzi*.

Infection in mice

Female BALB/c mice (18–22 g) were infected with bloodstream trypomastigotes by intraperitoneal inoculation of 10^4 parasites in 100 μl of saline solution and then mice were randomly divided in groups (six animals per group). After the day 5 of infection, treatment with 50 or 100 mg/kg weight of EEPA was given orally for 5 consecutive days. For the control group, benznidazole was given orally at dose of 100 mg/kg weight. Saline containing 20% DMSO was used as a vehicle and administrated on untreated and infected group. Animal infection was monitored daily by counting the number of motile parasites in 5 μl of fresh blood sample drawn from the lateral tail veins, as recommended by standard protocol (Brener 1962). Survival was monitored for 30 days after treatment. The one-way ANOVA and Bonferroni for multiple comparisons were used to determine the statistical significance of the group comparisons.

Results

Extraction and phytochemical analysis of EEPA revealed that this extract is rich in *seco*-steroids, mainly physalins B, D, F and G. By HPLC–UV, it was estimated that each 100 mg of EEPA contains 0.84% of physalin B, 0.90% of physalin D, 0.37% of physalin F and 0.36% of physalin G. This is in agreement with the literature showing that this plant contains a number of steroids (Nogueira et al. 2013; Tomassini et al. 2000).

The trypanocidal activity of EEPA was initially evaluated against epimastigotes and trypomastigotes (Y and Colombian strains) through the determination of IC_{50} and EC_{50} , respectively. The plant extract showed a potent anti-*T. cruzi* activity, being able to inhibit epimastigote proliferation and lyse trypomastigotes. The IC_{50} of EEPA

Table 1

Antiparasitic activity of EEPA on extracellular forms of *T. cruzi* and host cell cytotoxicity.

Sample	Epimastigotes $\text{IC}_{50} \pm \text{S.D}$ ($\mu\text{g/ml}$) ^a		Trypomastigotes $\text{EC}_{50} \pm \text{S.D}$ ($\mu\text{g/ml}$) ^b		$\text{M}\emptyset$ $\text{CC}_{50} \pm \text{S.D}$. ($\mu\text{g/ml}$) ^c
	Y strain	Colombian strain	Y strain	Colombian strain	
EEPA	2.9 \pm 0.1	7.4 \pm 0.2	1.7 \pm 0.5	2.3 \pm 0.2	6.1 \pm 0.8
BDZ	2.8 \pm 0.7	4.1 \pm 1.1	2.8 \pm 0.7	3.3 \pm 0.1	>50
GV	–	–	–	–	0.21 \pm 0.02

Values were calculated using concentrations in triplicate and three independent experiments were performed. IC_{50} = inhibitory concentration at 50%. EC_{50} = effective concentration at 50%. CC_{50} = cytotoxic concentration at 50%. S.D = standard deviation. BDZ = benznidazole. GV = gentian violet. $\text{M}\emptyset$ = macrophage.

^a Determined 120 h after incubation with compounds.

^b Determined 24 h after incubation with compounds.

^c Cell viability of BALB/c mouse macrophages determined 72 h after treatment.

treatment was 2.9 and 7.4 $\mu\text{g/ml}$ for epimastigotes of Y and Colombian strains, respectively, while benznidazole exhibited an IC_{50} of 2.8 and 4.1 $\mu\text{g/ml}$, respectively. For trypomastigotes, the EC_{50} calculated of EEPA was 1.7 and 2.8 $\mu\text{g/ml}$ for Y and Colombian strains, respectively. Under the same assay conditions, the standard drug benznidazole presented an EC_{50} of 2.8 and 3.3 $\mu\text{g/ml}$ for Y and Colombian strains, respectively. Next, the cytotoxicity of EEPA was determined in mammalian cells. The plant extract exhibited a CC_{50} value of 6.1 $\mu\text{g/ml}$, being several times less cytotoxicity than the reference drug, gentian violet ($\text{CC}_{50} = 0.21 \mu\text{g/ml}$) (Table 1).

The activity of EEPA against intracellular amastigotes (Y strain) was also investigated. The plant extract induced a concentration-dependent reduction in the analyzed parameters: percentage of infected macrophages (Fig. 1A) and the mean number of intracellular amastigotes per infected macrophage (Fig. 1B). Under the same conditions, a similar reduction was observed on treated-benznidazole macrophages. No signs of cytotoxicity were observed on macrophage cultures (data not shown).

After confirming that EEPA was able to decrease parasite viability, the mechanism of EEPA-induced cell death was investigated. In untreated cultures, most cells were negative for annexin V and PI staining, demonstrating cell viability (Fig. 2A). Cultures treated with EEPA showed a concentration and time-dependent increase in the number of PI-positive parasites when compared with untreated parasites (Fig. 2B–D). Treatment with 3.4 $\mu\text{g/ml}$ of EEPA for 72 h resulted in 11.5 and 41.3% of cells positive for PI and PI + annexin V, respectively, whereas 1.1% cells were stained only for annexin V. These results indicate that EEPA treatment increases the number of PI staining, which is characteristic of a parasite cell death caused by a necrotic process.

Next, *in vivo* studies to evaluate the effects of EEPA against *T. cruzi* infection in mice (acute phase) were performed. As shown in Fig. 3, EEPA treatment significantly ($P < 0.001$) reduced blood parasitaemia when compared with mice treated with vehicle (Fig. 3). At doses of 50 and 100 mg/kg, EEPA administration caused a reduction in blood parasitaemia of 42.6 and 72.7%, respectively (Table 2). In the group treated with benznidazole, it was observed >99% of inhibition of blood parasitaemia, indicating that eradication of infection was achieved. Treatment with EEPA, similar to the treatment with benznidazole, had a protective effect on mortality. Mice from benznidazole or EEPA treated groups did not show any behavioral alteration or signs of toxicity (data not shown).

Finally, the antiparasitic effect of EEPA and benznidazole in combination was investigated against trypomastigotes. In comparison to drug alone, the combination of EEPA and benznidazole reduced both EC_{50} and EC_{90} values. In fact, the EC_{50} and EC_{90} of benznidazole decreased in average by 59% when combined with EEPA (Table 3). The combination index values revealed that EEPA and benznidazole have synergistic effects.

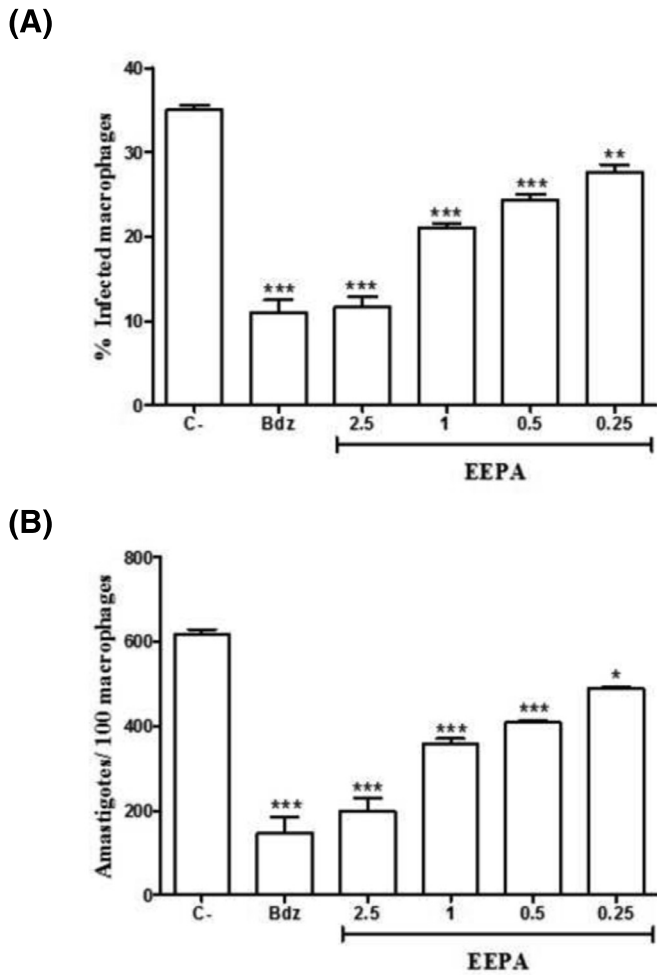


Fig. 1. EEPA inhibited amastigote proliferation in *T. cruzi*-infected macrophages. Mouse peritoneal exudate macrophages were infected with Y strain trypomastigotes for 2 h and treated with different concentrations of EEPA (2.5, 1, 0.5 or 0.25 µg/ml) or benznidazole (2.5 µg/ml), a standard drug. Cells were stained with hematoxylin and eosin and analyzed by optical microscopy. The percentage of infected macrophages (A) and the relative number of amastigotes per 100 macrophages (B) were determined by counting hematoxylin and eosin-stained cultures. BDZ is benznidazole. Values represent the mean ± SEM of triplicates. **P* < 0.05; ***P* < 0.01; ****P* < 0.001 compared to the control group.

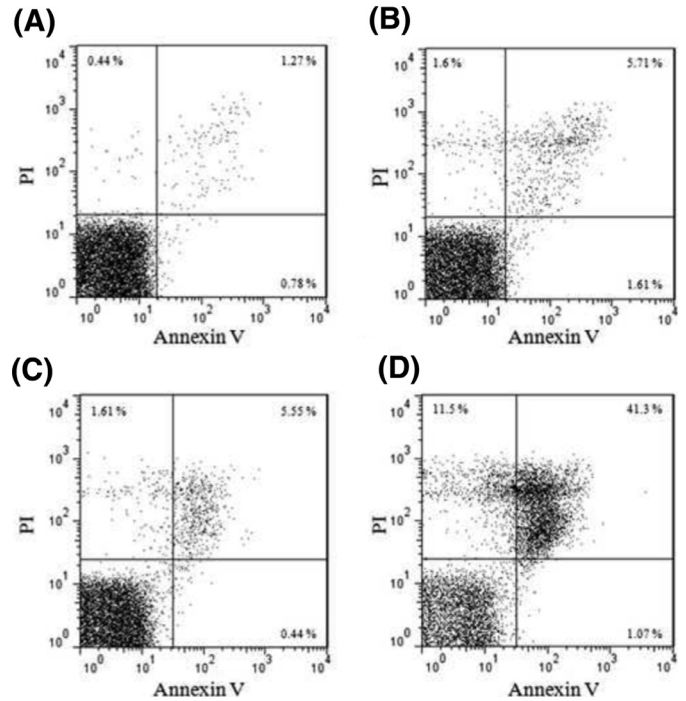


Fig. 2. Flow cytometry analysis of trypanomastigotes treated with EEPA for 24 or 72 h and stained with propidium iodide (PI) and annexin V. (A) Representative untreated trypanomastigotes (24 h); (B) trypanomastigotes treated with EEPA (5 µg/ml) for 24 h; (C) trypanomastigotes treated with EEPA (1.7 µg/ml) for 72 h; (D) trypanomastigotes treated with EEPA (3.4 µg/ml) for 72 h.

Discussion

In this study, the potent anti-*T. cruzi* activity of concentrated ethanolic extract from *P. angulata* (EEPA) rich in physalins was demonstrated *in vitro* on different strains of *T. cruzi* and *in vivo* on an acute model of infection. EEPA was chosen mainly because the isolation of the active molecule is costly, time consuming and gives a small fraction of material. On the other hand, the extract is easily obtained, has low cytotoxicity and high stability (Nogueira et al. 2013).

EEPA effectively inhibits the growth of epimastigotes and was toxic against bloodstream trypomastigotes of *T. cruzi*. More importantly, has potent activity against amastigotes inside infected

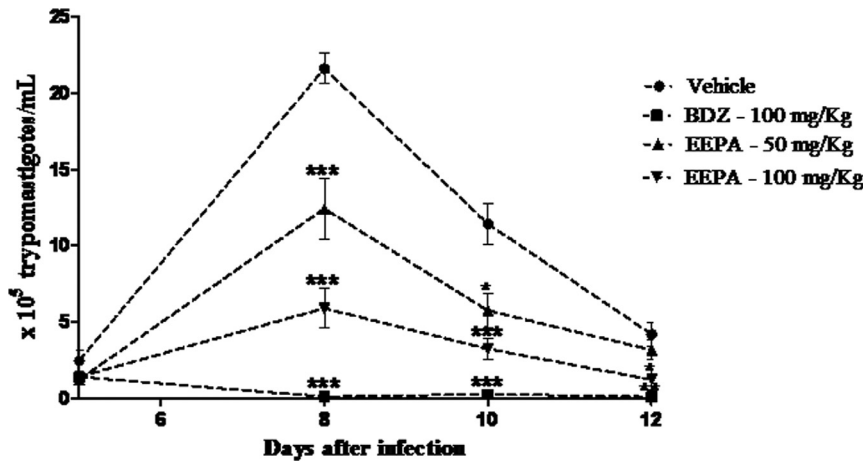


Fig. 3. Parasitemia of BALB/c mice infected with *T. cruzi* and treated with EEPA. Female BALB/c mice were infected with 10⁴ Y strain trypomastigotes. Five days after infection, mice were treated orally with EEPA (50 or 100 mg/kg) or benznidazole (100 mg/kg) once a day during 5 consecutive days. Parasitemia was monitored by counting the number of trypanomastigotes in fresh blood samples. Values represent the mean ± SEM of 6 mice per group. Results are from one experiment of two replicates performed. **P* < 0.05; ****P* < 0.001 compared to untreated-infected group (vehicle).

Table 2Parasitemia and mortality evaluation in mice infected with Y strain *T. cruzi* and treated daily with EEPA or benznidazole for 5 days.

Sample	Dose (mg/kg)	% Blood parasitemia reduction in mice ^a		Mortality ^b
		8 dpi	10 dpi	
EEPA	50	42.6	49.7	0/6
EEPA	100	72.7	71.7	0/6
BDZ	100	>99	>99	0/6
Vehicle	–	–	–	4/6

Dpi = days post-infection. BDZ = benznidazole. Vehicle = untreated and infected group.

^a Calculated as $[(\text{average vehicle group} - \text{average treated group}) / \text{average vehicle group}] \times 100\%$.^b Mortality was monitored until 30 days after treatment.**Table 3**

Antiparasitic activity of EEPA or benznidazole in Y strain trypomastigotes alone or in combination.

Sample	EC ₅₀ ± S.D. (μg/ml) ^a		EC ₉₀ ± S.D. (μg/ml) ^a		CI at ^b	
	Drug alone	Combination	Drug alone	Combination	EC ₅₀	EC ₉₀
EEPA	1.7 ± 0.5	0.58 ± 0.05	3.1 ± 0.2	1.3 ± 0.1	0.8 ± 0.07	0.83 ± 0.1
BDZ	2.8 ± 0.7	1.17 ± 0.1	6.7 ± 0.2	2.7 ± 0.2		

S.D. = standard deviation. BDZ = benznidazole.

^a EC₅₀ and EC₉₀ values were calculated using concentrations in triplicates and two independent experiments were performed.^b Combination index (CI). Cutoff: CI value of 0.3–0.7, synergism; 0.7–0.85, moderate synergism; 0.85–0.9, slight synergism; 0.9–1.1, additivity; >1.1, antagonism.

macrophages (the clinically relevant form), without affecting mammalian cells. These observations confirm and extend the antiparasitic activity of EEPA recently reported by Nogueira et al. (2013). The authors demonstrated that even in a low dose of EEPA is enough to reduce the percentage of infected cells, as well as the parasite burden in *L. amazonensis*-infected macrophages. Moreover, a high selectivity index was observed, pointing out the great efficacy against *L. amazonensis* (Nogueira et al. 2013).

To identify the mechanism of cell death induced by EEPA treatment, analyses of the classical necrosis/apoptosis processes were performed. From the literature, it is well known that activation of cell death pathway depends on type, time, and intensity of the stimulus (Kessler et al. 2013). Necrosis is usually defined as a process of cell collapse that involves oncosis (increase in cell volume), rupture of plasma membrane and the unorganized dismantling of swollen organelles. Apart from the presence of plasma membrane permeabilization, necrosis lacks specific biochemical markers (Kroemer et al. 2009). In this study, EEPA treatment caused an increase time-dependent in the number of PI-positive parasites, suggestive of cell death by necrosis. PI-positive parasites also were observed after 24 h of treatment with physalin B (Meira et al. 2013). In addition, ultrastructural analyses showed remarkable alterations in the morphology of the Golgi complex, kinetoplast, endoplasmic reticulum and plasma membrane of trypomastigotes, confirming a pattern consistent with necrotic cell death.

Combination therapies can be a valuable tool to improve treatment efficacy and reduce dose levels and toxicity, as well as to prevent the potential development of resistance, which may be advantages for the treatment of parasitic diseases (Vivas et al. 2008; Diniz et al. 2013). In this study, EEPA demonstrates synergistic effects with benznidazole against the bloodstream parasites *in vitro*, showing a promising profile for drug combination.

In spite of the great potential of natural products for infectious disease treatment, the literature is relatively scarce of anti-*T. cruzi* natural products (Altei et al. 2014; Da Rocha et al. 2014; Sanchez et al. 2013; Santos et al. 2012; Valli et al. 2013). Therefore the investigation of both crude and fractionated plant extracts is important. The findings reported here not only demonstrate that EEPA is a rich source

of antiparasitic natural products, but also points out the necessity of more efforts toward exploring biodiversity for identifying anti-*T. cruzi* compounds.

Conclusion

EEPA demonstrated a strong, selective, and broad-spectrum antiparasitic activity against *T. cruzi*. Consistent with this strong *in vitro* activity, EEPA reduced parasite burden by rapidly interrupting the cell cycle in the obligated host. Mechanistically, this natural product achieved antiparasitic activity through induction cell death *via* necrosis. EEPA was able to reduce the course of an aggressive acute infection murine model and provided to a suitable partner for drug combination. The results presented herein reinforce the investigation of other members of this family for antiparasitic compounds.

Conflict of interest

All authors have no conflict of interest to disclose.

Acknowledgments

This work was supported by grants from CNPq, PRONEX, FAPESB, FINEP, RENORBIO and FIOCRUZ/FARMANGUINHOS.

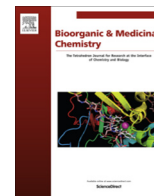
References

- Altei, W.F., Picchi, D.G., Abissi, B.M., Giesel, G.M., Flausino Jr., O., Reboud-Ravaux, M., Verli, H., Crusca Jr., E., Silveira, E.R., Cilli, E.M., Bolzani, V.S., 2014. Jatrophidin I, a cyclic peptide from Brazilian *Jatropha curcas* L.: isolation, characterization, conformational studies and biological activity. *Phytochemistry* 107, 91–96.
- Bahia, T.M., Andrade, I.M., Martins, T.A.F., Nascimento, A.F.S., Diniz, L.F., Caldas, I.S., Talvani, A., Trunz, B.B., Torrele, E., Ribeiro, I., 2012. Fexinidazole: a potential new drug candidate for Chagas disease. *PLoS Negl. Trop. Dis.* 6, e1870.
- Brener, Z., 1962. Therapeutic activity and criterion of cure in mice experimentally infected with *Trypanosoma cruzi*. *Rev. Inst. Med. Trop. São Paulo* 4, 386–396.
- Chou, T.C., Talalay, P., 2005. Quantitative analysis of dose–effect relationships: the combined effects of multiple drugs or enzyme inhibitors. *Adv. Enzyme Regul.* 22, 27–55.
- Coura, J.R., Viñas, P.A., 2010. Chagas disease: a new worldwide challenge. *Nature* 465 (Suppl.), S6–S7.

- Da Rocha, C.Q., Queiroz, E.F., Meira, C.S., Moreira, D.R., Soares, M.B., Marcourt, L., Vilegas, W., Wolfender, J.L., 2014. Dimeric flavonoids from *Arrabidaea brachypoda* and assessment of their anti-*Trypanosoma cruzi* activity. *J. Nat. Prod.* 77, 1345–1350.
- Da Silva, C.F., Junqueira, A., Lima, M.M., Romanha, A.J., Junior, P.A.S., Stephens, C.E., Som, P., Boykin, D.W., Soeiro, M.N.C., 2012. *In vitro* trypanocidal activity of DB745B and other novel arylimidamides against *Trypanosoma cruzi*. *J. Antimicrob. Chem.* 66, 1295–1297.
- Diniz, L.F., Urbina, J.A., Andrade, I.M., Mazzeti, A.L., Martins, T.A., Caldas, I.S., Talvani, A., Ribeiro, I., Bahia, M.T., 2013. Benzimidazole and posaconazole in experimental Chagas disease: positive interaction in concomitant and sequential treatments. *PLoS Negl. Trop. Dis.* 7, e2367.
- Federici, E.E., Abelman, W.B., Neva, F.A., 1964. Chronic and progressive myocarditis and myositis in C3H mice infected with *Trypanosoma cruzi*. *Am. J. Trop. Med. Hyg.* 13, 272–280.
- Guimarães, E.T., Lima, M.S., Santos, L.A., Ribeiro, I.M., Tomassini, T.B., Ribeiro-dos-Santos, R., Soares, M.B., 2009. Activity of physalins purified from *Physalis angulata* in *in vitro* and *in vivo* models of cutaneous leishmaniasis. *J. Antimicrob. Chemother.* 64, 84–87.
- Guimarães, E.T., Lima, M.S., Santos, L.A., Ribeiro, I.V., Tomassini, T.B.C., Ribeiro-dos-Santos, R., Santos, W.L.C., Soares, M.B.P., 2010. Effects of seco-steroids purified from *Physalis angulata* L., Solanaceae, on the viability of *Leishmania* sp. *Rev. Bras. Farmacogn.* 20, 945–949.
- Gupta, S., Wan, X., Zago, M.P., Sellers, V.C., Silva, T.S., Assiah, D., Dhiman, M., Nuñez, S., Petersen, J.R., Vásquez-Chagoyán, J.C., Estrada-Franco, J.G., Garg, N.J., 2013. Antigenicity and diagnostic potential of vaccine candidates in human Chagas disease. *PLoS Negl. Trop. Dis.* 7, e2018.
- Kessler, L.K., Soares, M.J., Probst, C.M., Krieger, M.C., 2013. *Trypanosoma cruzi* responses to sterol biosynthesis inhibitors: morphophysiological alterations leading cell death. *PLoS One* 8, e55497.
- Kroemer, G., Galluzzi, L., Vandenabeele, P., Abrams, J., Alnemri, E.S., Baehrecke, E.H., Blagosklonny, M.V., El-Deiry, W.S., Golstein, P., Green, D.R., Hengartner, M., Knight, R.A., Kumar, S., Lipton, S.A., Malorni, W., Nuñez, G., Peter, M.E., Tschopp, J., Yuan, J., Piacentini, M., Zhivotovskiy, B., Melino, G. Nomenclature Committee on Cell Death 2009, 2009. Classification of cell death: recommendations of the nomenclature committee on cell death 2009. *Cell Death Differ.* 16, 3–11.
- Maya, J.A., Cassels, B.K., Iturriaga-Vásquez, P., Ferreira, J., Fáunder, M., Galanti, N., Ferreira, A., Morello, A., 2007. Mode of action of natural and synthetic drugs against *Trypanosoma cruzi* and their interaction with the mammalian host. *Comp. Biochem. Physiol. A Mol. Integr. Physiol.* 146, 601–620.
- Meira, C.S., Guimarães, E.T., Bastos, T.M., Moreira, D.R.M., Tomassini, T.C.B., Ribeiro, I.M., Ribeiro-dos-Santos, R., Soares, M.B.P., 2013. Physalins B and F, seco-steroids isolated from *Physalis angulata* L., strongly inhibit proliferation, ultrastructure and infectivity of *Trypanosoma cruzi*. *Parasitology* 140, 1811–1821.
- Negi, A.S., Gupta, A., Hamid, A.A., 2014. Combating malaria with plant molecules: a brief update. *Curr. Med. Chem.* 21, 458–500.
- Newman, D.J., Cragg, G.M., 2012. Natural products as sources of new drugs over the 30 years from 1981 to 2010. *J. Nat. Prod.* 75, 311–335.
- Nogueira, R.C., Rocha, V.P.C., Nonato, F.R., Tomassini, T.C.B., Ribeiro, I.M., Ribeiro-dos-Santos, R., Soares, M.B.P., 2013. Genotoxicity and antileishmanial activity evaluation of *Physalis angulata* concentrated ethanolic extract. *Environ. Toxicol. Pharmacol.* 36, 1304–1311.
- Rassi Jr., A., Rassi, A., Marin-Neto, J.A., 2010. Chagas disease. *Lancet* 375, 1388–1402.
- Rocha, L.G., Almeida, J.R., Macêdo, R.O., Barbosa-Filho, J.M., 2005. A review of natural products with antileishmanial activity. *Phytomedicine* 12, 514–535.
- Sá, M.S., Menezes, M.N., Krettli, A.U., Ribeiro, I.M., Tomassini, T.C.B., Ribeiro-dos-Santos, R., Azevedo Jr., W.F., Soares, M.B., 2011. Antimalarial activity of physalins B, D, F and G. *J. Nat. Prod.* 74, 2269–2272.
- Sanchez, L.M., Knudsen, G.M., Helbig, C., De Muylder, G., Mascuch, S.M., Mackey, Z.B., Gerwick, L., Clayton, C., Mckerrow, J.H., Linington, R.G., 2013. Examination of the mode of action of the almiramide family of natural products against kinetoplastid parasite *Trypanosoma brucei*. *J. Nat. Prod.* 76, 630–641.
- Santos, V.A., Regasini, L.O., Nogueira, C.R., Passerini, G.D., Martinez, I., Bolzani, V.S., Graminha, M.A., Cicarelli, R.M., Furian, M., 2012. Antiprotozoal sesquiterpene pyridine alkaloids from *Maytenus ilicifolia*. *J. Nat. Prod.* 75, 991–995.
- Silva, L.H.P., Nussenzweig, V., 1953. Sobre a cepa de *Trypanosoma cruzi* altamente virulenta para o camundongo branco. *Folia Clin. Biol.* 20, 191–207.
- Singh, N., Mishra, B.B., Bajpai, S., Singh, R.K., Tiwari, V.K., 2014. Natural products based leads to fight against leishmaniasis. *Bioorg. Med. Chem.* 22, 18–45.
- Soares, M.B.P., Bellintani, M.C., Ribeiro, I.M., Tomassini, T.C.B., Ribeiro-dos-Santos, R., 2003. Inhibition of macrophage activation and lipopolysaccharide-induced death by seco steroids purified from *Physalis angulata* L. *Euro. J. Pharmacol.* 459, 107–112.
- Tomassini, T.C.B., Barbi, N.S., Ribeiro, I.M., Xavier, D.C.D., 2000. Genus *Physalis* – a revision of withasteroids. *Quím. Nova* 23, 47–57. doi:10.1590/S0100-4042200000100011.
- Urbina, J.A., 2009. Specific chemotherapy of Chagas disease: relevance, current limitations and new approaches. *Acta Trop.* 115, 55–68.
- Valli, M., dos Santos, R.N., Figueira, L.D., Nakajima, C.H., Castro-Gamboa, I., Andricopulo, A.D., Bolzani, V.S., 2013. Development of a natural products database from the biodiversity of Brazil. *J. Nat. Prod.* 76, 439–444.
- Vivas, L., Rattray, L., Stewart, L., Bongard, E., Robinson, B.L., et al., 2008. Anti-malarial efficacy of pyronaride and artesunate in combination *in vitro* and *in vivo*. *Acta Trop.* 105, 222–228.
- Wink, M., 2012. Medicinal plants: a source of anti-parasitic secondary metabolites. *Molecules* 17, 12771–12791.

ANEXO 6

FILHO, G. B. O.; CARDOSO, M. V. O.; ESPÍNOLA, J. W. P.; FERREIRA, L. F. G. R.; SIMONE, C. A.; FERREIRA, R. S.; COELHO, P. L.; **MEIRA, C. S.**; MOREIRA, D. R. M.; SOARES, M. B. P.; LEITE, A. C. L. Structural design, synthesis and pharmacological evaluation of 4-thiazolidinones against *Trypanosoma cruzi*, **Bioorganic & Medicinal Chemistry**, v. 23, p. 7478-7486, 2015.



Structural design, synthesis and pharmacological evaluation of 4-thiazolidinones against *Trypanosoma cruzi*



Gevanio Bezerra de Oliveira Filho^{a,*}, Marcos Veríssimo de Oliveira Cardoso^a, José Wanderlan Pontes Espíndola^a, Luiz Felipe Gomes Rebello Ferreira^a, Carlos Alberto de Simone^b, Rafaela Salgado Ferreira^c, Pollyanne Lacerda Coelho^c, Cássio Santana Meira^d, Diogo Rodrigo Magalhaes Moreira^d, Milena Botelho Pereira Soares^{d,e}, Ana Cristina Lima Leite^a

^a Departamento de Ciências Farmacêuticas, Centro de Ciências da Saúde, Universidade Federal de Pernambuco, 50740-520 Recife, PE, Brazil

^b Departamento de Física e Informática, Instituto de Física, Universidade de São Paulo, CEP 13560-970, São Carlos, SP, Brazil

^c Departamento de Bioquímica e Imunologia, Universidade Federal de Minas Gerais, CEP 31270-901, Belo Horizonte, MG, Brazil

^d Centro de Pesquisas Gonçalo Moniz, Fundação Oswaldo Cruz, CEP 40296-710, Salvador, BA, Brazil

^e Centro de Biotecnologia e Terapia Celular, Hospital São Rafael, Salvador, BA, Brazil

ARTICLE INFO

Article history:

Received 6 August 2015

Revised 20 October 2015

Accepted 31 October 2015

Available online 2 November 2015

Keywords:

Chagas disease

Trypanosoma cruzi

Thiosemicarbazones

Thiazolidinones

Bioisosterism

ABSTRACT

Chagas disease is an infection caused by protozoan *Trypanosoma cruzi*, which affects approximately 8–10 million people worldwide. Benznidazole is the only drug approved for treatment during the acute and asymptomatic chronic phases of Chagas disease; however, it has poor efficacy during the symptomatic chronic phase. Therefore, the development of new pharmaceuticals is needed. Here, we employed the bioisosterism to modify a potent antiparasitic and cruzain-inhibitor aryl thiosemicarbazone (**4**) into 4-thiazolidinones (**7–21**). Compounds (**7–21**) were prepared by using a straightforward synthesis and enabled good to excellent yields. As a chemical elucidation tool, X-ray diffraction of compound (**10**) revealed the geometry and conformation of this class compounds. The screening against cruzain showed that 4-thiazolidinones were less active than thiosemicarbazone (**4**). However, the antiparasitic activity in Y strain trypomastigotes and host cell cytotoxicity in J774 macrophages revealed that compounds (**10** and **18–21**) are stronger and more selective antiparasitic agents than thiosemicarbazone (**4**). Specifically, compounds (**18–20**), which carry a phenyl at position N3 of heterocyclic ring, were the most active ones, suggesting that this is a structural determinant for activity. In infected macrophages, compounds (**18–20**) reduced intracellular amastigotes, whereas Benznidazole did not. In *T. cruzi*-infected mice treated orally with 100 mg/kg of compound (**20**), a decreased of parasitemia was observed. In conclusion, we demonstrated that the conversation of thiosemicarbazones into 4-thiazolidinones retains pharmacological property while enhances selectivity.

© 2015 Elsevier Ltd. All rights reserved.

1. Introduction

It is estimated that 5–10% of the Latin American population has Chagas disease, which is caused by the protozoan *Trypanosoma cruzi*.¹ This situation is alarming, because there are no vaccines available and the current treatment using Benznidazole is of low efficacy and followed by several side effects.^{2,3} Benznidazole has antiparasitic effects against bloodstream parasites, but its activity is limited against parasites in tissues.^{4,5} Additionally, many

patients experience drug intolerance and adverse effects.⁶ Thus, new drugs to treat Chagas disease are necessary.

To address this need, a number of molecular targets for anti-*T. cruzi* drugs have been investigated, increasing the quality of drug identification for Chagas disease treatment. Examples of such targets are the lanosterol 14 α -demethylase,⁷ trypanothione reductase,⁸ cruzain,⁹ *trans*-sialidase,¹⁰ phosphatidylinositol 3-kinase¹¹ and cytochrome *b*.¹² By using structure-based drug design, two small-molecules were developed and are considered strong drug candidates: **K11777**, a vinyl sulfone peptide that inhibits cruzain,¹³ and **VNI**, an oxadiazole derivative inhibitor of 14- α -demethylase activity.^{14,15}

More recently, compound **VFV** reveals a broader antiprotozoal spectrum of action. It has stronger antiparasitic activity in cellular

* Corresponding author. Tel.: +55 81 21268511; fax: +55 81 21268510.

E-mail addresses: gev_filho@hotmail.com, acilb2003@yahoo.com.br (G.B. de Oliveira Filho).

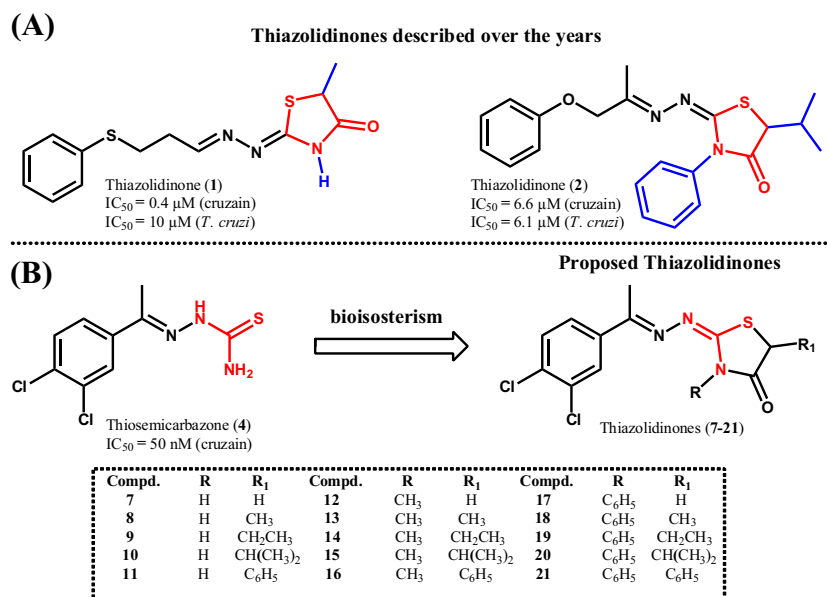


Figure 1. Bioisosterism-based design of novel thiazolidinones as potential anti-parasitic compounds. (A) Thiazolidinones described over the years (compounds **1**³⁵ and **2**³⁸ were previously investigated), (B) thiazolidinones proposed here.

experiments, and cures the experimental Chagas disease with 100% of efficacy, and suppresses visceral leishmaniasis by 89% (vs 60% for **VNI**).¹⁶ These compounds are likely to enter into clinical trials; however, the chances of any drug being approved in the clinical stage are very low. Given the outcomes observed for **K11777**, **VNI** and **VFV** as anti-*T. cruzi* agents, the design of compounds to inhibit cruzain and the 14- α -demethylase activity have received special attention.^{17,18}

Additionally, with the goal of avoiding the development of resistant *T. cruzi* strains, an enhanced of the number of potential drug candidates by combined drug therapy is necessary.^{19,20}

Thiosemicarbazones have been largely investigated as anti-*T. cruzi* agents.^{21–27} Among this class, the 3,4-dichlorophenyl thiosemicarbazone (**4**) was identified as one of the most potent cruzain inhibitor. The structure–activity relationships studies identified that the 3,4-dichlorophenyl is an important structural determinant for trypanocidal activity.²⁸

Due to the poor drugability of thiosemicarbazones, many attempts have been made to identify thiosemicarbazone-like compounds with improved antiparasitic effects.^{29–34} Following this line of research, our research group demonstrated an existing bioisosteric relationship between thiosemicarbazones and thiazolidinones, which led to the identification of strong antiparasitic thiazolidinones.^{35–38}

Based on these findings, here new thiazolidinones (**7–21**) were planned by employing the thiosemicarbazone (**4**) as a structural prototype (Fig. 1). We synthesized compounds (**7–21**) and evaluated their activity against cruzain and *T. cruzi*. The choice of substituents attached in compounds (**7–21**) was oriented by observing previously described structure–activity relationships.³⁸

2. Results

2.1. Synthesis and chemical characterization

The general route to preparing thiazolidinones is shown in Scheme 1. Firstly, thiosemicarbazones (**4–6**) were prepared by reacting commercially available 3',4'-dichloroacetophenone (**3**) with the appropriate thiosemicarbazide in an ultrasound bath in

the presence of catalytic H₂SO₄ or HCl (thiosemicarbazone **6**). Thiazolidinones (**7–21**) were prepared by reacting the respective aryl thiosemicarbazone with commercially available ethyl 2-bromoacetate or by preparing the desired 2-substituted-2-bromoacetates. These reactions were carried out in the presence of an excess of anhydrous NaOAc under reflux. This afforded compounds (**7–21**) in variable yields (38–84%) and acceptable purity (>95%).

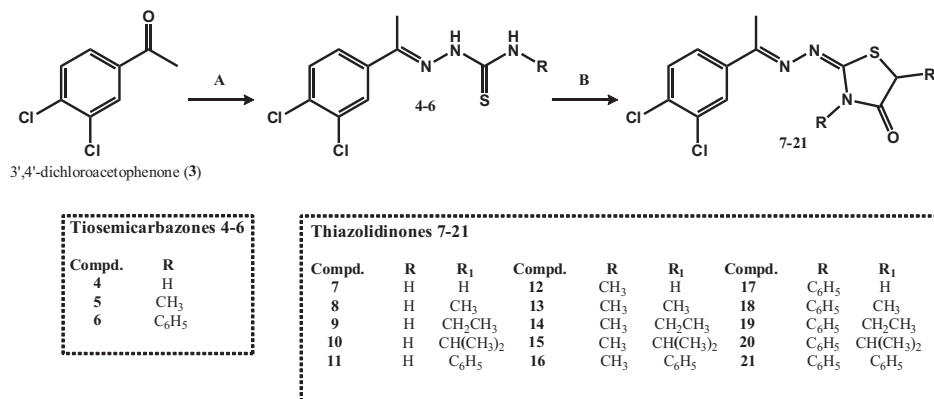
Structures of compounds were determined by nuclear magnetic resonance (NMR, ¹H and ¹³C), infrared (IR) and mass (HR-MS) spectral, while purity was determined by elemental analysis (E.A.). To define the relative configuration of the iminic bond, we executed X-ray diffraction of single crystals of compound (**10**). As observed in Figure 2, this compound adopts an *E*-geometry. In addition, it was observed that iminic bond in C1 is located in an exocyclic position in regard to the heterocyclic ring.

2.2. Pharmacological evaluation

We assessed the host cell cytotoxicity in J774 macrophages, while the in vitro anti-*T. cruzi* activity was determined against bloodstream trypomastigotes of Y strain (Table 1). Compounds that showed IC₅₀ values comparable to Benznidazole were considered active.

The inhibitory activity for thiazolidinones (**5–19**) against cruzain was also investigated. We measured cruzain mediated enzymatic activity inhibition by using an assay based on competition with the substrate Z-Phe-Arg-aminomethylcoumarin (Z-FR-AMC). Compounds were screened at 100 μM, the maximum concentration at which they were soluble in the assay buffer. However, cruzain inhibition by these compounds was not observed (Table S1).³⁹

The structure–activity relationship study began with two modifications on 4-thiazolidinone ring: (a) substituents at C5 position and (b) attachment of a methyl or phenyl group at nitrogen N3. These modifications yielded compounds (**7–21**). Among the tested compounds, compound (**20**) was the most potent antiparasitic, with an IC₅₀ value of 1.7 ± 0.17 μM for bloodstream trypomastigotes. This compound presented better antiparasitic properties than Benznidazole. Importantly, this did not affect host cells viability in concentrations up to 100 μM.



Scheme 1. Synthetic procedures for thiazolidinones (7–21). Reagents and conditions: (A) thiosemicarbazides, EtOH, H₂SO₄, or HCl, ultrasound bath, rt, 1–2 h, yields of 80–89%; (B) ethyl 2-bromoacetate or ethyl 2-substituted-2-bromoacetates; NaOAc, EtOH, reflux, overnight, yields of 38–84%.

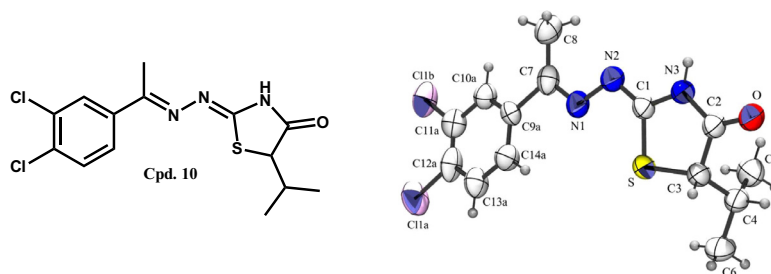


Figure 2. (Left) chemical structure of compound (10). (Right) ORTEP-3 projection of compound (10) showing atom-numbering and displacement ellipsoids at the 50% probability level.

Comparing thiosemicarbazones (4–6), it is observed that with the increase of lipophilicity in substituents at N3, with methyl (5) or phenyl (6), the trypanocidal activity decrease with an improvement in toxicity for macrophages. This trend is not observed for cyclic derivatives (7–21), otherwise an improvement in toxicity profile is observed with the cyclization of the thioamide into thiazolidinone moiety.

The good trypanocidal activity observed in unsubstituted thiosemicarbazone (4) was not kept in their cyclic derivatives (7, 12 and 17), however, their present lower cytotoxicity for macrophages, in opposition to (4). Among cyclic derivatives, only compounds (18), (19) and (20) present better trypanocidal activity than thiosemicarbazone (4).

In general, substitutions at N3 improved the antiparasitic activity, with *N*-phenyl compounds (17–21) exhibiting the strongest activity among all tested compounds. For instance, the methyl (18), ethyl (19), and isopropyl (20) compounds were, respectively, 12-, 16- and 25-times more potent antiparasitic agents than unsubstituted compound (17).

Given the selectivity of these compounds against bloodstream trypomastigotes of *T. cruzi*, we next examined their activity against intracellular parasites. To this end, we assessed an *in vitro* model of parasite infection using mouse macrophages infected with Y strain trypomastigotes. Three days after infection, 35–40% of the untreated macrophages were infected, and a high number of amastigotes per 100 macrophages were observed. Treatment with 50 μ M Benznidazole reduced the number of infected cells and the number of intracellular amastigotes ($P < 0.001$). We then tested the three most potent compounds, thiazolidinones (18), (19), and (20) at concentration of 50 μ M. As shown in Figure 3, these compounds inhibited *T. cruzi* infection with potency higher than Benznidazole ($P < 0.001$). When tested at different concentrations, it was possible to calculate the IC₅₀ values for compounds (18), (19) and (20)

against intracellular amastigotes. IC₅₀ values of 5.9 ± 0.52 , 3.2 ± 0.3 , and 3.1 ± 0.64 μ M for compounds (18), (19) and (20) were found, respectively. These values were lower than Benznidazole (IC₅₀ = 13.9 ± 0.39 μ M).

Finally, we evaluated the *in vivo* efficacy of compound (20). Starting on day 5 post-infection (dpi), compound (20) was administered at 100 mg/kg orally once per day for five consecutive days in BALB/c mice infected with 10⁴ Y strain trypomastigotes. Controls included untreated and Benznidazole-treated mice. The course of infection was monitored by counting blood parasites and animal survival was followed for 1 month. As seen in Figure 4, compound (20) reduced blood parasitemia ($P < 0.001$) compared to untreated control. At dose of 100 mg/kg, administration of (20) caused a reduction in blood parasitaemia of 86.7 (10 days post-infection (dpi)) and 97.1% (12 dpi) (Table 2). In the group treated with Benznidazole, it was observed >99% of inhibition of blood parasitaemia, indicating that eradication of infection was achieved. Treatment with (20), similar to the treatment with Benznidazole, had a protective effect on mortality. No signs of toxicity or body weight loss were observed in animals in the treatment group (data not shown).

3. Discussion

Here, we examined the chemistry and pharmacology of thiazolidinones derived from a thiosemicarbazone which is a highly potent cruzain inhibitor but a poor selective antiparasitic agent. The employed route to preparing thiazolidinones was efficient to produce compounds in acceptable yield and purity. X-ray diffraction revealed the conformation and geometry of iminic bound as well as the tautomerism of heterocyclic ring. By varying substituents attached at heterocyclic ring, it was possible to screen active compounds and to identify the main structural determi-

Table 1
Anti-*T. cruzi* activity of thiazolidinones (7–21)

Compd	R ₁	Trypomastigotes, Y strain <i>T. cruzi</i> IC ₅₀ ± SD ^a (μM)	Macrophages CC ₅₀ ± SD ^b (μM)	Selectivity index ^c
4	H	7.1 ± 0.76	13.4 ± 0.82	1.7
5	Methyl	11.2 ± 1.62	>100	8.8
6	Phenyl	>50	>100	–
7	H	>50	76.5 ± 3.18	–
8	Methyl	49.5 ± 0.51	>100	2.0
9	Ethyl	>50	76.7 ± 0.46	–
10	Isopropyl	16.9	>100	5.9
11	Phenyl	>50	96.9 ± 1.37	–
12	H	>50	>100	–
13	Methyl	>50	>100	–
14	Ethyl	48.5	>100	2.0
15	Isopropyl	>50	>100	–
16	Phenyl	41.5	97.6	–
17	H	>50	>100	–
18	Methyl	4.2 ± 0.28	26.1 ± 0.90	6
19	Ethyl	2.9 ± 0.91	23.3 ± 0.96	8
20	Isopropyl	1.7 ± 0.17	>100	>58
21	Phenyl	17.7 ± 0.09	27.1 ± 0.51	1.5
Bdz	–	10.6 ± 0.87	>100	>9.4
GV	–	–	0.45 ± 0.04	–

ND = not determined. Bdz = Benznidazole, GV = violet gentian. SD = standard deviation.

^a Determined after 24 h of incubation in the presence of compounds.

^b Determined in J774 cells for 72 h after incubation.

^c (CC₅₀ macrophages)/(IC₅₀ trypomastigotes).

nants of thiazolidinones for antiparasitic activity. We observed that the nonsubstituted or those containing a methyl at N3 presented poor antiparasitic activity. In contrast, thiazolidinones containing a phenyl group at N3 exhibited trypanocidal properties and were active against intracellular parasites, corroborating with a previously work of our group.³⁸ In addition, it is worth mentioning that these compounds presented low cytotoxicity in host cell viability, therefore showing good selectivity indexes.

Compounds (1) (Fig. 1) and (2) were previously synthesized by our group, with good trypanocidal activities (10 μM and 6.1 μM, respectively). The compounds with similar structure are compounds (8) and (20), with the same substituents at N3 and C5, respectively. The main structural difference between these

compounds (1–2 and 8, 20) are the substituents linked at N1 (phenylthiopropyl for (1), phenoxypropan-2-yl for (2) and 3,4-dichlorophenyl for (8) and (20). Comparing compound 1 with compound (8), it was not observed an improvement in trypanocidal activity. However, an improvement in trypanocidal activity was observed for compound (20), being 3-times more potent than compound (2), the lead compound identified by Moreira et al.³⁸ (6.1 μM vs 1.7 μM). This result highlight the importance of the 3,4-dichloro moiety for the trypanocidal activity (Fig. 5).

Regarding the mechanism of action, the thiazolidinones did not inhibit cruzain activity, while the thiosemicarbazone prototype did. These findings show that the mechanism of action of these antiparasitic thiazolidinones is different from thiosemicarbazones-inhibiting cruzain. In addition to displaying activity against axenic parasite, the thiazolidinones exhibited strong activity against intracellular amastigotes. In comparison to untreated infected macrophages, the compounds not only reduced the in vitro infection but also the parasite burden. Importantly, this activity was superior to Benznidazole-treated cells. Compound (20), the most potent in vitro thiazolidinone, was efficient in reducing the blood parasitemia in acutely-infected mice.

In overall, the substitution at N3 with phenyl and C5 with alkyl groups were benefic for the trypanocidal activity, generating compounds (18), (19) and (20), the most potent compounds presented in this study. It is worth to mention that compounds (18) (4.2 ± 0.28 μM), (19) (2.9 ± 0.91 μM) and (20) (1.7 ± 0.17 μM) were, respectively, 2-, 3- and 6-times more potent than the reference drug, Benznidazole (10.6 ± 0.87 μM) for trypomastigote form of the parasite. About intracellular amastigotes, compounds (18), (19) and (20) also present good trypanocidal activity, being 2-, 4- and 4-times more potent than Benznidazole, the unique drug available for treatment.

4. Conclusions

The search for antiparasitic compounds against *T. cruzi* based on heterocyclic chemistry led us to develop a new series of thiazolidinones. This study enabled molecular modifications at positions N3 and C5 on the thiazolidinic ring. The X-ray diffraction of compound (10) revealed that an *E*-geometry for iminic bond is observed. The in vitro screening showed that the presence of a phenyl group at position N3 improves the antiparasitic activity. This led to the identification of the potent *N*-phenyl substituted compounds (18–20), which were more potent trypanocidal agents than Benznidazole and previously described thiazolidinones (1–2). Compound (20) reduced parasitemia in both in vitro and in an acutely-infected mice model, thereby corroborating to the general notion that this class of heterocyclic compounds are strong antiparasitic agents.

5. Experimental section

5.1. Reagents and spectra analysis

All reagents were used as purchased from commercial sources (Sigma–Aldrich, Vetec, or Fluka). Progress of the reactions was followed by thin-layer chromatography (silica gel 60 F₂₅₄ in aluminum foil). Purity of the target compounds was confirmed by combustion analysis (for C, H, N and S) performed by a Carlo-Erba instrument (model EA 1110). IR was determined in KBr pellets. For NMR, we used a Varian UnityPlus 400 MHz (400 MHz for ¹H and 100 MHz for ¹³C) and Bruker AMX-300 MHz (300 MHz for ¹H and 75.5 MHz for ¹³C) instruments. DMSO-*d*₆, acetone-*d*₆, or D₂O were purchased from CIL. Chemical shifts are reported in ppm, and multiplicities are given as s (singlet),

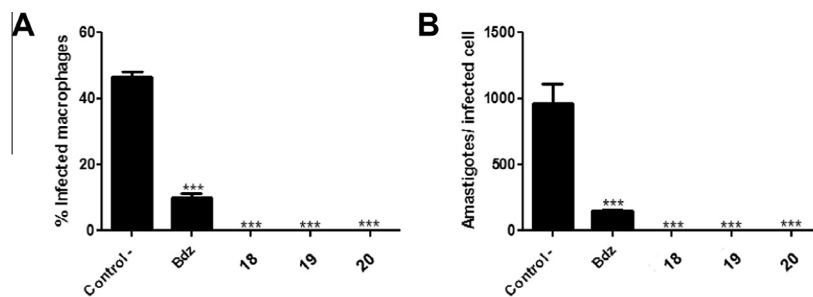


Figure 3. Thiazolidinones (**18**), (**19**), and (**20**) affect intracellular parasite development. The percentage of infected macrophages (A) and the relative number of amastigotes per 100 macrophages (B) are higher in untreated controls than in cultures treated with test compounds (**18**), (**19**), and (**20**), or Bdz. Macrophages were infected with Y strain trypomastigotes for 2 h, and test inhibitors were then added at 50 μ M. Cell cultures were incubated for 3 days. *** $P < 0.001$ compared to untreated controls. All compounds were tested in triplicate, and two independent experiments were performed. Bars indicate standard deviation. Bdz was used as a positive control.

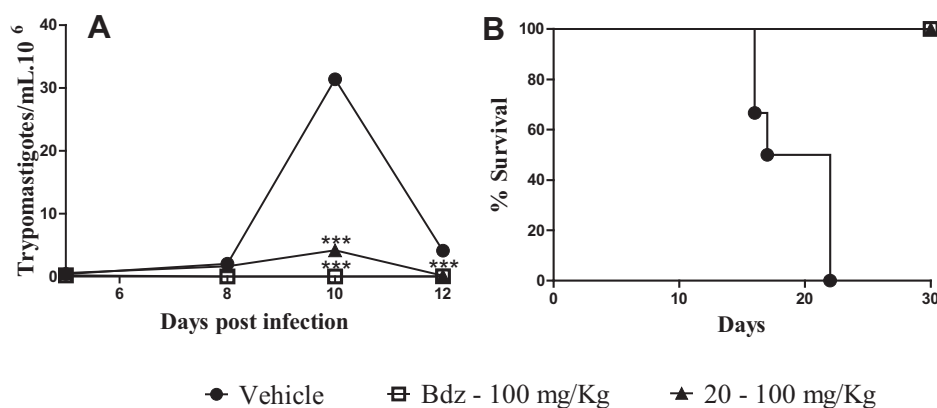


Figure 4. (A) Compound (**20**) substantially reduced parasitemia in mice. Female BALB/c mice were infected with 10^4 Y strain trypomastigotes. Five days after infection, mice were treated orally with compound (**20**) or Bdz with one daily dose (100 mg/kg) for five consecutive days. Parasitemia was monitored by counting the number of trypomastigotes in fresh blood samples. Values represent the mean \pm SEM of 6 mice per group. *** $P < 0.001$ compared to untreated-infected group (vehicle). (B) Treatment with compound (**20**) increases survival rates in infected mice. The animals were monitored for 30 days after infection. Results are from one experiment done with 6 mice per group.

Table 2

Parasitemia and mortality evaluation in mice infected with Y strain *T. cruzi* and treated daily with (**20**) or Benznidazole for 5 days

Compounds	Dose (mg/kg)	% Blood parasitemia reduction in mice ^a		Mortality ^b
		10 dpi	12 dpi	
20	100	86.7	97.1	0/6
Bdz	100	>99	>99	0/6
Vehicle	—	—	—	6/6

dpi = days post-infection. Bdz = Benznidazole. Vehicle = untreated and infected group.

^a Calculated as $([\text{average vehicle group} - \text{average treated group}]/\text{average vehicle group}) \times 100\%$.

^b Mortality was monitored until 30 days after treatment.

d (doublet), t (triplet), q (quartet), m (multiplet), and dd (double doublet), and coupling constants (J) in hertz. NH signals were localized in each spectrum after the addition of a few drops of D_2O . Structural assignments were corroborated by DEPT analysis. Mass spectrometry experiments were performed on a Q-TOF spectrometer LC-IT-TOF (Shimadzu). When otherwise specified, ESI was carried out in the positive ion mode. Reactions in an ultrasound bath were carried out under frequency of 40 kHz (180 W) and without external heating.

5.1.1. General procedure for the synthesis of thiosemicarbazones (4–6). Example for compound (4): Synthesis of 1-(3,4-dichlorophenyl)-ethylidene-thiosemicarbazone (4)

Under magnetic stirring: in a 100 mL round-bottom flask, 1.06 mmol (0.097 g) of thiosemicarbazide, 1.06 mmol (0.2 g) of 3',4'-dichloroacetophenone (**3**), 4 drops of H_2SO_4 and 20 mL of ethanol were added and maintained under magnetic stirring and reflux for 20 h. After cooling back to rt, the precipitate was filtered in a Büchner funnel with a sintered disc filter, washed with cold ethanol, and then dried over SiO_2 . Product was purified by recrystallization in hot toluol. Colorless crystals, mp: 187–189 °C; yield: 0.10 g (38%).

Under ultrasound irradiation: in a 10 mL round-bottom flask, 1.06 mmol (0.097 g) of thiosemicarbazide, 1.06 mmol (0.2 g) of 3',4'-dichloroacetophenone (**3**), 4 drops of H_2SO_4 and 20 mL of ethanol were added and maintained in a ultrasound bath for 30 min. After cooling back to rt, the precipitate was filtered in a Büchner funnel with a sintered disc filter, washed with cold ethanol, and then dried over SiO_2 . Product was purified by recrystallization in hot toluol. Colorless crystals, mp: 187–189 °C; yield: 0.22 g (80%); $R_f = 0.56$ (toluol/ethyl acetate 6:4). IR (KBr): 3427 (NH_2), 3399 (NH), 3138 (C–H), 1591 (C=N) cm^{-1} . 1H NMR (300 MHz, $DMSO-d_6$): δ 2.27 (s, 3H, CH_3), 7.58 (d, 1H, J 9.37 Hz, Ar), 7.86 (dd, 1H, J 9.37 and 3.75 Hz, Ar), 8.18 (s, 1H, NH_2), 8.26 (d, 1H, J 3.75 Hz, Ar), 8.36 (s, 1H, NH_2), 10.29 (s, 1H, NH). Signals at δ

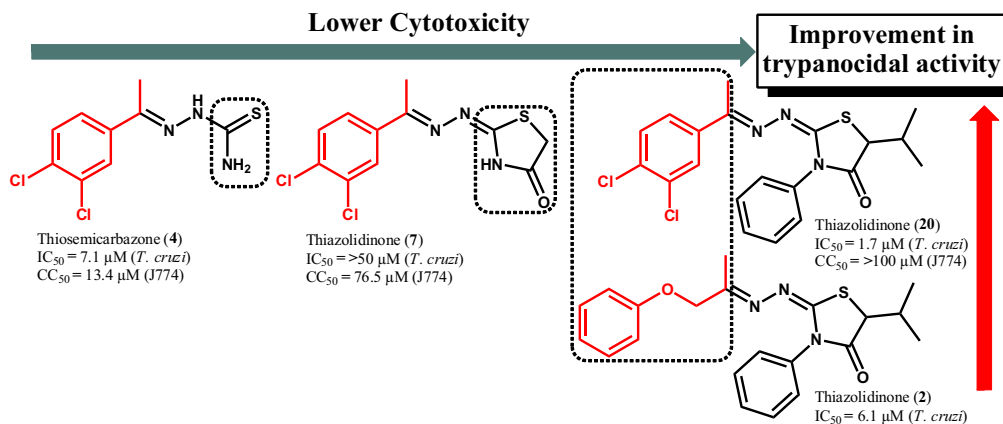


Figure 5. Structural improvements of proposed compounds.

8.18, 8.36 and 10.29 ppm disappear after adding D_2O . ^{13}C NMR (75.5 MHz, $DMSO-d_6$): δ 13.8 (CH_3), 126.7 (CH, Ar), 128.2 (CH, Ar), 130.2 (CH, Ar), 131.3 (C, Ar), 131.6 (3CIC, Ar), 138.2 (4CIC, Ar), 145.312 (C=N), 179.0 (C=S). HRMS (ESI): 259.9565 $[M-H]^+$. Anal. calcd for $C_9H_9Cl_2N_3S$: C, 41.23; H, 3.46; N, 16.03; S, 12.23. Found: C, 41.21; H, 3.61; N, 16.36; S, 12.78.

5.1.1.1. 1-(3,4-Dichlorophenyl)ethylideno-4-methylthiosemicarbazone (5).

Recrystallization in hot toluol afforded colorless crystal, mp: 195–197 °C; yield: 0.24 g (84%); $R_f = 0.7$ (toluol/ethyl acetate 6:4). IR (KBr): 3343 and 3219 (NH), 1547 (C=N) cm^{-1} . 1H NMR (300 MHz, $DMSO-d_6$): δ 2.28 (s, 3H, CH_3), 3.04 (d, 3H, J 6 Hz, N- CH_3 , coupling with N-H), 7.63 (d, 1H, J 8.57 Hz, Ar), 7.88 (dd, 1H, J 8.57 and 2.14 Hz, Ar), 8.23 (d, 1H, J 2.14 Hz, Ar), 8.61 (broad d, 1H, J 6 Hz, CH_3-NH), 10.33 (s, 1H, NH). ^{13}C NMR (75.5 MHz, $DMSO-d_6$): δ 13.8 (CH_3), 31.1 (N- CH_3), 126.7 (CH, Ar), 128.1 (CH, Ar), 130.2 (CH, Ar), 131.3 (C, Ar), 131.5 (3CIC, Ar), 138.3 (4CIC, Ar), 145.0 (C=N), 178.6 (C=S). HRMS (ESI): 275.9475 $[M+H]^+$. Anal. calcd for $C_{10}H_{11}Cl_2N_3S$: C, 43.49; H, 4.01; N, 15.21; S, 11.61. Found: C, 43.34; H, 3.98; N, 15.55; S, 11.74.

5.1.1.2. 1-(3,4-Dichlorophenyl)ethylidene-4-phenylthiosemicarbazone (6).

Recrystallization in hot toluol afforded colorless crystal, mp: 200–202 °C; yield: 0.32 g (89%); $R_f = 0.73$ (toluol/ethyl acetate 6:4). IR (KBr): 3309 and 3239 (NH), 3046 (C-H), 1523 (C=N) cm^{-1} . 1H NMR (300 MHz, $DMSO-d_6$): δ 2.36 (s, 3H, CH_3), 7.23 (t, 1H, J 7.21 Hz, Ar), 7.38 (t, 2H, J 7.21 Hz, Ar), 7.51 (d, 2H, J 7.21 Hz, Ar), 7.64 (d, 1H, J 9.09 Hz, Ar), 7.97 (dd, 1H, J 9.09 and 2.72 Hz, Ar), 8.34 (d, 1H, J 2.72 Hz, Ar), 10.18 (s, 1H, NH), 10.66 (s, 1H, ArNH). ^{13}C NMR (75.5 MHz, $DMSO-d_6$): δ 14.2 (CH_3), 125.6 (CH, Ar), 126.5 (CH, Ar), 127.0 (CH, Ar), 128.1 (CH, Ar), 128.4 (CH, Ar), 130.2 (CH, Ar), 131.3 (C, Ar), 131.8 (3CIC, Ar), 138.1 (4CIC, Ar), 139.2 (C-N, Ar), 146.3 (C=N), 177.3 (C=S). HRMS (ESI): 337.9678 $[M+H]^+$. Anal. calcd for $C_{15}H_{13}Cl_2N_3S$: C, 53.26; H, 3.87; N, 12.42; S, 9.48. Found: C, 53.23; H, 3.84; N, 12.31; S, 9.32.

5.1.2. General procedure for the synthesis of thiazolidinones 7–21. Example for compound (7)

Synthesis of 2-[1-(3,4-dichlorophenyl)ethylideno]thiazolidin-4-one (7). In a 100 mL round-bottom flask, 3.81 mmol (1.0 g) of thiosemicarbazone (4) was dissolved in 30 mL of ethanol, followed by adding 15.24 mmol (1.25 g) anhydrous sodium acetate under magnetic stirring and warming. After 15 min, 5.73 mmol (0.8 g) of ethyl 2-bromoacetate was added in portions and the mixture was maintained under reflux for 20 h. After cooling back to rt, the precipitate was filtered in a Büchner funnel with a sintered disc

filter, washed with cold ethanol, and then dried over SiO_2 . Product was purified by recrystallization in hot cyclohexane. Colorless crystals were obtained. Mp: 234–236 °C; yield: 0.75 g (65%); R_f : 0.53 (toluol/ethyl acetate 6:4). IR (KBr): 3143 (NH), 2985 (C-H), 1715 (C=O), 1628 (C=N) cm^{-1} . 1H NMR (300 MHz, $DMSO-d_6$): δ 2.36 (s, 3H, CH_3), 3.89 (s, 2H, S- CH_2), 7.69 (d, 1H, J 10 Hz, Ar), 7.80 (d, 1H, J 10 Hz, Ar), 8.00 (s, 1H, Ar), 12.06 (s, 1H, NH). ^{13}C NMR and DEPT (75.5 MHz, $DMSO-d_6$): δ 14.8 (CH_3), 33.3 (CH_2 , heterocycle), 126.8 (CH, Ar), 128.4 (CH, Ar), 131.0 (CH, Ar), 131.8 (C, Ar), 132.7 (3CIC, Ar), 138.7 (4CIC, Ar), 158.6 (C=N), 166.0 (S-C=N), 174.3 (C=O). HRMS (ESI): 301.9364 $[M+H]^+$. Anal. calcd for $C_{11}H_9Cl_2N_3OS$: C, 43.72; H, 3.00; N, 13.91; S, 10.61. Found: C, 44.00; H, 3.20; N, 13.47; S, 10.11.

5.1.2.1. 2-[1-(3,4-Dichlorophenyl)ethylideno]thiazolidin-4-one (8).

Recrystallization in toluol/cyclohexane 2:1 afforded colorless. Mp: 208–210 °C; yield: 0.68 g (56%); R_f : 0.52 (toluol/ethyl acetate 6:4). IR (KBr): 3422 (NH), 3139 (C-H), 1704 (C=O), 1627 (C=N) cm^{-1} . 1H NMR (300 MHz, $DMSO-d_6$): δ 1.48 (d, 3H, J 7.5 Hz, CH_3 heterocycle), 2.27 and 2.35 (s, 3H, CH_3), 4.15 (q, 1H, J 7.5 Hz, CH heterocycle), 7.60 and 7.68 (d, 1H, J 8.75 Hz, Ar), 7.78 and 7.87 (d, 1H, J 8.75 Hz, Ar), 7.99 and 8.26 (s, 1H, Ar), 8.36 and 10.30 (s, 1H, NH). ^{13}C NMR (75.5 MHz, $DMSO-d_6$): δ 13.8 and 14.3 (CH_3 heterocycle), 18.8 (CH_3), 41.0 (CH, heterocycle), 126.4 and 126.8 (CH, Ar), 127.8 and 128.2 (CH, Ar), 130.2 (CH, Ar), 131.3 and 131.6 (C, Ar), 132.2 (3CIC, Ar), 138.2 and 138.3 (4CIC, Ar), 145.3 (C=N), 157.9 (S-C=N), 177.3 (C=O). HRMS (ESI): 315.9491 $[M+H]^+$. Anal. calcd for $C_{12}H_{11}Cl_2N_3OS$: C, 45.58; H, 3.51; N, 13.29; S, 10.14. Found: C, 45.86; H, 3.68; N, 12.90; S, 10.00.

5.1.2.2. 2-[1-(3,4-Dichlorophenyl)ethylideno]thiazolidin-4-one (9).

Recrystallization in hot toluol afforded colorless. Mp: 175–177 °C; yield: 0.94 g (75%); R_f : 0.63 (toluol/ethyl acetate 6:4). IR (KBr): 2975 (C-H), 1704 (C=O), 1623 (C=N) cm^{-1} . 1H NMR (300 MHz, $DMSO-d_6$): δ 0.95 (broad s, 3H, CH_3), 1.88 (m, 2H, CH_2), 2.36 (s, 3H, CH_3), 4.20 (broad s, 1H, CH heterocycle), 7.69 (d, 1H, J 8 Hz, Ar), 7.80 (d, 1H, J 8 Hz, Ar), 7.99 (s, 1H, Ar), 12.05 (s, 1H, NH). ^{13}C NMR (75.5 MHz, $DMSO-d_6$): δ 10.3 (CH_3), 14.3 (CH_3), 25.4 (CH_2), 49.0 (CH, heterocycle), 126.4 (CH, Ar), 127.9 (CH, Ar), 130.6 (CH, Ar), 131.3 (C, Ar), 132.2 (3CIC, Ar), 138.3 (4CIC, Ar), 158.2 (C=N), 164.1 (S-C=N), 176.0 (C=O). HRMS (ESI): 329.9624 $[M+H]^+$. Anal. calcd for $C_{13}H_{13}Cl_2N_3OS$: C, 47.28; H, 3.97; N, 12.72; S, 9.71. Found: C, 47.20; H, 3.60; N, 12.34; S, 9.55.

5.1.2.3. 2-[1-(3,4-Dichlorophenyl)ethylidenehydrazono]-5-isopropylthiazolidin-4-one (10). Recrystallization in toluol/cyclohexane 2:1 afforded colorless. Mp: 193–195 °C; yield: 0.73 g (56%); R_f : 0.6 (toluol/ethyl acetate 6:4). IR (KBr): 2953 (C—H), 1707 (C=O), 1616 (C=N) cm^{-1} . ^1H NMR (300 MHz, DMSO- d_6): δ 0.87 (d, 3H, J 6 Hz, CH₃), 0.98 (d, 3H, J 6 Hz, CH₃), 2.36 (s, 3H, CH₃), 2.50 (m, 1H, CH), 4.30 (d, 1H, J 3 Hz, CH heterocycle), 7.69 (d, 1H, J 10 Hz, Ar), 7.81 (d, 1H, J 10 Hz, Ar), 7.99 (s, 1H, Ar), 12.06 (s, 1H, NH). ^{13}C NMR (75.5 MHz, DMSO- d_6): δ 14.4 (CH₃), 16.4 (CH₃), 20.3 (CH₃), 29.9 (CH), 54.7 (CH, heterocycle), 126.4 (CH, Ar), 128.0 (CH, Ar), 130.6 (CH, Ar), 131.3 (C, Ar), 132.3 (3CIC, Ar), 138.3 (4CIC, Ar), 158.6 (C=N), 163.7 (S—C=N), 175.4 (C=O). HRMS (ESI): 343.9749 [M—H]⁺. Anal. calcd for C₁₄H₁₅Cl₂N₃OS: C, 48.84; H, 4.39; N, 12.21; S, 9.31. Found: C, 49.19; H, 4.56; N, 12.16; S, 9.49.

5.1.2.4. 2-[1-(3,4-Dichlorophenyl)ethylidenehydrazono]-5-phenylthiazolidin-4-one (11). Recrystallization in hot toluol afforded colorless. Mp: 245–247 °C; yield: 0.95 g (65%); R_f : 0.57 (toluol/ethyl acetate 6:4). IR (KBr): 1711 (C=O), 1618 (C=N) cm^{-1} . ^1H NMR (300 MHz, DMSO- d_6): δ 2.41 (s, 3H, CH₃), 5.49 (s, 1H, CH heterocycle), 7.39 (m, 5H, Ar), 7.68 (d, 1H, J 9 Hz, Ar), 7.81 (dd, 1H, J 9 and 2.25 Hz, Ar), 8.01 (d, 1H, J 2.25 Hz, Ar), 12.35 (s, 1H, NH). ^{13}C NMR (75.5 MHz, DMSO- d_6): δ 14.9 (CH₃), 51.4 (CH, heterocycle), 126.9 (CH, Ar), 128.4 (CH, Ar), 128.7 (CH, Ar), 128.9 (CH, Ar), 129.3 (CH, Ar), 131.1 (CH, Ar), 131.8 (C, Ar), 132.8 (C, Ar), 137.2 (3CIC, Ar), 138.6 (4CIC, Ar), 159.2 (C=N), 162.0 (S—C=N), 175.0 (C=O). HRMS (ESI): 378.0310 [M+H]⁺. Anal. calcd for C₁₇H₁₃Cl₂N₃OS: C, 53.98; H, 3.46; N, 11.11; S, 8.48. Found: C, 53.75; H, 3.53; N, 11.12; S, 8.78.

5.1.2.5. 2-[1-(3,4-Dichlorophenyl)ethylidenehydrazono]-3-methylthiazolidin-4-one (12). Recrystallization in hot toluol afforded colorless. Mp: 195–197 °C; yield: 0.70 g (61%); R_f : 0.73 (toluol/ethyl acetate 6:4). IR (KBr): 2942 (C—H), 1717 (C=O), 1613 and 1570 (C=N) cm^{-1} . ^1H NMR (400 MHz, DMSO- d_6): δ 2.43 (s, 3H, CH₃), 3.20 (s, 3H, N—CH₃), 3.95 (s, CH₂ heterocycle), 7.72 (d, 1H, J 11.42 Hz, Ar), 7.83 (dd, 1H, J 11.42 and 1.43 Hz, Ar), 8.03 (d, 1H, J 1.43 Hz, Ar). ^{13}C NMR (100 MHz, DMSO- d_6): δ 14.2 (CH₃), 29.2 (N—CH₃), 32.0 (CH₂ heterocycle), 126.3 (CH, Ar), 127.9 (CH, Ar), 130.5 (CH, Ar), 131.2 (C, Ar), 132.3 (3CIC, Ar), 138.1 (4CIC, Ar), 159.4 (C=N), 164.5 (S—C=N), 172.0 (C=O). HRMS (ESI): 315.9498 [M+H]⁺. Anal. calcd for C₁₂H₁₁Cl₂N₃OS: C, 45.58; H, 3.51; N, 13.29; S, 10.14. Found: C, 45.48; H, 3.33; N, 13.18; S, 9.90.

5.1.2.6. 2-[1-(3,4-Dichlorophenyl)ethylidenehydrazono]-3,5-dimethylthiazolidin-4-one (13). Recrystallization in cyclohexane/toluol 3:1 afforded colorless. Mp: 178–180 °C; yield: 0.90 g (75%); R_f : 0.8 (toluol/ethyl acetate 6:4). IR (KBr): 1704 (C=O), 1606 and 1570 (C=N) cm^{-1} . ^1H NMR (400 MHz, DMSO- d_6): δ 1.53 (d, 3H, J 7.14 Hz, CH₃), 2.42 (s, 3H, CH₃), 3.22 (s, 3H, N—CH₃), 4.24 (q, J 7.14 Hz, CH heterocycle), 7.70 (d, 1H, J 8.51 Hz, Ar), 7.82 (dd, 1H, J 8.51 and 2.12 Hz, Ar), 8.02 (d, 1H, J 2.12 Hz, Ar). ^{13}C NMR (100 MHz, DMSO- d_6): δ 14.1 (CH₃, position 5 of the heterocycle), 18.5 (CH₃), 29.3 (N—CH₃), 41.1 (CH heterocycle), 126.3 (CH, Ar), 127.8 (CH, Ar), 130.4 (CH, Ar), 131.2 (C, Ar), 132.2 (3CIC, Ar), 138.1 (4CIC, Ar), 159.3 (C=N), 163.0 (S—C=N), 175.0 (C=O). HRMS (ESI): 329.9630 [M+H]⁺. Anal. calcd for C₁₃H₁₃Cl₂N₃OS: C, 47.28; H, 3.97; N, 12.72; S, 9.71. Found: C, 47.33; H, 3.81; N, 12.63; S, 9.69.

5.1.2.7. 2-[1-(3,4-Dichlorophenyl)ethylidenehydrazono]-5-ethyl-3-methylthiazolidin-4-one (14). Recrystallization in hot cyclohexane afforded colorless. Mp: 167–168 °C; yield: 0.80 g (64%); R_f : 0.81 (toluol/ethyl acetate 6:4). IR (KBr): 2970 (C—H), 1716 (C=O), 1610 and 1567 (C=N) cm^{-1} . ^1H NMR (400 MHz,

DMSO- d_6): δ 0.95 (t, 3H, CH₃), 1.83 (m, 1H, CH₂), 2.02 (m, 1H, CH₂), 2.42 (s, 3H, CH₃), 3.19 (s, 3H, N—CH₃), 4.27 (m, 1H, CH heterocycle), 7.70 (d, 1H, J 8 Hz, Ar), 7.83 (dd, 1H, J 8 and 2 Hz, Ar), 8.02 (d, 1H, J 2 Hz, Ar). ^{13}C NMR (100 MHz, DMSO- d_6): δ 10.1 (CH₃), 14.2 (CH₃), 25.3 (CH₂), 29.2 (N—CH₃), 48.1 (CH heterocycle), 126.3 (CH, Ar), 127.9 (CH, Ar), 130.4 (CH, Ar), 131.2 (C, Ar), 132.3 (3CIC, Ar), 138.1 (4CIC, Ar), 159.5 (C=N), 162.9 (S—C=N), 174.0 (C=O). Anal. calcd for C₁₄H₁₅Cl₂N₃OS: C, 48.84; H, 4.39; N, 12.21; S, 9.31. Found: C, 48.83; H, 4.09; N, 12.15; S, 9.58.

5.1.2.8. 2-[1-(3,4-Dichlorophenyl)ethylidenehydrazono]-5-isopropyl-3-methylthiazolidin-4-one (15). Recrystallization in cyclohexane/toluol 3:1 afforded colorless. Mp: 137–140 °C; yield: 0.70 g (53%); R_f : 0.84 (toluol/ethyl acetate 6:4). IR (KBr): 2947 (C—H), 1713 (C=O), 1610 and 1563 (C=N) cm^{-1} . ^1H NMR (300 MHz, DMSO- d_6): δ 0.84 (d, 3H, J 6.42 Hz, CH₃), 1.00 (d, 3H, J 6.42 Hz, CH₃), 2.43 (s, 3H, CH₃), 2.45 (m, 1H, CH), 3.21 (s, 3H, N—CH₃), 4.38 (d, 1H, J 2.5 Hz, CH heterocycle), 7.72 (d, 1H, J 7.5 Hz, Ar), 7.85 (dd, 1H, J 7.5 and 1.25 Hz, Ar), 8.03 (d, 1H, J 1.25 Hz, Ar). ^{13}C NMR (75.5 MHz, DMSO- d_6): δ 14.4 (CH₃), 16.4 (CH₃), 20.2 (CH₃), 29.3 (CH), 30.1 (N—CH₃), 53.9 (CH heterocycle), 126.5 (CH, Ar), 128.1 (CH, Ar), 130.7 (CH, Ar), 131.3 (C, Ar), 132.4 (3CIC, Ar), 138.1 (4CIC, Ar), 159.9 (C=N), 163.2 (S—C=N), 173.8 (C=O). HRMS (ESI): 357.9853 [M+H]⁺. Anal. calcd for C₁₅H₁₇Cl₂N₃OS: C, 50.28; H, 4.78; N, 11.73; S, 8.95. Found: C, 50.29; H, 4.64; N, 11.71; S, 9.19.

5.1.2.9. 2-[1-(3,4-Dichlorophenyl)ethylidenehydrazono]-3-methyl-5-phenylthiazolidin-4-one (16). Recrystallization in hot toluol afforded colorless. Mp: 194–196 °C; yield: 0.91 g (87%); R_f : 0.82 (toluol/ethyl acetate 6:4). IR (KBr): 1709 (C=O), 1603 and 1565 (C=N) cm^{-1} . ^1H NMR (300 MHz, DMSO- d_6): δ 2.47 (s, 3H, CH₃), 2.50 (s, 3H, N—CH₃), 5.55 (s, 1H, CH heterocycle), 7.39 (m, 5H, Ar), 7.71 (d, 1H, J 8.57 Hz, Ar), 7.84 (dd, 1H, J 8.57 and 2.14 Hz, Ar), 8.03 (d, 1H, J 2.14 Hz, Ar). ^{13}C NMR (75.5 MHz, DMSO- d_6): δ 14.4 (CH₃), 29.9 (N—CH₃), 50.1 (CH heterocycle), 126.5 (CH, Ar), 128.0 (CH, Ar), 128.3 (CH, Ar), 128.5 (CH, Ar), 128.8 (CH, Ar), 130.6 (CH, Ar), 131.3 (C, Ar), 136.5 (3CIC, Ar), 138.0 (4CIC, Ar), 160.0 (C=N), 163.0 (S—C=N), 173.0 (C=O). HRMS (ESI): 392.0450 [M+H]⁺. Anal. calcd for C₁₈H₁₅Cl₂N₃OS: C, 55.11; H, 3.85; N, 10.71; S, 8.17. Found: C, 55.37; H, 3.92; N, 10.58; S, 8.44.

5.1.2.10. 2-[1-(3,4-Dichlorophenyl)ethylidenehydrazono]-3-phenylthiazolidin-4-one (17). Recrystallization in hot toluol afforded colorless. Mp: 232–233 °C; yield: 0.8 g (71%); R_f : 0.79 (toluol/ethyl acetate 6:4). IR (KBr): 2970 (C—H), 1728 (C=O), 1606 and 1562 (C=N) cm^{-1} . ^1H NMR (400 MHz, DMSO- d_6): δ 2.16 (s, 3H, CH₃), 4.10 (s, 2H, CH₂ heterocycle), 7.41 (d, 2H, J 7.54 Hz, Ar), 7.45 (t, 1H, J 7.54 Hz, Ar), 7.53 (t, 2H, J 7.54 Hz, Ar), 7.70 (d, 1H, J 9.05 Hz, Ar), 7.79 (d, 1H, J 9.05 Hz, Ar), 7.99 (s, 1H, Ar). ^{13}C NMR (100 MHz, DMSO- d_6): δ 14.3 (CH₃), 32.2 (CH₂), 126.3 (CH, Ar), 127.8 (CH, Ar), 128.4 (CH, Ar), 128.7 (CH, Ar), 130.5 (CH, Ar), 134.9 (C, Ar), 136.8 (C, Ar), 163.0 (C=N), 171.6 (S—C=N), 198.6 (C=O). HRMS (ESI): 377.9950 [M+H]⁺. Anal. calcd for C₁₇H₁₃Cl₂N₃OS: C, 53.98; H, 3.46; N, 11.11; S, 8.48. Found: C, 53.68; H, 3.42; N, 10.89; S, 7.94.

5.1.2.11. 2-[1-(3,4-Dichlorophenyl)ethylidenehydrazono]-3-phenyl-5-methylthiazolidin-4-one (18). Recrystallization in cyclohexane/toluol 3:1 afforded colorless. Mp: 208–209 °C; yield: 0.78 g (67%); R_f : 0.83 (toluol/ethyl acetate 6:4). IR (KBr): 1712 (C=O), 1609 and 1571 (C=N) cm^{-1} . ^1H NMR (300 MHz, DMSO- d_6): δ 1.63 (d, 3H, J 6.9 Hz, CH₃), 2.16 (s, 3H, CH₃), 4.41 (q, 1H, J 6.9 Hz, CH heterocycle), 7.41–7.55 (m, 5H, Ar), 7.70 (d, 1H, J 8.4 Hz, Ar), 7.79 (dd, 1H, J 8.4 and 1.8 Hz, Ar), 7.99 (d, 1H, J 1.8 Hz, Ar). ^{13}C NMR (75.5 MHz, DMSO- d_6): δ 14.3 (CH₃), 18.7

(CH₃), 41.0 (CH heterocycle), 126.4 (CH, Ar), 127.9 (CH, Ar), 128.5 (CH, Ar), 128.8 (CH, Ar), 130.6 (CH, Ar), 131.3 (C, Ar), 132.4 (3CIC, Ar), 135.0 (C, Ar), 138.0 (4CIC, Ar), 159.7 (C=N), 163.2 (S=C=N), 174.8 (C=O). Anal. calcd for C₁₈H₁₅Cl₂N₃O₅: C, 55.11; H, 3.85; N, 10.71; S, 8.17. Found: C, 55.36; H, 4.01; N, 10.44; S, 7.64.

5.1.2.12. 2-[1-(3,4-Dichlorophenyl)ethylideno]hydrazono]-3-phenyl-5-ethylthiazolidin-4-one (19). Recrystallization in hot cyclohexane afforded colorless. Mp: 154 °C; yield: 0.42 g (35%); R_f: 0.86 (toluol/ethyl acetate 6:4). IR (KBr): 1708 (C=O), 1607 and 1568 (C=N) cm⁻¹. ¹H NMR (300 MHz, DMSO-*d*₆): δ 1.03 (t, 3H, CH₃), 1.98 (m, 1H, CH₂), 2.08 (m, 1H, CH₂), 2.16 (s, 3H, CH₃), 4.45 (m, 1H, CH heterocycle), 7.39–7.55 (m, 5H, Ar), 7.71 (d, 1H, *J* 8.7 Hz, Ar), 7.80 (dd, 1H, *J* 8.7 and 1.8 Hz, Ar), 7.99 (d, 1H, *J* 1.8 Hz, Ar). ¹³C NMR (75.5 MHz, DMSO-*d*₆): δ 10.1 (CH₃), 14.4 (CH₃), 25.5 (CH₂), 48.2 (CH heterocycle), 126.4 (CH, Ar), 127.9 (CH, Ar), 128.5 (CH, Ar), 128.9 (CH, Ar), 130.6 (CH, Ar), 131.3 (C, Ar), 132.4 (3CIC, Ar), 134.9 (C, Ar), 138.0 (4CIC, Ar), 160.0 (C=N), 163.0 (S=C=N), 173.9 (C=O). HRMS (ESI): 405.9517 [M+H]⁺. Anal. calcd for C₁₉H₁₇Cl₂N₃O₅: C, 56.16; H, 4.22; N, 10.34; S, 7.89. Found: C, 55.80; H, 4.23; N, 9.96; S, 7.97.

5.1.2.13. 2-[1-(3,4-Dichlorophenyl)ethylideno]hydrazono]-3-phenyl-5-isopropylthiazolidin-4-one (20). Recrystallization in hot cyclohexane afforded colorless. Mp: 158–160 °C; yield: 0.76 g (61%); R_f: 0.9 (toluol/ethyl acetate 6:4). IR (KBr): 2964 (C—H), 1720 (C=O), 1603 and 1564 (C=N) cm⁻¹. ¹H NMR (300 MHz, DMSO-*d*₆): δ 0.98 (d, 3H, CH₃), 1.06 (d, 3H, CH₃), 2.16 (s, 3H, CH₃), 2.36 (m, 1H, CH), 4.53 (d, 1H, CH heterocycle), 7.36–7.56 (m, 5H, Ar), 7.71 (d, 1H, *J* 8.4 Hz, Ar), 7.81 (dd, 1H, *J* 8.4 and 1.8 Hz, Ar), 7.99 (d, 1H, *J* 1.8 Hz, Ar). ¹³C NMR (75.5 MHz, DMSO-*d*₆): δ 14.5 (CH₃), 16.5 (CH₃), 20.1 (CH₃), 30.5 (CH), 53.8 (CH heterocycle), 126.5 (CH, Ar), 127.9 (CH, Ar), 128.4 (CH, Ar), 128.7 (CH, Ar), 130.2 (CH, Ar), 131.3 (C, Ar), 132.5 (3CIC, Ar), 134.8 (C, Ar), 138.0 (4CIC, Ar), 160.3 (C=N), 163.1 (S=C=N), 173.5 (C=O). HRMS (ESI): 419.9888 [M+H]⁺. Anal. calcd for C₂₀H₁₉Cl₂N₃O₅: C, 57.15; H, 4.56; N, 10.00; S, 7.63. Found: C, 57.16; H, 4.49; N, 9.90; S, 7.68.

5.1.2.14. 2-[1-(3,4-Dichlorophenyl)ethylideno]hydrazono]-3,5-diphenylthiazolidin-4-one (21). Recrystallization in hot toluol afforded colorless. Mp: 210–212 °C; yield: 0.77 g (58%); R_f: 0.88 (toluol/ethyl acetate 6:4). IR (KBr): 3053 (C—H), 1715 (C=O), 1605 and 1566 (C=N) cm⁻¹. ¹H NMR (300 MHz, DMSO-*d*₆): δ 2.20 (s, 3H, CH₃), 5.70 (s, 1H, CH heterocycle), 7.36–7.58 (m, 10H, Ar), 7.69 (d, 1H, *J* 8.4 Hz, Ar), 7.80 (dd, 1H, *J* 8.4 and 2.1 Hz, Ar), 7.99 (d, 1H, *J* 2.1 Hz, Ar). ¹³C NMR (75.5 MHz, DMSO-*d*₆): δ 14.0 (CH₃), 50.1 (CH heterocycle), 126.3 (CH, Ar), 127.8 (CH, Ar), 128.0 (CH, Ar), 128.1 (CH, Ar), 128.4 (CH, Ar), 128.7 (CH, Ar), 129.2 (CH, Ar), 129.6 (CH, Ar), 130.5 (CH, Ar), 133.5 (C, Ar), 133.7 (C, Ar), 134.8 (C, Ar), 134.9 (C, Ar), 136.8 (C, Ar), 163.0 (C=N), 171.2 (S=C=N), 198.0 (C=O). HRMS (ESI): 452.0380 [M+H]⁺. Anal. calcd for C₂₃H₁₇Cl₂N₃O₅: C, 60.80; H, 3.77; N, 9.25; S, 7.06. Found: C, 60.68; H, 3.74; N, 9.26; S, 7.08.

5.3. Cruzain inhibition

Cruzain activity was measured by monitoring the cleavage of the fluorogenic substrate Z-FR-AMC. Assays were performed in 0.1 M sodium acetate buffer pH 5.5, in the presence of 1 mM beta-mercaptoethanol and 0.01% Triton X-100. The final concentrations of cruzain was 0.5 nM, and the Z-FR-AMC substrate concentration was 2.5 μM (*K*_m = 1 μM) to a final volume of 200 μL and at 25 °C. In all assays, the enzyme was pre-incubated with the compounds for 10 min. before adding a solution containing the Z-FR-AMC substrate. Enzyme kinetic was followed by continuous reading for 5 min at 12 s intervals and readings were deter-

mined in a Synergy 2 (Biotek), from the Center of Flow Cytometry and Fluorimetry at the Biochemistry and Immunology Department (UFMG). The filters employed were 340 nM for excitation and 440 nM for emission. Activity was calculated based on initial velocity rates, compared to a DMSO control, since all compound stocks were prepared in DMSO. All compounds were evaluated at 10 μM and inhibition was measured in at least two independent experiments, each case in triplicate.

4.3. Animals

Female BALB/c mice (6–8 weeks old) were supplied by the animal breeding facility at Centro de Pesquisas Gonçalo Moniz (Fundação Oswaldo Cruz, Bahia, Brazil) and maintained in sterilized cages under a controlled environment, receiving a balanced diet for rodents and water ad libitum. All experiments were carried out in accordance with the recommendations of Ethical Issues Guidelines, and were approved by the local Animal Ethics Committee.

4.4. Parasites

Bloodstream trypomastigotes forms of *T. cruzi* were obtained from supernatants of LLC-MK2 cells previously infected and maintained in RPMI-1640 medium (Sigma-Aldrich, St. Louis, MO) supplemented with 10% fetal bovine serum (FBS; Cultilab, Campinas, Brazil), and 50 μg/mL gentamycin (Novafarma, Anápolis, Brazil) at 37 °C and 5% CO₂.

4.5. Host cell toxicity

J774 macrophages were dispensed on 96-well plates at a cell number of 5 × 10⁴ cells/mL in 200 μL of RPMI medium supplemented with 10% of FBS and 50 μg/mL of gentamycin and incubated for 24 h at 37 °C and 5% CO₂. After that time each compound, dissolved in DMSO was added at six concentrations (0.41–100 μM) in triplicate and incubated for 72 h. Cell viability was determined by AlamarBlue assay (Invitrogen, Carlsbad, CA, USA) according to the manufacturer instructions. Colorimetric readings were performed after 6 h at 570 and 600 nm. Cytotoxic concentration to 50% (CC₅₀) was calculated using data-points gathered from three independent experiments. Gentian violet (Synth, São Paulo, Brazil) was used as positive control. The final concentration of DMSO was less than 1% in all in vitro experiments.

4.6. Toxicity for Y strain trypomastigotes

Trypomastigotes collected from the supernatant of LLC-MK2 cells were dispensed into 96-well plates at a cell density of 4 × 10⁵ cells/well. Test inhibitors, were diluted into five different concentrations and added into their respective wells, and the plate was incubated for 24 h at 37 °C and 5% of CO₂. Aliquots of each well were collected and the number of viable parasites, based on parasite motility, was assessed in a Neubauer chamber. The percentage of inhibition was calculated in relation to untreated cultures. IC₅₀ calculation was also carried out using non-linear regression with Prism 4.0 GraphPad software. Benznidazole was used as the reference drug.

4.7. Intracellular parasite development

Peritoneal exudate macrophages were obtained by washing, with cold RPMI medium, the peritoneal cavity of BALB/c mice 4–5 days after injection of 3% thioglycolate (Sigma) in saline (1.5 mL per mice). Then, cells were seeded at a cell density of 2 × 10⁵ cells/well in a 24 well-plate with rounded coverslips on

the bottom in RPMI supplemented with 10% FBS and incubated for 24 h. Cells were then infected with Y strain trypomastigotes at a ratio of 10 parasites per macrophage for 2 h. Free trypomastigotes were removed by successive washes using saline solution. Next, cultures were incubated in complete medium alone or with the test inhibitors at 50 μ M for 6 h. The medium was replaced by a fresh medium and the plate was incubated for 3 days. Cells were fixed in methanol and the percentage of infected macrophages and the relative number of amastigotes per 100 macrophages were determined by manual counting after Giemsa staining in an optical microscope (Olympus, Tokyo, Japan). The percentage of infected macrophages and the number of amastigotes per 100 macrophages was determined by counting 100 cells per slide. To estimate IC₅₀ values, compounds were tested at five concentrations (1–50 μ M).

4.8. Infection in mice

Female BALB/c mice (6–8 weeks old) were infected with bloodstream trypomastigotes by intraperitoneal injection of 10⁴ parasites in 100 μ L of saline solution. Mice were then randomly divided in groups (six mice per group). After five days post-infection, treatment with 100 mg/kg weight of compound (**20**) was given orally once a day for five consecutive days. For the control group, Benznidazole was also given orally at dose of 100 mg/kg weight. Infection was monitored by counting the number of motile parasites in 5 μ L of fresh blood sample drawn from the lateral tail veins as recommended by standard protocols.⁴⁰ Survival was monitored for 30 days after treatment. The one-way ANOVA and Bonferroni for multiple comparisons were used to determine the statistical significance of the group comparisons.

Acknowledgements

This work received support from CNPq (grant reference 471461/2011–3 to A.C.L.L.) and FAPESP (PRONEX program, grant reference 6596 to M.B.P.S.). G.B.O.F. received a FACEPE Masters scholarship. A.C.L.L., C.A.S. and M.B.P.S. hold a CNPq senior fellowship. C.A.S. also thanks the Instituto de Física de São Carlos (University of São Paulo, Brazil) for the use of KappaCCD diffractometer.

Supplementary data

Supplementary data associated with this article can be found, in the online version, at <http://dx.doi.org/10.1016/j.bmc.2015.10.048>. These data include MOL files and InChIKeys of the most important compounds described in this article.

References and notes

1. WHO Chagas Disease (American trypanosomiasis), 2015.
2. Urbina, J. A. *Acta Trop.* **2010**, *115*, 55.
3. Olivieri, B. P.; Molina, J. T.; de Castro, S. L.; Pereira, M. C.; Calvet, C. M.; Urbina, J. A.; Araújo-Jorge, T. C. *Int. J. Antimicrob. Agents* **2010**, *36*, 79.
4. Rassi, A.; Marin-Neto, J. A. *Lancet* **2010**, *375*, 1388.
5. Barrett, M. P.; Burchmore, R. J. S.; Stich, A.; Lazzari, J. O.; Frasc, A. C.; Cazzulo, J. J.; Krishna, S. *Lancet* **2003**, *362*, 1469.
6. Pinazo, M.-J.; Muñoz, J.; Posada, E.; López-Chejade, P.; Gállego, M.; Ayala, E.; del Cacho, E.; Soy, D.; Gascon, J. *Antimicrob. Agents Chemother.* **2010**, *54*, 4896.
7. Buckner, F. S.; Urbina, J. A. *Int. J. Parasitol. Drugs Drug Resist.* **2012**, *2*, 236.
8. Lantwin, C. B.; Schlichting, I.; Kabsch, W.; Pai, E. F.; Krauth-Siegel, R. L. *Proteins Struct. Funct. Genet.* **1994**, *18*, 161.
9. Engel, J. C.; Doyle, P. S.; Hsieh, I.; McKerrow, J. H. *J. Exp. Med.* **1998**, *188*, 725.
10. dC-Rubin, S. S. C.; Schenkman, S. *Cell. Microbiol.* **2012**, *14*, 1522.
11. Wilkowsky, S.; Barbieri, M.; Stahl, P.; Isola, E. L. *Exp. Cell Res.* **2001**, *264*, 211.
12. Khare, S.; Roach, S. L.; Barnes, S. W.; Hoepfner, D.; Walker, J. R.; Chatterjee, A. K.; Neitz, R. J.; Arkin, M. R.; McNamara, C. W.; Ballard, J.; Lai, Y.; Fu, Y.; Molteni, V.; Yeh, V.; McKerrow, J. H.; Glynn, R. J.; Supek, F. *Plos Pathog.* **2015**, *11*, e1005058.
13. Doyle, P. S.; Zhou, Y. M.; Engel, J. C.; McKerrow, J. H. *Antimicrob. Agents Chemother.* **2007**, *51*, 3932.
14. Villalta, F.; Dobish, M. C.; Nde, P. N.; Kleshchenko, Y. Y.; Hargrove, T. Y.; Johnson, C. A.; Waterman, M. R.; Johnston, J. N.; Lepesheva, G. I. *J. Infect. Dis.* **2013**, *208*, 504.
15. Soeiro, M. d. N. C.; de Souza, E. M.; da Silva, C. F.; Batista, D. d. G. J.; Batista, M. M.; Pavao, B. P.; Araujo, J. S.; Aiub, C. A. F.; da Silva, P. B.; Lionel, J.; Britto, C.; Kim, K.; Sulikowski, G.; Hargrove, T. Y.; Waterman, M. R.; Lepesheva, G. I. *Antimicrob. Agents Chemother.* **2013**, *57*, 4151.
16. Lepesheva, G. I.; Hargrove, T. Y.; Rachakonda, G.; Wawrzak, Z.; Pomel, S.; Cojean, S.; Nde, P. N.; Nes, W. D.; Locuson, C. W.; Calcutt, M. W.; Waterman, M. R.; Daniels, J. S.; Loiseau, P. M.; Villalta, F. *J. Infect. Dis.* **2015**.
17. Rascon, A.; McKerrow, J. *Curr. Med. Chem.* **2013**, *20*, 3078.
18. Magalhaes Moreira, D. R.; Lima Leite, A.; Santos, R. R.; Soares, M. *Curr. Drug Targets* **2009**, *10*, 212.
19. Arantes, J. M.; Francisco, A. F.; de Abreu Vieira, P. M.; Silva, M.; Araújo, M. S. S.; de Carvalho, A. T.; Pedrosa, M. L.; Carneiro, C. M.; Tafuri, W. L.; Martins-Filho, O. A.; Elói-Santos, S. M. *Exp. Parasitol.* **2011**, *128*, 401.
20. Cencig, S.; Coltel, N.; Truyens, C.; Carlier, Y. *Int. J. Antimicrob. Agents* **2012**, *40*, 527.
21. Espindola, J. W. P.; de O. Cardoso, M. V.; de O. Filho, G. B.; Oliveira e Silva, D. A.; M. Moreira, D. R.; Bastos, T. M.; de Simone, C. A.; Soares, M. B. P.; Villela, F. S.; Ferreira, R. S.; de Castro, M. C. A. B.; Pereira, V. R. A.; Murta, S. M. F.; Sales, P. A., Junior; Romanha, A. J.; L. Leite, A. C. *Eur. J. Med. Chem.* **2015**, *101*, 818.
22. Du, X.; Guo, C.; Hansell, E.; Doyle, P. S.; Caffrey, C. R.; Holler, T. P.; McKerrow, J. H.; Cohen, F. E. *J. Med. Chem.* **2002**, *45*, 2695.
23. Greenbaum, D. C.; Mackey, Z.; Hansell, E.; Doyle, P.; Gut, J.; Caffrey, C. R.; Lehrman, J.; Rosenthal, P. J.; McKerrow, J. H.; Chibale, K. *J. Med. Chem.* **2004**, *47*, 3212.
24. Fujii, N.; Mallari, J. P.; Hansell, E. J.; Mackey, Z.; Doyle, P.; Zhou, Y. M.; Gut, J.; Rosenthal, P. J.; McKerrow, J. H.; Guy, R. K. *Bioorg. Med. Chem. Lett.* **2005**, *15*, 121.
25. Chiyanzu, I.; Hansell, E.; Gut, J.; Rosenthal, P. J.; McKerrow, J. H.; Chibale, K. *Bioorg. Med. Chem. Lett.* **2003**, *13*, 3527.
26. Fonseca, N. C.; da Cruz, L. F.; da Silva Villela, F.; do Nascimento Pereira, G. A.; de Siqueira-Neto, J. L.; Kellar, D.; Suzuki, B. M.; Ray, D.; de Souza, T. B.; Alves, R. J.; Sales, P. A., Junior; Romanha, A. J.; Murta, S. M. F.; McKerrow, J. H.; Caffrey, C. R.; de Oliveira, R. B.; Ferreira, R. S. *Antimicrob. Agents Chemother.* **2015**, *59*, 2666.
27. M. Moreira, D. R.; Lima Leite, A. C.; O. Cardoso, M. V.; Srivastava, R. M.; Hernandes, M. Z.; Rabello, M. M.; da Cruz, L. F.; Ferreira, R. S.; de Simone, C. A.; Meira, C. S.; Guimarães, E. T.; da Silva, A. C.; Dos Santos, T. A. R.; Pereira, V. R. A.; Pereira Soares, M. B. *ChemMedChem* **2014**, *9*, 177.
28. de Carvalho, L. P.; Gomes, M. A. G. B.; Rocha, B. S.; de Oliveira, R. R.; Maria, E. J.; de Melo, E. J. T. *J. Dev. Drugs* **2014**, *3*, 126.
29. Siles, R.; Chen, S.-E.; Zhou, M.; Pinney, K. G.; Trawick, M. L. *Bioorg. Med. Chem. Lett.* **2006**, *16*, 4405.
30. Porcal, W.; Hernández, P.; Boiani, M.; Aguirre, G.; Boiani, L.; Chidichimo, A.; Cazzulo, J. J.; Campillo, N. E.; Paez, J. A.; Castro, A.; Krauth-Siegel, R. L.; Davies, C.; Basombrio, M. A.; González, M.; Cerecetto, H. *J. Med. Chem.* **2007**, *50*, 6004.
31. Guido, R. V. C.; Trossini, G. H. G.; Castilho, M. S.; Oliva, G.; Ferreira, E. I.; Andricopulo, A. D. *J. Enzyme Inhib. Med. Chem.* **2008**, *23*, 964.
32. Pizzo, C.; Faral-Tello, P.; Salinas, G.; Fló, M.; Robello, C.; Wipf, P.; Graciela Mahler, S. *Medchemcomm* **2012**, *3*, 362.
33. Merlino, A.; Benitez, D.; Campillo, N. E.; Páez, J. A.; Tinoco, L. W.; González, M.; Cerecetto, H. *Medchemcomm* **2012**, *3*, 90.
34. de O. Cardoso, M. V.; de Siqueira, L. R. P.; da Silva, E. B.; Costa, L. B.; Hernandes, M. Z.; Rabello, M. M.; Ferreira, R. S.; da Cruz, L. F.; M. Moreira, D. R.; Pereira, V. R. A.; de Castro, M. C. A. B.; Bernhardt, P. V.; L. Leite, A. C. *Eur. J. Med. Chem.* **2014**, *86*, 48.
35. Hernandes, M. Z.; Rabello, M. M.; L. Leite, A. C.; O. Cardoso, M. V.; M. Moreira, D. R.; Brondani, D. J.; Simone, C. A.; Reis, L. C.; Souza, M. A.; Pereira, V. R. A.; Ferreira, R. S.; McKerrow, J. H. *Bioorg. Med. Chem.* **2010**, *18*, 7826.
36. L. Leite, A. C.; de Lima, R. S.; D.M. Moreira, D. R.; D.O. Cardoso, M. V.; Gouveia de Brito, A. C.; Farias Dos Santos, L. M.; Hernandes, M. Z.; Kiperstok, A. C.; de Lima, R. S.; Soares, M. B. P. *Bioorg. Med. Chem.* **2006**, *14*, 3749.
37. L. Leite, A. C.; de M. Moreira, D. R.; de O. Cardoso, M. V.; Hernandes, M. Z.; Alves Pereira, V. R.; Silva, R. O.; Kiperstok, A. C.; Lima, M. daS.; Soares, M. B. P. *ChemMedChem* **2007**, *2*, 1339.
38. M. Moreira, D. R.; Costa, S. P. M.; Hernandes, M. Z.; Rabello, M. M.; de Oliveira Filho, G. B.; de Melo, C. M. L.; da Rocha, L. F.; de Simone, C. A.; Ferreira, R. S.; Fradico, J. R. B.; Meira, C. S.; Guimarães, E. T.; Srivastava, R. M.; Pereira, V. R. A.; Soares, M. B. P.; L. Leite, A. C. *J. Med. Chem.* **2012**, *55*, 10918.
39. Ferreira, R. S.; Bryant, C.; Ang, K. H.; McKerrow, J. H.; Shoichet, B. K.; Renslo, A. R. *J. Med. Chem.* **2009**, *52*, 5005.
40. Brenner, Z. *Rev. Inst. Med. Trop. Sao Paulo* **1962**, *4*, 389.

ANEXO 7

CORRÊA, R. S.; SILVA, M. M.; GRAMINHA, A. E.; **MEIRA, C. S.**; SANTOS, J. A. F.; MOREIRA, D. R. M.; SOARES, M. B. P.; POELHSITZ, G. V.; CASTELLANO, E. E.; JR, C. B.; COMINETTI, M. R.; BATISTA, A. A. Ruthenium(II) complexes of 1,3-thizolidine-2-thione: Cytotoxicity against tumor cells and anti-*Trypanosoma cruzi* activity enhanced upon combination with benznidazole. **Journal of Inorganic Biochemistry**, v. 156, p. 153-163, 2016.



Ruthenium(II) complexes of 1,3-thiazolidine-2-thione: Cytotoxicity against tumor cells and anti-*Trypanosoma cruzi* activity enhanced upon combination with benznidazole



Rodrigo S. Corrêa^{a,b,*}, Monize M. da Silva^a, Angelica E. Graminha^a, Cássio S. Meira^c, Jamyle A.F. dos Santos^c, Diogo R.M. Moreira^c, Milena B.P. Soares^{c,d}, Gustavo Von Poelhsitz^e, Eduardo E. Castellano^f, Carlos Bloch Jr^g, Marcia R. Cominetti^h, Alzir A. Batista^{a,*}

^a Departamento de Química, Universidade Federal de São Carlos, CP 676, CEP 13565-905 São Carlos, SP, Brazil

^b Departamento de Química, ICEB, Universidade Federal de Ouro Preto, CEP 35400-000 Ouro Preto, MG, Brazil

^c Centro de Pesquisas Gonçalo Moniz, Fiocruz, CEP:40296-710 Salvador, BA, Brazil

^d Centro de Biotecnologia e Terapia Celular, Hospital São Rafael, Avenida São Rafael, 2152, São Marcos, CEP 41253-190 Salvador, BA, Brazil

^e Instituto de Química, Universidade Federal de Uberlândia, CP 593, CEP 38400-902 Uberlândia, MG, Brazil

^f Instituto de Física, Universidade de São Paulo, CP 369, CEP 13560-970 São Carlos, SP, Brazil

^g Centro Nacional de Pesquisa de Recursos Genéticos e Biotecnologia, EMBRAPA, Estação Parque Biológico, CEP 70910-900 Brasília, DF, Brazil

^h Departamento de Gerontologia, Universidade Federal de São Carlos, CP 676, CEP 13565-905 São Carlos, SP, Brazil

ARTICLE INFO

Article history:

Received 2 September 2015

Received in revised form 16 December 2015

Accepted 28 December 2015

Available online 2 January 2016

Keywords:

Ru(II) complexes

Cytotoxicity

Trypanosoma cruzi

ctDNA-binding

1,3-Thiazolidine-2-thione

ABSTRACT

Three new mixed and mononuclear Ru(II) complexes containing 1,3-thiazolidine-2-thione (tzdtH) were synthesized and characterized by spectroscopic analysis, molar conductivity, cyclic voltammetry, high-resolution electrospray ionization mass spectra and X-ray diffraction. The complexes presented unique stereochemistry and the proposed formulae are: [Ru(tzdt)(bipy)(dppb)]PF₆ (**1**), *cis*-[Ru(tzdt)₂(PPh₃)₂] (**2**) and *trans*-[Ru(tzdt)(PPh₃)₂(bipy)]PF₆ (**3**), where dppb = 1,4-bis(diphenylphosphino)butane and bipy = 2,2'-bipyridine. These complexes demonstrated strong cytotoxicity against cancer cell lines when compared to cisplatin. Specifically, complex **2** was the most potent cytotoxic agent against MCF-7 breast cells, while complexes **1** and **3** were more active in DU-145 prostate cells. Binding of complexes to ctDNA was determined by UV-vis titration and viscosity measurements and revealed binding constant (K_b) values in range of $1.0\text{--}4.9 \times 10^3 \text{ M}^{-1}$, which are characteristic of compounds possessing weak affinity to ctDNA. In addition, these complexes presented antiparasitic activity against *Trypanosoma cruzi*. Specifically, complex **3** demonstrated strong potency, moderate selectivity index and acted in synergism with the approved antiparasitic drug, benznidazole. Additionally, complex **3** caused parasite cell death through a necrotic process. In conclusion, we demonstrated that Ru(II) complexes have powerful pharmacological activity, while the metal-free tzdtH does not provoke the same outcome.

© 2015 Elsevier Inc. All rights reserved.

1. Introduction

Cancer is considered a group of complex and multifaceted diseases [1]. Carcinogenesis is thought to be initiated by changes to the DNA within cells and also by inhibition of growth suppressors, which, in turn, gives rise to the uncontrolled cell proliferation, invasion of surrounding and distant tissues, and ultimately leads to a risk of aggressive metastasis [2]. Prostate and breast cancers are of high incidence and mortality around the world and the development of new drugs is of interest [3]. Drugs containing transition metals hold a promising possibility for cancer

treatment. Although cisplatin has been largely employed alone or in drug combinations against prostate and breast cancers, limitations regarding resistance has been observed [4,5]. To overcome cisplatin limitation, Satraplatin, the first orally available Pt drug, is currently undergoing clinical investigation [6]. Ruthenium compounds are promising pharmaceuticals because of many biological features, such as reduced toxicity, suitable biodistribution, and mechanisms of action different than platinum-based compounds [7,8]. In the last years, Ru(III) complexes have entered clinical trials: NAMI-A [ImH][*trans*-RuCl₄(DMSO)(Im)], KP1019 (indazolium *trans*-[tetrachloridobis(1H-indazole)ruthenate(III)]) and NKP-1339 [sodium *trans*-[tetrachloridobis(1H-indazole)ruthenate(III)]] [9,10]. The half-sandwich η^6 -arene-Ru(II) complexes are a promising class of antitumor compounds with particular emphasis on the [RuCl₂(η^6 -p-cymene)(PTA)], PTA = 1,3,5-triaza-7-phosphaadamantane, named as RAPTA-C [11]. This compound is highly active in vivo against metastatic

* Corresponding authors.

E-mail addresses: rodrigocorre@iceb.ufop.br (R.S. Corrêa), daab@ufscar.br (A.A. Batista).

cells by inhibiting cathepsin B, a protease related to tumor invasion and metastasis [12,13].

Regarding parasitic infections, American trypanosomiasis (Chagas disease) is an important health problem in Latin America, affecting 8–14 million people (14,000 deaths per year) with different forms of the pathology [14,15]. It is of great concern due to the development of chronic cardiomyopathy and other related health problems [16]. Chemotherapy is only based on nifurtimox and benznidazole (Bdz), drugs that are more than 50 years old and suffer from low efficacy and high levels of toxicity [17]. Since the discovery of an efficient Ru(II) complex containing clotrimazole against *Trypanosoma cruzi*, a large number of metal complexes have been evaluated for this purpose [18]. Strategies for the development of new anti-trypanosomal metallodrugs generally involve: coordination of antiparasitic ligands to the metal, and coordination of DNA intercalators to the metal and metal compounds as direct inhibitors of parasite enzymes [19,20].

In view of this, our research group has been studying a number of pharmacological properties for Ru(II) complexes containing phosphines and diimines ligands as anticancer and anti-infectious agents [21–27]. Remarkable activities were observed for complexes with general formulae $[\text{Ru}(\text{pic})(\text{dppb})(\text{N}-\text{N})]\text{PF}_6$, where pic = 2-pyridinecarboxylate; N–N = 2,2-bipyridine or 1,10'-phenanthroline. These complexes displayed strong in vitro activity against *Mycobacterium tuberculosis* and more importantly, presented activity against multi-resistant strains. In view of these results with bidentate *N,O*-ligand (pic), we sought to investigate Ru complexes containing bidentate *N,S*-ligands. In fact, heterocyclic *N,S*-ligands have been extensively used in the preparation of metal complexes for therapeutic application [27–29]. Among them, an interesting ligand is 1,3-thiazolidine-2-thiol (tzdtH), which has a classical thiol/thione tautomerism as shown in Fig. 1. Crystallographic studies for tzdtH structure indicate that the thione tautomer (form II; Fig. 1) is present in the solid state [30]. However, two tautomeric forms can be found in aqueous and in organic solutions (i.e., 1,4-dioxane, CCl_4 , benzene, CHCl_3 , CH_2Cl_2 , $\text{C}_2\text{H}_4\text{Cl}_2$, EtOH, MeOH, CH_3CN , DMF and DMSO) [31,32]. Given this promising outlook and considering the different coordination sites of the tzdtH [33–35], this work aimed to study the reactivity of this ligand with Ru(II) phosphine precursors. To the best of our knowledge, only three ruthenium organometallic compounds with anionic tzdt[−] are described in the literature, however no detailed structural as well as pharmacological evaluation were carried out [36,37]. Thus, here three new Ru(II) complexes with the formulae $[\text{Ru}(\text{tzdt})(\text{bipy})(\text{dppb})]\text{PF}_6$ (**1**), *cis*- $[\text{Ru}(\text{tzdt})_2(\text{PPh}_3)_2]$ (**2**) and *trans*- $[\text{Ru}(\text{tzdt})(\text{PPh}_3)_2(\text{bipy})]\text{PF}_6$ (**3**), were obtained and evaluated as cytotoxic and antiparasitic agents.

2. Experimental

2.1. General

Reactions and chemicals were handled under Argon atmosphere. Solvents were purified by standard methods. Chemicals used were of reagent grade or comparable purity. $\text{RuCl}_3 \cdot 3\text{H}_2\text{O}$, dppb, bipy and

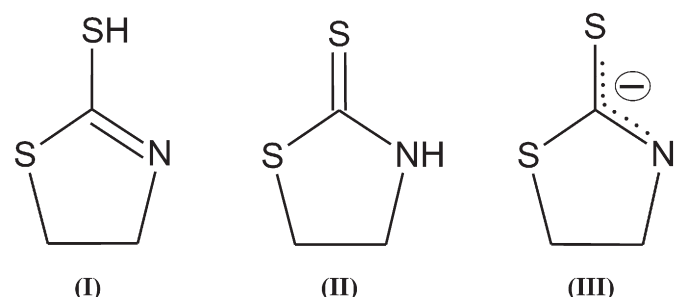


Fig. 1. The tautomeric (I and II) and anionic (III) structures of the tzdtH ligand.

tzdtH were purchased from Sigma-Aldrich (St. Louis, MO) and used as supplied. The reactants *cis*- $[\text{RuCl}_2(\text{dppb})(\text{bipy})]$ [38], $[\text{RuCl}_2(\text{PPh}_3)_3]$ [39] and *cis*- $[\text{RuCl}_2(\text{PPh}_3)_2(\text{bipy})]$ [40] precursors were prepared according to literature. The IR spectra were recorded on a FT-IR Bomem-Michelson 102 spectrometer in the 4000–250 cm^{-1} region, using CsI pellets. Conductivity values were obtained at room temperature using 10^{-3} M solutions of the complexes in CH_2Cl_2 by using a Meter Lab CDM2300 instrument. ^1H , $^{31}\text{P}\{^1\text{H}\}$ and $^{13}\text{C}\{^1\text{H}\}$ NMR were recorded on a Bruker DRX 400 MHz using tetramethylsilane as reference and solvent CDCl_3 to the complexes **1** and **2** and acetone- d_6 to complex **3**. The $^{31}\text{P}\{^1\text{H}\}$ chemical shifts are reported in relation to H_3PO_4 , 85%. The UV–vis spectra of the complexes, (concentration c.a. 10^{-4} M), were recorded in CH_2Cl_2 on a Hewlett Packard diode array–8452 A. Cyclic voltammetry experiments were performed in an electrochemical analyzer BAS, model 100B and carried out at room temperature. Typical conditions were: CH_2Cl_2 containing 0.10 M Bu_4NClO_4 (TBAP) as supporting electrolyte, and using a one-compartment cell, both working and auxiliary electrodes were stationary Pt foils, and the reference electrode was Ag/AgCl, 0.10 M TBAP in CH_2Cl_2 . Ferrocene (Fc) was employed for calibrating the electrochemical system and the redox potential. Under these conditions, (Fc⁺/Fc) couple presented 430 mV. High resolution mass spectra of complexes were obtained by direct infusion in a MicroTof-Q II Bruker Daltonics Mass Spectrometer (Le) in the positive ion mode, employing methanol as solvent (LC/MS grade from Honeywell/B&J Brand). Elemental analyses were carried out in the Microanalytical Laboratory of Federal University of São Carlos, with an EA 1108 FISON Instruments CHNS microanalyzer.

2.2. Synthesis and characterization

2.2.1. $[\text{Ru}(\text{tzdt})(\text{bipy})(\text{dppb})]\text{PF}_6$ (**1**)

In a Schlenk flask, 16 mg (0.14 mmol) of tzdtH was dissolved in 10 mL of a CH_2Cl_2 solution containing 20 μL of triethylamine. After, 100 mg (0.12 mmol) of *cis*- $[\text{RuCl}_2(\text{dppb})(\text{bipy})]$ reactant was added and maintained under stirring at room temperature for 3 h. Then, 30 mg (0.18 mmol) of NH_4PF_6 was added and the volume concentrated under reduced pressure to ca. 2 mL. Orange crystals were separated by filtration, washed with dry diethyl ether and dried under vacuum to yield 94 mg (83%). Anal. Calc. for $[\text{RuC}_{41}\text{H}_{40}\text{N}_3\text{P}_2\text{S}_2]\text{PF}_6$: exp. (calc) 51.90 (52.01); H, 4.21 (4.26); N, 4.28 (4.44); S, 6.55 (6.77)%. Molar conductance ($\text{S cm}^2 \text{mol}^{-1}$, CH_2Cl_2) 46.5. IR (cm^{-1}): ($\nu\text{C}-\text{H}$) 3076, 3053, 2949, 2924; (νCH_2) 2854, 2679; (νCN) 1535, 1433; ($\nu\text{CC}(\text{ring}) + \nu\text{CC}(\text{dppb})$) 1483, 1309; ($\nu\text{C}-\text{S}$) 1159; ($\nu\text{C}-\text{P}$) 1094; (ν_{ring}) 1043, 997; ($\nu\text{P}-\text{F}$) 843; (γCS) 764; (γ_{ring}) 698; ($\nu\text{Ru}-\text{P}$) 517, 507; ($\nu\text{Ru}-\text{S}$) 492; ($\nu\text{Ru}-\text{N}$) 426. $^{31}\text{P}\{^1\text{H}\}$ NMR (162 MHz, CDCl_3 , 298 K): δ (ppm) (d, 43.2 and 44.6, $^2J = 35.1$ Hz); ^1H NMR (400 MHz, CDCl_3 , 298 K): δ (ppm): 8.96 (1H, d, bipy); 8.74 (1H, br. s, bipy); 8.09 (1H, m, bipy); 8.03 (1H, m, bipy); 7.85 (1H, m, bipy); 7.73 (1H, m, bipy); 7.45 (2H, t, H_p of dppb); 7.41–6.93 (16H, m, H_o and H_m of dppb); 6.89 (2H, t, bipy); 6.38 (2H, t, H_p of dppb); 3.40–2.30 (4H, m, CH_2 of tzdt); 2.30–1.03 (8H, m, CH_2 of dppb). $^{13}\text{C}\{^1\text{H}\}$ NMR (125.74 MHz, CDCl_3 , 298 K): δ (ppm) 183.75 (CS); 158.09–151.45 (C-Bipy), 139.93–121.92 (C-dppb and C-Bipy); 55.26 (1C, CH_2-N of tzdt) and 32.03 (1C, CH_2-S of tzdt); 31.75–21.29 (C- CH_2 of dppb). UV–vis (CH_2Cl_2 , 1.6×10^{-4} M): λ/nm ($\epsilon/\text{M}^{-1} \text{cm}^{-1}$) 296 (15,970), 420 (2850).

2.2.2. *cis*- $[\text{Ru}(\text{tzdt})_2(\text{PPh}_3)_2]$ (**2**)

In the Schlenk flask, 20 mg (0.17 mmol) of tzdtH was dissolved in 60 mL of ethanol. To this, 60 mL of CH_2Cl_2 containing 30 μL of Et_3N followed by 70 mg of $[\text{RuCl}_2(\text{PPh}_3)_3]$ reactant were added. After stirring for 30 min, under room temperature, color mixture changed from a brownish to a yellowish suspension. Solvent was removed under reduced pressure and the yellowish solid was filtered and washed with ethanol and diethyl ether and then dried under vacuum to yield 50 mg (79%). Anal. Calc. for $[\text{RuC}_{42}\text{H}_{38}\text{N}_2\text{S}_4\text{P}_2] \cdot \frac{1}{2}\text{H}_2\text{O}$: exp. (calc) 57.76 (57.91); H, 4.22 (4.51); N, 3.33 (3.22); S, 15.17 (14.73)%. Molar conductance ($\text{S cm}^2 \text{mol}^{-1}$,

CH₂Cl₂) 1.8. IR (cm⁻¹) (νC–H) 3072, 3049, 2947, 2928; (νCH₂) 2849; (νCN) 1527; 1508; (νCC_(ring) + νCC_(dppb)) 1479, 1385; (νC–S) 1188; (νC–P) 1088; (ν_{ring}) 1045, 993; (γCS) 750; (γ_{ring}) 696; (νRu–P) 520; (νRu–S) 497; (νRu–N) 435. ³¹P{¹H} NMR (162 MHz, CDCl₃, 298 K): δ (ppm) 54.2 (s); ¹H NMR (400 MHz, CDCl₃, 298 K): δ (ppm): 7.32 (12H, m, H_o of PPh₃); 7.23 (6H, t, H_p of PPh₃); 7.10 (12H, t, H_m of PPh₃); 3.27 (2H, ddd, CH₂ of tzdt); 3.20 (2H, dd, CH₂ of tzdt); 2.94 (2H, ddd, CH₂ of tzdt); 2.65 (2H, dd, CH₂ of tzdt). ¹³C{¹H} NMR (125.74 MHz, CDCl₃, 298 K): δ (ppm) 181.88 (CS); 137.33–127.09 (36C, C-PPh₃); 56.49 (2C, CH₂-N of tzdt) and 31.72 (2C, CH₂-S of tzdt). UV–vis (CH₂Cl₂, 4 × 10⁻⁵ M): λ/nm (ε/M⁻¹ cm⁻¹) 310 (1993).

2.2.3. *trans*-[Ru(Tzdt)(Pph₃)₂(Bipy)]PF₆ (**3**)

In the Schlenk flask, 33 mg (0.137 mmol) of tzdtH was dissolved in a mixture of CH₂Cl₂:MeOH (80:20) containing 20 μL Et₃N. Then, 100 mg (0.114 mmol) of *cis*-[RuCl₂(PPh₃)₂(bipy)] reactant was added and the mixture was stirred under reflux temperature for 24 h. After this, the resulting orange solution was concentrated under reduced pressure to 2 mL and 10 mL of water was added. The resulting orange solid was filtered, washed with warmed water, diethyl ether and then dried under vacuum to yield 113 mg (92%). Anal. Calc. for [RuC₄₉H₄₂N₃S₂P₂]₂PF₆·2H₂O: exp. (calc) 54.69 (54.44); H, 4.12 (4.29); N, 3.97 (3.89); S, 6.23 (5.93) %. Molar conductance (S cm² mol⁻¹, CH₂Cl₂) 50.2. IR (cm⁻¹): (νC–H) 3076; 3055; 2951; 2924; (νCH₂) 2852; (νCN) 1528, 1433; (νCC_(ring) + νCC_(dppb)) 1384; 1307; (νC–S) 1159; (νC–P) 1090; (ν_{ring}) 1051, 999; (νP–F) 840; (γCS) 762; (γ_{ring}) 698; (νRu–P) 519; (νRu–S) 492; (νRu–N) 438. ³¹P{¹H} NMR (162 MHz, CDCl₃, 298 K): δ (ppm) 33.3 (s); ¹H NMR (400 MHz, CDCl₃, 298 K): δ (ppm): 9.75 (1H, d, bipy); 9.02 (1H, d, bipy); 7.71 (2H, m, bipy); 7.65 (2H, m, bipy); 7.57 (1H, m, bipy); 7.35 (6H, m, H_p of PPh₃); 7.28 (12H, m, H_o of PPh₃); 7.20 (12H, m, H_m of PPh₃); 7.11 (1H, m, bipy); 3.37 (2H, t, CH₂ of tzdt); 2.57 (2H, t, CH₂ of tzdt). ¹³C{¹H} NMR (125.74 MHz, CDCl₃, 298 K): δ (ppm) 182.52 (CS); 158.68–153.62 (C-Bipy), 136.58–123.77 (C-PPh₃ and C-Bipy); 57.41 (1C, CH₂-N, tzdt), 31.77 (1C, CH₂-S, tzdt). UV–vis (CH₂Cl₂, 8 × 10⁻⁵ M): λ/nm (ε/M⁻¹ cm⁻¹) 280 (26266), 302 (17927), 348 (5488), 444 (3434).

2.3. X-ray diffraction

Single crystals of the complexes were grown from diethyl ether diffusion into a dichloromethane solution of complex at room temperature (293 K). X-ray diffraction experiments were carried out at room temperature using a suitable crystal mounted on glass fiber, and positioned on the goniometer head. Intensity data were measured on an Enraf-Nonius Kappa-CCD diffractometer with graphite monochromated MoKα radiation (λ = 0.71073 Å). The cell refinements were performed using the software Collect [41] and Scalepack [42], and the final cell parameters were obtained on all reflections. The structures were solved by direct method using SHELXS-97 and refined using the software SHELXL-97. In all complexes' structures, the Gaussian method was used for the absorption corrections [43]. Non-hydrogen atoms of the complexes were unambiguously located, and a full-matrix, least-squares refinement of these atoms with anisotropic thermal parameters was carried out. In all ligands of the complexes, aromatic C–H hydrogen atoms were positioned stereochemically and were refined with fixed individual displacement parameters [U_{iso}(H) = 1.2 U_{eq}(Csp²)] using a riding model with aromatic, C–H bond lengths which were fixed at 0.93 Å. Methylene groups of tzdt ligand were also set as isotropic with a thermal parameter 20% greater than the equivalent isotropic displacement parameter of the atom to which each one was bonded and C–H bond lengths were fixed at 0.97 Å. Tables were generated by WinGX and the structure representations by MERCURY. The CrystalExplorer 2.1 program was used to generate the Hirshfeld surfaces and the fingerprint plot. The Hirshfeld surfaces were employed to define the intermolecular environment of molecules within the crystal of each complex

[44–46]. The fingerprint plot or 2D-fingerprint graphics is constructed by the plot of *de* versus *di* (*de* = external distance is defined as the distance between the calculated Hirshfeld surface and the nearest atom of an adjacent molecule; *di* = internal distance is distance between the nearest nucleus internal and the calculated Hirshfeld surface). Relationships between crystal packing pattern and molecular geometry were determined by analyzing parameters present in Hirshfeld fingerprint plots. The 2D-fingerprint also provides the percentage of each intermolecular contact occurring in the complex structure. Crystallography data were registered in the Cambridge Crystallographic Data Centre (CCDC), with the respective deposit numbers: 1037025 (**1**), 1037026 (**2**) and 1037027 (**3**).

2.4. DNA binding

2.4.1. Spectroscopic titration

A solution of calf thymus DNA (ctDNA, Sigma-Aldrich) was prepared in Tris–HCl buffer (5 mM Tris–HCl, pH 7.2). A solution of ctDNA in the buffer gave a ratio of UV absorbance at 260 and 280 nm of about 1.8:1, indicating that the solution is protein-free. The concentration of ctDNA was measured from its absorption intensity at 260 nm using the molar absorption coefficient value of 6600 M⁻¹ cm⁻¹ [47]. Solutions of Ru(II) complexes used in the experiments were prepared in Tris–HCl buffer containing 5% DMSO. To the ctDNA titration experiments, different concentrations of the ctDNA were used (ranging 3.8 × 10⁻⁵ to 7.6 × 10⁻⁴ M), while the concentration of ruthenium complexes were maintained at 1.6 × 10⁻⁴, 4.4 × 10⁻⁵ and 8.6 × 10⁻⁵ M for **1**, **2** and **3**, respectively. Sample correction was done for the absorbance of DNA and the spectra were recorded after solution equilibration for 2 min. It is worth mentioning that complex **2** and **3** structures change after incubating in the buffered medium, such as observed in the ³¹P NMR spectrum of complexes **2** and **3** (see the Supplementary material). These changes can be attributed to exchange of the monodentate PPh₃ ligand. As a result, the signal of PPh₃ free is observed at around –6.3 ppm. The intrinsic equilibrium binding constant (K_b) of the complexes to ctDNA was obtained using the McGhee–von Hippel (MvH) method [48] by using the expression of Wolfe and co-workers [49]:

$$[\text{ctDNA}]/(\varepsilon_a - \varepsilon_f) = [\text{ctDNA}]/(\varepsilon_b - \varepsilon_f) + 1/K_b(\varepsilon_b - \varepsilon_f)$$

in which [ctDNA] is the concentration of ctDNA in base pairs, ε_a is the ratio of the absorbance/[Ru(II) complex], ε_f is the extinction coefficient of the free Ru(II) complex, and ε_b is the extinction coefficient of the complex in the fully bound form. The ratio of the slope to the intercept in the plot of [ctDNA]/(ε_a–ε_f) vs. [ctDNA] gives the value of K_b, which was calculated from the metal to ligand charge transfer (MLCT) absorption band (λ_{max}). Changes in the absorption intensity increasing concentration of ctDNA was monitored and analyzed by regression analysis. The nonlinear least-squares analysis was calculated by using OriginLab.

2.4.2. Viscosity measurements

Viscometric titrations of **1–3** were performed using an Ostwald viscometer in a constant temperature (37 °C). The concentration of ctDNA was 4.2 × 10⁻³ μM, and the flow times were measured with an automated timer. Each sample was measured 5 times and an average flow time was calculated. Data were presented as (η/η₀)^{1/3} versus [complex]/[ctDNA], where η is the viscosity of ctDNA in the presence of the complex and η₀ is that of ctDNA alone. Relative viscosity for ctDNA in either the presence or absence of complex was calculated from the relation: η = (t – t₀) / (t₀), where t is the observed flow time of the ctDNA containing solution and t₀ is the flow time of buffer alone.

2.5. Cytotoxicity against cancer cells

Human tumor breast cell line MCF-7 (ATCC No. HTB-22) and human prostate tumor cell line DU-145 (ATCC: HTB-81) were cultured in RPMI-1640 medium (Sigma-Aldrich) supplemented with 20% fetal bovine serum (FBS; Cultilab, Campinas, Brazil) at 37 °C in 5% CO₂. Aliquots of 200 µL containing 1×10^4 cells were seeded in 96-well microplates and incubated for 12 h. Drugs were dissolved in sterile DMSO (stock solution with maximum concentration of 20 mM) and diluted in RPMI-1640 medium from 0.05 to 200 µM (final concentration of 1% DMSO per well). Negative control (without drug) and positive control (cisplatin) were included in the plate and then incubated for 48 h at 37 °C in 5% CO₂. After incubation, cells were washed twice with phosphate buffer saline, 50 µL of MTT (MTT, Life, Carlsbad, USA) at 0.5 mg mL⁻¹ was added and incubated for 4 h, followed by adding 100 µL of isopropanol. Colorimetric reading was performed in a microplate reader at 595 nm. Cell viability was measured in comparison to the negative control (cells receiving only DMSO). Inhibitory concentration to 50% (IC₅₀) was determined by using non-linear regression. Three independent experiments were performed.

2.6. Host cell toxicity

J774 macrophages were seeded on 96-well plates at a cell number of 5×10^4 cells mL⁻¹ in 200 µL of RPMI medium (Sigma-Aldrich) supplemented with 10% of FBS (Life, Carlsbad, USA) and 50 µg mL⁻¹ of gentamycin (Life) and incubated for 24 h at 37 °C and 5% CO₂. After that time each compound was added at six concentrations (0.04 to 10 µM) in triplicate and incubated for 72 h. Cell viability was determined by AlamarBlue assay (Life) according to the manufacturer's instructions. Colorimetric readings were performed after 6 h at 570 and 600 nm. Cytotoxic concentration to 50% (CC₅₀) was calculated using data-points gathered from three independent experiments. Gentian violet (Synth, São Paulo, Brazil) was used as positive control.

2.7. Antiparasitic activity

2.7.1. Cytotoxicity for trypomastigotes

Trypomastigotes collected from the supernatants of previously infected LLC-MK2 cells were dispensed into 96-well plates at a cell number of 2×10^6 cells mL⁻¹ in 200 µL of RPMI medium. Compounds were tested at concentration range of 0.02 to 10 µM, in triplicate. The plate was incubated for 24 h at 37 °C and 5% CO₂. Aliquots from each well were collected and the number of viable parasites was assessed in a Neubauer chamber and compared to untreated parasite culture. This experiment was performed three times. Benznidazole (LAFEPE, Recife, Brazil) was used as the positive control. Cytotoxic concentration to 50% (CC₅₀) was calculated using data-points gathered from three independent experiments.

2.7.2. Inhibition of parasite infection

Peritoneal macrophages (2×10^5 cells mL⁻¹) obtained from BALB/c mice were seeded in a 24 well-plate with rounded coverslips on the bottom in RPMI supplemented with 10% FBS and incubated for 24 h. Cells were then infected with trypomastigotes (10:1) for 2 h. Free trypomastigotes were removed by successive washes using saline solution and the cells were incubated for 24 h for internalization and differentiation of trypomastigotes into amastigotes. Following this, cultures were incubated in complete medium alone or with compounds for 72 h. Cells were fixed in absolute alcohol and the percentage of infected macrophages and the number of amastigotes/100 macrophages was determined by manual counting after hematoxylin and eosin staining using an optical microscope (Olympus, Tokyo, Japan). The percentage of infected macrophages and the number of amastigotes per 100 macrophages was determined by counting 100 cells per slide.

The one-way ANOVA and Bonferroni for multiple comparisons were used to determine the statistical significance of the group comparisons. Benznidazole was used as the positive control.

2.8. Propidium iodide and annexin V staining

Trypomastigotes (1×10^7) were incubated for 24 h at 37 °C in the absence or presence of Ru(II) complex **3** (0.01, 0.015 or 0.02 µM). After incubation, the parasites were labeled for propidium iodide (PI) and annexin V using the annexin V-FITC apoptosis detection kit (Sigma-Aldrich), according to the manufacturer's instructions. Acquisition and analyses was performed using a FACS Calibur flow cytometer (Becton Dickinson, CA, USA), with FlowJo software (Tree Star, CA, USA). A total of 30,000 events were acquired in the region previously established as trypomastigote forms of *T. cruzi*. Two independent experiments were performed.

3. Results

3.1. Synthesis, infrared spectroscopy and mass spectrometry

The chemical reactivity of tzdtH in triethylamine was studied under the presence of metal complexes *cis*-[RuCl₂(dppb)(bipy)], [RuCl₂(PPh₃)₃] and *cis*-[RuCl₂(PPh₃)₂(bipy)]. This led to the formation of complexes with formulae [Ru(tzdt)(bipy)(dppb)]PF₆ (**1**), *cis*-[Ru(tzdt)₂(PPh₃)₂] (**2**) and *trans*-[Ru(tzdt)(PPh₃)₂(bipy)]PF₆ (**3**) containing the monoanionic tzdt⁻ as chelated ligand as shown in Scheme 1. Each synthetic procedure was straightforward, provided good yields and analytically pure complexes as determined by elemental analyses.

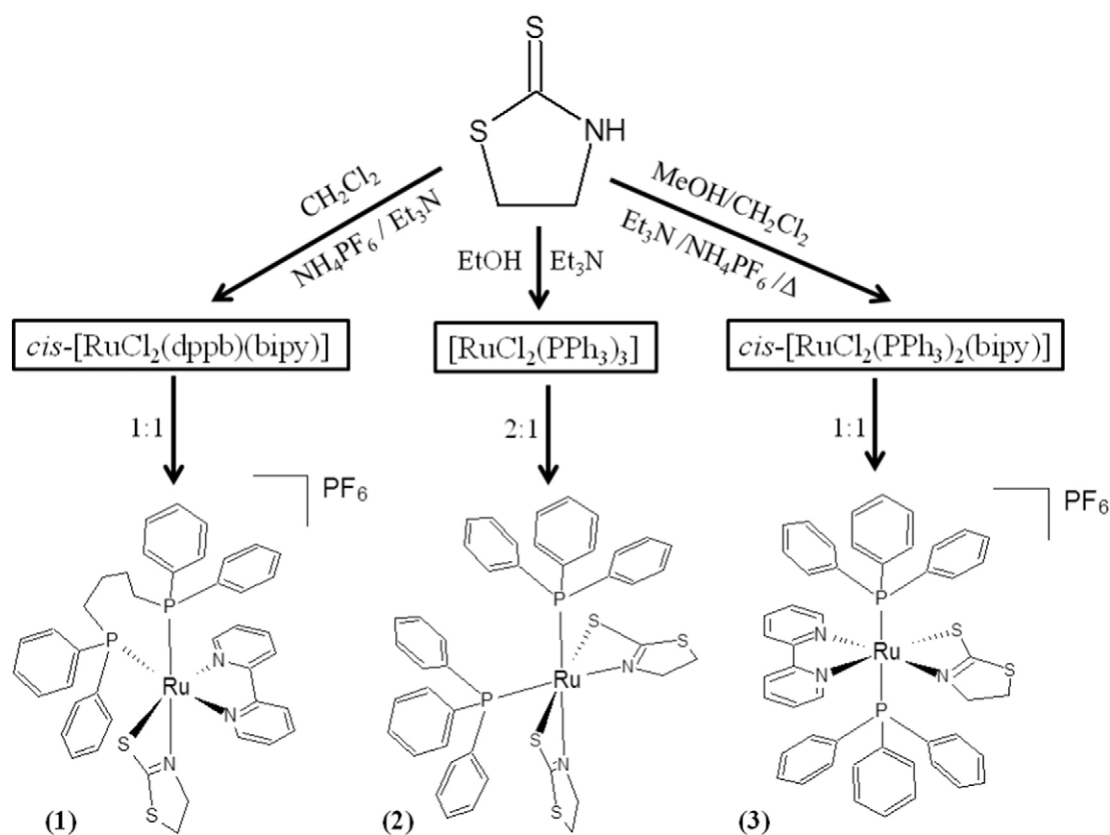
Infrared spectra of complexes **1–3** confirmed the presence of the tzdt⁻ ligand coordinated to the metal center. High energy region of each spectrum exhibited bands at 2854–2849 cm⁻¹, which were assigned to the νCH₂ stretching vibration of tzdt ligand. The νN–H stretching vibration at 3138 cm⁻¹ in the spectrum of metal-free tzdtH was absent in the spectra of the ruthenium complexes, suggesting that ligand is coordinated into its deprotonated form. Strong bands found in the region of 1535–1300 cm⁻¹ are characteristic of νCN and νCC stretching vibrations of the tzdt⁻, dppb and bipy ligands. In the complexes, the bands related to νC=S and δC=S absorptions of tzdt⁻ occur in the regions around 1188–1159 and 764–750 cm⁻¹, respectively.

Regarding ESI-MS(+) spectra, complex **1** presented the most intense molecular peak at 802.1179 Da, while its predicted monoisotopic mass is 802.1186 Da. For complexes **2** and **3**, M⁺ peaks occurred at 862.0428 and 900.1345 Da, respectively. In both complexes **2** and **3**, peaks corresponding to [M – PPh₃]⁺ were observed.

3.2. Electrochemical study

The redox behavior of metal complexes was investigated by cyclic voltammetry (Fig. 2). Complexes **1–3** revealed one-electron waves for Ru(II)/Ru(III) redox process with quasi-reversible behavior at +1150, +690 and +926 mV. These values highlight the different stereochemistry around the Ru(II) center. Complex **2** exhibited redox process in lower potential than complexes **1** and **3**. This can be explained because of two molecules of tzdt⁻ and the absence of bipy, which is a well-known π-electron acceptor ligand. In fact, the bipy-containing complexes **1** and **3** presented Ru(II)/Ru(III) oxidation peaks around 1000 mV, which are similar values to Ru(II) complexes described in the literature [25,26]. Despite complexes **1** and **3** presenting the same ligands, **3** has a redox potential much lower than **1**. This may be explained by the competition for electron density around the metal between the phosphorus atoms in *trans* position observed in complex **3** [27].

The half-wave potential (E_{1/2}) values for these complexes were more anodic than the starting reactants by approximately 0.60 V (Table 1).



Scheme 1. Routes used to prepare Ru(II)/tzdt[−] complexes.

This indicates that ruthenium is more easily oxidized in metal precursors than complexes (1–3), therefore complexes (1–3) are more stable than their starting reactants. This stabilization is possible due to the replacement of two σ and π donor chlorides by a negative and monocharged chelating tzdt[−], which contains an acceptor group.

3.3. NMR spectroscopy

Resonance for complexes 1 and 2 was carried out in CDCl₃, while acetone-*d*₆ was used in complex 3. In the ³¹P{¹H} NMR spectrum of complex 1, a typical AB spin system was observed with chemical shifts at 43.2(d) and 44.5(d) ppm, indicating the magnetic nonequivalence

of the two phosphorus atoms of dppb. The precursor complex *cis*-[RuCl₂(dppb)(bipy)] shows a pair of doublets at 32.0 and 43.0 ppm with the high field signal corresponding to the P *trans* N, as previously described [40]. These assignments are based on an empirical linear correlation established between crystallographic determined Ru–P distances in a series of Ru–dppb complexes and the corresponding ³¹P chemical shift observed in solution, in which the chemical shift become more high-field with increasing Ru–P bond length [50]. In view of this information, we suggest that in complex 1 the high-field doublet belongs to the P *trans* to nitrogen from bipy, because the Ru–P2 distance of 2.3299(9) Å (*trans* bipy) is longer than that observed for the Ru–P1 *trans* of nitrogen of the 2-MT ligand [2.3069(9) Å].

In contrast, only one singlet is observed in the ³¹P{¹H} NMR spectra of complexes 2 and 3, due to the presence of two equivalent PPh₃ phosphorus atoms (Table 1). For complex 2 the singlet signal at 54.2 ppm is typical of PPh₃ *trans* to nitrogen of N-heterocyclic ligands as observed for similar compounds such as the *cis*-[Ru(pymS)₂(PPh₃)₂], pymS = deprotonated 2-mercaptopyrimidine [51]. For complex 3 the singlet is observed at 33.3 ppm, a chemical shift in low field is shifted when compared to *cis*-[RuCl₂(PPh₃)₂(bipy)], where a singlet is presented at 21.5 ppm [52]. These values are typical of PPh₃ *trans* to PPh₃ as observed for a series of ruthenium compounds [53,54]. The ¹H NMR spectrum of metal-free tzdtH in CDCl₃ displayed a broad singlet corresponding to the proton of the N–H group around 7.30 ppm and a pair of triplets in the range 3.50–4.00 ppm corresponding to the methylenic protons.

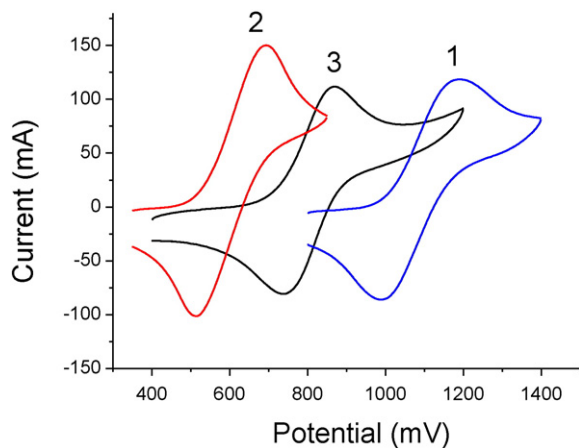


Fig. 2. Cyclic voltammograms of Ru(II) complexes 1, 2 and 3. Conditions: CH₂Cl₂, 0.10 M Bu₄NClO₄ as supporting electrolyte, scan rate 100 mV s^{−1}; working and auxiliary electrodes stationary Pt foils, and Ag/AgCl as reference electrode.

Table 1
³¹P{¹H} NMR and cyclic voltammetry data for complexes 1–3.

Complex	δ (ppm)	$^2J_{P-P}$ (Hz)	$E_{1/2}$ (mV)	ΔE_p (mV)
1	43.2(d); 44.6(d)	35.1	1082	135
2	54.2(s)	–	602	176
3	33.3(s)	–	860	132

For complexes **1–3** the signal at 7.30 is absent confirming that tzdtH is coordinated to Ru(II) in a deprotonated form and the methylenic protons appeared as multiplet signals in the range 2.30–3.40 ppm, considerably high-field shifted when compared with free-ligand. In the aromatic region protons of dppb (complex **1**) and PPh₃ (complexes **2** and **3**) displayed the typical pattern of multiplet signals for *ortho*, *meta* and *para* hydrogens of the aromatic rings in ranges of 6.38–7.45; 7.10–7.32 and 7.20–7.35 ppm, respectively. In addition, complexes **1** and **3** exhibited the expected deshielded doublets corresponding to the *ortho* hydrogens of the bipy ligands at 8.96; 8.74 and 9.75; 9.02 ppm, respectively. The ¹³C NMR spectra of complexes **1–3** displayed signals around 183–181 ppm, depending on the complex, typical of the CS coordinated group. This signal is shielded compared with that observed for the free ligand which occurs at 201.7 ppm, indicating that sulfur is coordinated to the metal. In addition, complexes displayed signals in the range 57.4–55.3 and 32.0–31.7 ppm, typically assigned to carbon atoms of the N-CH₂ and S-CH₂ groups of the thiazolidine ring, respectively.

3.4. X-ray crystal structures

Suitable crystals for a single crystal X-ray structure determination were obtained by slow evaporation of a chloroform solution. The MERCURY plots in Fig. 3 show that these complexes possess a distorted octahedral geometry. Crystal data collections and structure refinement parameters are summarized in Table 1S. The crystallographic analysis of metal-free tzdtH described in the literature shows that C1–S1 is a

double bond, while C1–N1 single-bond [54]. When tzdtH is coordinated to Ru, the length of these bonds significantly changes in which the C1–S1 is longer whereas C1–N1 is shorter in all the complexes. This suggests that the ligand adopts the canonical form (III) depicted in Fig. 1. In the crystal structure of complex **3**, the Ru–P bond lengths are longer than the other two complexes, possible due to the P to P *trans* influence. In contrast, the Ru–N1 length in **3** is shorter than that the observed for complexes **1** and **2**, because of the P to N *trans* influence which slightly affects the Ru–N bond length.

When we analyze the tzdt[−] conformation, a planar conformation in complexes **1** and **3** is observed, while in complex **2** a twisted ring is observed in the ligand structure. Due to the intermolecular interaction and crystal packing, the free tzdtH in solid state adopts either a distorted or a planar conformation. In the crystal structure of the neutral complex **2**, a sulfur···sulfur contact is observed, which explains the tzdtH distorted conformation. The distance of S···S atoms in the structure of complex **2** is at 3.543 Å as shown in Fig. 4, being shorter than the sum of the van der Waals radius (3.60 Å).

To examine the spatial arrangement of Ru complexes, the intermolecular contacts of each crystal structure were determined by using the Hirshfeld surfaces and their corresponding 2D-fingerprint plots (Supplementary material). The relative contribution of the intermolecular contacts present in these complexes shares interesting structural features. In complex (**1**), the contribution is: H···H (55.1%), C···H (17.2%), F···H (15.9%), S···H (7.9%), C···C (1.4%), C···F (0.5%), S···F (0.4%), and N···H (0.4%). In comparison to complex **1**, the intermolecular contribution found in **2** is slightly different [H···H (63.6%), C···H (17.5%),

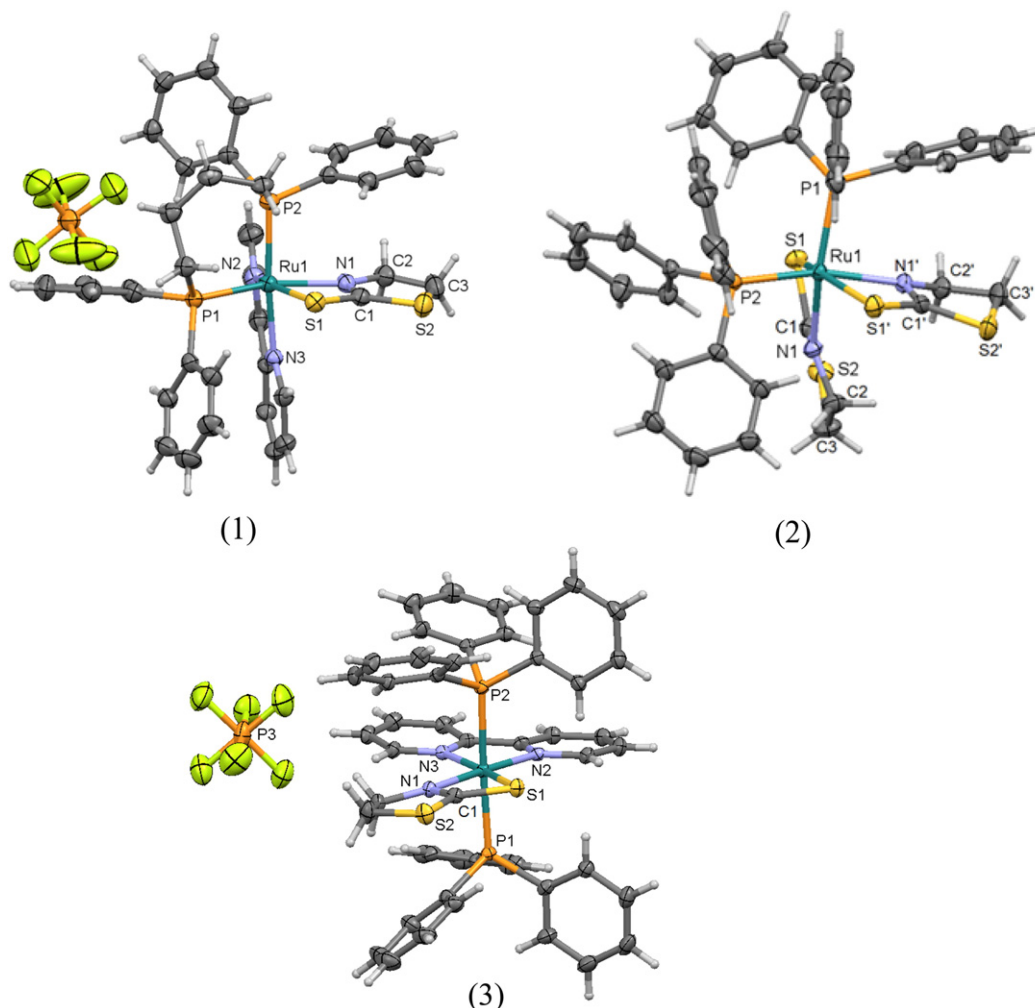


Fig. 3. Crystal structures of complexes **1**, **2** and **3** with selected atoms labeled. Ellipsoids are represented at 30% of probability.

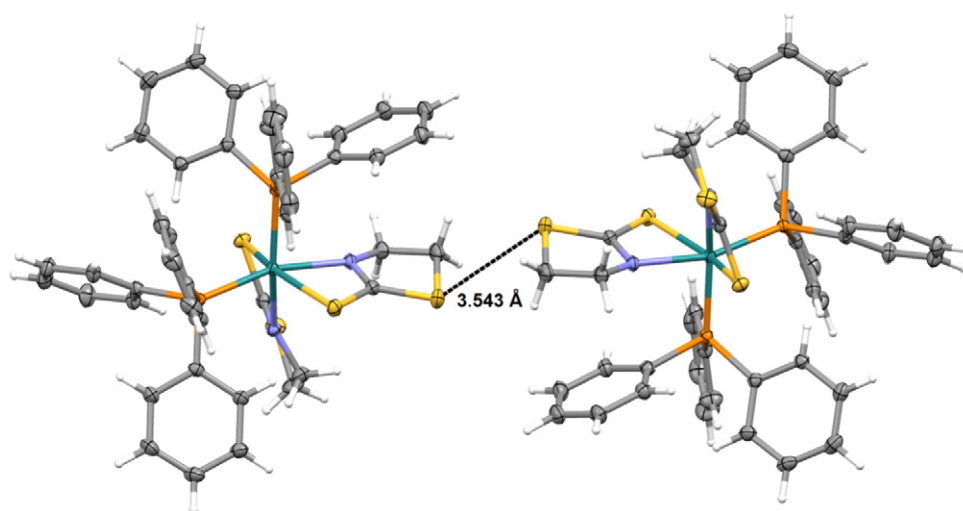


Fig. 4. Representation of S...S contact occurring in complex 2.

S...H (17.5%), C...C (0.8%), S...C (0.2%]). For complex **2**, the Hirshfeld surface analysis highlights the intermolecular contacts between S...S with contribution of 0.3%, which is absent in other complexes, this kind of contact can be seen in Fig. 4. The contribution to Hirshfeld surface in complex **3** [H...H (48.7%), C...H (19.0%), F...H (13.7%), S...H (6.3%), C...C (0.6%)] is similar to that observed in complex **1**. In all of them, the H...H contacts compose about 50% of the Hirshfeld surface, evidencing the importance of van der Waals forces to crystal packing stabilization.

3.5. Pharmacological evaluation

3.5.1. Cytotoxicity in cancer cells and ctDNA binding

In vitro cytotoxicity against DU-145 prostate and MCF-7 breast cancer cells was examined 48 h after incubation with drugs and the results were expressed by determining the IC_{50} values. Cisplatin was the reference cytotoxic drug. For comparison reason only, metal-free ligands tzdtH, dppb, bipy and PPh_3 were tested as well. The results are summarized in Table 2.

All the complexes displayed cytotoxicity against cancer cells, while none metal-free ligands were cytotoxic in concentrations up to 200 μM . These observations strongly suggests that Ru(II) associated with the ligands are responsible for the cytotoxicity in cancer

cells. Importantly, the Ru(II) complexes were more active than cisplatin. A comparison between the complexes revealed that compound **1** is potent against the two cancer cell lines, while **2** is more cytotoxic against breast than prostate cells. Complex **1** was particularly more potent against prostate cells, while compound **3** was against breast cells. Complex **2** was less active among the complexes.

Based on the cytotoxicity of these Ru(II) complexes against cancer cells, it was hypothesized that these complexes may interact with ctDNA. To verify this, the interaction with ctDNA was studied via spectroscopic titration (Fig. 5a). Under the presence of the Ru(II) complexes, a ctDNA hypochromism in the range of 29–35% was observed, which indicates that metal complexes form a ternary complex with ctDNA. In addition, the binding constant (K_b) were determined and the respective values found were: 1.0, 1.7 and $4.9 \times 10^3 M^{-1}$ for complexes **1**, **2** and **3**. These values indicate a weak interaction with ctDNA when compared to a classical ctDNA intercalator ethidium bromide ($K_b 10^6 M^{-1}$) [55]. Interestingly, complex **1** was the most active anticancer drug, but it presented lower ctDNA than complex **3**, which was less cytotoxic. Moreover, viscosity analysis of ctDNA-binding revealed that viscosity is not modified when the concentration of a Ru(II) complex increases. This supports the idea that ruthenium complexes have a weak

Table 2

Cytotoxicity and antitrypanosomal activities of complexes **1–3**, metal-free tzdtH and reference drugs.

Compounds	$IC_{50} \pm S.E.M.$ (μM)			J774 macrophages, $CC_{50} \pm S.E.M.$ (μM) ^c	SI ^d
	DU-145 ^a	MCF-7 ^a	<i>T. cruzi</i> trypomastigotes ^b		
tzdtH	>200	>200	>10	>10	–
1	0.3 ± 0.2	1.1 ± 0.9	0.23 ± 0.09	1.0 ± 0.16	3.7
2	4.9 ± 0.2	0.98 ± 0.2	>10	>10	–
3	0.9 ± 0.9	3.3 ± 1.3	0.010 ± 0.001	0.34 ± 0.3	34
Cisplatin	2.0 ± 0.5	8.9 ± 2.6	–	–	–
Benzimidazole	–	–	10.6 ± 0.8	–	–
Gentian violet	–	–	–	0.82 ± 0.1	–
Dppb	>200	>200	–	–	–
PPh_3	180.1 ± 1.6	>200	–	–	–
Bipy	>200	>200	–	–	–

IC_{50} = inhibitory concentration to 50%; and CC_{50} = cytotoxic concentration to 50%. SI = selectivity index. IC_{50} and CC_{50} values were determined from at least two independent experiments using concentration in triplicate.

^a Determined in cancer cells after 48 h incubation with drugs.

^b Determined in Y strain of *T. cruzi* trypomastigotes after 24 h incubation.

^c Determined in J774 macrophage cell lines after 72 h incubation.

^d SI determined as $(CC_{50} \text{ macrophages}) / (IC_{50} T. cruzi)$.

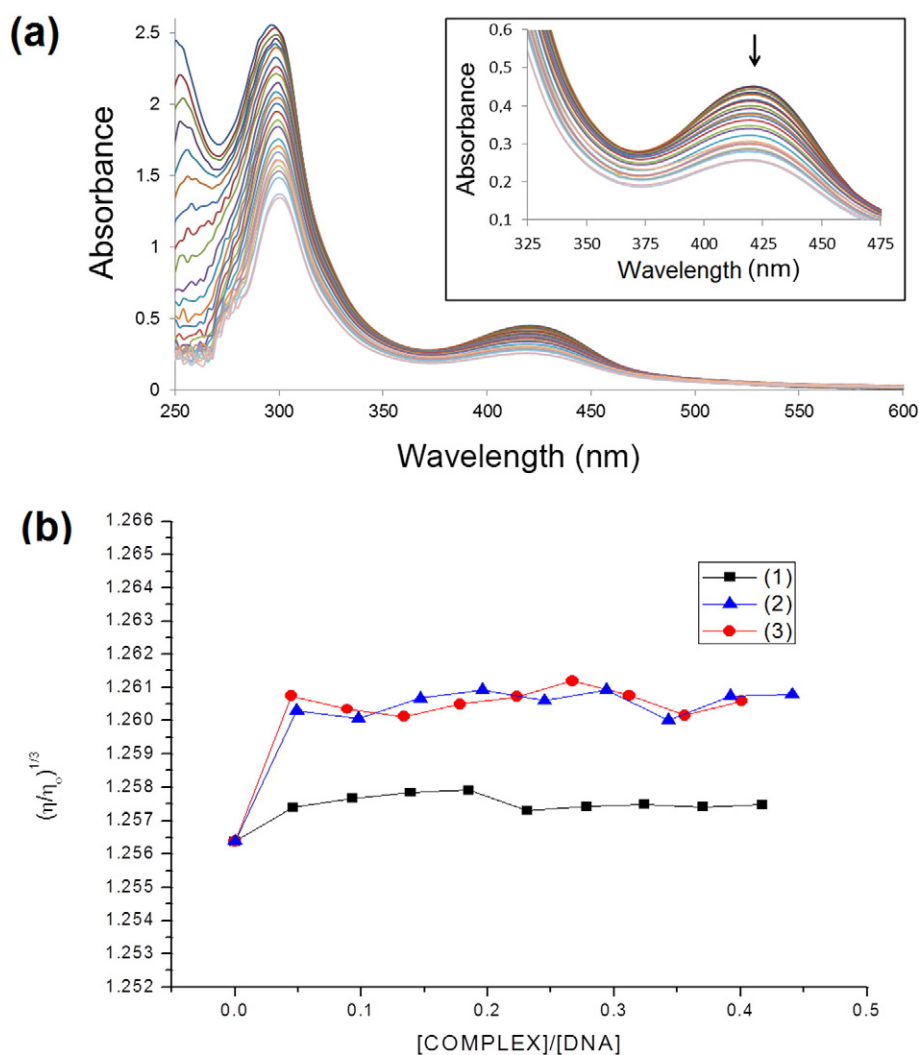


Fig. 5. (a) Electronic absorption spectra of complex **1** at a concentration of 1.6×10^{-4} M, showing the changes when concentration of ctDNA is increased (ranging from 3.8×10^{-5} to 7.6×10^{-4} M). ctDNA has no absorption at $\lambda > 325$ nm. (b) Viscosity of ctDNA $(\eta/\eta_0)^{1/3}$ in the presence of complexes **1–3** at increasing amounts. Experiments carried out at 298 K, in a Tris–HCl buffer, pH 7.4.

interaction, possibly by an electrostatic mode [56]. A plausible interpretation for this observation is that the binding of Ru(II) complexes to ctDNA is not via intercalation, due to the absence of planar ligands.

3.5.2. Antiparasitic activity

The antiparasitic evaluation against bloodstream trypomastigotes of *T. cruzi* parasite revealed that metal-free tzdtH and complex **2** have no activity in a concentration up to 10 μ M. In contrast, complexes **1** and **3**

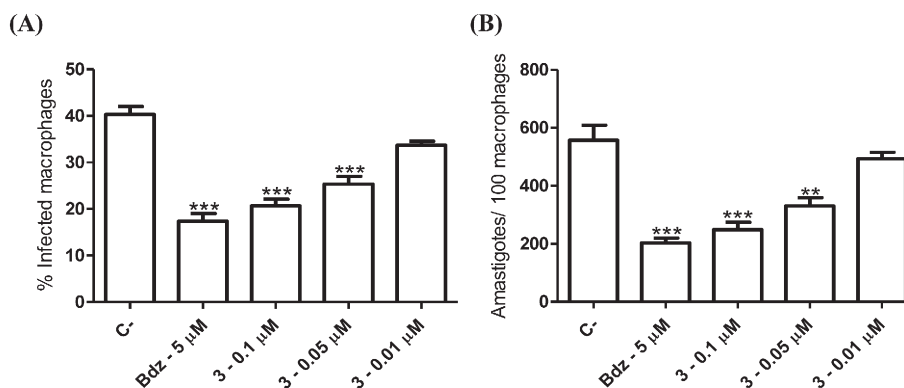


Fig. 6. Complex **3** inhibited *T. cruzi* amastigote proliferation in macrophages. Mouse peritoneal macrophages were infected with Y strain trypomastigotes for 2 h and treated with the complex (0.01, 0.05 or 0.1 μ M) or benznidazole (BdZ) (5 or 10 μ M). Cells were stained with hematoxylin and eosin and analyzed by optical microscopy. The percentage of infected macrophages (A) and the relative number of amastigotes per 100 macrophages (B) are higher in untreated infected controls than in cultures treated with the complex. (C–) is negative control. Values represent the mean \pm S.E.M. of triplicates. ** $P < 0.01$; and *** $P < 0.001$ compared to untreated cultures.

exhibited strong activity (Table 2). Complex **3** displayed the highest antiparasitic activity, being more potent than benznidazole, the reference antiparasitic drug. Additionally, complex **3** had little effect on J774 macrophage viability, therefore showing that the antiparasitic activity for this complex was achieved with great selectivity index. Regarding the structure–activity relationships, active antiparasitic complexes containing a bipy ligand were observed, while complex **2** lacking bipy was inactive. Therefore, these observations suggest that the presence of bipy as well as a positive charge present in the structures of complexes **1** and **3** contribute to antiparasitic activity.

3.5.3. Evaluation in *T. cruzi*-infected macrophages

After observing that complex **3** has potent and selective activity against the extracellular parasite, its antiparasitic activity against the intracellular form of *T. cruzi* was investigated (Fig. 6). In comparison to untreated infected macrophages, complex **3** treatment reduced the percentage of infected macrophages. Moreover, this treatment reduced the mean number of amastigotes per 100 macrophages. Importantly, complex **3** at 0.1 μM has comparable antiparasitic activity to benznidazole, the positive control. Therefore, these results show that this complex has antiparasitic activity against the intracellular and proliferative amastigote form. Since amastigote proliferation is pivotal within parasite cell cycle, it is plausible that these compounds impair the parasite cell cycle development inside host cells.

Given this strong antiparasitic activity, it was investigated whether the Ru(II) complexes have enhanced activity in drug combination with benznidazole. As shown in Fig. 7, drug combination of benznidazole at 5 μM plus complex **3** at 0.05 μM reduced the percentage of infected macrophages as well as the number of amastigotes more than each drug alone (Fig. 7, panels A, B). Importantly, the drug

combination displayed stronger activity than benznidazole alone at a high concentration (10 μM). When the concentration of complex **3** was increased at 0.1 μM and added in combination to benznidazole at 5 μM , in practice no intracellular parasites were observed (Fig. 7, panels C, D). These results indicate that drug combination of benznidazole and complex **3** has enhanced antiparasitic activity.

3.5.4. Parasite cell death

After ascertaining the antiparasitic activity of complex **3**, it was investigated how this complex causes parasite cell death. In comparison to untreated trypomastigotes (Fig. 8, panel A), complex **3** treatment lead to single PI staining and double PI + annexin V staining, which are characteristics of necrosis and late apoptosis, respectively. As observed by comparing panels B–D, complex **3** causes cell death in a concentration-dependent manner. Therefore, the Ru complex causes parasite cell death mainly by inducing necrosis.

4. Conclusions

Here we demonstrated the great chemical versatility of tzdtH, which is able to react with phosphine-, diamine- and phosphine/diamine-Ru precursors. The X-ray crystallography analyses revealed the exact structures of the complexes $[\text{Ru}(\text{tzdt})(\text{bipy})(\text{dppb})]\text{PF}_6$ (**1**), $\text{cis-}[\text{Ru}(\text{tzdt})_2(\text{PPh}_3)_2]$ (**2**) and $\text{trans-}[\text{Ru}(\text{tzdt})(\text{PPh}_3)_2(\text{bipy})]\text{PF}_6$ (**3**) and highlighted that the tzdt heterocyclic ring can assume a planar or twisted conformation under metal coordination. The electrochemical profile of these Ru complexes pointed out that tzdt provided resistance toward oxidation than the precursor complexes. These complexes exhibited strong anticancer and antiparasitic activity, while the metal-free tzdtH do not provoke the same outcome. Regarding the anticancer activity,

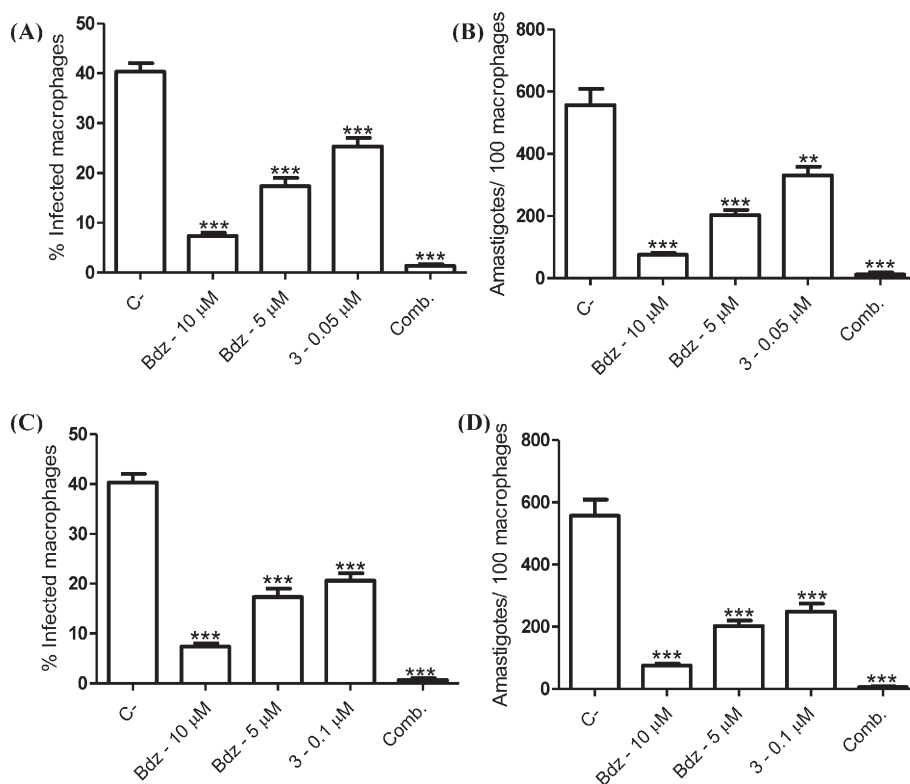


Fig. 7. Combination of complex **3** and benznidazole (Bdz) is more potent to inhibit *T. cruzi* amastigote proliferation in macrophages than each compound used alone. Mouse peritoneal macrophages were infected with Y strain trypomastigotes for 2 h and treated with complex **3** (0.05 or 0.1 μM) alone or in combination with benznidazole at (5.0 μM). Cells were stained with hematoxylin and eosin and analyzed by optical microscopy. (A and B) Combination of 0.05 μM of complex **3** plus 5 μM of benznidazole. (C and D) Combination of 0.1 μM of complex **3** plus 5 μM of benznidazole. (C –) is negative control. Values represent the mean \pm S.E.M. of triplicates. *** P < 0.001 compared to untreated cultures.

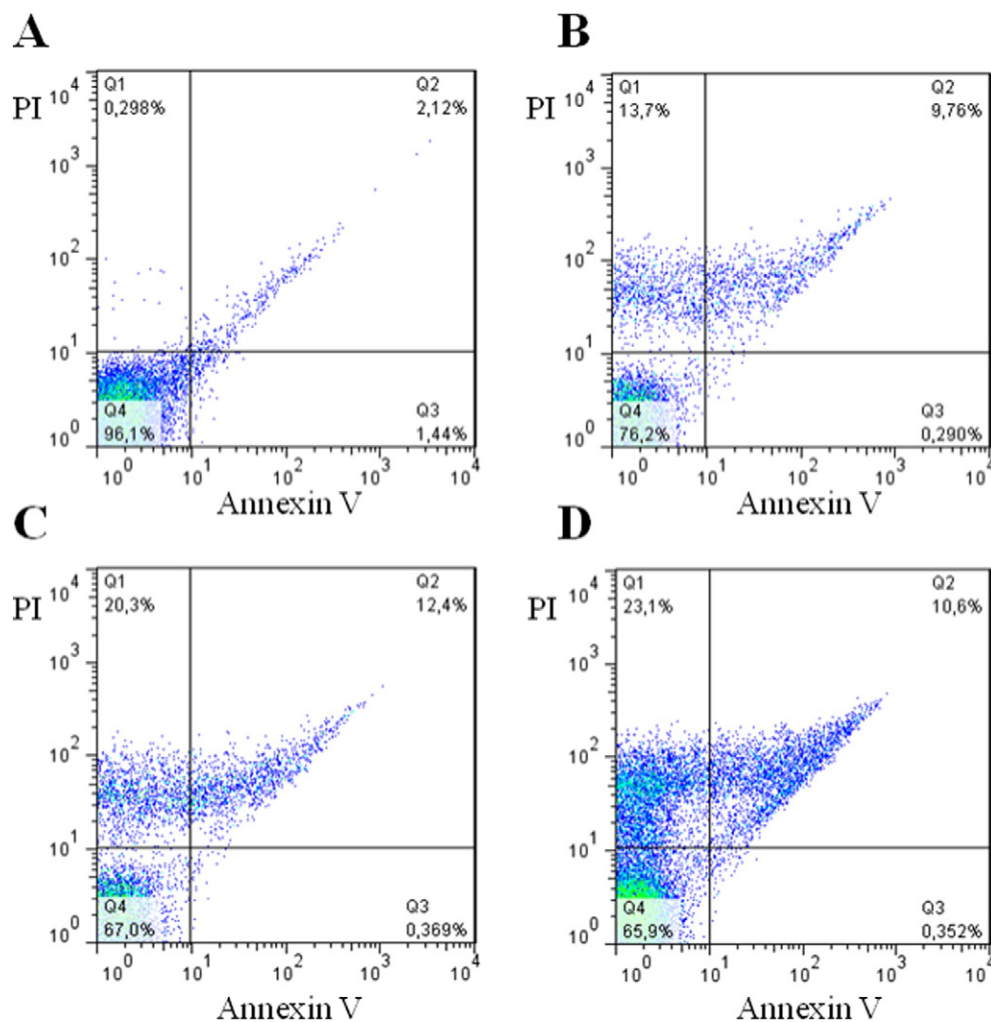


Fig. 8. Cell death analysis under complex **3** treatment. Trypanostigotes were treated with the complex for 24 h. Parasites were examined by flow cytometry with annexin V and PI staining. Cells plotted in each quadrant represent the following: lower left, double negative; upper left, PI single positive; lower right, annexin V single positive; and upper right, PI and annexin V double positive. (A) Untreated; (B) complex at 0.01 μ M; (C) complex at 0.015 μ M; and (D) complex at 0.02 μ M.

the new complexes exhibited cytotoxicity against prostate and breast cancer cells. They were more potent than cisplatin and more cytotoxic for cancer than normal cells (macrophages), indicating a degree of selectivity. Regarding the antiparasitic activity against *T. cruzi*, these complexes exhibited a broad spectrum of action (extracellular, intracellular forms). Flow cytometry analysis revealed that complex **3** destroys parasite cells, indicating this is more likely a parasitocidal than a cytostatic drug. These complexes arrested the parasite cell cycle and strongly affected the intracellular development and ultimately caused irreversible parasite death through a necrotic process. An important aspect in the anticancer and antiparasitic therapy is the drug combination. Here it was observed that Ru(II) complexes exhibit enhanced antiparasitic activity when given in combination with the antiparasitic drug benznidazole. This points out that these complexes are suitable molecules for drug combination compositions.

Acknowledgments

We thank the Brazilian Agencies of Research: CNPq, CAPES, FAPESP and FAPESP (grant number 2012/06013-4). R.S.C. thanks FAPESP (Fundação de Amparo à Pesquisa do Estado de São Paulo) for a post-doctoral fellowship (grant numbers 2009/08131-1 and 2013/26559-4). C.S.M. is receiving a FAPESP (Fundação de Amparo à Pesquisa do Estado da Bahia) (Grant 0417/2012) scholarship. G.V.P. thanks FAPEMIG (Fundação de Amparo à Pesquisa do Estado de Minas Gerais) (Grant

APQ-04010-10). The authors acknowledge Dr. Marília I. F. Barbosa and Prof. Javier Ellena for the helpful discussions during the preparation of the manuscript.

Supplementary data

Coordinates and other crystallographic data have been deposited with the deposition codes CCDC 1037025, CCDC 1037026 and CCDC 1037027, for **1**, **2** and **3**, respectively. Copies of this information may be obtained from The Director, CCDC, 12 Union Road, Cambridge CB2 1EZ, UK, Fax: +44 1233 336,033, E-mail: deposit@ccdc.cam.ac.uk or www.ccdc.cam.ac.uk. Supplementary data to this article can be found online at <http://dx.doi.org/10.1016/j.jinorgbio.2015.12.024>.

References

- [1] B.L.D.M. Bruecher, G. Lyman, R. van Hillegersberg, R.E. Pollock, F. Lordick, H. Yang, T. Ushijima, K.G. Yeoh, T. Skricka, W. Polkowski, G. Wallner, V. Verwaal, A. Garofalo, D. D'Ugo, F. Roviello, H.U. Steinau, T.J. Wallace, M. Daumer, N. Mähle, T.J. Reid, M. Ducreux, Y. Kitagawa, A. Knuth, B. Zilberstein, S.R. Steele, I.S. Jamall, I.S. Jamall, *BMC Cancer* 14 (2014) 186.
- [2] K.C. Oeffinger, S.S. Baxi, D.N. Friedman, C.S. Moskowitz, *Semin. Oncol.* 40 (2013) 676–689.
- [3] J. Ferlay, E. Steliarova-Foucher, J. Lortet-Tieulent, S. Rosso, J.W.W. Coebergh, H. Comber, D. Forman, F. Bray, *Eur. J. Cancer* 49 (2013) 1374–1403.
- [4] N.J. Wheate, S. Walker, G.E. Craig, R. Oun, *Dalton Trans.* 39 (2010) 8113–8127.
- [5] S. Dasari, P.B. Tchounwou, *Eur. J. Pharmacol.* 740 (2014) 364–378.

- [6] J. Cetnar, G. Wilding, D. McNeel, N.K. LoConte, T.A. McFarland, J. Eickhoff, G. Liu, *Urol. Oncol.-Sem. Orig. Investig.* 31 (2013) 436–441.
- [7] K.D. Mjos, C. Orvig, *Chem. Rev.* 114 (2014) 4540–4563.
- [8] R.S. Correa, K.M.d. Oliveira, F.G. Delolo, A. Alvarez, R. Mocelo, A.M. Plutini, M.R. Cominetti, E.E. Castellano, A.A. Batista, *J. Inorg. Biochem.* 150 (2015) 63–71.
- [9] S. Pillozzi, L. Gasparoli, M. Stefanini, M. Ristori, M. D'Amico, E. Alessio, F. Scaletti, A. Beccchetti, A. Arcangeli, L. Messori, *Dalton Trans.* 43 (2014) 12150–12155.
- [10] R. Trondl, P. Heffeter, C.R. Kowol, M.A. Jakupc, W. Berger, B.K. Keppler, *Chem. Sci.* 5 (2014) 2925–2932.
- [11] C. Scolaro, A. Bergamo, L. Brescacin, R. Delfino, M. Cocchietto, G. Laurenczy, T.J. Geldbach, G. Sava, P.J. Dyson, *J. Med. Chem.* 48 (2005) 4161–4171.
- [12] C.G. Hartinger, N. Metzler-Nolte, P.J. Dyson, *Organometallics* 31 (2012) 5677–5685.
- [13] M.V. Babak, S.M. Meier, K.V.M. Huber, J. Reynisson, A.A. Legin, M.A. Jakupc, A. Roller, A. Stukalov, M. Gridling, K.L. Bennett, J. Colinge, W. Berger, P.J. Dyson, G. Superti-Furga, B.K. Keppler, C.G. Hartinger, *Chem. Sci.* 6 (2015) 2449–2456.
- [14] P.J. Hotez, D.H. Molyneux, A. Fenwick, J. Kumaresan, S.E. Sachs, J.D. Sachs, L. Savioli, *N. Engl. J. Med.* 357 (2007) 1018–1027.
- [15] I. Ribeiro, A.-M. Sevcik, F. Alves, G. Diap, R. Don, M.O. Harhay, S. Chang, B. Pecoul, *PLoS Negl. Trop. Dis.* 3 (2009).
- [16] J.A. Urbina, *Acta Trop.* 115 (2010) 55–68.
- [17] C.A. Morillo, J.A. Marin-Neto, A. Avezum, S. Sosa-Estani, A. Rassi-Jr, F. Rosas, E. Villena, R. Quiroz, R. Bonilla, C. Britto, F. Guhl, E. Velazquez, L. Bonilla, B. Meeks, P. Rao-Melacini, J. Pogue, A. Mattos, J. Lazdins, A. Rassi, S.J. Connolly, S. Yusuf, BENEFIT Investigators, *N. Engl. J. Med.* 373 (2015) 1295–1306.
- [18] M. Navarro, C. Gabbiani, L. Messori, D. Gambino, *Drug Discov. Today* 15 (2010) 1070–1078.
- [19] D. Gambino, *Coord. Chem. Rev.* 255 (2011) 2193–2203.
- [20] D.R. Moreira, A.C. Leite, R.R. dos Santos, M.B. Soares, *Curr. Drug Targets* 10 (2009) 212–231.
- [21] F.B. Nascimento, G. Von Poelhsitz, F.R. Pavan, D.N. Sato, C.Q.F. Leite, H.S. Selistre-de-Araújo, J. Ellena, E.E. Castellano, V.M. Deflon, A.A. Batista, *J. Inorg. Biochem.* 102 (2008) 1783–1789.
- [22] F.R. Pavan, G. Von Poelhsitz, M.I.F. Barbosa, S.R.A. Leite, A.A. Batista, J. Ellena, L.S. Sato, S.G. Franzblau, V. Moreno, D. Gambino, C.Q.F. Leite, *Eur. J. Med. Chem.* 46 (2011) 5099–5107.
- [23] E.R. dos Santos, M.A. Mondelli, L.V. Pozzi, R.S. Correa, H.S. Salistre-de-Araujo, F.R. Pavan, C.Q.F. Leite, J. Ellena, V.R.S. Malta, S.P. Machado, A.A. Batista, *Polyhedron* 51 (2013) 292–297.
- [24] F.R. Pavan, G. Von Poelhsitz, L.V.P. da Cunha, M.I.F. Barbosa, S.R.A. Leite, A.A. Batista, S.H. Cho, S.G. Franzblau, M.S. de Camargo, F.A. Resende, E.A. Varanda, C.Q.F. Leite, *PLoS One* 8 (2013).
- [25] M.A. Mondelli, A.E. Graminha, R.S. Correa, M.M. da Silva, A.P. Carnizello, G. Von Poelhsitz, J. Ellena, V.M. Deflon, G.F. Caramori, M.H. Torre, D.C. Tavares, A.A. Batista, *Polyhedron* 68 (2014) 312–318.
- [26] M.I.F. Barbosa, R.S. Corrêa, K.M.d. Oliveira, C. Rodrigues, J. Ellena, O.R. Nascimento, V.P.C. Rocha, F.R. Nonato, T.S. Macedo, J.M. Barbosa-Filho, M.B.P. Soares, A.A. Batista, *J. Inorg. Biochem.* 136 (2014) 33–39.
- [27] M.A.P. Almeida, F.B.d. Nascimento, A.E. Graminha, A.G. Ferreira, J. Ellena, F.M.d.S. Mello, A.P.d. Lima, E.d.P. Silveira-Lacerda, A.A. Batista, *Polyhedron* 81 (2014) 735–742.
- [28] R. Corona-Sanchez, R.A. Toscano, M. Carmen Ortega-Alfaro, C. Sandoval-Chavez, J.G. Lopez-Cortes, *Dalton Trans.* 42 (2013) 11992–12004.
- [29] L. Li, K. Du, Y. Wang, H. Jia, X. Hou, H. Chao, L. Ji, *Dalton Trans.* 42 (2013) 11576–11588.
- [30] E.S. Raper, R.E. Oughtred, I.W. Nowell, *Inorg. Chim. Acta Lett.* 77 (1983) L89–L93.
- [31] U.M. Rabie, M.H.M. Abou-El-Wafa, H. Nassar, *Spectrochim. Acta A* 78 (2011) 512–517.
- [32] C. Abbehausen, R.E.F. de Paiva, A.L.B. Formiga, P.P. Corbi, *Chem. Phys.* 408 (2012) 62–68.
- [33] E.S. Raper, J.R. Creighton, W. Clegg, L. Cucurull-Sanchez, M.N.S. Hill, P.D. Akrivos, *Inorg. Chim. Acta* 271 (1998) 57–64.
- [34] P.G. Jones, S. Friedrichs, *Acta Crystallogr. C* 62 (2006) (M623–M7).
- [35] D. Atzei, D. De Filippo, A. Rossi, M. Porcelli, *Spectrochim. Acta A* 57 (2001) 1073–1083.
- [36] W.S. Sheldrick, C. Landgrafe, *Inorg. Chim. Acta* 208 (1993) 145–151.
- [37] J.D.E.T. Wilton-Ely, M. Wang, D.M. Benoit, D.A. Tocher, *Eur. J. Inorg. Chem.* (2006) 3068–3078.
- [38] S.L. Queiroz, A.A. Batista, G. Oliva, M. Gambardella, R.H.A. Santos, K.S. MacFarlane, S.J. Rettig, B.R. James, *Inorg. Chim. Acta* 267 (1998) 209–221.
- [39] T.A. Stephens, G. Wilkinson, *J. Inorg. Nucl. Chem.* 28 (1966) 945–956.
- [40] A.A. Batista, M.O. Santiago, C.L. Donnici, I.S. Moreira, P.C. Healy, S.J. Berners-Price, S.L. Queiroz, *Polyhedron* 20 (2001) 2123–2128.
- [41] Enraf-Nonius, Collect, Nonius BV, Delft, The Netherlands (1997–2000).
- [42] Z. Otwinowski, W. Minor, *Macromolecular Crystallography, Part A*, Academic Press, New York, 1997.
- [43] P. Coppens, L. Leiserowitz, D. Rabinovich, *Acta Crystallogr.* 18 (1965) 1035–1038.
- [44] M.A. Spackman, D. Jayatilaka, *CrystEngComm* 11 (2009) 19–32.
- [45] J.J. McKinnon, M.A. Spackman, A.S. Mitchell, *Acta Crystallogr. B* 60 (2004) 627–668.
- [46] M.A. Spackman, J.J. McKinnon, *CrystEngComm* (2002) 378–392.
- [47] M.E. Reichmann, S.A. Rice, C.A. Thomas, P. Doty, *J. Am. Chem. Soc.* 76 (1954) 3047–3053.
- [48] J.D. McGhee, P.H.V. Hippel, *J. Mol. Biol.* 86 (1974) 469–489.
- [49] A. Wolfe, G.H. Shimer, T. Meehan, *Biochemistry* 26 (1987) 6392–6396.
- [50] K.S. MacFarlane, A.M. Joshi, S.J. Rettig, B.R. James, *Inorg. Chem.* 35 (1996) 7304–7310.
- [51] T.S. Lobana, P. Kaur, A. Castineiras, *J. Coord. Chem.* 58 (2005) 429–435.
- [52] M.O. Santiago, A.A. Batista, M.P. de Araujo, C.L. Donnici, I.D. Moreira, E.E. Castellano, J. Ellena, S. dos Santos, S.L. Queiroz, *Transit. Met. Chem.* 30 (2005) 170–175.
- [53] K. Wohnrath, A.A. Batista, A.G. Ferreira, J. Zukerman-Schpector, L.A.A. de Oliveira, E.E. Castellano, *Polyhedron* 17 (1998) 2013–2020.
- [54] R.S. Correa, S.A. Santana, R. Salloum, R.M. Silva, A.C. Doriguetto, *Acta Crystallogr. C* 62 (2006) (O115–O7).
- [55] M. Cory, D.D. McKee, J. Kagan, D.W. Henry, J.A. Miller, *J. Am. Chem. Soc.* 107 (1985) 2528–2536.
- [56] T.S. Kamachi, N. Chitrapriya, H. Lee, C.F. Fronczek, F.R. Fronczek, K. Natarajan, *Dalton Trans.* 41 (2012) 2066–2077.

ANEXO 8

ESPÍRITO-SANTO, R. F.; **MEIRA, C. S.**; COSTA, R. S.; FILHO, O. P. S.; EVANGELISTA, A. F.; TROSSINI, G. H. G.; FERREIRA, G. M.; VELOZO, E. S.; VILARREAL, C. F.; SOARES, M. B. P. The anti-inflammatory and immunomodulatory potential of braylin: Pharmacological properties and mechanisms by *in silico*, *in vitro* and *in vivo* approaches. PLOS One, v. 12, p. 0179174, 2017.

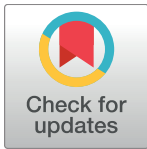
RESEARCH ARTICLE

The anti-inflammatory and immunomodulatory potential of braylin: Pharmacological properties and mechanisms by *in silico*, *in vitro* and *in vivo* approaches

Renan Fernandes Espirito-Santo¹, Cassio Santana Meira², Rafael dos Santos Costa¹, Otávio Passos Souza Filho¹, Afranio Ferreira Evangelista², Gustavo Henrique Goulart Trossini³, Glaucio Monteiro Ferreira³, Eudes da Silva Velozo¹, Cristiane Flora Villarreal^{1,2*}, Milena Botelho Pereira Soares^{2,4}

1 Faculdade de Farmácia, Universidade Federal da Bahia, Salvador, Bahia, Brazil, **2** Instituto Gonçalo Moniz, Fundação Oswaldo Cruz (FIOCRUZ), Salvador, Bahia, Brazil, **3** Faculdade de Ciências Farmacêuticas, Universidade São Paulo, São Paulo, São Paulo, Brazil, **4** Centro de Biotecnologia e Terapia Celular, Hospital São Rafael, Salvador, Bahia, Brazil

* cfv@ufba.br



OPEN ACCESS

Citation: Espirito-Santo RF, Meira CS, Costa RdS, Souza Filho OP, Evangelista AF, Trossini GHG, et al. (2017) The anti-inflammatory and immunomodulatory potential of braylin: Pharmacological properties and mechanisms by *in silico*, *in vitro* and *in vivo* approaches. PLoS ONE 12(6): e0179174. <https://doi.org/10.1371/journal.pone.0179174>

Editor: Zhengqi Wang, Emory University, UNITED STATES

Received: February 12, 2017

Accepted: May 24, 2017

Published: June 8, 2017

Copyright: © 2017 Espirito-Santo et al. This is an open access article distributed under the terms of the [Creative Commons Attribution License](https://creativecommons.org/licenses/by/4.0/), which permits unrestricted use, distribution, and reproduction in any medium, provided the original author and source are credited.

Data Availability Statement: All relevant data are within the paper and its Supporting Information files.

Funding: This work was supported by Fundação de Amparo à Pesquisa do Estado da Bahia — FAPESB, grant numbers: DTE 0046/2011 CFV, PNX0009/2009 MBPS. The funders had no role in study design, data collection and analysis, decision to publish, or preparation of the manuscript.

Abstract

Braylin belongs to the group of natural coumarins, a group of compounds with a wide range of pharmacological properties. Here we characterized the pharmacological properties of braylin *in vitro*, *in silico* and *in vivo* in models of inflammatory/immune responses. In *in vitro* assays, braylin exhibited concentration-dependent suppressive activity on activated macrophages. Braylin (10–40 μM) reduced the production of nitrite, IL-1β, TNF-α and IL-6 by J774 cells or peritoneal exudate macrophages stimulated with LPS and IFN-γ. Molecular docking calculations suggested that braylin present an interaction pose to act as a glucocorticoid receptor ligand. Corroborating this idea, the inhibitory effect of braylin on macrophages was prevented by RU486, a glucocorticoid receptor antagonist. Furthermore, treatment with braylin strongly reduced the NF-κB-dependent transcriptional activity on RAW 264.7 cells. Using the complete Freund's adjuvant (CFA)-induced paw inflammation model in mice, the pharmacological properties of braylin were demonstrated *in vivo*. Braylin (12.5–100 mg/kg) produced dose-related antinociceptive and antiedematogenic effects on CFA model. Braylin did not produce antinociception on the tail flick and hot plate tests in mice, suggesting that braylin-induced antinociception is not a centrally-mediated action. Braylin exhibited immunomodulatory properties on the CFA model, inhibiting the production of pro-inflammatory cytokines IL-1β, TNF-α and IL-6, while increased the anti-inflammatory cytokine TGF-β. Our results show, for the first time, anti-inflammatory, antinociceptive and immunomodulatory effects of braylin, which possibly act through the glucocorticoid receptor activation and by inhibition of the transcriptional activity of NF-κB. Because braylin is a phosphodiesterase-4 inhibitor, this coumarin could represent an ideal prototype of glucocorticoid receptor ligand, able to induce synergic immunomodulatory effects.

Competing interests: The authors have declared that no competing interests exist.

Introduction

Immune-mediated disorders, such as rheumatoid arthritis, Crohn's disease, asthma and ulcerative colitis, are a group of diseases associated with inflammatory pathogenetic mechanisms that involve an inappropriate or excessive immune response [1]. They affect approximately 5–7 percent of the population in Western countries [2,3]. The immune dysregulation causes inflammatory injury in various organs, resulting in morbidity, reduced quality of life and premature death [3]. The ideal drug to treat immune-mediated inflammatory disorders needs to establish early control of inflammation, preventing the tissue damage, parallel to a favorable profile of adverse effects. Currently, the available anti-inflammatory drugs do not meet these requirements, often displaying more adverse effects than is acceptable, less therapeutic effects than desirable, or both.

Natural products have been considered a plentiful source in the search for new chemical entities that modulate the immune system with reduced adverse effects. Plant secondary metabolites are important for flavoring of food, resistance against pests and as drugs, including substances with immunosuppressive activity [4]. Coumarins, a group of plant-derived polyphenolic compounds, have attracted intense interest in recent years due to their diverse and potent pharmacological properties. The structural characteristic of coumarins depicts a framework consisting of fused benzene and α -pyrone ring systems [5]. This type of special benzo-pyrone structure enables its derivatives to exert noncovalent interactions with various active sites in organisms, such as enzymes and receptors, and thus display a wide range of biological activities [6]. In fact, these compounds have been considered to possess wide potential as medicinal drugs and have served as valuable leads for further design and synthesis of more active analogues.

Among the multiple pharmacological properties of coumarins, their potent anti-inflammatory activity has been evidenced [7]. The anti-inflammatory properties of coumarin are associated with several mechanisms, including reduction of inflammatory molecules expression, inhibition of cyclooxygenase and lipoxygenase enzymes and inhibition of nuclear translocation of the transcription factor κ B, NF- κ B [7–10]. Braylin (Fig 1) is a coumarin first described in 1949, with limited data on their pharmacological properties already described [11]. Recently, Lin et al. showed that braylin presents potent phosphodiesterase-4 (PDE4) inhibitory activity [12]. Phosphodiesterases are enzymes that regulate the cellular levels of the second messengers cAMP and cGMP, by controlling their rates of degradation [13]. PDE4 is the predominant cyclic AMP degrading enzyme in a variety of inflammatory cells, and its inhibition elevates intracellular cAMP, which in turn down-regulates the inflammatory response [14,15]. Thus, this enzyme has been identified as a therapeutic target of high interest for immune-mediated inflammatory diseases [15–18]. Therefore, the present study was designed to evaluate whether braylin presents anti-inflammatory and immunomodulatory properties. Using *in vitro*, *in silico* and *in vivo* assays, we show here the pharmacological properties of braylin, including its possible mechanisms of action.

Materials and Methods

Extraction and isolation of braylin

Braylin was isolated from the roots of *Zanthoxylum tingoassuiba* A. St. Hil (Rutaceae) collected in August 2009 in Feira de Santana, Brazil, 12° 12' 52.9" S, 38° 52' 44.1" W. A voucher specimen (n°. 88005) has been identified and deposited at the Herbarium Alexandre Leal Costa (ALCB) of the Federal University of Bahia, Brazil. Braylin (837 mg) was isolated from the root bark (76.423 g) of *Zanthoxylum tingoassuiba* as a yellow amorphous solid and was identified by

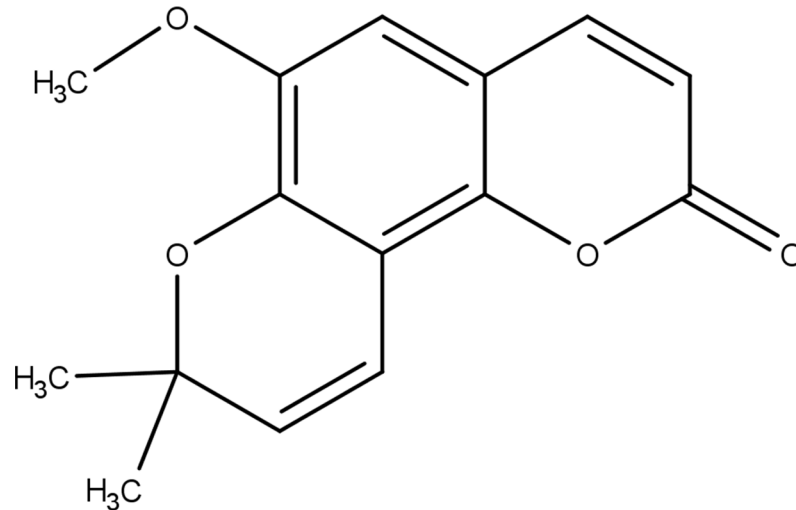


Fig 1. Chemical structure of braylin.

<https://doi.org/10.1371/journal.pone.0179174.g001>

spectroscopic data comparison according to literature procedures [19]. ^1H (500 MHz) and ^{13}C (125 MHz) NMR spectra were acquired at room temperature on a VARIAN Inova-500 spectrometer, with CD_3OD as solvent (S1 Table). The HPLC/MS analysis was obtained with a HPLC Shimadzu 20A with Bruker micrO-TOF II spectrometer, using (N_2) 10 eV for MS and 45 eV for MS/MS, in positive ionization mode with a Phenomenex Luna C_{18} column (4.6×250 mm, $5 \mu\text{m}$ particle size, $0.6 \text{ mL}\cdot\text{min}^{-1}$ oven at 35°C) (S1 Fig). Analytical HPLC analysis was carried out on a Shimadzu Prominence LC-6A instrument with Kromasil® C_{18} column (4.6×250 mm, 100A $5 \mu\text{m}$ particle size, $0.6 \text{ mL}\cdot\text{min}^{-1}$) and guard column (4.6×20 mm, $5 \mu\text{m}$ particle size). All methods analyses were performed with isocratic flow of solvent A (MeOH) and solvent B (H_2O) in proportion 50:50. HPLC eluates were monitored using UV detection at wavelengths of 254 nm. All solvents used were of analytical grade (Merck, Kenilworth, NJ, USA). The percent purity of braylin used in the pharmacological experiments carried out was greater than 98%, as determined by HPLC.

Chemicals and drugs

Dexamethasone, antagonist of glucocorticoid receptor R486, complete Freund's adjuvant (CFA), phosphate buffered saline (PBS), Tween 20, phenylmethylsulphonyl fluoride (PMSF), benzamethonium chloride, EDTA, aprotinin A, Dulbecco's Modified Eagle's Medium (DMEM), and 3,3',5,5'-tetramethylbenzidine (TMB) were obtained from Sigma Chemical Company (St. Louis, MO, USA). Diazepam and morphine were obtained from Cristália (Itapira, SP, Brazil). Dexamethasone was dissolved in ethanol (10% in normal saline). Braylin was dissolved in 50% propylene glycol plus saline, and remaining substances were dissolved directly in saline. Drugs were administrated by intraperitoneal (ip) route 40 minutes before testing, and the control group only received vehicle.

Peritoneal exudate macrophages cultures

Peritoneal exudate cells were obtained by washing, with cold saline, the peritoneal cavity of mice 5 days after injection of 3% thioglycolate in saline (1.5 mL per mouse). Cells were washed twice with DMEM, resuspended in DMEM supplemented with 10% fetal bovine serum (Cultilab, Campinas, Brazil) and $50 \mu\text{g}/\text{mL}$ of gentamycin (Novafarma, Anápolis, Brazil), and plated

in 96-well tissue culture plates at 2×10^5 cells per 0.2 mL per well. After 2 hours of incubation at 37°C, non-adherent cells were removed by two washes with DMEM. Macrophages were then submitted to the protocol of cytotoxicity, cytokine and nitric oxide determinations, as described below.

Cytotoxicity to mammalian cells

To determine the cytotoxicity of braylin, murine macrophage-like cell line J774, kindly provided by Dr. Patricia S. T. Veras (Gonçalo Moniz Institute, Fiocruz/BA), Raw 264.7 Luc cells or peritoneal exudate macrophages were plated into 96-well plates at a cell density of 2×10^5 cells/well in Dulbecco's modified Eagle medium (DMEM; Life Technologies, GIBCO-BRL, Gaithersburg, MD, USA) supplemented with 10% fetal bovine serum (FBS; GIBCO), and 50 µg/mL of gentamycin (Novafarma, Anápolis, GO, Brazil) and incubated for 2 hours at 37°C and 5% CO₂. Braylin was added at four concentrations ranging from 10 to 80 µM in four replicates, and plates were incubated for 72 hours. Twenty µL/well of Alamar Blue (Invitrogen, Carlsbad, CA) was added to the plates during 12 hours. Colorimetric readings were performed at 570 and 600 nm. Gentian violet (Synth, São Paulo, Brazil) at 10 µM was used as positive control. Three independent experiments were performed.

Measurement of cytokine and nitric oxide concentrations on macrophages

For cytokine and nitric oxide (NO) determinations, J774 cells or peritoneal exudate macrophages were seeded in 96-well tissue culture plates at 2×10^5 cells/well in DMEM medium supplemented with 10% of FBS and 50 µg/mL of gentamycin for 2 hours at 37°C and 5% CO₂. Cells were then stimulated with LPS (500 ng/mL, Sigma) and IFN-γ (5 ng/mL; Sigma) in the presence of braylin, vehicle or dexamethasone at different concentrations, and incubated at 37°C. Cell-free supernatants were collected 4 hours (for TNF-α measurement) and 24 hours (for IL-1β, IL-6 and nitrite quantification) and kept at -80°C. Cytokine concentrations in supernatants from macrophage cultures were determined by enzyme-linked immunosorbent assay (ELISA), using the DuoSet kit from R&D Systems (Minneapolis, MN, USA), according to the manufacturer's instructions. For the antagonism assay, the glucocorticoid receptor antagonist RU486 was added in some cultures at a final concentration of 10 µM. Quantification of nitric oxide was done using the Griess method [20].

NF-κB luciferase assay

The murine mouse leukemic monocyte macrophage cell line Raw 264.7 Luc cells bearing the pBIIX-luciferase (pBIIX-luc) targeting vector containing the firefly luciferase gene (luc) driven by two NF-κB binding sites from the kappa light chain enhancer in front of a minimal fos promoter [21] was kindly provided by Maria Célia Jamur (University of São Paulo, Ribeirão Preto, Brazil). Cells were cultured in RPMI medium (Sigma) supplemented with 20% FBS and 50 µg/mL of gentamycin at 37°C in a humidified environment containing 5% CO₂. For luciferase reporter assays, 5×10^5 cells/ml were pretreated with different concentrations of braylin (40, 20 or 10 µM) for 1 hour prior to stimulated with LPS (500 ng/mL) and IFN-γ (5 ng/mL) for 3 hours. Then each well was washed with cold-PBS and cells were incubated with TNT lysis buffer (200 mM Tris, pH 8.0, 200 mM NaCl, 1% Triton X-100) for 20 minutes at 4°C. The luciferase activity in the cell lysates was determined using the Luciferase Assay System (Promega, Madison, WI, USA). The samples were analyzed in a Globomax 20/20 luminometer (Promega). Data were then expressed as relative light units.

Molecular docking

Molecular docking and scoring protocols were used as implemented in GOLD version 5.2 (CCDC, Cambridge, UK) [22] to investigate the possible ligand binding conformations within the glucocorticoid receptor (GR) binding pocket. X-ray crystallographic data for GR complexed with R486 group 2.3 A (PDB ID 1NHZ) used in the docking simulations were retrieved from the Protein Data Bank (PDB). The ligand and water molecules were removed from the binding pocket and hydrogen atoms were added in standard geometry using the Biopolymer module implemented in SYBYL 2.0 (Sybyl x 2.1. Tripos, 2010). The residues within the binding sites were manually checked for possible flipped orientation, protonation, and tautomeric states with Pymol 1.3 (Delano Scientific, San Carlos, USA) side-chain wizard script. The binding sites were defined as all the amino acid residues encompassed within a 10.0 Å radius sphere centered on catalytic. Docking method was validated by redocking of the GR structure to crystal structure (PDB: 1NHZ) with R486.

Animals

Experiments were performed on male Swiss Webster mice obtained from the Animal Facilities at the Instituto Gonçalo Moniz (FIOCRUZ; Salvador, Brazil). Animals (22–28 g) were housed in temperature-controlled rooms (22–25°C), under a 12:12 hours light-dark cycle, with access to water and food ad libitum until experimental initiation. All behavioral tests were performed between 8:00 a.m. and 5:00 p.m., and animals were only used once. Animal care and handling procedures were in strict accordance with the recommendations in the Guide for the Care and Use of Laboratory Animals of the National Institutes of Health and Brazilian College of Animal Experimentation. The protocol was approved by the Institutional Animal Care and Use Committee, Ethics Committee for Animal Experimentation of FIOCRUZ (CEUA/FIOCRUZ. Permit Number: L-IGM-015/2013). Every effort was made to minimize the number of animals used and any discomfort. Behavioral tests were performed without knowing to which experimental group each mouse belonged. Results shown are from two independent experiments performed.

Inflammatory model

Mice were lightly anesthetized with halothane and received 20 µL of complete Freund's adjuvant (CFA 1 mg/mL of heat killed *Mycobacterium tuberculosis* in 85% paraffin oil and 15% mannideimonoleate; Sigma) in the plantar region of the right hind paw, according to a previously reported method [23]. Inflammatory hyperalgesia, edema, and local cytokines levels were measured by von Frey filaments, plethysmometer and ELISA, respectively, as described below. Mice were injected with braylin (12.5 to 100 mg/kg), vehicle (50% propylene glycol in physiological saline; control group) or dexamethasone (2 mg/kg, reference drug) by ip route 40 minutes before CFA.

Inflammatory hyperalgesia evaluation

The threshold to mechanical stimulation was measured with von Frey filaments (Stoelting, Chicago, IL, USA). In a quiet room, mice were placed in acrylic cages (12×10×17 cm) with wire grid floors, 30 minutes before the beginning of the test. This consisted of evoking a hind paw flexion reflex with one of a series of filaments with logarithmically incremental stiffness (0.0045–28.84 g). A positive response was characterized by the removal of the paw followed by clear flinching movements. A tilted mirror placed under the grid provided a clear view of the

hind paws of the mice. An up-down method was used to record the threshold, which was represented as the filament weight (g) in which the animal responds in 50% of presentations [24].

Plethysmometer test

The volume of each mouse paw was measured (mm^3) with a plethysmometer (Ugo Basile, Comerio, Italy) before (V_0) and after (V_T) the CFA injection, as described previously [23]. The amount of paw swelling was determined for each mouse and data were represented as paw volume variation (Δ , mm^3).

Cytokine measurement by ELISA

The paw levels of cytokines were determined as previously described [25]. Treatments were performed 40 minutes before the CFA injection. Skin tissues were removed from the paws 2, 4, 8 or 24 hours after CFA, in mice terminally anesthetized with halothane from each experimental group. Tissue proteins were extracted from 100 mg tissue/mL phosphate buffered saline (PBS) to which 0.4 M NaCl, 0.05% Tween 20 and protease inhibitors (0.1 mM PMSF, 0.1 mM benzethonium chloride, 10 mM EDTA, and 20 KI aprotinin A/100 ml) were added (Sigma). The samples were centrifuged for 10 minutes at 3000 g and the supernatant was frozen at -70°C for later quantification. Interleukin- 1β (IL- 1β), tumor necrosis factor α (TNF- α), interleukin-6 (IL-6), interleukin-13 (IL-13), interleukin-10 (IL-10) and transforming growth factor β (TGF- β) levels were estimated using commercially available immunoassay ELISA kits for mice (R&D System, Minneapolis, MN, USA), according to the manufacturer's instructions. The results are expressed as picograms of cytokine per milligram of protein.

Tail flick and hot plate tests

The tail flick test in mice was conducted as described elsewhere [26]. Before the experiment, each animal was habituated to the restraint cylinder for 20 minutes/day for 5 consecutive days. On the day of the experiment, mice were placed in the restraint cylinder and the tail tip (2 cm) was submersion in a water bath at $50 \pm 0.5^\circ\text{C}$. The latency of the tail withdrawal reflex was measured in seconds. Each submersion was terminated after 16 seconds to minimize potential skin damage. Tail flick latency was measured before (baseline) and after treatments. The hot plate test in mice was conducted as described elsewhere, with minor modifications [27]. On the experiment day, mice were placed on the equipment (TECA Corporation, Chicago, IL, USA), which was maintained at $52 \pm 0.5^\circ\text{C}$, and latencies to hind-paw licking or jumping (nociceptive thermal threshold) were recorded with a cut-off time of 16 s. The threshold was measured before (baseline) and after treatments.

Motor function assay

To evaluate possible non-specific muscle-relaxant or sedative effects of braylin, mice were submitted to the rota-rod test, as previously described [26]. The rota-rod apparatus (Insight, Ribeirão Preto, SP, Brazil) consisted of a bar with a diameter of 3 cm, subdivided into five compartments. The bar rotated at a constant speed of 6 revolutions per minute. The animals were selected 24 hours previously by eliminating those mice that did not remain on the bar for two consecutive periods of 120 s. Animals were treated and 40 minutes afterwards were placed on a rotating rod. The resistance to falling was measured for up to 120 s. The results are expressed as the average time (s) the animals remained on the rota-rod in each group. Diazepam (10 mg/kg) was the reference drug.

Statistical analysis

Data are presented as means \pm standard error of the means (SEM) of measurements made on 6–9 animals in each group. Comparisons between three or more treatments were made using one-way ANOVA with Tukey’s post-hoc test, or for repeated measures, two-way ANOVA with Bonferroni’s post-hoc test, as appropriate. All data were analyzed using Prism 5 Computer Software (GraphPad, San Diego, CA, USA). Statistical differences were considered to be significant at $p < 0.05$.

Results

Initially, the pharmacological effects of braylin were investigated on a set of *in vitro* assays. The effects of braylin on cell viability was determined by a colorimetric Alamar Blue assay 24 hours after treatment. As revealed in Fig 2, braylin at a concentration of 40 μM or lower did not induce cytotoxic effect on J774 cells or peritoneal exudate macrophages, stimulated with LPS

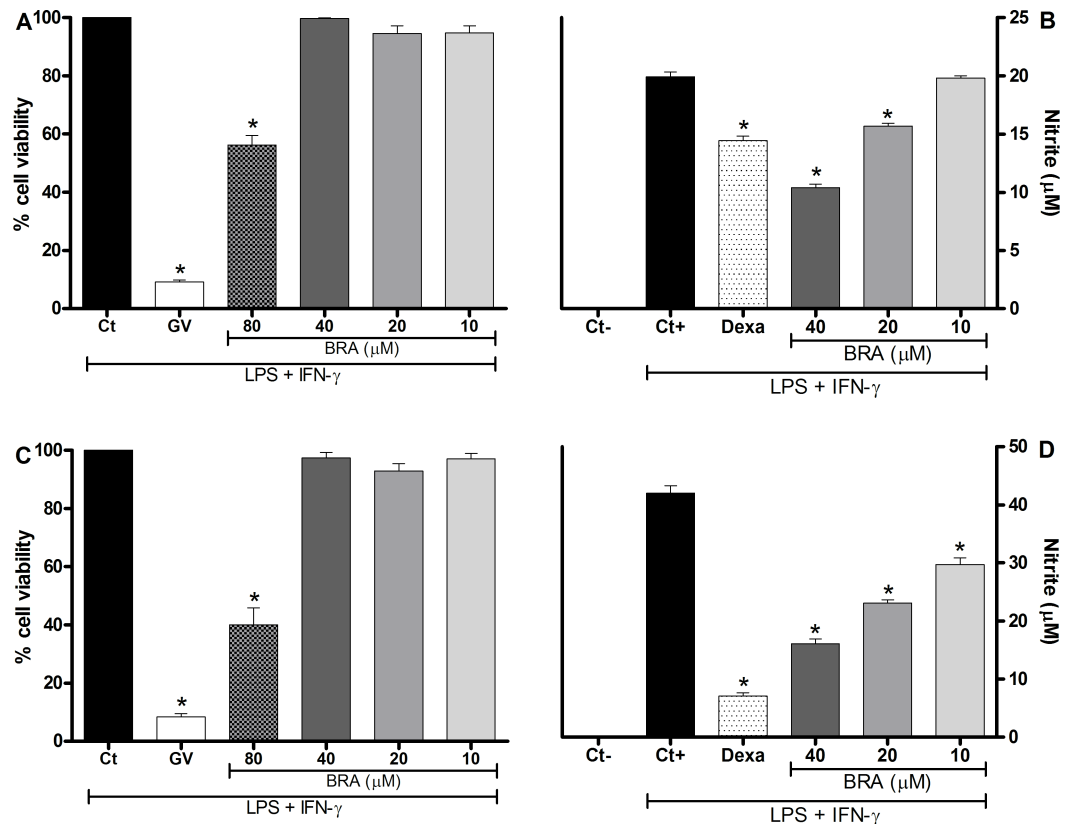


Fig 2. Cytotoxic effect of braylin and its modulation of nitric oxide production on macrophages. Panels A and C: J774 cells (A) or peritoneal exudate macrophages (C) were incubated with vehicle (50% propylene glycol in saline, Ct, control group) or different concentrations of braylin (BRA; 10, 20, 40 or 80 μM) for 72 hours and cell viability was determined by Alamar Blue assay. Gentian violet (GV) was used as positive control. Data are expressed as means \pm SEM; $n = 9$ determinations per group. *Significantly different from the vehicle treated cultures ($p < 0.05$). ANOVA followed by Tukey’s multiple comparison test. Panels B and D: Concentrations of nitrite were determined in J774 macrophages (B) or peritoneal exudate macrophages (D) treated with vehicle (50% propylene glycol in saline, Ct+, control group), braylin (BRA; 10, 20 or 40 μM) or dexamethasone (Dexa; 40 μM) in the presence of LPS (500 ng/mL) + IFN- γ (5 ng/mL). Cell-free supernatants were collected 24 hours after treatments for nitrite quantification by the Griess method. Ct- shows concentrations of nitrite in unstimulated cells. Data are expressed as means \pm SEM; $n = 9$ determinations per group. *Significantly different from the vehicle treated cultures stimulated with LPS + IFN- γ ($p < 0.05$). ANOVA followed by Tukey’s multiple comparison test.

<https://doi.org/10.1371/journal.pone.0179174.g002>

and IFN- γ . Therefore, subsequent experiments were performed with braylin at 40 μ M. The modulatory effects of braylin on macrophages were investigated through the quantification of the inflammatory mediators NO and cytokines, produced by activated macrophages. As shown in Fig 2B and 2D, braylin treatment reduced, in a concentration-dependent manner, the production of nitrite on macrophages stimulated with LPS and IFN- γ , suggesting a reduction of NO production. The inhibitory effect of braylin on J774 cells and peritoneal exudate macrophages was statistically significant until 20 and 10 μ M, respectively. Dexamethasone at 40 μ M reduced nitrite production.

Fig 3 shows that braylin treatment was able to reduce, in a concentration-dependent manner, the production of TNF- α , IL-1 β and IL-6 by macrophages stimulated with LPS and IFN- γ . Braylin reduced the production of TNF- α on J774 macrophages (Fig 3A) at concentrations of 20 and 40 μ M. The inhibitory effect of braylin on the TNF- α production by peritoneal exudate macrophages was statistically significant at 10, 20 and 40 μ M (Fig 3B). The braylin-induced reduction of IL-1 β (Fig 3C) and IL-6 (Fig 3E) production on J774 macrophages was statistically significant at 10, 20 and 40 μ M. In addition, braylin reduced the production of IL-1 β (Fig 3D) and IL-6 (Fig 3F) on peritoneal exudate macrophages at 20 and 40 μ M. Under the same conditions, dexamethasone (40 μ M) caused a similar reduction of TNF- α , IL-1 β and IL-6 production (Fig 3).

To assess the possible interactions of braylin in the binding pocket of glucocorticoid receptor (GR), docking studies were performed. The validation of the method showed a good superimposition between the crystal pose and the docked pose of RU486, a GR antagonist, suggesting that the docking method is sufficiently robust to determine the correct ligand poses in the active site of GR. The results were compared with docking poses of the antagonist RU486 and the agonist dexamethasone to suggest best fit interactions and supposed mechanism of action. The best poses obtained to RU486, braylin and dexamethasone in the glucocorticoid receptor (PDB: 1HNZ) are showed in Fig 4.

Based on docking studies RU486, dexamethasone and braylin, presented interactions on the same site of the GR. When the occupancy was analyzed, RU486 showed interactions in two different subpockets, which are promoted by groups prop-1-yne and N,N-dimethylaniline. Dexamethasone presented a different subpocket interaction, promoted by ketone group and terminal ring (A) of the molecule. On other hand, braylin occupies only the active site of GR. The analyses of the interaction residues suggested by docking have shown that RU486 presents three hydrogen bonds, with GLN 642, ARG 611 and GLN 570 (Fig 5A). For dexamethasone, the major interactions were observed in relation to dextrane group and two important hydrogen bonds with the carbonyl group of the TRY-735 and GLY-567 (Fig 5B). For braylin, the docking studies suggest the stabilization in the GR by hydrophobic interactions, hydrogen bond with GLY-567 like dexamethasone, and the PHE-623 promote a π -stack with aromatic ring (Fig 5C).

The possible antagonism of RU486 on the braylin-induced inhibitory effect in stimulated macrophage cultures was then evaluated. Addition of RU486 (10 μ M) to J774 macrophage cultures stimulated with LPS and IFN- γ partially prevented the inhibitory effect of braylin (40 μ M) on the TNF- α production (Fig 6A). As expected, in the presence of RU486, the inhibitory effect of dexamethasone (40 μ M) on the TNF- α production by macrophages was reduced.

Next the NF- κ B reporter system, in Raw 264.7 cells transfected with p-NF- κ B-Luc reporter plasmid, was used to evaluate the effect of braylin on NF- κ B activation. Initially, the effects of braylin on Raw 264.7 cell viability was determined. Braylin, at a concentration of 80 μ M or lower, did not induce cytotoxic effect on Raw 264.7 cells 72 hours after treatment (S3 Fig). As revealed in Fig 6B, macrophage cultures stimulated with LPS and IFN- γ showed high levels of NF- κ B dependent transcriptional activity. Treatment with braylin (10, 20 and 40 μ M)

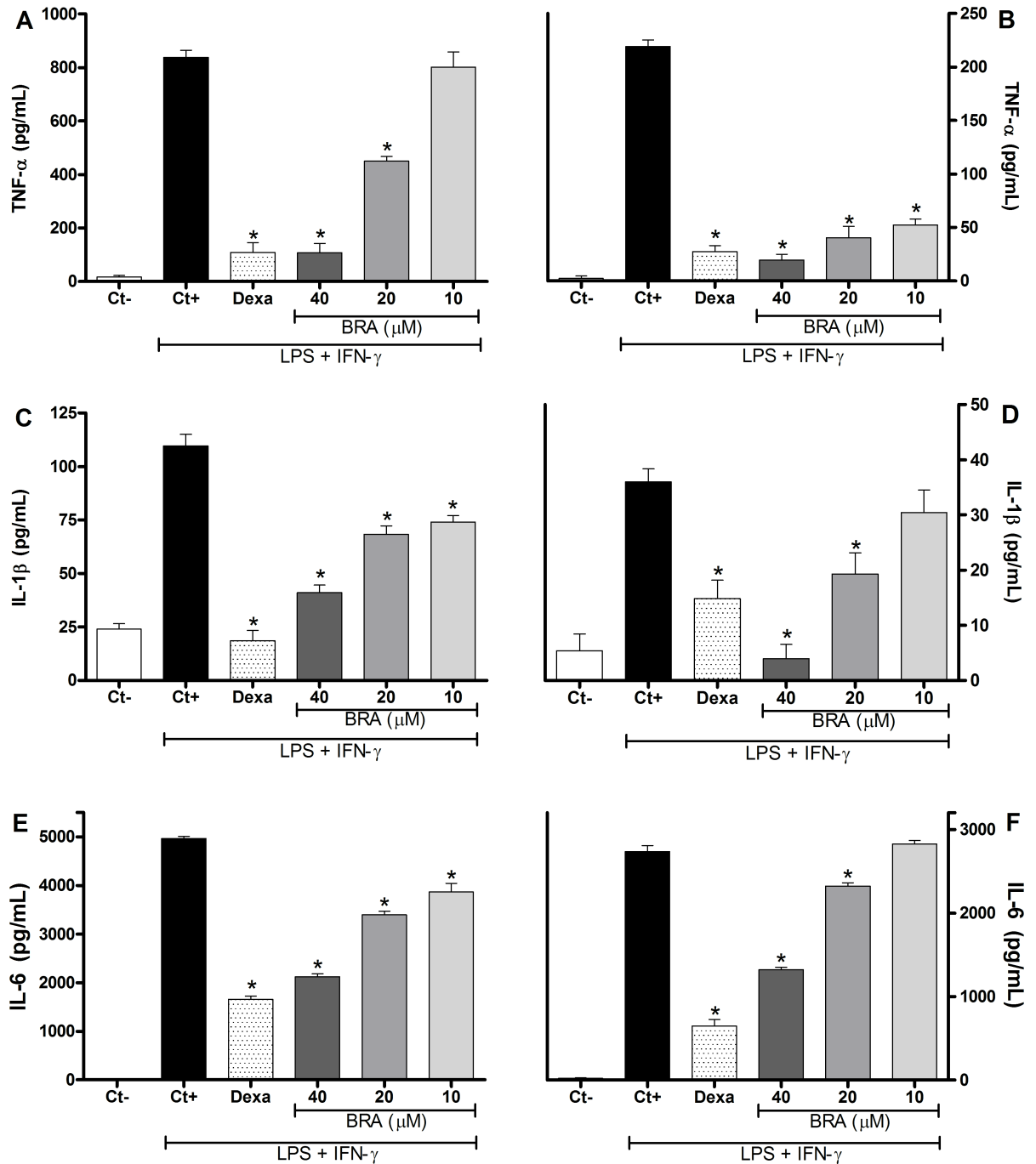


Fig 3. Effect of braylin on cytokine production by activated macrophages. Concentrations of TNF- α , IL-1 β and IL-6 were determined in cultures of J774 macrophages (panels A, C and E) or peritoneal exudate macrophages (panels B, D and F) treated with vehicle (50% propylene glycol in saline, Ct+, control group), braylin (BRA; 10, 20 or 40 μ M) or dexamethasone (Dexa; 40 μ M) in the presence of LPS (500 ng/mL) plus IFN- γ (5 ng/mL). Cell-free supernatants were collected 4 hours (for TNF- α measurement) and 24 hours (for IL-1 β and IL-6) after treatments for ELISA assay. Ct- shows cytokine concentrations in unstimulated cells. Data are expressed as means \pm SEM; $n = 10$ determinations per group. *Significantly different from the vehicle treated cultures stimulated with LPS + IFN- γ ($p < 0.05$). ANOVA followed by Tukey's multiple comparison test.

<https://doi.org/10.1371/journal.pone.0179174.g003>

dramatically reduced NF- κ B dependent transcriptional activity when compared with vehicle-treated cultures. Treatment with dexamethasone (40 μ M) also was able to reduce the NF- κ B

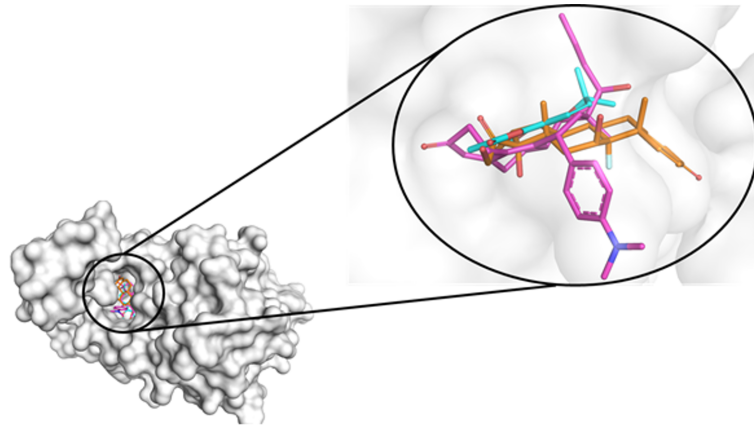


Fig 4. Best poses of the docking results to RU486 (pink), dexamethasone (orange) and braylin (cyan) superimposed in GR (pdb 1NHZ).

<https://doi.org/10.1371/journal.pone.0179174.g004>

dependent transcriptional activity, but the effect of braylin, at all tested concentrations, was higher than that of dexamethasone.

Based on the reliable results from the *in vitro* assays, the potential of braylin as an immunomodulatory agent was next evaluated on the CFA-induced paw inflammation model. The effects of braylin on inflammatory hyperalgesia, paw edema and local levels of cytokines was assessed. Administration of braylin (25–100 mg/kg) by ip route, 40 minutes before CFA, significantly reduced inflammatory hyperalgesia at 2, 4 and 8 hours after the stimulus (Fig 7A). The pre-treatment with braylin (12–100 mg/kg, ip) significantly reduced paw edema 2, 4 and 8 hours post-stimulus (Fig 7B). Supporting data from braylin, vehicle treatment (50% propylene glycol in saline) yielded no activity, while the reference drug, dexamethasone (2 mg/kg), inhibited CFA-induced hyperalgesia and edema. Braylin had a greater efficacy than dexamethasone, considering both hyperalgesia (Fig 7A) and edema (Fig 7B) signs; however, its effects were short-lasting.

The effects of braylin were also evaluated on the tail flick and hot plate tests, which mainly identify central analgesics. The ip administration of braylin (100 mg/kg) did not alter the latency time in the tail-flick (Fig 8A) and hot plate (Fig 8B) tests. The administration of morphine (5 mg/kg ip), the reference drug, resulted in a significant increase in the latency time at both, tail flick and hot plate tests (Fig 8). Moreover, relaxing or motor deficit effects were discarded, since administration of braylin (100 mg/kg, ip) did not affect the motor performance in mice on the rota-rod test (S4 Fig). As expected, diazepam (10 mg/kg ip), a central nervous

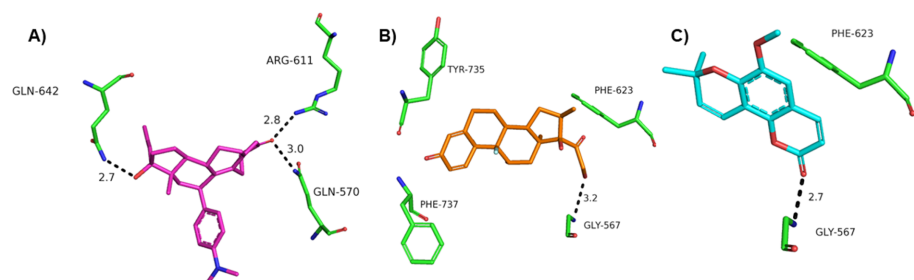


Fig 5. Docking solutions showing the main interactions for (A) RU486 (pink), (B) dexamethasone (orange) and (C) braylin (cyan) superimposed in GR (pdb 1NHZ).

<https://doi.org/10.1371/journal.pone.0179174.g005>

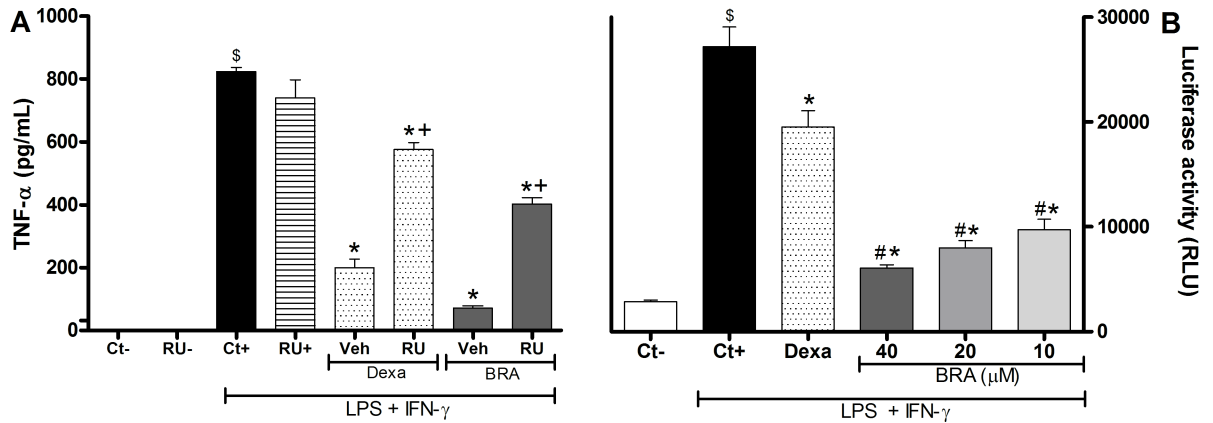


Fig 6. Involvement of glucocorticoid receptors and NF-κB dependent transcriptional activity in the immunomodulatory effect of braylin. Panel A shows data from glucocorticoid receptor antagonism assay. Concentrations of TNF-α were determined in J774 macrophages treated with vehicle (50% propylene glycol in saline, Ct+, control group), braylin (BRA, 40 μM), RU486 (GR antagonist, 10 μM) + braylin 40 μM, dexamethasone (Dexa; 40 μM) or RU486 (10 μM) + dexamethasone (40 μM) in the presence of LPS (500 ng/mL) and IFN-γ (5 ng/mL). Cell-free supernatants were collected 4 hours after treatments for TNF-α measurement by ELISA. Ct- and RU- show concentrations of TNF-α in unstimulated cells, treated with vehicle and RU486, respectively. Data are expressed as means ± SEM; n = 10 determinations per group. [§]Significantly different from the vehicle treated cultures unstimulated (p < 0.05); *Significantly different from the vehicle treated cultures stimulated with LPS + IFN-γ (p < 0.05). ⁺Significantly different from the group untreated with antagonist (p < 0.05). Panel B shows the effect of braylin on the activation of NF-κB on RAW 264.7 Luc macrophages. Cells were pretreated with vehicle (50% propylene glycol in saline, Ct+, control group), braylin (BRA; 10, 20 or 40 μM) or dexamethasone (Dexa; 40 μM) for 1 hour prior to stimulated with LPS (500 ng/mL) and IFN-γ (5 ng/mL) for 3 hours. Ct- shows luciferase activity in unstimulated cells. Luciferase activity was measured in a luminometer. [§]Significantly different from the vehicle treated cultures unstimulated (p < 0.05); *Significantly different from the vehicle treated cultures stimulated with LPS + IFN-γ (p < 0.05). [#]Significantly different from the Dexa group (p < 0.05). ANOVA followed by Tukey's multiple comparison test.

<https://doi.org/10.1371/journal.pone.0179174.g006>

system depressant used as standard drug, reduced the permanence time of mice on the rotarod (S4 Fig).

Considering the inhibitory effect of braylin on macrophage cells, its possible modulatory action on cytokine production during inflammation was evaluated. Data obtained by ELISA analyses shows that braylin (50 mg/kg) and dexamethasone (2 mg/kg) reduced the local levels of IL-1β (Fig 9A), TNF-α (Fig 9B) and IL-6 (Fig 9C) during CFA-induced paw inflammation. The inhibitory effects of braylin on TNF-α and IL-1β levels were statistically significant 2 and 4 hours after CFA, while on IL-6, a significant inhibition was seen 2 hours after stimulus. Dexamethasone reduced the IL-1β and TNF-α levels until 8 hours after stimulus, but the IL-6 level was reduced just until 4 hours. The modulatory effects of braylin on anti-inflammatory cytokines production were also investigated. Treatment with braylin (50 mg/kg) enhanced the paw levels of TGF-β (Fig 9F), while IL-13 (Fig 9D) and IL-10 (Fig 9E) were not modulated by this coumarin. Instead, dexamethasone enhanced IL-10, but not TGF-β or IL-13 concentrations.

Discussion

The present study demonstrated, for the first time, the consistent anti-inflammatory and immunomodulatory properties of braylin. Braylin exhibited low cytotoxicity and consistent suppressive activities on macrophages cultures. Braylin acts, at least in part, through activation of GR, since the GR antagonist RU486 prevented the *in vitro* effects of braylin. Docking data corroborated with this hypothesis. In addition, using the NF-κB luciferase assay, the treatment with braylin dramatically reduced the NF-κB dependent transcriptional activity on macrophages. Systemic administration of braylin inhibited *in vivo* events related to inflammation, namely hyperalgesia and edema. Furthermore, this coumarin induced evident immunomodulatory

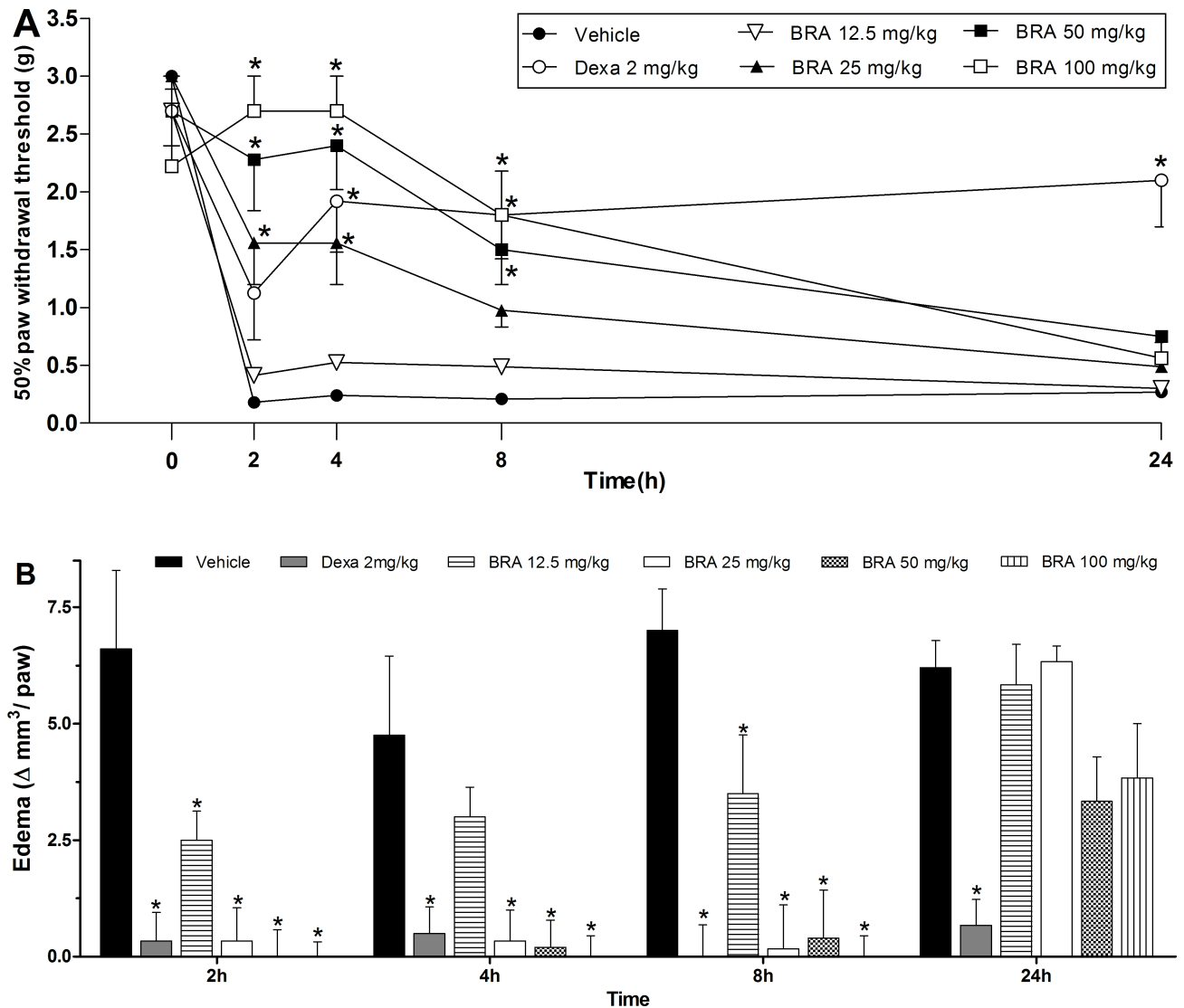


Fig 7. Effects of braylin on complete Freund's adjuvant (CFA)-induced paw inflammation. Mice were injected with braylin (BRA; 12.5–100 mg/kg), vehicle (50% propylene glycol in saline; control group) or dexamethasone (Dexa; 2 mg/kg; reference drug) by ip route 40 minutes before CFA (injected at time zero). (A) Inflammatory hyperalgesia measured at 2, 4, 8 and 24 hours after the CFA stimulus. The mechanical nociceptive threshold (axis of ordinates) is represented as the filament weight (g) in which the animal responds in 50% of presentations. (B) Paw edema measured at 2, 4, 8 and 24 hours after CFA, represented as paw volume variation. Data are expressed as means \pm SEM; $n = 6$ mice per group. * Significantly different from the control group ($p < 0.05$). Two-way ANOVA followed by the Bonferroni's test.

<https://doi.org/10.1371/journal.pone.0179174.g007>

property *in vivo* through the modulation of pro- and anti-inflammatory cytokines levels. These results describe the pharmacological properties of braylin, indicating this coumarin as a potential candidate to drug development.

Because macrophages play a central role in the immune regulation and inflammatory responses, the possible suppressive effect of braylin was initially evaluated on these cells. Activated macrophages release cytokines such as IL-1, IL-6, TNF- α , IL-10 and IL-18, that coordinate immune/inflammatory responses. They are activated by different signals, including inflammatory cytokines such as TNF- α , and deactivated by anti-inflammatory cytokines, such as TGF- β [28]. Activated macrophages are also capable of releasing high levels of NO, and this mediator has been implicated as a pro-inflammatory agent [29]. Braylin, at non-cytotoxic

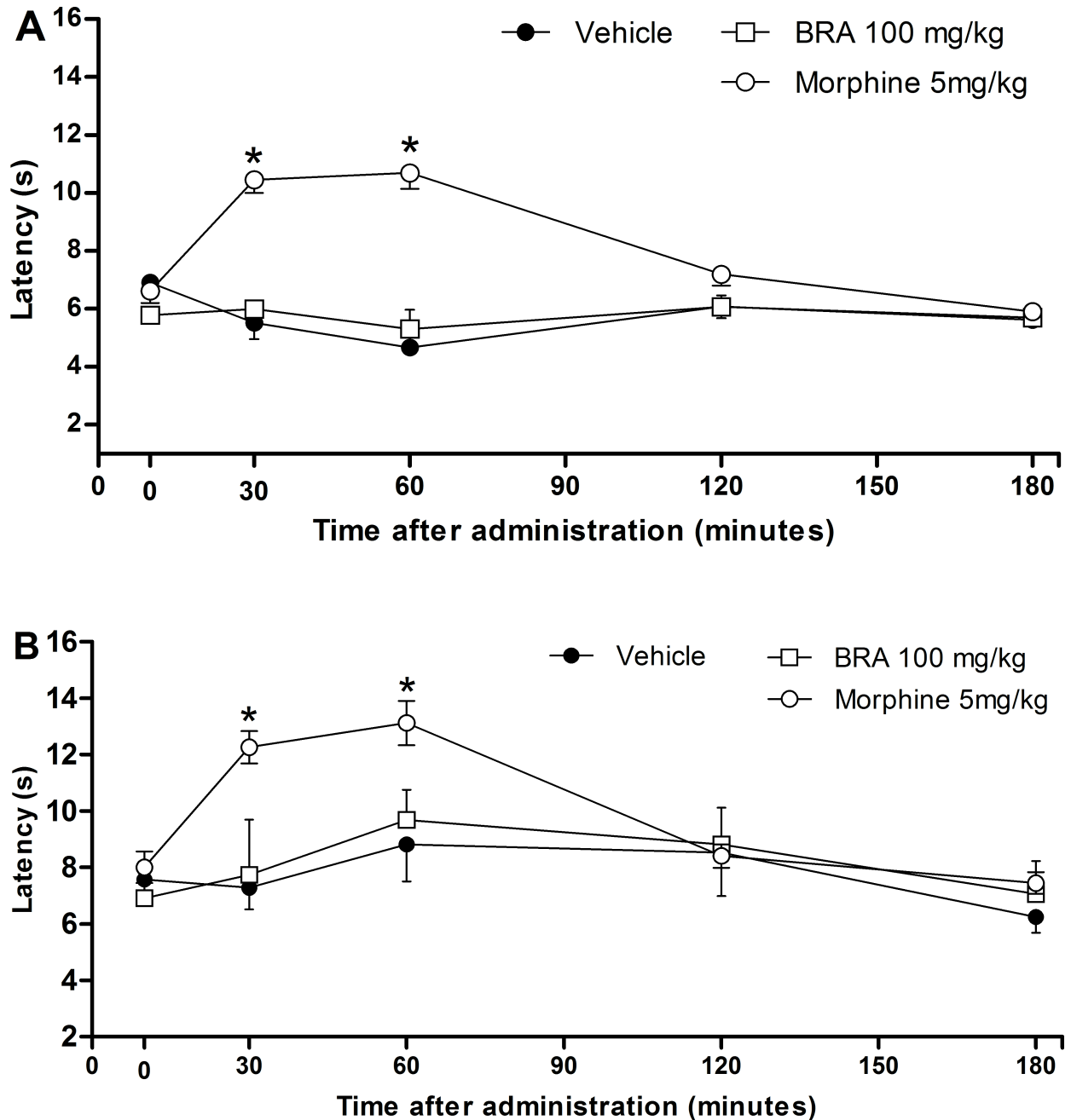


Fig 8. Effects of braylin on tail flick and hot plate tests in mice. Panels representing the latency in seconds in the tail flick (panel A) and hot plate (panel B) tests, after ip injection of braylin (BRA; 100 mg/kg), vehicle (50% propylene glycol in saline; control group) or morphine (5 mg/kg; reference drug). Data are reported as means \pm SEM; $n = 6$ mice per group. * Significantly different from the control group ($p < 0.05$). Two-way ANOVA followed by the Bonferroni's test.

<https://doi.org/10.1371/journal.pone.0179174.g008>

concentrations, reduced the production of nitrite, TNF- α , IL-1 β and IL-6 by stimulated macrophages in a concentration-dependent manner, suggesting the anti-inflammatory and immunomodulatory potential of this coumarin.

To understand how braylin inhibits the production of inflammatory mediators by macrophages, the contribution of glucocorticoid receptor (GR) was first investigated by theoretical

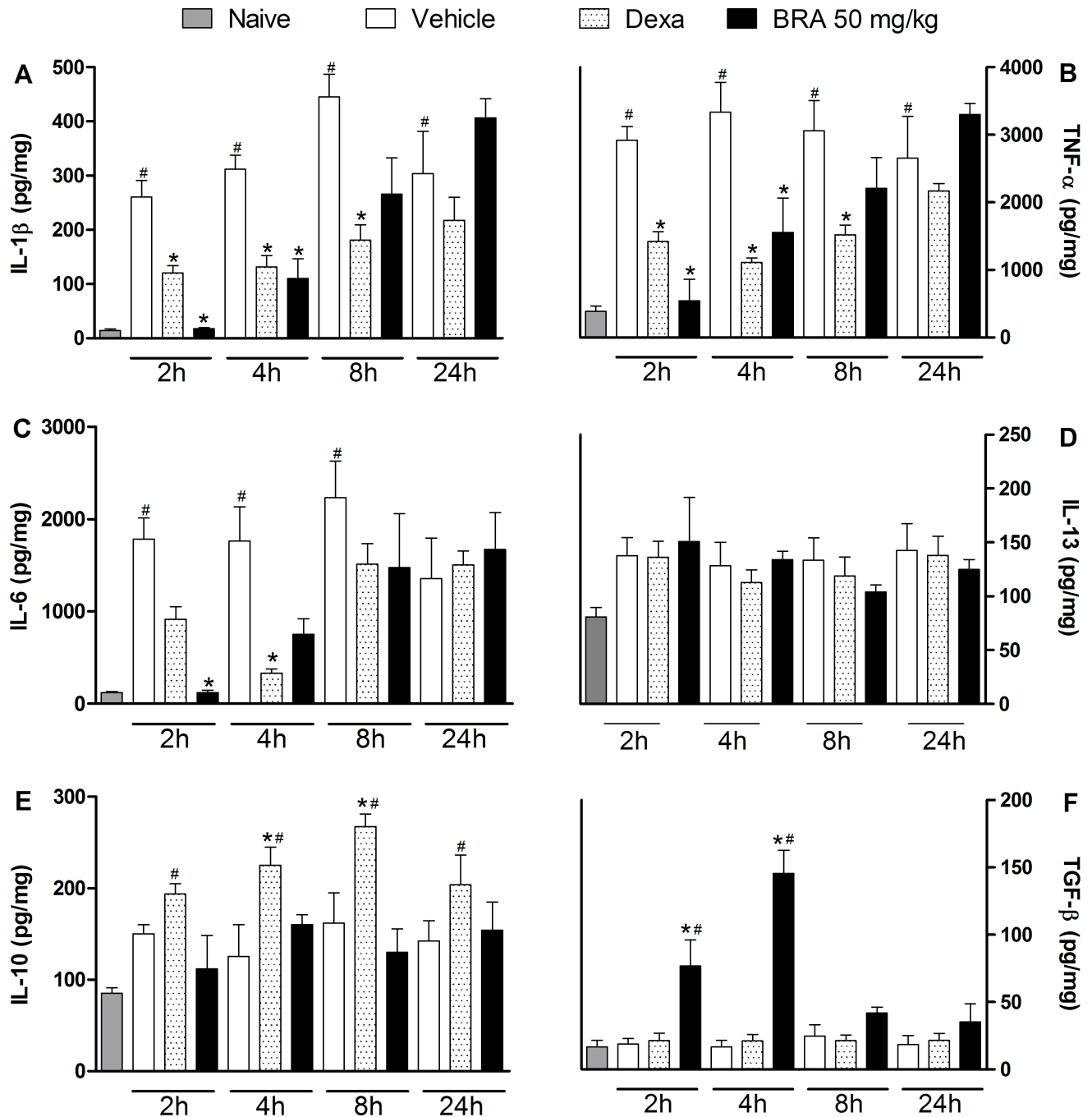


Fig 9. Effects of braylin on cytokines paw levels during CFA-induced inflammation. Mice were injected with braylin (BRA; 50 mg/kg), vehicle (50% propylene glycol in saline; control group) or dexamethasone (Dexa; 2 mg/kg; reference drug) by ip route 40 minutes before CFA (injected at time zero). The naïve group consists of mice that did not receive any experimental manipulation. Panels shows the paw levels of (A) interleukin-1 β (IL-1 β), (B) tumor necrosis factor- α (TNF- α), (C) interleukin-6 (IL-6), (D) interleukin-13 (IL-13), (E) interleukin-10 (IL-10) and (F) transforming growth factor- β (TGF- β), determined in skin tissues samples by ELISA, 3 hours after the CFA injection. The results are expressed as picograms of cytokine per milligram of protein. Data are expressed as means \pm SEM; $n = 6$ mice per group. * Significantly different from the vehicle group in the same time ($p < 0.05$); # significantly different from the naïve group ($p < 0.05$). ANOVA followed by Tukey's multiple comparison test.

<https://doi.org/10.1371/journal.pone.0179174.g009>

methods. Based on docking studies RU486, dexamethasone and braylin presented interactions on the same site of the GR. Analyzing the possible mode of interaction between the GR and RU486, dexamethasone and braylin (S2 Fig), it was possible to verify that an important characteristic is the influence of the N,N-dimethylaniline group of RU486, which by steric hindrance displaces an alpha-helix, number 12, as previously observed [30–32]. In the mode of binding of dexamethasone and braylin, however, there is insufficient molecular volume to promote changes in conformation of the 12 alpha-helix due to the absence of groups that can confer this displacement. However, the mode of interaction with GR4, the specific receptor for dexamethasone, showed no withdrawal from this alpha-helix, thus suggesting a selectivity of dexamethasone and braylin by the GR receptor. The contribution of GR activation to the immunomodulatory effect of braylin was confirmed in an antagonism assay, in which RU486 partially prevented the inhibitory effect of braylin on stimulated macrophages.

Although glucocorticoids remain the most effective therapy for inflammatory and immune diseases, their use is associated with side effects and many patients with chronic diseases become resistant to glucocorticoids requiring higher doses [33]. Aiming to overcome this clinical problem, research has been focused on the development of more potent GR agonists or combination pharmacological strategies that target the GR, as well as other targets [34]. On the “combination therapy”, a second drug is added to potentiate the effects of the glucocorticoid. It has been demonstrated that the combined use with phosphodiesterase-4 inhibitors enhance the clinical efficacy of glucocorticoids, probably by elevating intracellular cAMP [35]. Importantly, braylin presents potent phosphodiesterase-4 inhibitory activity [12], in addition to a partially GR-dependent immunomodulatory effect of braylin demonstrated herein. Thus, according to the current goals of drug development, braylin can represent an ideal GR ligand prototype, able to cross-talk with other signaling pathways and inducing synergic immunomodulatory effects.

The GR activation mediates transactivation or transrepression of several genes involved with the reduction of inflammation and immune function [36]. Glucocorticoids induce their transcriptional effects by direct DNA binding of the GR or by binding to other transcription factors, such as NF- κ B and AP-1, to repress their function [34]. In addition, an important signaling pathway used by Toll-like receptors in activated macrophages results in NF- κ B activation. The genes that are expressed in response to NF- κ B transcriptional activation encode several pro-inflammatory proteins, such as IL-1 β , TNF- α , and inducible nitric oxide synthase [28]. Considering the inhibitory effects of braylin on these mediators, as well as the well-described crosstalk between NF- κ B and glucocorticoid signaling, the effect of braylin on NF- κ B activation was also evaluated.

We found here that braylin treatment was able to intensely reduce the transcriptional activity of NF- κ B. Considering that NF- κ B is a central regulator of inflammatory response, it is possible to propose that the mechanism of action of braylin, involved with its anti-inflammatory and immunomodulatory effects, is through the inhibition of the transcriptional activity of NF- κ B. On the other hand, braylin possesses inhibitory activity on PDE₄ [12], and PDE₄ inhibitors present a broad range of anti-inflammatory activities in experimental and clinical conditions [16,37]. Whether or not the PDE₄ inhibition contributes to the pharmacological effects of braylin presented here is still on investigation.

The potential of braylin as an immunomodulatory agent was also demonstrated *in vivo* using the CFA-induced paw inflammation model, a well-established experimental protocol for study of inflammation and anti-inflammatory drugs. CFA induces local release of mediators, such as cytokines and prostanoids, involved in the inflammatory signs, such as edema, hyperalgesia and vasodilation [38–42]. Importantly, systemic administration of braylin reduced the CFA-induced hyperalgesia with a greater efficacy than dexamethasone, considered the gold

standard drug, showing an important and dose-related antinociceptive effect of braylin. The lack of effects in motor performance of mice on the rota-rod test reinforced the antinociceptive properties of braylin. The tail flick and hot plate tests, which mainly identify central-acting analgesics [43], indicated that the braylin-induced antinociception is not a centrally-mediated action, but likely an effect associated with anti-inflammatory properties.

Peripheral inflammation is associated with the local production of neuroactive inflammatory cytokines and growth factors. It has already been established that the local injection of CFA produces inflammatory hyperalgesia initiated by peripheral nociceptor activation and local release of mediators, such as IL-1 β and TNF- α , which has a major role in the production of inflammatory pain hypersensitivity [38,44]. In addition to the inhibitory effect of braylin on macrophage cells *in vitro*, we showed that braylin reduced the local levels of IL-1 β , TNF- α and IL-6 during CFA-induced paw inflammation. Cytokines play an essential role in the development of inflammatory signs and symptoms, and the first cytokines described as participating in the development of inflammatory pain were IL-1 β , TNF- α and IL-6 [39,45,46]. In addition, upon inflammatory stimulation, the activation of the cytokine pathways precedes the release of final mediators such as prostaglandins, which are involved with nociceptive sensitization, in addition to its ability to trigger acute inflammation producing vasodilatation, vascular permeability and edema [46–51]. Considering the key role of IL-1 β , TNF- α and IL-6 to the inflammatory response, it may be suggested that the antinociceptive and antiedematogenic effects of braylin are related to its ability to inhibit the release of inflammatory cytokines.

During the course of an inflammatory process, pro- and anti-inflammatory mediators are produced and the balance between these two signals determines the magnitude of the inflammatory response. In the present study, the antiedematogenic and antinociceptive effects of braylin were simultaneous to a substantial increase in the production of TGF- β . The TGF- β family members are cytokines that have been implicated in a broad range of biological functions including modulation of cell proliferation or cell differentiation, immunosuppression, tissue repair, and neuroprotection [52–54], and their immune functions are mostly anti-inflammatory. Chen *et al* demonstrated a pivotal role for TGF- β in the regulation of immune response leading to suppression of synovial inflammation and matrix destruction in streptococcal cell wall-induced erosive polyarthritis [55]. Systemic administration of TGF- β prevents the relapse of autoimmune encephalomyelitis [56]. In addition, TGF- β inhibits the proliferation of glial cells and induces anti-inflammatory and immunosuppressive effects on these cells [57,58]. Considering the above described properties of TGF- β , it is possible to propose that the braylin-induced pharmacological effects are mediated by this anti-inflammatory cytokine. In addition, under inflammatory conditions, TGF- β inhibits TNF- α production [59], corroborating the results showed here. In fact, beneficial effects of TGF- β on models of pain have been evidenced. TGF- β induces antinociceptive effect, inhibits the activation and proliferation of microglia and astrocytes and reduces the expression of pro-inflammatory cytokines involved with neuropathic pain maintenance [58,60].

Conclusions

In conclusion, to the best of our knowledge, this is the first *in vivo* demonstration of pharmacological properties of braylin. Using *in vivo* and *in vitro* approach, antinociceptive, anti-inflammatory and immunomodulatory properties of braylin were demonstrated, likely linked to GR activation and its ability to induce inhibition of the transcriptional activity of NF- κ B. Our results demonstrate a strong potential of braylin as a candidate drug for the treatment of immune-inflammatory diseases.

Supporting information

S1 Table. NMR data of braylin (CD3OD, ¹H 500 MHz; ¹³C 125 MHz).
(TIF)

S1 Fig. HPLC/MS analysis of braylin (250 mm; 4.6 mm; 5 μm, flow 0.6 mL/min, 35°C).
(TIF)

S2 Fig. Interactions of (A) RU486 (pink), (B) dexamethasone (orange) and (C) braylin (cyan) with the GR. In A it is possible to see the steric hindrance displaced by N,N-dimethylaniline group of the RU486 in the alpha-helix 12. Dexamethasone and braylin did not induce changes in alpha-helix 12.
(TIFF)

S3 Fig. Cytotoxic effect of braylin on RAW 264.7 Luc macrophages.
(TIF)

S4 Fig. Effects of braylin on motor function assessed by rota-rod test in mice.
(TIF)

Author Contributions

Conceptualization: CFV GHGT MBPS ESV.

Data curation: RFES GHGT ESV CFV MBPS.

Formal analysis: RFES GMF GHGT.

Funding acquisition: ESV CFV MBPS.

Investigation: RFES CSM RSC OPSF AFE GMF.

Methodology: ESV GHGT CFV MBPS.

Project administration: CFV MBPS.

Resources: CFV MBPS ESV.

Software: GMF GHGT.

Supervision: CFV MBPS.

Validation: MBPS ESV ESV GHGT.

Visualization: GHGT CFV.

Writing – original draft: CFV MBPS GHGT.

Writing – review & editing: CFV MBPS.

References

1. Williams JP, Meyers JA. Immune-mediated inflammatory disorders (I.M.I.D.s): the economic and clinical costs. *Am J Manag Care* 2002; 21: S664–681.
2. Davidson A, Diamond B. Autoimmune diseases. *N Engl J Med*. 2001; 345: 340–350. <https://doi.org/10.1056/NEJM200108023450506> PMID: [11484692](https://pubmed.ncbi.nlm.nih.gov/11484692/)
3. Kuek A, Hazleman BL, Ostor AJK. Immune-mediated inflammatory diseases (IMIDs) and biologic therapy: a medical revolution. *Postgrad Med J*. 2007; 83: 251–260. <https://doi.org/10.1136/pgmj.2006.052688> PMID: [17403952](https://pubmed.ncbi.nlm.nih.gov/17403952/)

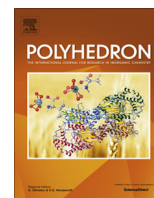
4. Verpoorte R, Vander Heijden R, Memelink J. Engineering the plant cell factory for secondary metabolite production. *Transgenic Res.* 2000; 9: 323–343. PMID: [11131010](#)
5. Venugopala KN, Rashmi V, Odhav B. Review on natural coumarin lead compounds for their pharmacological activity. *Biomed Res Int.* 2013. <https://doi.org/10.1155/2013/963248> PMID: [23586066](#)
6. Peng XM, Damu GL, Zhou C. Current developments of coumarin compounds in medicinal chemistry. *Curr Pharm Des.* 2013; 19: 3884–3930. PMID: [23438968](#)
7. Fylaktakidou KC, Hadjipavlou-Litina DJ, Litinas KE, Nicolaides DN. Natural and synthetic coumarin derivatives with anti-inflammatory/antioxidant activities. *Current Pharm Design* 2004; 10: 3813–3833.
8. Lima FO, Nonato FR, Couto RD, Barbosa-Filho JM, Nunes XP, Ribeiro dos Santos R, et al. Mechanisms involved in the antinociceptive effects of 7-hydroxycoumarin. *J Nat Prod.* 2011; 74: 596–602. <https://doi.org/10.1021/np100621c> PMID: [21417376](#)
9. Li ZP, Hu JF, Sun MN, Ji HJ, Zhao M, Wu DH, et al. Effect of compound IMMLG5521, a novel coumarin derivative, on carrageenan-induced pleurisy in rats. *Eur J Pharmacol.* 2011; 661: 118–123. <https://doi.org/10.1016/j.ejphar.2011.04.024> PMID: [21549112](#)
10. Huang GJ, Deng JS, Liao JC, Hou WC, Wang SY, Sung PJ, et al. Inducible nitric oxide synthase and cyclooxygenase-2 participate in anti-inflammatory activity of imperatorin from *Glehnia littoralis*. *J Agric Food Chem.* 2012; 60: 1673–1681. <https://doi.org/10.1021/jf204297e> PMID: [22188242](#)
11. Aneja R, Mukerjee SK, Seshadri TR. Synthesis of benzo-furan derivatives-I: karanj ketone, karanjin and pongapin. *Tetrahedron* 1958; 2: 203–210.
12. Lin TT, Huang YY, Tang GH, Cheng ZB, Liu X, Luo HB, et al. Prenylated coumarins: natural phosphodiesterase-4 inhibitors from *Toddalia asiatica*. *J Nat Prod.* 2014; 77: 955–962. <https://doi.org/10.1021/np401040d> PMID: [24597921](#)
13. Bender AT, Beavo JA. Cyclic nucleotide phosphodiesterases: molecular regulation to clinical use. *Pharmacol Rev.* 2006; 58: 488–520. <https://doi.org/10.1124/pr.58.3.5> PMID: [16968949](#)
14. Serezani CH, Ballinger MN, Aronoff DM, Peters-Golden M. Cyclic AMP: master regulator of innate immune cell function. *Am J Respir Cell Mol Biol.* 2008; 39: 127–132. <https://doi.org/10.1165/rcmb.2008-0091TR> PMID: [18323530](#)
15. Salari P, Abdollahi M. Phosphodiesterase inhibitors in inflammatory bowel disease. *Expert Opin Investig Drugs* 2012; 21: 261–264. <https://doi.org/10.1517/13543784.2012.658915> PMID: [22303952](#)
16. Houslay MD, Schafer P, Zhang KY. Keynote review: phosphodiesterase-4 as a therapeutic target. *Drug Discov Today* 2005; 10: 1503–1519. [https://doi.org/10.1016/S1359-6446\(05\)03622-6](https://doi.org/10.1016/S1359-6446(05)03622-6) PMID: [16257373](#)
17. Baumer W, Hoppmann J, Rundfeldt C, Kietzmann M. Highly selective phosphodiesterase 4 inhibitors for the treatment of allergic skin diseases and psoriasis. *Inflamm Allergy Drug Targets* 2007; 6: 17–26. PMID: [17352685](#)
18. Strand V, Fiorentino D, Hu C, Day RM, Stevens RM, Papp KA. Improvements in patient-reported outcomes with apremilast, an oral phosphodiesterase 4 inhibitor, in the treatment of moderate to severe psoriasis: results from a phase IIb randomized, controlled study. *Health Qual Life Outcomes* 2013. <https://doi.org/10.1186/1477-7525-11-82> PMID: [23663752](#)
19. Randrianarivelojosia M, Mulholland DA, Farland KMC. Prenylated coumarins from *Cedrelopsis longibracteata* (Ptaeroxylaceae). *Biochem Syst Ecol.* 2005; 33: 301–304.
20. Green LC, Wagne DA, Glogowski J, Skipper PL, Wishnok JS, Tannenbaum SR. Analysis of nitrate, nitrite, and [¹⁵N] nitrate in biological fluids. *Anal Biochem.* 1982; 126: 131–138. PMID: [7181105](#)
21. Zhong H, SuYang H, Erdjument-Bromage H, Tempst P, Ghosh S. The transcriptional activity of NF- κ B is regulated by the I κ B-associated PKAc subunit through a cyclic AMP-independent mechanism. *Cell* 1997; 89(3): 413–424. PMID: [9150141](#)
22. Verdonk ML, Cole JC, Hartshorn MJ, Murray CW, Taylor RD. Improved protein-ligand docking using GOLD. *Proteins* 2003; 52: 609–623. <https://doi.org/10.1002/prot.10465> PMID: [12910460](#)
23. Lima MS, Quintans LJ jr, Santana WA, Kaneto CM, Soares MBP, Villarreal CF. Anti-inflammatory effects of carvacrol: evidence for a key role of interleukin-10. *Eur J Pharmacol.* 2013; 699: 112–117. <https://doi.org/10.1016/j.ejphar.2012.11.040> PMID: [23220159](#)
24. Chaplan SR, Bach FW, Pogrel JW, Chung JM, Yaksh TL. Quantitative assessment of tactile allodynia in the rat paw. *J Neurosci Meth.* 1994; 53: 55–63.
25. Oliveira CM, Nonato FR, Lima FO, Couto RD, David JP, David JM, et al. Antinociceptive properties of bergenin. *J Nat Prod.* 2011; 74: 2062–2068. <https://doi.org/10.1021/np200232s> PMID: [21939182](#)
26. Gama KB, Quintans JS, Antonioli AR, Quintans LJ Jr, Santana WA, Branco A, et al. Evidence for the involvement of descending pain-inhibitory mechanisms in the antinociceptive effect of hecogenin acetate. *J Nat Prod.* 2013; 76: 559–563. <https://doi.org/10.1021/np3007342> PMID: [23437926](#)

27. Woolfe G, MacDonald A. The evaluation of the analgesic action of pethidine hydrochloride (demerol). *J Pharmacol Exp Ther.* 1944; 80: 300–307.
28. Fujiwara N, Kobayashi K. Macrophages in inflammation. *Curr Drug Targets Inflamm Allergy* 2005; 4: 281–286. PMID: [16101534](https://pubmed.ncbi.nlm.nih.gov/16101534/)
29. Korhonen R, Lahti A, Kankaanranta H, Moilanen E. Nitric oxide production and signaling in inflammation. *Curr Drug Targets Inflamm Allergy* 2005; 4: 471–479. PMID: [16101524](https://pubmed.ncbi.nlm.nih.gov/16101524/)
30. Kauppi B, Jakob C, Färnegårdh M, Yang J, Ahola H, Alarcon M, et al. The three-dimensional structures of antagonistic and agonistic forms of the glucocorticoid receptor ligand-binding domain: RU-486 induces a transconformation that leads to active antagonism. *J Biol Chem.* 2003; 278(25): 22748–22754. <https://doi.org/10.1074/jbc.M212711200> PMID: [12686538](https://pubmed.ncbi.nlm.nih.gov/12686538/)
31. Edman K, Hosseini A, Bjursell MK, Aagaard A, Wissler L, Gunnarsson A, et al. Ligand Binding Mechanism in Steroid Receptors: From Conserved Plasticity to Differential Evolutionary Constraints. *Structure* 2015; 23(12): 2280–2290. <https://doi.org/10.1016/j.str.2015.09.012> PMID: [26602186](https://pubmed.ncbi.nlm.nih.gov/26602186/)
32. Matsuo Y, Yamada A, Tsukamoto K, Tamura H, Ikezawa H, Nakamura H, et al. A distant evolutionary relationship between bacterial sphingomyelinase and mammalian DNase I. *Protein Sci.* 1996; 5(12): 2459–2467. <https://doi.org/10.1002/pro.5560051208> PMID: [8976554](https://pubmed.ncbi.nlm.nih.gov/8976554/)
33. Barnes PJ, Adcock IM. Glucocorticoid resistance in inflammatory diseases. *Lancet* 2009; 373: 1905–1917. [https://doi.org/10.1016/S0140-6736\(09\)60326-3](https://doi.org/10.1016/S0140-6736(09)60326-3) PMID: [19482216](https://pubmed.ncbi.nlm.nih.gov/19482216/)
34. Hapgood JP, Avenant C, Moliki JM. Glucocorticoid-independent modulation of GR activity: Implications for immunotherapy. *Pharmacol Ther.* 2016; 165: 93–113. <https://doi.org/10.1016/j.pharmthera.2016.06.002> PMID: [27288728](https://pubmed.ncbi.nlm.nih.gov/27288728/)
35. Giembycz MA, Newton R. Potential mechanisms to explain how LABAs and PDE4 inhibitors enhance the clinical efficacy of glucocorticoids in inflammatory lung diseases. *F1000Prime Rep.* 2015. <https://doi.org/10.12703/P7-16> PMID: [25750734](https://pubmed.ncbi.nlm.nih.gov/25750734/)
36. Schacke H, Docke WD, Asadullah K. Mechanisms involved in the side effects of glucocorticoids. *Pharmacol Ther.* 2002; 96: 23–43. PMID: [12441176](https://pubmed.ncbi.nlm.nih.gov/12441176/)
37. Pagès L, Gavaldà A, Lehner MD. PDE4 inhibitors: a review of current developments (2005–2009). *Expert Opin Ther Pat.* 2009; 19: 1501–1519. <https://doi.org/10.1517/13543770903313753> PMID: [19832118](https://pubmed.ncbi.nlm.nih.gov/19832118/)
38. Woolf CJ, Allchorne A, Safieh-Garabedian B, Poole S. Cytokines, nerve growth factor and inflammatory hyperalgesia: the contribution of tumour necrosis factor alpha. *Br J Pharmacol.* 1997; 121: 417–424. <https://doi.org/10.1038/sj.bjp.0701148> PMID: [9179382](https://pubmed.ncbi.nlm.nih.gov/9179382/)
39. Dinarello CA. Proinflammatory cytokines. *Chest* 2000; 118: 503–508. PMID: [10936147](https://pubmed.ncbi.nlm.nih.gov/10936147/)
40. Cunha FQ, Ferreira SH. Peripheral hyperalgesic cytokines. *Adv Exp Med Biol.* 2003; 521: 22–39. PMID: [12617562](https://pubmed.ncbi.nlm.nih.gov/12617562/)
41. Conti B, Tabarean I, Andrei C, Bartfai T. Cytokines and fever. *Front Biosci.* 2004; 9: 1433–1449. PMID: [14977558](https://pubmed.ncbi.nlm.nih.gov/14977558/)
42. Fehrenbacher JC, Vasko MR, Duarte DB. Models of inflammation: Carrageenan- or complete Freund's Adjuvant (CFA)-induced edema and hypersensitivity in the rat. *Curr Protoc Pharmacol.* 2012. <https://doi.org/10.1002/0471141755.ph0504s56> PMID: [22382999](https://pubmed.ncbi.nlm.nih.gov/22382999/)
43. Le Bars D, Gozariu M, Cadden SW. Animal models of nociception. *Pharmacol Rev.* 2001; 53: 597–652. PMID: [11734620](https://pubmed.ncbi.nlm.nih.gov/11734620/)
44. Safieh-Garabedian B, Poole S, Allchorne A, Winter J, Woolf CJ. Contribution of interleukin-1 beta to the inflammation-induced increase in nerve growth factor levels and inflammatory hyperalgesia. *Br J Pharmacol.* 1995; 115: 1265–1275. PMID: [7582555](https://pubmed.ncbi.nlm.nih.gov/7582555/)
45. Faccioli LH, Souza GE, Cunha FQ, Poole S, Ferreira SH. Recombinant interleukin-1 and tumor necrosis factor induce neutrophil migration "in vivo" by indirect mechanisms. *Agents Actions* 1990; 30: 344–349. PMID: [2201176](https://pubmed.ncbi.nlm.nih.gov/2201176/)
46. Verri WA Jr, Cunha TM, Parada CA, Poole S, Cunha FQ, Ferreira SH. Hypernociceptive role of cytokines and chemokines: targets for analgesic drug development? *Pharmacol Ther.* 2006; 112: 116–138. <https://doi.org/10.1016/j.pharmthera.2006.04.001> PMID: [16730375](https://pubmed.ncbi.nlm.nih.gov/16730375/)
47. Cunha FQ, Poole S, Lorenzetti BB, Ferreira SH. The pivotal role of tumour necrosis factor alpha in the development of inflammatory hyperalgesia. *Br J Pharmacol.* 1992; 107: 660–664. PMID: [1472964](https://pubmed.ncbi.nlm.nih.gov/1472964/)
48. Cunha TM, Verri WA Jr, Silva JS, Poole S, Cunha FQ, Ferreira SH. A cascade of cytokines mediates mechanical inflammatory hypernociception in mice. *Proc Natl Acad Sci. USA* 2005; 102: 1755–1760. <https://doi.org/10.1073/pnas.0409225102> PMID: [15665080](https://pubmed.ncbi.nlm.nih.gov/15665080/)
49. Zucali JR, Dinarello CA, Oblon DJ, Gross MA, Anderson L, Weiner RS. Interleukin 1 stimulates fibroblasts to produce granulocyte-macrophage colony-stimulating activity and prostaglandin E2. *J Clin Invest.* 1986; 77: 1857–1863. <https://doi.org/10.1172/JCI112512> PMID: [3486886](https://pubmed.ncbi.nlm.nih.gov/3486886/)

50. Gitter BD, Labus JM, Lees SL, Scheetz ME. Characteristics of human synovial fibroblast activation by IL-1 beta and TNF alpha. *Immunology* 1989; 66: 196–200. PMID: [2784408](#)
51. Hohjoh H, Inazumi T, Tsuchiya S, Sugimoto Y. Prostanoid receptors and acute inflammation in skin. *Biochimie* 2014. <https://doi.org/10.1016/j.biochi.2014.08.010> PMID: [25179301](#)
52. Letterio JJ, Roberts AB. TGF-beta: A critical modulator of immune cell function. *Clin Immunol Immunopathol.* 1997; 84: 244–250. PMID: [9281382](#)
53. Grande JP. Role of transforming growth factor-beta in tissue injury and repair. *Proc Soc Exp Biol Med.* 1997; 214: 27–40. PMID: [9012358](#)
54. Dobolyi A, Vincze C, Pal G, Lovas G. The neuroprotective functions of transforming growth factor beta proteins. *Int J Mol Sci.* 2012; 13: 8219–8258. <https://doi.org/10.3390/ijms13078219> PMID: [22942700](#)
55. Chen W, Jin W, Cook M, Weiner HL, Wahl SM. Oral delivery of group a streptococcal cell walls augments circulating TGF-beta and suppresses streptococcal cell wall arthritis. *J Immunol.* 1998; 161: 6297–6304. PMID: [9834119](#)
56. Jin YX, Xu LY, Guo H, Ishikawa M, Link H, Xiao BG. TGF-beta1 inhibits protracted-relapsing experimental autoimmune encephalomyelitis by activating dendritic cells. *J Autoimmun.* 2000; 14: 213–220. <https://doi.org/10.1006/jaut.2000.0364> PMID: [10756083](#)
57. Bottner M, Kriegelstein K, Unsicker K. Transforming growth factor-beta 1 impairs neuropathic pain through pleiotropic effects. *J Neurochem.* 2000; 75: 2227–2240. PMID: [11080174](#)
58. Echeverry S, Shi XQ, Haw A, Liu H, Zhang ZW, Zhang J. Transforming growth factor-beta1 impairs neuropathic pain through pleiotropic effects. *Mol Pain* 2009. <https://doi.org/10.1186/1744-8069-5-16> PMID: [19327151](#)
59. Benveniste EN, Tang LP, Law RM. Differential regulation of astrocyte TNF-alpha expression by the cytokines TGF-beta, IL-6 and IL-10. *Int J Dev Neurosci.* 1995; 13: 341–349. PMID: [7572286](#)
60. Chen NF, Huang SY, Chen WF, Chen CH, Lu CH, Chen CL, et al. TGF-beta1 attenuates spinal neuroinflammation and the excitatory amino acid system in rats with neuropathic pain. *J Pain* 2013; 14: 1671–1685. <https://doi.org/10.1016/j.jpain.2013.08.010> PMID: [24290447](#)

ANEXO 9

PLUTÍN, A. M.; ALVAREZ, A.; MOCELO, R.; RAMOS, R.; CASTELLANO, E. E.; SILVA, M. M.; VILARREAL, W.; PAVAN, F. R.; **MEIRA, C. S.**; FILHO, J. S. R.; MOREIRA, D. R. M.; SOARES, M. B. P.; BATISTA, A. A. Palladium(II)/N,N-disubstituted-N'-acythioureas complexes as anti-*Mycobacterium tuberculosis* and anti-*Trypanosoma cruzi* agents. **Polyhedron**, v. 132, p. 70-77, 2017.



Palladium(II)/*N,N*-disubstituted-*N'*-acylthioureas complexes as anti-*Mycobacterium tuberculosis* and anti-*Trypanosoma cruzi* agents



Ana M. Plutín^{a,*}, Anislay Alvarez^a, Raúl Mocoelo^a, Raúl Ramos^a, Eduardo E. Castellano^b, Monize M. da Silva^c, Wilmer Villarreal^c, Fernando R. Pavan^d, Cássio Santana Meira^e, José Simão Rodrigues Filho^e, Diogo Rodrigo M. Moreira^e, Milena Botelho P. Soares^{e,f}, Alzir A. Batista^{c,*}

^aLaboratório de Síntese Orgânica, Facultad de Química, Universidad de La Habana, La Habana, Cuba

^bInstituto de Física de São Carlos, Universidade de São Paulo, São Carlos, SP, Brazil

^cDepartamento de Química, Universidade Federal de São Carlos, CEP 13.565-905 São Carlos, SP, Brazil

^dFaculdade de Ciências Farmacêuticas, UNESP, Araraquara, SP, Brazil

^eInstituto Gonçalo Moniz, Fundação Oswaldo Cruz, CEP 40296-750 Salvador, BA, Brazil

^fCentro de Biotecnologia e Terapia Celular, Hospital São Rafael, CEP 41253-190 Salvador, BA, Brazil

ARTICLE INFO

Article history:

Received 30 January 2017

Accepted 1 May 2017

Available online 10 May 2017

Keywords:

Metal complexes

Palladium

Thioureas

Tuberculosis

Trypanosoma cruzi

ABSTRACT

The new complexes of Pd(II) with *N,N*-disubstituted-*N'*-acylthioureas: [(**1**) [Pd(dppf)(*N,N*-dimethyl-*N'*-benzoylthioureato-*k*²O,S)]PF₆, (**2**) [Pd(dppf)(*N,N*-diethyl-*N'*-benzoylthioureato-*k*²O,S)]PF₆, (**3**) [Pd(dppf)(*N,N*-dibutyl-*N'*-benzoylthioureato-*k*²O,S)]PF₆, (**4**) [Pd(dppf)(*N,N*-diphenyl-*N'*-benzoylthioureato-*k*²O,S)]PF₆, (**5**) [Pd(dppf)(*N,N*-diethyl-*N'*-furoylthioureato-*k*²O,S)]PF₆, (**6**) [Pd(dppf)(*N,N*-diphenyl-*N'*-furoylthioureato-*k*²O,S)]PF₆, (**7**) [Pd(dppf)(*N,N*-dimethyl-*N'*-thiophenylthioureato-*k*²O,S)]PF₆, and (**8**) [Pd(dppf)(*N,N*-diphenyl-*N'*-thiophenylthioureato-*k*²O,S)]PF₆, were prepared and characterized by elemental analysis, and spectroscopic techniques. The structures of complexes (**2**), (**3**), (**5**), (**6**) and (**8**) had their structures determined by X-ray crystallography, confirming the coordination of the ligands with the metal through sulfur and oxygen atoms, forming distorted square-planar geometries. These complexes have shown antibacterial activity against anti-*Mycobacterium tuberculosis* H37Rv ATCC 27294. The complexes exhibited antiparasitic activity against *Trypanosoma cruzi*, while the metal-free thioureas did not. The results demonstrated that the compounds described here can be considered as promising anti-*Mycobacterium tuberculosis* and anti-*T. cruzi* agents, since in both cases their *in vitro* activity were better than reference drugs available for the treatment of both diseases.

© 2017 Elsevier Ltd. All rights reserved.

1. Introduction

The *Mycobacterium tuberculosis* (MTB), causative agent of tuberculosis, is responsible for the death of around 2–3 million people, annually, and a global economic toll of US\$12 billion each year [1]. The rise of multidrug resistance (MDR) in MTB has complicated and prolonged the treatment. Therefore, no new drugs have been developed specifically against mycobacteria since the 1960s [2]. Thus, there is a great need to develop new therapeutic agents to treat tuberculosis, so as to reduce the total duration of treatment and to provide more effective drugs against MDR TB and latent tuberculosis infection. This involves the development of new therapeutic strategies against bacterial infection, which becomes more

stringent, and one reason for this is mainly due the bacterial drug resistance to currently administered treatments.

Also, Chagas disease, caused by the protozoan parasite *Trypanosoma cruzi* (*T. cruzi*), affects approximately 10 million people worldwide, with a high prevalence in Latin America [3]. The few drugs available, benznidazole and nifurtimox, are only effective in curing when administered during the acute phase, but not effective in patients that have progressed to the chronic phase [4]. Furthermore, these drugs are not considered ideal, due to their severe side effects [5]. Thus, the search for new anti-*T. cruzi* compounds is also needed.

One strategy for the development of antimycobacterial and antiparasitic agents from the inorganic point of view is to use an organic compound, which already exhibit antibacterial property, as ligand, to form metal complexes. Thus, good candidates for this purpose are thiourea and their derivatives, which are known for their antiviral, antibacterial and cytotoxic properties [6]. There

* Corresponding author. Fax: +55 16 3351 8350.

E-mail address: daab@ufscar.br (A.A. Batista).

are several works in the literature demonstrating the activity of this class of compounds, against parasites such as *Plasmodium falciparum*, *Trypanosoma brucei* and *T. cruzi* [7]. In recent years, a number of urea, thiourea and acylthiourea derivatives containing (R)-2-amino-1-butanol were evaluated against *Mycobacterium tuberculosis* strains H37Rv ATCC 27294, showing good anti-tuberculosis effect, and the complexing capacity of thiourea derivatives have been reported [8–9].

The biological activity of complexes containing thiourea derivatives has been successfully screened for various biological processes and they exhibit a wide range of biological activities, including antifungal, anticancer [9–10] and insecticidal activities [11]. Therefore, in order to extend the research on potential metallodrugs aiming the *M. Tuberculosis* and Chagas disease we report here on some palladium complexes containing the bis(diphenylphosphine)ferrocene and *N,N*-disubstituted-*N'*-acyl thioureas as ligands. Detailed descriptions of synthesis and characterization of the ligands have been reported elsewhere [12]. The Pd(II)/*N,N*-disubstituted-*N'*-acyl thioureas complexes described in this work were synthesized, structurally characterized and were tested for their anti-*M. tuberculosis* and anti-*T. cruzi* activity, showing good results.

2. Experimental

2.1. Materials and measurements

The dichloro[bis(diphenylphosphino)ferrocene]palladium (II) was obtained from Stream. All reagents were purchased with reagent grade and used without further purification. Solvents were dried and used freshly distilled, unless otherwise specifically indicated. Thin layer chromatography (TLC) was performed on 0.25 mm silic gel pre-coated plastic sheets (40/80 mm) (Polygram_{SIL} G/UV254, Macherey & Nagel, Düren, Germany) using benzene/methanol (9/1) as eluent. The IR spectra were recorded on a FTIR Bomem-Michelson 102 spectrometer in the 4000–200 cm⁻¹ region using CsI pellets. Conductivity values were obtained using 1.0 mmol·L⁻¹ solutions of complexes in CH₂Cl₂, using a Meter Lab CDM2300 instrument. The molar conductance measurements (Λ_m) were carried out in dichloromethane at 25 °C, using concentrations of 1.0 × 10⁻³ mol·L⁻¹ for the complexes. ¹H, ³¹P{¹H} and ¹³C NMR spectra were recorded on a Bruker DRX 400 MHz, internally referenced to TMS for hydrogen chemical shift (δ). The ³¹P chemical shifts are reported in relation to H₃PO₄, 85%. CDCl₃ was used as solvent, unless mentioned. Partial elemental analyses were carried out on the Department of Chemistry of the Federal University of São Carlos, in an instrument of CHNS staff EA 1108 of the FISONs.

2.2. Synthesis of *N,N*-dialkyl-*N'*-(acyl/aroil)thioureas

The *N,N*-disubstituted-*N'*-acylthioureas HL(1–8) used in this work were synthesized by the procedure previously reported in the literature [12]. A solution of an appropriate acyl chloride (30 mmol) in acetone (50 mL) was added dropwise to a suspension of KSCN (0.01 mol) in acetone (30 mL). The mixture was stirred until a precipitate appeared (ammonium chloride), indicating the formation of the respective organic isothiocyanate. The corresponding amine (40 mmol), dissolved in acetone was added slowly and with constant stirring to the resulting solution. The solution was cooled in an ice-water bath and the stirring was continued at room temperature during 2–9 h, until the reaction was completed (the reaction progress was monitored by TLC). The reaction mixture was then poured into 600 mL of cold water. The solid *N,N*-disubstituted-*N'*-(acyl/aroil)thioureas were collected by filtration

and finally purified by recrystallization from ethanol. The compounds were obtained as crystalline solids, in good yields. The identity of the products was confirmed by comparing their ¹H and ¹³C NMR data with those reported in the literature [12]. The structures of the *N,N*-disubstituted-*N'*-acyl thioureas used as ligands in this work are shown in Fig. 1.

2.3. Synthesis of the complexes

The complexes were prepared as yellow solid products by a similar method to that used for [Pd(PPh₃)₂Cl₂] [9] from direct reactions with the precursor [Pd(dppf)Cl₂], with the *N,N*-disubstituted-*N'*-acylthioureas, in methanol solutions. The complexes were separated from the reaction mixtures as yellow crystalline solids. Filtration and further washing with hot water and hot hexane were enough to afford pure and stable compounds, in about 80% yields. Thus, the general procedure for the synthesis of the complexes is described: A solution of [Pd(dppf)Cl₂] (1.46 g; 2.00 mmol) in 5 mL of methanol, was added dropwise to a solution of corresponding *N,N*-dialkyl-*N'*-(acyl/aroil)thiourea (2.00 mmol), dissolved in 30 mL of the same solvent, and 0.368 g (2.00 mmol) of KPF₆. The reaction was heated under magnetic stirring at about 80 °C, for 2 h. The reaction mixture was left in the refrigerator overnight. The yellow solids obtained were filtered off and washed, successively, with hot water and hot hexane (3 × 20 mL). The obtained compounds are stable in the air and in dimethylsulphoxide solutions, for at least 72 h, as showed ³¹P{¹H} NMR experiments.

The ¹H, ¹³C and ³¹P{¹H} NMR, IR and the elemental analyses, melting point temperature and molar conductivity (Λ_m , 1.0 × 10⁻³ mol L⁻¹ in CH₂Cl₂) for the complexes (1–8) are listed below and the other data used for the characterization of the complexes will be found in the text:

(1) [Pd(dppf)(*N,N*-dimethyl-*N'*-benzoylthioureato-k²O,S)]PF₆: ¹H NMR, δ : 7.86–7.81 (m, 5H, Ph), 7.64–7.51 (m, 5H), 7.37–7.17 (m, 10H), 3.48 (3H, s, CH₃), and 3.18 (3H, s, CH₃). NMR ¹³C, δ : 169.7 (C=S); 161.8 (C=O); 134.5, 134.4, 134.4, 134.2, 134.1, 132.7–127.7 (C-Ph), 29.7 (CH₃), 15.3 (CH₃). ³¹P{¹H} NMR, δ , 41.12 (d); 28.06 (d); ²J_{P-P} = 19.43 Hz; IR, cm⁻¹: ν (C=O) 1416, ν (C=S) 747; ν (C=N) 1502; Anal. (%): Found (Calc) for C₄₄H₃₉F₆FeN₂OP₃PdS: C, 52.26 (52.17); H, 3.90 (3.88); N, 2.82 (2.77); S, 3.21 (3.17). Λ_m = 48.6 Ω^{-1} cm² mol⁻¹.

(2) [Pd(dppf)(*N,N*-diethyl-*N'*-benzoylthioureato-k²O,S)]PF₆: ¹H NMR, δ : 7.87–7.82 (m, 1H), 7.61–7.48 (m, 5H), 7.36–7.31 (m, 5H), 7.15–6.99 (m, 10H), 3.81 (d, J = 7.07 Hz, 2H, CH₂), 3.58 (d, J = 7.07 Hz, 2H, CH₂), 1.28 (t, J = 7.02, 7.02 Hz, 3H, CH₃), 1.31 (t, J = 7.02, 7.02 Hz, 3H, CH₃); NMR ¹³C, δ : 170.0 (C=S); 169.6 (C=O); 135.7, 135.6, 134.6, 134.5, 134.2–127.5 (C-Ph), 47.3 (CH₂), 46.5 (CH₂), 13.1 (CH₃), 12.1 (CH₃); ³¹P{¹H}, δ : 41.27 (d); 27.41 (d); ²J_{P-P} = 21.86 Hz; IR, cm⁻¹: ν (C=O) 1414, ν (C=S) 750; ν (C=N) 1501; Anal. (%): Found (Calc) for C₄₆H₄₃F₆FeN₂OP₃PdS: C, 53.15 (53.07); H, 4.08 (4.16); N, 2.70 (2.69); S, 3.00 (3.08). MP: 270–272 °C, Λ_m = 44.6 Ω^{-1} cm² mol⁻¹.

(3) [Pd(dppf)(*N,N*-dibutyl-*N'*-benzoylthioureato-k²O,S)]PF₆: ¹H NMR, δ : 8.04–7.99 (m, 1H), 7.80–7.08 (m, 34H), 4.88 (d, J = 7.08 Hz, 2H, CH₂), 3.68 (4H, q, CH₂), 2.07–1.70 (2H, m, CH₂), 0.93 (3H, t, CH₃, J = 7.01 Hz). NMR ¹³C, δ : 170.6 (C=S), 168.5 (C=O), 135.6, 135.3, 135.2, 133.6–128.8 (C-Ph), 53.6 (CH₂), 52.4 (CH₂), 20.9 (CH₂), 14.2 (CH₃); ³¹P{¹H}, δ : 41.18 (d); 27.63 (d); ²J_{P-P} = 20.26 Hz; IR, cm⁻¹: ν (C=O) 1495, ν (C=S) 747; ν (C=N) 1495; Anal. (%): Found (Calc) for C₅₀H₅₁F₆FeN₂OP₃PdS: C, 54.54 (54.74); H, 4.65 (4.68); N, 2.53 (2.55); S, 2.85 (2.92), MP: 230–232 °C, Λ_m = 47.6 Ω^{-1} cm² mol⁻¹.

(4) [Pd(dppf)(*N,N*-diphenyl-*N'*-benzoylthioureato-k²O,S)]PF₆: ¹H NMR, δ : 7.86–7.82 (m, 1H), 7.14 (s, 1H), 6.73 (d, J = 1.60 Hz, 1H), 6.86–6.83 (m, 1H), NMR ¹³C, δ : 174.6 (C=S); 172.9 (C=O); 144.0, 143.1, 134.4, 134.3, 134.2, 134.1–127.3 (C/Ph). ³¹P{¹H}, δ :

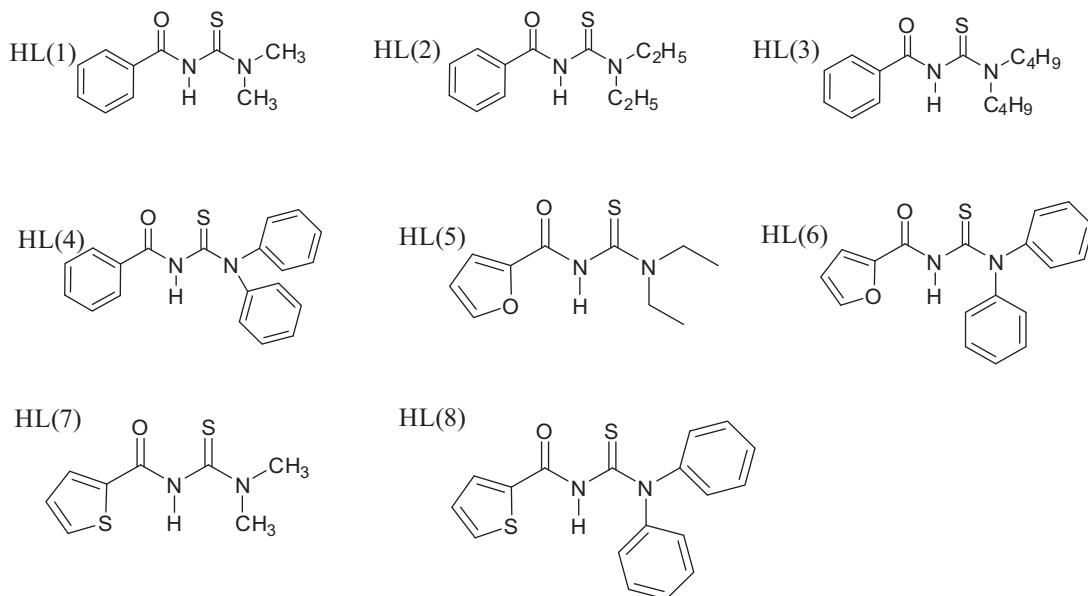


Fig. 1. Structures of the *N,N*-disubstituted-*N'*-acyl thioureas used as ligands in this work.

41.25 (d), 27.58 (d) $^2J_{P-P} = 20.26$; IR, cm^{-1} : $\nu(\text{C}=\text{O})$ 1430, $\nu(\text{C}=\text{S})$ 752; $\nu(\text{C}=\text{N})$ 1494; Anal. (%): Found (Calc) for $\text{C}_{54}\text{H}_{43}\text{F}_6\text{FeN}_2\text{OP}_3\text{PdS}$: C, 56.98 (57.03); H, 3.90 (3.81); N, 2.37 (2.46); S, 2.78 (2.82). MP: 275–277 °C, $A_M = 48.6 \Omega^{-1} \text{cm}^2 \text{mol}^{-1}$.

(5) $[\text{Pd}(\text{dppf})(\text{N,N}$ -diethyl-*N'*-furoylthioureato- $\text{k}^2\text{O,S})]\text{PF}_6$: ^1H NMR, δ : 7.85–7.80 (m, 1H), 7.60–6.18 (3H, m, furoyl), 3.74 (2H, d, CH_2), 3.34 (2H, d, CH_2), 1.22 (3H, t, CH_3), 0.95 (3H, t, CH_3). NMR ^{13}C , δ : 165.7 (C=S), 159.8 (C=O), 145.9, 134.6, 134.5, 134.1–129.4 (C-Ph), 128.8–112.0 (C-Ph and furan ring), 47.2 (CH_2), 46.5 (CH_2), 13.1 (CH_3), 11.9 (CH_3). $^{31}\text{P}\{^1\text{H}\}$, δ : 41.45 (d), 27.32 (d); $^2J_{P-P} = 19.43$, IR, cm^{-1} : $\nu(\text{C}=\text{O})$ 1474, $\nu(\text{C}=\text{S})$ 747; $\nu(\text{C}=\text{N})$ 1504; Anal. (%): Found (Calc): Anal. (%): Found (Calc) for $\text{C}_{44}\text{H}_{41}\text{F}_6\text{FeN}_2\text{O}_2\text{P}_3\text{PdS}$: C, 51.15 (51.26); H, 3.97 (4.00); N, 2.68 (2.72); S, 3.09 (3.11). MP: 242–244 °C, $A_M = 48.6 \Omega^{-1} \text{cm}^2 \text{mol}^{-1}$.

(6) $[\text{Pd}(\text{dppf})(\text{N,N}$ -diphenyl-*N'*-furoylthioureato- $\text{k}^2\text{O,S})]\text{PF}_6$: ^1H NMR, δ : 7.91–7.80 (m, 1H), 7.63–7.43 (m, 1H), 7.20–6.99 (m, 1H), 6.53–6.16 (m, 1H), 4.98 (s, 2H, CH_2), 4.77 (s, 2H, CH_2). NMR ^{13}C , δ : 167.7 (C=S); 162.0 (C=O); 149.5, 146.8, 146.1, 145.7, 145.2–112.3 (C-Ph), 53.5 (CH_2), 52.8 (CH_2). $^{31}\text{P}\{^1\text{H}\}$, δ : 41, 30 (d), 27.54 (d); $^2J_{P-P} = 19.43$; IR, cm^{-1} : $\nu(\text{C}=\text{O})$ 1486, $\nu(\text{C}=\text{S})$ 741; $\nu(\text{C}=\text{N})$ 1573; Anal. (%): Found (Calc) for $\text{C}_{52}\text{H}_{41}\text{F}_6\text{FeN}_2\text{O}_2\text{P}_3\text{PdS}$: C, 55.39 (55.41); H, 3.61 (3.66); N, 2.45 (2.49); S, 2.80 (2.84). MP: 264–266 °C, $A_M = 52.6 \Omega^{-1} \text{cm}^2 \text{mol}^{-1}$.

(7) $[\text{Pd}(\text{dppf})(\text{N,N}$ -dimethyl-*N'*-thiophenylthioureato- $\text{k}^2\text{O,S})]\text{PF}_6$: ^1H NMR, δ : 8.02 (1H, dd, $J_1 = 7.2$ Hz, $J_2 = 8.1$ Hz, thiophene CH), 7.87 (1H, dd, $J_1 = 7.59$ Hz, $J_2 = 8.2$ Hz, thiophene CH), 6.70 (1H, dd, $J_1 = 6.7$ Hz, $J_2 = 8.6$ Hz, thiophene CH), 7.59–7.27 (C-Ph) 0.97 (6H, t, CH_3 , $J = 7.1$ Hz), NMR ^{13}C , δ : 166.7 (C=S); 164.1 (C=O); 141.2, 134.6, 134.5, 134.5, 134.4, 132.4, 132.3, 132.2, 131.7, 128.9–125.6 (C-Ph); 21.8 (2 CH_3). $^{31}\text{P}\{^1\text{H}\}$, δ : 41.58 (d), 27.97 (d), $^2J_{P-P} = 19.47$; IR, cm^{-1} : $\nu(\text{C}=\text{O})$ 1418, $\nu(\text{C}=\text{S})$ 745; $\nu(\text{C}=\text{N})$ 1494; Anal. (%): Found (Calc) for $\text{C}_{42}\text{H}_{37}\text{F}_6\text{FeN}_2\text{OP}_3\text{PdS}_2$: C, 49.35 (49.50); H, 3.60 (3.66); N, 2.71 (2.75); S, 6.20 (6.29). MP: 245–247 °C, $A_M = 50.6 \Omega^{-1} \text{cm}^2 \text{mol}^{-1}$.

(8) $[\text{Pd}(\text{dppf})(\text{N,N}$ -diphenyl-*N'*-thiophenylthioureato- $\text{k}^2\text{O,S})]\text{PF}_6$: ^1H NMR, δ : 8.02 (1H, dd, $J_1 = 7.2$ Hz, $J_2 = 8.1$ Hz, thiophene CH), 7.90 (1H, dd, $J_1 = 7.5$ Hz, $J_2 = 8.2$ Hz, thiophene CH), 7.89 (1H, dd, $J_1 = 6.7$ Hz, $J_2 = 8.3$ Hz, thiophene CH), 7.82–7.13 (m, 10H, arom-H). NMR ^{13}C , δ : 173.7 (C=S); 166.2 (C=O); 144.1, 143.2, 140.8, 140.7, 134.7, 134.2, 134.1, 134.0, 133.9, 132.3, 128.5–127.8 (C-Ph); $^{31}\text{P}\{^1\text{H}\}$, δ : 41.62 (d); 27.63 (d); $^2J_{P-P} = 19.43$ Hz; IR,

cm^{-1} : $\nu(\text{C}=\text{O})$ 1420, $\nu(\text{C}=\text{S})$ 743; $\nu(\text{C}=\text{N})$ 1479; Anal. (%): Found (Calc) for $\text{C}_{52}\text{H}_{41}\text{F}_6\text{FeN}_2\text{OP}_3\text{PdS}_2$: C, 54.45 (54.63); H, 3.49 (3.61); N, 2.41 (2.45); S, 5.54 (5.61). MP: 256–258 °C, $A_M = 49.6 \Omega^{-1} \text{cm}^2 \text{mol}^{-1}$.

2.4. Crystal structure determination

Single crystals suitable for X-ray diffraction were obtained by slow evaporation of CHCl_3 :*n*-hexane (3:1) solutions of the complexes **2**, **3**, **5**, **6** and **8**. Diffraction data were collected on an Enraf–Nonius Kappa-CCD diffractometer with graphite-monochromated Mo K α radiation ($\lambda = 0.71073$ Å). The final unit cell parameters were based on all reflections. Data collections were performed using the COLLECT program [13]; integration and scaling of the reflections were performed with the HKL Denzo–Scalepack system of programs [14]. Absorption corrections were carried out using the Gaussian method [15]. The structures were solved by direct methods with SHELXS-97 [16]. The models were refined by full-matrix least-squares on F^2 by means of SHELXL-97 [17]. The projection views of the structures were prepared using ORTEP-3 for Windows [18]. Hydrogen atoms were stereochemically positioned and refined with the riding model. Data collections and experimental details are summarized in Table 1. Relevant interatomic bond lengths and angles are listed in Table 2. Also included are the CCDC deposit numbers for Supplementary crystallographic data.

2.5. Antimycobacterial activity assay

Antimycobacterial activities of each tested compound and of the standard drug ethambutol were determined in triplicate, in sterile 96-well flat bottom microplates. The tested compound concentrations ranged from 0.087 to 25 $\mu\text{g}/\text{mL}$, and the ethambutol from 0.015 to 1.0 $\mu\text{g}/\text{mL}$. The microplate Alamar Blue assay [19] was used to measure the minimal inhibitory concentration (MIC) for the tested compounds (minimum concentration necessary to inhibit 90 % growth of *M. tuberculosis* H₃₇Rv ATCC 27294). The development of a pink color in the wells was taken as indicating bacterial growth and the maintenance of a blue color as the contrary. The fluorescence of the dye was measured in a SPECTRAfluor Plus microplate reader (Tecan*) in bottom reading mode with excitation at 530 nm and emission at 590 nm.

Table 1
Crystal data and refinement parameters for **2**, **3**, **5**, **6**, and **8** complexes.

Compound	2	3	5	6	8
Empirical formula	C ₄₆ H ₄₃ F ₆ FeN ₂ O ₃ PdS. CH ₂ Cl ₂	C ₅₀ H ₅₁ F ₆ FeN ₂ O ₃ PdS	C ₄₄ H ₄₁ F ₆ FeN ₂ O ₂ P ₃ PdS	C ₅₂ H ₄₁ F ₆ FeN ₂ O ₂ P ₃ PdS	C ₅₂ H ₄₁ F ₆ FeN ₂ O P ₃ PdS ₂
Formula weight	1125.97	1097.15	1031.01	1127.09	1143.15
Crystal system	monoclinic	monoclinic	monoclinic	triclinic	triclinic
Space group	<i>P2₁/c</i>	<i>Pc</i>	<i>P2₁/a</i>	<i>P1̄</i>	<i>P1̄</i>
<i>T</i> (K)	293	296		296	296
<i>a</i> (Å)	10.5650(2)	10.6147(5)	10.8430(2)	12.5827(3)	12.5960(3)
<i>b</i> (Å)	27.6270(8)	14.557(1)	28.8291(5)	13.8101(4)	13.8000(4)
<i>c</i> (Å)	16.8200(4)	16.325(1)	14.1096(2)	14.9739(4)	15.0780(4)
<i>V</i> (Å ³)	4861.2(2)	2506.2(3)	4406.77(13)	2453.78(12)	2479.3(1)
<i>Z</i>	4	2	4	2	2
<i>D</i> _{calc} (mg/m ³)	1.538	1.454	1.554	1.525	1.531
Absorption coefficient (mm ⁻¹)	0.981	0.846	0.958	0.868	0.899
<i>F</i> (000)	2280	1120	2088	1140	1156
θ range for data collection (°)	2.555–25.999	2.875–25.997	2.565–25.997	2.972–25.999	2.84–26.00
Index ranges	–11 ≤ <i>h</i> ≤ 13 –32 ≤ <i>k</i> ≤ 34 –20 ≤ <i>l</i> ≤ 12	–12 ≤ <i>h</i> ≤ 13 –17 ≤ <i>k</i> ≤ 17 –20 ≤ <i>l</i> ≤ 16	–12 ≤ <i>h</i> ≤ 13 –35 ≤ <i>k</i> ≤ 35 –16 ≤ <i>l</i> ≤ 17	–15 ≤ <i>h</i> ≤ 15 –17 ≤ <i>k</i> ≤ 16 –18 ≤ <i>l</i> ≤ 18	–15 ≤ <i>h</i> ≤ 15 –17 ≤ <i>k</i> ≤ 17 –18 ≤ <i>l</i> ≤ 18
Reflections collected	25156	12255	38378	25632	28331
Independent reflections (<i>R</i> _{int})	9351 [<i>R</i> _{int} = 0.0386]	7966 [<i>R</i> _{int} = 0.0592]	8639 [<i>R</i> _{int} = 0.0926]	9547 [<i>R</i> _{int} = 0.0481]	9719 [<i>R</i> _{int} = 0.0387]
Goodness-of-fit on <i>F</i> ²	1.024	1.044	1.026	1.019	1.070
Final <i>R</i> indices	<i>R</i> ₁ = 0.0518	<i>R</i> ₁ = 0.0603	<i>R</i> ₁ = 0.0509	<i>R</i> ₁ = 0.0479	<i>R</i> ₁ = 0.0461
[<i>I</i> N 2σ (<i>I</i>)]	<i>wR</i> ₂ = 0.1345	<i>wR</i> ₂ = 0.1537	<i>wR</i> ₂ = 0.1275	<i>wR</i> ₂ = 0.1247	<i>wR</i> ₂ = 0.1314
Largest diff. peak and hole (eÅ ⁻³)	0.848 and –0.631	0.779 and –0.487	0.888 and –0.810	0.623 and –0.794	1.160 and –0.794
CCDC deposit number	1502550	1502551	1502552	1502553	1502554

Table 2
Selected bond lengths (Å) and angles (°) for **2**, **3**, **5**, **6** and **8** complexes.

	2	3	5	6	8
<i>Bond lengths</i> (Å)					
Pd–O	2.046(3)	2.067(7)	2.032(3)	2.049(2)	2.053(2)
Pd–P(1)	2.261(1)	2.266(2)	2.255(1)	2.2578(9)	2.2620(8)
Pd–P(2)	2.356(1)	2.359(2)	2.35(1)	2.3478(9)	2.3527(8)
Pd–S	2.290(1)	2.295(2)	2.300(1)	2.2979(9)	2.2991(9)
S–C1	1.740(4)	1.73(1)	1.748(5)	1.721(4)	1.731(4)
O–C2	1.274(5)	1.26(1)	1.259(5)	1.267(4)	1.270(4)
C1–N1	1.335(6)	1.37(1)	1.333(6)	1.334(5)	1.329(5)
C2–N1	1.297(6)	1.29(1)	1.309(6)	1.317(5)	1.322(4)
<i>Angles</i> (°)					
O–Pd–S	91.88(9)	92.2(2)	90.9(1)	91.94(7)	92.16(7)
O–Pd–P(1)	178.8(1)	178.8(2)	176.0(1)	179.41(8)	178.67(9)
O–Pd–P(2)	84.53(9)	84.6(2)	84.1(1)	83.25(7)	83.86(7)
P(2)–Pd–S	175.94(4)	176.8(1)	174.41(4)	174.64(3)	174.29(3)
P(1)–Pd–S	88.43(4)	88.24(9)	90.42(4)	88.14(3)	87.58(3)
P(2)–Pd–P(1)	95.12(4)	94.99(8)	94.74(4)	96.70(3)	96.49(3)

2.6. Antiparasitic activity

Y strain trypomastigotes of *T. cruzi* collected from the LLC-MK2 cell supernatant were dispensed into 96-well plates at a cell density of 2.0×10^6 cells/mL in 200 μ L of RPMI medium. Compounds were tested at eight concentrations from (10–0.01 μ M), in triplicate. The plate was incubated for 24 h at 37 °C and 5% CO₂. Aliquots from each well were collected and the number of viable parasites, based on parasite viability, was assessed in a Neubauer chamber and compared to untreated parasite culture. This experiment was performed three times. Inhibitory concentration for 50 % (IC₅₀) was calculated using data-points gathered from three independent experiments. Benznidazole was used as a positive control.

2.7. Cytotoxicity in murine cells

J774 cells (murine macrophages cell line, established from a tumor that arose in female BALB/c mouse) were placed on 96-well plates at a cell density of 5×10^4 cells/ML in 200 μ L of RPMI-1640 medium (no phenol red) and supplemented with 10% FBS and 50 μ g/mL of gentamycin and incubated for 24 h at 37 °C and 5%

CO₂. Compounds were added in a series of eight concentrations, in triplicate, and incubated for 72 h. Then, 20 μ L/well of AlamarBlue (Invitrogen, Carlsbad, USA) was added to all wells and incubated during 6 h. Colorimetric readings were performed at 570 and 600 nm. Cytotoxic concentration for 50% (CC₅₀) was calculated using data-points gathered from three independent experiments. Gentian violet was used as a positive control.

2.8. Propidium iodide (PI) and annexin V staining

T. cruzi trypomastigotes from Y strain (1×10^7) were incubated for 24 h at 37 °C in the absence or presence of **1** (0.61 or 1.22 μ M) or **4** (1.91 or 3.82 μ M). After incubation, the parasites were labeled for PI and FITC-annexin V using the annexin V-FITC apoptosis detection kit (Sigma–Aldrich), according to the manufacturer's instructions. Acquisition and analyses was performed using a FACS Calibur flow cytometer (Becton Dickinson, San Diego, CA), with FlowJo software (Tree Star, Ashland, OR). A total of 10,000 events were acquired in the region previously established as that corresponding to trypomastigotes.

3. Results and discussion

The ligands were prepared following the procedures previously reported in the literature [12] and were obtained in yields ranging from 79% to 91%. The complexes of the type $[\text{Pd}(\text{dppf})(\text{L})]$ were obtained by the reactions between $[\text{Pd}(\text{dppf})\text{Cl}_2]$ and the ligands (see Scheme 1). The synthesized complexes were yellowish crystals and their elemental analyses, melting point temperatures, and molar conductivities are listed in the experimental section. Complexes **2**, **3**, **5**, **6** and **8** were also characterized by single crystal X-ray diffraction.

The IR spectra of the complexes were compared with those of the free ligands. The N–H stretching vibrations which exist in the ligands disappear. A broad peak ascribed to the C–N bond appears around $1580\text{--}1600\text{ cm}^{-1}$, indicating deprotonation of the acylthioureido group of the ligands during the complexes formation and therefore their coordination through the oxygen and sulfur atoms [20–22]. The bands observed around $471\text{--}490\text{ cm}^{-1}$ were assigned to M–O [23,24]. Assignment of the Pd–S stretching vibration bands at about 360 cm^{-1} are in accordance to the reported literature [25,26]. The bands in the $551\text{--}556\text{ cm}^{-1}$ range are assigned to M–N (imino nitrogen) [20]. Strong bands in the region of about 1500 cm^{-1} , are shown by the IR spectra of the complexes which may reasonably be assigned to the coordinated C–O groups. The absorption bands at $815\text{--}878\text{ cm}^{-1}$ in the spectra of free *N,N*-disubstituted-*N'*-acylthioureas, attributed to the $\nu(\text{C}=\text{S})$ stretching vibrations, shift to the $837\text{--}845\text{ cm}^{-1}$ range in the complexes spectra, corresponding to the weakening of the C–S double bond character [21].

In the ^1H NMR spectra (CDCl_3) of the ligands HL(**1–8**), the NH proton appears at $8.79\text{--}8.45\text{ ppm}$ as broad singlets. This signal is absent in the ^1H NMR spectra of the corresponding palladium complexes, in the same solvent, as a consequence of the deprotonation of the nitrogen atom. Similarly, the IR spectra of the ligands HL(**1–8**) show NH stretching vibrations in the range $3150\text{--}3260\text{ cm}^{-1}$, but these signals are absent in the spectra of the corresponding metal complexes. In the ^{13}C NMR spectra, the carbon atom of the thiocarbonyl group appears at $\delta = 165.67\text{--}173.67$ in the metal complexes, as mentioned in the experimental section.

The $^{31}\text{P}\{^1\text{H}\}$ NMR spectra of the precursor $[\text{Pd}(\text{dppf})\text{Cl}_2]$, in CH_2Cl_2 solution, shows a singlet peak for phosphorus atoms at $\delta = 35.12$. For all complexes two doublets arise, at about $\delta = 41.34$ and 27.64 , indicating the presence of two magnetically different phosphorus atoms coordinated to the palladium(II) ion. Also in the region of $\delta = -138\text{--}158$ a multiple signal of the PF_6^- , functioning as outer-sphere anions for the complexes is observed, in accordance to the molar conductivity measurements for these complexes (see experimental section). These data are consistent with those obtained for some thiosemicarbazones and *N,N*-disubstituted-*N'*-acyl thioureas complexes [10,21,27].

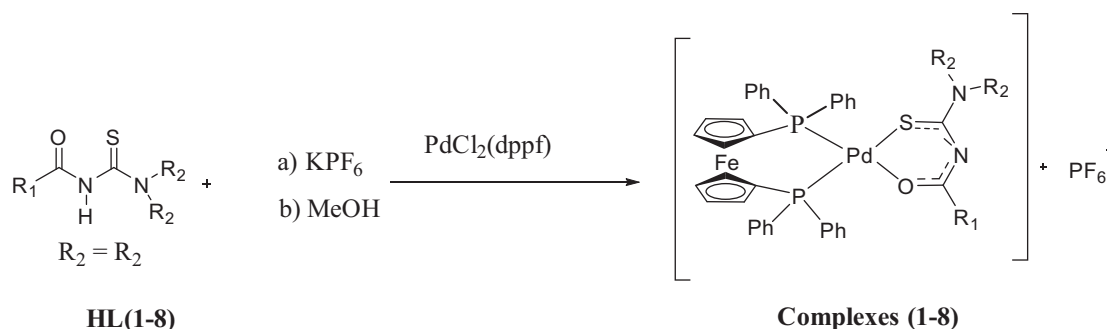
The molecular structures of **2**, $[\text{Pd}(\text{dppf})(\text{N,N}\text{-diethyl-}N'\text{-benzoylthioureato-}k^2\text{O,S})]\text{PF}_6$, **3**, $[\text{Pd}(\text{dppf})(\text{N,N}\text{-dibutyl-}N'\text{-benzoylthioureato-}k^2\text{O,S})]\text{PF}_6$, **5**, $[\text{Pd}(\text{dppf})(\text{N,N}\text{-diethyl-}N'\text{-furoylthioureato-}k^2\text{O,S})]\text{PF}_6$, **6**, $[\text{Pd}(\text{dppf})(\text{N,N}\text{-diphenyl-}N'\text{-furoylthioureato-}k^2\text{O,S})]\text{PF}_6$, and **8**, $[\text{Pd}(\text{dppf})(\text{N,N}\text{-diphenyl-}N'\text{-thiophenylthioureato-}k^2\text{O,S})]\text{PF}_6$, are shown in Fig. 2, and selected bond lengths and angles ($^\circ$) for these structures are listed in Table 2.

In all complexes the Pd(II) ion is nearly planar, in a fourfold environment. The thione C–S bond in the coordinated anionic ligands becomes formally a single bond making it longer (average = 1.734 \AA) than the C=S bond of the neutral moieties [27,28] (Fig. 2, Table 2). Thus the metal is coordinated to the negatively charged organic molecules, which act as bidentate ligands, through oxygen (average distance Pd–O = 2.0494 \AA) and sulfur (average distance Pd–S = 2.2964 \AA) atoms. The Pd–S average distance is close to the ones found for other palladium(II) thiosemicarbazones complexes [21]. The remaining binding sites are occupied by biphosphines (dppf) (average distance Pd–P1 = 2.2604 \AA and Pd–P2 = 2.3531 \AA). The distances for the C–S and C–O bonds in the chelate rings, listed in Table 2, are the characteristic of single and double bond lengths, respectively [9,21,27]. The N1–C1 and N2–N1 bond distances (average 1.3402 \AA and 1.307 \AA , respectively) present typical bond lengths of double bond character, suggesting an electron delocalization in the acyl thiourea moiety [21–27]. The C–O bond distances are slightly sensitive to the coordination of the ligand to the metal. In previously work it was reported, on the bis-triphenylphosphine-*N,N*-diethyl-*N'*-furoylthioureato- $k^2\text{O,S}$, that the C–O distance for the free ligand is $1.226(3)\text{ \AA}$ (average for two independent molecules per asymmetric unit), and $1.266(9)\text{ \AA}$ (average), after its coordination to the metal [28].

After structural characterization, the metal-free *N,N*-disubstituted-*N'*-acylthioureas and metal complexes were investigated for their *in vitro* antimycobacterial activity against *M. tuberculosis* H37Rv strain and antiparasitic activity against Y strain *T. cruzi* trypanomastigotes. The results are displayed in Table 3.

None the metal-free ligands presented antimycobacterial activity in concentration below $70\text{ }\mu\text{M}$, while the palladium complexes presented activity in the same micromolar range as observed under Ethambutol treatment. Therefore, the presence of palladium is essential to improve the antimycobacterial activity of the free ligands. Regarding structure–activity relationships, the main difference between most and less active Pd(II) complexes is the presence of a linear and alkyl side chain attached at R2 in the ligand structure. This may be the reason for the decreased the antimycobacterial activity of complexes **4**, **6** and **8** in comparison to **1**, **2**, **3**, **5** and **7**.

Next, the antiparasitic activity was analyzed and the results were compared to the reference drug benznidazole, which displayed an IC_{50} value of $10.61 \pm 0.87\text{ }\mu\text{M}$. None the metal-free ligands displayed antiparasitic activity, while the Pd(II) complexes



Scheme 1. Route for the syntheses of $[\text{Pd}(\text{dppf})(\text{N,N}\text{-disubstituted-}N'\text{-acylthiourea})]\text{PF}_6$ complexes.

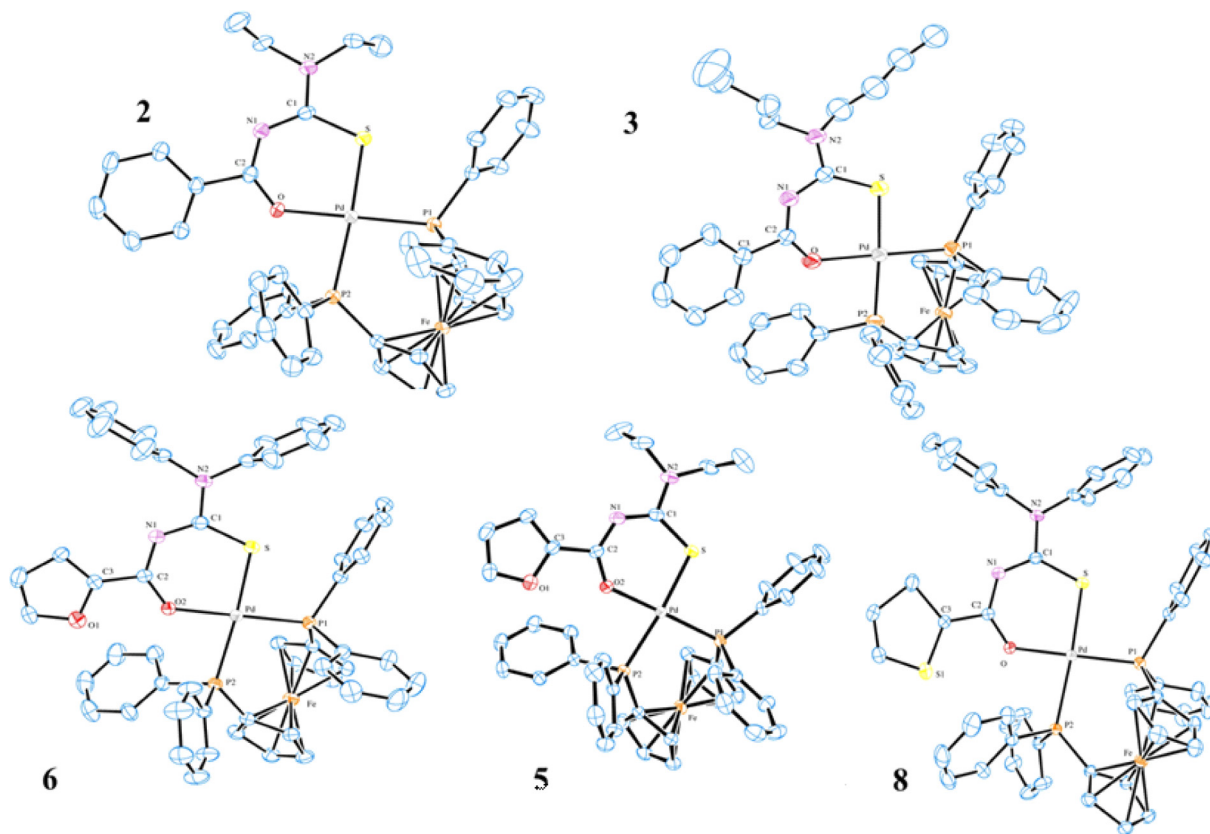


Fig. 2. ORTEP view of complexes **2**, **3**, **5**, **6** and **8** showing 50% probability ellipsoids. The $(PF_6)^-$ anion and some labels of the ligands are omitted for clarity. For complex **2** there is a CH_2Cl_2 solvated molecule, which was also omitted.

Table 3
Antimycobacterial, antiparasitic and cytotoxicity activity of ligands and complexes **1–8**.

Compound	<i>M. tuberculosis</i> H ₃₇ Rv MIC (μM) ^(a)	<i>T. cruzi</i> IC ₅₀ ± S.E.M. (μM) ^(b)	Cytotoxicity CC ₅₀ ± S.D. (μM) ^(c)	SI ^(d)
HL (1)	>119.6	>10	>30	–
HL (2)	>100.3	>10	>30	–
HL (3)	>85.6	>10	>30	–
HL (4)	>75.3	>10	>30	–
HL (5)	>110.6	>10	>30	–
HL (6)	>75.3	>10	>30	–
HL (7)	>116.8	>10	>30	–
HL (8)	>73.9	>10	>30	–
1	2.58 ± 0.38	0.61 ± 0.27	2.63 ± 1.25	4.3
2	2.82 ± 0.04	0.53 ± 0.21	1.53 ± 0.50	2.9
3	5.24 ± 0.33	1.47 ± 0.47	4.14 ± 1.35	2.8
4	17.32 ± 0.20	1.91 ± 0.50	8.83 ± 1.60	4.6
5	2.98 ± 0.02	0.76 ± 0.20	2.27 ± 0.64	3.0
6	6.36 ± 0.16	1.91 ± 0.70	3.86 ± 0.35	2.0
7	2.88 ± 0.07	0.55 ± 0.07	1.85 ± 0.48	3.3
8	9.71 ± 1.12	1.59 ± 0.04	5.83 ± 0.72	3.7
Ethambutol	5.62	–	–	–
Benznidazole	–	10.61 ± 0.87	>30	>2.8
Gentian Violet	–	–	0.82 ± 0.12	–

^(a) Determined after 7 days incubation time with the drugs.

^(b) Determined in trypomastigotes after 24 h incubation.

^(c) Determined in J774 macrophages after 72 h incubation.

^(d) SI = selectivity index for antiparasitic activity, determined as $CC_{50}(\text{cytotoxicity})/IC_{50}(\text{trypomastigotes})$.

exhibit antiparasitic activity. In general, the metal complexes were more potent antiparasitic agents than benznidazole, however, they presented lower selectivity indexes than benznidazole. After observing that palladium complexes exhibit antiparasitic activity, it was investigated how the complexes can cause parasite cell death. To this end, trypomastigotes were treated with the IC₅₀ or

IC₉₉ concentration of complexes **1** and **4** for 24 h and then stained with PI/annexin (Fig. 3).

In comparison to untreated parasites, treatment with complex **1** at IC₅₀ concentration increased from 2.2 to 11.5 % cells positively stained for annexin. When the complex **1** was added at IC₉₉ concentration, the % of annexin-stained cells changed from 11.5 to

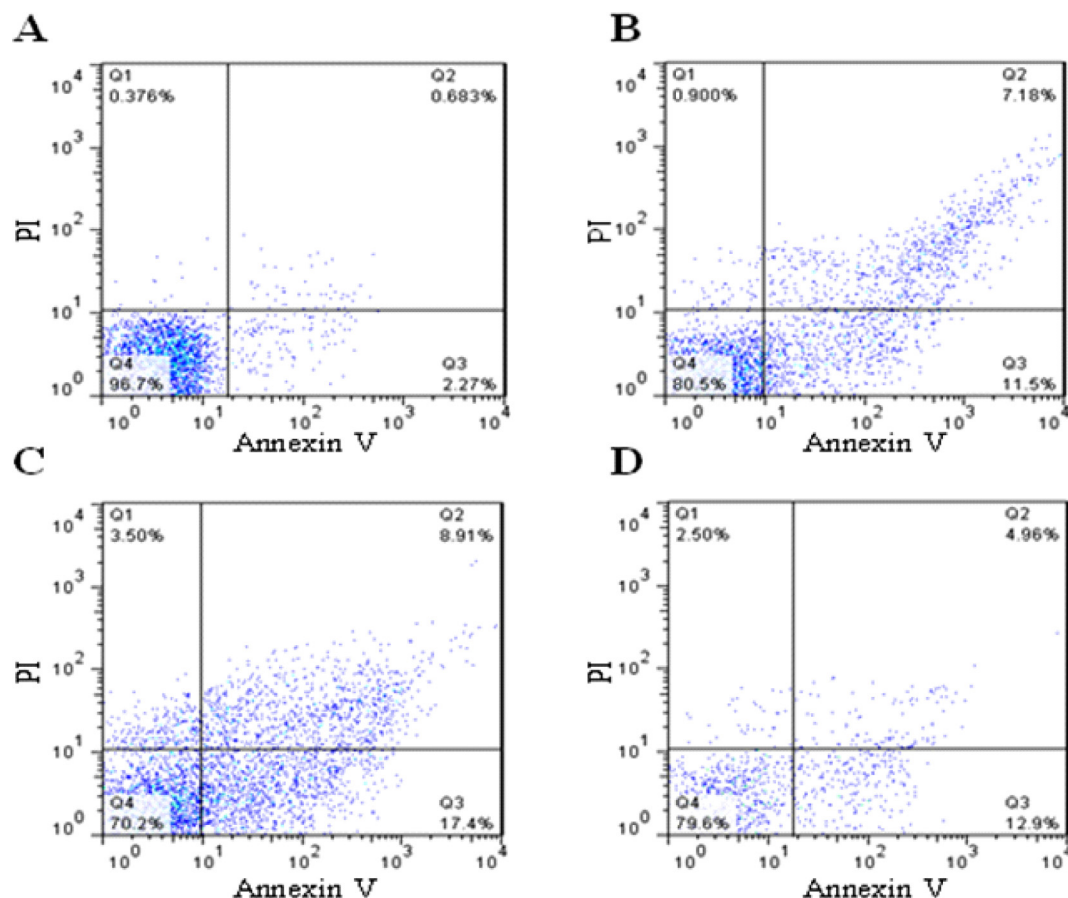


Fig. 3. Flow cytometry analysis of trypomastigotes (Ystrain) treated with **1** or **4** for 24 h and stained with PI and annexin V. (A) Representative untreated trypomastigotes; (B) trypomastigotes treated with **1** ($0.61 \mu\text{mol L}^{-1}$); (C) trypomastigotes treated with **1** ($1.22 \mu\text{M}$); (D) trypomastigotes treated with **4** ($1.91 \mu\text{M}$). Three independent experiments were performed, here on representative experiment is shown.

17.4, indicating that complex acts in a concentration-dependent manner. It was also observed that complex **1** treatment increased the double staining for PI/annexin. A similar cell death was also observed when complex **4** was evaluated. The single and double staining observed here for these complexes are indicative that parasite cell death occurs through an apoptosis process. Antiparasitic properties of palladium complexes have been observed as causing apoptotic cell death [29], while other metal transition complexes usually cause a necrotic death [30].

4. Conclusions

A novel series of Pd(II)/*N,N*-disubstituted-*N*-acyl thioureas is here reported. The IR and NMR data suggest the coordination of the ligands to the metal center occurs bidentately, through the oxygen and sulfur atoms, which was confirmed by X-ray crystallographic characterization for complexes **2**, **3**, **5**, **6** and **8**. *In vitro* screening of complexes against *M. tuberculosis* and *T. cruzi* revealed that metal-free ligands were inactive, while complexes were activity. Structure–activity relationship indicated that their activity are dependent of the R2 group present in the amine nitrogen, while the nature of R1, attached in the acyl group, was less important for activity. The findings observed here reinforce that palladium are valuable antiparasitic agents.

Acknowledgments

This work was supported by the Brazilian sponsors: CAPES (Project Oficio/CSS/CGCI/ 23038009487/2011-25/DRI/CAPES, AUX

CAPES-MES-Cuba, 339/2011), CNPq, FAPESP (Processo 2014/13691-4) and FAPESP.

Appendix A. Supplementary data

CCDC 1502550, 1502551, 1502552, 1502553 and 1502554 contains the supplementary crystallographic data for complexes **2**, **3**, **5**, **6** and **8**. These data can be obtained free of charge via <http://dx.doi.org/10.1016/j.poly.2017.05.003>, or from the Cambridge Crystallographic Data Centre, 12 Union Road, Cambridge CB2 1EZ, UK; fax: (+44) 1223-336-033; or e-mail: deposit@ccdc.cam.ac.uk.

References

- [1] Global Alliance for TB Drug Development. www.tb Alliance.org [accessed 01.06.2016].
- [2] T.D. Primm, S.G. Franzblau, *Curr. Bioact. Compd.* 6 (2007) 201.
- [3] C.J. Schofield, C.J. Jannin, J.R. Salvatella, *Trends Parasitol.* 12 (2006) 583.
- [4] S. Antinori, R. Grande, R. Bianco, L. Traversi, C. Cogliati, D. Torzillo, E. Repetto, M. Corbellino, L. Milazzo, M. Galli, L. Galimberti, *Clin. Infect. Dis.* 60 (2015) 1873.
- [5] J.A. Urbina, *Acta Trop.* 115 (2010) 55.
- [6] H. Pervze, H.P. Iqbal, M.Y. Tahir, F.H. Nasim, M.I. Choudhary, K.M. Khan, *J. Enzym. Inhib. Med. Chem.* 23 (2008) 848.
- [7] D.C. Greenbaum, Z. Mackey, E. Hansell, P. Doyle, J. Gut, C.R. Caffrey, J. Lehrman, P.J. Rosenthal, J.H. Mckerrow, K. Chibale, *J. Med. Chem.* 47 (2004) 3212.
- [8] G.M. Dobrikov, V. Valcheva, Y. Nikolova, I. Ugrinova, E. Pasheva, V. Dimitrov, *Eur. J. Med. Chem.* 63 (2013) 468.
- [9] A.M. Plutín, R. Mocelo, A. Alvarez, R. Ramos, E.E. Castellano, Marcia R. Cominetti, A.E. Graminha, A.G. Ferreira, A.A. Batista, *J. Inorg. Biochem.* 134 (2014) 76.
- [10] R.S. Correa, K.M. de Oliveira, F.G. Delolo, A. Alvarez, R. Mocelo, A.M. Plutín, M.R. Cominetti, E.E. Castellano, A.A. Batista, *J. Inorg. Biochem.* 150 (2015) 63.

- [11] H. Arslan, N. Duran, G. Borekci, C.K. Ozer, C. Akbay, *Molecules* 14 (2009) 519.
- [12] A. Plutín, H. Márquez, M. Morales, M. Sosa, L. Morán, Y. Rodríguez, M. Suárez, C. Seoane, N. Martín, *Tetrahedron* 56 (2000) 1533.
- [13] Enraf-Nonius, Collect, Nonius BV, Delft, The Netherlands, 1997–2000.
- [14] Z. Otwinowski, W. Minor, Processing of X-ray diffraction data collected in oscillation mode, *Macromol. Crystallogr. A* 276 (1997).
- [15] R.H. Blessing, *Acta Crystallogr. A* 51 (1995) 33.
- [16] G.M. Sheldrick, ShelXS-97 Program for Crystal Structure Resolution, University of Göttingen, Göttingen, Germany, 1997.
- [17] G.M. Sheldrick, ShelXL-97, University of Göttingen, Göttingen, Germany, Program for Crystal Structures Analysis, 1997.
- [18] L.J. Farrugia, *J. Appl. Crystallogr.* 30 (1997) 565.
- [19] L.A. Collins, S.G. Franzblan, *Antimicrob. Agents Chemother.* 41 (1997) 1004.
- [20] A.E. Graminha, C. Rodrigues, A.A. Batista, L.R. Teixeira, E.S. Fagundes, H. Beraldo, *Spectrochim. Acta A* 69 (2008) 1073.
- [21] P. I. da S. Maia, A.E. Graminha, F.R. Pavan, C.Q.F. Leite, A.A. Batista, D.F. Back, E.S. Lang, J. Ellena, S. de S. Lemos, H.S. Salistre-de-Araujo, V.M. Deflon, *J. Braz. Chem. Soc.* 21 (2010) pp. 1177.
- [22] A.P. Rebolledo, M. Vieites, D. Gambino, O.E. Piro, E.E. Castellano, C.L. Zani, E.M. Souza-Fagundes, L.R. Teixeira, A.A. Batista, H. Beraldo, *J. Inorg. Biochem.* 99 (2005) 698.
- [23] K. Nakamoto, *Infrared and Raman Spectra of Inorganic and Coordination Compounds*, fourth ed., Wiley, New York, 1986.
- [24] A. Pérez-Rebolledo, O.E. Piro, E.E. Castellano, L.R. Teixeira, A.A. Batista, H. Beraldo, *J. Mol. Struct.* 794 (2006) 18.
- [25] B.H. Abdullah, Y.M. Salh, *Orient. J. Chem.* 26 (2010) 763.
- [26] M.N. Patel, C.R. Patel, H.N. Joshi, P.A. Vekariya, *Appl. Biochem. Biotechnol.* 172 (2014) 1846.
- [27] A.M. Plutín, A. Alvarez, R. Mocio, R. Ramos, E.E. Castellano, M.M. da Silva, L. Colina-Vegas, Fernando R. Pavan, A.A. Batista, *Inorg. Chem. Com.* 63 (2016) 74.
- [28] B. O'Reilly, A.M. Plutín, H. Pérez, O. Calderón, R. Ramos, R. Martínez, R.A. Toscano, J. Duque, H. Rodríguez-Solla, R. Martínez-Alvarez, M. Suárez, N. Martín, *Polyhedron* 36 (2010) 133.
- [29] A.L. Matsuo, L.S. Silva, A.C. Torrecilhas, B.S. Pascoalino, T.C. Ramos, E.G. Rodrigues, S. Schenkman, A.C. Caires, L.R. Travassos, *Antimicrob. Agents Chemother.* 54 (2010) 3318.
- [30] T. M. Bastos, M. I. Barbosa, M. M. da Silva, J. W. da C. Júnior, C. S. Meira, E. T. Guimaraes, J. Ellena, D. R. Moreira, A. A. Batista, M. B. Soares, *Antimicrob. Agents Chemother.* 58 (2014) pp. 6044.

ANEXO 10

FILHO, G. B. O.; CARDOSO, M. V. O.; ESPÍNOLA, J. W. P.; SILVA, D. A. O.; FERREIRA, R. S.; COELHO, P. L.; ANJOS, P. S.; SANTOS, E. S.; **MEIRA, C. S.**; MOREIRA, D. R. M.; SOARES, M. B. P.; LEITE, A. C. L. Structural design, synthesis and pharmacological evaluation of thiazoles against *Trypanosoma cruzi*. **European Journal of Medicine Chemistry**, v. 141, p. 346-361, 2017.



Contents lists available at ScienceDirect

European Journal of Medicinal Chemistry

journal homepage: <http://www.elsevier.com/locate/ejmech>

Research paper

Structural design, synthesis and pharmacological evaluation of thiazoles against *Trypanosoma cruzi*

Gevanio Bezerra de Oliveira Filho ^{a, b, *}, Marcos Veríssimo de Oliveira Cardoso ^c, José Wanderlan Pontes Espíndola ^a, Dayane Albuquerque Oliveira e Silva ^a, Rafaela Salgado Ferreira ^d, Pollyanne Lacerda Coelho ^d, Pâmela Silva dos Anjos ^e, Emanuelle de Souza Santos ^e, Cássio Santana Meira ^e, Diogo Rodrigo Magalhaes Moreira ^e, Milena Botelho Pereira Soares ^{e, f}, Ana Cristina Lima Leite ^a

^a Laboratório de Planejamento em Química Medicinal - LpQM, Departamento de Ciências Farmacêuticas, Centro de Ciências da Saúde, Universidade Federal de Pernambuco - UFPE, 50740-520, Recife, PE, Brazil

^b Faculdade de Integração do Sertão - FIS, Rua João Luiz de Melo, 2110, COHAB, Serra Talhada, PE, Brazil

^c Colegiado de Nutrição, Universidade de Pernambuco, CEP 56328-903, Petrolina, PE, Brazil

^d Departamento de Bioquímica e Imunologia, Universidade Federal de Minas Gerais, CEP 31270-901, Belo Horizonte, MG, Brazil

^e Instituto Gonçalo Moniz, Fundação Oswaldo Cruz, CEP 40296-710, Salvador, BA, Brazil

^f Centro de Biotecnologia e Terapia Celular, Hospital São Rafael, Salvador, BA, Brazil

ARTICLE INFO

Article history:

Received 5 July 2017

Received in revised form

29 August 2017

Accepted 21 September 2017

Available online 22 September 2017

Keywords:

Chagas disease

Thiosemicarbazones

Thiazoles

Trypanosoma cruzi

ABSTRACT

Chagas disease is one of the most significant health problems in the American continent. benznidazole (BDZ) and nifurtimox (NFX) are the only drugs approved for treatment and exhibit strong side effects and ineffectiveness in the chronic stage, besides different susceptibility among *T. cruzi* DTUs (Discrete Typing Units). Therefore, new drugs to treat this disease are necessary. Thiazole compounds have been described as potent trypanocidal agents. Here we report the structural planning, synthesis and anti-*T. cruzi* evaluation of a new series of 1,3-thiazoles (**7–28**), which were designed by placing this heterocycle instead of thiazolidin-4-one ring. The synthesis was conducted in an ultrasonic bath with 2-propanol as solvent at room temperature. By varying substituents attached to the phenyl and thiazole rings, substituents were observed to retain, enhance or greatly increase their anti-*T. cruzi* activity. In some cases, methyl at position 5 of the thiazole (compounds **9**, **12** and **23**) increased trypanocidal property. The exchange of phenyl for pyridinyl heterocycle resulted in increased activity, giving rise to the most potent compound against the trypanosigote form (**14**, IC₅₀trypo = 0.37 μM). Importantly, these new thiazoles were toxic for trypomastigotes without affecting macrophages and cardiomyoblast viability. The compounds were also evaluated against cruzain, and five of the most active compounds against trypomastigotes (**7**, **9**, **12**, **16** and **23**) inhibited more than 70% of enzymatic activity at 10 μM, among which compound **7** had an IC₅₀ in the submicromolar range, suggesting a possible mechanism of action. In addition, examination of *T. cruzi* cell death showed that compound **14** induces apoptosis. We also examined the activity against intracellular parasites, revealing that compound **14** inhibited *T. cruzi* infection with potency similar to benznidazole. The antiparasitic effect of **14** and benznidazole in combination was also investigated against trypomastigotes and revealed that they have synergistic effects, showing a promising profile for drug combination. Finally, in mice acutely-infected with *T. cruzi*, **14** treatment significantly reduced the blood parasitaemia and had a protective effect on mortality. In conclusion, we report the identification of compounds (**7**), (**12**), (**15**), (**23**) and (**26**) with similar trypanocidal activity of benznidazole; compounds (**9**) and (**21**) as trypanocidal agents equipotent with BDZ, and compound **14** with potency 28 times better than the reference drug without affecting macrophages and cardiomyoblast viability. Mechanistically, the

* Corresponding author. Laboratório de Planejamento em Química Medicinal - LpQM, Departamento de Ciências Farmacêuticas, Centro de Ciências da Saúde, Universidade Federal de Pernambuco - UFPE, 50740-520, Recife, PE, Brazil.

E-mail addresses: gev_filho@hotmail.com (G.B. de Oliveira Filho), acllb2003@yahoo.com.br (A.C.L. Leite).

compounds inhibit cruzain, and **14** induces *T. cruzi* cell death by an apoptotic process, being considered a good starting point for the development of new anti-Chagas drug candidates.

© 2017 Elsevier Masson SAS. All rights reserved.

1. Introduction

One of the most significant health problems in the American continent in terms of human health (i.e., number of people infected with and dying from it), socioeconomic impact and geographic distribution is the Chagas disease, caused by the protozoan parasite *Trypanosoma cruzi* (*T. cruzi*) [1]. In Brazil, losses of over US\$ 1.3 billion in wages and industrial productivity are estimated due to workers with Chagas disease [2]. Regardless of the decreased incidence of new infections in Brazil and other countries due to urbanization and improved living conditions, an estimated number of 6–8 million people remains infected [1–3].

Benznidazole (BDZ) and Nifurtimox (NFX), launched in the early 1970s, are the only drugs approved for human treatment. Both compounds share some characteristics: better tolerance by children, higher effectiveness during the acute phase of *T. cruzi* infection, higher toxicity in adults, and different susceptibility among *T. cruzi* DTUs (Discrete Typing Units). Private-funded laboratories lack interest on Chagas disease research, while equipment and technological restrictions in public laboratories hamper the development of new drugs and treatment strategies. This scenario generates the current situation where the available drugs are the same as in 1970, have strong side effects and ineffectiveness in the chronic phase of the disease [1,4]. Thus, new drugs to treat Chagas disease are necessary.

Trypanosoma cruzi contains cysteine, serine, threonine and metallo proteinases. The most abundant among these enzymes is cruzipain, a cysteine proteinase expressed as a complex mixture of isoforms by the major developmental stages of the parasite, including some membrane-bound isoforms. This enzyme is an immunodominant antigen in human chronic Chagas disease and seems to be important in the host/parasite relationship. Inhibitors of cruzipain kill the parasite and cure infected mice, thus making the enzyme a very promising target for the development of new drugs against Chagas disease [5–12].

The importance of this enzyme has recently been emphasized in a study by Sbaraglini et al. whose computer-guided drug repositioning strategy led to the discovery of the trypanocidal effects of clofazimine and benidipine. These compounds showed inhibitory effects on cruzipain, on different parasite stages and in a murine model of acute Chagas disease. Benidipine and clofazimine were able to reduce the parasite burden in cardiac and skeletal muscles of chronically infected mice compared with untreated mice as well as diminish the inflammatory process in these tissues [12].

Regarding the identification of cruzain inhibitors, most of the efforts have been conducted through the investigation of peptides and peptide-like compounds, such as ureas [13,14], hydrazones [15–17], triazoles [18,19], thiosemicarbazones [20–25], thiazolidin-4-ones [26–28] and 1,3-thiazoles [29–31].

Recently, our research group identified the thiazolidin-4-one (**5**) [32], a cyclic bioisoster of the potent cruzain inhibitor 3,4-dichlorophenyl thiosemicarbazone (**6**) [20]. Compound (**5**) was less active against cruzain than thiosemicarbazone (**6**). However, the antiparasitic activity against Y strain of *T. cruzi* trypomastigotes and host cell cytotoxicity in J774 macrophages revealed that compound (**5**) is a stronger and more selective antiparasitic agent than thiosemicarbazone (**6**). In *T. cruzi* infected mice treated orally with

100 mg/kg of compound (**5**), a decreased of parasitaemia was observed [32].

Thiazoles compounds (**1**, **2**, **3** and **4**) have been described as potent trypanocidal agents [28–31], then this work devised a series of 1,3-thiazoles for bioisosteric exchange thiazolidin-4-one ring through thiazole heterocycle (Fig. 1). The compounds of this series (**7–28**) were designed in such a way as to vary the group linked to position 4 of the thiazole ring, through insertion of alkyl substituents and aromatic rings with different substitutions in *ortho*, *meta* and *para*.

2. Results and discussion

2.1. Synthesis and chemical characterization

The general route to prepare thiazoles (**7–28**) is shown in Schemes 1–3. Firstly, thiosemicarbazones (**6a–c**) were prepared by reacting commercially available 3',4'-dichloroacetophenone with the appropriate thiosemicarbazide in an ultrasound bath in the presence of catalytic H₂SO₄ (or HCl in the case of thiosemicarbazone **6c**). Thiazoles (**7–9**) were prepared according to the methodology described by Hantzsch [33], by reacting the respective aryl thiosemicarbazone with commercially available chloroacetones (Scheme 1). These reactions were carried out in the presence of an excess of anhydrous NaOAc under reflux, affording compounds (**7–9**) in variable yields (46–88%) and acceptable purity (>95%).

For the series of thiazoles (**10–28**), due to previous experience of our research group [28–31] and literature reports [34], the synthesis was conducted in an ultrasonic bath (40 MHz, 30–120 min) with 2-propanol as solvent at room temperature. For these conditions the reaction proceeded faster and with similar yields to the Hantzsch method. The 2-bromoacetophenones used were purchased from commercial sources (Scheme 2).

To investigate the effect of substituents inserted on the N3 position for pharmacological activity, we prepared the aryl-thiazoles (**11**) and (**13**) (Scheme 3), in the same manner as compounds (**10–28**).

The chemical structures of compounds were determined by nuclear magnetic resonance (N.M.R., ¹H and ¹³C), infrared (I.R.) and mass spectra (HR-MS), while purity was determined by elemental analysis (E.A.). The analysis of ¹H and ¹³C NMR spectra of compounds (**7–28**) has highlighted the signals relating to the methine located at the C-5 position in the heterocyclic ring, which are diagnostic for this class of compounds. In NMR ¹³C, the carbon referring to this methine is easy to locate, in $\delta = 101–117$ ppm. In IR, the presence of the band relating iminics links as well as the absence of absorption in the carbonyl region are also suggestive of the formation of compounds (**7–28**).

Another important structural feature of these compounds is the position of the double bond involving the C2 carbon of the heterocycle ring. Depending on imino-lactam tautomerism, the C2 carbon double bond present in compounds (**7–10**, **12**, **14–28**) can be endocyclic or exocyclic in relation to the heterocycle (Fig. 2). Compounds **11** and **13** possess a methyl or phenyl group respectively in N-4 of thiazole nucleus, thus they presented an exocyclic bond.

In the NMR ¹H of compounds (**7–10**, **12**, **14–28**), the chemical

shift of the N-H ranges between 10.5 and 11.5 ppm (DMSO-d₆), while in thiosemicarbazone (**6a-c**), the chemical shift of hidrazinic protons varies between 10.29 and 10.66 ppm. The data from literature for amidic proton of lactams, thiazolidin-4-ones and thiazolidin-2,4-diones show the chemical shift in the range of 11.4–12.3 ppm [35,36]. In view of these reports, we can suggest that the N-H signal in the compounds (**7–10**, **12**, **14–28**) is characteristic of hidrazinic protons (Fig. 2, form I).

For an unambiguous assignment of this connection, we try to obtain crystals of the compounds (**7–28**) suitable for the diffraction of X-rays, but without success. Recently, Cardoso et al. (2014) [29] identified by X-ray crystallography that the position of the double bond involving the C2 carbon of the heterocycle ring of 2-pyridyl thiazoles is endocyclic. Based on this, we can suggest this is also true for compounds (**7–10**, **12**, **14–28**) (Fig. 2, form I).

Another important structural feature of these compounds is the isomerism *Z* or *E* in hydrazine double-bond C2=N2. Based on compounds previously crystallized by our group to define the relative configuration, we suggest that the major isomer formed presents the *E* configuration in hydrazine double-bond C2=N2 (Fig. 3) [26–29,37,38]. Besides, a representative NMR-¹H spectrum of compound **25** is presented in Supplementary Material.

2.2. Pharmacological evaluation

We assessed host cell cytotoxicity in J774 macrophages and H9c2 rat cardiomyoblasts, while *in vitro* anti-*T. cruzi* activity was determined against bloodstream trypomastigotes of Y strain (Table 1). Compounds that showed IC₅₀ values comparable to benznidazole were considered active.

Regarding cytotoxicity of the compounds (**7–28**) in J774 macrophages, five compounds (**7**, **9**, **14**, **15**, and **21**) were toxic at

concentrations less than 50 μM, and for H9c2 rat cardiomyoblast cells, only four compounds (**7**, **14**, **15** and **21**) were toxic at concentrations less than 50 μM. Beside these compounds, other thiazoles did not affect the cell viability of macrophages or cardiomyoblast at concentrations below 50 μM. The most toxic congener (**14**) was about 22 (J774) and 7 (H9c2) times less toxic than the reference inhibitor (gentian violet).

Compound (**7**, IC_{50trypo} = 17.1 μM), which has a methyl in position 4 of the thiazole ring, was one of the most potent compounds in the series, showed trypanocidal property similar to that of benznidazole (IC_{50trypo} = 10.6 μM). Similarly, compound (**9**, IC_{50trypo} = 10.5 μM), which differs to (**7**) only by one methyl at position 5 of the thiazole ring, demonstrated increased trypanocidal property, being equipotent to benznidazole. Also, compared to the compound unsubstituted in the phenyl ring (**10**, IC_{50trypo} = >50 μM) that did not show trypanocidal activity, inserting a methyl at position 5 of the thiazole ring (**12**), greatly increased pharmacological activity, to give a compound (**12**, IC_{50trypo} = 17.8 μM) equipotent to benznidazole. This suggests that substitution of alkyl groups at position 4 and 5 of the thiazole ring are beneficial for trypanocidal activity, corroborating the recent work of de Moraes Gomes [30,31]. On the other hand, the insertion of a chloromethyl (**8**, IC_{50trypo} = >50 μM) at position 4 of the thiazole ring has been shown deleterious for trypanocidal activity.

The mono-*para*-substituted compound with methoxy (**26**, IC_{50trypo} = 17.1 μM) was also equipotent to benznidazole. In the same position, substitution with methyl (**16**, IC_{50trypo} = 47.74 μM), fluorine (**17**, IC_{50trypo} = >50 μM), chlorine (**18**, IC_{50trypo} = >50 μM) or bromine (**22**, IC_{50trypo} = >50 μM) was deleterious for trypanocidal activity. Insertion of nitro groups in the *meta* and *para* positions, (**24**) and (**25**) also were not beneficial for pharmacological activity.

Interestingly, the simple insertion of a methyl at position 5 of

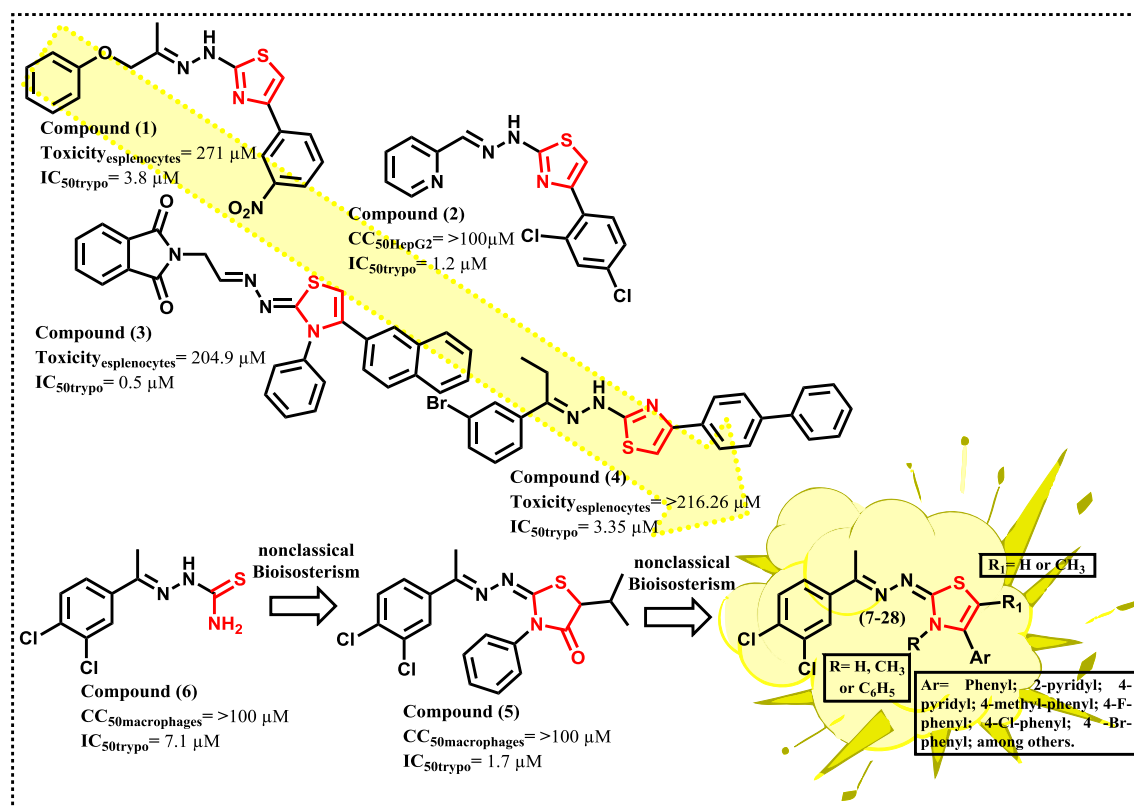
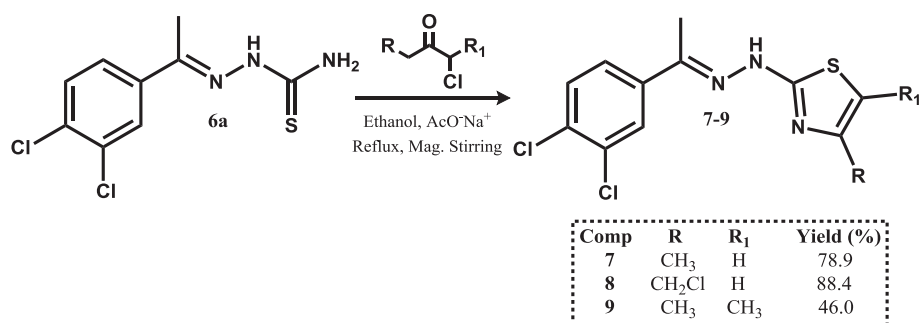
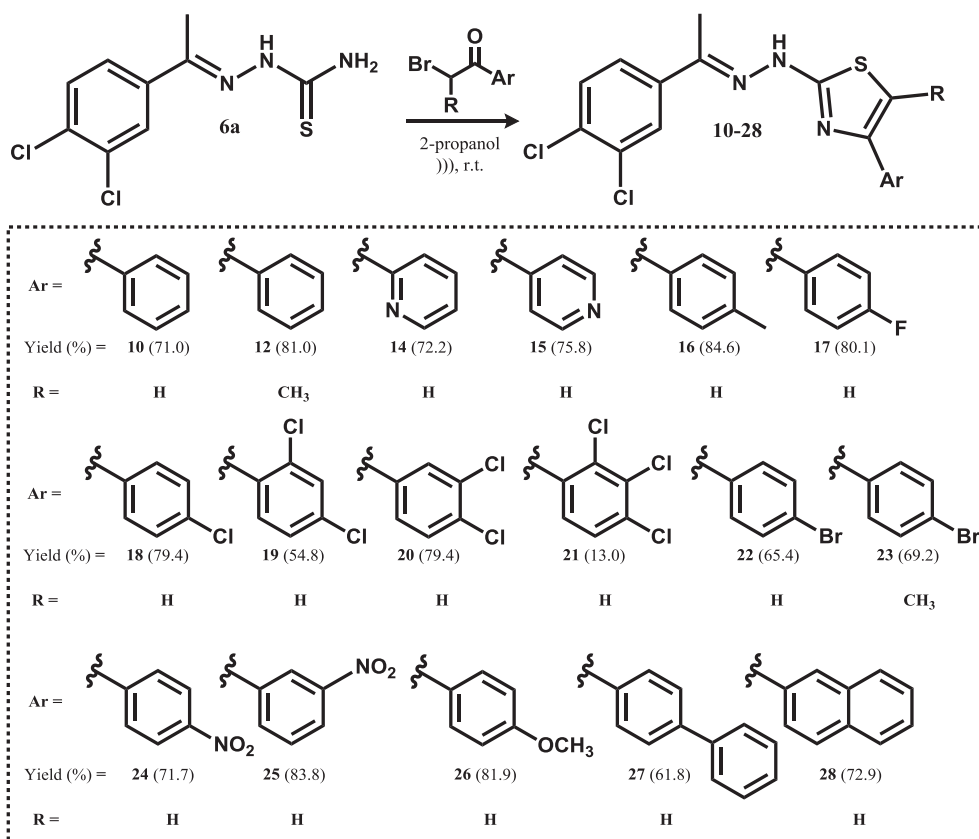


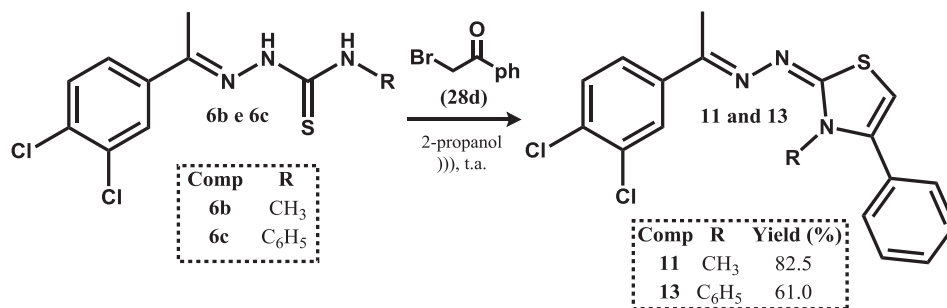
Fig. 1. Planning structural of 1,3-thiazoles serie **7–28**. Replace the thiazolidin-4-one heterocycle by other structurally equivalent (1,3-thiazole).



Scheme 1. Synthetic procedures for thiazoles (7–9).



Scheme 2. Synthetic procedures for thiazoles (10–28).



Scheme 3. Synthetic procedures for thiazoles (11 and 13).

the thiazole ring, generating compound (23, IC₅₀trypano = 19.1 μM) mono-*para*-bromo-substituted, produced a compound with similar trypanocidal activity of benzimidazole, which corroborates results of

compound (9) and (12), wherein inserting alkyl substituents at the 5-position of the heterocycle increased pharmacological activity, and should be explored by our research group. The tri-substituted

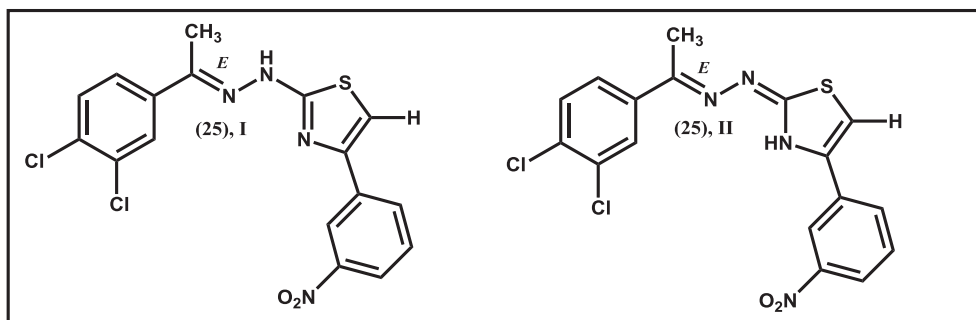


Fig. 2. Position of the C = N bond at the C2 carbon of the compound (25).

2',3',4'-tri-chloro compound (**21**, $IC_{50\text{trypo}} = 6 \mu\text{M}$) also showed similar potency compared to benzimidazole, while the simple substitution for dichlorinated compounds at the 2',4'- (**19**) and 3', 4'- (**20**) was not beneficial for trypanocidal activity. We tried to evaluate the influence of exchange of H by methyl (**11**) or (**13**) phenyl in the N3 position of the thiazole ring, but neither insertion was beneficial for trypanocidal activity, in agreement with the recent work of de Moraes Gomes [30,31].

The exchange of phenyl (**10**, $IC_{50\text{trypo}} = >50 \mu\text{M}$) for heterocycle 2-pyridyl (**14**, $CC_{50\text{trypo}} = 0.37 \mu\text{M}$) and 4-pyridyl (**15**, $IC_{50\text{trypo}} = 16.8 \mu\text{M}$) resulted in increased activity, giving rise to the most potent compound of series (**14**, $IC_{50\text{trypo}} = 0.37 \mu\text{M}$), which reminds us of the importance of the 2-pyridyl heterocycle, which might facilitate binding with a possible biological target, since it possesses a hydrogen bond acceptor. Compound **14** was approximately 28-fold more potent than benzimidazole. On the other hand, exchange for phenyl-phenyl (**27**) or naphthyl (**28**) did not result in increased trypanocidal activity.

Altogether, results obtained for the series (**7–28**) corroborate literature reports [28–31,39] that thiazoles are compounds with potent trypanocidal activity and low toxicity to mammalian cells, as observed also in the work of da Silva et al. where compounds **4d** and **4k** presented the best activities $IC_{50\text{trypo}} = 1.2$ and $1.6 \mu\text{M}$, respectively [40]. Compounds **4d** and **4k** have a 2-pyridyl group as a structural feature similar to compound **14** described herein. This leads us to note the importance of this group. Compound **14** was approximately 4-fold more potent than **4d** and **4k** (Fig. 4).

Finally, it is noteworthy that although the molecular target involved in trypanocidal properties of 1,3-thiazoles (**7–28**) is not known, the pharmacological properties profile identified is relevant. Screening of the series revealed compounds (**7**), (**12**), (**15**), (**23**) and (**26**) with trypanocidal activity similar to benzimidazole; compounds (**9**) and (**21**) as trypanocidal agents equipotent with the reference drug (BDZ), and compound **14** about 28 times more potent than benzimidazole.

The summary of structure activity relationship (SAR) is presented in Fig. 5.

The inhibitory activity for thiazoles (**7–28**) against cruzain was also investigated. We measured cruzain enzymatic activity inhibition by using an assay based on competition with the substrate Z-Phe-Arg-aminomethylcoumarin (Z-FR-AMC). Compounds were screened at $10 \mu\text{M}$, the maximum concentration at which they were soluble in the assay buffer (Table 2) [41].

As proposed by Du et al. [20], the thioamide moiety has an important role in the cruzain inhibition mechanism, however it has been demonstrated that cyclic derivatives, as 1,3-thiazoles [29], thiazolidin-4-ones [28] and 2,4-oxadiazoles [42], may also inhibit this enzyme. In this work, most cyclic derivatives present only modest inhibitory activity of cruzain, however, five of most active compounds for trypomastigote form (**7**, **9**, **12**, **16** and **23**) inhibit this enzyme by more than 70%, corroborating with the literature [29]. Compounds **7** and **9** were most active, respectively with IC_{50} values of 0.6 and $9 \mu\text{M}$, suggesting a possible mechanism of action these compounds. Compound **14** (the most active of all series), did not

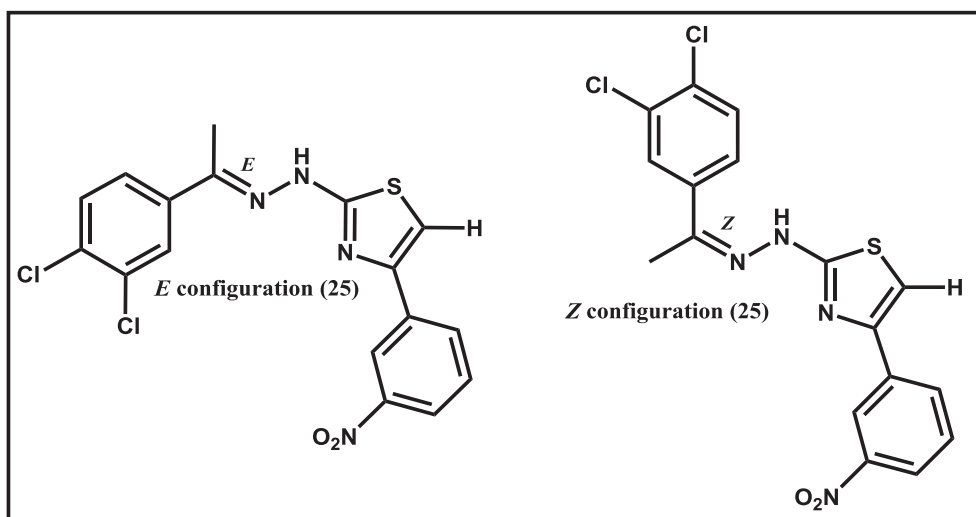
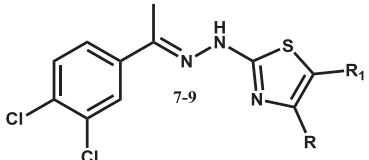
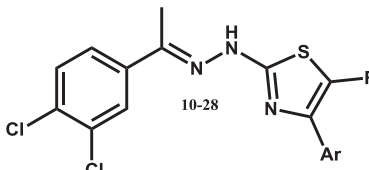
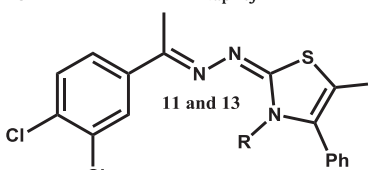


Fig. 3. Isomerism Z or E in hydrazine double-bond C2=N2.

Table 1
Anti-*T. cruzi* activity and cytotoxicity effects of thiazoles 7–28.

Cpd.	Ar/R	R ₁	Trypomastigotes, Y strain <i>T. cruzi</i> IC ₅₀ ± S.D. (μM) ^a	Macrophages CC ₅₀ ± S.D. (μM) ^b	H9c2 CC ₅₀ ± S.D. (μM) ^c
					
7	CH ₃	H	17.1 (±0.7)	33.71 (±0.63)	26.12 (±0.55)
8	CH ₂ Cl	H	>50	>50	>50
9	CH ₃	CH ₃	10.5 (±1.5)	41.76 (±2.98)	>50
					
10	Ph	H	>50	>50	>50
12	Ph	CH ₃	17.8 (±2.1)	>50	>50
14	2-Py	H	0.37 (±0.1)	10.06 (±1.18)	10.18 (±2.52)
15	4-Py	H	16.8 (±0.7)	39.81 (±0.03)	41.94 (±1.52)
16	4-CH ₃ Ph	H	47.74 (±2.38)	>50	>50
17	4-FPh	H	>50	>50	>50
18	4-ClPh	H	>50	>50	>50
19	2,4-diClPh	H	>50	>50	>50
20	3,4-diClPh	H	>50	>50	>50
21	2,3,4-triClPh	H	6 (±1.52)	21.28 (±1.98)	16.97 (±1.84)
22	4-BrPh	H	>50	>50	>50
23	4-BrPh	CH ₃	19.1 (±0.4)	>50	>50
24	4-NO ₂ Ph	H	>50	>50	>50
25	3-NO ₂ Ph	H	>50	>50	>50
26	4-OCH ₃ Ph	H	17.1 (±1.68)	>50	>50
27	4-PhPh	H	>50	>50	>50
28	2-Naphtyl	H	>50	>50	>50
					
11	CH ₃	H	>50	>50	>50
13	Ph	H	>50	>50	>50
Bdz	–	–	10.61 (±0.87)	>50	>50
GV	–	–	NT	0.45 (±0.04)	1.5 (±0.7)

^a Determined after 24 h of incubation in the presence of compounds.^b Determined in J774 cells for 72 h after incubation.^c Determined in H9c2 rat cardiomyoblast cells for 72 h after incubation. NT = not tested. Bdz = benznidazole. GV = gentian violet. S.D. = standard deviation.

inhibit cruzain, suggesting that it kills the parasite by acting on another target.

To understand how compound **14** affects parasite cells, we performed a staining with Rhodamine 123, to detect changes in the mitochondrial membrane potential in *T. cruzi* trypomastigotes. As seen in Fig. 6, treatment with **14**, at its IC₅₀ or two times the IC₅₀, induced mitochondria depolarization evidenced by a decrease in Rhodamine 123 fluorescence intensity, which typically lead to apoptosis.

To confirm the hypothesis of cell death by apoptosis a double staining with annexin V and propidium iodide was performed for flow cytometry analysis. Eventual phosphatidylserine flipping in the membrane surface is an alteration observed in the apoptotic process, while the collapse of the cell, making it permeable to propidium iodide, is an alteration observed in the process of necrosis [43]. As shown in Fig. 7, in untreated cultures, most trypomastigotes

were negative for annexin V and PI staining, demonstrating cell viability. In comparison to untreated parasites, a significant increase in the number of Annexin V-positive parasites was observed under treatment with **14** (0.4 μM) for 24 h, indicating parasite cell death through apoptosis induction.

Given the selectivity of these compounds against bloodstream trypomastigotes of *T. cruzi*, we also examined their activity against intracellular parasites. To this end, we assessed an *in vitro* model of parasite infection using mouse macrophages infected with Y strain trypomastigotes. Three days after infection, 15–20% of the untreated macrophages were infected, and a high number of amastigotes per 100 macrophages were observed. Treatment with 5 μM of benznidazole reduced the number of infected cells and the number of intracellular amastigotes ($P < 0.001$). We then tested the most potent compound, thiazole (**14**), at concentrations of 8, 2 and 0.5 μM. As shown in Fig. 8, this compound inhibited *T. cruzi*

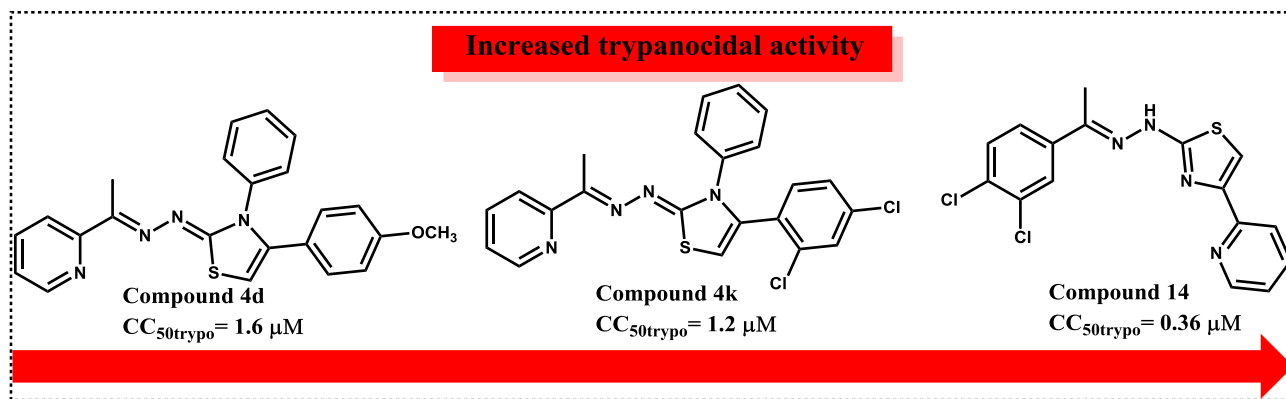


Fig. 4. Summary of SAR for thiazole compounds.

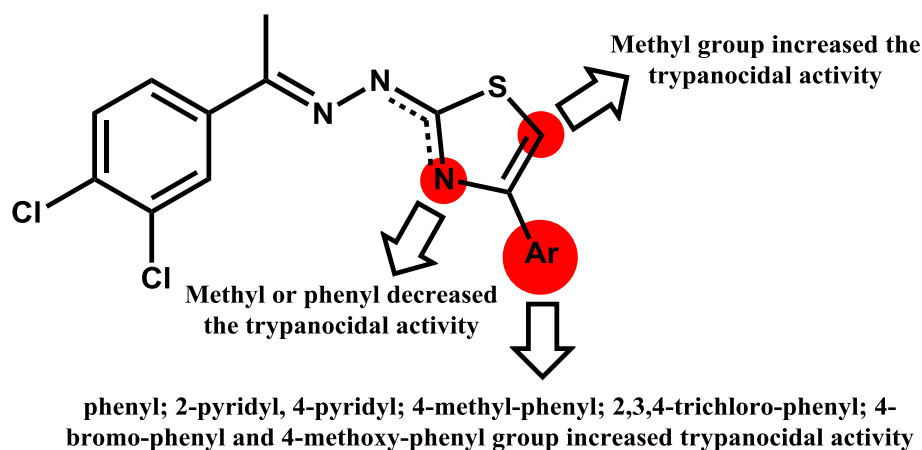


Fig. 5. Summary of SAR of trypanocidal activity.

Table 2
Cruzain inhibition of thiazoles 7–28.

Cpd.	% cruzain inhibition \pm S.D. at 10 μ M ^a	IC ₅₀ (μ M) ^b
7	97 \pm 1	0.6 \pm 0.2
8	50 \pm 5	ND
9	84 \pm 5	9 \pm 3
10	59 \pm 8	ND
11	12 \pm 5	ND
12	76 \pm 4	ND
13	31 \pm 4	ND
14	17 \pm 1	ND
15	32 \pm 2	ND
16	75 \pm 5	ND
17	32 \pm 3	ND
18	31 \pm 2	ND
19	35 \pm 9	ND
20	ND	ND
21	38 \pm 8	ND
22	43 \pm 3	ND
23	74 \pm 4	ND
24	ND	ND
25	33 \pm 7	ND
26	41 \pm 2	ND
27	44 \pm 8	ND
28	44 \pm 5	ND

^a Determined in a competition assay with ZFR-AMC, average for two screens, each in triplicate.

^b Means relating to at least two IC₅₀ determinations. All errors calculated by the formula: σ/\sqrt{n} , at where σ = standard deviation and n = number of experiments. S.D. = standard deviation. ND = Not determined.

infection in a concentration dependent manner, being equipotent to benznidazole at concentration of 2 μ M, and showing higher potency than benznidazole at concentration of 8 μ M ($P < 0.001$).

The antiparasitic effect of **14** and benznidazole in combination was also investigated against trypomastigotes. Such experiment is important because combination therapies can be a valuable tool to improve treatment efficacy and reduce dose levels and toxicity, as well as to prevent the potential development of resistance, which may be advantages for the treatment of parasitic diseases [44,45]. The combination index value of 0.37 ± 0.09 associated with a concave isobologram reveals that **14** demonstrates synergistic effects with benznidazole against the bloodstream parasites *in vitro*, showing a promising profile for drug combination (Fig. 9).

Next, *in vivo* studies to evaluate the effects of **14** against *T. cruzi* infection in mice (acute phase) were performed. As shown in Fig. 10, treatment with compound **14** significantly ($P < 0.001$) reduced blood parasitaemia when compared with mice treated with vehicle (Fig. 10). At dose of 25 mg/kg, administration of compound **14** caused a reduction in blood parasitaemia of 54.6 and 64.1% at days 8 and 12 post infection respectively (Table 3). In the group treated with benznidazole, it was observed >99% of inhibition of blood parasitaemia, indicating that eradication of infection was achieved. Treatment with **14**, similar to the treatment with benznidazole, had a protective effect on mortality (Table 3). Mice from benznidazole or **14** treated groups did not show any behavioral alteration or signs of toxicity (data not shown).

Finally, we evaluated if the compounds synthesized that properties within the Lipinski's Rule of Five, which are important for

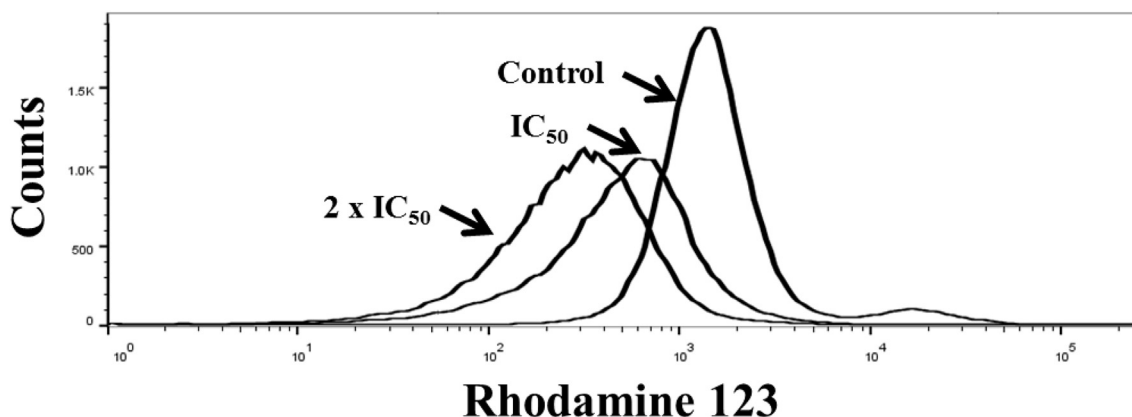


Fig. 6. Effects of **14** on the mitochondrial membrane potential. Overlay flow cytometric histograms of the control and the **14**-treated parasites labeled with Rhodamine 123. The reduction of Rhodamine 123 fluorescence intensity, mainly at the $2 \times IC_{50}$ of **14**, indicates the depolarization of the mitochondrial membrane.

pharmacokinetics and drug development. Compound obeying at least three of the four criteria are to considered to adhere to the Lipinski Rule [47]. Other interest property is the polar surface area (PSA), since compounds with a low PSA ($\leq 140 \text{ \AA}^2$) tend to have higher oral bioavailability [48,49]. All compounds synthesized, except **24** and **25**, are compatible with Lipinski Rule and present appropriate PSA (Table 4).

Considering the aim to identify a new antitrypanosomatid, the analysis of the results depicted in Table 1, allowed the selection of compound **14** as a trypanosomicidal agent. Therefore, its physico-chemical and ADME properties were calculated using the SwissADME (a free web tool to evaluate pharmacokinetics, drug-likeness and medicinal chemistry friendliness of small molecules) and the results were compared to those obtained for benznidazole (Table 5).

As demonstrated in Table 5, the druglikeness of compound **14** was very similar to benznidazole, with no violations of Lipinsky's rule of 5 [47]. Regardless of the poor solubility (predicted in buffer at pH of 6.5), compound **14** was shown to be highly permeable based on gastrointestinal absorption (GI), according to the BOILED-Egg predictive model (Brain Or Intestinal EstimateD permeation method). These results were similar to benznidazole. Compound **14** was expected to have an oral bioavailability score of 0.55 as well as benznidazole (Table 5). Taken together, this data, suggests a good *in silico* druglikeness profile and great chemical stabilities for compound **14**. In fact, the *in vivo* efficacy of **14** reinforces this idea.

3. Conclusions

The 1,3-thiazoles were structurally designed by employing the non-classical bioisosteric exchange of a thiazolidin-4-one ring by a thiazole heterocycle. This led to the synthesis and chemical characterization of compounds **7–28**, which were evaluated concerning their anti-*T. cruzi*, cytotoxicity and cruzain inhibition activities. The pharmacological evaluation led to the identification of thiazoles (**7**, **9**, **12**, **14**, **15**, **21**, **23** and **26**) as potents anti-*T. cruzi* agent. Concerning their mechanism of action, some of these compounds inhibit cruzain and compound **14** was observed to induce parasite cell death through an apoptotic process, as indicated by the induced depolarization of the mitochondrial membrane in Rhodamine 123 labeling assay. Compound **14** was also able to inhibit *in vitro* infection by *T. cruzi*, showed synergistic effect with the reference drug, showing a promising profile for drug combination, and at dose of

25 mg/kg caused a reduction in blood parasitaemia of 54.6 and 64.1% at days 8 and 10 post infection respectively. These results suggest that the strategies used are promising to obtain novel potent and selective antiparasitic agents.

4. Experimental protocols

4.1. Reagents and spectra analysis

All reagents were used as purchased from commercial sources (Sigma-Aldrich, Acros Organics, Vetec, or Fluka). Progress of the reactions was followed by thin-layer chromatography (silica gel 60 F254 in aluminum foil). Purity of the target compounds was confirmed by combustion analysis (for C, H, N, S) performed by a Carlo-Erba instrument (model EA 1110). IR was determined in KBr pellets. For NMR, we used a Bruker AMX-300 MHz (300 MHz for ^1H and 75.5 MHz for ^{13}C) instruments. DMSO- d_6 or D_2O were purchased from CIL. Chemical shifts are reported in ppm, and multiplicities are given as s (singlet), d (doublet), t (triplet), q (quartet), m (multiplet), and dd (double doublet), and coupling constants (J) in hertz. NH signals were localized in each spectrum after the addition of a few drops of D_2O . Structural assignments were corroborated by DEPT analysis. Mass spectrometry experiments were performed on a Q-TOF spectrometer LC-IT-TOF (Shimadzu). When otherwise specified, ESI was carried out in the positive ion mode. Reactions in an ultrasound bath were carried out under frequency of 40 kHz (180 W) and without external heating.

4.1.1. General procedure for the synthesis of thiosemicarbazones (6a-c)

Example for compound (**6a**): Synthesis of 1-(3,4-dichlorophenyl)-ethylidenethiosemicarbazone (**6a**). Under magnetic stirring: in a 100 mL round-bottom flask, 1.06 mmol (0.097 g) of thiosemicarbazide, 1.06 mmol (0.2 g) of 3',4'-dichloroacetophenone, 4 drops of H_2SO_4 and 20 mL of ethanol were added and maintained under magnetic stirring and reflux for 20 h. After cooling back to rt, the precipitate was filtered in a Büchner funnel with a sintered disc filter, washed with cold ethanol, and then dried over SiO_2 . Product was purified by recrystallization in hot toluol. Colorless crystals, m.p.: 187–189 °C; yield: 0.10 g (38%).

Under ultrasound irradiation: in a 10 mL round-bottom flask, 1.06 mmol (0.097 g) of thiosemicarbazide, 1.06 mmol (0.2 g) of 3',4'-dichloroacetophenone, 4 drops of H_2SO_4 and 20 mL of ethanol

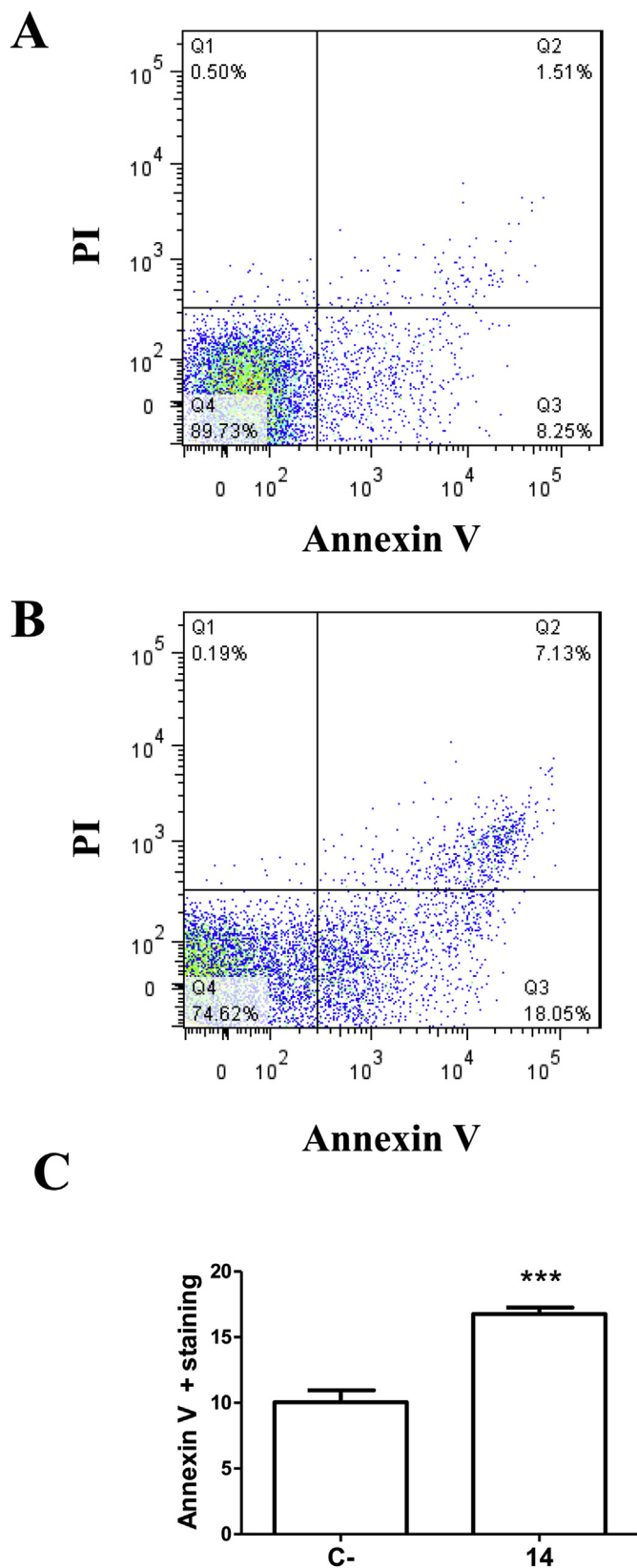


Fig. 7. Flow cytometry analysis of trypanomastigotes treated with **14** and stained with annexin V. (A) Untreated trypanomastigotes; (B) trypanomastigotes treated with **14** (0.4 μ M); (C) Percentage of stained cells with annexin V after 24 h of treatment with **14**. Values represent the means \pm SEM of six determinations. *** $P < 0.01$.

were added and maintained in an ultrasound bath for 30 min. After cooling back to rt, the precipitate was filtered in a Büchner funnel with a sintered disc filter, washed with cold ethanol, and then dried over SiO₂. Product was purified by recrystallization in hot toluol. Colorless crystals, m.p.: 187–189 °C; yield: 0.22 g (80%); $R_f = 0.56$ (toluol/ethyl acetate 6:4). IR (KBr): 3427 (NH₂), 3399 (NH), 3138 (C–H), 1591 (C=N) cm⁻¹. ¹H NMR (300 MHz, DMSO-*d*₆): δ 2.27 (s, 3H, CH₃), 7.58 (d, 1H, *J* 9.37 Hz, Ar), 7.86 (dd, 1H, *J* 9.37 and 3.75 Hz, Ar), 8.18 (s, 1H, NH₂), 8.26 (d, 1H, *J* 3.75 Hz, Ar), 8.36 (s, 1H, NH₂), 10.29 (s, 1H, NH). Signals at δ 8.18, 8.36 and 10.29 ppm disappear after adding D₂O. ¹³C NMR (75.5 MHz, DMSO-*d*₆): δ 13.8 (CH₃), 126.7 (CH, Ar), 128.2 (CH, Ar), 130.2 (CH, Ar), 131.3 (C, Ar), 131.6 (3CIC, Ar), 138.2 (4CIC, Ar), 145.312 (C=N), 179.0 (C=S). HRMS (ESI): 259.9565 [M + H]⁺. Anal. calcd for C₉H₉Cl₂N₃S: C, 41.23; H, 3.46; N, 16.03; S, 12.23. Found: C, 41.21; H, 3.61; N, 16.36; S, 12.78.

4.1.1.1. 1-(3,4-dichlorophenyl)ethylidene-4-methylthiosemicarbazone (6b). Recrystallization in hot toluol afforded colorless crystal, m.p.: 195–197 °C; yield: 0.24 g (84%); $R_f = 0.7$ (toluol/ethyl acetate 6:4). IR (KBr): 3343 e 3219 (NH), 1547 (C=N) cm⁻¹. ¹H NMR (300 MHz, DMSO-*d*₆): δ 2.28 (s, 3H, CH₃), 3.04 (d, 3H, *J* 6 Hz, N–CH₃, coupling with N–H), 7.63 (d, 1H, *J* 8.57 Hz, Ar), 7.88 (dd, 1H, *J* 8.57 and 2.14 Hz, Ar), 8.23 (d, 1H, *J* 2.14 Hz, Ar), 8.61 (broad d, 1H, *J* 6 Hz, CH₃–NH), 10.33 (s, 1H, NH). ¹³C NMR (75.5 MHz, DMSO-*d*₆): δ 13.8 (CH₃), 31.1 (N–CH₃), 126.7 (CH, Ar), 128.1 (CH, Ar), 130.2 (CH, Ar), 131.3 (C, Ar), 131.5 (3CIC, Ar), 138.3 (4CIC, Ar), 145.0 (C=N), 178.6 (C=S). HRMS (ESI): 275.9475 [M + H]⁺. Anal. calcd for C₁₀H₁₁Cl₂N₃S: C, 43.49; H, 4.01; N, 15.21; S, 11.61. Found: C, 43.34; H, 3.98; N, 15.55; S, 11.74.

4.1.1.2. 1-(3,4-dichlorophenyl)ethylidene-4-phenylthiosemicarbazone (6c). Recrystallization in hot toluol afforded colorless crystal, m.p.: 200–202 °C; yield: 0.32 g (89%); $R_f = 0.73$ (toluol/ethyl acetate 6:4). IR (KBr): 3309 and 3239 (NH), 3046 (C–H), 1523 (C=N) cm⁻¹. ¹H NMR (300 MHz, DMSO-*d*₆): δ 2.36 (s, 3H, CH₃), 7.23 (t, 1H, *J* 7.21 Hz, Ar), 7.38 (t, 2H, *J* 7.21 Hz, Ar), 7.51 (d, 2H, *J* 7.21 Hz, Ar), 7.64 (d, 1H, *J* 9.09 Hz, Ar), 7.97 (dd, 1H, *J* 9.09 and 2.72 Hz, Ar), 8.34 (d, 1H, *J* 2.72 Hz, Ar), 10.18 (s, 1H, NH), 10.66 (s, 1H, ArNH). ¹³C NMR (75.5 MHz, DMSO-*d*₆): δ 14.2 (CH₃), 125.6 (CH, Ar), 126.5 (CH, Ar), 127.0 (CH, Ar), 128.1 (CH, Ar), 128.4 (CH, Ar), 130.2 (CH, Ar), 131.3 (C, Ar), 131.8 (3CIC, Ar), 138.1 (4CIC, Ar), 139.2 (C–N, Ar), 146.3 (C=N), 177.3 (C=S). HRMS (ESI): 337.9678 [M + H]⁺. Anal. calcd for C₁₅H₁₃Cl₂N₃S: C, 53.26; H, 3.87; N, 12.42; S, 9.48. Found: C, 53.23; H, 3.84; N, 12.31; S, 9.32.

4.1.2. General procedure for the synthesis of 1,3-thiazoles (7–9)

Example for compound (**7**): Synthesis of 2-[1-(3,4-dichlorophenyl)ethylidenehydrazinyl]-4-methyl-1,3-thiazole (**7**). In a 50 mL round-bottom flask, 0.76 mmol (0.2 g) of thiosemicarbazone (**6a**) was dissolved in 30 mL of ethanol followed by addition of 3.04 mmol (0.25 g) of sodium acetate. After stirring and heating for 15 min, 1.14 mmol (0.105 g) of 2-chloroacetone was added in portions and the mixture was maintained under stirring and reflux for 5 h. After cooling back to rt, the precipitate was filtered off and the solvent was evaporated under reduced pressure. The crude mixture was crystallized in hot water, affording brown crystals, m.p.: 102–104 °C; yield: 0.18 g (78%). $R_f = 0.57$ (toluol/ethyl acetate 6:4). IR (KBr): 3190 (NH), 1568 (C=N) cm⁻¹. ¹H NMR (300 MHz, DMSO-*d*₆): δ 1.88 (s, 3H, CH₃), 2.15 (s, 3H, CH₃), 6.30 (s, 1H, CH thiazole), 7.63 (d, 1H, *J* 8.4 Hz, Ar), 7.71 (dd, 1H, *J* 8.4 and 1.8 Hz, Ar), 7.90 (d, 1H, *J* 1.8 Hz, Ar), 11.99 (s, 1H, NH). ¹³C NMR (75.5 MHz, DMSO-*d*₆): δ 16.4 (CH₃), 21.4 (CH₃), 101.8 (CH thiazole), 125.5 (CH, Ar), 127.0 (CH, Ar), 130.5 (CH, Ar), 130.7 (C, Ar), 131.2 (3CIC, Ar), 138.8 (4CIC, Ar), 144.5 (C, thiazole), 169.5 (C=N), 172.2 (S–C=N). HRMS (ESI): 300.0168 [M + H]⁺. Anal. calcd for C₁₂H₁₁Cl₂N₃S: C, 48.01; H, 3.69; N, 14.00; S, 10.68. Found: C, 48.07;

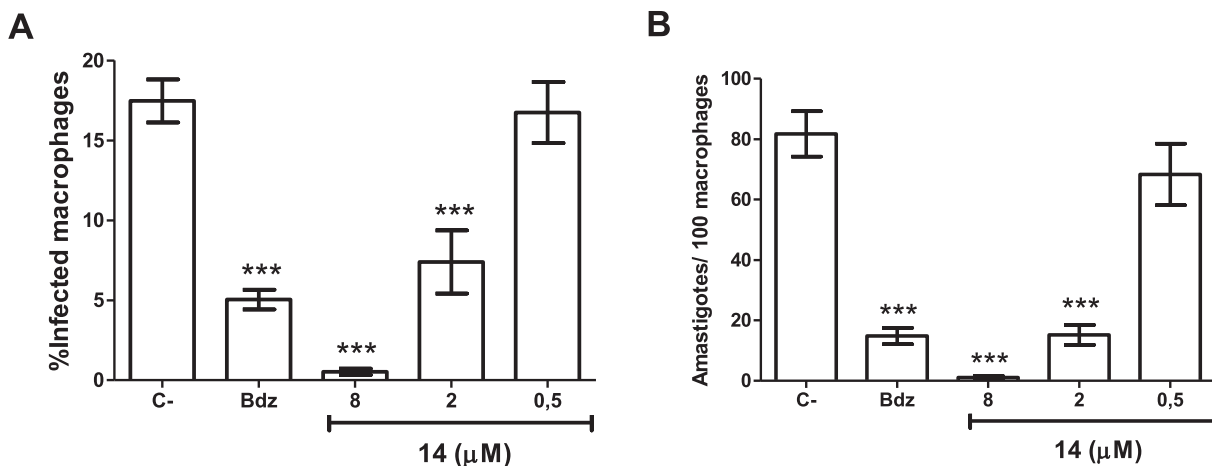


Fig. 8. Thiazole **14** affects intracellular parasite development. The percentage of infected macrophages (A) and the relative number of amastigotes per 100 macrophages (B) are higher in untreated controls than in cultures treated with test compound **14** or Bdz. Infected macrophages were treated for 3 days with compounds and then analyzed in Perkin-Elmer Opera confocal microscope after staining with hoeschst. Values represent the means \pm SEM of six determinations. *** P < 0.001; ** P < 0.01; * P < 0.05. Bdz (benznidazole; 5 μ M) was used as a positive control.

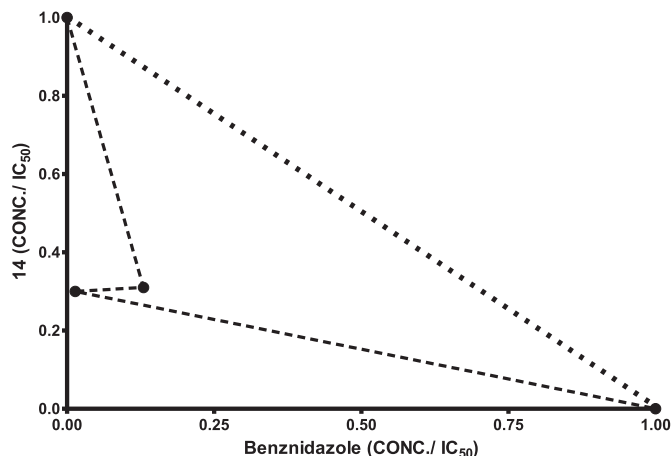


Fig. 9. Isobologram describing the synergistic effects of **14** and benznidazole on trypanostigote viability. Broken lines correspond to the predicted positions of the experimental points for additive effects. A combination index of 0.37 ± 0.09 was calculated according to Chou & Talalay [46].

H, 3.96; N, 14.07; S, 10.65.

4.1.2.1. 4-(chloromethyl)-2-[1-(3,4-dichlorophenyl)ethylidene-hydrazinyl]-thiazole (8). Recrystallization in hot ethanol afforded brown crystals, m.p.: 124–126 °C; yield: 1.12 g (88%); $R_f = 0.64$ (toluol/ethyl acetate 6:4). IR (KBr): 3065 (C-H), 1561 (C=N) cm^{-1} . ^1H NMR (300 MHz, DMSO- d_6): δ 2.68 (s, 3H, CH₃), 4.64 (s, 2H, CH₂), 6.96 (s, 1H, CH thiazole), 7.15 (dd, 1H, J 8.4 and 2.1 Hz, Ar), 7.28 (d, 1H, J 2.1 Hz, Ar), 7.42 (d, 1H, J 8.4 Hz, Ar). ^{13}C NMR (75.5 MHz, DMSO- d_6): δ 15.8 (CH₃), 46.5 (CH₂), 111.6 (CH thiazole), 126.3 (CH, Ar), 130.2 (CH, Ar), 131.1 (CH, Ar), 132.4 (C, Ar), 132.6 (C, Ar), 133.2 (C, Ar), 147.8 (C, Ar), 151.6 (C=N), 162.2 (S-C=N). HRMS (ESI): 333.9613 [M - H]⁺. Anal. calcd for C₁₂H₁₀Cl₃N₃S: C, 43.07; H, 3.01; N, 12.56; S, 9.58. Found: C, 43.07; H, 3.00; N, 12.42, S, 9.69.

4.1.2.2. 2-[1-(3,4-dichlorophenyl)ethylidene-hydrazinyl]-4,5-dimethylthiazole (9). Recrystallization in hot ethanol afforded yellow crystals, m.p.: 157–159 °C; yield: 0.55 g (46%); $R_f = 0.51$ (toluol/ethyl acetate 6:4). IR (KBr): 3197 (NH), 2918 (C-H), 1546 (C=N) cm^{-1} . ^1H NMR (300 MHz, DMSO- d_6): δ 2.04 (s, 3H, CH₃), 2.12 (s, 3H,

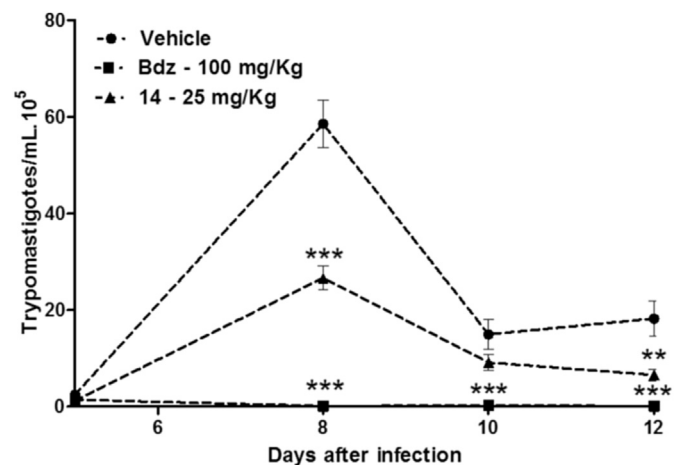


Fig. 10. Parasitaemia of BALB/c mice infected with *T. cruzi* and treated with **14**. Female BALB/c mice were infected with 10^4 Y strain trypomastigotes. Five days after infection, mice were treated orally with **14** (25 mg/kg) or benznidazole (100 mg/kg) once a day during five consecutive days. Parasitaemia was monitored by counting the number of trypomastigotes in fresh blood samples. Values represent the mean \pm SEM of 6 mice per group. ** P < 0.01; *** P < 0.001 compared to untreated-infected group (vehicle).

Table 3

Parasitaemia and mortality evaluation in mice infected with Y strain *T. cruzi* and treated daily with **14** or benznidazole for 5 days.

Sample	Dose (mg/Kg)	% Blood parasitaemia reduction in mice ^a		Mortality ^b
		8dpi	12 dpi	
14	25	54.6%	64.1	1/6
BDZ	100	>99	>99	0/6
Vehicle	—	—	—	5/6

^a Calculated as ((average vehicle group – average treated group)/average vehicle group) \times 100%.

^b Mortality was monitored until 30 days after treatment. Dpi = days post-infection. BDZ = benznidazole. Vehicle = untreated and infected group.

CH₃), 2.25 (s, 3H, CH₃), 7.63 (d, 1H, J 8.4 Hz, Ar), 7.71 (dd, 1H, J 8.4 and J 2.1 Hz, Ar), 7.90 (d, 1H, J 2.1 Hz, Ar), 11.52 (s, 1H, NH). ^{13}C NMR (75.5 MHz, DMSO- d_6): δ 11.3 (CH₃), 13.8 (CH₃), 21.5 (CH₃), 112.0 (S-

Table 4
Physicochemical properties calculated for the thiazoles.

Compd.	MW (g/mol)	C log P	H bond donors	H bond acceptors	Criteria met	PSA Å ²
Desirable Value	<500	<5	<5	<10	3 at least	≤140
7	300.2	4.33	1	3	All	37.28
8	334.64	4.86	1	4	All	37.28
9	314.23	4.97	1	3	All	37.28
10	362.27	6.22	1	3	3	37.28
11	376.3	4.84	0	3	All	27.96
12	376.3	6.87	1	3	3	37.28
13	438.37	6.51	0	3	3	27.96
14	363.26	4.29	1	4	4	50.17
15	363.26	5.01	1	4	3	50.17
16	376.3	6.74	1	3	3	37.28
17	380.26	6.37	1	3	3	37.28
18	396.71	6.83	1	3	3	37.28
19	431.16	7.44	1	3	3	37.28
20	431.16	7.44	1	3	3	37.28
21	465.6	8.04	1	3	3	37.28
22	441.17	7.00	1	3	3	37.28
23	455.2	7.64	1	3	3	37.28
24	407.27	6.17	1	5	2	80.42
25	407.27	6.17	1	5	2	80.42
26	392.3	6.07	1	4	3	46.51
27	438.37	7.88	1	3	3	37.28
28	412.33	7.22	1	3	3	37.28

Table 5
Physico-chemistry properties and ADME profile of compounds **14** and benznidazole calculated using the Program SwissADME.

Predicted properties	Compounds	
	14	Benznidazole
MW (g/mol)	363.23	260.25
H-Donors	1	1
H-Acceptors	4	4
Rotatable Bonds	4	6
LogP	4.29	0.66
Solubility	1.07 mg/mL	2.27 mg/mL
GI absorption	High	High
Bioavailability Score	0.55	0.55

C-CH₃ thiazole), 125.9 (CH, Ar), 127.3 (CH, Ar), 130.9 (CH, Ar), 130.98 (C, Ar), 131.6 (3ClC, Ar), 139.4 (4ClC, Ar), 145.2 (N-C-CH₃, thiazole), 167.4 (C=N), 172.5 (S-C=N). HRMS (ESI): 313.9612 [M+H]⁺. Anal. calcd for C₁₃H₁₃Cl₂N₃S: C, 49.69; H, 4.17; N, 13.37; S, 10.20. Found: C, 49.35; H, 4.28; N, 13.27, S, 10.30.

4.1.3. General procedure for the synthesis of 1,3-thiazoles (**10**–**28**)

Example for compound (**10**): Synthesis of 2-[1-(3,4-dichlorophenyl)ethylidene-hydrazinyl]-4-phenylthiazole (**10**). Under ultrasound irradiation: in a 100 mL round-bottom flask, 3.81 mmol (0.76 g) of 2-bromoacetophenone and 25 mL of isopropanol were added and maintained in an ultrasound bath, the mixture was sonicated at room temperature until complete solubilization of the reagents. Then it was added 3.81 mmol (1.0 g) of the compound (**6a**). Immediately after addition, there was complete solubilization and change of color of the reaction mixture from light yellow to gray. The mixture was kept under ultrasonic bath at room temperature for 2 h. Thereafter, the precipitate formed was filtered, washed with isopropanol and dried in over SiO₂. The product was recrystallized in hot ethanol/methanol 2: 1, affording gray crystals, m.p.: 259–261 °C; yield: 0.98 g (71%). R_f: 0.62 (toluol/ethyl acetate 6:4). IR (KBr): 2918 (CH), 1612 (C=N) cm⁻¹. ¹H NMR (300 MHz, DMSO-*d*₆): δ 2.31 (s, 3H, CH₃), 7.30–7.43 (m, 4H, Ar), 7.65–7.94 (m, 5H, Ar), 11.25 (s, 1H, NH). ¹³C NMR (75.5 MHz, DMSO-*d*₆): δ 11.5 (CH₃), 102.1 (CH thiazole), 123.2 (CH,

Ar), 123.4 (CH, Ar), 124.9 (CH, Ar), 125.3 (CH, Ar), 126.3 (CH, Ar), 128.2 (CH, Ar), 130.98 (C, Ar), 131.6 (3ClC, Ar), 135.0 (C, Ar), 139.4 (4ClC, Ar), 143.9 (C, Ar), 150.0 (C=N), 170.0 (S-C=N). HRMS (ESI): 361.9579 [M+H]⁺. Anal. calcd for C₁₇H₁₃Cl₂N₃S: C, 56.36; H, 3.62; N, 11.60; S, 8.85. Found: C, 56.34; H, 3.69; N, 11.51; S, 8.84.

4.1.3.1. 2-[1-(3,4-dichlorophenyl)ethylidene-hydrazono]-3-methyl-4-phenyl-2,3-dihydrothiazole (**11**). Recrystallization in hot ethanol afforded yellow crystals, m.p.: 247–248 °C; yield: 1.12 g (82%); R_f = 0.93 (toluol/ethyl acetate 6:4). IR (KBr): 3035 (C-H), 1593 (C=N) cm⁻¹. ¹H NMR (300 MHz, DMSO-*d*₆): δ 2.40 (s, 3H, CH₃), 3.40 (s, 3H, N-CH₃), 6.59 (s, 1H, CH thiazole), 7.51 (m, 5H, Ar), 7.67 (d, 1H, J 8.4 Hz, Ar), 7.80 (d, 1H, J 8.4 Hz, Ar), 7.98 (s, 1H, Ar). ¹³C NMR (75.5 MHz, DMSO-*d*₆): δ 14.2 (CH₃), 34.1 (N-CH₃), 101.8 (CH thiazole), 125.9 (CH, Ar), 127.4 (CH, Ar), 128.8 (CH, Ar), 129.4 (CH, Ar), 130.0 (CH, Ar), 130.6 (C, Ar), 131.3 (3ClC, Ar), 138.8 (4ClC, Ar), 141.0 (N-C-C, thiazole), 152.5 (C=N), 170.1 (S-C=N). HRMS (ESI): 375.9459 [M+H]⁺. Anal. calcd for C₁₈H₁₅Cl₂N₃S: C, 57.45; H, 4.02; N, 11.17; S, 8.52. Found: C, 57.51; H, 3.98; N, 11.43; S, 8.55.

4.1.3.2. 2-[1-(3,4-dichlorophenyl)ethylidene-hydrazinyl]-5-methyl-4-phenylthiazole (**12**). Recrystallization in hot ethanol afforded beige crystals, m.p.: 234–236 °C; yield: 1.16 g (81%); R_f = 0.54 (toluol/ethyl acetate 6:4). IR (KBr): 3022 (C-H), 1619 (C=N) cm⁻¹. ¹H NMR (300 MHz, DMSO-*d*₆): δ 2.35 (s, 3H, CH₃), 2.38 (s, 3H, N-CH₃), 7.42–7.62 (m, 5H, Ar), 7.69 (d, 1H, J 8.4 Hz, Ar), 7.83 (d, 1H, J 8.4 Hz, Ar), 8.65 (s, 1H, Ar). ¹³C NMR (75.5 MHz, DMSO-*d*₆): δ 12.4 (CH₃), 14.7 (CH₃), 117.9 (S-C-CH₃ thiazole), 126.6 (CH, Ar), 127.6 (CH, Ar), 128.0 (CH, Ar), 128.1 (CH, Ar), 128.9 (CH, Ar), 131.0 (C, Ar), 131.8 (3ClC, Ar), 132.0 (4ClC, Ar), 138.4 (N-C-C, thiazole), 165.9 (C=N), 167.2 (S-C=N). HRMS (ESI): 375.9648 [M+H]⁺. Anal. calcd for C₁₈H₁₅Cl₂N₃S: C, 57.45; H, 4.02; N, 11.17; S, 8.52. Found: C, 57.34; H, 3.95; N, 11.21; S, 8.58.

4.1.3.3. 2-[1-(3,4-dichlorophenyl)ethylidene-hydrazono]-3,4-diphenyl-2,3-dihydrothiazole (**13**). Recrystallization in hot toluol afforded beige crystals, m.p.: 170–172 °C; yield: 0.23 g (61%); R_f = 0.96 (toluol/ethyl acetate 6:4). IR (KBr): 1597 and 1515 (C=N) cm⁻¹. ¹H NMR (300 MHz, DMSO-*d*₆): δ 2.16 (s, 3H, CH₃), 6.67 (s, 1H, CH thiazole), 7.16–7.52 (m, 10H, Ar), 7.65 (d, 1H, J 8.4 Hz, Ar), 7.76

(dd, 1H, *J* 8.4 and 1.8 Hz, Ar), 7.95 (d, 1H, *J* 1.8 Hz, Ar). ¹³C NMR (75.5 MHz, DMSO-*d*₆): δ 14.1 (CH₃), 102.1 (CH thiazole), 125.6 (CH, Ar), 125.8 (CH, Ar), 126.5 (CH, Ar), 127.0 (CH, Ar), 127.3 (CH, Ar), 127.7 (CH, Ar), 128.1 (CH, Ar), 128.2 (CH, Ar), 128.4 (CH, Ar), 128.7 (CH, Ar), 130.2 (CH, Ar), 130.5 (CH, Ar), 130.6 (CH, Ar), 131.1 (C, Ar), 131.2 (C, Ar), 137.5 (C, Ar), 138.9 (C, Ar), 139.6 (C, Ar), 153.2 (C=N), 169.9 (S–C=N). HRMS (ESI): 438.0271 [M+H]⁺. Anal. calcd for C₂₃H₁₇Cl₂N₃S: C, 63.02; H, 3.91; N, 9.59; S, 7.31. Found: C, 62.45; H, 4.08; N, 9.63; S, 6.86.

4.1.3.4. 2-[1-(3,4-dichlorophenyl)ethylidene-hydrazinyl]-4-(pyridin-2-yl)thiazole (**14**). Recrystallization in hot ethanol afforded green crystals, m.p.: 227 °C; yield: 1.0 g (72%); R_f = 0.46 (toluol/ethyl acetate 6:4). IR (KBr): 3360 (NH), 3165 (CH), 1615 and 1597 (C=N) cm⁻¹. ¹H NMR (300 MHz, DMSO-*d*₆): δ 2.35 (s, 3H, CH₃), 7.68–7.79 (m, 3H, Ar), 7.97–8.10 (m, 2H, Ar), 8.24–8.36 (m, 2H, Ar), 8.64–8.72 (m, 1H, Ar), 11.00 (s, 1H, NH). ¹³C NMR (75.5 MHz, DMSO-*d*₆): δ 14.0 (CH₃), 117.1 (CH thiazole), 124.3 (CH, Ar), 125.8 (CH, Ar), 127.3 (CH, Ar), 130.6 (CH, Ar), 131.3 (CH, Ar), 138.2 (C, Ar), 138.9 (C, Ar), 139.6 (C, Ar), 145.5 (C, Ar), 153.2 (C=N), 169.9 (S–C=N). HRMS (ESI): 362.9710 [M+H]⁺. Anal. calcd for C₁₆H₁₂Cl₂N₄S: C, 52.90; H, 3.33; N, 15.42; S, 8.83. Found: C, 52.85; H, 3.38; N, 15.72; S, 8.88.

4.1.3.5. 2-[1-(3,4-dichlorophenyl)ethylidene-hydrazinyl]-4-(pyridin-4-yl)thiazole (**15**). Recrystallization in hot ethanol afforded green crystals, m.p.: 197 °C; yield: 1.05 g (75%); R_f = 0.5 (toluol/ethyl acetate 6:4). IR (KBr): 1630 and 1561 (C=N) cm⁻¹. ¹H NMR (300 MHz, DMSO-*d*₆): δ 2.31 (s, 3H, CH₃), 7.63 (d, 1H, *J* 7.8 Hz), 7.71 (d, 1H, *J* 7.8 Hz, Ar), 7.89 (s, 1H, Ar), 8.36 (d, 2H, *J* 5.7 Hz, Ar), 8.72 (s, 1H, CH thiazole), 8.93 (d, 2H, *J* 5.7 Hz, Ar), 11.72 (s, 1H, NH). ¹³C NMR (75.5 MHz, DMSO-*d*₆): δ 14.0 (CH₃), 117.0 (CH thiazole), 122.0 (CH, Ar), 125.7 (CH, Ar), 127.3 (CH, Ar), 130.6 (CH, Ar), 131.3 (CH, Ar), 138.1 (C, Ar), 142.1 (C, Ar), 145.1 (C, Ar), 145.9 (C, Ar), 149.1 (C, Ar), 153.2 (C=N), 170.3 (S–C=N). HRMS (ESI): 363.7868 [M+H]⁺. Anal. calcd for C₁₆H₁₂Cl₂N₄S: C, 52.90; H, 3.33; N, 15.42; S, 8.83. Found: C, 52.70; H, 3.37; N, 15.41; S, 8.88.

4.1.3.6. 2-[1-(3,4-dichlorophenyl)ethylidene-hydrazinyl]-4-(*p*-tolyl)thiazole (**16**). Recrystallization in hot ethanol afforded beige crystals, m.p.: 256–258 °C; yield: 1.21 g (84%); R_f = 0.75 (toluol/ethyl acetate 6:4). IR (KBr): 3030 (CH), 1608 (C=N) cm⁻¹. ¹H NMR (300 MHz, DMSO-*d*₆): δ 2.30 (s, 3H, CH₃), 2.31 (s, 3H, CH₃), 7.19–7.26 (m, 3H, Ar), 7.63–7.76 (m, 4H, Ar), 7.94 (s, 1H, Ar), 11.50 (s, 1H, NH). ¹³C NMR (75.5 MHz, DMSO-*d*₆): δ 13.9 (CH₃), 20.8 (CH₃), 103.6 (CH thiazole), 125.6 (CH, Ar), 125.8 (CH, Ar), 127.3 (CH, Ar), 129.2 (CH, Ar), 130.6 (CH, Ar), 131.2 (C, Ar), 131.3 (C, Ar), 137.1 (C, Ar), 138.3 (C, Ar), 144.8 (C, Ar), 149.4 (C, Ar), 169.3 (C=N), 172.2 (S–C=N). HRMS (ESI): 375.9742 [M+H]⁺. Anal. calcd for C₁₈H₁₅Cl₂N₃S: C, 57.45; H, 4.02; N, 11.17; S, 8.52. Found: C, 57.15; H, 4.00; N, 10.86; S, 8.42.

4.1.3.7. 2-[1-(3,4-dichlorophenyl)ethylidene-hydrazinyl]-4-(4-fluorophenyl)thiazole (**17**). Recrystallization in hot ethanol afforded beige crystals, m.p.: 267–269 °C; yield: 0.85 g (80%); R_f = 0.66 (toluol/ethyl acetate 6:4). IR (KBr): 2923 (CH), 1615 (C=N) cm⁻¹. ¹H NMR (300 MHz, DMSO-*d*₆): δ 2.29 (s, 3H, CH₃), 7.20–7.25 (m, 2H, Ar), 7.31 (s, 1H, CH thiazole), 7.62 (d, 1H, *J* 8.4 Hz, Ar), 7.72 (d, 1H, *J* 8.4 Hz, Ar), 7.85–7.89 (m, 2H, Ar), 7.91 (s, 1H, Ar). ¹³C NMR (75.5 MHz, DMSO-*d*₆): δ 13.9 (CH₃), 104.3 (CH thiazole), 115.4 (CH, Ar), 115.7 (CH, Ar), 125.7 (CH, Ar), 127.3 (CH, Ar), 127.6 (CH, Ar), 127.7 (CH, Ar), 130.6 (CH, Ar), 131.2 (C, Ar), 131.3 (C, Ar), 138.3 (C, Ar), 144.8 (C, Ar), 148.6 (C=N), 160.1 and 163.3 (d, C–F, Ar), 169.5 (S–C=N). HRMS (ESI): 379.9738 [M+H]⁺. Anal. calcd for C₁₇H₁₂Cl₂FN₃S: C, 53.69; H, 3.18; N, 11.05; S, 8.43. Found: C, 53.53; H, 3.52; N, 10.95; S, 8.42.

4.1.3.8. 4-(4-chlorophenyl)-2-[1-(3,4-dichlorophenyl)ethylidene-hydrazinyl]thiazole (**18**). Recrystallization in hot ethanol afforded beige crystals, m.p.: 266–268 °C; yield: 1.2 g (79%); R_f = 0.72 (toluol/ethyl acetate 6:4). IR (KBr): 3047 (CH), 1611 (C=N) cm⁻¹. ¹H NMR (300 MHz, DMSO-*d*₆): δ 2.28 (s, 3H, CH₃), 7.38 (s, 1H, CH thiazole), 7.43 (d, 2H, *J* 8.1 Hz, Ar), 7.61 (d, 1H, *J* 8.4 Hz, Ar), 7.70 (d, 1H, *J* 8.4 Hz, Ar), 7.84 (d, 2H, *J* 8.1 Hz, Ar), 7.90 (s, 1H, Ar), 10.59 (s, 1H, NH). ¹³C NMR (75.5 MHz, DMSO-*d*₆): δ 13.9 (CH₃), 105.3 (CH thiazole), 125.7 (CH, Ar), 127.3 (CH, Ar), 128.4 (CH, Ar), 128.6 (CH, Ar), 128.7 (CH, Ar), 129.5 (CH, Ar), 130.6 (CH, Ar), 131.2 (C, Ar), 131.3 (C, Ar), 132.1 (C, Ar), 133.1 (C, Ar), 138.3 (C, Ar), 144.6 (N–C–C, Ar), 148.6 (C=N), 169.5 (S–C=N). HRMS (ESI): 395.9470 [M+H]⁺. Anal. calcd for C₁₇H₁₂Cl₃N₃S: C, 51.47; H, 3.05; N, 10.59; S, 8.08. Found: C, 51.35; H, 3.22; N, 10.58; S, 7.93.

4.1.3.9. 4-(2,4-dichlorophenyl)-2-[1-(3,4-dichlorophenyl)ethylidene-hydrazinyl]thiazole (**19**). Recrystallization in hot ethanol afforded gray crystals, m.p.: 244–246 °C; yield: 0.9 g (54%); R_f = 0.65 (toluol/ethyl acetate 6:4). IR (KBr): 2923 (CH), 1623 (C=N) cm⁻¹. ¹H NMR (300 MHz, DMSO-*d*₆): δ 2.31 (s, 3H, CH₃), 7.44 (s, 1H, CH thiazole), 7.51 (dd, 1H, *J* 8.4 and 2.1 Hz, Ar), 7.69 (d, 1H, *J* 8.4 Hz, Ar), 7.70–7.74 (m, 1H, Ar), 7.77 (d, 1H, *J* 2.1 Hz, Ar), 7.94–7.95 (m, 2H, Ar), 11.51 (s, 1H, NH). ¹³C NMR (75.5 MHz, DMSO-*d*₆): δ 15.8 (CH₃), 119.0 (CH thiazole), 128.3 (CH, Ar), 128.4 (CH, Ar), 128.6 (CH, Ar), 128.7 (CH, Ar), 129.5 (CH, Ar), 132.6 (CH, Ar), 131.2 (C, Ar), 131.3 (C, Ar), 132.1 (C, Ar), 133.1 (C, Ar), 138.3 (C, Ar), 144.6 (C, Ar), 151.6 (C=N), 170.1 (S–C=N). HRMS (ESI): 429.9246 [M+H]⁺. Anal. calcd for C₁₇H₁₁Cl₄N₃S: C, 47.36; H, 2.57; N, 9.75; S, 7.44. Found: C, 47.60; H, 2.61; N, 9.71; S, 7.50.

4.1.3.10. 4-(3,4-dichlorophenyl)-2-[1-(3,4-dichlorophenyl)ethylidene-hydrazinyl]thiazole (**20**). Recrystallization in hot ethanol afforded beige crystals, m.p.: 266–268 °C; yield: 1.2 g (79%); R_f = 0.76 (toluol/ethyl acetate 6:4). IR (KBr): 3043 (CH), 1616 (C=N) cm⁻¹. ¹H NMR (300 MHz, DMSO-*d*₆): δ 2.29 (s, 3H, CH₃), 7.56 (s, 1H, CH thiazole), 7.64 (d, 2H, *J* 8.4 Hz, Ar), 7.72 (dd, 1H, *J* 8.4 and 1.8 Hz, Ar), 7.83 (dd, 1H, *J* 8.4 and 1.8 Hz, Ar), 7.91 (d, 1H, *J* 1.8 Hz, Ar), 8.08 (d, 1H, *J* 1.8 Hz, Ar), 9.20 (s, 1H, NH). ¹³C NMR (75.5 MHz, DMSO-*d*₆): δ 14.5 (CH₃), 107.3 (CH thiazole), 126.2 (CH, Ar), 126.3 (CH, Ar), 127.9 (CH, Ar), 130.3 (CH, Ar), 131.2 (CH, Ar), 131.5 (CH, Ar), 131.8 (C, Ar), 132.0 (C, Ar), 132.0 (C, Ar), 132.1 (C, Ar), 135.8 (C, Ar), 139.0 (C, Ar), 144.9 (C, Ar), 148.6 (C=N), 170.3 (S–C=N). HRMS (ESI): 429.8872 [M+H]⁺. Anal. calcd for C₁₇H₁₁Cl₄N₃S: C, 47.36; H, 2.57; N, 9.75; S, 7.44. Found: C, 47.34; H, 2.30; N, 9.71; S, 7.43.

4.1.3.11. 2-[1-(3,4-dichlorophenyl)ethylidene-hydrazinyl]-4-(2,3,4-trichlorophenyl)thiazole (**21**). Recrystallization in hot ethanol afforded orange crystals, m.p.: 214–217 °C; yield: 0.23 g (13%); R_f = 0.55 (toluol/ethyl acetate 6:4). IR (KBr): 2922 (CH), 1621 and 1567 (C=N) cm⁻¹. ¹H NMR (300 MHz, DMSO-*d*₆): δ 2.74 (s, 3H, CH₃), 7.12 (s, 1H, CH thiazole), 7.18 (dd, 1H, *J* 8.1 and 1.8 Hz, Ar), 7.26 (d, 1H, *J* 8.7 Hz, Ar), 7.29 (d, 1H, *J* 1.8 Hz, Ar), 7.40 (d, 1H, *J* 8.7 Hz, Ar), 7.50 (d, 1H, *J* 8.1 Hz, Ar). ¹³C NMR (75.5 MHz, DMSO-*d*₆): δ 15.0 (CH₃), 119.5 (CH thiazole), 124.2 (CH, Ar), 126.3 (CH, Ar), 129.2 (CH, Ar), 130.2 (CH, Ar), 131.1 (CH, Ar), 131.7 (C, Ar), 132.4 (C, Ar), 132.6 (C, Ar), 132.2 (C, Ar), 133.4 (C, Ar), 137.5 (C, Ar), 143.5 (C, Ar), 152.0 (C=N), 170.1 (S–C=N). HRMS (ESI): 465.8882 [M+H]⁺. Anal. calcd for C₁₇H₁₀Cl₅N₃S: C, 43.85; H, 2.16; N, 9.02; S, 6.89. Found: C, 43.90; H, 1.94; N, 9.06; S, 6.81.

4.1.3.12. 4-(4-bromophenyl)-2-[1-(3,4-dichlorophenyl)ethylidene-hydrazinyl]thiazole (**22**). Recrystallization in hot ethanol afforded gray crystals, m.p.: 265–267 °C; yield: 1.10 g (65%); R_f = 0.71 (toluol/ethyl acetate 6:4). IR (KBr): 2925 (CH), 1616 (C=N) cm⁻¹. ¹H NMR (300 MHz, DMSO-*d*₆): δ 2.30 (s, 3H, CH₃), 5.19 (s, 1H, NH), 7.42

(s, 1H, CH thiazole), 7.59 (d, 2H, *J* 8.4 Hz, Ar), 7.65 (d, 1H, *J* 8.4 Hz, Ar), 7.73 (dd, 1H, *J* 8.4 and 1.8 Hz, Ar), 7.81 (d, 2H, *J* 8.4 Hz, Ar), 7.92 (d, 1H, *J* 1.8 Hz, Ar). ¹³C NMR (75.5 MHz, DMSO-*d*₆): δ 13.8 (CH₃), 105.3 (CH thiazole), 120.6 (C, Ar), 125.7 (CH, Ar), 127.3 (CH, Ar), 127.6 (CH, Ar), 129.8 (CH, Ar), 130.6 (CH, Ar), 131.1 (C, Ar), 131.3 (CH, Ar), 131.5 (CH, Ar), 133.7 (C, Ar), 138.4 (C, Ar), 144.2 (C, Ar), 149.1 (C=N), 169.5 (S–C=N). HRMS (ESI): 437.9016 [M – H]⁺. Anal. calcd for C₁₇H₁₂BrCl₂N₃S: C, 46.28; H, 2.74; N, 9.52; S, 7.27. Found: C, 46.29; H, 2.92; N, 8.55; S, 7.30.

4.1.3.13. 4-(4-bromophenyl)-2-[1-(3,4-dichlorophenyl)ethylidenehydrazinyl]-5-methylthiazole (**23**). Recrystallization in hot ethanol afforded beige crystals, m.p.: 270 °C; yield: 1.20 g (69%); R_f = 0.65 (toluol/ethyl acetate 6:4). IR (KBr): 2923 (CH), 1622 (C=N) cm⁻¹. ¹H NMR (300 MHz, DMSO-*d*₆): δ 2.31 (s, 3H, CH₃), 2.38 (s, 3H, CH₃), 7.56 (d, 1H, *J* 8.7 Hz, Ar), 7.64 (d, 2H, *J* 3.3 Hz, Ar), 7.67 (d, 2H, *J* 3.3 Hz, Ar), 7.76 (dd, 1H, *J* 8.7 and 1.5 Hz, Ar), 7.97 (d, 1H, *J* 1.5 Hz, Ar). ¹³C NMR (75.5 MHz, DMSO-*d*₆): δ 12.1 (CH₃), 14.0 (CH₃), 118.4 (C5 thiazole), 120.8 (C, Ar), 125.9 (CH, Ar), 127.4 (CH, Ar), 130.2 (CH, Ar), 130.5 (CH, Ar), 131.3 (CH, Ar), 131.5 (CH, Ar), 133.7 (C, Ar), 138.2 (C, Ar), 144.2 (C, Ar), 149.1 (C=N), 165.5 (S–C=N). Anal. calcd for C₁₈H₁₄BrCl₂N₃S: C, 47.49; H, 3.10; N, 9.23; S, 7.04. Found: C, 47.52; H, 3.02; N, 9.83; S, 7.05.

4.1.3.14. 2-[1-(3,4-dichlorophenyl)ethylidenehydrazinyl]-4-(4-nitrophenyl)thiazole (**24**). Recrystallization in hot ethanol afforded orange crystals, m.p.: 226–228 °C; yield: 1.11 g (71%); R_f = 0.61 (toluol/ethyl acetate 6:4). IR (KBr): 3304 (NH), 1597 and 1565 (C=N) cm⁻¹. ¹H NMR (300 MHz, DMSO-*d*₆): δ 2.32 (s, 3H, CH₃), 7.69 (d, 1H, *J* 8.7 Hz, Ar), 7.70 (s, 1H, CH thiazole), 7.76 (dd, 1H, *J* 8.7 and 2.1 Hz, Ar), 7.95 (d, 1H, *J* 2.1 Hz, Ar), 8.13 (d, 2H, *J* 8.7 Hz, Ar), 8.29 (d, 2H, *J* 8.7 Hz, Ar). ¹³C NMR (75.5 MHz, DMSO-*d*₆): δ 16.2 (CH₃), 106.5 (CH thiazole), 121.4 (CH, Ar), 123.4 (CH, Ar), 127.0 (CH, Ar), 128.6 (CH, Ar), 131.6 (CH, Ar), 132.7 (C, Ar), 132.9 (C, Ar), 137.6 (C, Ar), 139.8 (C, Ar), 144.5 (C, Ar), 148.6 (C, Ar), 158.6 (C=N), 171.1 (S–C=N). HRMS (ESI): 404.9496 [M – H]⁺. Anal. calcd for C₁₇H₁₂Cl₂N₄O₂S: C, 50.13; H, 2.97; N, 13.76; S, 7.87. Found: C, 50.12; H, 3.00; N, 13.69; S, 8.07.

4.1.3.15. 2-[1-(3,4-dichlorophenyl)ethylidenehydrazinyl]-4-(3-nitrophenyl)thiazole (**25**). Recrystallization in hot ethanol afforded orange crystals, m.p.: 234–236 °C; yield: 1.30 g (83%); R_f = 0.63 (toluol/ethyl acetate 6:4). IR (KBr): 3089 (C–H), 1614 and 1565 (C=N) cm⁻¹. ¹H NMR (300 MHz, DMSO-*d*₆): δ 2.32 (s, 3H, CH₃), 7.64 (d, 1H, *J* 8.4 Hz, Ar), 7.67 (s, 1H, CH thiazole), 7.69–7.74 (m, 2H, Ar), 7.91 (d, 1H, *J* 2.1 Hz, Ar), 8.13 (dd, 1H, *J* 8.4 and 2.1 Hz, Ar), 8.30 (d, 1H, *J* 7.8 Hz, Ar), 8.69 (s, 1H, Ar). ¹³C NMR (75.5 MHz, DMSO-*d*₆): δ 14.2 (CH₃), 107.5 (CH thiazole), 120.4 (CH, Ar), 122.4 (CH, Ar), 126.0 (CH, Ar), 127.6 (CH, Ar), 130.6 (CH, Ar), 130.9 (CH, Ar), 131.5 (CH, Ar), 131.7 (C, Ar), 131.9 (C, Ar), 136.6 (C, Ar), 138.8 (C, Ar), 144.5 (C, Ar), 148.6 (C=N), 170.1 (S–C=N). HRMS (ESI): 406.9958 [M+H]⁺. Anal. calcd for C₁₇H₁₂Cl₂N₄O₂S: C, 50.13; H, 2.97; N, 13.76; S, 7.87. Found: C, 50.33; H, 2.87; N, 13.77; S, 7.88.

4.1.3.16. 2-[1-(3,4-dichlorophenyl)ethylidenehydrazinyl]-4-(4-methoxyphenyl)thiazole (**26**). Recrystallization in hot ethanol afforded yellow crystals, m.p.: 216–218 °C; yield: 1.22 g (81%); R_f = 0.6 (toluol/ethyl acetate 6:4). IR (KBr): 2914 (C–H), 1611 (C=N) cm⁻¹. ¹H NMR (300 MHz, DMSO-*d*₆): δ 2.31 (s, 3H, CH₃), 3.77 (s, 3H, O–CH₃), 6.97 (d, 2H, *J* 8.7 Hz, Ar), 7.17 (s, 1H, CH thiazole), 7.66 (d, 1H, *J* 8.4 Hz, Ar), 7.75 (d, 2H, *J* 8.7 Hz, Ar), 7.78 (d, 1H, *J* 8.4 Hz, Ar), 7.95 (s, 1H, Ar), 10.29 (s, 1H, NH). ¹³C NMR (75.5 MHz, DMSO-*d*₆): δ 13.8 (CH₃), 55.1 (O–CH₃), 102.2 (CH thiazole), 114.0 (CH, Ar), 125.7 (CH, Ar), 126.9 (CH, Ar), 127.2 (CH, Ar), 130.6 (CH, Ar), 131.1 (C, Ar), 131.3 (C, Ar), 138.4 (C, Ar), 144.4 (C, Ar), 149.5 (C, Ar), 158.9 (C=N), 169.3 (S–C=N). HRMS (ESI): 392.0213 [M+H]⁺. Anal. calcd for

C₁₈H₁₅Cl₂N₃OS: C, 55.11; H, 3.85; N, 10.71; S, 8.17. Found: C, 55.09; H, 3.62; N, 10.50; S, 8.23.

4.1.3.17. 4-([1,1'-biphenyl]-4-yl)-2-[1-(3,4-dichlorophenyl)ethylidenehydrazinyl]thiazole (**27**). Recrystallization in hot toluol afforded beige crystals, m.p.: 269–271 °C; yield: 1.15 g (61%); R_f = 0.78 (toluol/ethyl acetate 6:4). IR (KBr): 2925 (C–H), 1608 (C=N) cm⁻¹. ¹H NMR (300 MHz, DMSO-*d*₆): δ 2.32 (s, 3H, CH₃), 7.33–7.48 (m, 5H, Ar), 7.66–7.78 (m, 6H, Ar), 7.93–7.96 (m, 3H, Ar). ¹³C NMR (75.5 MHz, DMSO-*d*₆): δ 15.0 (CH₃), 104.7 (CH thiazole), 125.8 (CH, Ar), 126.2 (CH, Ar), 126.5 (CH, Ar), 126.9 (CH, Ar), 127.3 (CH, Ar), 127.5 (CH, Ar), 128.8 (CH, Ar), 129.0 (CH, Ar), 130.6 (C, Ar), 131.2 (C, Ar), 131.3 (C, Ar), 133.2 (C, Ar), 138.4 (C, Ar), 139.2 (C, Ar), 139.6 (C, Ar), 150.0 (C=N), 169.4 (S–C=N). Anal. calcd for C₂₃H₁₇Cl₂N₃S: C, 63.02; H, 3.91; N, 9.59; S, 7.31. Found: C, 63.08; H, 3.98; N, 9.55; S, 7.21.

4.1.3.18. 2-[1-(3,4-dichlorophenyl)ethylidenehydrazinyl]-4-(naphthalen-2-yl)thiazole (**28**). Recrystallization in hot toluol afforded beige crystals, m.p.: 259–260 °C; yield: 1.14 g (72%); R_f = 0.68 (toluol/ethyl acetate 6:4). IR (KBr): 3047 (C–H), 1621 (C=N) cm⁻¹. ¹H NMR (300 MHz, DMSO-*d*₆): δ 2.32 (s, 3H, CH₃), 7.49 (m, 3H, Ar), 7.62–7.75 (m, 2H, Ar), 7.88–8.00 (m, 5H, Ar), 8.38 (s, 1H, CH, Ar). ¹³C NMR (75.5 MHz, DMSO-*d*₆): δ 13.9 (CH₃), 105.3 (CH thiazole), 123.9 (CH, Ar), 124.2 (CH, Ar), 125.7 (CH, Ar), 126.1 (CH, Ar), 126.5 (CH, Ar), 127.3 (CH, Ar), 127.6 (CH, Ar), 128.1 (CH, Ar), 130.6 (C, Ar), 131.1 (C, Ar), 131.3 (C, Ar), 131.6 (C, Ar), 132.4 (C, Ar), 133.1 (C, Ar), 138.4 (C, Ar), 144.6 (C, Ar), 149.7 (C=N), 169.5 (S–C=N). HRMS (ESI): 411.9917 [M+H]⁺. Anal. calcd for C₂₁H₁₅Cl₂N₃S: C, 61.17; H, 3.67; N, 10.19; S, 7.78. Found: C, 61.18; H, 3.94; N, 10.21; S, 7.99.

4.2. Cruzain inhibition

Cruzain activity was measured by monitoring the cleavage of the fluorogenic substrate Z-FR-AMC, as previously described [50]. Assays were performed in 0.1 M sodium acetate buffer pH 5.5, in the presence of 1 mM beta-mercaptoethanol and 0.01% Triton X-100, to a final volume of 200 μL and at 25 °C. The final concentrations of cruzain was 0.5 nM, and the Z-FR-AMC substrate concentration was 2.5 μM (K_m = 1 μM). In all assays, the enzyme was pre-incubated with the compounds for 10 min before adding a solution containing the Z-FR-AMC substrate. Enzyme kinetic was followed by continuous reading for 5 min at 12s intervals, employing a Synergy 2 (Biotek) from the Center of Flow Cytometry and Fluorimetry at the Biochemistry and Immunology Department (UFMG). The filters employed were 340 nM for excitation and 440 nM for emission. Activity was calculated based on initial velocity rates, compared to a DMSO control, since all compound stocks were prepared in DMSO. All compounds were evaluated at 10 μM and inhibition was measured in at least two independent experiments, in each case in triplicate. IC₅₀ curves were determined based on at least seven compound concentrations, employing the nonlinear regression analysis of “log (inhibitor) vs response with variable slope – four parameters” in the software GraphPad Prism 5.0. The reported values refer to the average and standard deviation between the values obtained for at least two curves, in which each concentration was evaluate in triplicate.

4.3. Animals

Female BALB/c mice (6–8 weeks old) were supplied by the animal breeding facility at Centro de Pesquisas Gonçalo Moniz (Fundação Oswaldo Cruz, Bahia, Brazil) and maintained in sterilized cages under a controlled environment, receiving a balanced diet for rodents and water *ad libitum*. All experiments were carried out in

accordance with the recommendations of Ethical Issues Guidelines, and were approved by the local Animal Ethics Committee (Approved number: L-IGM-016/13).

4.4. Parasites

Bloodstream trypomastigotes forms of *T. cruzi* were obtained from supernatants of LLC-MK2 cells previously infected and maintained in Dulbecco's modified Eagle medium (DMEM; Life Technologies, GIBCO-BRL, Gaithersburg, MD) supplemented with 10% fetal bovine serum (FBS; GIBCO), and 50 µg/mL of gentamycin (Novafarma, Anápolis, GO, Brazil) at 37 °C and 5% CO₂.

4.5. Host cell toxicity

Cytotoxicity of the compounds was determined initially in the rat cardiomyoblast cell line H9c2 and the murine macrophage cell line J774. Cells were seeded into 96-well plates at a cell density of 1×10^4 cells/well in Dulbecco's modified Eagle medium supplemented with 10% FBS, and 50 µg/mL of gentamycin and incubated for 24 h at 37 °C and 5% CO₂. After that time each compound, dissolved in DMSO was added at six concentrations (0.41–100 µM) in triplicate and incubated for 72 h. Cell viability was determined by AlamarBlue assay (Invitrogen, Carlsbad, CA, USA) according to the manufacturer instructions. Colorimetric readings were performed after 6 h at 570 and 600 nm. Cytotoxic concentration to 50% (CC₅₀) was calculated using data-points gathered from three independent experiments. Gentian violet (Synth, São Paulo, Brazil) was used as positive control. The final concentration of DMSO was less than 1% in all *in vitro* experiments.

4.6. Toxicity for *Y* strain trypomastigotes

Trypomastigotes collected from the supernatant of LLC-MK2 cells were dispensed into 96-well plates at a cell density of 4×10^5 cells/well. Test inhibitors, were diluted into five different concentrations and added into their respective wells, and the plate was incubated for 24 h at 37 °C and 5% of CO₂. Aliquots of each well were collected and the number of viable parasites, based on parasite motility, was assessed in a Neubauer chamber. The percentage of inhibition was calculated in relation to untreated cultures. IC₅₀ calculation was also carried out using non-linear regression with Prism 4.0 GraphPad software. Benznidazole was used as the reference drug.

4.7. Propidium iodide and annexin V staining

Trypomastigotes 1×10^7 /mL in 24 well-plates were treated with **14** (0.4 µM) in DMEM supplemented with FBS at 37 °C for 24 h and labeled for propidium iodide (PI) and annexin V using the annexin V-FITC apoptosis detection kit (Sigma), according to the manufacturer's instructions. Acquisition and analyses was performed using a FACS Calibur flow cytometer (Becton Dickinson, San Diego, CA), with FlowJo software (Tree Star, Ashland, OR). A total of 10,000 events were acquired in the region previously established as that corresponding to trypomastigotes forms of *T. cruzi*.

4.8. Rhodamine 123 staining

Trypomastigotes 1×10^7 /mL in 24 well-plates were treated or not with **14** (0.4 or 0.8 µM) in DMEM supplemented with FBS at 37 °C for 24 h. Then, cells were washed twice with PBS solution and resuspended in 0.5 mL PBS containing 5 µg/mL of Rhodamine 123 (Sigma) for 15 min. After staining, the parasites were washed twice with PBS solution and immediately analyzed using a FACS Calibur

flow cytometer (Becton Dickinson, San Diego, CA), with FlowJo software (Tree Star, Ashland, OR). A total of 10,000 events were acquired in the region previously established as that corresponding to trypomastigotes forms of *T. cruzi*.

4.8.1. Intracellular parasite development

Peritoneal exudate macrophages (5×10^4 cells/well) obtained from BALB/c mice were seeded in a 96 well-plate in DMEM supplemented with 10% FBS and incubated for 24 h. Cells were then infected with trypomastigotes (10:1) for 2 h. Free trypomastigotes were removed by successive washes using saline solution and the cells were incubated for 24 h to allow full internalization and differentiation of trypomastigotes to amastigotes. Next, cultures were incubated in complete medium alone or with the thiazole **14** (8, 2 and 0.5 µM) or benznidazole (5 µM) for 72 h. Cells were fixed in formaldehyde 4% and stained with hoeschst (100 µg/mL; Invitrogen, Carlsbad, CA). Plates were then imaged and analyzed in a Perkin-Elmer Opera confocal microscope to quantify the number of infected cells and the number of amastigotes per 100 cells, as previously described [51]. The one-way ANOVA and Bonferroni for multiple comparisons were used to determine the statistical significance of the group comparisons.

4.9. Drug combination

For *in vitro* drug combinations, doubling dilutions of each drug (**14** and benznidazole), used alone or in fixed combinations were incubated with trypomastigotes followed the protocol described above. The analysis of the combined effects was performed by determining the combination index (CI), used as cutoff to determine synergism, by using Chou-Talalay CI method [46] and through the construction of isobologram using the fixed ratio method, as described previously [52].

4.10. Infection in mice

Female BALB/c mice (18–22 g) were infected with bloodstream trypomastigotes by intraperitoneal inoculation of 10^4 parasites in 100 µL of saline solution and then mice were randomly divided in three groups (six animals per group). After the day 5 of infection, treatment with 25 mg/kg weight of **14** was given orally for five consecutive days. For the control group, benznidazole was given orally at dose of 100 mg/kg weight. Saline containing 20% DMSO was used as a vehicle and administrated on untreated and infected group. Animal infection was monitored daily by counting the number of motile parasites in 5 µL of fresh blood sample drawn from the lateral tail veins, as recommended by standard protocol [53]. Survival was monitored for 30 days after treatment. The one-way ANOVA and Bonferroni for multiple comparisons were used to determine the statistical significance of the group comparisons.

Acknowledgement

This work received support from CNPq (grant reference 471461/2011-3 to A.C.L.L.), FAPESB (PRONEX program, grant reference 6596 to M.B.P.S.), FAPEMIG (Grant PPM-00342-16 to R.S.F.) and CAPES (Grant PVE A118/2013 to R.S.F.). G.B.O.F. received a FACEPE Masters scholarship. A.C.L.L., M.B.P.S., R.S.F. and D.R.M.M. hold a CNPq fellowship. We are thankful to the Center of Flow Cytometry and Fluorimetry at the Biochemistry and Immunology Department (UFMG) for access to the fluorimeter. We also thank the Department of Fundamental Chemistry - Federal University of Pernambuco (DQF-UFPE) and Center for Strategic Technologies of the Northeast (CETENE) for recording the ¹H NMR, ¹³C NMR, LCMS and IR spectra of all compounds.

Appendix A. Supplementary data

Supplementary data related to this article can be found at <https://doi.org/10.1016/j.ejmech.2017.09.047>.

References

- [1] J. Bermudez, C. Davies, A. Simonazzi, J.P. Real, S. Palma, J. Pablo Real, S. Palma, Current drug therapy and pharmaceutical challenges for Chagas disease, *Acta Trop.* 156 (2016) 1–16, <https://doi.org/10.1016/j.actatropica.2015.12.017>.
- [2] DNDI, About Chagas Disease – DNDI, 2017. <https://www.dndi.org/diseases-projects/chagas/>. (Accessed 22 May 2017).
- [3] WHO, WHO | Chagas Disease (American Trypanosomiasis), WHO, 2014. <http://www.who.int/mediacentre/factsheets/fs340/en/>. (Accessed 18 November 2015).
- [4] I. Molina, F. Salvador, A. Sánchez-Montalvá, Actualización en enfermedad de Chagas, *Enferm. Infecc. Microbiol. Clin.* 34 (2016) 132–138, <https://doi.org/10.1016/j.eimc.2015.12.008>.
- [5] J.A. Urbina, R. Docampo, Specific chemotherapy for Chagas disease: controversies and advances, *Trends Parasitol.* 19 (2003) 495–501, <https://doi.org/10.1016/j.pt.2003.09.001>.
- [6] J.H. McKerrow, P.S. Doyle, J.C. Engel, L.M. Podust, S.A. Robertson, R. Ferreira, T. Saxton, M. Arkin, I.D. Kerr, L.S. Brinen, C.S. Craik, Two approaches to discovering and developing new drugs for Chagas disease, *Mem. Inst. Oswaldo Cruz* 104 (Suppl) (2009) 263–269. <http://www.ncbi.nlm.nih.gov/pubmed/19753483>.
- [7] J. Clayton, Chagas disease: pushing through the pipeline, *Nature* 465 (2010) S12–S15, <https://doi.org/10.1038/nature09224>.
- [8] E. Chatelain, Chagas disease drug discovery: toward a new era, *J. Biomol. Screen* 20 (2015) 22–35, <https://doi.org/10.1177/1087057114550585>.
- [9] J.A. Urbina, Specific chemotherapy of Chagas disease: relevance, current limitations and new approaches, *Acta Trop.* 115 (2010) 55–68, <https://doi.org/10.1016/j.actatropica.2009.10.023>.
- [10] N. Shang, Q. Li, T.-P. Ko, H.-C. Chan, J. Li, Y. Zheng, C.-H. Huang, F. Ren, C.-C. Chen, Z. Zhu, M. Galizzi, Z.-H. Li, C.A. Rodrigues-Poveda, D. Gonzalez-Pacanoska, P. Veiga-Santos, T.M.U. de Carvalho, W. de Souza, J.A. Urbina, A.H.-J. Wang, R. Docampo, K. Li, Y.-L. Liu, E. Oldfield, R.-T. Guo, Squalene synthase as a target for Chagas disease therapeutics, *PLoS Pathog.* 10 (2014) e1004114, <https://doi.org/10.1371/journal.ppat.1004114>.
- [11] R.J. Neitz, C. Bryant, S. Chen, J. Gut, E. Hugo Caselli, S. Ponce, S. Chowdhury, H. Xu, M.R. Arkin, J.A. Ellman, A.R. Renslo, Tetrafluorophenoxymethyl ketone cruzain inhibitors with improved pharmacokinetic properties as therapeutic leads for Chagas' disease, *Bioorg. Med. Chem. Lett.* 25 (2015) 4834–4837, <https://doi.org/10.1016/j.bmcl.2015.06.066>.
- [12] M.L. Sbaraglini, C.L. Bellera, L. Fraccaroli, L. Larocca, C. Carrillo, A. Talevi, C.D. Alba Soto, Novel cruzain inhibitors for the chemotherapy of chronic Chagas disease, *Int. J. Antimicrob. Agents* 48 (2016) 91–95, <https://doi.org/10.1016/j.ijantimicag.2016.02.018>.
- [13] X. Du, E. Hansell, J.C. Engel, C.R. Caffrey, F.E. Cohen, J.H. McKerrow, Aryl ureas represent a new class of anti-trypanosomal agents, *Chem. Biol.* 7 (2000) 733–742, [https://doi.org/10.1016/S1074-5521\(00\)00018-1](https://doi.org/10.1016/S1074-5521(00)00018-1).
- [14] H.J. Wiggers, J.R. Rocha, W.B. Fernandes, R. Sesti-Costa, Z.A. Carneiro, J. Cheleski, A.B.F. da Silva, L. Juliano, M.H.S. Cezari, J.S. Silva, J.H. McKerrow, C.A. Montanari, Non-peptidic cruzain inhibitors with trypanocidal activity discovered by virtual screening and in vitro assay, *PLoS Negl. Trop. Dis.* 7 (2013) e2370, <https://doi.org/10.1371/journal.pntd.0002370>.
- [15] J.M. dos Santos Filho, A.C.L. Leite, B.G. de Oliveira, D.R.M. Moreira, M.S. Lima, M.B.P. Soares, L.F.C.C. Leite, Design, synthesis and cruzain docking of 3-(4-substituted-aryl)-1,2,4-oxadiazole-N-acylhydrazones as anti-Trypanosoma cruzi agents, *Bioorg. Med. Chem.* 17 (2009) 6682–6691, <https://doi.org/10.1016/j.bmc.2009.07.068>.
- [16] N.C. Romeiro, G. Aguirre, P. Hernández, M. González, H. Cerecetto, I. Aldana, S. Pérez-Silanes, A. Monge, E.J. Barreiro, L.M. Lima, Synthesis, trypanocidal activity and docking studies of novel quinoxaline-N-acylhydrazones, designed as cruzain inhibitors candidates, *Bioorg. Med. Chem.* 17 (2009) 641–652, <https://doi.org/10.1016/j.bmc.2008.11.065>.
- [17] T. Franklim, L. Freire-De-Lima, J. de Nazareth Sá Diniz, J. Previato, R. Castro, L. Mendonça-Previato, M. de Lima, Design, synthesis and trypanocidal evaluation of novel 1,2,4-Triazoles-3-thiones derived from natural piperine, *Molecules* 18 (2013) 6366–6382, <https://doi.org/10.3390/molecules18066366>.
- [18] K. Brak, P.S. Doyle, J.H. McKerrow, J.A. Ellman, Identification of a new class of nonpeptidic inhibitors of cruzain, *J. Am. Chem. Soc.* 130 (2008) 6404–6410, <https://doi.org/10.1021/ja710254m>.
- [19] K. Brak, I.D. Kerr, K.T. Barrett, N. Fuchi, M. Debnath, K. Ang, J.C. Engel, J.H. McKerrow, P.S. Doyle, L.S. Brinen, J.A. Ellman, Nonpeptidic tetrafluorophenoxymethyl ketone cruzain inhibitors as promising new leads for Chagas disease chemotherapy, *J. Med. Chem.* 53 (2010) 1763–1773, <https://doi.org/10.1021/jm901633v>.
- [20] X. Du, C. Guo, E. Hansell, P.S. Doyle, C.R. Caffrey, T.P. Holler, J.H. McKerrow, F.E. Cohen, Synthesis and Structure–Activity relationship study of potent trypanocidal thio semicarbazone inhibitors of the trypanosomal cysteine protease cruzain, *J. Med. Chem.* 45 (2002) 2695–2707, <https://doi.org/10.1021/jm010459j>.
- [21] D.C. Greenbaum, Z. Mackey, E. Hansell, P. Doyle, J. Gut, C.R. Caffrey, J. Lehrman, P.J. Rosenthal, J.H. McKerrow, K. Chibale, Synthesis and Structure–Activity relationships of parasiticidal thiosemicarbazone cysteine protease inhibitors against plasmodium falciparum, trypanosoma brucei, and trypanosoma cruzi, *J. Med. Chem.* 47 (2004) 3212–3219, <https://doi.org/10.1021/jm030549j>.
- [22] R. Siles, S.-E. Chen, M. Zhou, K.G. Pinney, M.L. Trawick, Design, synthesis, and biochemical evaluation of novel cruzain inhibitors with potential application in the treatment of Chagas' disease, *Bioorg. Med. Chem. Lett.* 16 (2006) 4405–4409, <https://doi.org/10.1016/j.bmcl.2006.05.041>.
- [23] N. Beatriz Huaman Lozano, V. Goncalves Maltarollo, K. Cacilda Weber, K. Maria Honorio, R. Victorio Carvalho Guido, A. Defini Andricopulo, A. Borges Ferreira Da Silva, Molecular features for antitrypanosomal activity of thiosemicarbazones revealed by OPS-PLS QSAR studies, *Med. Chem. Los Angeles* 8 (2012) 1045–1056, <https://doi.org/10.2174/157340612804075043>.
- [24] D.R. Magalhaes Moreira, A.D.T. de Oliveira, P.A. Teixeira de Moraes Gomes, C.A. de Simone, F.S. Villela, R.S. Ferreira, A.C. da Silva, T.A.R. dos Santos, M.C.A. Brelaz de Castro, V.R.A. Pereira, A.C.L. Leite, Conformational restriction of aryl thiosemicarbazones produces potent and selective anti-Trypanosoma cruzi compounds which induce apoptotic parasite death, *Eur. J. Med. Chem.* 75 (2014) 467–478, <https://doi.org/10.1016/j.ejmech.2014.02.001>.
- [25] J.W.P. Espíndola, M.V. de O. Cardoso, G.B. de O. Filho, D.A. Oliveira e Silva, D.R.M. Moreira, T.M. Bastos, C.A. de Simone, M.B.P. Soares, F.S. Villela, R.S. Ferreira, M.C.A.B. de Castro, V.R.A. Pereira, S.M.F. Murta, P.A. Sales Junior, A.J. Romanha, A.C.L. Leite, Synthesis and structure–activity relationship study of a new series of antiparasitic aryl-oxo thiosemicarbazones inhibiting Trypanosoma cruzi cruzain, *Eur. J. Med. Chem.* 101 (2015) 818–835, <https://doi.org/10.1016/j.ejmech.2015.06.048>.
- [26] A.C.L. Leite, D.R. de M. Moreira, M.V. de O. Cardoso, M.Z. Hernandez, V.R. Alves Pereira, R.O. Silva, A.C. Kiperstok, M. da S. Lima, M.B.P. Soares, Synthesis, cruzain docking, and in vitro studies of aryl-4-oxothiazolylhydrazones Against Trypanosoma cruzi, *ChemMedChem* 2 (2007) 1339–1345, <https://doi.org/10.1002/cmdc.200700022>.
- [27] M. Zaldini Hernandez, M. Montenegro Rabello, A. Cristina Lima Leite, M. Verissimo Oliveira Cardoso, D. Rodrigo Magalhaes Moreira, D. José Brondani, C. Alberto Simone, L. Campos Reis, M. Assis Souza, V. Rego Alves Pereira, R. Salgado Ferreira, J. Hobson McKerrow, M.Z. Hernandez, M.M. Rabello, A.C.L. Leite, M.V.O. Cardoso, D.R.M. Moreira, D.J. Brondani, C.A. Simone, L.C. Reis, M.A. Souza, V.R.A. Pereira, Studies toward the structural optimization of novel thiazolylhydrazone-based potent antitrypanosomal agents, *Bioorg. Med. Chem.* 18 (2010) 7826–7835, <https://doi.org/10.1016/j.bmc.2010.09.056>.
- [28] D.R.M. Moreira, S.P.M. Costa, M.Z. Hernandez, M.M. Rabello, G.B. de Oliveira Filho, C.M.L. de Melo, L.F. da Rocha, C.A. de Simone, R.S. Ferreira, J.R.B. Fradico, C.S. Meira, E.T. Guimarães, R.M. Srivastava, V.R.A. Pereira, M.B.P. Soares, A.C.L. Leite, Structural investigation of anti-trypanosoma cruzi 2-Iminothiazolidin-4-ones allows the identification of agents with efficacy in infected mice, *J. Med. Chem.* 55 (2012) 10918–10936, <https://doi.org/10.1021/jm301518v>.
- [29] M.V. de O. Cardoso, L.R.P. de Siqueira, E.B. da Silva, L.B. Costa, M.Z. Hernandez, M.M. Rabello, R.S. Ferreira, L.F. da Cruz, D.R. Magalhaes Moreira, V.R.A. Pereira, M.C.A.B. de Castro, P.V. Bernhardt, A.C.L. Leite, 2-Pyridyl thiazoles as novel anti-Trypanosoma cruzi agents: structural design, synthesis and pharmacological evaluation, *Eur. J. Med. Chem.* 86 (2014) 48–59, <https://doi.org/10.1016/j.ejmech.2014.08.012>.
- [30] P.A.T. de Moraes Gomes, M. de Oliveira Barbosa, E. Farias Santiago, M.V. de Oliveira Cardoso, N.T. Capistrano Costa, M.Z. Hernandez, D.R.M. Moreira, A.C. da Silva, T.A.R. dos Santos, V.R.A. Pereira, F.A. Brayner dos Santos, G.A. do Nascimento Pereira, R.S. Ferreira, A.C.L. Leite, New 1,3-thiazole derivatives and their biological and ultrastructural effects on Trypanosoma cruzi, *Eur. J. Med. Chem.* 121 (2016) 387–398, <https://doi.org/10.1016/j.ejmech.2016.05.050>.
- [31] P.A.T. de M. Gomes, A.R. Oliveira, M.V. de O. Cardoso, E. de F. Santiago, M. de O. Barbosa, L.R.P. de Siqueira, D.R.M. Moreira, T.M. Bastos, F.A. Brayner, M.B.P. Soares, A.P. de O. Mendes, M.C.A.B. de Castro, V.R.A. Pereira, A.C.L. Leite, L. Siqueira, D.R.M. Moreira, T.M. Bastos, F.A. Brayner, M.B.P. Soares, A.P. de O. Mendes, M. Castro, V.R.A. Pereira, A.C.L. Leite, Phthalimido-thiazoles as building blocks and their effects on the growth and morphology of Trypanosoma cruzi, *Eur. J. Med. Chem.* 111 (2016) 46–57, <https://doi.org/10.1016/j.ejmech.2016.01.010>.
- [32] G.B. de Oliveira Filho, M.V. de Oliveira Cardoso, J.W.P. Espíndola, L.F.G.R. Ferreira, C.A. de Simone, R.S. Ferreira, P.L. Coelho, C.S. Meira, D.R. Magalhaes Moreira, M.B.P. Soares, A.C. Lima Leite, Structural design, synthesis and pharmacological evaluation of 4-thiazolidinones against Trypanosoma cruzi, *Bioorg. Med. Chem.* 23 (2015) 7478–7486, <https://doi.org/10.1016/j.bmc.2015.10.048>.
- [33] A.V. Erian, S.M. Sherif, H.M. Gaber, The chemistry of β -Haloketones and their utility in heterocyclic synthesis, *Molecules* 8 (2003) 793–865, <https://doi.org/10.3390/81100793>.
- [34] D.-N. Zhang, J.-T. Li, Y.-L. Song, H.-M. Liu, H.-Y. Li, Efficient one-pot three-component synthesis of N-(4-arylthiazol-2-yl) hydrazones in water under ultrasound irradiation, *Ultrason. Sonochem.* 19 (2012) 475–478, <https://doi.org/10.1016/j.ultrsonch.2011.10.017>.
- [35] P. Vicini, A. Geronikaki, K. Anastasia, M. Incerti, F. Zani, Synthesis and antimicrobial activity of novel 2-thiazolylimino-5-arylidene-4-thiazolidinones,

- Bioorg. Med. Chem. 14 (2006) 3859–3864, <https://doi.org/10.1016/j.bmc.2006.01.043>.
- [36] C. Pizzo, C. Saiz, A. Talevi, L. Gavernet, P. Palestro, C. Bellera, L.B. Blanch, D. Benítez, J.J. Cazzulo, A. Chidichimo, P. Wipf, S.G. Mahler, Synthesis of 2-hydrazolyl-4-thiazolidinones based on multicomponent reactions and biological evaluation against *Trypanosoma cruzi*, *Chem. Biol. Drug Des.* 77 (2011) 166–172, <https://doi.org/10.1111/j.1747-0285.2010.01071.x>.
- [37] A.C.L. Leite, R.S.R.S. de Lima, D.R. de M. Moreira, M.V. de O. Cardoso, A.C. Gouveia de Brito, L.M. Farias dos Santos, M.Z. Hernandez, A.C. Kiperstok, R.S.R.S. de Lima, M.B.P.P. Soares, Synthesis, docking, and in vitro activity of thiosemicarbazones, aminoacyl-thiosemicarbazides and acyl-thiazolidinones against *Trypanosoma cruzi*, *Bioorg. Med. Chem.* 14 (2006) 3749–3757, <https://doi.org/10.1016/j.bmc.2006.01.034>.
- [38] D.R.M. Moreira, A.C. Lima Leite, M.V.O. Cardoso, R.M. Srivastava, M.Z. Hernandez, M.M. Rabello, L.F. Da Cruz, R.S. Ferreira, C.A. De Simone, C.S. Meira, E.T. Guimaraes, A.C. Da Silva, T.A.R. Dos Santos, V.R.A. Pereira, M.B. Pereira Soares, Structural design, synthesis and structure-activity relationships of thiazolidinones with enhanced anti-*Trypanosoma cruzi* activity, *ChemMedChem* 9 (2014) 177–188, <https://doi.org/10.1002/cmdc.201300354>.
- [39] M.E. Caputto, A. Ciccarelli, F. Frank, A.G. Moglioni, G.Y. Moltrasio, D. Vega, E. Lombardo, L.M. Finkielstein, Synthesis and biological evaluation of some novel 1-indanone thiazolylhydrazones derivatives as anti-*Trypanosoma cruzi* agents, *Eur. J. Med. Chem.* 55 (2012) 155–163, <https://doi.org/10.1016/j.ejmech.2012.07.013>.
- [40] E.B. da Silva, D.A. Oliveira e Silva, A.R. Oliveira, C.H. da Silva Mendes, T.A.R. dos Santos, A.C. da Silva, M.C.A. de Castro, R.S. Ferreira, D.R.M. Moreira, M.V. de O. Cardoso, C.A. de Simone, V.R.A. Pereira, A.C.L. Leite, Design and synthesis of potent anti-*Trypanosoma cruzi* agents new thiazoles derivatives which induce apoptotic parasite death, *Eur. J. Med. Chem.* 130 (2017) 39–50, <https://doi.org/10.1016/j.ejmech.2017.02.026>.
- [41] R.S. Ferreira, C. Bryant, K.K.H. Ang, J.H. McKerrow, B.K. Shoichet, A.R. Renslo, Divergent modes of enzyme inhibition in a homologous structure-activity series, *J. Med. Chem.* 52 (2009) 5005–5008, <https://doi.org/10.1021/jm9009229>.
- [42] J.M. dos Santos Filho, D.R.M. Moreira, C.A. de Simone, R.S. Ferreira, J.H. McKerrow, C.S. Meira, E.T. Guimarães, M.B.P. Soares, Optimization of anti-*Trypanosoma cruzi* oxadiazoles leads to identification of compounds with efficacy in infected mice, *Bioorg. Med. Chem.* 20 (2012) 6423–6433, <https://doi.org/10.1016/j.bmc.2012.08.047>.
- [43] A.L. Matsuo, L.S. Silva, A.C. Torrecilhas, B.S. Pascoalino, T.C. Ramos, E.G. Rodrigues, S. Schenkman, A.C.F. Caires, L.R. Travassos, In vitro and in vivo trypanocidal effects of the cyclopalladated compound 7a, a drug candidate for treatment of Chagas' disease, *Antimicrob. Agents Chemother.* 54 (2010) 3318–3325, <https://doi.org/10.1128/AAC.00323-10>.
- [44] L. Vivas, L. Rattray, L. Stewart, E. Bongard, B.L. Robinson, W. Peters, S.L. Croft, Anti-malarial efficacy of pyronaridine and artesunate in combination in vitro and in vivo, *Acta Trop.* 105 (2008) 222–228, <https://doi.org/10.1016/j.actatropica.2007.12.005>.
- [45] L. de F. Diniz, J.A. Urbina, I.M. de Andrade, A.L. Mazzeti, T.A.F. Martins, I.S. Caldas, A. Talvani, I. Ribeiro, M.T. Bahia, Benznidazole and posaconazole in experimental Chagas disease: positive interaction in concomitant and sequential treatments, *PLoS Negl. Trop. Dis.* 7 (2013) e2367, <https://doi.org/10.1371/journal.pntd.0002367>.
- [46] T.C. Chou, P. Talalay, Quantitative analysis of dose-effect relationships: the combined effects of multiple drugs or enzyme inhibitors, *Adv. Enzyme Regul.* 22 (1984) 27–55, <http://www.ncbi.nlm.nih.gov/pubmed/6382953>.
- [47] C.A. Lipinski, F. Lombardo, B.W. Dominy, P.J. Feeney, Experimental and computational approaches to estimate solubility and permeability in drug discovery and development settings, *Adv. Drug Deliv. Rev.* 23 (1997) 3–25, [https://doi.org/10.1016/S0169-409X\(96\)00423-1](https://doi.org/10.1016/S0169-409X(96)00423-1).
- [48] N.A. Meanwell, Improving drug candidates by design: a focus on physico-chemical properties as a means of improving compound disposition and safety, *Chem. Res. Toxicol.* 24 (2011) 1420–1456, <https://doi.org/10.1021/tx200211v>.
- [49] D.F. Veber, S.R. Johnson, H.-Y. Cheng, B.R. Smith, K.W. Ward, K.D. Kopple, Molecular properties that influence the oral bioavailability of drug candidates, *J. Med. Chem.* 45 (2002) 2615–2623, <http://www.ncbi.nlm.nih.gov/pubmed/12036371>.
- [50] N.C. Fonseca, L.F. da Cruz, F. da Silva Villela, G.A. do Nascimento Pereira, J.L. de Siqueira-Neto, D. Kellar, B.M. Suzuki, D. Ray, T.B. de Souza, R.J. Alves, P.A.S. J?nior, A.J. Romanha, S.M.F. Murta, J.H. McKerrow, C.R. Caffrey, R.B. de Oliveira, R.S. Ferreira, Synthesis of a sugar-based thiosemicarbazone series and structure-activity relationship versus the parasite cysteine proteases rhodesain, cruzain, and schistosoma mansonii cathepsin B1, *Antimicrob. Agents Chemother.* 59 (2015) 2666–2677, <https://doi.org/10.1128/AAC.04601-14>.
- [51] J. Alonso-Padilla, I. Cotillo, J.L. Presa, J. Cantizani, I. Peña, A.I. Bardera, J.J. Martín, A. Rodríguez, Automated high-content assay for compounds selectively toxic to *trypanosoma cruzi* in a myoblastic cell line, *PLoS Negl. Trop. Dis.* 9 (2015) e0003493, <https://doi.org/10.1371/journal.pntd.0003493>.
- [52] Q.L. Fivelman, I.S. Adagu, D.C. Warhurst, Modified fixed-ratio isobologram method for studying in vitro interactions between atovaquone and proguanil or dihydroartemisinin against drug-resistant strains of *Plasmodium falciparum*, *Antimicrob. Agents Chemother.* 48 (2004) 4097–4102, <https://doi.org/10.1128/AAC.48.11.4097-4102.2004>.
- [53] Z. BRENER, Therapeutic activity and criterion of cure on mice experimentally infected with *Trypanosoma cruzi*, *Rev. Inst. Med. Trop. Sao Paulo.* 4 (n.d.) 389–396.